THE 11TH EDITION OF THE INTERNATIONAL MEETING OF THE SPCE-TC: ADVANCES IN STEM CELLS AND CELL THERAPIES

EDITED BY: Susana Solá and Joana Paiva Miranda
PUBLISHED IN: Frontiers in Cell and Developmental Biology

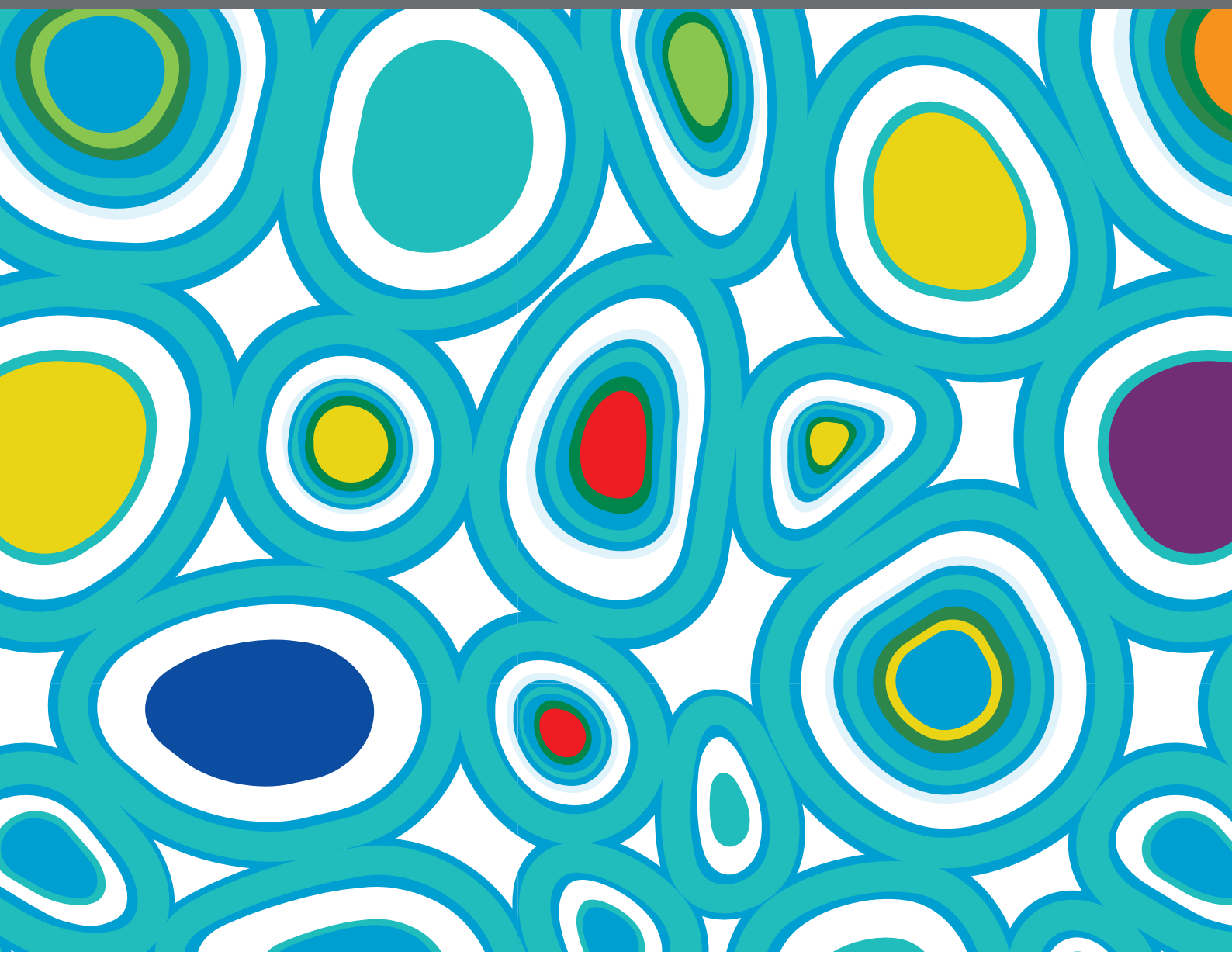

frontiers Research Topics

ISSN 1664-8714
ISBN 978-2-88971-321-9
DOI 10.3389/978-2-88971-321-9

About Frontiers

Frontiers is more than just an open-access publisher of scholarly articles: it is a pioneering approach to the world of academia, radically improving the way scholarly research is managed. The grand vision of Frontiers is a world where all people have an equal opportunity to seek, share and generate knowledge. Frontiers provides immediate and permanent online open access to all its publications, but this alone is not enough to realize our grand goals.

Frontiers Journal Series

The Frontiers Journal Series is a multi-tier and interdisciplinary set of open-access, online journals, promising a paradigm shift from the current review, selection and dissemination processes in academic publishing. All Frontiers journals are driven by researchers for researchers; therefore, they constitute a service to the scholarly community. At the same time, the Frontiers Journal Series operates on a revolutionary invention, the tiered publishing system, initially addressing specific communities of scholars, and gradually climbing up to broader public understanding, thus serving the interests of the lay society, too.

Dedication to Quality

Each Frontiers article is a landmark of the highest quality, thanks to genuinely collaborative interactions between authors and review editors, who include some of the world's best academicians. Research must be certified by peers before entering a stream of knowledge that may eventually reach the public - and shape society; therefore, Frontiers only applies the most rigorous and unbiased reviews.
Frontiers revolutionizes research publishing by freely delivering the most outstanding research, evaluated with no bias from both the academic and social point of view. By applying the most advanced information technologies, Frontiers is catapulting scholarly publishing into a new generation.

What are Frontiers Research Topics?

Frontiers Research Topics are very popular trademarks of the Frontiers Journals Series: they are collections of at least ten articles, all centered on a particular subject. With their unique mix of varied contributions from Original Research to Review Articles, Frontiers Research Topics unify the most influential researchers, the latest key findings and historical advances in a hot research area! Find out more on how to host your own Frontiers Research Topic or contribute to one as an author by contacting the Frontiers Editorial Office: frontiersin.org/about/contact

THE 11TH EDITION OF THE INTERNATIONAL MEETING OF THE SPCE-TC: ADVANCES IN STEM CELLS AND CELL THERAPIES

Topic Editors:
Susana Solá, University of Lisbon, Portugal
Joana Paiva Miranda, University of Lisbon, Portugal

Citation: Solá, S., Miranda, J. P., eds. (2021). The 11th Edition of the International Meeting of the SPCE-TC: Advances in Stem Cells and Cell Therapies. Lausanne: Frontiers Media SA. doi: 10.3389/978-2-88971-321-9

Table of Contents

frontiers in Cell and Developmental Biology

EDITORIAL
published: 14 July 2021
doi: 10.3389/fcell.2021.720554

Editorial: The 11th Edition of the International Meeting of the SPCE-TC: Advances in Stem Cells and Cell Therapies

Joana P. Miranda and Susana Solá**

Faculty of Pharmacy, Research Institute for Medicines (iMed.ULisboa), Universidade de Lisboa, Lisbon, Portugal

Keywords: stem cell repair mechanisms, neuroscience, cancer, tissue engineering, cell development, hepatology

Editorial on the Research Topic

The 11th Edition of the International Meeting of the SPCE-TC: Advances in Stem Cells and Cell Therapies

OPEN ACCESS

Edited and reviewed by:
Valerie Kouskoff,
The University of Manchester, United Kingdom

****Correspondence:***
Joana P. Miranda
jmiranda@ff.ulisboa.pt
Susana Solá
susana.sola@ff.ulisboa.pt

Specialty section:
This article was submitted to Stem Cell Research, a section of the journal Frontiers in Cell and Developmental Biology

Received: *04 June 2021*
Accepted: *21 June 2021*
Published: *14 July 2021*

Citation:
Miranda JP and Solá S (2021) Editorial: The 11th Edition of the International Meeting of the SPCE-TC: Advances in Stem Cells and Cell Therapies. Front. Cell Dev. Biol. 9:720554. doi: 10.3389/fcell.2021.720554

The key role of stem cells on tissue development, maintenance, and repair is becoming increasingly evident in health and disease. The special issue on *The 11th Edition of the International Meeting of the SPCE-TC: Advances in Stem Cells and Cell Therapies* gathers several scientific contributions in this area while featuring the collaborative and interdisciplinary approach among Portuguese scientists within the stem cell community.

With the main focus on stem cells and regenerative medicine, our selected content embraces novel discoveries on metabolic and cell reprogramming, tissue engineering, regenerative medicine and cell transplantation while highlighting major advances in developmental biology, cancer and neuroscience scientific fields.

Original research articles include novel stem cell engineering approaches to breakthrough neuroscience. For example, Rocha et al. reveal that the combination of two type of cells in 3D biodegradable hydrogels promotes an efficient re-vascularization in trauma-related injuries of the central nervous system. In fact, acute traumatic spinal cord injury is a devastating event without effective therapeutic approach (Ahuja et al., 2017). In this study, the authors show that, under specific bio-engineering conditions, adipose-derived stem cells are capable of regulating protein expression in human umbilical vein endothelial cells to stimulate neuritogenesis and increase vascularization of dorsal root ganglia explants. These data open up promising avenues toward the implantion of this biomaterial-based cell therapy after spinal cord injury, possibly inducing revascularization and functional recovery. Regarding the value of neural organoids for disease modeling and therapy, Gomes et al. have managed to derive both dorsal and ventral 3D structures from health individuals- and Rett patient-specific induced pluripotent stem cells (hiPSCs) and study the organization and functional network complexity of the Rett Syndrome. Although brain organoids derived from Rett patients have been already used to identify promising treatments (Samarasinghe et al., 2019; Trujillo et al., 2021) this work provides a deeper understanding of the neural defects associated early stages of the developmental process in this Syndrome. Noteworthy, a premature development of the deep-cortical layer and a lower expression of neural progenitor cells were observed in dorsal organoids of female Rett-derived organoids, along with impairments of interneuron's migration and other electrophysiological and functional defects. In line with

the previous works, Serras et al. further demonstrate the value of tissue organoids, in particular, 3D liver models for drug development. Around 40–50% of the drug candidates associated with hepatotoxicity in humans do not present the same toxicological concern in animal models (van Tonder et al., 2013). This has led to the proposal that the better the quality of non-clinical safety profiles, the higher the success rates for moving phase II upward (Cook et al., 2014; Walker et al., 2020). Consequently, *in vitro* liver models are growing strong while new drugs advance into clinical trials. This comprehensive review addresses the drug-induced hepatotoxicity mechanisms and the currently available 3D liver *in vitro* models, their characteristics, as well as their advantages and limitations for human hepatotoxicity assessment.

In addition, and going back to neuroscience field, the use of hiPSC to dissect neuropathological mechanisms was also performed by Lopes et al., who reveal profound alterations on mitochondrial biogenesis, function and morphology in both iPSC and neural stem cells derived from Huntington disease (HD) patients. HD is caused by CAG repeat expansion in the HTT gene and, like other neurodegenerative conditions, this disease continues to lack an effective cure. In this work, the authors demonstrate that deletion of CAG repeat by CRISPR/Cas9 technology ameliorates all mitochondrial phenotypes of HD-derived cells, bringing significant new information to tackle metabolic dysfunction associated with this neurological condition.

The remarkable contribution of Garcez et al. is another step toward our understanding on the role of mitochondrial dynamics and morphology in stem cell activity. Here, it has been elegantly revealed that mitochondrial dynamics are pivotal to assure basal oxidative phosphorylation levels in female germ stem cells of Drosophila ovary, and, importantly, that the number and morphology of these cells is greatly dependent on their basal respiration levels. Indeed, these findings are absolutely in line with recent studies demonstrating that aging-induced germline stem cell loss is dependent on mitochondrial dynamic shifts (Amartuvshin et al., 2020) and that maintenance of male germline stem cells relies on mitochondrial fusion processes (Demarco et al., 2019).

Still in the developmental biology field, this Research Topic also includes two personal perspectives from Seco et al. and from Soares-da-Silva et al. Specifically, Seco et al. discuss the embryonic source of aortic hematopoietic stem cells, a matter of intense debate within in the hematopoietic development field. The authors reflect on recent fate-mapping discoveries to re-interpretate classical studies in avian embryos and unify principles that better clarify the identity and origin of aortic hematopoietic stem cells. They also present conflicted data and discuss how future research may contribute to clarify some controversies, while also providing exciting data in chick embryos. On the other hand, Soares-da-Silva et al. explore hematopoietic and hepatic fetal systems concurrent establishment and evaluate to what degree they modulate their respective development. Indeed, deeper insights on the dynamics of fetal liver composition along development, and on how these different cell types impact hematopoiesis, are needed (Ema and Nakauchi, 2000). As insights into the molecular networks governing physiological hematopoietic stem cell (HSC) expansion accumulate, it is foreseeable that strategies to enhance HSC proliferation will be also improved.

Moving to cancer biology, Boemi et al. reveal for the first time that tamoxifen has no significant effect on cellular functions of adipose-derived stem cells. This ex-vivo single-center study come to contradict previous *in vitro* reports showing that tamoxifen inhibits proliferation and multi-lineage differentiation rates of adipose-derived stem cells (Pike et al., 2015), rising the discussion in this area of research. Further insights on the fast-growing cancer stem cells research area can also be found on our review collection, in which Pádua et al. emphasize the relevance of several transcription factors as potential biomarkers for cancer stem cells, but also as putative therapeutic targets in gastric and colorectal cancer. Still within the cancer field, but with a different approach, Silva M. et al., hold a promising future for the use of human mesenchymal stromal cells (MSCs), as cell delivery systems for anticancer proteins, due to their unique biological features (Ayuzawa et al., 2009). Upon treatment with hazurin-MSC-secretome, the authors observed a decrease in cancer cell proliferation, migration, and invasion, as well as an increase in cell death of lung and breast cancer cell lines, suggesting that MSC-derived secretome containing azurin elicits an anticancer effect.

Other important potential of stem cells is their application for regenerative medicine and developing new Advanced therapeutic medicinal products (ATMPs), namely for cell therapies (Samsonraj et al., 2017). In particular, human MSCs have gather special interest as a universal and feasible add-on therapy for several pathologies. This has been also extensively explored in this issue by Coelho et al., Laundos et al., and Silva M. et al.. Coelho et al., in a critical and very actual revision paper, approach MSCs as a potential therapeutic strategy in COVID-19 patients. On the other hand, Laundos et al., in a murine myocardial infarction model, show that umbilical cord matrix (UCM)-MSC based cellular products improved cardiac function and limited adverse cardiac remodeling post-ischemic injury, supporting the sustained and long-term beneficial therapeutic effect of MSCs. Silva A. C. et al., in turn, review the impact of extracellular matrix (ECM) alterations on cardiac cells, throughout heart ontogeny and disease, a hot topic as well (Bonnans et al., 2014). They further debate on available strategies based on cell–ECM interactions, toward the design of new regenerative therapies. Finally, Inácio et al., further highlight the importance of deciphering the regenerative mechanisms of mammalian adult heart. Indeed, heart failure, due to cardiomyocyte loss, is still one of the significant health burdens worldwide. In order to further contribute to the field, the authors demonstrate that DAN domain family member 5 precursor (DAND5) is a key driver for the generation and expansion of iPSC-derived cardiomyocytes systems, and therefore with further clinical application purposes.

We are particularly pleased to present this Collection and hope our readers will consider this a useful resource for the state of the art in the emerging field of stem cells and cell

therapies. We also thank all contributing authors, referees and Frontiers journals.

AUTHOR CONTRIBUTIONS

JPM and SS wrote the Editorial based on their critical analysis of all articles submitted in the special issue on the 11th Edition of the International Meeting of the SPCE-TC: Advances in Stem Cells and Cell Therapies. Both authors contributed to the article and approved the submitted version.

FUNDING

This work was supported by grants PTDC/MED-NEU/29650/2017, PTDC/MED-TOX/29183-2017, UIDB/04138/2020, and UIDP/04138/2020 from Fundação para a Ciência e a Tecnologia, Lisbon, Portugal.

ACKNOWLEDGMENTS

We thank all contributing authors, referees and Frontiers journal.

REFERENCES

Ahuja, C. S., Wilson, J. R., Nori, S., Kotter, M. R. N., Druschel, C., Curt, A., et al. (2017). Traumatic spinal cord injury. *Nat. Rev. Dis. Primers* 3:17018. doi: 10.1038/nrdp.2017.18

Amartuvshin, O., Lin, C., Hsu, S., Kao, S. H., Chen, A., Tang, W. C., et al. (2020). Aging shifts mitochondrial dynamics toward fission to promote germline stem cell loss. *Aging Cell*. 19:e13191. doi: 10.1111/acel.13191

Ayuzawa, R., Doi, C., Rachakatla, R. S., Pyle, M. M., Maurya, D. K., Troyer, D., et al. (2009). Naïve human umbilical cord matrix derived stem cells significantly attenuate growth of human breast cancer cells *in vitro* and *in vivo*. *Cancer Lett.* 280, 31–37. doi: 10.1016/j.canlet.2009.02.011

Bonnans, C., Chou, J., and Werb, Z. (2014). Remodelling the extracellular matrix in development and disease. *Nat. Rev. Mol. Cell Biol.* 15, 786–801. doi: 10.1038/nrm3904

Cook, D., Brown, D., Alexander, R., March, R., Morgan, P., Satterthwaite, G., et al. (2014). Lessons learned from the fate of AstraZeneca's drug pipeline: a five-dimensional framework. *Nat. Rev. Drug Discov.* 13, 419–431. doi: 10.1038/nrd4309

Demarco, R. S., Uyemura, B. S., D'Alterio, C., and Jones, D. L. (2019). Mitochondrial fusion regulates lipid homeostasis and stem cell maintenance in the Drosophila testis. *Nat. Cell Biol.* 21, 710–720. doi: 10.1038/s41556-019-0332-3

Ema, H., and Nakauchi, H. (2000). Expansion of hematopoietic stem cells in the developing liver of a mouse embryo. *Blood* 95, 2284–2289. doi: 10.1182/blood.V95.7.2284

Pike, S., Zang, P., and Wei, Z. (2015). In vitro effects of tamoxifen on adipose-derived stem cells. *Wound Repair. Regen.* 23, 728–736. doi: 10.1111/wrr.12322

Samarasinghe, R. A., Miranda, A. O., Mitchel, S., Ferando, I., Watanabe, M., Buth, J. E., et al. (2019). Identification of neural oscillations and epileptiform changes in human brain organoids. *Biorxiv [Preprint]*. doi: 10.1101/820183

Samsonraj, R. M., Raghunath, M., Nurcombe, V., Hui, J. H., van Wijnen, A. J., and Cool, S. M. (2017). Concise Review: Multifaceted Characterization of Human Mesenchymal Stem Cells for Use in Regenerative Medicine. *Stem Cells Transl. Med.* 6, 2173–2185. doi: 10.1002/sctm.17-0129

Trujillo, C. A., Adams, J. W., Negraes, P. D., Carromeu, C., Tejwani, L., Acab, A., et al. (2021). Pharmacological reversal of synaptic and network pathology in human MECP2-KO neurons and cortical organoids. *EMBO Mol. Med.* 13:e12523. doi: 10.15252/emmm.202012523

van Tonder, J. J., Steenkamp, V., and Gulumi, M. (2013). "Pre-clinical assessment of the potential intrinsic hepatotoxicity of candidate drugs," in *New Insights Into Toxicity and Drug Testing*, ed S. Gowder (London: IntechOpen).

Walker, P. A., Ryder, S., Lavado, A., Dilworth, C., and Riley, R. J. (2020). The evolution of strategies to minimise the risk of human drug-induced liver injury (DILI) in drug discovery and development. *Arch. Toxicol.* 94, 2559–2585. doi: 10.1007/s00204-020-02763-w

Conflict of Interest: The authors declare that the research was conducted in the absence of any commercial or financial relationships that could be construed as a potential conflict of interest.

frontiers in Cell and Developmental Biology

ORIGINAL RESEARCH
published: 16 June 2020
doi: 10.3389/fcell.2020.00489

In vitro Evaluation of ASCs and HUVECs Co-cultures in 3D Biodegradable Hydrogels on Neurite Outgrowth and Vascular Organization

*Luís A. Rocha[1,2,3], Eduardo D. Gomes[1,2], João L. Afonso[1,2], Sara Granja[1,2], Fatima Baltazar[1,2], Nuno A. Silva[1,2], Molly S. Shoichet[4], Rui A. Sousa[3], David A. Learmonth[3] and Antonio J. Salgado[1,2]**

[1] Life and Health Sciences Research Institute (ICVS), School of Medicine, University of Minho, Braga, Portugal, [2] ICVS/3B's – PT Government Associate Laboratory, Guimaraes, Portugal, [3] Stemmatters, Biotecnologia e Medicina Regenerativa SA, Barco, Portugal, [4] Institute of Biomaterials and Biomedical Engineering, University of Toronto, Toronto, ON, Canada

OPEN ACCESS

Edited by:
Joana Paiva Miranda,
University of Lisbon, Portugal

Reviewed by:
Hae-Won Kim,
Institute of Tissue Regeneration Engineering (ITREN), South Korea
Christian Dani,
INSERM U1091 Institut de biologie de Valrose, France

***Correspondence:**
Antonio J. Salgado
asalgado@med.uminho.pt

Specialty section:
This article was submitted to Stem Cell Research, a section of the journal Frontiers in Cell and Developmental Biology

Received: 15 March 2020
Accepted: 25 May 2020
Published: 16 June 2020

Citation:
Rocha LA, Gomes ED, Afonso JL, Granja S, Baltazar F, Silva NA, Shoichet MS, Sousa RA, Learmonth DA and Salgado AJ (2020) In vitro Evaluation of ASCs and HUVECs Co-cultures in 3D Biodegradable Hydrogels on Neurite Outgrowth and Vascular Organization. Front. Cell Dev. Biol. 8:489. doi: 10.3389/fcell.2020.00489

Vascular disruption following spinal cord injury (SCI) decisively contributes to the poor functional recovery prognosis facing patients with the condition. Using a previously developed gellan gum hydrogel to which the adhesion motif GRGDS was grafted (GG-GRGDS), this work aimed to understand the ability of adipose-derived stem cells (ASCs) to impact vascular organization of human umbilical vein endothelial cells (HUVECs), and how this in turn affects neurite outgrowth of dorsal root ganglia (DRG) explants. Our data shows that culturing these cells together lead to a synergistic effect as showed by increased stimulation of neuritogenesis on DRG. Importantly, HUVECs were only able to assemble into vascular-like structures when cultured in the presence of ASCs, which shows the capacity of these cells in reorganizing the vascular milieu. Analysis of selected neuroregulatory molecules showed that the co-culture upregulated the secretion of several neurotrophic factors. On the other hand, ASCs, and ASCs + HUVECs presented a similar profile regarding the presence of angiotrophic molecules herein analyzed. Finally, the implantation of GG-GRGDS hydrogels encapsulating ASCs in the chick chorioallantoic membrane (CAM) lead to increases in vascular recruitment toward the hydrogels in comparison to GG-GRGDS alone. This indicates that the combination of ASCs with GG-GRGDS hydrogels could promote re-vascularization in trauma-related injuries in the central nervous system and thus control disease progression and induce functional recovery.

Keywords: vascularization, spinal cord injury, neurovascular, biomaterial, cell therapy, secretome, adipose-derived stem cells

INTRODUCTION

According to latest estimations, approximately 27 million people worldwide live with disabilities caused by spinal cord injury (SCI; James et al., 2019). This condition causes severe motor, autonomic, and sensory deficits. To date, treatment options are restricted to palliative care (Silva et al., 2014). Disruption of the vascular architecture of the spinal cord occurs concomitantly with injury and originates intraparenchymal hemorrhage, tissue edema, and swelling that leads to tissue ischemia (Mautes et al., 2000). Consequently, the blood spinal cord barrier (BSCB) is compromised and blood-borne molecules and inflammatory cells infiltrate the tissue indiscriminately (Bartanusz et al., 2011). Vascular damage initiates in gray matter and progressively extends into surrounding white matter leading to disrupted myelin and axonal and periaxonal swelling (Tator and Koyanagi, 1997). Altogether, these events exacerbate the already deleterious injury environment and contribute to the poor recovery scenario facing SCI patients. Endogenous attempts of revascularization (through angiogenesis) are observed from day 3 and peak about 1 week following injury, where some reports showed a return to basal vascular levels or even a 5-fold increase in vascular density at SCI injury site (Casella et al., 2002; Whetstone et al., 2003; Dray et al., 2009). This compensatory mechanism fails to integrate newly formed vessels into functional neurovascular units and most are pruned 2 weeks after injury. Additionally, Glut-1 transporters, which act as constant glucose transporters across the BSCB, are only reestablished at this time point and leave surviving neurons in a persistent metabolic imbalance (Whetstone et al., 2003). Recently it was shown that vascular perfusion below injury during the chronic phase of SCI was half that in comparison to normal spinal cords or above injury, resulting in local chronic hypoxia, and that transiently reestablishing oxygenation levels lead to brief motor recovery (Li et al., 2017). This finding highlights the relevance of vascularization therapies for SCI, showing that even though specific neuronal circuits bellow injury may remain functional, chronic hypoxia, and insufficient nutrient supply dictates their inability to undergo normal homeostasis. Thus, different approaches, either directly targeting vascularization (Rauch et al., 2009; Han et al., 2010; De Laporte et al., 2011; Yu et al., 2016) or not, concretely using neurotrophin-3-loaded chitosan (Duan et al., 2015), chitosan microhydrogels (Chedly et al., 2017), or a poly(lactic-co-glycolic) acid scaffold to deliver mesenchymal stem cells (MSCs; Ropper et al., 2017), revealed that modulation of this parameter is intricately involved in enhanced SCI recovery.

In this regard, transplantation of MSCs following SCI has shown protective effects to local vasculature (Matsushita et al., 2015; Morita et al., 2016; Vawda et al., 2019). Additionally, MSCs are also capable of promoting neuroprotection and modulation of the immune response toward a more regenerative-prone environment, which broadens the range of their effect and make them a promising candidate to treat SCI (Novikova et al., 2011; Spejo et al., 2013; Ribeiro et al., 2015). These effects have been extensively connected to the panel of molecules that MSCs secrete (secretome), including neurotrophic factors [brain derived nerve growth factor (BDNF), nerve growth factor (NGF), or glial-derived growth factor (GDNF)], pro-angiogenic molecules [vascular endothelial growth factor (VEGF), basic fibroblast growth factor (bFGF), or angiopoietin-1 (Ang-1)], or immunomodulatory molecules [monocyte chemoattractant protein-1 (MCP-1), transforming growth factor beta (TGF beta), or tumor necrosis factor alpha (TNF alpha)] though this profile varies across distinct MSC sources (Salgado et al., 2015; Pires et al., 2016). Among MSCs, adipose-derived stem cells (ASCs) are a clinically-relevant population for cell therapy applications as their isolation takes advantage of otherwise discarded tissue, being minimally invasive, and their transplantation does not elicit host immune response (Bunnell et al., 2008; Bronckaers et al., 2014). Despite the richness of ASCs' secretome in angiogenic factors, different reports demonstrated limited capacity to produce fully branched vascular networks, contrasting to direct contact experiments where ASCs lead to the development of matured vascular structures, highlighting the advantage of including these cells in SCI therapies targeting vascularization (Merfeld-Clauss et al., 2010; Verseijden et al., 2010; Rohringer et al., 2014). Thus, including this type of MSCs in such therapies is appealing as it could possibly enable the modulation of vasculature toward homeostasis and overcome the host deficient response. Furthermore, endothelial cells positively affect neuronal proliferation and neurogenesis, being able to act as physical tracks for axonal growth (Li et al., 2013; Lange et al., 2016; Himmels et al., 2017; Paredes et al., 2018). The development of a cell therapy based on the transplantation of ASCs benefits from their capacity in protecting spared neurons, modulating the environment to a regenerative phenotype, whilst acting on the preservation of the BSCB and enhancing vascular organization following SCI. This can, in turn, contribute to quickly restore the compromised BSCB, controlling the infiltration of inflammatory cells and other inappropriate agents, preventing prolonged tissue hypoxia, providing simultaneously physical cues for neuronal regeneration.

To improve poor survival rates associated with cell transplantation, hydrogels are being used as they enable replication of the physical properties of the native central nervous system (CNS), whilst providing appropriate cues for cell survival, proliferation, and integration into host tissue (Orive et al., 2009; Khaing et al., 2014). Taking this into consideration, in this work we intended to develop a co-culture system based on the encapsulation of ASCs and human umbilical vein endothelial cells (HUVECs) within an in-house developed gellan gum (GG) matrix modified with the adhesion motif GRGDS (Silva et al., 2012; Gomes et al., 2016). This GG-based biomaterial has been previously reported as suitable to culture distinct neuronal cells and ASCs, which later translated into improved functional outcomes following its implantation in a SCI animal model.

The main goals of the present work were to study the simultaneous impact of ASCs in the vascular organization of HUVECs and neurite extension of dorsal root ganglia (DRG) explants, as well as to understand how the angiogenic and neuroregulatory nature of their secretome is altered by the presence of HUVECs in 3D conditions. Finally, we assessed

the capacity of ASCs encapsulated in GG-GRGDS hydrogels to recruit blood vessels in a simple *in vivo setting* using the chick chorioallantoic membrane (CAM) assay.

MATERIALS AND METHODS

Coupling of Maleimide-GRGDS to Furan-Gellan Gum

The coupling of GRGDS to GG was done using a two-step methodology where first GG is modified with furan by creating an amide bond, through the activation of its -COOH groups, and then coupled to maleimide-modified GRGDS (mal-GRGDS) taking advantage of Diels-Alder cyclization chemistry between the maleimide group of the peptide and the furan group of GG in accordance to previously described protocols (Silva et al., 2012; Gomes et al., 2016). A 1% (w/V) gellan gum (GG, Sigma, United States) solution was dissolved in 100 mM 2-(N-morpholino)ethanesulfonic acid (MES, Sigma, United States) buffer at pH 5.5 and 37°C. Then, a 750 mM 4-(4,6-Dimethoxy-1,3,5-triazin-2-yl)-4-methylmorpholinium chloride (DMT-MM, Sigma, United States) solution is added in a 1:4 molar ratio (GG:DMT-MM) to activate the-COOH groups of the polymer, which is followed by the addition of furfurylamine (Acros Organics, Belgium) using the same molar ratio. The reaction continues for 24 h and afterwards the obtained products are dialyzed in membranes with a cutoff of 12–14 kDa (Spectrum Labs, United States) to purify the modified polymer from reaction by-products alternatively against distilled water and PBS (0.1 M, pH 7.2) for 5 days. GG-furan was recovered as a white powder by removing its aqueous content by lyophilization. To immobilize the peptide in furan-GG, 1.2 mg/mL of the modified polymer was dissolved in 100 mM MES buffer at pH 5.5 and 37°C. After complete dissolution, mal-GRGDS peptide (Anaspec, United States) was added in a 1:5 molar ration (furan:maleimide), and the reaction continued under vigorous stirring for 48 h. The purification of the peptide-modified GG is done by dialysis (Mw cutoff 12–14 kDa) against distilled water and PBS (0.1 M, pH 7.2) in alternance. Removal of water by lyophilization allowed to obtain GRGDS-modified GG (GG-GRGDS) as a white powder. To quantify the amount of peptide immobilized onto the backbone of GG we performed an amino acid analysis. The protocol consists on the acidic hydrolysis of the peptide with 6 N HCl for 24 h followed by derivatization with phenylisothiocyanate. HPLC was used to quantify the derivatized hydrolizates. A defined amount of mal-GRGDS previously incubated with native GG suffered the same derivatization protocol and amino acid analysis and was used as a control.

Cell Isolation and Culture

Adipose-derived stem cells were isolated by LaCell LLC from the lipoaspirates of consenting donors according to Dubois and coworkers (Dubois et al., 2008) under a protocol previously approved by an institutional review panel at LaCell LLC. Upon isolation, ASCs were cultured in α-MEM (Invitrogen, United States) supplemented with 10% Fetal Bovine Serum (FBS, Biochrom AG, Germany), and 1% (V/V) penicillin-streptomycin (pen/strep, Invitrogen, United States) at 37°C and 5% CO_2 (V/V) with medium exchanges every 3 days.

Human umbilical vein endothelial cells were obtained from the umbilical cord of healthy consenting patients from the Gynecology and Obstetrics Service of Hospital de Braga using a protocol approved by the review board of the Ethical Commission for Health of Braga Hospital (CESHB). After rinsing and cleaning the umbilical cord with PBS, a cannula was inserted into the umbilical vein. Then, the vein was washed with PBS to remove blood clots and excesses of blood. Afterwards, the other extremity of the umbilical cord was closed with forceps and the vein was filled with α-MEM containing 0.2% (w/V; 210 U/mL) Type I Collagenase (Gibco, Thermo Fischer Scientific, United States) and 1% pen/strep. To allow for digestion, the umbilical cord was transferred into a cell culture incubator [T = 37°C and 5% (V/V) CO_2] for 15 min. Before opening, the cord was massaged to guarantee a homogenous digestion and then its content transferred to a 50 mL Falcon, being subsequently washed with α-MEM having 10% FBS (w/V) and 1% pen/strep, PBS, and finally with a syringe filled with air. This was followed by the centrifugation of the suspension for 10 min at 1200 rpm, removal of the supernatant and resuspension of the pellet in Endothelial Growth Media (EGM, R&D Systems, United States) supplemented with 1× Endothelial Growth Supplement (EGS, R&D Systems, United States), and 1% (V/V) pen/strep. The cellular suspension was then equally divided into the wells of a 6-well plate pre-coated with 1% (w/V) Type B bovine gelatin (Sigma, United States) and cultured in Endothelial Growth Media (EGM, R&D Systems, United States) supplemented with 1× Endothelial Growth Supplement (EGS, R&D Systems, United States) and 1% (V/V) pen/strep at 37°C and 5% (V/V) CO_2 overnight to allow the attachment of HUVECs. The following day media was changed to remove unattached cells and debris and from this point onwards media is exchanged every two days to keep purifying the culture. Upon confluence, part of the cells were stored in liquid nitrogen until further use and the rest were transferred to a T75 flask pre-coated with gelatin and cultured as previously described.

Hydrogel Preparation

Lyophilized GG-GRGDS and unmodified GG was exposed to UV lights for 15 min (Silva et al., 2013). To produce hydrogels for the 3D environment experiments, a 1% (w/V) solution composed of equal parts of GG-GRGDS and unmodified GG was prepared and dissolved at 40°C in ultra-pure water. Prior to the experiments the polymeric solution was ionically crosslinked by adding 10% (V/V) of a 0.3% (w/V) $CaCl_2$ [to a final concentration of 0.03% (w/V)]. The volume of hydrogels for the experiments was 50 μL.

3D Cell Cultures – ASCs, HUVECs and Their Co-Culture

Prior to their encapsulation in GG-GRGDS ASCs and HUVECs were cultured as detailed in section "Cell isolation and culture"

and the hydrogels prepared according to section "Hydrogel preparation." The pellets with the appropriate number of ASCs and HUVECs were resuspended homogenously in the corresponding volume of GG-GRGDS at a cell density of 30,000 cells/50 μL of hydrogel and cultured under previously described conditions for each cell type. The encapsulation of cells for co-culture experiments was done in a 1:1 ASCs:HUVECs ratio by mixing the appropriate volume of each cell suspension obtained subsequently to individual 2D cultures which was followed by centrifugation at 1200 rpm for 5 min to obtain the cell mixture pellet. The appropriate volume of GG-RGDS was then added to the pellet allowing formation of hydrogels with the previously referred density (15,000 ASCs + 15,000 HUVECs/50 μL of hydrogel) being cultured using α-MEM with 10% (V/V) FBS and 1% (V/V) pen/strep.

Dorsal Root Ganglia (DRG) Isolation and Culture

Dorsal root ganglia explants were used to understand the capacity that co-culturing ASCs and HUVECs in GG-GRGDS has in inducing neurite outgrowth from the explants in comparison to each cell type cultured alone and GG-GRGDS without cells. Furthermore, using the same experimental setting this organotypic model allowed to assess the modulation of genes related to axonal growth and cytoskeleton dynamics (GAP43 and β-Tubulin III, respectively) along their time in culture. The isolation of DRG explants was effectuated using a previously detailed protocol (Gomes et al., 2016, 2018). Thus, DRG from the thoracic regions of the spine of neonatal pups (P5-7) were removed and placed in cold 1 × HBSS without Ca^{2+} and Mg^{2+} (Invitrogen, United States) with 1% (V/V) pen/strep. The remains of peripheral nerve processes were properly cleaned from DRG and then the explants were placed on top of the hydrogels across the 4 groups (no cells, ASCs, HUVECs, ASCs + HUVECs). The cell culture continued for 7 days in Neurobasal medium supplemented with 1 × B27 (Invitrogen, United States), 2 mM L-glutamine (Invitrogen, United States), 6 mg/mL D-glucose (Sigma, United States), and 1% (V/V) pen/strep with medium changes every two days and under a humidified atmosphere [37°C and 5% (V/V) CO_2] before fixating the samples using PFA and performing immunocytochemistry (ICC) to understand neurite outgrowth as well as the morphology of ASCs and HUVECs inside the hydrogels.

Dorsal root ganglia collection for PCR analysis followed the same extraction and culture methodology and was done at multiple timepoints: 12 h, 24 h, 1 day, 4 days, and 7 days following culture in the hydrogels referring to the 4 s. Pools of 2 DRG were collected at each timepoint to eppendorfs containing TripleXtractor (Grisp, Portugal; a phenol and guanidine isothiocyanate-based solution to extract high quality RNA) and then subjected to RNA isolation or in alternative were rapidly frozen at −80°C until further use.

Cell encapsulation was performed 24 h before DRG culture and followed the methodology detailed in section "3D cell cultures – ASCs, HUVECs and their co-culture."

Immunocytochemistry (ICC) and Phalloidin/DAPI Staining

After 7 days of culture hydrogels and explants were fixed in 4% paraformaldehyde (PFA, Panreac, Spain) for 45 min at room temperature (RT). This step was followed by washing the samples 3 times with PBS and by permeabilizing cell membranes with 0.3% (V/V) Triton X-100 (Sigma, United States) for 10 min. To block non-specific binding sites, samples were incubated in PBS with 10% (V/V) fetal calf serum (FCS, Biochrom AG, Germany) for 1 h 30 min. Primary antibodies were then properly diluted in PBS 10% FCS and added to the samples for 48 h at 4°C. Mouse anti-neurofilament 200 kDa antibody (1:200, Millipore, United States) was used to unveil neurites and rabbit anti-CD 31 (1:20, Abcam, United Kingdom) to identify HUVECs. Following 3 washes using PBS with 0.5% (V/V) FCS, Alexa Fluor 488 goat anti-rabbit (1:1000, Invitrogen, United States) and Alexa Fluor 647 goat anti-mouse (1:1000, Invitrogen, United States) were diluted in PBS and added to the hydrogels overnight at 4°C. Following 3 washes with PBS, a PBS solution with 1 μg/mL of DAPI (Invitrogen, United States), and 0.1 μg/mL (Sigma, United States) was added to the hydrogels for 45 min at RT. Imaging was performed on a confocal point-scanning microscope Olympus FV1000.

Neurite Extension and Outgrowth Analysis

The area occupied by the neurites of each DRG explant was calculated using the ImageJ (NIH) plugin Neurite-J (Torres-Espín et al., 2014) and using a previously developed protocol (Gomes et al., 2018). Therefore, after defining the scale, the area referring to the body of the DRG was defined and the threshold contrast properly corrected to emphasize its neurites. The image is automatically translated to 8 bits and using the function "Analyze particles" the area corresponding to the extension the neurites is calculated. The longest neurite was also quantified using Neurite-J after identifying again the DRG body the plugin automatically creates concentric rings with 25 μm intervals and is defining as the length at which the last ring is capable of intersecting neurites.

Analysis of the Vascular Organization of HUVECs in GG-GRGDS

To analyze the vascular arrangement of HUVECs encapsulated in GG-GRGDS either in the presence or not of ASCs, AngioTool64 Version 0.6a was used (Zudaire et al., 2011). After opening the images referring to the fluorescence channel utilized for CD31 and defining the scale, the background and small particles were removed by defining the appropriate signal threshold in the software. After this correction the software automatically quantifies different parameters related to vascular organization such as total vessel length, vessel area, vessel percentage area, and number of junctions.

RNA Extraction and qRT-PCR Analysis

Total RNA was extracted from pools of 2 DRG using TripleXtractor and following the instructions provided by the

manufacturers. After quantifying the RNA using a NanoDrop 1000 spectrophotometer (ThermoFisher Scientific, United States) the samples were diluted to approximately 1 μg/μL and 1 μg of sample transcribed into cDNA using the Xpert cDNA Synthesis Mastermix (Grisp, Portugal) to the manufacturer's protocol. Primers were designed using the Primer-BLAST tool (NCBI, United States) and the name of the genes, GenBank accession numbers and sequences are found on **Table 1**. The qRT-PCR reactions were done in a CFX96 real-time instrument (BioRad, United States) with the XPert Fast SYBR. mastermix and using equal cDNA concentrations for each sample following the manufacturer's instructions. The expression levels of target genes (GAP-43 and β-Tubulin III) were normalized against housekeeping genes (GAPDH and HPRT-1) and presented as fold-change mRNA levels in comparison to the control group. The fold-change levels were calculated using the $2^{\Delta\Delta CT}$ method.

Secretome Collection From 3D Cultures

The collection of the secretome from 3D cell culture sections was performed after culturing and maintaining cells across the 3 conditions (ASCs, HUVECs and their co-culture) for 6 days as detailed in section "3D cell cultures – ASCs, HUVECs and their co-culture." Subsequently, the hydrogels were washed 3 times with PBS and Neurobasal with 1% (V/V) pen/strep. This is followed by their incubation with Neurobasal with 1% (V/V) pen/strep during 24 h after which their secretome is collected, centrifuged at 1200 rpm for 5 min and the supernatant recovered and stored at −80°C until further use.

Neurotrophic and Angiogenic Profile of 3D Secretomes

The evaluation of the angiogenic and neurotrophic profile of the previously obtained secretomes was performed using the Human Neuro Discovery Array C1 and Human Angiogenesis Array C1 (RayBiotech, United States) following the manufacturer's guidelines. Briefly, each membrane was blocked for unspecific interactions using blocking buffer for 30 min at RT which was followed by its removal and incubation with 1 mL of secretome overnight at 4°C. Afterwards, the secretome was aspirated and the membranes washed using the washing buffers provided by the kit. Subsequently, 1 mL of biotinylated antibody cocktail was pipetted into each membrane and incubated for 2 h at RT. The antibody cocktail was removed, and the membranes washed using the same washing protocol. Then, 2 mL of 1 × HRP-Streptavidin was added to each well and incubated for 2 h at RT. The membranes were once again washed and prior to their revealing, 500 μL of a 1:1 mixture containing Detection buffer C and D was added for 2 min at RT. Finally, the chemiluminescence image of each membrane was obtained using a Sapphire Biomolecular Imager (Azure Biosystems, United States). The intensity of each dot was quantified using the AzureSpot software (Azure Biosystems, United States) by designing an 8 × 8 dot grid adjusted to include each individual point. Absolute values were normalized for the mean of the positive control of each membrane and the background subtracted to allow the comparison between membranes and secretomes.

Chick Chorioallantoic Membrane (CAM) Assay

This simple *in vivo* system was used to evaluate the chemotactic capacity of GG-GRGDS hydrogels encapsulating ASCs in recruiting blood vessels toward the hydrogel in comparison to GG-GRGDS alone and collagen. The protocol was initiated by incubating white fertilized chicken eggs at 37°C and under a 40% humidified atmosphere for 3 days. After carefully cleaning the eggs with chlorohexidine and putting the egg racks in a laminar-flow hood a small hole in the smallest extremity of the egg was made 2 mL of albumin removed with a 20 G needle in a syringe to dissociate the CAM from the egg shell. Embryo viability was assessed after creating a circular window (approximately 3 cm) that allowed to check it and granted access to the CAM. Then, the opening was sealed with parafilm and the remaining eggs allowed to return to the incubated where they stayed for 1 week. At this point, GG-GRGDS hydrogels encapsulating ASCs, GG-GRGDS alone, and collagen were transferred to a zone with no major vascularization on top of a CAM, following opening the eggs and checking for their viability. GG-GRGDS hydrogels were produced 24 h before implantation as detailed in section "Hydrogel preparation" and ASCs encapsulated according to section "3D cell cultures – ASCs, HUVECs and their co-culture." GG-GRGDS hydrogels with no cells were incubated in α-MEM supplemented with 10% (w/V) FBS and 1% pen/strep. Collagen hydrogels were done at the same time by mixing rat tail Collagen Type I [3.61 mg/mL, 89.6% (V/V), BD Biosciences, United States] with 10% (V/V) of 10× DMEM concentrated medium (Invitrogen, United States) and 0.4% (V/V) of a 7.5%

TABLE 1 | Forward and reverse sequences of the primers used for qRT-PCR analysis and respective GenBank accession number, gene symbol, name, and product size.

GenBank accession number	Gene symbol	Gene name	Primer sequence (5′→3′)	Size (bp)
NM_017195.3	GAP43	Growth Associated Protein 43	**Fw:** CAA GCT GAG GAG GAG AAA GAA GC **Rv:** GCA GGA GAG ACA GGG TTC AGG T	158
NM_139254.2	Tubb3	Tubulin beta III	**Fw:** AGA CCC CAG CGG CAA CTA TGT **Rv:** CCA GCA CCA CTC TGA CCG AA	204
NM_017008.4	GAPDH	Glyceraldehyde 3-phosphate dehydrogenase	**Fw:** CAG TGC CAG CCT CGT CTC AT **Rv:** TGG TGA TGG GTT TCC CGT TGA	247
NM_012583.2	HPRT1	hypoxanthine phosphoribosyltransferase 1	**Fw:** CCT CAG TCC CAG CGT CGT GAT TA **Rv:** TCC AGC AGG TCA GCA AAG AAC T	231

(w/V) $NaHCO_3$ solution. 50 μL hydrogel drops were then made and incubated for 2 h at 37°C and 5% CO_2 (Gomes et al., 2018) for polymerization to occur. Then, the collagen hydrogels were incubated in α-MEM supplemented with 10% (w/V) FBS and 1% pen/strep until CAM implantation. Following 3 days of implantation the hydrogels were photographed *in ovo* using a stereomicroscope (Olympus S2x16) and the embryos sacrificed at −80°C for 10 min and fixated in 4% PFA at RT. The CAM portion harboring each hydrogel was dissected and excised using small scissors and transferred to 6-well plates. *Ex ovo* images of each CAM were taken and the total number of vessels directly converging to the hydrogels quantified using ImageJ which allowed to discriminate differences in this parameter between experimental groups.

Statistical Analysis

Statistical analysis was performed using GraphPad Prism version 7.04 for Windows (GraphPad Software). Neurite outgrowth as well as CAM experiments were analyzed by performing one-way ANOVA followed by the Bonferroni *post-hoc* test. Welch's *t*-test allowed to assess differences among groups for the vascular arrangement experiments and two-way ANOVA with Tukey's multiple comparisons test to assess differences between groups at each timepoint. Differences were considered statistically significant if a p-value ≤ 0.05 was observed (95 % confidence level).

RESULTS

Successful GRGDS Engraftment in GG

The modification of GG followed a click chemistry approach previously optimized and published by our group (Silva et al., 2012; Gomes et al., 2016). Quantification of the total peptide bound to GG using HPLC-based amino acid analysis showed 92.85 nmol of GRGDS per mg of GG (**Figure 1**).

The Presence of ASCs Is Fundamental to Increase Neurite Outgrowth on DRG Explants and the Vascular Assembly of HUVECs

Given the lack of self-regenerative capacity observed in SCI, understanding how this parameter is affected is of pivotal importance during the initial steps of the development of a therapeutic approach to treat the condition (biomaterial-based or not). Thus, modulation of neuritogenesis by co-culturing ASCs and HUVECs in GG-GRGDS was compared to each cell type alone and the hydrogel by itself using a DRG organotypic model for axonal regeneration. Following 7 days of culture it was observed that both ASCs and the co-culture promoted increased neurite outgrowth (**Figure 2A**). Quantification of the area occupied by neurites provided similar values for GRGDS-GG encapsulating ASCs and the co-culture ($7.83 \pm 0.75 \times 10^5$ μm^2 and $8.0 \pm 1.2 \times 10^5$ μm^2, respectively), being superior to HUVECs alone ($608757 \pm 0.86 \times 10^5$ μm^2), and statistically significantly higher ($p < 0.01$) than GG-GRGDS ($2.99 \pm 0.35 \times 10^5$ μm^2; **Figure 2B**).

A biomaterial-based strategy that aims to promote a revascularization therapy for SCI must provide furnish adequate conditions for ECs to assemble into vascular structures. Therefore, this was another parameter analyzed during these experiments. When encapsulated alone in GG-GRGDS hydrogels, HUVECs were found to be interspersed along the hydrogel with no obvious assembly into vascular-like structures. This was in complete contrast to what occurred when co-culturing these ECs with ASCs, where the vascular organization of HUVECs was noticeable (**Figure 3A**). The presence of ASCs statistically significantly increased several parameters related to vasculature such as vessel area (0.28 ± 0.07 mm vs 1.32 ± 0.16 mm; $p < 0.001$), vessel percentage area (6.1 ± 0.90% vs 14.16 ± 1.78%; $p < 0.01$), average vessel length (0.12 ± 0.08 mm vs 0.31 ± 0.07 mm; $p < 0.001$), total vessel length (7.79 ± 1.58 mm vs 39.72 ± 5.02 mm; $p < 0.001$), and the number of junctions formed by the vascular bed (19.50 ± 5.39 mm vs 121.30 ± 27.10 mm; $p < 0.01$; **Figures 3B–F**). These results show that ASCs have the capacity to induce vascular re-organization of biomaterials and how this modulation can be important to create a positive interplay on ECs and finally impact axonal growth.

GAP-43 Expression Rapidly Increases in DRG From GG-GRGDS Encapsulating ASCs and Co-Culture Groups as ß-Tubulin III Decreases

The temporal dynamics of the genetic expression of GAP-43 (highly expressed in the growth cone of regenerating neurons) and ß-Tubulin III (Tubb3, neuronal cytoskeleton) allowed to understand how the use of ASCs, HUVECs and their co-culture could be modulating neurite extension from DRG in comparison to the hydrogel without cells. Analyzing **Figure 4A** it is possible to conclude that ASCs and the co-culture upregulated the expression of GAP-43 in DRG neurons as early as 12 h following culture (2.71 ± 0.14 fold for ASCs and 3.47 ± 0.71 fold for ASCs + HUVECs), reaching its maximum at 24 h (ASCs: 5.53 ± 2.8 fold, ASCs + HUVECs: 9.1 ± 4.33 fold) where statistically significant differences were found to HUVECs ($p < 0.05$ for ASCs and $p < 0.01$ for ASCs + HUVECs) and GG-GRGDS alone ($p < 0.01$ for ASCs and $p < 0.001$ for ASCs + HUVECs) during the same timepoint. The genetic expression of this axonal growth-related protein markedly decreased at the 4 days timepoint for both conditions where ASCs presented a lesser decrease following 7 days of culture.

GAP-43 expression in DRG cultured together with HUVECs encapsulated in GG-GRGDS was increased at the 12 and 24 h timepoints relative to the hydrogel alone (1.71 ± 0.10 and 1.94 ± 0.46 fold, respectively) but without the dramatic increase detailed for the other two conditions. Interestingly, the expression of Tubb3 followed the opposite path (**Figure 4B**). Thus, the expression of this neuronal cytoskeleton gene was downregulated for ASCs and ASCs + HUVECs at 12 h (ASCs: 0.69 ± 0.23 fold; ASCs + HUVECs: 0.81 ± 0.20 fold), and 24 h of

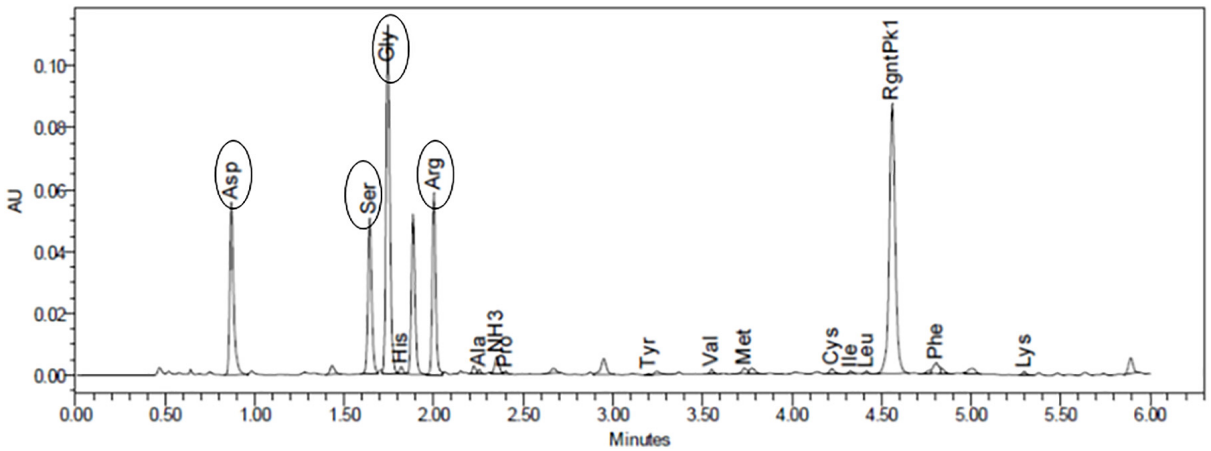

FIGURE 1 | Amino acid analysis allowed to quantify the amount of peptide bound to gellan (92.85 nmol of GRGDS/mg of gellan). Oval forms identify each peptide.

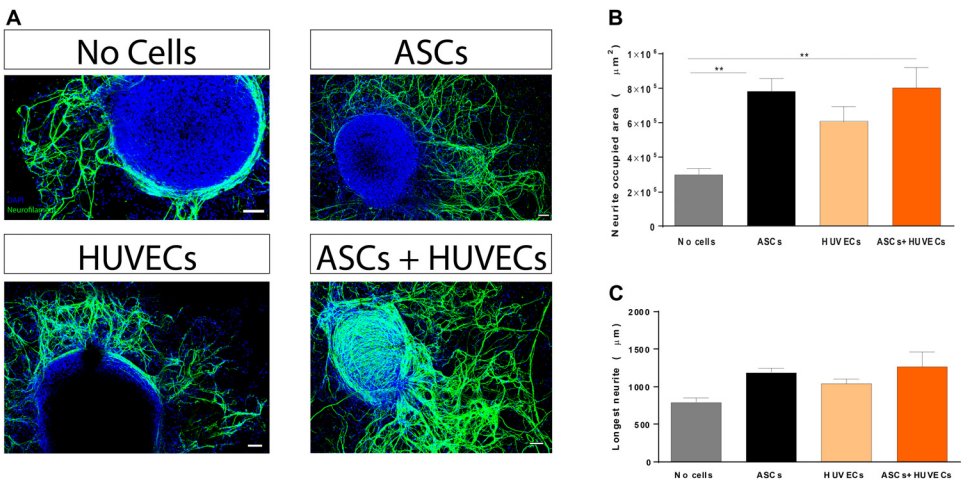

FIGURE 2 | Effect of co-culturing ASCs and HUVECs on GRGDS-modified gellan gum in the neurite outgrowth of DRG explants in comparison to each cell type alone. **(A)** Representative images of the conditions. **(B)** Co-culture promoted a similar outgrowth to ASCs, being statistically significantly higher than the hydrogel without cells. **(C)** The longest neurite followed the same trend but without statistical differences. Scale bar: 100 μm. Values are shown as mean ± SEM (n = 8/10); $^{**}p < 0.01$.

culture (ASCs: 0.42 ± 0.06 fold; ASCs + HUVECs: 0.53 ± 0.31 fold). This gene, however, was slightly upregulated at 4 days of culture for both conditions (1.39 ± 0.50 fold for ASCs and 2.00 ± 0.92 fold for ASCs + HUVECs) which was followed by its downregulation at 7 days of culture (ASCs: 0.54 ± 0.09 fold; ASCs + HUVECs: 0.62 ± 0.11 fold). The expression of Tubb3 for DRG cultured with HUVECs presented a more homogeneous dynamic (1.046 ± 0.29 fold at 12 h; 0.60 ± 0.10 fold at 24 h; 1.23 ± 0.25 fold at 4 days; and 0.646 ± 0.12 fold at 7 days). These results show that the combination of GG-GRGDS hydrogels with ASCs or ASCS+HUVECs was able to stimulate axonal growth, which was reflected by increased GAP-43 levels at 12 h and 24 h following culture, contrarily to HUVECs where upregulation of this gene was not as markedly as seen for the other two conditions. On the other hand, it seemed that for neurite outgrowth to occur the cytoskeleton of DRG neurons had to be disturbed. These results are in line with what was observed in the neurite outgrowth experiments described in **Figure 2**.

Neurotrophic and Angiogenic Signature of the Secretome of ASCs + HUVECs Is Distinct From Each Cell Type Alone

The results obtained on DRG experiments showed a clear beneficial effect on HUVECs by the presence of ASCs, with enhancement on their organization into vascular-like structures. This was followed by an increased capacity of the co-culture and ASCs in promoting neurite outgrowth from the explants in relation to HUVECs and prompted the study of the neurotrophic and angiogenic character of their secretomes. The full array of biomolecules detected, and their relative expression can be found in **Supplementary Figure S1**.

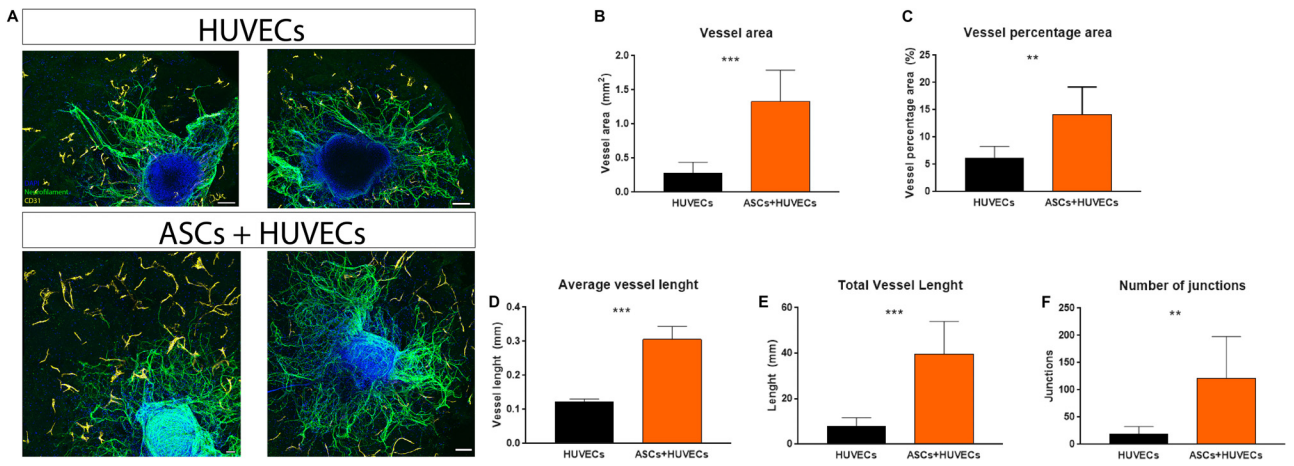

FIGURE 3 | (A) Vascular organization of HUVECs inside GG-GRGDS when cultured alone and in co-culture with ASCs. These MSCs promoted the organization of the endothelial cells in vascular-like structures with a statistically significant increase on **(B)** vessel area, **(C)** vessel percentage area, **(D)** average vessel length, **(E)** total vessel length, and **(F)** number of junctions. Scale bar: 100 μm. Data is shown as mean± SEM with $n = 8/10$. $^{**}p < 0.01$, $^{***}p < 0.001$.

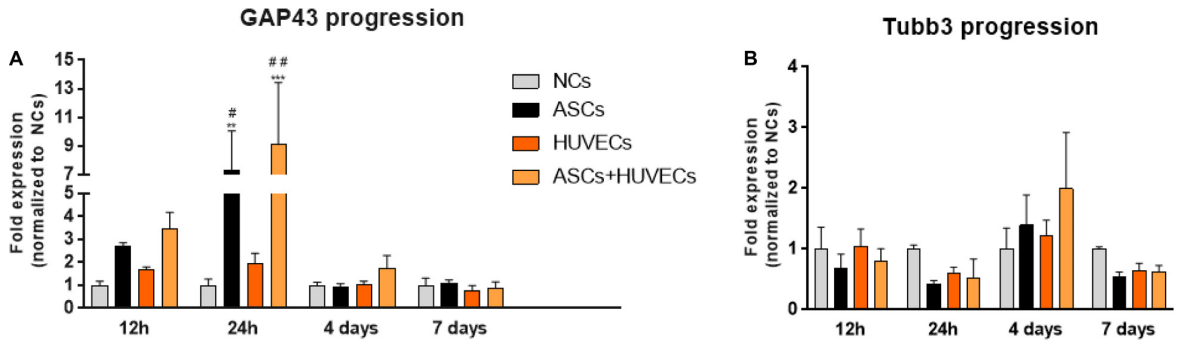

FIGURE 4 | Temporal dynamics of the expression of GAP-43 and βIII-tubulin in DRG cultured on GG-GRGDS encapsulating ASCs, HUVECs, ASCs+HUVECs, or no cells. **(A)** The co-culture condition increases the expression of GAP43 as early as 12 h in comparison to all the other conditions, reaching the maximum at 24 h (statistically significant to no cells and HUVECs), and decreasing at latter timepoints (4 and 7 days). **(B)** The expression of βIII-tubulin follows an opposite dynamic and shows that the induction of plasticity is dependent on the downregulation of cytoskeleton genes. Scale bar: 100 μm. Results are shown as mean ± SEM ($n = 4$, each represents a pool of 2 DRG). $^{**}p < 0.01$ and $^{***}p < 0.001$ in comparison to no cells; $^{\#}p < 0.05$ and $^{\#\#}p < 0.01$ in comparison to HUVECs.

Starting with the neuroregulatory component of the conditioned media, the secretome of HUVECs showed markedly decreased amounts of growth factors associated with neuronal growth and survival, including BDNF, GDNF, β-NGF, IGF-1, or S100-B (**Figure 5A**). This is the opposite to the other two conditions (ASCs and ASCs + HUVECs) where these neuroregulatory factors were upregulated. In fact, the highest relative expression values for BDNF, GDNF, β-NGF IGF-1, and S100 B were seen in the co-culture (**Figure 5A**). Additionally, it was also observed high amounts of IL-6 and MCP-1 on the secretome of ASCs and ASCs + HUVECs, two cytokines that have an important role in immune response following neuronal trauma (**Supplementary Figure S1A**). The analysis of angiogenic components followed the same trend, with the secretome of HUVECs in general presenting decreased expression of the factors, excepting EGF which presented increased relative amounts in the secretome of the ECs. These include TIMP-1 and TIMP-2, being the latter increased in the secretome of the co-culture, and CXCL-1/2/3 which was upregulated in the conditioned media of ASCs. The presence of Angiogenin and CXCL-5 was only observed whenever ASCs were present, showing both relative higher quantities in the secretome of ASCs + HUVECs (**Figure 5B**). Additionally, we also found similar amounts of bFGF, VEGF-A, and VEGF-D in the secretome of ASCs and ASCs + HUVECs (**Supplementary Figure S1B**).

Altogether, these results help to shed some insight in the way the secretome dynamics of ASCs might be affected by the presence of other cells on the environment. Thus, we observed a positive impact on the expression of neurotrophic factors when HUVECs were in culture together with ASCs and a very similar angiogenic profile for the secretome of ASCs and ASCs + HUVECs, a fact that may indicate that this modulation might be specific for some components of the secretome.

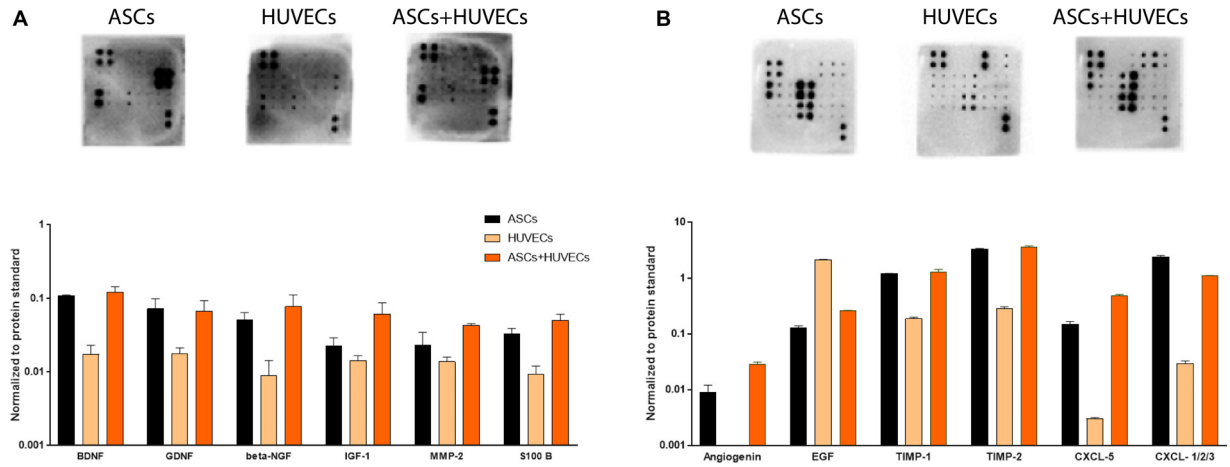

FIGURE 5 | Analysis of the secretomes of ASCs, HUVECs, and their co-culture after 7 days of culture in GG-GRGDS allowed to understand the relative expression of a panel of neuroregulatory and angiotrophic molecules. **(A)** The secretome of ASCs+HUVECs showed an upregulation on different neurotrophic factors (BDNF, β-NGF, IGF-1, and S-100 B) showing a positive effect of the interaction of both cells on the secretion of these molecules. **(B)** The secretome of HUVECs presented decreased amounts of the quantified angiogenic molecules, with exception to EGF, whereas ASCs+HUVECs upregulated Angiogenin and CXCL-5 and ASCs promoted increased expression of CXCL-1/2/3.

Vascular Recruitment Is Potentiated by the Presence of ASCs

To understand the capacity of GRGDS-modified GG encapsulating ASCs in recruiting blood vessels and induce vascular reorganization these were tested against the biomaterial without cells in an *in vivo* setting: the CAM assay. This model takes advantage of the highly vascularized CAM (grows by day 7 of chick embryonic development and matures by day 12) to study angiogenesis. It is a cheap and relatively quick way to study angiogenesis, especially for drug screening and implantation of biomaterial-based therapies aiming to transplant cells (due to limited immune responses, which allow the transplant of xenografts) serving as proof-of-concept before evolving to more complex *in vivo* models (Nowak-Sliwinska et al., 2014). Following 3 days of implantation (**Figure 6A**), the combination of hydrogel and ASCs exerted a chemoattractant effect on blood vessels as it significantly increased their convergence (70.17 ± 3.76 blood) when comparing to GRGDS alone (38.71 ± 4.09 blood vessels; **Figure 6B**). As previously detailed, this recruitment is likely to be mediated by the secretome of ASCs due to its highly rich angiogenic content. Therefore, these results show that ASCs have the potential to redesign the vascular milieu of SCI by promoting vascular attraction and reorganization of spared blood vessels (helping to revascularize the lesion site and prevent damage associated to vascular damage in SCI).

DISCUSSION

Vascular damage leading to BSCB disruption occurs in spinal cord trauma or laceration, playing a critical role in defining the severity of SCI. In fact, Noble and Wrathall (Noble and Wrathall, 1989a,b) demonstrated that the extension of the cystic cavity was similar to the intraparenchymal hemorrhage originated by vessel destruction and opened up the possibility that controlling this phenomena could lead to attenuate the severity of the condition. Even though the permeability of the BSCB is restored 14 days following injury, it is important to highlight that most vessels are not associated in neurovascular units, which are crucial in regulating appropriate blood flow to the spinal cord (Casella et al., 2002; Goritz et al., 2011).

Li et al. (2017) recently demonstrated that spinal cord tissue caudal to the lesion site is in permanent hypoxia. By artificially elevating O_2 levels, the authors observed a prolonged increased on tissue oxygenation (in opposition to rostral to lesion where the values got back to normal 1 min after the stimulus) probably due to triggering neurovascular coupling, which further dilates vessels and increases oxygen and neuronal activity, originating transient locomotor gains of function (Li et al., 2017). This elegant study clearly underlines the importance of appropriate vascular functional for neuronal homeostasis.

Aiming to reshape the vascular milieu following SCI, in this work we started by understanding the potential of ASCs in modulating this parameter and how it would affect axonal growth. Thus, these MSCs were encapsulated with HUVECs in an in-house biomaterial-based approach (GG-GRGDS hydrogels) and the neurite outgrowth experiments showed that the co-culture provided potential for axonal regeneration similar to ASCs alone and superior to HUVECs or the hydrogel, opening the possibility of positive between both types of cells in the injury environment. In fact, the co-culture (as ASCs alone) proved to impact the internal neuronal growth machinery from early timepoints (12 h at least) as shown by the upregulation of a protein directly connected to axonal growth (GAP-43). This protein is highly expressed in regenerating axons where it acts to potentiate filopodia formation in growth cones (if phosphorylated) or induces microtubule-based outgrowth (if

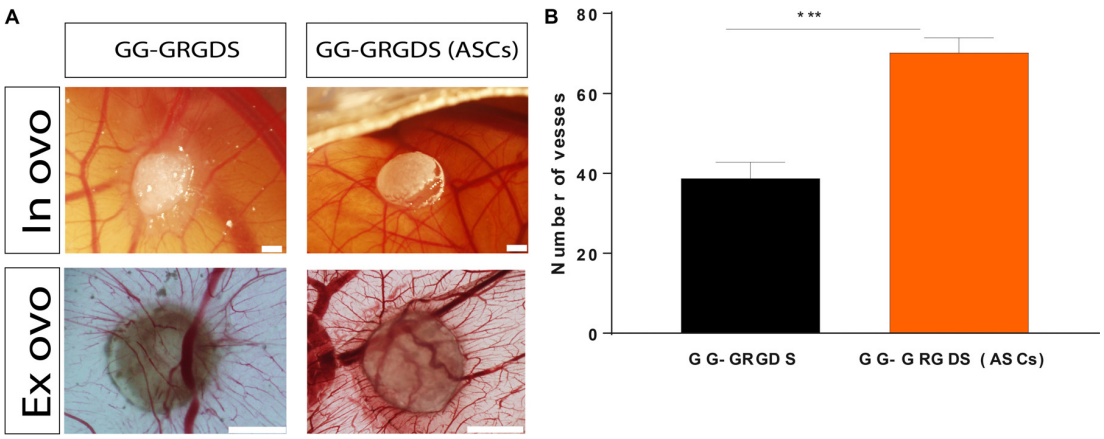

FIGURE 6 | Vessel recruitment capacity of ASCs encapsulated in GG-GRGDS following 3 days of implantation on CAM. **(A)** Representative *in ovo* and *ex ovo* images of each condition. **(B)** Quantification of the number of vessels converging to the hydrogels demonstrated that these ASCs significantly impacted this parameter in comparison to the hydrogel without cells, which shows how these cells may affect the SCI vascular milieu following implantation. Scale bar: 1 mm. Results are shown as mean ± SEM (n = 12/14); ***$p < 0.001$.

unphosphorylated; He et al., 1997; Dent and Meiri, 1998). One of the molecules that has been shown to upregulate GAP-43 is BDNF (Segal et al., 1995; Gupta et al., 2009), being essential for the neurotrophic action of the latter. Therefore, this is one of the mechanisms we propose for the neurite outgrowth results here reported.

The beneficial effects of ASCs on the organization of HUVECs were quite visible within the hydrogels, since these ECs were only capable of organizing in vascular-like structures when cultured in the presence of the MSCs. The characterization of the secretome of ASCs by our (Pires et al., 2016) and other groups (Nakagami et al., 2005; Kachgal and Putnam, 2011; Nakanishi et al., 2011) has showed an enrichment in angiogenic growth factors which could explain the impact of these MSCs on the vascular organization of HUVECs. Nevertheless, in line with our findings, others reported increased tube-formation capacity and vessel network stability of ECs when co-cultured in the presence of ASCs or other types of MSCs (Merfeld-Clauss et al., 2010; Holnthoner et al., 2015). These studies showed that ASCs induced an increased expression of CD31 in ECs and acted on VEGF, HGF and PDGF-BB pathways being their presence imperative for the formation and stabilization of such networks.

The present work also showed that the effect of ASCs on HUVECs probably created a positive synergy that can upregulate a different variety of neurotrophic factors. These molecules belong to the PI3K-Akt pathway, which our group previously identified as one of the effectors of the secretome of ASCs in injured spinal cord (Gomes et al., 2018). This pathway contributes to cell growth, proliferation and nutrient uptake and its activation has been shown to promote the regeneration of corticospinal tract neurons (Liu et al., 2010), and optic nerve axons (Park et al., 2008), making it a central signaling cascade to drive regeneration.

Moving away from classical neurotrophic factors, we desired to highlight the prevalence of IL-6, and MCP-1 in the secretome of ASCs and ASCs + HUVECs which are classically defined as mediators of the inflammatory response and can also impact neuronal regeneration (Leibinger et al., 2013; Kwon et al., 2015; Willis et al., 2020). Willis et al. (2020) showed that IL-6 induces neuroprotection in neurons following traumatic brain injury by a *trans*-signaling mechanism. MCP-1 seems to mediate the crosstalk between DRG neurons and macrophages, inducing neurite outgrowth, and mobilizing M2 macrophages (Kwon et al., 2015).

The analysis of angiotrophic molecules revealed the presence of several angiotrophic factors such as Angiogenin, EGF, bFGF, PDGF-BB, TPO as well as VEGF-A, and VEGF-D in the secretome of ASCs and ASCs+HUVECs. During these experiments it was clear that the secretome of HUVECs showed a clear downregulation, in some cases lack of expression of these factors, a fact that highlights the importance of adding ASCs to provoke their normal homeostasis in GG-GRGDS and might help to explain their incapacity to assembly into vascular-like networks in the absence of the MSCs. Two type of VEGF isoforms (VEGF-A and -D), a key family of angiogenic proteins, were detected on the analyzed secretomes. VEGF-A binds VEGFR1 and VEGFR2 and is crucial for vascular development during embryogenesis, continuing to stimulate angiogenesis postnatally, and having also a role in pathological angiogenesis (Holmes and Zachary, 2005). In addition this isoform is capable exerting neurotrophic and neuroprotective effects (trough flk-1), being a molecule capable of connecting angiogenesis with neuronal development (Sondell et al., 2000).

We also found increased levels of TIMP-1 and TIMP-2 in all the conditioned media collected from ASCs and ASCs+HUVECs collected in GG-GRGDS hydrogels, a possible reflection of the cellular interactions at the time of recollection. These were collected after 7 days of culture when the cells colonized the entire hydrogel and vascular networks (for the co-culture) were established leading to the inhibition of cellular migration, and the stabilization of the vascular networks formed.

CXCL5 and CXCL1/2/3 also showed increased relative amounts in the secretomes of ASCs + HUVECs and ASCs, respectively. Both chemokines impact angiogenesis after binding to CXCR2 (Mehrad et al., 2007; Chen et al., 2019). CXCL5 exerts angiogenic effects through the induction of VEGF-A by binding FOXD1 protein to a promoter of the growth factor (Chen et al., 2019). CXCL1/2/3 through CXCR2, leads to the activation and migration of ECs (Mehrad et al., 2007). These results allowed us to understand the relative expression of a myriad of angiogenic and neurotrophic effectors present in the secretome of ASCs and how it can be modulated by the presence of other cells in a 3D environment (in this case HUVECs).

Otherwise a bionert polymer, previous works have demonstrated that the insertion of RGD motifs into the backbone of GG allows the polymer to activate cellular integrins which in turn induces cellular adhesion, proliferation, survival, and regular homeostasis (Silva et al., 2012; Gomes et al., 2016). Accordingly, this chemical modification also impacts the quality of the secretome of MSCs since secretome collected from MSCs on GRGDS-modified GG enhanced neuronal survival, their proliferation and metabolism in comparison to native GG (Silva et al., 2013). Apart from these chemical cues, the physical properties of the three dimensional environment provided by hydrogels also have a profound impact on cellular behavior (Lee and Kim, 2018). Chaudhuri et al. (2016) designed RGD-modified alginate hydrogels with different stress relaxation properties and elegantly showed how the simple modulation of this physical parameter directed MSC differentiation and impacted cellular proliferation independently of RGD density. Taking this example into consideration, the elucidation on how such parameters govern the capacity of GRGDS-GG in promoting for instance the assembling HUVECs into vascular-like structures or the impact the physical properties of the hydrogel have on the secretome of ASCs should be explored in future studies.

Even though our *in vitro* results showed the potential ASCs have to influence angiogenesis and vascular organization of transplanted ECs, these still needed to be validated in an *in vivo-like* setting. The CAM assay enabled to observe that ASCs encapsulated in GG-GRGDS had a significantly higher capacity in recruiting blood vessels toward the hydrogel when compared to GG-GRGDS, a feature that shows the impact of their secretome on reshaping vascular organization and recruitment. This feature is of primordial importance when thinking on the implantation of a vascularization strategy in an animal model of SCI. Therefore, it shows that it might have the capacity to stimulate angiogenesis and with this induce the revascularization of the lesion site and possibly control the infiltration of inflammatory cells from the acute phase of the condition. Finally, this might allow to modulate the severity of the condition.

CONCLUSION

In this work we started by validating *in vitro* the potential of developing a therapeutic approach aiming to restore normal homeostatic vasculature following SCI and with this to positively modulate inflammation with the final goal of impacting disease severity and motor and autonomic recovery. The co-culture ASCs + HUVECs in GG-GRGDS hydrogels lead to a similar neurite outgrowth and arborization in DRG explants as ASCs alone, impacting genetic expression of proteins involved in regeneration as early as 12 h following culture. Moreover, ASCs were pivotal for the arrangement of HUVECs into vascular-like structures a feature probably due not only to their paracrine action but also to cell-to-cell communication. The neurotrophic part of the secretome of ASCs and HUVECs showed an upregulation in some of these molecules, proving that the interaction between these MSCs and ECs may induce benefits to SCI environment. Regarding the angiotrophic molecules analyzed, the profile of ASCs and co-culture was similar, which helps to prove that the major changes in vascular assembly are majorly mediated by cell-cell contact. Finally, implantation of the hydrogel together with ASCs in the CAM lead to increased recruitment of blood vessels which shows the potential of these cell in reshaping the vascular milieu *in vivo*. Altogether, these results open up a promising possibility of implanting this biomaterial-based cell therapy in a SCI animal to study its impact on revascularization and functional recovery.

DATA AVAILABILITY STATEMENT

The raw data supporting the conclusions of this article will be made available by the authors, without undue reservation, to any qualified researcher.

ETHICS STATEMENT

The studies involving human participants were reviewed and approved by LaCell LLC; Ethical Commission for Health of Braga Hospital. The patients/participants provided their written informed consent to participate in this study.

AUTHOR CONTRIBUTIONS

LR conducted the experiments, analyzed data, and wrote the manuscript. EG, JA, and SG helped during the cell culture and CAM experiments, contributing to data analysis. FB, NS, RS, and DL helped to draft the manuscript and revised it critically. AS conceived the analysis, participated in its design and coordination, helped to draft the manuscript, and gave the final approval of the version to be published. All authors read and approved the final manuscript.

FUNDING

The authors want to acknowledge the financial support from Prémios Santa Casa Neurociências – Prize Melo e Castro for Spinal Cord Injury Research (MC-04/17); from Portuguese

Foundation for Science and Technology [Doctoral fellowship (PD/BDE/127835/2016) to LR; Post-doctoral fellowship (SFRH/BPD/117858/2016) to SG and Scientific Employment Stimulus to NS (CEECIND/04794/2017)]. This work was funded by FEDER, through the Competitiveness Internationalization Operational Program (POCI), and by National funds, through the Foundation for Science and Technology (FCT), under the scope of the projects POCI-01-0145-FEDER-007038; TUBITAK/0007/2014; PTDC/DTP-FTO/5109/2014; POCI-01-0145-FEDER-029206; POCI-01-0145-FEDER-031392; PTDC/MED-NEU/31417/2017; and NORTE-01-0145-FEDER-029968. This work has also been developed under the scope of the project NORTE-01-0145-FEDER-000013, supported by the Northern Portugal Regional Operational Program (NORTE 2020), under the Portugal 2020 Partnership Agreement, and through the European Regional Development Fund (FEDER).

ACKNOWLEDGMENTS

We want to acknowledge Professor Jeffrey Gimble at the Tulane University Center for Stem Cell Research and Regenerative Medicine and LaCell LLC (New Orleans, Louisiana, United States) for kindly providing the ASCs used in this study.

SUPPLEMENTARY MATERIAL

The Supplementary Material for this article can be found online at: https://www.frontiersin.org/articles/10.3389/fcell.2020.00489/full#supplementary-material

FIGURE S1 | Total panel of molecules detected on **(A)** Neurodiscovery and **(B)** Angiogenesis Array and their relative expression.

REFERENCES

Bartanusz, V., Jezova, D., Alajajian, B., and Digicaylioglu, M. (2011). The blood-spinal cord barrier: morphology and clinical implications. *Ann. Neurol.* 70, 194–206. doi: 10.1002/ana.22421

Bronckaers, A., Hilkens, P., Martens, W., Gervois, P., Ratajczak, J., Struys, T., et al. (2014). Mesenchymal stem/stromal cells as a pharmacological and therapeutic approach to accelerate angiogenesis. *Pharmacol. Ther.* 143, 181–196. doi: 10.1016/j.pharmthera.2014.02.013

Bunnell, B. A., Flaat, M., Gagliardi, C., Patel, B., and Ripoll, C. (2008). Adipose-derived stem cells: isolation, expansion and differentiation. *Methods* 45, 115–120. doi: 10.1016/j.ymeth.2008.03.006

Casella, G. T. B., Marcillo, A., Bunge, M. B., and Wood, P. M. (2002). New vascular tissue rapidly replaces neural parenchyma and vessels destroyed by a contusion injury to the rat spinal cord. *Exp. Neurol.* 173, 63–76. doi: 10.1006/exnr.2001.7827

Chaudhuri, O., Gu, L., Klumpers, D., Darnell, M., Bencherif, S. A., Weaver, J. C., et al. (2016). Hydrogels with tunable stress relaxation regulate stem cell fate and activity. *Nat. Mater.* 15, 326–334. doi: 10.1038/nmat4489

Chedly, J., Soares, S., Montembault, A., von Boxberg, Y., Veron-Ravaille, M., Mouffle, C., et al. (2017). Physical chitosan microhydrogels as scaffolds for spinal cord injury restoration and axon regeneration. *Biomaterials* 138, 91–107. doi: 10.1016/j.biomaterials.2017.05.024

Chen, C., Xu, Z.-Q., Zong, Y.-P., Ou, B.-C., Shen, X.-H., Feng, H., et al. (2019). CXCL5 induces tumor angiogenesis via enhancing the expression of FOXD1 mediated by the AKT/NF-κB pathway in colorectal cancer. *Cell Death Dis.* 10:178. doi: 10.1038/s41419-019-1431-6

De Laporte, L., Des Rieux, A., Tuinstra, H. M., Zelivyanskaya, M. L., De Clerck, N. M., Postnov, A. A., et al. (2011). Vascular endothelial growth factor and fibroblast growth factor 2 delivery from spinal cord bridges to enhance angiogenesis following injury. *J. Biomed. Mater. Res. A* 98A, 372–382. doi: 10.1002/jbm.a.33112

Dent, E. W., and Meiri, K. F. (1998). Distribution of phosphorylated GAP-43 (neuromodulin) in growth cones directly reflects growth cone behavior. *J. Neurobiol.* 35, 287–299. doi: 10.1002/(sici)1097-4695(19980605)35:3<287::aid-neu6>3.0.co;2-v

Dray, C., Rougon, G., and Debarbieux, F. (2009). Quantitative analysis by in vivo imaging of the dynamics of vascular and axonal networks in injured mouse spinal cord. *Proc. Natl. Acad. Sci. U.S.A.* 106, 9459–9464. doi: 10.1073/pnas.0900222106

Duan, H., Ge, W., Zhang, A., Xi, Y., Chen, Z., Luo, D., et al. (2015). Transcriptome analyses reveal molecular mechanisms underlying functional recovery after spinal cord injury. *Proc. Natl. Acad. Sci. U.S.A.* 112:201510176. doi: 10.1073/pnas.1510176112

Dubois, S. G., Floyd, E. Z., Zvonic, S., Kilroy, G., Wu, X., Carling, S., et al. (2008). Isolation of human adipose-derived stem cells from biopsies and liposuction specimens. *Methods Mol. Biol.* 449, 69–79. doi: 10.1007/978-1-60327-169-1_5

Gomes, E. D., Mendes, S. S., Assunção-Silva, R. C., Teixeira, F. G., Pires, A. O., Anjo, S. I., et al. (2018). Co-transplantation of adipose tissue-derived stromal cells and olfactory ensheathing cells for spinal cord injury repair. *Stem Cells* 36, 696–708. doi: 10.1002/stem.2785

Gomes, E. D., Mendes, S. S., Leite-Almeida, H., Gimble, J. M., Tam, R. Y., Shoichet, M. S., et al. (2016). Combination of a peptide-modified gellan gum hydrogel with cell therapy in a lumbar spinal cord injury animal model. *Biomaterials* 105, 38–51. doi: 10.1016/j.biomaterials.2016.07.019

Goritz, C., Dias, D. O., Tomilin, N., Barbacid, M., Shupliakov, O., and Frisen, J. (2011). A pericyte origin of spinal cord scar tissue. *Science* 333, 238–242. doi: 10.1126/science.1203165

Gupta, S. K., Mishra, R., Kusum, S., Spedding, M., Meiri, K. F., Gressens, P., et al. (2009). GAP-43 is essential for the neurotrophic effects of BDNF and positive AMPA receptor modulator S18986. *Cell Death Differ.* 16, 624–637. doi: 10.1038/cdd.2008.188

Han, S., Arnold, S. A., Sithu, S. D., Mahoney, E. T., Geralds, J. T., Tran, P., et al. (2010). Rescuing vasculature with intravenous angiopoietin-1 and αvβ3 integrin peptide is protective after spinal cord injury. *Brain* 133, 1026–1042. doi: 10.1093/brain/awq034

He, Q., Dent, E. W., and Meiri, K. F. (1997). Modulation of actin filament behavior by GAP-43 (neuromodulin) is dependent on the phosphorylation status of serine 41, the protein kinase C site. *J. Neurosci.* 17, 3515–3524. doi: 10.1523/jneurosci.17-10-03515.1997

Himmels, P., Paredes, I., Adler, H., Karakatsani, A., Luck, R., Marti, H. H., et al. (2017). Motor neurons control blood vessel patterning in the developing spinal cord. *Nat. Commun.* 8:14583. doi: 10.1038/ncomms14583

Holmes, D. I. R., and Zachary, I. (2005). The vascular endothelial growth factor (VEGF) family: angiogenic factors in health and disease. *Genome Biol.* 6:209. doi: 10.1186/gb-2005-6-2-209

Holnthoner, W., Hohenegger, K., Husa, A.-M., Muehleder, S., Meinl, A., Peterbauer-Scherb, A., et al. (2015). Adipose-derived stem cells induce vascular tube formation of outgrowth endothelial cells in a fibrin matrix. *J. Tissue Eng. Regen. Med.* 9, 127–136. doi: 10.1002/term.1620

James, S. L., Theadom, A., Ellenbogen, R. G., Bannick, M. S., Montjoy-Venning, W., Lucchesi, L. R., et al. (2019). Global, regional, and national burden of traumatic brain injury and spinal cord injury, 1990–2016: a systematic analysis for the global burden of disease study 2016. *Lancet Neurol.* 18, 56–87. doi: 10.1016/S1474-4422(18)30415-0

Kachgal, S., and Putnam, A. J. (2011). Mesenchymal stem cells from adipose and bone marrow promote angiogenesis via distinct cytokine and protease expression mechanisms. *Angiogenesis* 14, 47–59. doi: 10.1007/s10456-010-9194-9

Khaing, Z. Z., Thomas, R. C., Geissler, S. A., and Schmidt, C. E. (2014). Advanced biomaterials for repairing the nervous system: what can hydrogels do for the brain? *Mater. Today* 17, 332–340. doi: 10.1016/j.mattod.2014.05.011

Kwon, M. J., Shin, H. Y., Cui, Y., Kim, H., Thi, A. H. L., Choi, J. Y., et al. (2015). CCL2 mediates neuron-macrophage interactions to drive proregenerative macrophage activation following preconditioning injury. *J. Neurosci.* 35, 15934–15947. doi: 10.1523/JNEUROSCI.1924-15.2015

Lange, C., Turrero Garcia, M., Decimo, I., Bifari, F., Eelen, G., Quaegebeur, A., et al. (2016). Relief of hypoxia by angiogenesis promotes neural stem cell differentiation by targeting glycolysis. *EMBO J.* 35, 924–941. doi: 10.15252/embj.201592372

Lee, J. H., and Kim, H. W. (2018). Emerging properties of hydrogels in tissue engineering. *J. Tissue Eng.* 9:2041731418768285. doi: 10.1177/2041731418768285

Leibinger, M., Müller, A., Gobrecht, P., Diekmann, H., Andreadaki, A., and Fischer, D. (2013). Interleukin-6 contributes to CNS axon regeneration upon inflammatory stimulation. *Cell Death Dis.* 4:e609. doi: 10.1038/cddis.2013.126

Li, S., Haigh, K., Haigh, J. J., and Vasudevan, A. (2013). Endothelial VEGF sculpts cortical cytoarchitecture. *J. Neurosci.* 33, 14809–14815. doi: 10.1523/JNEUROSCI.1368-13.2013

Li, Y., Lucas-Osma, A. M., Black, S., Bandet, M. V., Stephens, M. J., Vavrek, R., et al. (2017). Pericytes impair capillary blood flow and motor function after chronic spinal cord injury. *Nat. Med.* 23, 733–741. doi: 10.1038/nm.4331

Liu, K., Lu, Y., Lee, J. K., Samara, R., Willenberg, R., Sears-Kraxberger, I., et al. (2010). PTEN deletion enhances the regenerative ability of adult corticospinal neurons. *Nat. Neurosci.* 13, 1075–1081. doi: 10.1038/nn.2603

Matsushita, T., Lankford, K. L., Arroyo, E. J., Sasaki, M., Neyazi, M., Radtke, C., et al. (2015). Diffuse and persistent blood-spinal cord barrier disruption after contusive spinal cord injury rapidly recovers following intravenous infusion of bone marrow mesenchymal stem cells. *Exp. Neurol.* 267, 152–164. doi: 10.1016/j.expneurol.2015.03.001

Mautes, A. E., Weinzierl, M. R., Donovan, F., and Noble, L. J. (2000). Vascular events after spinal cord injury: contribution to secondary pathogenesis. *Phys. Ther.* 80, 673–687. doi: 10.1093/ptj/80.7.673

Mehrad, B., Keane, M. P., and Strieter, R. M. (2007). Chemokines as mediators of angiogenesis. *Thromb. Haemost.* 80, 755–762. doi: 10.1160/TH07-01-0040

Merfeld-Clauss, S., Gollahalli, N., March, K. L., and Traktuev, D. O. (2010). Adipose tissue progenitor cells directly interact with endothelial cells to induce vascular network formation. *Tissue Eng. A* 16, 2953–2966. doi: 10.1089/ten.tea.2009.0635

Morita, T., Sasaki, M., Kataoka-Sasaki, Y., Nakazaki, M., Nagahama, H., Oka, S., et al. (2016). Intravenous infusion of mesenchymal stem cells promotes functional recovery in a model of chronic spinal cord injury. *Neuroscience* 335, 221–231. doi: 10.1016/j.neuroscience.2016.08.037

Nakagami, H., Maeda, K., Morishita, R., Iguchi, S., Nishikawa, T., Takami, Y., et al. (2005). Novel autologous cell therapy in ischemic limb disease through growth factor secretion by cultured adipose tissue-derived stromal cells. *Arterioscler. Thromb. Vasc. Biol.* 25, 2542–2547. doi: 10.1161/01.ATV.0000190701.92007.6d

Nakanishi, C., Nagaya, N., Ohnishi, S., Yamahara, K., Takabatake, S., Konno, T., et al. (2011). Gene and protein expression analysis of mesenchymal stem cells derived from rat adipose tissue and bone marrow. *Circ. J.* 75, 2260–2268. doi: 10.1253/circj.cj-11-0246

Noble, L. J., and Wrathall, J. R. (1989a). Correlative analyses of lesion development and functional status after graded spinal cord contusive injuries in the rat. *Exp. Neurol.* 103, 34–40. doi: 10.1016/0014-4886(89)90182-9

Noble, L. J., and Wrathall, J. R. (1989b). Distribution and time course of protein extravasation in the rat spinal cord after contusive injury. *Brain Res.* 482, 57–66. doi: 10.1016/0006-8993(89)90542-8

Novikova, L. N., Brohlin, M., Kingham, P. J., Novikov, L. N., and Wiberg, M. (2011). Neuroprotective and growth-promoting effects of bone marrow stromal cells after cervical spinal cord injury in adult rats. *Cytotherapy* 13, 873–887. doi: 10.3109/14653249.2011.574116

Nowak-Sliwinska, P., Segura, T., and Iruela-Arispe, M. L. (2014). The chicken chorioallantoic membrane model in biology, medicine and bioengineering. *Angiogenesis* 17, 779–804. doi: 10.1007/s10456-014-9440-7

Orive, G., Anitua, E., Pedraz, J. L., and Emerich, D. F. (2009). Biomaterials for promoting brain protection, repair and regeneration. *Nat. Rev. Neurosci.* 10, 682–692. doi: 10.1038/nrn2685

Paredes, I., Himmels, P., and Ruiz de Almodóvar, C. (2018). Neurovascular Communication during CNS Development. *Dev. Cell* 45, 10–32. doi: 10.1016/j.devcel.2018.01.023

Park, K. K., Liu, K., Hu, Y., Smith, P. D., Wang, C., Cai, B., et al. (2008). Promoting axon regeneration in the adult CNS by modulation of the PTEN/mTOR pathway. *Science* 322, 963–966. doi: 10.1126/science.1161566

Pires, A. O., Mendes-Pinheiro, B., Teixeira, F. G., Anjo, S. I., Ribeiro-Samy, S., Gomes, E. D., et al. (2016). Unveiling the differences of secretome of human bone marrow mesenchymal stem cells, adipose tissue derived stem cells and human umbilical cord perivascular cells: a proteomic analysis. *Stem Cells Dev.* 25, 1073–1083. doi: 10.1089/scd.2016.0048

Rauch, M. F., Hynes, S. R., Bertram, J., Redmond, A., Robinson, R., Williams, C., et al. (2009). Engineering angiogenesis following spinal cord injury: a coculture of neural progenitor and endothelial cells in a degradable polymer implant leads to an increase in vessel density and formation of the blood-spinal cord barrier. *Eur. J. Neurosci.* 29, 132–145. doi: 10.1111/j.1460-9568.2008.06567.x

Ribeiro, T. B., Duarte, A. S. S., Longhini, A. L. F., Pradella, F., Farias, A. S., Luzo, A. C. M., et al. (2015). Neuroprotection and immunomodulation by xenografted human mesenchymal stem cells following spinal cord ventral root avulsion. *Sci. Rep.* 5:16167. doi: 10.1038/srep16167

Rohringer, S., Hofbauer, P., Schneider, K. H., Husa, A. M., Feichtinger, G., Peterbauer-Scherb, A., et al. (2014). Mechanisms of vasculogenesis in 3D fibrin matrices mediated by the interaction of adipose-derived stem cells and endothelial cells. *Angiogenesis* 17, 921–933. doi: 10.1007/s10456-014-9439-0

Ropper, A. E., Thakor, D. K., Han, I., Yu, D., Zeng, X., Anderson, J. E., et al. (2017). Defining recovery neurobiology of injured spinal cord by synthetic matrix-assisted hMSC implantation. *Proc. Natl. Acad. Sci. U.S.A.* 114, E820–E829. doi: 10.1073/pnas.1616340114

Salgado, A. J., Sousa, J. C., Costa, B. M., Pires, A. O., Mateus-Pinheiro, A., Teixeira, F. G., et al. (2015). Mesenchymal stem cells secretome as a modulator of the neurogenic niche: basic insights and therapeutic opportunities. *Front. Cell. Neurosci.* 9:249. doi: 10.3389/fncel.2015.00249

Segal, R. A., Pomeroy, S. L., and Stiles, C. D. (1995). Axonal growth and fasciculation linked to differential expression of BDNF and NT3 receptors in developing cerebellar granule cells. *J. Neurosci.* 15(7 Pt 1), 4970–4981. doi: 10.1523/jneurosci.15-07-04970.1995

Silva, N. A., Cooke, M. J., Tam, R. Y., Sousa, N., Salgado, A. J., Reis, R. L., et al. (2012). The effects of peptide modified gellan gum and olfactory ensheathing glia cells on neural stem/progenitor cell fate. *Biomaterials* 33, 6345–6354. doi: 10.1016/j.biomaterials.2012.05.050

Silva, N. A., Moreira, J., Ribeiro-Samy, S., Gomes, E. D., Tam, R. Y., Shoichet, M. S., et al. (2013). Modulation of bone marrow mesenchymal stem cell secretome by ECM-like hydrogels. *Biochimie* 95, 2314–2319. doi: 10.1016/j.biochi.2013.08.016

Silva, N. A., Sousa, N., Reis, R. L., and Salgado, A. J. (2014). From basics to clinical: a comprehensive review on spinal cord injury. *Prog. Neurobiol.* 114, 25–57. doi: 10.1016/j.pneurobio.2013.11.002

Sondell, M., Sundler, F., and Kanje, M. (2000). Vascular endothelial growth factor is a neurotrophic factor which stimulates axonal outgrowth through the flk-1 receptor. *Eur. J. Neurosci.* 12, 4243–4254. doi: 10.1046/j.0953-816X.2000.01326.x

Spejo, A. B., Carvalho, J. L., Goes, A. M., and Oliveira, A. L. R. (2013). Neuroprotective effects of mesenchymal stem cells on spinal motoneurons following ventral root axotomy: synapse stability and axonal regeneration. *Neuroscience* 250, 715–732. doi: 10.1016/j.neuroscience.2013.07.043

Tator, C. H., and Koyanagi, I. (1997). Vascular mechanisms in the pathophysiology of human spinal cord injury. *J. Neurosurg.* 86, 483–492. doi: 10.3171/jns.1997.86.3.0483

Torres-Espín, A., Santos, D., González-Pérez, F., del Valle, J., and Navarro, X. (2014). Neurite-J: an Image-J plug-in for axonal growth analysis in organotypic cultures. *J. Neurosci. Methods* 236, 26–39. doi: 10.1016/j.jneumeth.2014.08.005

Vawda, R., Badner, A., Hong, J., Mikhail, M., Lakhani, A., Dragas, R., et al. (2019). Early intravenous infusion of mesenchymal stromal cells exerts a tissue source age-dependent beneficial effect on neurovascular integrity and neurobehavioral recovery after traumatic cervical spinal cord injury. *Stem Cells Transl. Med.* 8, 639–649. doi: 10.1002/sctm.18-0192

Verseijden, F., Posthumus-van Sluijs, S. J., Pavljasevic, P., Hofer, S. O. P., van Osch, G. J. V. M., and Farrell, E. (2010). Adult human bone marrow- and adipose

tissue-derived stromal cells support the formation of prevascular-like structures from endothelial cells in vitro. *Tissue Eng. A* 16, 101–114. doi: 10.1089/ten.TEA.2009.0106

Whetstone, W. D., Hsu, J. Y. C., Eisenberg, M., Werb, Z., and Noble-Haeusslein, L. J. (2003). Blood-spinal cord barrier after spinal cord injury: relation to revascularization and wound healing. *J. Neurosci. Res.* 74, 227–239. doi: 10.1002/jnr.10759

Willis, E. F., MacDonald, K. P. A., Nguyen, Q. H., Garrido, A. L., Gillespie, E. R., Harley, S. B. R., et al. (2020). Repopulating microglia promote brain repair in an IL-6-dependent manner. *Cell* 180, 833.e16–846.e16. doi: 10.1016/j.cell.2020.02.013

Yu, S., Yao, S., Wen, Y., Wang, Y., Wang, H., and Xu, Q. (2016). Angiogenic microspheres promote neural regeneration and motor function recovery after spinal cord injury in rats. *Sci. Rep.* 6:33428. doi: 10.1038/srep33428

Zudaire, E., Gambardella, L., Kurcz, C., and Vermeren, S. (2011). A computational tool for quantitative analysis of vascular networks. *PLoS One* 6:e27385. doi: 10.1371/journal.pone.0027385

Conflict of Interest: The authors declare that the research was conducted in the absence of any commercial or financial relationships that could be construed as a potential conflict of interest.

frontiers in Cell and Developmental Biology

MINI REVIEW
published: 18 June 2020
doi: 10.3389/fcell.2020.00442

The Relevance of Transcription Factors in Gastric and Colorectal Cancer Stem Cells Identification and Eradication

*Diana Pádua[1,2], Paula Figueira[1,2], Inês Ribeiro[1,2], Raquel Almeida[1,2,3,4] and Patrícia Mesquita[1,2]**

[1] i3S – Institute for Research and Innovation in Health, University of Porto, Porto, Portugal, [2] Institute of Molecular Pathology and Immunology, University of Porto, Porto, Portugal, [3] Faculty of Medicine, University of Porto, Porto, Portugal, [4] Department of Biology, Faculty of Sciences, University of Porto, Porto, Portugal

Gastric and colorectal cancers have a high incidence and mortality worldwide. The presence of cancer stem cells (CSCs) within the tumor mass has been indicated as the main reason for tumor relapse, metastasis and therapy resistance, leading to poor overall survival. Thus, the elimination of CSCs became a crucial goal for cancer treatment. The identification of these cells has been performed by using cell-surface markers, a reliable approach, however it lacks specificity and usually differs among tumor type and in some cases even within the same type. In theory, the ideal CSC markers are those that are required to maintain their stemness features. The knowledge that CSCs exhibit characteristics comparable to normal stem cells that could be associated with the expression of similar transcription factors (TFs) including SOX2, OCT4, NANOG, KLF4 and c-Myc, and signaling pathways such as the Wnt/β-catenin, Hedgehog (Hh), Notch and PI3K/AKT/mTOR directed the attention to the use of these similarities to identify and target CSCs in different tumor types. Several studies have demonstrated that the abnormal expression of some TFs and the dysregulation of signaling pathways are associated with tumorigenesis and CSC phenotype. The disclosure of common and appropriate biomarkers for CSCs will provide an incredible tool for cancer prognosis and treatment. Therefore, this review aims to gather the new insights in gastric and colorectal CSC identification specially by using TFs as biomarkers and divulge promising drugs that have been found and tested for targeting these cells.

Keywords: gastric cancer, colorectal cancer, transcription factors, cancer stem cells, signaling pathways, targeted therapy

OPEN ACCESS

Edited by:
Susana Solá, University of Lisbon, Portugal

Reviewed by:
Asfar S. Azmi, Wayne State University Karmanos Cancer Institute, United States
Borhane Guezguez, German Cancer Research Center, Germany

***Correspondence:**
Patrícia Mesquita
pmesquita@ipatimup.pt

Specialty section:
This article was submitted to Stem Cell Research, a section of the journal Frontiers in Cell and Developmental Biology

Received: *20 March 2020*
Accepted: *11 May 2020*
Published: *18 June 2020*

Citation:
Pádua D, Figueira P, Ribeiro I, Almeida R and Mesquita P (2020) The Relevance of Transcription Factors in Gastric and Colorectal Cancer Stem Cells Identification and Eradication. Front. Cell Dev. Biol. 8:442. doi: 10.3389/fcell.2020.00442

INTRODUCTION

Gastrointestinal malignancies are listed among the major causes of cancer death worldwide, being associated with environmental and genetic risk factors such as older age, chronic inflammation, family history, smoking, dietary patterns, overweight and physical inactivity, as well as gut microbiota (Lochhead and El-Omar, 2008; Mattiuzzi et al., 2019). Gastric cancer (GC) and colorectal cancer (CRC) are among the top five most incident and deadly cancers worldwide

(Bray et al., 2018). As surgical techniques improve, as well as radiotherapy, chemotherapy and neoadjuvant therapies, the 5-year survival rate can reach up to 95% for early GC and 90% for localized CRC (Song et al., 2017; Sonbol et al., 2019). However, most patients have advanced-stage disease at diagnosis and so the best surgical window is missed (Song et al., 2017; Bray et al., 2018). They develop recurrent loco-regional disease or distant metastases with consequent decrease in survival. The heterogeneity of cancer at molecular, histological and phenotypic levels plays an important role in therapy resistance and tumor recurrence, being cancer stem cells (CSCs) among the major causative factors of cancer heterogeneity and treatment failure (Iseghohi, 2016; Gullo et al., 2018). The CSC model of tumor progression hypothesizes that a small subpopulation of cancer cells that display stem-like properties sustains tumor growth, metastasis, relapse and resistance to chemotherapy (Iseghohi, 2016). CSCs can undergo symmetric and asymmetric divisions, having the ability to give rise to all the different types of cancer cells within the tumor (Marjanovic et al., 2013). The origin of CSCs is still unclear and controversial (Dalerba et al., 2007a; Brunner et al., 2012). Various hypotheses suggest that depending on the tumor type, CSCs might be derived from adult stem cells, adult progenitor cells that underwent mutations, or differentiated cells that gained stem-like properties through dedifferentiation (Basu et al., 2016; Phi et al., 2018). A large number of studies demonstrate that CSCs share biomarkers with normal stem cells, thus specific markers for their identification have been explored in recent years. It is known that some transcription factors (TFs) can be re-expressed or reactivated in CSCs, playing a crucial role in the reprogramming of these cells. This review aims to provide a better understanding on how TFs associated with gastric and colorectal CSCs phenotype can be used for CSCs identification, characterization and targeted therapy.

THE CHALLENGES OF CANCER STEM CELL IDENTIFICATION

The identification of normal stem cells is now an easy process due to their well-recognized set of biomarkers whereas the identification of CSCs is a challenging task resulting from their complex phenotype, that differs from one tumor to another (Pattabiraman and Weinberg, 2014). Additionally, CSCs represent a very small percentage of tumor cells within the total tumor mass making even harder their detection in heterogeneous tumors (Kim Y. et al., 2009). The use of different combinations of cell-surface markers has been the main strategy to identify CSCs in several tumor types (Magee et al., 2012). The cell-surface markers are chosen according to their expression and relevance in the tumor type allowing the separation of CSCs from non-CSCs (Pattabiraman and Weinberg, 2014). In GC and CRC, the list of cell-surface markers capable of identifying CSCs is growing (**Table 1**). This means that the interest in gastric and colorectal CSCs identification and targeting is rising but also means that the already used markers are not uniformly advantageous for CSCs detection. In particular, inconsistencies remain concerning which cell-surface marker may be the ideal marker to identify gastric and colorectal CSCs from cell lines and primary tumors (Takaishi et al., 2009; Zhang et al., 2011; Jiang Y. et al., 2012; Rocco et al., 2012; Wakamatsu et al., 2012; Brungs et al., 2016).

Gastric Cancer

Several cell-surface markers have emerged for gastric CSC identification. The transmembrane glycoprotein CD44 was the first described cell-surface marker used in gastric CSC identification. Takaishi et al. (2009) and his collaborators analyzed a panel of six GC cell lines and in three of them – NCI-N87, MKN-45 and MKN-74 – a small $CD44^+$ cell subpopulation displayed CSC features such as self-renewal, asymmetric division, spheroid colony formation, and *in vivo* tumorigenic ability. They also observed that the $CD44^+$ subpopulation had a higher resistance to anticancer drugs when compared to $CD44^-$ cells (Takaishi et al., 2009). However, in the other three cell lines – AGS, Kato III and MKN28 – the CD44 cell-surface marker was not able to mark cells with stem cell properties (Takaishi et al., 2009). Clinically, $CD44^+$ cancer cells at the invasive GC front are associated with poor patient survival (Nosrati et al., 2014; Kodama et al., 2017). Later, Zhang et al. (2011) combined CD44 with CD24, a signal transducer, and successfully detected a $CD44^+CD24^+$ cellular subpopulation with CSCs characteristics, such as the capability to self-renew and to originate differentiated progeny (Zhang et al., 2011). Additionally, they showed that $CD44^+CD24^+$ cells had higher ability to form tumors when injected into immunodeficient mice, compared to the $CD44^-CD24^-$ cells (Zhang et al., 2011). The CD54 cell-surface marker, also known as ICAM-1 (intercellular adhesion molecule 1), was combined with CD44 to isolate gastric CSCs from tumor tissues and peripheral blood of patients with GC (Chen et al., 2012). The $CD44^+CD54^+$ cells exhibited *in vitro* and *in vivo* self-renewal ability, formed gastric tumorspheres and originated tumors similar to the original human tumor when injected into immunodeficient mice (Chen et al., 2012). The epithelial cell adhesion molecule (EpCAM) has also been used in combination with CD44 to mark gastric CSCs. The small $EpCAM^+/CD44^+$ subpopulation isolated from primary human GC tissues was more resistant to anticancer drugs including 5-fluorouracil (5-FU), doxorubicin, vinblastine and paclitaxel, when compared with $EpCAM^+/CD44^-$, $EpCAM^-/CD44^+$ and $EpCAM^-/CD44^-$ cells (Brabletz et al., 2005; Han et al., 2011). It also showed capacity to form sphere-like structures in serum free conditions and greater ability to originate tumors in immunocompromised mice (Han et al., 2011). The tumors formed after inoculation of the $EpCAM^+/CD44^+$ cells recapitulated the heterogeneous morphology and phenotype present in the original gastric tumor (Han et al., 2011). Moreover, Fukamachi et al. (2013) identified another potential gastric CSC marker, the CD49f, an integrin α6 (ITGA6) that is a subunit of laminin receptors. Their work showed that $CD49f^+$ cells from GC originated tumors when subcutaneously injected into immunodeficient mice, while $CD49f^-$ cells did not (Fukamachi et al., 2013). They also demonstrated that some of the $CD49f^+$ sphere-forming cells were more resistant to doxorubicin, 5-FU and doxifluridine than the other GC cells studied (Fukamachi et al., 2013). Another cell-surface marker identified as a gastric

TABLE 1 | Cancer stem cell (CSC) biomarkers for gastric and colorectal cancer.

	Gastric Cancer	Colorectal Cancer
CSCs biomarkers	**References**	**References**
CD44	Takaishi et al., 2009; Zhang X. et al., 2016	Du et al., 2008; Huang et al., 2015
CD44 combined with CD24	Zhang et al., 2011	—
CD44 combined with CD54	Chen et al., 2012	—
CD44 combined with EpCAM	Han et al., 2011	Dalerba et al., 2007b
CD44 combined with CD133	—	Huang et al., 2015
CD49f	Fukamachi et al., 2013	Haraguchi et al., 2013
CD71	Ohkuma et al., 2012	—
CD90	Jiang J. et al., 2012	—
CD133	Fukamachi et al., 2011; Zhang X. et al., 2016	O'Brien et al., 2007; Ricci-Vitiani et al., 2007; Huang et al., 2015
CD133 combined with CD166	—	Dalerba et al., 2007b
CD184 (CXCR4)	Fujita et al., 2015	—
CD200	—	Zhang S.S. et al., 2016
Lgr5	Gong et al., 2016	—
Lgr5 combined with EpCAM	—	Kemper et al., 2012
Lgr5 combined with EpCAM and CD44	—	Leng et al., 2018
ALDH	Zhi et al., 2011	Huang et al., 2009
SOX2	Pádua et al., 2020	Takeda et al., 2018

The table contains some of the most reported CSCs markers used for both tumor types.

CSC marker is the CD71 transferrin receptor. In this case, it was demonstrated that the $CD71^-$ subpopulation from the MKN-1 GC cell line displayed CSC features, contrary to $CD71^+$ cells. The $CD71^-$ cells were more resistant to 5-FU than $CD71^+$, had higher tumorigenic ability and were mostly present in the invasive front of the tumor (Ohkuma et al., 2012). The cell-surface glycoprotein CD90 (Thy-1) appeared as a potential gastric CSC marker since it was capable of identifying a small population with *in vivo* tumorigenic and self-renewal ability (Jiang J. et al., 2012). Additionally, 25% of the gastric primary tumors possessed higher expression of erb-b2 receptor tyrosine kinase 2 (HER2), which was correlated with the higher expression of CD90 (Jiang J. et al., 2012). CD133 (prominin-1), a pentaspan transmembrane glycoprotein, is described as a gastric CSC marker due to the fact that its expression is positively correlated with tumor aggressiveness in GC patients (Fukamachi et al., 2011; Lee et al., 2012; Wakamatsu et al., 2012; Hashimoto et al., 2014; Nosrati et al., 2014). Zhao et al. showed that the frequency of $CD133^+$ in gastric primary tumors samples was higher than $CD133^-$ cells and CD133 was associated with poor prognosis in GC (Zhao et al., 2010). Also, spheroid cells from GC cell lines and primary GC tissues presented CD133 expression and displayed several features of CSCs (Zhang X. et al., 2016). New cell-surface markers have emerged in the study of gastric CSCs and demonstrated to be able to mark a small population in GC with stem-like features, specifically Lgr5 (leucine-rich repeat-containing G-protein coupled receptor 5) and CXCR4 (C-X-C chemokine receptor type 4) also known as CD184 (Fujita et al., 2015; Gong et al., 2016). Also, the intracellular enzyme aldehyde dehydrogenase (ALDH) has been used to identify gastric CSCs (Zhi et al., 2011; Wakamatsu et al., 2012). Zhi et al. (2011) were able to divide NCI-N87 and SNU-1 GC cell lines into $ALDH^+$ and $ALDH^-$ cells. The $ALDH^+$ cells presented CSC features such as higher levels of SOX2, NANOG and Nestin, formed more sphere-like structures and had higher resistance to 5-FU and cisplatin (Zhi et al., 2011). They also showed that $ALDH^+$ cells were more sensitive to salinomycin, a drug proposed to target CSCs (Zhi et al., 2011).

Colorectal Cancer

Several specific cell-surface markers were used to identify colorectal CSCs (Todaro et al., 2010; Vaiopoulos et al., 2012; Rassouli et al., 2016; Wahab et al., 2017; Zhou et al., 2017; Boesch et al., 2018; Munro et al., 2018; Parizadeh et al., 2019; van der Heijden and Vermeulen, 2019). CD133 was shown to be a robust CSC-surface marker in CRC (O'Brien et al., 2007; Ricci-Vitiani et al., 2007; Akbari et al., 2020). Positive expression of CD133 was, for the first time, associated with a significantly worse survival and poorer clinical response to 5-FU-based chemotherapy in CRC patients (Ong et al., 2010). CD44 is also a valid marker of colorectal CSCs (Du et al., 2008). In combination with EpCAM it has already been considered a better strategy, when compared to CD133 (Dalerba et al., 2007b). Furthermore, CD166 (another transmembrane glycoprotein) could be used to co-purify CSCs (Dalerba et al., 2007b). More recently, colonospheres and chemoresistant CRC cells were found to be enriched with CD133 and CD44 (Huang et al., 2015). A strategy that combines CD133 with CD44, seems to be more reliable to isolate colorectal CSCs from both cell lines and primary tumors (Abbasian et al., 2019). Horst et al. (2009) showed that CD133 may have a better prognostic capacity *per se*, but the combination of CD133, CD44, and CD166 markers may stratify better the risk of CRC. Lgr5 positivity identifies human colorectal CSCs and is a prognostic factor for CRC (Kemper et al., 2012; Jiang Y. et al., 2016). Lgr5 overexpression has been shown to be important in

CRC progression, as a result of its role in potentiating the Wnt signaling pathway (Carmon et al., 2012). de Sousa e Melo et al. (2017) have shown that $Lgr5^+$ CSCs are crucial for the formation of liver metastases, while in the primary tumor $Lgr5^-$ cells proliferate and are capable of originating $Lgr5^+$ cells, assuring a rapid tumor growth when treatment ends. Lgr5 combined with CD44 and EpCAM can further improve the identification of CSCs in CRC (Leng et al., 2018). Vermeulen et al. (2008) have shown that spheroid cultures of colon CSCs express CD133, CD166, CD44, CD29, CD24, Lgr5, and nuclear β-catenin, all of which described markers of the CSC population. Also, CD200 showed a role as a CSC marker in colon cancer, and CD49f was associated with tumor cell invasion and metastasis in colon cancer working as an important marker for identifying colorectal CSCs (Robertson et al., 2009; Haraguchi et al., 2013; Zhang S.S. et al., 2016). ALDH1 also appears as a specific marker for colonic CSCs and as an independent prognostic factor for patients with CRC (Huang et al., 2009; Lugli et al., 2010; Kahlert et al., 2012; Goossens-Beumer et al., 2014; Zhou et al., 2017; Munro et al., 2018). In patients with stage II-III rectal cancer that received radio-chemotherapy, ALDH1 expression was correlated with poor prognosis, cancer relapse and metastasis (Huang et al., 2009; Deng et al., 2014).

TRANSCRIPTION FACTORS AS POTENTIAL CSC MARKERS

One of the challenges to target CSCs is to identify specific markers as well as to uncover targetable molecular features associated with their phenotype. It is known that normal stem cells and CSCs share core stemness signaling pathways such as Notch, Hedgehog, WNT/β-catenin and JAK/STAT, that have pivotal roles in maintaining stem cell properties and regulating their transcriptional program (Chen K. et al., 2013). SOX2, OCT4, KLF4, and NANOG are some of the key TFs known to promote stemness by upregulating genes involved in self-renewal and pluripotency, while suppressing genes involved in differentiation (Young, 2011; Tang et al., 2015; Buczek et al., 2018). Key stem cell TFs like SOX2, OCT4, and NANOG have been proven to be overexpressed in CSCs. For that reason, fluorescence reporter systems driven by portions of promoters where these proteins bind were developed to allow CSCs to be labeled and tracked in various types of cancer. These reporter systems seem to be a powerful tool to identify and study CSCs more efficiently than cell-surface markers (Saygin et al., 2016). Tang et al. (2015) developed a flexible lentiviral-based reporter system (SORE6-GFP) that allows direct visualization of CSCs based on SOX2 and OCT4 expression. By using this novel reporter system, our group was able to isolate gastric CSCs from two phenotypically different GC cell lines (AGS and Kato III) (Pádua et al., 2020). Using the same principle, other authors have been developing similar systems to identify and characterize CSCs in a variety of solid tumors. Buczek et al. (2018) established a method using a lentiviral construct carrying the promoter of NANOG to identify prostate CSCs and more recently, Ghanei et al. (2020) introduced a similar approach for the isolation of CSCs in a breast cancer cell line based on the single expression of OCT4. Although the use of cell-surface markers is the most trusted approach to detect these cells, several studies demonstrated that they lack specificity and cannot be used for real time assessment of CSCs behavior, which could give new insights about their properties and possible targets (Tang et al., 2015). Growing evidences support that specific TFs overexpressed in normal gastrointestinal stem cells may contribute to the self-renewal characteristics of CSCs in GC and CRC and are related with patient prognosis (Hadjimichael et al., 2015; Zhao et al., 2017). This makes them a powerful tool in CSCs identification and study.

SOX2 (SRY-Box Transcription Factor 2)

SOX2 is a master regulator that belongs to the family of high-mobility group TFs. It plays many roles throughout development and cell differentiation in normal tissues, namely in mammalian embryogenesis, morphogenesis and homeostasis of the foregut-derived epithelia of the esophagus, lung and trachea (Avilion et al., 2003; Sarkar and Hochedlinger, 2013). SOX2 role in stemness was strengthen with Takahashi and Yamanaka's findings when reprogramming mouse embryonic fibroblasts into induced pluripotent stem (iPS) cells, by introducing SOX2 along with OCT3/4, c-Myc and KLF4 (Takahashi and Yamanaka, 2006). In cancer, SOX2 has increasingly been associated with a CSC phenotype in several tumors (Wuebben and Rizzino, 2017; Takeda et al., 2018). In GC, SOX2 role is still controversial: some authors associate its high expression with a more aggressive phenotype, poor prognosis and worse response to therapy whereas others have shown the opposite (Hütz et al., 2013; Camilo et al., 2014; Carrasco-Garcia et al., 2016; Zhang X. et al., 2016; Wuebben and Rizzino, 2017; Basati et al., 2020; Pádua et al., 2020). Our group identified subpopulations of gastric CSCs in two human cell lines based on the expression of SOX2 and showed that $SORE6^+$ cells presented CSCs properties, including higher proliferation and ability to form gastrospheres, enhanced *in vivo* tumorigenesis and increased resistance to 5-FU (Pádua et al., 2020). Additionally, Hütz et al. (2013) observed that inhibition of SOX2 resulted in reduced cell proliferation and migration, increased apoptosis, changes in cell cycle and reduced tumorigenic potential of cells *in vivo*. Similar results were observed *in vivo*, where suppression of SOX2 resulted in reduced tumor growth and decreased tumorigenicity (Tian et al., 2012; Hütz et al., 2013). In CRC, SOX2 overexpression has been associated with tumor progression and disease recurrence and SOX2 *de novo* expression was associated with poorly differentiated and more invasive tumors and poor patient overall survival (Lundberg et al., 2014; Lundberg et al., 2016). Takeda et al. (2018) have shown that $SOX2^+$ cells developed chemoresistance to oxaliplatin and 5-FU, exhibiting typical asymmetric cell division and higher CSC markers expression. They concluded that colon cancer cells expressing SOX2 behave like CSCs and are therefore associated with poor prognosis (Lundberg et al., 2016; Takeda et al., 2018). Taken together, these findings indicate that SOX2 has a critical role in several aspects of CSCs biology.

OCT4 (POU Class 5 Homeobox 1)

OCT4, a homeodomain TF of the Pit-Oct-Unc family, is expressed in embryonic stem cells, where it maintains stem cell-like properties, and in adult stem cells, being involved in their proliferation and differentiation (Loh et al., 2006; Han et al., 2014). Abnormal expression of OCT4 has been observed in different tumor types, including GC and CRC (Dai et al., 2013; Basati et al., 2020). Studies report that its expression is positively correlated with more aggressive and metastatic tumors, as well as with poorer overall prognosis (Zhang X. et al., 2016; Basati et al., 2020). Chen and collaborators demonstrated that overexpression of OCT4 in GC cells led differentiated cancer cells to become undifferentiated and acquiring self-renewal capacity (Chen et al., 2009) and another study reported that downregulation of OCT4 induced differentiation in GC cells (Tai et al., 2005). Additionally, Zhang X. et al. (2016) demonstrated a p-ERK mediated positive feedback loop between the cell surface marker CD44 and OCT4, responsible for sustaining gastric CSCs properties. OCT4 has also been reported in colon CSCs and its knockdown inhibits cell migration and invasion, suggesting it may act as a novel prognostic marker in CRC (Miyoshi et al., 2010, 2018; Dai et al., 2013; Amini et al., 2014).

KLF4 (Kruppel Like Factor 4)

KLF4, also known as the gut-enriched Kruppel like factor (GKLF), is strongly expressed in post-mitotic and terminally differentiated epithelial tissues, along with those of the gastrointestinal tract (Cho et al., 2007; Cui et al., 2013). It is suggested that it may have an anticancer role in GC, being downregulated due to hypermethylation and loss of heterozygosity in gastric CSCs (Cho et al., 2007). Several studies have shown that KLF4 low expression is negatively associated with patient overall survival and may be a useful prognostic marker in GC patients (Li et al., 2012; Zhang et al., 2012; Hsu et al., 2013; Hashimoto et al., 2017; Zhao et al., 2020). Regarding CRC, KLF4 role is still not clear. Some studies reveal KLF4 is overexpressed in colon CSCs and its knockdown affects the stemness phenotype and decreases the cells malignant profile, while others demonstrate that loss of expression is associated with stem-like features namely formation of colonospheres, cell growth arrest, uncontrolled cell proliferation, pluripotency and self-renewal (Shie et al., 2000; Wei et al., 2006; Leng et al., 2013; Hadjimichael et al., 2015).

NANOG (Nanog Homeobox)

NANOG was first discovered in embryonic stem cells (ESCs) and is a key TF involved in self-renewal and multipotency (Chambers et al., 2003). It is typically silenced in normal somatic cells, though abnormal expression has been reported in malignant tumors, such as GC and CRC (Lin et al., 2012; Hadjimichael et al., 2015). Previous studies demonstrate that NANOG is highly expressed in GC and significantly associated with tumor size and grade, along with decreased overall survival (Iv Santaliz-Ruiz et al., 2014; Basati et al., 2020). Although studies indicate NANOG is associated with a CSC phenotype, it remains unclear its role in CSC maintenance in GC (Iv Santaliz-Ruiz et al., 2014). With respect to CRC, NANOG overexpression has been associated with colony formation and stem cell properties, as well as worse prognosis (Ibrahim et al., 2012; Zhang et al., 2013; Hadjimichael et al., 2015).

c-Myc (MYC Proto-Oncogene, bHLH Transcription Factor)

c-Myc is an essential TF that regulates genes that take part in biological processes such as self-renewal, differentiation, growth and metabolism (Dang, 2013; Bretones et al., 2015). Although it is one of the most commonly activated oncogenes involved in the pathogenesis of cancer, its overexpression alone is unable to induce the transformation of normal cells into tumor cells (Yang et al., 2020). The role of c-Myc in GC is less studied than in other tumor types. It has been suggested as a CSC marker in some tumors such as small-cell lung cancer, prostate cancer, neuroblastoma, glioblastoma and hematopoietic malignancies, but the expression and relevance in GC has not yet been clarified (Yang et al., 2020). Some authors associate c-Myc deregulation with poor prognostic features (Han et al., 1999; de Souza et al., 2013; Wang et al., 2016). Upregulation of c-Myc is common in 70% of CRC cases and it has been shown to have a crucial role in maintaining chemoresistance and self-renewal, being overexpressed in colon CSCs (Muzny et al., 2012; Zhang et al., 2019). Despite some controversial results, it has been shown that high expression of c-Myc is an independent poor prognostic factor in CRC (Lee et al., 2015; Wang et al., 2017).

SOX9 (SRY-Box Transcription Factor 9)

SOX9 regulates developmental processes such as male sex determination, chondrogenesis, neurogenesis, and neural crest development (Jo et al., 2014). Also, it plays a vital role in cell fate decisions and stem cell maintenance during embryonic development and adulthood in several organs, including the gastrointestinal tract (Bastide et al., 2007; Huch and Clevers, 2011). Its role in GC is still conflicting, while some studies defend an association between lower survival and SOX9 high expression, others demonstrate poor prognosis with a decreased level of SOX9 expression (Sun et al., 2012; Santos et al., 2016; Mesquita et al., 2019). Also, both oncogenic and tumor suppressor activity of SOX9 have been implicated in CRC (Darido et al., 2008; Lu et al., 2008; Matheu et al., 2012; Prévostel and Blache, 2017). Previous studies suggest that this TF can influence tumor proliferation and progression, mainly through the regulation of the CSC pool, and could correlate with poor prognosis (Lu et al., 2008; Espersen et al., 2015; Javier et al., 2016).

GLI1 (GLI Family Zinc Finger 1)

GLI1 is part of the Sonic Hedgehog (SHH) pathway and seems to be essential for the maintenance of cancer cells with stem like properties in both GC and CRC (Zhang X. et al., 2016; Yang et al., 2018). In GC, its expression is significantly higher in metastatic cancer tissues and is positively correlated with a more aggressive tumor phenotype (Zhang X. et al., 2016). Furthermore, it has been observed that GLI1 overexpression promotes a CSC phenotype enhancing cell proliferation, migration and therapy

resistance (Dong et al., 2019; Yao et al., 2019). GLI1 also plays an important role in CSC characteristics related with aggressiveness and metastatic spread of CRC cells leading to decreased survival. Furthermore, GLI1 knockdown downregulates CD133/SOX9 expression and clonogenic ability of CRC cells, indicating this TF could be a potential marker for CSCs in CRC (Yang et al., 2018).

STAT3 (Signal Transducer and Activator of Transcription 3)

STAT3 plays an important role in the regulation of various physiological functions, such as inflammation, proliferation and invasion, being highly expressed in gastric and colorectal CSCs (Yu H. et al., 2009; Lin et al., 2011; Hajimoradi et al., 2016; Sonbol et al., 2019). In gastric CSCs, high expression of STAT3 has been reported to be involved in stemness properties and invasive ability (Hajimoradi et al., 2016; Jiang et al., 2017; Sonbol et al., 2019). Regarding its prognostic value several studies report STAT3 activation as a marker of unfavorable outcome (Kim D.Y. et al., 2009; Deng et al., 2010, 2013; Ji et al., 2016). In CRC, STAT3 is one of the major oncogenic proteins associated with proliferation, angiogenesis, invasion and chemo-radiotherapy resistance (Lin et al., 2005, 2011; Munro et al., 2018). Also, its inhibition prevents tumor initiation, being an attractive therapeutic target for CRC (Lin et al., 2011).

SALL4 (Spalt Like Transcription Factor 4)

As a TF, SALL4 plays essential roles in maintaining pluripotency and self-renewal of ESCs, being downregulated or silenced in differentiated cells (Zhang et al., 2006, 2015; Yang et al., 2008). SALL4 acts as an oncogene and it is associated with cancer initiation, development, and progression (Ma et al., 2006). Zhang et al. (2014) showed that the overexpression of SALL4 is associated with gastric CSC features and could be involved in the generation and maintenance of these cells. Later, Yuan et al. (2016) suggested a novel mechanism for SALL4 role in GC, showing that this TF binds to the promoter region of CD44 and activates it expression, enhancing cell proliferation, migration and invasion. Increasing evidence indicates that upregulation of SALL4 is associated with lymph node metastasis and poorer overall prognosis (Zhang et al., 2014, 2018b). In CRC, SALL4 overexpression is detected in 87% of tumor tissues and it is correlated with tumor cell metastasis to lymph nodes being associated with poor prognosis and showing its essential role in maintaining the properties of CSCs (Forghanifard et al., 2013; Zhang et al., 2015).

β-Catenin (Catenin Beta 1)

The Wnt/β-catenin pathway is implicated in the regulation of the epithelial stem cell self-renewal (Behrens et al., 1996). Alone, β-catenin signaling has been shown as necessary for the maintenance of CSC features (Huang et al., 2007; Kanwar et al., 2010; Jiang R. et al., 2016). The dysregulation of the Wnt/β-catenin signaling pathway has been implicated in colon carcinogenesis and plays a critical role in regulating the growth and maintenance of colonospheres (Kolligs et al., 2002; Kanwar et al., 2010). The activation of this pathway can lead to the conversion of intestinal stem cells into CSCs, where expression levels of β-catenin are higher (Kanwar et al., 2010). Some studies revealed that high levels of nuclear β-catenin, in CRC patients, were associated with a poor prognosis and could be used as a biomarker for late phase CRC (Chen Z. et al., 2013). Gastric CSCs self-renewal and proliferation ability, both *in vitro* and *in vivo*, are also improved by the Wnt/β-catenin signaling (Mao et al., 2014; Chiurillo, 2015).

CSCs AND TUMOR MICROENVIRONMENT

The close interaction between CSCs and their niche is fundamental for maintaining the stemness of CSCs and tumor progression. The CSC niche, a specific tumor microenvironment, which consists of stroma, micro-vessels, hypoxic regions, cancer-associated fibroblasts (CAFs), cancer-associated mesenchymal stem cells (MSCs), tumor-associated macrophages (TAMs) and extracellular matrix, secretes soluble factors (e.g., cytokines and growth factors) that are necessary for cancer cell survival (Quante et al., 2013; Lau et al., 2017; Yang et al., 2020). Growth factors and cytokines regulate Wnt, Notch, JAK-STAT3 and other signaling pathways thereby stimulating growth, epithelial-to-mesenchymal transition (EMT), invasion, angiogenesis, metastasis and inhibiting apoptosis (Yang et al., 2020). These pathways are required for the self-renewal and maintenance of CSCs. For instance, growth factors like hepatocyte growth factor (HGF), secreted by the stromal myofibroblasts, activate the Wnt-signaling in a subset of colon cancer cells that maintain the CSC phenotype (Vermeulen et al., 2010). Another example is hypoxia, which also maintains a stem-like phenotype in CRC and GC through the increased expression of hypoxia-inducible factors (HIFs), the transcription factors HIF-1α and HIF-2α, that maintain the Wnt/β-catenin signaling pathway and activate stemness-related TFs such as OCT4 (Gidekel et al., 2003; Liu et al., 2008; Mazumdar et al., 2010; Yeung et al., 2011; Vadde et al., 2017). On the other hand, cancer cells also secrete growth factors and proteases to promote changes in their microenvironment (Ishimoto et al., 2014). One significant example of this crosstalk between cancer cells and the microenvironment is the secretion of cytokines like interleukin-6 (IL-6) by the cancer-associated mesenchymal stem cells that enhance the progression of CRC through the IL-6/JAK2/STAT3 signaling (Zhang et al., 2018a). The same is observed in GC through the secretion of interleukin-8 (Li W. et al., 2015). On the other hand, cancer cells mediate the production of inflammatory cytokines with pro-tumorigenic roles or the inhibition of cytokines involved in immune surveillance, altering the composition of the immune cells in the tumor microenvironment (Quante et al., 2013; West et al., 2015). Specifically, Rezalotfi et al. (2019) suggested that CSCs could alter the cytokines in the tumor microenvironment by demonstrating that the balance between suppressive regulatory T cells (Treg) and T helper cells producing IL17 (Th17) could be affected. Chaudhry et al. (2009) disclosed further that STAT3 is fundamental for the inhibition of Treg cells development and

Th17 differentiation. In fact, the STAT3 transcription factor, in collaboration with NFκB, regulates the expression of these genes encoding critical cancer-promoting inflammatory mediators, establishing a crosstalk between cancer and immune cells of the microenvironment and perpetuating the effects of STAT3 activation in cancer cells (Yu et al., 2007; Grivennikov and Karin, 2010; Yang et al., 2019). However, despite the growing evidences on the interaction of gastric and colorectal CSCs with the tumor microenvironment, the specific molecules involved and their signaling pathways still need further investigation in order to design safe therapies.

THERAPEUTIC APPROACHES TO TARGET CSCs

The therapeutic approach in GC and CRC is determined by the stage of the disease at the time of diagnosis. Patients are treated with surgery, chemotherapy and/or radiation. In GC, surgery remains the main treatment for stage I. It can also be performed at stages II and III but chemotherapy (perioperative, neoadjuvant or adjuvant) is necessary to improve overall survival of the patients. For stage IV, chemotherapy with doublet or triplet platinum/fluoro-pyrimidine combinations or capecitabine is the main treatment (Neri et al., 2007; Smyth et al., 2016). Resective surgery is the main curative treatment used in non-metastasized CRC, although neo-adjuvant treatments are also administered in rectal carcinoma (Kuipers et al., 2015). After surgery, 5-FU-based chemotherapy is used to reduce the risk of tumor recurrence and improve overall survival of patients (Dienstmann et al., 2017). Currently, the decision of giving adjuvant treatment to early-stage CRC patients is recommended to high risk patients with one or more risk factors (Kannarkatt et al., 2017). Patients with very high risk – microsatellite stable (MSS) and T4 may be considered for the addition of oxaliplatin (Labianca et al., 2013). However, in some cases of GC and CRC, after a believed efficacious treatment, the cancer reappears locally or in distant metastasis. This results from the presence of CSCs that were able to resist the therapy applied, revealing that the existence of CSCs is one of the biggest difficulties in cancer treatment (Dean et al., 2005). Thus, direct targeting of CSCs seems to be the key for tumor complete elimination. The therapy against CSCs using specific molecules should eradicate these cells while the conventional therapy eliminates the non-CSCs present in the tumor bulk. Nevertheless, this type of treatment should be administrated in combination due to the possibility of cell plasticity that facilitates the appearance of *de novo* CSCs from non-CSCs. Moreover, targeting specific TFs or signaling pathways responsible for maintaining the CSC phenotype could become novel therapies against GC and CRC. For that reason, several clinical trials are being undertaken to explore the efficacy of diverse compounds, that are capable of modulating or inactivating proteins that gastric and colorectal CSCs use to grow and survive, allowing their elimination. Additionally, it is worth to mention that several studies have been conducted to evaluate the efficacy of small molecules in targeting CSCs *in vitro* and *in vivo*, compounds capable of eliminating or reducing the CSC population that could also be part of the path in cancer therapy targeting CSCs (Gupta et al., 2009; Abetov et al., 2015; Shapiro et al., 2016; Müller et al., 2017; Park et al., 2017; Pádua et al., 2020). **Table 2** lists the drugs that have been or are being investigated in clinical trials, alone or in combination with other compounds, to treat GC and CRC.

Immunotherapy

Cancer immunotherapy has emerged as a potential tool for cancer treatment (Farkona et al., 2016). Several immunotherapeutic strategies have been developed including cancer vaccines, oncolytic viruses, monoclonal antibodies or recombinant proteins, chimeric antigen receptor T cell (CAR-T) cells and other cellular therapies, lymphocyte-activating cytokines and checkpoint inhibitors (Riley et al., 2019). Immunotherapy aims to improve the immune system response against cancer cells through natural mechanisms (Riley et al., 2019). Therefore, it can be used to target cancer cells and also CSCs in the tumor microenvironment (Badrinath and Yoo, 2019). Many immunotherapeutic agents targeting CSCs have been tested in clinical trials (Menon et al., 2016). Monoclonal antibodies that specifically target CSC surface biomarkers have been used in gastric and colorectal cancer. Ongoing there is a Phase I study of RO5429083, a monoclonal antibody against CD44 in patients with metastatic and/or locally advanced malignant solid tumors (NCT01358903). Also used were EpCAM antibodies, such as edrecolomab, that was tested in patients with resected stage II adenocarcinoma of the colon (Niedzwiecki et al., 2011) and adecatumumab, that is being tested in a Phase II study to evaluate efficacy and safety, alone or with FOLFOX, in metastasized CRC (NCT00866944). A Phase I dose finding study is evaluating the bispecific antibody targeting EGFR and Lgr5 (MCLA-158) in metastatic CRC and other advanced solid tumors (NCT03526835). In addition, CAR-T cell therapies, have been developed to target CSCs in GC and CRC. There are three Phase I or II clinical trials in GC using CAR-T cells targeting EpCAM (NCT03013712, NCT03563326, and NCT02725125), one of them consisting in the intraperitoneal infusion in advanced GC with peritoneal metastasis. NCT03013712 includes patients with colon cancer. Moreover, there is a Phase I/II clinical study of CAR-T cells targeting CD133 in relapsed and/or chemotherapy refractory malignancies including CRC (NCT02541370).

Targeting the Transcription Factor STAT3

From the list of TFs strongly associated with CSC phenotype in GC and CRC, STAT3 became crucial as a molecular target for cancer therapy because napabucasin (BBI608), the first-in-class cancer stemness (CSCs) inhibitor that works by targeting STAT3, effectively blocks cancer relapse and metastasis in xenografted human cancers (Li Y. et al., 2015; Zhang Y. et al., 2016). Napabucasin is a naturally occurring drug orally administered. It inhibits CSC self-renewal and induces apoptosis in CSCs by targeting CSC signaling pathways (STAT3, NANOG and β-catenin) in GC (Bekaii-Saab and El-Rayes, 2017). In CRC, napabucasin has been investigated in several studies. A phase I/II clinical trial investigated napabucasin with other standard therapeutic treatments for advanced gastrointestinal malignancies (Bendell et al., 2017). Another

TABLE 2 | Complete and ongoing clinical trials of therapeutic agents targeting gastric and/or colorectal CSCs, correlated signaling pathways and the transcription factor STAT3.

Drug/Antibody	Targets	Disease/Condition	NCT Identifier	Phase	Routes of administration	Recruitment status	Last update	Sponsor
Immunotherapy								
RO5429083	CD44	Metastatic and/or locally advanced malignant solid tumors	NCT01358903	I	Intravenous (IV)	Completed, no results posted	November 2016	Hoffmann-La Roche
Adecatumumab alone or in combination with FOLFOX	EpCAM	R0 resection of colorectal liver metastases	NCT00866944	II	Intravenous (IV)	Completed, no results posted	November 2011	Amgen Research (Munich) GmbH
MCLA-158	EGFR and Lgr5	Advanced/metastatic solid tumors, including CRC	NCT03526835	I	Intravenous (IV)	Recruiting	August 2018	Merus N.V.
EpCAM CAR-T	EpCAM	Relapsed or refractory EpCAM positive cancer	NCT03013712	I/II	Intravenous (IV)	Recruiting	January 2017	First Affiliated Hospital of Chengdu Medical College
EpCAM CAR-T	EpCAM	Advanced GC with peritoneal metastasis	NCT03563326	I	Intravenous (IV)	Recruiting	September 2018	Jian-Kun Hu
EpCAM CAR-T	EpCAM	GC	NCT02725125	—	Intravenous (IV)	Unknown	March 2017	Sinobioway Cell Therapy Co., Ltd.
CART-133	CD133	Chemotherapy refractory advanced malignancies, including CRC	NCT02541370	I/II	Intravenous (IV)	Completed, no results posted	December 2019	Chinese PLA General Hospital
Transcription Factor inhibitors								
BBI608 or BNC105 in combination with nivolumab	STAT3	Metastatic CRC	NCT03647839	II	Oral and Intravenous (IV)	Recruiting	February 2019	Australasian Gastro-Intestinal Trials Group
Danvatirsen (AZD9150) in combination with Durvalumab (MEDI4736)	STAT3	Advanced and refractory pancreatic, non-small cell lung cancer, and mismatch repair deficient CRC	NCT02983578	II	Intravenous (IV)	Recruiting	March 2020	M.D. Anderson Cancer Center
Napabucasin (GB201) in combination with FOLFIRI	STAT3	Metastatic CRC	NCT03522649	III	Oral and Intravenous (IV)	Recruiting	June 2019	1Globe Health Institute LLC
TTI-101	STAT3	Advanced cancers, including gastric adenocarcinoma and CRC	NCT03195699	I	Oral	Recruiting	February 2020	Tvardi Therapeutics, Incorporated

(Continued)

TABLE 2 | Continued

Drug	Targets	Disease/Condition	NCT Identifier	Phase	Routes of administration	Recruitment status	Last update	Sponsor
Wnt/β -catenin pathway inhibitors								
Artesunate, prior to surgery	β-catenin	Stage II/III CRC	NCT02633098	II	Oral	Recruiting	April 2019	St George's, University of London
DKN-01 in combination with atezolizumab	DKK1	GC	NCT04166721	I/II	Intravenous (IV)	Recruiting	February 2020	Royal Marsden NHS Foundation Trust
ETC-1922159 in combination with pembrolizumab	PORCN	Advanced solid tumors	NCT02521844	I	Oral and Intravenous (IV)	Active, not recruiting	October 2019	EDDC (Experimental Drug Development Centre), A*STAR Research Entities
Foxy-5	Wnt-5A	CRC	NCT02020291	I	Intravenous (IV)	Completed, no results posted	February 2016	WntResearch AB
Foxy-5	Wnt-5A	Metastatic breast, colon or prostate cancer	NCT02655952	I	Intravenous (IV)	Completed, no results posted	December 2018	WntResearch AB
Foxy-5 as neo-adjuvant therapy	Wnt-5A	Colon cancer	NCT03883802	II	Intravenous (IV)	Recruiting	April 2019	WntResearch AB
Genistein in combination with FOLFOX or FOLFOX-Avastin	tyrosine kinase and topoisomerase-II	Metastatic CRC	NCT01985763	I/II	Oral and Intravenous (IV)	Completed, has results	May 2019	Sofya Pintova
LGK974	PORCN	Malignancies dependent on Wnt ligands, including BRAF mutant CRC	NCT01351103	I	Oral	Recruiting	February 2020	Novartis Pharmaceuticals
LGK974 in combination with LGX818 and cetuximab	PORCN	BRAF-mutant metastatic CRC and Wnt pathway mutations metastatic CRC	NCT02278133	I/II	Oral	Completed, no results posted	October 2017	Array BioPharma
MCLA-158	EGFR and LGR5	Advanced/metastatic solid tumors, including CRC	NCT03526835	I	Intravenous (IV)	Recruiting	August 2018	Merus N.V.
Mesalazine	induces the expression of μ-protocadherin	CRC	NCT02077777	II	Oral	Completed, no results posted	December 2016	SOFAR S.p.A.
OMP-18R5 (Vantictumab)	Wnt receptor	Solid tumors	NCT01608867	I	Intravenous (IV)	Completed, no results posted	September 2016	OncoMed Pharmaceuticals, Inc.
OMP-54F28 (Ipafricept)	Wnt receptor	Solid tumors	NCT01608867	I	Intravenous (IV)	Completed, no results posted	July 2017	OncoMed Pharmaceuticals, Inc.

(Continued)

TABLE 2 | Continued

Drug	Targets	Disease/Condition	NCT Identifier	Phase	Routes of administration	Recruitment status	Last update	Sponsor
Hedgehog (Hh) pathway inhibitors								
BMS-833923 (XL139)	Smoothened	Advanced or metastatic solid tumors	NCT01413906	I	Oral	Completed, no results posted	June 2013	Bristol-Myers Squibb
BMS-833923 in combination with cisplatin and capecitabine	Smoothened	Metastatic gastric, gastroesophageal, or esophageal adenocarcinomas	NCT00909402	I	Oral and Intravenous (IV)	Completed, no results posted	June 2013	Bristol-Myers Squibb
LDE255 (Sonidegib) in combination with BKM120 (Buparlisib)	Smoothened (and PI3K)	Advanced solid tumors	NCT01576666	I	Oral	Completed, no results posted	February 2016	Novartis Pharmaceuticals
LEQ-506	Smoothened	Advanced solid tumors	NCT01106508	I	Oral	Completed, no results posted	February 2020	Novartis Pharmaceuticals
Vismodegib in combination with standard chemotherapy	Smoothened	Advanced GC or gastroesophageal junction cancer	NCT00982592	II	Oral and Intravenous (IV)	Completed, has results	January 2016	National Cancer Institute (NCI)
Vismodegib (GDC-0449) with concurrent chemotherapy and bevacizumab as first-line therapy	Smoothened	Metastatic CRC	NCT00636610	II	Oral	Completed, has results	June 2017	Genentech, Inc.
NOTCH pathway inhibitors								
BMS-906024	Pan-Notch	Advanced or metastatic solid tumors	NCT01292655	I	Intravenous (IV)	Completed, no results posted	January 2020	Bristol-Myers Squibb
CB-103	Pan-Notch	Advanced or metastatic solid tumors, including CRC	NCT03422679	I/II	Oral	Recruiting	May 2019	Cellestia Biotech AG
LY3039478 (Crenigacestat)	Pan-Notch	Advanced solid tumors	NCT02836600	I	Oral	Active, not recruiting	December 2019	Eli Lilly and Company
LY3039478 (Crenigacestat) in combination with other anticancer agents	Pan-Notch	Advanced or metastatic solid tumors	NCT02784795	I	Oral and Intravenous (IV)	Completed, no results posted	March 2020	Eli Lilly and Company
LY900009	γ-Secretase	Advanced cancer	NCT01158404	I	Oral	Completed, has results	August 2019	Eli Lilly and Company
MEDI0639	DLL4	Advanced solid tumors	NCT01577745	I	Intravenous (IV)	Completed, has results	May 2017	MedImmune LLC
REGN421 (SAR153192; Enoticumab)	DLL4	Advanced solid malignancies	NCT00871559	I	Intravenous (IV)	Completed, no results posted	March 2014	Regeneron Pharmaceuticals

(Continued)

TABLE 2 | Continued

Drug	Targets	Disease/Condition	NCT Identifier	Phase	Routes of administration	Recruitment status	Last update	Sponsor
RO4929097	γ-Secretase	Recurrent and metastatic CRC	NCT01116687	II	Oral	Completed, has results	May 2014	National Cancer Institute (NCI)
RO4929097 in combination with capecitabine	γ-Secretase	Refractory solid tumors	NCT01158274	I	Oral	Completed, no results posted	November 2014	National Cancer Institute (NCI)
RO4929097 in combination with cediranib maleate	γ-Secretase	Advanced solid tumors including CRC	NCT01131234	I	Oral	Completed, no results posted	December 2014	National Cancer Institute (NCI)
			PI3K/AKT/mTOR pathway inhibitors					
Acetylsalicylic acid (aspirin)	—	CRC stage I-III with mutations in the PI3K signaling pathway	NCT02647099	III	Oral	Recruiting	August 2019	Anna Martling
Acetylsalicylic acid (aspirin)	—	Resected colon cancer with PI3K mutation stage II or III high risk	NCT02945033	III	Oral	Recruiting	October 2019	University Hospital, Rouen
Acetylsalicylic acid (aspirin)	—	Dukes C and high-risk dukes B CRCs	NCT00565708	III	Oral	Recruiting	September 2019	National Cancer Centre, Singapore
Acetylsalicylic acid (aspirin) and metformin	—	Stage I–III CRC patients	NCT03047837	II	Oral	Recruiting	February 2019	Ente Ospedaliero Ospedali Galliera
AZD2014 (Vistusertib)	mTORC1 and mTORC2	RICTOR amplified GC	NCT03061708	II	Oral	Terminated (lack of efficacy)	May 2019	Samsung Medical Center
AZD2014 (Vistusertib)	mTORC1 and mTORC2	TSC1/2 mutated or TSC1/2 null GC	NCT03082833	II	Oral	Terminated (lack of efficacy)	May 2019	Samsung Medical Center
AZD5363 in combination with paclitaxel	AKT	Advanced gastric adenocarcinoma	NCT02451956	II	Oral and Intravenous (IV)	Completed, no results posted	December 2019	Samsung Medical Center
AZD8186 in combination with paclitaxel	PI3K β/δ	Advanced GC	NCT04001569	I/II	Oral and Intravenous (IV)	Recruiting	June 2019	Seoul National University Bundang Hospital
BKM120 (Buparlisib) in combination with LDE255 (Sonidegib)	PI3K and Smoothened	Advanced solid tumors	NCT01576666	I	Oral	Completed, no results posted	February 2016	Novartis Pharmaceuticals
BYL719 (Alpelisib) in combination with AUY922	PI3K	Advanced or metastatic GC	NCT01613950	I	Oral and Intravenous (IV)	Completed, no results posted	February 2020	Novartis Pharmaceuticals
BYL719 (Alpelisib) in combination with LGX818 (Encorafenib) and Cetuximab	BRAF, EGFR and PI3K	in BRAF Mutant Metastatic CRC	NCT01719380	I/II	Oral and Intravenous (IV)	Completed, no results posted	April 2019	Array BioPharma

(Continued)

TABLE 2 | Continued

Drug	Targets	Disease/Condition	NCT Identifier	Phase	Routes of administration	Recruitment status	Last update	Sponsor
Cabozantinib	Multikinases	Refractory metastatic CRC	NCT03542877	II	Oral	Active, not recruiting	April 2019	Academic Thoracic Oncology Medical Investigators Consortium
CB-839 (Telaglenastat) in combination with capecitabine	Glutaminase	Solid tumors and fluoropyrimidine resistant PIK3CA mutant CRC	NCT02861300	I/II	Oral	Recruiting	March 2020	Case Comprehensive Cancer Center
Copanlisib in combination with anti-PD-1 antibody Nivolumab	PI3K	Relapsed/refractory solid tumors, mismatch-repair proficient (MSS) CRC	NCT03711058	I/II	Intravenous (IV)	Recruiting	July 2019	Sidney Kimmel Comprehensive Cancer Center at Johns Hopkins
DS-7423	PI3K and mTOR	Advanced solid malignant tumors	NCT01364844	I	Oral	Completed, no results posted	February 2014	Daiichi Sankyo, Inc.
Ipatasertib (GDC-0068) in combination with oxaliplatin, 5-FU and leucovorin	AKT	Advanced or metastatic GC or gastroesophageal junction cancer	NCT01896531	II	Oral and Intravenous (IV)	Active, not recruiting	February 2020	Genentech, Inc.
MK-2206	AKT	Advanced GC or gastroesophageal junction cancer	NCT01260701	II	Oral	Completed, has results	January 2016	National Cancer Institute (NCI)
MK-2206	AKT	CRC that is metastatic or locally advanced and cannot be removed by surgery	NCT01802320	II	Oral	Completed, has results	September 2019	National Cancer Institute (NCI)
MK-2206 in combination with AZD6244 (Selumetinib)	AKT and MEK	Advanced CRC	NCT01333475	II	Oral	Completed, has results	September 2015	National Cancer Institute (NCI)
Neratinib in combination with Trastuzumab or with Cetuximab	HER2 and EGFR	KRAS/NRAS/BRAF/ PIK3CA wild-type metastatic CRC by HER2 status	NCT03457896	II	Oral	Recruiting	November 2019	NSABP Foundation Inc
Pembrolizumab (MK-3475) combined with **INCB050465** or with Itacitinib (INCB039110)	JAK1 and PI3K-delta	Advanced solid tumors, including CRC	NCT02646748	I	Oral	Active, not recruiting	December 2019	Incyte Corporation

(Continued)

TABLE 2 | Continued

Drug	Targets	Disease/Condition	NCT Identifier	Phase	Routes of administration	Recruitment status	Last update	Sponsor
PX-866 (Sonolisib) in combination with Cetuximab	PIP3	Incurable metastatic CRC	NCT01252628	I/II	Oral	Completed	May 2018	Cascadian Therapeutics Inc.
RAD001 (Everolimus)	TOR serine-threonine kinases	Previously treated unresectable or metastatic esophageal cancer or GC	NCT00985192	II	Oral	Completed, has results	February 2020	Translational Oncology Research International
RAD001 (Everolimus)	TOR serine-threonine kinases	Advanced GC	NCT00519324	II	Oral	Completed, no results posted	November 2015	Novartis Pharmaceuticals
RAD001 (Everolimus) in combination with AV-951(Tivozanib)	TOR serine-threonine kinases and VEGFRs 1, 2, and 3	Gastrointestinal cancer	NCT01058655	I/II	Oral	Completed, has results	April 2017	Dana-Farber Cancer Institute
RAD001 (Everolimus) in combination with Capecitabine and Oxaliplatin	TOR serine-threonine kinases	Advanced GC	NCT01049620	I	Oral and Intravenous (IV)	Completed, no results posted	January 2020	Asan Medical Center
RAD001 (Everolimus) in combination with cisplatin and HDFL (high-dose 5-FU and leucovorin)	TOR serine-threonine kinases	Advanced GC	NCT00632268	II	Oral and Intravenous (IV)	Completed, no results posted	August 2013	National Taiwan University Hospital
SAR245409 (Voxtalisib) in combination with MSC1936369B (pimasertib)	PI3K, MTOR, MEK1 and 2	Advanced or metastatic solid tumors (GC not included)	NCT01390818	I	Oral	Completed, has results	March 2017	EMD Serono
Serabelisib in combination with Canagliflozin	PI3Kα and SGLT2	Advanced solid tumors	NCT04073680	I/II	Oral	Not yet recruiting	February 2020	Petra Pharma
SF1126	PI3K	Solid tumors	NCT00907205	I	Intravenous (IV)	Completed, no results posted	June 2013	Semafore Pharmaceuticals
Trametinib in combination with Trifluridine and Tipiracil Hydrochloride	MEK	Chemotherapy-resistant RAS-mutated (PIK3CA/PTEN-Wild-Type) metastatic CRC	NCT03317119	I	Oral	Recruiting	January 2020	City of Hope Medical Center

GC corresponds to gastric cancer and CRC to colorectal cancer. FOLFOX corresponds to a chemotherapy regimen with folinic acid (leucovorin), fluorouracil (5-FU) and oxaliplatin (Eloxatin) and FOLFIRI corresponds to a chemotherapy regimen with folinic acid (leucovorin), fluorouracil (5-FU) and irinotecan (Camptosar).

study – CanStem303C – a randomized phase III clinical trial done in adult patients with previously treated metastatic CRC evaluated napabucasin in combination with FOLFIRI (Grothey et al., 2017). Napabucasin monotherapy has been reported in a published phase III trial. The CO.23 trial evaluated the efficacy of napabucasin monotherapy versus placebo in metastasized CRC, which failed to demonstrate a significant difference in the napabucasin group survival. However, in a pre-specified biomarker analysis, phosphorylated STAT3 (pSTAT3)-positive patients experienced a significant survival benefit from napabucasin over placebo (Jonker et al., 2018; Sonbol et al., 2019). Another ongoing trial involving STAT3 inhibition is the phase II trial MODULATE (NCT03647839) which specifically aims to study the modulation of the tumor microenvironment using either vascular disrupting agents (BNC105) or STAT3 inhibition (BBI608), in synergy with an immune checkpoint protein (PD1) inhibitor (nivolumab). This trial is recruiting microsatellite stable, refractory CRC cases.

Targeting the Wnt/β-Catenin Signaling Pathway

Wnt/β-catenin signaling pathway is a major regulator of normal intestinal development and its over-activation behaves as a hallmark of CRC, being particularly significant in drug resistance and stemness maintenance of colorectal CSCs (Takebe et al., 2011; Basu et al., 2016). The activation of the Wnt/β-catenin signaling pathway is associated with poor prognosis (Janssen et al., 2006). It results mostly from the accumulation of mutations in the APC tumor suppressor gene, oncogenic KRAS-signaling pathway, β-catenin and p53. Mutations that do not allow the formation of the APC/Axin/GSK3β destruction complex result in the accumulation and nuclear translocation of β-catenin that binds to transcription factors of T cell factor family (TCF4) and activates target genes like c-Myc, cyclinD1 and survivin, some involved in maintaining stemness (Myant et al., 2013; Lee et al., 2015; Zhou et al., 2017). It has been shown that loss of APC in CRC triggered the expression of a Rac1 GTPase via the induced expression of c-Myc, necessary to intestinal stem cell proliferation and CRC initiation (Myant et al., 2013). On the other hand, p53 may affect the outcome of Wnt signaling in CRC development (Voorneveld et al., 2015), having a role in the acquisition of pluripotency during reprogramming (Takahashi and Yamanaka, 2006; Krizhanovsky and Lowe, 2009). The Wnt signaling pathway is also dysregulated in GC (Chiurillo, 2015). However, the involvement and mechanisms are not yet as fully understood as in CRC. A number of studies suggest β-catenin and APC as driver genes, revealing somatic mutations in both genes that might have relevance in GC (Horii et al., 1992; Nakatsuru et al., 1993; Woo et al., 2001; Clements et al., 2002; Zhang and Xue, 2008). Genomic analysis of several gastric primary tumors disclosed that Wnt/β-catenin, together with NF-κB and proliferation/stem cell pathways, were deregulated in more than 70% of the primary tumors. Patient stratification by combinations of these oncogenic pathways revealed to be a great tool for GC clinical behavior assessment (Ooi et al., 2009). Many molecules have been used to target the Wnt/β-catenin in gastrointestinal CSCs (Chiurillo, 2015; Parizadeh et al., 2019; Patel et al., 2019; Yang et al., 2020). Genistein, a soy-derived compound, was tested in a Phase I/II research trial, in combination with FOLFOX or FOLFOX-Bevacizumab, where it was demonstrated to be well tolerated by patients and may have improved efficacy in the treatment of metastatic CRC (Pintova et al., 2019). *In vitro* and *in vivo* studies have shown that Genistein affects mainly Wnt/β-catenin and PI3K/AKT pathways (Su et al., 2003; Kim et al., 2005; Zhang and Chen, 2011; Wang et al., 2012).

Targeting the Hedgehog Signaling Pathway

The dysregulation of Hedgehog (Hh) signaling pathway has been reported as another main cause of CSCs self-renewal and chemoresistance, being associated with poor clinical outcome in patients with GC or CRC (Ma et al., 2005; Varnat et al., 2009; Takebe et al., 2011; Usui et al., 2018). In this pathway, target gene expression is predominantly regulated by the Smoothened (SMO) protein but GLI inhibitors are also used (Rimkus et al., 2016; Didiasova et al., 2018). In GC cells, SMO regulates nuclear translocation of GLI-1 that in turn promotes transcription of target genes, such as CD44 (Yoon et al., 2014). Yoon et al. (2014) showed that in AGS, MKN-45, and NCI-N87 GC cell lines, the Hh pathway inhibition using SMO shRNA or small-molecule inhibitors significantly decreased spheroid formation ability and tumor growth. Vismodegib (GDC-0449), the first Hh pathway inhibitor used in cancer research, is currently undergoing Phase II trials in advanced GC and in metastatic CRC (Gupta et al., 2010; Berlin et al., 2013). Examination of tumor samples revealed that Vismodegib has not increased progression-free or overall survival as a whole, but only in a limited subset of patients with high CD44 expression (Cohen et al., 2013; Yoon et al., 2014). Disappointingly, these treatments with Vismodegib, did not increase progression-free survival in CRC patients (Low and de Sauvage, 2010; McMillan and Matsui, 2012). When the SMO inhibitor AY9944 was used in combination with the GLI-1 inhibitor GANT61, there was an increased response to anti-cancer drugs in tumor organoids and a decreased capacity to form colonies in SW480 and HCT116 CRC cells (Usui et al., 2018). These results indicate that this strategy might be worthwhile in CRC.

Targeting the Notch Signaling Pathway

The Notch signaling pathway is one of the most activated signaling pathways in cancer, namely in GC and CRC, and promotes metastization (Du et al., 2014; Hayakawa et al., 2019). It has a key role in the maintenance and differentiation of CSCs (Quail et al., 2012; Lu et al., 2013; Yang et al., 2020). In GC and CRC, the expression of Notch1 or Jagged1 is associated with poor prognosis (Yeh et al., 2009; Kang et al., 2012; Jackstadt et al., 2019; Kim et al., 2019; Mohamed et al., 2019). In CRC, Notch1 is associated with more aggressive subtypes, recruiting neutrophils to drive metastasis (Jackstadt et al., 2019). Due to the fact that the Notch pathway is related to CSC self-renewal and angiogenesis, targeting this pathway became a potential anti-CSC therapeutic approach (Venkatesh et al., 2018). Strategies

used to inhibit Notch signaling include γ-secretase inhibition (GSI), Notch receptor (e.g., Notch1, Notch2, and Notch3) or ligand (e.g., Jagged1 and Jagged2) antibodies and combination therapy with inhibitors of other pathways. The inhibition of Notch receptors using two GSIs has allowed to disclose the importance of Notch pathway in the growth and survival of GC cells (Brzozowa et al., 2013). Furthermore, GSIs lead to the induction of apoptosis and inhibition of tumor-sphere formation of $CD44^{+}$ gastric CSCs (Barat et al., 2017). However, it is important to mention that GSIs do not only target Notch-related proteins but also proteases involved in numerous cellular processes, which could originate adverse effects *in vivo* (Shih Ie and Wang, 2007; Wang et al., 2010; Brzozowa et al., 2013). Nevertheless, various clinical trials have been performed to evaluate the efficacy of targeting the Notch signaling pathway in GC and CRC (**Table 2**). RO4929097, a selective GSI, showed good anti-tumor activity in preclinical and early trials but it was not good enough for metastatic CRC (Luistro et al., 2009; Strosberg et al., 2012; Tolcher et al., 2012). Combinations of RO4929097 with other drugs in advanced solid tumors, including CRC, were well tolerated and presented some clinical benefit (Sahebjam et al., 2013; LoConte et al., 2015). LY900009 is another GSI tested in advanced cancers, including those of gastrointestinal tract. It is currently in a phase I trial and revealed a safety profile, with the majority of patients experiencing low-grade gastrointestinal adverse effects (Pant et al., 2016). Furthermore, it was demonstrated to have an inhibitory effect on Notch signaling pathway, inducing goblet cell differentiation and increased mucin production, similarly to that observed in rats (Pant et al., 2016). Moreover, MEDI0639 is a monoclonal antibody that specifically binds to DLL4 and prevents its interaction with Notch receptors, thereby inhibiting Notch-mediated signaling and target gene transcription, which may block tumor angiogenesis and eventually tumor cell growth (Ishigami et al., 2013). A phase I study in advanced solid tumors demonstrated that MEDI0639 is well tolerated and preliminary results show evidence of antitumor activity (Falchook et al., 2015).

Targeting the PI3K/AKT/mTOR Signaling Pathway

The PI3K/AKT/mammalian target of rapamycin (mTOR) signaling pathway is typically abnormally activated in many carcinomas (Michl and Downward, 2005; Johnson et al., 2010; Narayanankutty, 2019). It is thought to be crucial in angiogenesis, cell proliferation, metabolism, survival, metastasis and drug resistance (Cantley, 2002; Edinger and Thompson, 2002; Fingar et al., 2004; Al-Batran et al., 2012; Tapia et al., 2014). AKT is commonly overexpressed in tumors and plays an important role in the metabolic reprogramming of cancer (Yap et al., 2011; Iida et al., 2013). Although the PI3K/AKT/mTOR pathway has been extensively studied, there are few studies in CSCs. In GC and CRC, activation of mTOR appears to cause tumor progression and poor patient survival (Lang et al., 2007; Murayama et al., 2009; Xiao et al., 2009; Yu G. et al., 2009; An et al., 2010). Thus, its inhibition seems to be fundamental for GC and CRC therapy. A phase II study using RAD001 (everolimus) in previously treated unresectable or metastatic esophageal cancer or GC was performed over the rational that everolimus may stop tumor growth by blocking some of the fundamental enzymes for cell growth and by blocking angiogenesis. Everolimus was well tolerated by the patients however this study displayed a strong weakness by being single-arm and non-comparative. However, mTOR suppression decreased ALDH1 activity, which is a marker of CSCs in CRC (Xia and Xu, 2015). Growth inhibition, using a dual PI3K/mTOR inhibitor, PF-04691502, was observed *in vitro* and in xenografted CRC tumors (Fang et al., 2013). Another mTOR inhibitor decreased survival and invasion of colorectal CSCs *in vitro*, and suppressed tumor growth *in vivo* (Francipane and Lagasse, 2013). The allosteric AKT inhibitor (MK-2206) led to a decrease in CSCs proliferation, and reduction of the capacity to form colonospheres *in vitro* and to initiate tumor formation *in vivo*. Mice with xenografted tumors showed a significant decrease in tumor progression. Also, MK-2206 significantly inhibited the growth of patient-derived tumorspheres (Malkomes et al., 2016). A phase II study in advanced gastric or gastroesophageal junction cancer has revealed that MK-2206, as second-line therapy, at a dose of 60 mg was well tolerated by patients and showed some modest evidence of activity, however, the overall survival (5.1 months) was lower than the study efficacy endpoint (6.5 months) (Ramanathan et al., 2015). However, there is a Phase II clinical trial with MK-2206, to study patients with previously treated colon or rectal cancer that has spread and cannot be removed by surgery, concluding that in contrast to robust preclinical data, it does not have effect in these tumors (Dasari et al., 2016). MK-2206 was also used in combination with AZD6244 (Selumetinib), a mitogen-activated protein extracellular signal-regulated kinase (MEK)1/2 inhibitor, in a Phase II trial but the level of target inhibition obtained with the maximum non-toxic dose was not the expected (Do et al., 2015). SAR245409 (Voxtalisib) was tested in a Phase I research trial in combination with another MEK inhibitor, MSC1936369B (Pimasertib), in advanced or metastatic solid tumors (Schram et al., 2018). The primary purpose of the study was to determine the maximum tolerated dose of the drug combination. The drug RAD001 (Everolimus) downregulates mTOR. A combination of RAD001, mFOLFOX-6 and Bevacizumab has been shown to be efficacious and safe in metastatic CRC (Weldon Gilcrease et al., 2019). A multicenter phase II study for patients with refractory, metastatic CRC concluded good tolerability and efficacy of Everolimus combined with Tivozanib (an oral VEGF receptor-1, -2, -3 inhibitor) with 50% of the patients having stable disease at 2 months (Wolpin et al., 2013).

DISCUSSION

The identification of CSCs remains a challenging task, particularly in solid tumors like GC and CRC. The use of cell surface markers as a primary tool to identify gastric and colorectal CSCs has disclosed some weaknesses and for that reason the uncovering of more reliable biomarkers must become a priority.

These biomarkers should include the TFs that are required for the maintenance of gastric and colorectal CSCs phenotype, as well as components of the signaling pathways that have key roles in CSC features. This explains why TFs such as STAT3 and signaling pathways like Wnt/β-catenin, Hedgehog, NOTCH and PI3K/AKT/mTOR emerged as powerful targets, whose inactivation or modulation could eliminate gastric and colorectal CSCs. This fact is corroborated by several completed and ongoing clinical trials targeting these potential biomarkers in both tumor types, where some of the molecules have shown promising results. The incapacity to achieve the wanted levels of target inhibition was the major shortcoming of the clinical trials. Yet, the use of higher doses is not possible due to toxicity problems, which led to the development of combinations of drugs targeting different pathways. Furthermore, it is more advisable to measure the outcome of the treatments in terms of CSCs behavior, by assessing capacity to metastasize and re-growth after removing the drug.

FUTURE PERSPECTIVES

The validation of potential gastric and colorectal CSCs biomarkers and their association with GC and CRC stage is imperative to understand patient prognosis and apply a more suitable therapy. The development of a robust therapy combining CSC targets with conventional chemotherapy could be the solution to overcome resistance to anti-cancer drugs and completely eliminate cancer. Considering these issues, it is crucial that future studies further explore the role of TFs and components of signaling pathways on cancer stemness in order to develop therapies that could eradicate CSCs.

AUTHOR CONTRIBUTIONS

All authors listed have made a substantial, direct and intellectual contribution to the work, and approved it for publication.

FUNDING

This work was supported by the FEDER – Fundo Europeu de Desenvolvimento Regional funds through the COMPETE 2020 – Operacional Programme for Competitiveness and Internationalisation (POCI), Portugal 2020, and by Portuguese funds through the FCT – Fundação para a Ciência e a Tecnologia/Ministério da Ciência, Tecnologia e Inovação in the framework of the project "Institute for Research and Innovation in Health Sciences" (POCI-01-0145-FEDER-007274); projects POCI-01-0145-FEDER-029017 and POCI-01-0145-FEDER-016390 funded by FCT. DP acknowledges FCT for financial support through a Ph.D. fellowship (SFRH/BD/146186/2019).

REFERENCES

Abbasian, M., Mousavi, E., Arab-Bafrani, Z., and Sahebkar, A. (2019). The most reliable surface marker for the identification of colorectal cancer stem-like cells: a systematic review and meta-analysis. *J. Cell. Physiol.* 234, 8192–8202. doi: 10.1002/jcp.27619

Abetov, D., Mustapova, Z., Saliev, T., Bulanin, D., Batyrbekov, K., and Gilman, C. P. (2015). Novel small molecule inhibitors of cancer stem cell signaling pathways. *Stem Cell Rev. Rep.* 11, 909–918. doi: 10.1007/s12015-015-9612-x

Akbari, M., Shomali, N., Faraji, A., Shanehbandi, D., Asadi, M., Mokhtarzadeh, A., et al. (2020). CD133: an emerging prognostic factor and therapeutic target in colorectal cancer. *Cell Biol. Int.* 44, 368–380. doi: 10.1002/cbin.11243

Al-Batran, S. E., Ducreux, M., and Ohtsu, A. (2012). mTOR as a therapeutic target in patients with gastric cancer. *Int. J. Cancer* 130, 491–496. doi: 10.1002/ijc.26396

Amini, S., Fathi, F., Mobalegi, J., Sofimajidpour, H., and Ghadimi, T. (2014). The expressions of stem cell markers: Oct4, Nanog, Sox2, nucleostemin, Bmi, Zfx, Tcl1, Tbx3, Dppa4, and Esrrb in bladder, colon, and prostate cancer, and certain cancer cell lines. *Anat. Cell Biol.* 47, 1–11. doi: 10.5115/acb.2014.47.1.1

An, J. Y., Kim, K. M., Choi, M. G., Noh, J. H., Sohn, T. S., Bae, J. M., et al. (2010). Prognostic role of p-mTOR expression in cancer tissues and metastatic lymph nodes in pT2b gastric cancer. *Int. J. Cancer* 126, 2904–2913. doi: 10.1002/ijc.24872

Avilion, A. A., Nicolis, S. K., Pevny, L. H., Perez, L., Vivian, N., and Lovell-Badge, R. (2003). Multipotent cell lineages in early mouse development depend on SOX2 function. *Genes Dev.* 17, 126–140. doi: 10.1101/gad.224503

Badrinath, N., and Yoo, S. Y. (2019). Recent advances in cancer stem cell-targeted immunotherapy. *Cancers* 11:310. doi: 10.3390/cancers11030310

Barat, S., Chen, X., Bui, C. K., Bozko, P., Götze, J., Christgen, M., et al. (2017). Gamma-secretase inhibitor IX (GSI) impairs concomitant activation of notch and wnt-beta-catenin pathways in CD44+ gastric cancer stem cells. *Stem Cells Transl. Med.* 6, 819–829. doi: 10.1002/sctm.16-0335

Basati, G., Mohammadpour, H., and Emami Razavi, A. (2020). Association of high expression levels of SOX2, NANOG, and OCT4 in gastric cancer tumor tissues with progression and poor prognosis. *J. Gastrointest. Cancer* 51, 41–47. doi: 10.1007/s12029-018-00200-x

Bastide, P., Darido, C., Pannequin, J., Kist, R., Robine, S., Marty-Double, C., et al. (2007). Sox9 regulates cell proliferation and is required for Paneth cell differentiation in the intestinal epithelium. *J. Cell Biol.* 178, 635–648. doi: 10.1083/jcb.200704152

Basu, S., Haase, G., and Ben-Ze'ev, A. (2016). Wnt signaling in cancer stem cells and colon cancer metastasis. *F1000Res.* 5:F1000 Faculty Rev-699. doi: 10.12688/f1000research.7579.1

Behrens, J., von Kries, J. P., Kuhl, M., Bruhn, L., Wedlich, D., Grosschedl, R., et al. (1996). Functional interaction of beta-catenin with the transcription factor LEF-1. *Nature* 382, 638–642. doi: 10.1038/382638a0

Bekaii-Saab, T., and El-Rayes, B. (2017). Identifying and targeting cancer stem cells in the treatment of gastric cancer. *Cancer* 123, 1303–1312. doi: 10.1002/cncr.30538

Bendell, J. C., Hubbard, J. M., O'Neil, B. H., Jonker, D. J., Starodub, A., Peyton, J. D., et al. (2017). Phase 1b/II study of cancer stemness inhibitor napabucasin (BBI-608) in combination with FOLFIRI +/- bevacizumab (bev) in metastatic colorectal cancer (mCRC) patients (pts). *J. Clin. Oncol.* 35, 3529–3529. doi: 10.1200/JCO.2017.35.15_suppl.3529

Berlin, J., Bendell, J. C., Hart, L. L., Firdaus, I., Gore, I., Hermann, R. C., et al. (2013). A randomized phase II trial of vismodegib versus placebo with FOLFOX or FOLFIRI and bevacizumab in patients with previously untreated metastatic colorectal cancer. *Clin. Cancer Res.* 19, 258–267. doi: 10.1158/1078-0432.CCR-12-1800

Boesch, M., Spizzo, G., and Seeber, A. (2018). Concise review: aggressive colorectal cancer: role of epithelial cell adhesion molecule in cancer stem cells and epithelial-to-mesenchymal transition. *Stem Cells Transl. Med.* 7, 495–501. doi: 10.1002/sctm.17-0289

Brabletz, T., Jung, A., Spaderna, S., Hlubek, F., and Kirchner, T. (2005). Opinion: migrating cancer stem cells - an integrated concept of malignant tumour progression. *Nat. Rev. Cancer* 5, 744–749. doi: 10.1038/nrc1694

Bray, F., Ferlay, J., Soerjomataram, I., Siegel, R. L., Torre, L. A., and Jemal, A. (2018). Global cancer statistics 2018: GLOBOCAN estimates of incidence and

mortality worldwide for 36 cancers in 185 countries. *CA Cancer J. Clin.* 68, 394–424. doi: 10.3322/caac.21492

Bretones, G., Delgado, M. D., and León, J. (2015). Myc and cell cycle control. *Biochim. Biophys. Acta* 1849, 506–516. doi: 10.1016/j.bbagrm.2014.03.013

Brungs, D., Aghmesheh, M., Vine, K. L., Becker, T. M., Carolan, M. G., and Ranson, M. (2016). Gastric cancer stem cells: evidence, potential markers, and clinical implications. *J. Gastroenterol.* 51, 313–326. doi: 10.1007/s00535-015-1125-5

Brunner, T. B., Kunz-Schughart, L. A., Grosse-Gehling, P., and Baumann, M. (2012). Cancer stem cells as a predictive factor in radiotherapy. *Semin. Radiat. Oncol.* 22, 151–174. doi: 10.1016/j.semradonc.2011.12.003

Brzozowa, M., Mielańczyk, L., Michalski, M., Malinowski, L., Kowalczyk-Ziomek, G., Helewski, K., et al. (2013). Role of Notch signaling pathway in gastric cancer pathogenesis. *Contemp. Oncol.* 17, 1–5. doi: 10.5114/wo.2013.33765

Buczek, M. E., Reeder, S. P., and Regad, T. (2018). "Identification and isolation of cancer stem cells using NANOG-EGFP reporter system," in *Cancer Stem Cells: Methods and Protocols*, eds G. Papaccio and V. Desiderio (New York, NY: Springer), 139–148.

Camilo, V., Barros, R., Celestino, R., Castro, P., Vieira, J., Teixeira, M. R., et al. (2014). Immunohistochemical molecular phenotypes of gastric cancer based on SOX2 and CDX2 predict patient outcome. *BMC Cancer* 14:753. doi: 10.1186/1471-2407-14-753

Cantley, L. C. (2002). The phosphoinositide 3-kinase pathway. *Science* 296, 1655–1657. doi: 10.1126/science.296.5573.1655

Carmon, K. S., Lin, Q., Gong, X., Thomas, A., and Liu, Q. (2012). LGR5 interacts and cointernalizes with Wnt receptors to modulate Wnt/β-catenin signaling. *Mol. Cell. Biol.* 32, 2054–2064.

Carrasco-Garcia, E., Santos, J. C., Garcia, I., Brianti, M., García-Puga, M., Pedrazzoli, J., et al. (2016). Paradoxical role of SOX2 in gastric cancer. *Am. J. Cancer Res.* 6, 701–713.

Chambers, I., Colby, D., Robertson, M., Nichols, J., Lee, S., Tweedie, S., et al. (2003). Functional expression cloning of nanog, a pluripotency sustaining factor in embryonic stem cells. *Cell* 113, 643–655.

Chaudhry, A., Rudra, D., Treuting, P., Samstein, R. M., Liang, Y., Kas, A., et al. (2009). CD4+ regulatory T cells control TH17 responses in a Stat3-dependent manner. *Science* 326, 986–991. doi: 10.1126/science.1172702

Chen, K., Huang, Y.-H., and Chen, J.-L. (2013). Understanding and targeting cancer stem cells: therapeutic implications and challenges. *Acta Pharmacol. Sin.* 34, 732–740. doi: 10.1038/aps.2013.27

Chen, T., Yang, K., Yu, J., Meng, W., Yuan, D., Bi, F., et al. (2012). Identification and expansion of cancer stem cells in tumor tissues and peripheral blood derived from gastric adenocarcinoma patients. *Cell Res.* 22, 248–258. doi: 10.1038/cr.2011.109

Chen, Z., He, X., Jia, M., Liu, Y., Qu, D., Wu, D., et al. (2013). β-catenin overexpression in the nucleus predicts progress disease and unfavourable survival in colorectal cancer: a meta-analysis. *PLoS One* 8:e63854. doi: 10.1371/journal.pone.0063854

Chen, Z., Xu, W. R., Qian, H., Zhu, W., Bu, X. F., Wang, S., et al. (2009). Oct4, a novel marker for human gastric cancer. *J. Surg. Oncol.* 99, 414–419. doi: 10.1002/jso.21270

Chiurillo, M. A. (2015). Role of the Wnt/β-catenin pathway in gastric cancer: an in-depth literature review. *World J. Exp. Med.* 5, 84–102. doi: 10.5493/wjem.v5.i2.84

Cho, Y. G., Song, J. H., Kim, C. J., Nam, S. W., Yoo, N. J., Lee, J. Y., et al. (2007). Genetic and epigenetic analysis of the KLF4 gene in gastric cancer. *APMIS* 115, 802–808. doi: 10.1111/j.1600-0463.2007.apm_643.x

Clements, W. M., Wang, J., Sarnaik, A., Kim, O. J., MacDonald, J., Fenoglio-Preiser, C., et al. (2002). beta-Catenin mutation is a frequent cause of Wnt pathway activation in gastric cancer. *Cancer Res.* 62, 3503–3506.

Cohen, D. J., Christos, P. J., Kindler, H. L., Catenacci, D. V. T., Bekaii-Saab, T. B., Tahiri, S., et al. (2013). Vismodegib (V), a hedgehog (HH) pathway inhibitor, combined with FOLFOX for first-line therapy of patients (pts) with advanced gastric and gastroesophageal junction (GEJ) carcinoma: a New York Cancer Consortium led phase II randomized study. *J. Clin. Oncol.* 31, 4011–4011. doi: 10.1200/jco.2013.31.15_suppl.4011

Cui, J., Shi, M., Quan, M., and Xie, K. (2013). Regulation of EMT by KLF4 in gastrointestinal cancer. *Curr. Cancer Drug Targets* 13, 986–995. doi: 10.2174/15680096113136660104

Dai, X., Ge, J., Wang, X., Qian, X., Zhang, C., and Li, X. (2013). OCT4 regulates epithelial-mesenchymal transition and its knockdown inhibits colorectal cancer cell migration and invasion. *Oncol. Rep.* 29, 155–160. doi: 10.3892/or.2012.2086

Dalerba, P., Cho, R. W., and Clarke, M. F. (2007a). Cancer stem cells: models and concepts. *Annu. Rev. Med.* 58, 267–284. doi: 10.1146/annurev.med.58.062105.204854

Dalerba, P., Dylla, S. J., Park, I.-K., Liu, R., Wang, X., Cho, R. W., et al. (2007b). Phenotypic characterization of human colorectal cancer stem cells. *Proc. Natl. Acad. Sci. U.S.A.* 104, 10158–10163. doi: 10.1073/pnas.0703478104

Dang, C. V. (2013). MYC, metabolism, cell growth, and tumorigenesis. *Cold Spring Harb. Perspect. Med.* 3:a014217. doi: 10.1101/cshperspect.a014217

Darido, C., Buchert, M., Pannequin, J., Bastide, P., Zalzali, H., Mantamadiotis, T., et al. (2008). Defective claudin-7 regulation by Tcf-4 and Sox-9 disrupts the polarity and increases the tumorigenicity of colorectal cancer cells. *Cancer Res.* 68, 4258–4268.

Dasari, A., Overman, M. J., Fogelman, D. R., Kee, B. K., Menter, D., Raghav, K. P. S., et al. (2016). A phase II and co-clinical study of an AKT inhibitor in patients (pts) with biomarker-enriched, previously treated metastatic colorectal cancer (mCRC). *J. Clin. Oncol.* 34, 3563–3563. doi: 10.1200/JCO.2016.34.15_suppl.3563

de Sousa e Melo, F., Kurtova, A. V., Harnoss, J. M., Kljavin, N., Hoeck, J. D., Hung, J., et al. (2017). A distinct role for Lgr5+ stem cells in primary and metastatic colon cancer. *Nature* 543, 676–680. doi: 10.1038/nature21713

de Souza, C. R. T., Leal, M. F., Calcagno, D. Q., Costa Sozinho, E. K., Borges, B. D. N., Montenegro, R. C., et al. (2013). MYC deregulation in gastric cancer and its clinicopathological implications. *PLoS One* 8:e64420. doi: 10.1371/journal.pone.0064420

Dean, M., Fojo, T., and Bates, S. (2005). Tumour stem cells and drug resistance. *Nat. Rev. Cancer* 5, 275–284. doi: 10.1038/nrc1590

Deng, J., Liang, H., Zhang, R., Sun, D., Pan, Y., Liu, Y., et al. (2013). STAT3 is associated with lymph node metastasis in gastric cancer. *Tumour Biol.* 34, 2791–2800. doi: 10.1007/s13277-013-0837-5

Deng, J.-Y., Sun, D., Liu, X.-Y., Pan, Y., and Liang, H. (2010). STAT-3 correlates with lymph node metastasis and cell survival in gastric cancer. *World J. Gastroenterol.* 16, 5380–5387. doi: 10.3748/wjg.v16.i42.5380

Deng, Y., Zhou, J., Fang, L., Cai, Y., Ke, J., Xie, X., et al. (2014). ALDH1 is an independent prognostic factor for patients with stages II-III rectal cancer after receiving radiochemotherapy. *Br. J. Cancer* 110, 430–434. doi: 10.1038/bjc.2013.767

Didiasova, M., Schaefer, L., and Wygrecka, M. (2018). Targeting GLI transcription factors in cancer. *Molecules* 23:1003. doi: 10.3390/molecules23051003

Dienstmann, R., Vermeulen, L., Guinney, J., Kopetz, S., Tejpar, S., and Tabernero, J. (2017). Consensus molecular subtypes and the evolution of precision medicine in colorectal cancer. *Nat. Rev. Cancer* 17, 79–92. doi: 10.1038/nrc.2016.126

Do, K., Speranza, G., Bishop, R., Khin, S., Rubinstein, L., Kinders, R. J., et al. (2015). Biomarker-driven phase 2 study of MK-2206 and selumetinib (AZD6244, ARRY-142886) in patients with colorectal cancer. *Invest. New Drugs* 33, 720–728. doi: 10.1007/s10637-015-0212-z

Dong, H., Liu, H., Zhou, W., Zhang, F., Li, C., Chen, J., et al. (2019). GLI1 activation by non-classical pathway integrin α(v)β(3)/ERK1/2 maintains stem cell-like phenotype of multicellular aggregates in gastric cancer peritoneal metastasis. *Cell Death Dis.* 10, 574–574. doi: 10.1038/s41419-019-1776-x

Du, L., Wang, H., He, L., Zhang, J., Ni, B., Wang, X., et al. (2008). CD44 is of functional importance for colorectal cancer stem cells. *Clin. Cancer Res.* 14, 6751–6760. doi: 10.1158/1078-0432.CCR-08-1034

Du, X., Cheng, Z., Wang, Y.-H., Guo, Z.-H., Zhang, S.-Q., Hu, J.-K., et al. (2014). Role of Notch signaling pathway in gastric cancer: a meta-analysis of the literature. *World J. Gastroenterol.* 20, 9191–9199. doi: 10.3748/wjg.v20.i27.9191

Edinger, A. L., and Thompson, C. B. (2002). Akt maintains cell size and survival by increasing mTOR-dependent nutrient uptake. *Mol. Biol. Cell* 13, 2276–2288.

Espersen, M. L., Olsen, J., Linnemann, D., Hogdall, E., and Troelsen, J. T. (2015). Clinical implications of intestinal stem cell markers in colorectal cancer. *Clin. Colorectal Cancer* 14, 63–71. doi: 10.1016/j.clcc.2014.12.004

Falchook, G. S., Dowlati, A., Naing, A., Gribbin, M. J., Jenkins, D. W., Chang, L. L., et al. (2015). Phase I study of MEDI0639 in patients with advanced solid tumors. *J. Clin. Oncol.* 33, 3024–3024. doi: 10.1200/jco.2015.33.15_suppl.3024

Fang, D. D., Zhang, C. C., Gu, Y., Jani, J. P., Cao, J., Tsaparikos, K., et al. (2013). Antitumor efficacy of the dual PI3K/mTOR inhibitor PF-04691502 in a Human Xenograft tumor model derived from colorectal cancer stem cells harboring a PIK3CA mutation. *PLoS One* 8:e67258. doi: 10.1371/journal.pone.0067258

Farkona, S., Diamandis, E. P., and Blasutig, I. M. (2016). Cancer immunotherapy: the beginning of the end of cancer? *BMC Med.* 14:73. doi: 10.1186/s12916-016-0623-5

Fingar, D. C., Richardson, C. J., Tee, A. R., Cheatham, L., Tsou, C., and Blenis, J. (2004). mTOR controls cell cycle progression through its cell growth effectors S6K1 and 4E-BP1/eukaryotic translation initiation factor 4E. *Mol. Cell. Biol.* 24, 200–216. doi: 10.1128/mcb.24.1.200-216.2004

Forghanifard, M. M., Moghbeli, M., Raeisossadati, R., Tavassoli, A., Mallak, A. J., Boroumand-Noughabi, S., et al. (2013). Role of SALL4 in the progression and metastasis of colorectal cancer. *J. Biomed. Sci.* 20:6. doi: 10.1186/1423-0127-20-6

Francipane, M. G., and Lagasse, E. (2013). Selective targeting of human colon cancer stem-like cells by the mTOR inhibitor Torin-1. *Oncotarget* 4, 1948–1962. doi: 10.18632/oncotarget.1310

Fujita, T., Chiwaki, F., Takahashi, R. U., Aoyagi, K., Yanagihara, K., Nishimura, T., et al. (2015). Identification and characterization of CXCR4-positive gastric cancer stem cells. *PLoS One* 10:e0130808. doi: 10.1371/journal.pone.0130808

Fukamachi, H., Seol, H. S., Shimada, S., Funasaka, C., Baba, K., Kim, J. H., et al. (2013). CD49f(high) cells retain sphere-forming and tumor-initiating activities in human gastric tumors. *PLoS One* 8:e72438. doi: 10.1371/journal.pone.0072438

Fukamachi, H., Shimada, S., Ito, K., Ito, Y., and Yuasa, Y. (2011). CD133 is a marker of gland-forming cells in gastric tumors and Sox17 is involved in its regulation. *Cancer Sci.* 102, 1313–1321. doi: 10.1111/j.1349-7006.2011.01947.x

Ghanei, Z., Jamshidizad, A., Joupari, M. D., and Shamsara, M. (2020). Isolation and characterization of breast cancer stem cell-like phenotype by Oct4 promoter-mediated activity. *J. Cell. Physiol.* doi: 10.1002/jcp.29437 [Epub ahead of print].

Gidekel, S., Pizov, G., Bergman, Y., and Pikarsky, E. (2003). Oct-3/4 is a dose-dependent oncogenic fate determinant. *Cancer Cell* 4, 361–370.

Gong, X., Azhdarinia, A., Ghosh, S. C., Xiong, W., An, Z., Liu, Q., et al. (2016). LGR5-targeted antibody–drug conjugate eradicates gastrointestinal tumors and prevents recurrence. *Mol. Cancer Ther.* 15, 1580–1590. doi: 10.1158/1535-7163.MCT-16-0114

Goossens-Beumer, I. J., Zeestraten, E. C., Benard, A., Christen, T., Reimers, M. S., Keijzer, R., et al. (2014). Clinical prognostic value of combined analysis of Aldh1, Survivin, and EpCAM expression in colorectal cancer. *Br. J. Cancer* 110, 2935–2944. doi: 10.1038/bjc.2014.226

Grivennikov, S. I., and Karin, M. (2010). Dangerous liaisons: STAT3 and NF-kappaB collaboration and crosstalk in cancer. *Cytokine Growth Factor Rev.* 21, 11–19. doi: 10.1016/j.cytogfr.2009.11.005

Grothey, A., Shah, M. A., Yoshino, T., Cutsem, E. V., Taieb, J., Xu, R., et al. (2017). CanStem303C trial: a phase III study of napabucasin (BBI-608) in combination with 5-fluorouracil (5-FU), leucovorin, irinotecan (FOLFIRI) in adult patients with previously treated metastatic colorectal cancer (mCRC). *J. Clin. Oncol.* 35, TS3619–TS3619. doi: 10.1200/JCO.2017.35.15_suppl.TPS3619

Gullo, I., Carneiro, F., Oliveira, C., and Almeida, G. M. (2018). Heterogeneity in gastric cancer: from pure morphology to molecular classifications. *Pathobiology* 85, 50–63. doi: 10.1159/000473881

Gupta, P. B., Onder, T. T., Jiang, G., Tao, K., Kuperwasser, C., Weinberg, R. A., et al. (2009). Identification of selective inhibitors of cancer stem cells by high-throughput screening. *Cell* 138, 645–659. doi: 10.1016/j.cell.2009.06.034

Gupta, S., Takebe, N., and Lorusso, P. (2010). Targeting the Hedgehog pathway in cancer. *Ther. Adv. Med. Oncol.* 2, 237–250. doi: 10.1177/1758834010366430

Hadjimichael, C., Chanoumidou, K., Papadopoulou, N., Arampatzi, P., Papamatheakis, J., and Kretsovali, A. (2015). Common stemness regulators of embryonic and cancer stem cells. *World J. Stem Cells* 7, 1150–1184. doi: 10.4252/wjsc.v7.i9.1150

Hajimoradi, M., Mohammad Hassan, Z., Ebrahimi, M., Soleimani, M., Bakhshi, M., Firouzi, J., et al. (2016). STAT3 is overactivated in gastric cancer stem-like cells. *Cell J.* 17, 617–628. doi: 10.22074/cellj.2016.3834

Han, M.-E., Jeon, T.-Y., Hwang, S.-H., Lee, Y.-S., Kim, H.-J., Shim, H.-E., et al. (2011). Cancer spheres from gastric cancer patients provide an ideal model system for cancer stem cell research. *Cell. Mol. Life Sci.* 68:3589. doi: 10.1007/s00018-011-0672-z

Han, S., Kim, H. Y., Park, K., Cho, H. J., Lee, M. S., Kim, H. J., et al. (1999). c-Myc expression is related with cell proliferation and associated with poor clinical outcome in human gastric cancer. *J. Korean Med. Sci.* 14, 526–530. doi: 10.3346/jkms.1999.14.5.526

Han, S.-M., Han, S.-H., Coh, Y.-R., Jang, G., Chan Ra, J., Kang, S.-K., et al. (2014). Enhanced proliferation and differentiation of Oct4- and Sox2-overexpressing human adipose tissue mesenchymal stem cells. *Exp. Mol. Med.* 46:e101. doi: 10.1038/emm.2014.28

Haraguchi, N., Ishii, H., Mimori, K., Ohta, K., Uemura, M., Nishimura, J., et al. (2013). CD49f-positive cell population efficiently enriches colon cancer-initiating cells. *Int. J. Oncol.* 43, 425–430. doi: 10.3892/ijo.2013.1955

Hashimoto, I., Nagata, T., Sekine, S., Moriyama, M., Shibuya, K., Hojo, S., et al. (2017). Prognostic significance of KLF4 expression in gastric cancer. *Oncol. Lett.* 13, 819–826. doi: 10.3892/ol.2016.5499

Hashimoto, K., Aoyagi, K., Isobe, T., Kouhuji, K., and Shirouzu, K. (2014). Expression of CD133 in the cytoplasm is associated with cancer progression and poor prognosis in gastric cancer. *Gastric Cancer* 17, 97–106. doi: 10.1007/s10120-013-0255-9

Hayakawa, Y., Tsuboi, M., Asfaha, S., Kinoshita, H., Niikura, R., Konishi, M., et al. (2019). BHLHA15-positive secretory precursor cells can give rise to tumors in intestine and colon in mice. *Gastroenterology* 156, 1066.e–1081.e. doi: 10.1053/j.gastro.2018.11.024

Horii, A., Nakatsuru, S., Miyoshi, Y., Ichii, S., Nagase, H., Kato, Y., et al. (1992). The APC gene, responsible for familial adenomatous polyposis, is mutated in human gastric cancer. *Cancer Res.* 52, 3231–3233.

Horst, D., Kriegl, L., Engel, J., Kirchner, T., and Jung, A. (2009). Prognostic significance of the cancer stem cell markers CD133, CD44, and CD166 in colorectal cancer. *Cancer Invest.* 27, 844–850. doi: 10.1080/07357900902744502

Hsu, L.-S., Chan, C.-P., Chen, C.-J., Lin, S.-H., Lai, M.-T., Hsu, J.-D., et al. (2013). Decreased Kruppel-like factor 4 (KLF4) expression may correlate with poor survival in gastric adenocarcinoma. *Med. Oncol.* 30:632. doi: 10.1007/s12032-013-0632-6

Huang, E. H., Hynes, M. J., Zhang, T., Ginestier, C., Dontu, G., Appelman, H., et al. (2009). Aldehyde dehydrogenase 1 is a marker for normal and malignant human colonic stem cells (SC) and tracks SC overpopulation during colon tumorigenesis. *Cancer Res.* 69, 3382–3389. doi: 10.1158/0008-5472.CAN-08-4418

Huang, R., Wang, G., Song, Y., Tang, Q., You, Q., Liu, Z., et al. (2015). Colorectal cancer stem cell and chemoresistant colorectal cancer cell phenotypes and increased sensitivity to Notch pathway inhibitor. *Mol. Med. Rep.* 12, 2417–2424. doi: 10.3892/mmr.2015.3694

Huang, W. S., Wang, J. P., Wang, T., Fang, J. Y., Lan, P., and Ma, J. P. (2007). ShRNA-mediated gene silencing of beta-catenin inhibits growth of human colon cancer cells. *World J. Gastroenterol.* 13, 6581–6587. doi: 10.3748/wjg.v13.i48.6581

Huch, M., and Clevers, H. (2011). Sox9 marks adult organ progenitors. *Nat. Genet.* 43, 9–10. doi: 10.1038/ng0111-9

Hütz, K., Mejías-Luque, R., Farsakova, K., Ogris, M., Krebs, S., Anton, M., et al. (2013). The stem cell factor SOX2 regulates the tumorigenic potential in human gastric cancer cells. *Carcinogenesis* 35, 942–950. doi: 10.1093/carcin/bgt410

Ibrahim, E. E., Babaei-Jadidi, R., Saadeddin, A., Spencer-Dene, B., Hossaini, S., Abuzinadah, M., et al. (2012). Embryonic NANOG activity defines colorectal cancer stem cells and modulates through AP1- and TCF-dependent mechanisms. *Stem Cells* 30, 2076–2087. doi: 10.1002/stem.1182

Iida, M., Brand, T. M., Campbell, D. A., Starr, M. M., Luthar, N., Traynor, A. M., et al. (2013). Targeting AKT with the allosteric AKT inhibitor MK-2206 in non-small cell lung cancer cells with acquired resistance to cetuximab. *Cancer Biol. Ther.* 14, 481–491. doi: 10.4161/cbt.24342

Iseghohi, S. O. (2016). Cancer stem cells may contribute to the difficulty in treating cancer. *Genes Dis.* 3, 7–10. doi: 10.1016/j.gendis.2016.01.001

Ishigami, S., Arigami, T., Uenosono, Y., Okumura, H., Kurahara, H., Uchikado, Y., et al. (2013). Clinical implications of DLL4 expression in gastric cancer. *J. Exp. Clin. Cancer Res.* 32:46. doi: 10.1186/1756-9966-32-46

Ishimoto, T., Sawayama, H., Sugihara, H., and Baba, H. (2014). Interaction between gastric cancer stem cells and the tumor microenvironment. *J. Gastroenterol.* 49, 1111–1120. doi: 10.1007/s00535-014-0952-0

Iv Santaliz-Ruiz, L. E., Xie, X., Old, M., Teknos, T. N., and Pan, Q. (2014). Emerging role of nanog in tumorigenesis and cancer stem cells. *Int. J. Cancer* 135, 2741–2748. doi: 10.1002/ijc.28690

Jackstadt, R., van Hooff, S. R., Leach, J. D., Cortes-Lavaud, X., Lohuis, J. O., Ridgway, R. A., et al. (2019). Epithelial NOTCH signaling rewires the tumor microenvironment of colorectal cancer to drive poor-prognosis subtypes and metastasis. *Cancer Cell* 36, 319.e–336.e. doi: 10.1016/j.ccell.2019.08.003

Janssen, K. P., Alberici, P., Fsihi, H., Gaspar, C., Breukel, C., Franken, P., et al. (2006). APC and oncogenic KRAS are synergistic in enhancing Wnt signaling in intestinal tumor formation and progression. *Gastroenterology* 131, 1096–1109. doi: 10.1053/j.gastro.2006.08.011

Javier, B. M., Yaeger, R., Wang, L., Sanchez-Vega, F., Zehir, A., Middha, S., et al. (2016). Recurrent, truncating SOX9 mutations are associated with SOX9 overexpression, KRAS mutation, and TP53 wild type status in colorectal carcinoma. *Oncotarget* 7, 50875–50882. doi: 10.18632/oncotarget.9682

Ji, K., Zhang, M., Chu, Q., Gan, Y., Ren, H., Zhang, L., et al. (2016). The role of p-STAT3 as a prognostic and clinicopathological marker in colorectal cancer: a systematic review and meta-analysis. *PLoS One* 11:e0160125. doi: 10.1371/journal.pone.0160125

Jiang, J., Zhang, Y., Chuai, S., Wang, Z., Zheng, D., Xu, F., et al. (2012). Trastuzumab (herceptin) targets gastric cancer stem cells characterized by CD90 phenotype. *Oncogene* 31, 671–682. doi: 10.1038/onc.2011.282

Jiang, R., Niu, X., Huang, Y., and Wang, X. (2016). β-Catenin is important for cancer stem cell generation and tumorigenic activity in nasopharyngeal carcinoma. *Acta Biochim. Biophys. Sin.* 48, 229–237. doi: 10.1093/abbs/gmv134

Jiang, Y., He, Y., Li, H., Li, H. N., Zhang, L., Hu, W., et al. (2012). Expressions of putative cancer stem cell markers ABCB1, ABCG2, and CD133 are correlated with the degree of differentiation of gastric cancer. *Gastric Cancer* 15, 440–450. doi: 10.1007/s10120-012-0140-y

Jiang, Y., Li, W., He, X., Zhang, H., Jiang, F., and Chen, Z. (2016). Lgr5 expression is a valuable prognostic factor for colorectal cancer: evidence from a meta-analysis. *BMC Cancer* 16:12. doi: 10.1186/s12885-015-1985-3

Jiang, Y. X., Yang, S. W., Li, P. A., Luo, X., Li, Z. Y., Hao, Y. X., et al. (2017). The promotion of the transformation of quiescent gastric cancer stem cells by IL-17 and the underlying mechanisms. *Oncogene* 36, 1256–1264. doi: 10.1038/onc.2016.291

Jo, A., Denduluri, S., Zhang, B., Wang, Z., Yin, L., Yan, Z., et al. (2014). The versatile functions of Sox9 in development, stem cells, and human diseases. *Genes Dis.* 1, 149–161. doi: 10.1016/j.gendis.2014.09.004

Johnson, S. M., Gulhati, P., Rampy, B. A., Han, Y., Rychahou, P. G., Doan, H. Q., et al. (2010). Novel expression patterns of PI3K/Akt/mTOR signaling pathway components in colorectal cancer. *J. Am. Coll. Surg.* 210, 767–776, 776–778. doi: 10.1016/j.jamcollsurg.2009.12.008

Jonker, D. J., Nott, L., Yoshino, T., Gill, S., Shapiro, J., Ohtsu, A., et al. (2018). Napabucasin versus placebo in refractory advanced colorectal cancer: a randomised phase 3 trial. *Lancet Gastroenterol. Hepatol.* 3, 263–270. doi: 10.1016/S2468-1253(18)30009-8

Kahlert, C., Gaitzsch, E., Steinert, G., Mogler, C., Herpel, E., Hoffmeister, M., et al. (2012). Expression analysis of aldehyde dehydrogenase 1A1 (ALDH1A1) in colon and rectal cancer in association with prognosis and response to chemotherapy. *Ann. Surg. Oncol.* 19, 4193–4201. doi: 10.1245/s10434-012-2518-9

Kang, H., An, H. J., Song, J. Y., Kim, T. H., Heo, J. H., Ahn, D. H., et al. (2012). Notch3 and Jagged2 contribute to gastric cancer development and to glandular differentiation associated with MUC2 and MUC5AC expression. *Histopathology* 61, 576–586. doi: 10.1111/j.1365-2559.2012.04274.x

Kannarkatt, J., Joseph, J., Kurniali, P. C., Al-Janadi, A., and Hrinczenko, B. (2017). Adjuvant chemotherapy for stage II colon cancer: a clinical dilemma. *J. Oncol. Pract.* 13, 233–241. doi: 10.1200/jop.2016.017210

Kanwar, S. S., Yu, Y., Nautiyal, J., Patel, B. B., and Majumdar, A. P. (2010). The Wnt/beta-catenin pathway regulates growth and maintenance of colonospheres. *Mol. Cancer* 9:212. doi: 10.1186/1476-4598-9-212

Kemper, K., Prasetyanti, P. R., De Lau, W., Rodermond, H., Clevers, H., and Medema, J. P. (2012). Monoclonal antibodies against Lgr5 identify human colorectal cancer stem cells. *Stem Cells* 30, 2378–2386. doi: 10.1002/stem.1233

Kim, D.-Y., Cha, S.-T., Ahn, D.-H., Kang, H.-Y., Kwon, C.-I., Ko, K.-H., et al. (2009). STAT3 expression in gastric cancer indicates a poor prognosis. *J. Gastroenterol. Hepatol.* 24, 646–651. doi: 10.1111/j.1440-1746.2008.05671.x

Kim, E. J., Shin, H.-K., and Park, J. H. Y. (2005). Genistein inhibits insulin-like growth factor-I receptor signaling in HT-29 human colon cancer cells: a possible mechanism of the growth inhibitory effect of Genistein. *J. Med. Food* 8, 431–438. doi: 10.1089/jmf.2005.8.431

Kim, H. B., Lim, H. J., Lee, H. J., Park, J. H., and Park, S. G. (2019). Evaluation and clinical significance of Jagged-1-activated notch signaling by APEX1 in colorectal cancer. *Anticancer Res.* 39, 6097–6105. doi: 10.21873/anticanres.13817

Kim, Y., Joo, K. M., Jin, J., and Nam, D.-H. (2009). Cancer stem cells and their mechanism of chemo-radiation resistance. *Int. J. Stem Cells* 2, 109–114. doi: 10.15283/ijsc.2009.2.2.109

Kodama, H., Murata, S., Ishida, M., Yamamoto, H., Yamaguchi, T., Kaida, S., et al. (2017). Prognostic impact of CD44-positive cancer stem-like cells at the invasive front of gastric cancer. *Br. J. Cancer* 116, 186–194. doi: 10.1038/bjc.2016.401

Kolligs, F. T., Bommer, G., and Goke, B. (2002). Wnt/beta-catenin/tcf signaling: a critical pathway in gastrointestinal tumorigenesis. *Digestion* 66, 131–144. doi: 10.1159/000066755

Krizhanovsky, V., and Lowe, S. W. (2009). Stem cells: the promises and perils of p53. *Nature* 460, 1085–1086. doi: 10.1038/4601085a

Kuipers, E. J., Grady, W. M., Lieberman, D., Seufferlein, T., Sung, J. J., Boelens, P. G., et al. (2015). Colorectal cancer. *Nat. Rev. Dis. Primers* 1:15065. doi: 10.1038/nrdp.2015.65

Labianca, R., Nordlinger, B., Beretta, G. D., Mosconi, S., Mandalà, M., Cervantes, A., et al. (2013). Early colon cancer: ESMO clinical practice guidelines for diagnosis, treatment and follow-up. *Ann. Oncol.* 24(Suppl. 6), vi64–vi72. doi: 10.1093/annonc/mdt354

Lang, S. A., Gaumann, A., Koehl, G. E., Seidel, U., Bataille, F., Klein, D., et al. (2007). Mammalian target of rapamycin is activated in human gastric cancer and serves as a target for therapy in an experimental model. *Int. J. Cancer* 120, 1803–1810. doi: 10.1002/ijc.22442

Lau, E. Y.-T., Ho, N. P.-Y., and Lee, T. K.-W. (2017). Cancer stem cells and their microenvironment: biology and therapeutic implications. *Stem Cells Int.* 2017:3714190. doi: 10.1155/2017/3714190

Lee, H. H., Seo, K. J., An, C. H., Kim, J. S., and Jeon, H. M. (2012). CD133 expression is correlated with chemoresistance and early recurrence of gastric cancer. *J. Surg. Oncol.* 106, 999–1004. doi: 10.1002/jso.23178

Lee, K. S., Kwak, Y., Nam, K. H., Kim, D. W., Kang, S. B., Choe, G., et al. (2015). c-MYC copy-number gain is an independent prognostic factor in patients with colorectal cancer. *PLoS One* 10:e0139727. doi: 10.1371/journal.pone.0139727

Leng, Z., Tao, K., Xia, Q., Tan, J., Yue, Z., Chen, J., et al. (2013). Kruppel-like factor 4 acts as an oncogene in colon cancer stem cell-enriched spheroid cells. *PLoS One* 8:e56082. doi: 10.1371/journal.pone.0056082

Leng, Z., Xia, Q., Chen, J., Li, Y., Xu, J., Zhao, E., et al. (2018). Lgr5+CD44+EpCAM+ strictly defines cancer stem cells in human colorectal cancer. *Cell. Physiol. Biochem.* 46, 860–872. doi: 10.1159/000488743

Li, M. X., Wang, Q., Wang, B., Yan, D. W., Tang, H. M., Peng, Z. H., et al. (2012). [Association between gut-enriched Kruppel-like factor and prognosis of patients with gastric cancer]. *Zhonghua Wei Chang Wai Ke Za Zhi* 15, 732–735.

Li, W., Zhou, Y., Yang, J., Zhang, X., Zhang, H., Zhang, T., et al. (2015). Gastric cancer-derived mesenchymal stem cells prompt gastric cancer progression through secretion of interleukin-8. *J. Exp. Clin. Cancer Res.* 34:52. doi: 10.1186/s13046-015-0172-3

Li, Y., Rogoff, H. A., Keates, S., Gao, Y., Murikipudi, S., Mikule, K., et al. (2015). Suppression of cancer relapse and metastasis by inhibiting cancer stemness. *Proc. Natl. Acad. Sci. U.S.A.* 112, 1839–1844. doi: 10.1073/pnas.1424171112

Lin, L., Liu, A., Peng, Z., Lin, H. J., Li, P. K., Li, C., et al. (2011). STAT3 is necessary for proliferation and survival in colon cancer-initiating cells. *Cancer Res.* 71, 7226–7237. doi: 10.1158/0008-5472.CAN-10-4660

Lin, Q., Lai, R., Chirieac, L. R., Li, C., Thomazy, V. A., Grammatikakis, I., et al. (2005). Constitutive activation of JAK3/STAT3 in colon carcinoma tumors and cell lines: inhibition of JAK3/STAT3 signaling induces apoptosis and cell cycle arrest of colon carcinoma cells. *Am. J. Pathol.* 167, 969–980. doi: 10.1016/s0002-9440(10)61187-x

Lin, T., Ding, Y.-Q., and Li, J.-M. (2012). Overexpression of Nanog protein is associated with poor prognosis in gastric adenocarcinoma. *Med. Oncol.* 29, 878–885. doi: 10.1007/s12032-011-9860-9

Liu, L., Ning, X., Sun, L., Zhang, H., Shi, Y., Guo, C., et al. (2008). Hypoxia-inducible factor-1 alpha contributes to hypoxia-induced chemoresistance in gastric cancer. *Cancer Sci.* 99, 121–128. doi: 10.1111/j.1349-7006.2007.00643.x

Lochhead, P., and El-Omar, E. M. (2008). Gastric cancer. *Br. Med. Bull.* 85, 87–100. doi: 10.1093/bmb/ldn007

LoConte, N. K., Razak, A. R. A., Ivy, P., Tevaarwerk, A., Leverence, R., Kolesar, J., et al. (2015). A multicenter phase 1 study of γ -secretase inhibitor RO4929097 in combination with capecitabine in refractory solid tumors. *Invest. New Drugs* 33, 169–176. doi: 10.1007/s10637-014-0166-6

Loh, Y.-H., Wu, Q., Chew, J.-L., Vega, V. B., Zhang, W., Chen, X., et al. (2006). The Oct4 and Nanog transcription network regulates pluripotency in mouse embryonic stem cells. *Nat. Genet.* 38, 431–440. doi: 10.1038/ng1760

Low, J. A., and de Sauvage, F. J. (2010). Clinical experience with Hedgehog pathway inhibitors. *J. Clin. Oncol.* 28, 5321–5326. doi: 10.1200/jco.2010.27.9943

Lu, B., Fang, Y., Xu, J., Wang, L., Xu, F., Xu, E., et al. (2008). Analysis of SOX9 expression in colorectal cancer. *Am. J. Clin. Pathol.* 130, 897–904. doi: 10.1309/ajcpw1w8gjbqgcni

Lu, J., Ye, X., Fan, F., Xia, L., Bhattacharya, R., Bellister, S., et al. (2013). Endothelial cells promote the colorectal cancer stem cell phenotype through a soluble form of Jagged-1. *Cancer Cell* 23, 171–185. doi: 10.1016/j.ccr.2012.12.021

Lugli, A., Iezzi, G., Hostettler, I., Muraro, M. G., Mele, V., Tornillo, L., et al. (2010). Prognostic impact of the expression of putative cancer stem cell markers CD133, CD166, CD44s, EpCAM, and ALDH1 in colorectal cancer. *Br. J. Cancer* 103, 382–390. doi: 10.1038/sj.bjc.6605762

Luistro, L., He, W., Smith, M., Packman, K., Vilenchik, M., Carvajal, D., et al. (2009). Preclinical profile of a potent γ-secretase inhibitor targeting notch signaling with *in vivo* efficacy and pharmacodynamic properties. *Cancer Res.* 69, 7672–7680. doi: 10.1158/0008-5472.Can-09-1843

Lundberg, I. V., Edin, S., Eklof, V., Oberg, A., Palmqvist, R., and Wikberg, M. L. (2016). SOX2 expression is associated with a cancer stem cell state and down-regulation of CDX2 in colorectal cancer. *BMC Cancer* 16:471. doi: 10.1186/s12885-016-2509-5

Lundberg, I. V., Lofgren Burstrom, A., Edin, S., Eklof, V., Oberg, A., Stenling, R., et al. (2014). SOX2 expression is regulated by BRAF and contributes to poor patient prognosis in colorectal cancer. *PLoS One* 9:e101957. doi: 10.1371/journal.pone.0101957

Ma, X., Chen, K., Huang, S., Zhang, X., Adegboyega, P. A., Evers, B. M., et al. (2005). Frequent activation of the hedgehog pathway in advanced gastric adenocarcinomas. *Carcinogenesis* 26, 1698–1705. doi: 10.1093/carcin/bgi130

Ma, Y., Cui, W., Yang, J., Qu, J., Di, C., Amin, H. M., et al. (2006). SALL4, a novel oncogene, is constitutively expressed in human acute myeloid leukemia (AML) and induces AML in transgenic mice. *Blood* 108, 2726–2735.

Magee, J. A., Piskounova, E., and Morrison, S. J. (2012). Cancer stem cells: impact, heterogeneity, and uncertainty. *Cancer Cell* 21, 283–296. doi: 10.1016/j.ccr.2012.03.003

Malkomes, P., Lunger, I., Luetticke, A., Oppermann, E., Haetscher, N., Serve, H., et al. (2016). Selective AKT inhibition by MK-2206 represses colorectal cancer-initiating stem cells. *Ann. Surg. Oncol.* 23, 2849–2857. doi: 10.1245/s10434-016-5218-z

Mao, J., Fan, S., Ma, W., Fan, P., Wang, B., Zhang, J., et al. (2014). Roles of Wnt/β-catenin signaling in the gastric cancer stem cells proliferation and salinomycin treatment. *Cell Death Dis.* 5:e1039. doi: 10.1038/cddis.2013.515

Marjanovic, N. D., Weinberg, R. A., and Chaffer, C. L. (2013). Cell plasticity and heterogeneity in cancer. *Clin. Chem.* 59, 168–179. doi: 10.1373/clinchem.2012.184655

Matheu, A., Collado, M., Wise, C., Manterola, L., Cekaite, L., Tye, A. J., et al. (2012). Oncogenicity of the developmental transcription factor Sox9. *Cancer Res.* 72, 1301–1315. doi: 10.1158/0008-5472.CAN-11-3660

Mattiuzzi, C., Sanchis-Gomar, F., and Lippi, G. (2019). Concise update on colorectal cancer epidemiology. *Ann. Transl. Med.* 7:609. doi: 10.21037/atm.2019.07.91

Mazumdar, J., O'Brien, W. T., Johnson, R. S., LaManna, J. C., Chavez, J. C., Klein, P. S., et al. (2010). O_2 regulates stem cells through Wnt/β-catenin signalling. *Nat. Cell Biol.* 12, 1007–1013. doi: 10.1038/ncb2102

McMillan, R., and Matsui, W. (2012). Molecular pathways: the hedgehog signaling pathway in cancer. *Clin. Cancer Res.* 18, 4883–4888.

Menon, S., Shin, S., and Dy, G. (2016). Advances in cancer immunotherapy in solid tumors. *Cancers* 8:E106. doi: 10.3390/cancers8120106

Mesquita, P., Freire, A. F., Lopes, N., Gomes, R., Azevedo, D., Barros, R., et al. (2019). Expression and clinical relevance of SOX9 in gastric cancer. *Dis. Markers* 2019:8267021. doi: 10.1155/2019/8267021

Michl, P., and Downward, J. (2005). Mechanisms of disease: PI3K/AKT signaling in gastrointestinal cancers. *Z. Gastroenterol.* 43, 1133–1139.

Miyoshi, N., Fujino, S., Ohue, M., Yasui, M., Takahashi, Y., Sugimura, K., et al. (2018). The POU5F1 gene expression in colorectal cancer: a novel prognostic marker. *Surg. Today* 48, 709–715. doi: 10.1007/s00595-018-1644-9

Miyoshi, N., Ishii, H., Nagai, K., Hoshino, H., Mimori, K., Tanaka, F., et al. (2010). Defined factors induce reprogramming of gastrointestinal cancer cells. *Proc. Natl. Acad. Sci. U.S.A.* 107, 40–45. doi: 10.1073/pnas.0912407107

Mohamed, S. Y., Kaf, R. M., Ahmed, M. M., Elwan, A., Ashour, H. R., and Ibrahim, A. (2019). The prognostic value of cancer stem cell markers (Notch1, ALDH1, and CD44) in primary colorectal carcinoma. *J. Gastrointest. Cancer* 50, 824–837. doi: 10.1007/s12029-018-0156-6

Müller, S., Cañeque, T., Acevedo, V., and Rodriguez, R. (2017). Targeting cancer stem cells with small molecules. *Isr. J. Chem.* 57, 239–250. doi: 10.1002/ijch.201600109

Munro, M. J., Wickremesekera, S. K., Peng, L., Tan, S. T., and Itinteang, T. (2018). Cancer stem cells in colorectal cancer: a review. *J. Clin. Pathol.* 71, 110–116. doi: 10.1136/jclinpath-2017-204739

Murayama, T., Inokuchi, M., Takagi, Y., Yamada, H., Kojima, K., Kumagai, J., et al. (2009). Relation between outcomes and localisation of p-mTOR expression in gastric cancer. *Br. J. Cancer* 100, 782–788. doi: 10.1038/sj.bjc.6604915

Muzny, D. M., Bainbridge, M. N., Chang, K., Dinh, H. H., Drummond, J. A., Fowler, G., et al. (2012). Comprehensive molecular characterization of human colon and rectal cancer. *Nature* 487, 330–337. doi: 10.1038/nature11252

Myant, K. B., Cammareri, P., McGhee, E. J., Ridgway, R. A., Huels, D. J., Cordero, J. B., et al. (2013). ROS production and NF-κB activation triggered by RAC1 facilitate WNT-driven intestinal stem cell proliferation and colorectal cancer initiation. *Cell Stem Cell* 12, 761–773. doi: 10.1016/j.stem.2013.04.006

Nakatsuru, S., Yanagisawa, A., Furukawa, Y., Ichii, S., Kato, Y., Nakamura, Y., et al. (1993). Somatic mutations of the APC gene in precancerous lesion of the stomach. *Hum. Mol. Genet.* 2, 1463–1465. doi: 10.1093/hmg/2.9.1463

Narayanankutty, A. (2019). PI3K/ Akt/ mTOR pathway as a therapeutic target for colorectal cancer: a review of preclinical and clinical evidence. *Curr. Drug Targets* 20, 1217–1226. doi: 10.2174/1389450120666190618123846

Neri, B., Pantaleo, P., Giommoni, E., Grifoni, R., Paoletti, C., Rotella, V., et al. (2007). Oxaliplatin, 5-fluorouracil/leucovorin and epirubicin as first-line treatment in advanced gastric carcinoma: a phase II study. *Br. J. Cancer* 96, 1043–1046. doi: 10.1038/sj.bjc.6603644

Niedzwiecki, D., Bertagnolli, M. M., Warren, R. S., Compton, C. C., Kemeny, N. E., Benson, A. B., et al. (2011). Documenting the natural history of patients with resected stage II adenocarcinoma of the colon after random assignment to adjuvant treatment with edrecolomab or observation: results from CALGB 9581. *J. Clin. Oncol.* 29, 3146–3152. doi: 10.1200/jco.2010.32.5357

Nosrati, A., Naghshvar, F., and Khanari, S. (2014). Cancer stem cell markers CD44, CD133 in primary gastric adenocarcinoma. *Int. J. Mol. Cell. Med.* 3, 279–286.

O'Brien, C. A., Pollett, A., Gallinger, S., and Dick, J. E. (2007). A human colon cancer cell capable of initiating tumour growth in immunodeficient mice. *Nature* 445, 106–110. doi: 10.1038/nature05372

Ohkuma, M., Haraguchi, N., Ishii, H., Mimori, K., Tanaka, F., Kim, H. M., et al. (2012). Absence of CD71 transferrin receptor characterizes human gastric adenosquamous carcinoma stem cells. *Ann. Surg. Oncol.* 19, 1357–1364. doi: 10.1245/s10434-011-1739-7

Ong, C. W., Kim, L. G., Kong, H. H., Low, L. Y., Iacopetta, B., Soong, R., et al. (2010). CD133 expression predicts for non-response to chemotherapy in colorectal cancer. *Mod. Pathol.* 23, 450–457. doi: 10.1038/modpathol.2009.181

Ooi, C. H., Ivanova, T., Wu, J., Lee, M., Tan, I. B., Tao, J., et al. (2009). Oncogenic pathway combinations predict clinical prognosis in gastric cancer. *PLoS Genet.* 5:e1000676. doi: 10.1371/journal.pgen.1000676

Pádua, D., Barros, R., Amaral, A. L., Mesquita, P., Freire, A. F., Sousa, M., et al. (2020). A SOX2 reporter system identifies gastric cancer stem-like cells sensitive to monensin. *Cancers* 12:495. doi: 10.3390/cancers12020495

Pant, S., Jones, S. F., Kurkjian, C. D., Infante, J. R., Moore, K. N., Burris, H. A., et al. (2016). A first-in-human phase I study of the oral Notch inhibitor, LY900009, in patients with advanced cancer. *Eur. J. Cancer* 56, 1–9. doi: 10.1016/j.ejca.2015.11.021

Parizadeh, S. M., Jafarzadeh-Esfehani, R., Hassanian, S. M., Parizadeh, S. M. R., Vojdani, S., Ghandehari, M., et al. (2019). Targeting cancer stem cells as therapeutic approach in the treatment of colorectal cancer. *Int. J. Biochem. Cell Biol.* 110, 75–83. doi: 10.1016/j.biocel.2019.02.010

Park, J. H., Chung, S., Matsuo, Y., and Nakamura, Y. (2017). Development of small molecular compounds targeting cancer stem cells. *Medchemcomm* 8, 73–80. doi: 10.1039/c6md00385k

Patel, S., Alam, A., Pant, R., and Chattopadhyay, S. (2019). Wnt signaling and its significance within the tumor microenvironment: novel therapeutic insights. *Front. Immunol.* 10:2872. doi: 10.3389/fimmu.2019.02872

Pattabiraman, D. R., and Weinberg, R. A. (2014). Tackling the cancer stem cells - what challenges do they pose? *Nat. Rev. Drug Discov.* 13, 497–512. doi: 10.1038/nrd4253

Phi, L. T. H., Sari, I. N., Yang, Y.-G., Lee, S.-H., Jun, N., Kim, K. S., et al. (2018). Cancer Stem Cells (CSCs) in drug resistance and their therapeutic implications in cancer treatment. *Stem Cells Int.* 2018:5416923. doi: 10.1155/2018/5416923

Pintova, S., Dharmupari, S., Moshier, E., Zubizarreta, N., Ang, C., and Holcombe, R. F. (2019). Genistein combined with FOLFOX or FOLFOX–Bevacizumab for the treatment of metastatic colorectal cancer: phase I/II pilot study. *Cancer Chemother. Pharmacol.* 84, 591–598. doi: 10.1007/s00280-019-03886-3

Prévostel, C., and Blache, P. (2017). The dose-dependent effect of SOX9 and its incidence in colorectal cancer. *Eur. J. Cancer* 86, 150–157. doi: 10.1016/j.ejca.2017.08.037

Quail, D. F., Taylor, M. J., and Postovit, L. M. (2012). Microenvironmental regulation of cancer stem cell phenotypes. *Curr. Stem Cell Res. Ther.* 7, 197–216. doi: 10.2174/157488812799859838

Quante, M., Varga, J., Wang, T. C., and Greten, F. R. (2013). The gastrointestinal tumor microenvironment. *Gastroenterology* 145, 63–78. doi: 10.1053/j.gastro.2013.03.052

Ramanathan, R. K., McDonough, S. L., Kennecke, H. F., Iqbal, S., Baranda, J. C., Seery, T. E., et al. (2015). Phase 2 study of MK-2206, an allosteric inhibitor of AKT, as second-line therapy for advanced gastric and gastroesophageal junction cancer: a SWOG cooperative group trial (S1005). *Cancer* 121, 2193–2197. doi: 10.1002/cncr.29363

Rassouli, F. B., Matin, M. M., and Saeinasab, M. (2016). Cancer stem cells in human digestive tract malignancies. *Tumor Biol.* 37, 7–21. doi: 10.1007/s13277-015-4155-y

Rezalotfi, A., Ahmadian, E., Aazami, H., Solgi, G., and Ebrahimi, M. (2019). Gastric cancer stem cells effect on Th17/Treg Balance; a bench to beside perspective. *Front. Oncol.* 9:226. doi: 10.3389/fonc.2019.00226

Ricci-Vitiani, L., Lombardi, D. G., Pilozzi, E., Biffoni, M., Todaro, M., Peschle, C., et al. (2007). Identification and expansion of human colon-cancer-initiating cells. *Nature* 445, 111–115. doi: 10.1038/nature05384

Riley, R. S., June, C. H., Langer, R., and Mitchell, M. J. (2019). Delivery technologies for cancer immunotherapy. *Nat. Rev. Drug Discov.* 18, 175–196. doi: 10.1038/s41573-018-0006-z

Rimkus, T. K., Carpenter, R. L., Qasem, S., Chan, M., and Lo, H. W. (2016). Targeting the sonic hedgehog signaling pathway: review of smoothened and GLI inhibitors. *Cancers* 8:22. doi: 10.3390/cancers8020022

Robertson, J. H., Yang, S. Y., Winslet, M. C., and Seifalian, A. M. (2009). Functional blocking of specific integrins inhibit colonic cancer migration. *Clin. Exp. Metastasis* 26, 769–780. doi: 10.1007/s10585-009-9276-5

Rocco, A., Liguori, E., Pirozzi, G., Tirino, V., Compare, D., Franco, R., et al. (2012). CD133 and CD44 cell surface markers do not identify cancer stem cells in primary human gastric tumors. *J. Cell. Physiol.* 227, 2686–2693. doi: 10.1002/jcp.23013

Sahebjam, S., Bedard, P. L., Castonguay, V., Chen, Z., Reedijk, M., Liu, G., et al. (2013). A phase I study of the combination of ro4929097 and cediranib in patients with advanced solid tumours (PJC-004/NCI 8503). *Br. J. Cancer* 109, 943–949. doi: 10.1038/bjc.2013.380

Santos, J. C., Carrasco-Garcia, E., Garcia-Puga, M., Aldaz, P., Montes, M., Fernandez-Reyes, M., et al. (2016). SOX9 elevation acts with canonical WNT signaling to drive gastric cancer progression. *Cancer Res.* 76, 6735–6746. doi: 10.1158/0008-5472.CAN-16-1120

Sarkar, A., and Hochedlinger, K. (2013). The sox family of transcription factors: versatile regulators of stem and progenitor cell fate. *Cell Stem Cell* 12, 15–30. doi: 10.1016/j.stem.2012.12.007

Saygin, C., Samour, M., Chumakova, A., Jarrar, A., Lathia, J. D., and Reizes, O. (2016). "Reporter systems to study cancer stem cells," in *Stem Cell Heterogeneity: Methods and Protocols*, ed. K. Turksen (New York, NY: Springer), 319–333.

Schram, A. M., Gandhi, L., Mita, M. M., Damstrup, L., Campana, F., Hidalgo, M., et al. (2018). A phase Ib dose-escalation and expansion study of the oral MEK inhibitor pimasertib and PI3K/MTOR inhibitor voxtalisib in patients with advanced solid tumours. *Br. J. Cancer* 119, 1471–1476. doi: 10.1038/s41416-018-0322-4

Shapiro, G., Bedard, P., Infante, J., Bauer, T., Prawira, A., Laksin, O., et al. (2016). Phase 1 results of PTC596, a novel small molecule targeting cancer stem cells (CSCs) by reducing levels of BMI1 protein. *Eur. J. Cancer* 69, S148.

Shie, J. L., Chen, Z. Y., O'Brien, M. J., Pestell, R. G., Lee, M. E., and Tseng, C. C. (2000). Role of gut-enriched Kruppel-like factor in colonic cell growth and differentiation. *Am. J. Physiol. Gastrointest. Liver Physiol.* 279, G806–G814. doi: 10.1152/ajpgi.2000.279.4.G806

Shih Ie, M., and Wang, T. L. (2007). Notch signaling, gamma-secretase inhibitors, and cancer therapy. *Cancer Res.* 67, 1879–1882.

Smyth, E. C., Verheij, M., Allum, W., Cunningham, D., Cervantes, A., Arnold, D., et al. (2016). Gastric cancer: ESMO Clinical Practice Guidelines for diagnosis, treatment and follow-up†. *Ann. Oncol.* 27(Suppl._5), v38–v49. doi: 10.1093/annonc/mdw350

Sonbol, M. B., Ahn, D. H., and Bekaii-Saab, T. (2019). Therapeutic targeting strategies of cancer stem cells in gastrointestinal malignancies. *Biomedicines* 7:17. doi: 10.3390/biomedicines7010017

Song, Z., Wu, Y., Yang, J., Yang, D., and Fang, X. (2017). Progress in the treatment of advanced gastric cancer. *Tumor Biol.* 39:1010428317714626. doi: 10.1177/1010428317714626

Strosberg, J. R., Yeatman, T., Weber, J., Coppola, D., Schell, M. J., Han, G., et al. (2012). A phase II study of RO4929097 in metastatic colorectal cancer. *Eur. J. Cancer* 48, 997–1003. doi: 10.1016/j.ejca.2012.02.056

Su, S.-J., Chow, N.-H., Kung, M.-L., Hung, T.-C., and Chang, K.-L. (2003). Effects of soy isoflavones on apoptosis induction and G2-M arrest in human hepatoma cells involvement of caspase-3 activation, Bcl-2 and Bcl-XL downregulation, and Cdc2 kinase activity. *Nutr. Cancer* 45, 113–123. doi: 10.1207/S15327914NC4501_13

Sun, M., Uozaki, H., Hino, R., Kunita, A., Shinozaki, A., Ushiku, T., et al. (2012). SOX9 expression and its methylation status in gastric cancer. *Virchows Arch.* 460, 271–279. doi: 10.1007/s00428-012-1201-7

Tai, M.-H., Chang, C.-C., Olson, L. K., and Trosko, J. E. (2005). Oct4 expression in adult human stem cells: evidence in support of the stem cell theory of carcinogenesis. *Carcinogenesis* 26, 495–502. doi: 10.1093/carcin/bgh321

Takahashi, K., and Yamanaka, S. (2006). Induction of pluripotent stem cells from mouse embryonic and adult fibroblast cultures by defined factors. *Cell* 126, 663–676. doi: 10.1016/j.cell.2006.07.024

Takaishi, S., Okumura, T., Tu, S., Wang, S. S. W., Shibata, W., Vigneshwaran, R., et al. (2009). Identification of gastric cancer stem cells using the cell surface marker CD44. *Stem Cells* 27, 1006–1020. doi: 10.1002/stem.30

Takebe, N., Harris, P. J., Warren, R. Q., and Ivy, S. P. (2011). Targeting cancer stem cells by inhibiting Wnt, Notch, and Hedgehog pathways. *Nat. Rev. Clin. Oncol.* 8, 97–106. doi: 10.1038/nrclinonc.2010.196

Takeda, K., Mizushima, T., Yokoyama, Y., Hirose, H., Wu, X., Qian, Y., et al. (2018). Sox2 is associated with cancer stem-like properties in colorectal cancer. *Sci. Rep.* 8:17639.

Tang, B., Raviv, A., Esposito, D., Flanders, K. C., Daniel, C., Nghiem, B. T., et al. (2015). A flexible reporter system for direct observation and isolation of cancer stem cells. *Stem Cell Rep.* 4, 155–169. doi: 10.1016/j.stemcr.2014.11.002

Tapia, O., Riquelme, I., Leal, P., Sandoval, A., Aedo, S., Weber, H., et al. (2014). The PI3K/AKT/mTOR pathway is activated in gastric cancer with potential prognostic and predictive significance. *Virchows Arch.* 465, 25–33. doi: 10.1007/s00428-014-1588-4

Tian, T., Zhang, Y., Wang, S., Zhou, J., and Xu, S. (2012). Sox2 enhances the tumorigenicity and chemoresistance of cancer stem-like cells derived from gastric cancer. *J. Biomed. Res.* 26, 336–345. doi: 10.7555/JBR.26.20120045

Todaro, M., Francipane, M. G., Medema, J. P., and Stassi, G. (2010). Colon cancer stem cells: promise of targeted therapy. *Gastroenterology* 138, 2151–2162. doi: 10.1053/j.gastro.2009.12.063

Tolcher, A. W., Messersmith, W. A., Mikulski, S. M., Papadopoulos, K. P., Kwak, E. L., Gibbon, D. G., et al. (2012). Phase I Study of RO4929097, a gamma

secretase inhibitor of notch signaling, in patients with refractory metastatic or locally advanced solid tumors. *J. Clin. Oncol.* 30, 2348–2353. doi: 10.1200/jco.2011.36.8282

Usui, T., Sakurai, M., Umata, K., Elbadawy, M., Ohama, T., Yamawaki, H., et al. (2018). Hedgehog signals mediate anti-cancer drug resistance in three-dimensional primary colorectal cancer organoid culture. *Int. J. Mol. Sci.* 19:1098. doi: 10.3390/ijms19041098

Vadde, R., Vemula, S., Jinka, R., Merchant, N., Bramhachari, P. V., and Nagaraju, G. P. (2017). Role of hypoxia-inducible factors (HIF) in the maintenance of stemness and malignancy of colorectal cancer. *Crit. Rev. Oncol. Hematol.* 113, 22–27. doi: 10.1016/j.critrevonc.2017.02.025

Vaiopoulos, A. G., Kostakis, I. D., Koutsilieris, M., and Papavassiliou, A. G. (2012). Colorectal cancer stem cells. *Stem Cells* 30, 363–371. doi: 10.1002/stem.1031

van der Heijden, M., and Vermeulen, L. (2019). Stem cells in homeostasis and cancer of the gut. *Mol. Cancer* 18:66. doi: 10.1186/s12943-019-0962-x

Varnat, F., Duquet, A., Malerba, M., Zbinden, M., Mas, C., Gervaz, P., et al. (2009). Human colon cancer epithelial cells harbour active HEDGEHOG-GLI signalling that is essential for tumour growth, recurrence, metastasis and stem cell survival and expansion. *EMBO Mol. Med.* 1, 338–351. doi: 10.1002/emmm.200900039

Venkatesh, V., Nataraj, R., Thangaraj, G. S., Karthikeyan, M., Gnanasekaran, A., Kaginelli, S. B., et al. (2018). Targeting Notch signalling pathway of cancer stem cells. *Stem Cell Investig.* 5:5. doi: 10.21037/sci.2018.02.02

Vermeulen, L., De Sousa, E., Melo, F., van der Heijden, M., Cameron, K., de Jong, J. H., et al. (2010). Wnt activity defines colon cancer stem cells and is regulated by the microenvironment. *Nat. Cell Biol.* 12, 468–476. doi: 10.1038/ncb2048

Vermeulen, L., Todaro, M., de Sousa Mello, F., Sprick, M. R., Kemper, K., Perez Alea, M., et al. (2008). Single-cell cloning of colon cancer stem cells reveals a multi-lineage differentiation capacity. *Proc. Natl. Acad. Sci. U.S.A.* 105, 13427–13432. doi: 10.1073/pnas.0805706105

Voorneveld, P. W., Kodach, L. L., Jacobs, R. J., van Noesel, C. J., Peppelenbosch, M. P., Korkmaz, K. S., et al. (2015). The BMP pathway either enhances or inhibits the Wnt pathway depending on the SMAD4 and p53 status in CRC. *Br. J. Cancer* 112, 122–130. doi: 10.1038/bjc.2014.560

Wahab, S. M. R., Islam, F., Gopalan, V., and Lam, A. K. (2017). The identifications and clinical implications of cancer stem cells in colorectal cancer. *Clin. Colorectal Cancer* 16, 93–102. doi: 10.1016/j.clcc.2017.01.011

Wakamatsu, Y., Sakamoto, N., Oo, H. Z., Naito, Y., Uraoka, N., Anami, K., et al. (2012). Expression of cancer stem cell markers ALDH1, CD44 and CD133 in primary tumor and lymph node metastasis of gastric cancer. *Pathol. Int.* 62, 112–119. doi: 10.1111/j.1440-1827.2011.02760.x

Wang, H., Li, Q., and Chen, H. (2012). Genistein affects histone modifications on Dickkopf-Related Protein 1 (DKK1) gene in SW480 human colon cancer cell line. *PLoS One* 7:e40955. doi: 10.1371/journal.pone.0040955

Wang, W., Deng, J., Wang, Q., Yao, Q., Chen, W., Tan, Y., et al. (2017). Synergistic role of Cul1 and c-Myc: prognostic and predictive biomarkers in colorectal cancer. *Oncol. Rep.* 38, 245–252. doi: 10.3892/or.2017.5671

Wang, X., Liu, Y., Shao, D., Qian, Z., Dong, Z., Sun, Y., et al. (2016). Recurrent amplification of MYC and TNFRSF11B in 8q24 is associated with poor survival in patients with gastric cancer. *Gastric Cancer* 19, 116–127. doi: 10.1007/s10120-015-0467-2

Wang, Z., Li, Y., Ahmad, A., Azmi, A. S., Banerjee, S., Kong, D., et al. (2010). Targeting Notch signaling pathway to overcome drug resistance for cancer therapy. *Biochim. Biophys. Acta* 1806, 258–267. doi: 10.1016/j.bbcan.2010.06.001

Wei, D., Kanai, M., Huang, S., and Xie, K. (2006). Emerging role of KLF4 in human gastrointestinal cancer. *Carcinogenesis* 27, 23–31. doi: 10.1093/carcin/bgi243

Weldon Gilcrease, G., Stenehjem, D. D., Wade, M. L., Weis, J., McGregor, K., Whisenant, J., et al. (2019). Phase I/II study of everolimus combined with mFOLFOX-6 and bevacizumab for first–line treatment of metastatic colorectal cancer. *Invest. New Drugs* 37, 482–489. doi: 10.1007/s10637-018-0645-2

West, N. R., McCuaig, S., Franchini, F., and Powrie, F. (2015). Emerging cytokine networks in colorectal cancer. *Nat. Rev. Immunol.* 15, 615–629. doi: 10.1038/nri3896

Wolpin, B. M., Ng, K., Zhu, A. X., Abrams, T., Enzinger, P. C., McCleary, N. J., et al. (2013). Multicenter phase II study of tivozanib (AV-951) and everolimus (RAD001) for patients with refractory, metastatic colorectal cancer. *Oncologist* 18, 377–378. doi: 10.1634/theoncologist.2012-0378

Woo, D. K., Kim, H. S., Lee, H. S., Kang, Y. H., Yang, H. K., and Kim, W. H. (2001). Altered expression and mutation of beta-catenin gene in gastric carcinomas and cell lines. *Int. J. Cancer* 95, 108–113.

Wuebben, E. L., and Rizzino, A. (2017). The dark side of SOX2: cancer - a comprehensive overview. *Oncotarget* 8, 44917–44943. doi: 10.18632/oncotarget.16570

Xia, P., and Xu, X. Y. (2015). PI3K/Akt/mTOR signaling pathway in cancer stem cells: from basic research to clinical application. *Am. J. Cancer Res.* 5, 1602–1609.

Xiao, L., Wang, Y. C., Li, W. S., and Du, Y. (2009). The role of mTOR and phospho-p70S6K in pathogenesis and progression of gastric carcinomas: an immunohistochemical study on tissue microarray. *J. Exp. Clin. Cancer Res.* 28:152. doi: 10.1186/1756-9966-28-152

Yang, J., Chai, L., Fowles, T. C., Alipio, Z., Xu, D., Fink, L. M., et al. (2008). Genome-wide analysis reveals Sall4 to be a major regulator of pluripotency in murine-embryonic stem cells. *Proc. Natl. Acad. Sci. U.S.A.* 105, 19756–19761. doi: 10.1073/pnas.0809321105

Yang, L., Shi, P., Zhao, G., Xu, J., Peng, W., Zhang, J., et al. (2020). Targeting cancer stem cell pathways for cancer therapy. *Signal Transduct. Target. Ther.* 5:8. doi: 10.1038/s41392-020-0110-5

Yang, Z., Zhang, C., Qi, W., Cui, Y., and Xuan, Y. (2018). GLI1 promotes cancer stemness through intracellular signaling pathway PI3K/Akt/NFkappaB in colorectal adenocarcinoma. *Exp. Cell Res.* 373, 145–154. doi: 10.1016/j.yexcr.2018.10.006

Yang, Z. H., Dang, Y. Q., and Ji, G. (2019). Role of epigenetics in transformation of inflammation into colorectal cancer. *World J. Gastroenterol.* 25, 2863–2877. doi: 10.3748/wjg.v25.i23.2863

Yao, Y., Zhou, D., Shi, D., Zhang, H., Zhan, S., Shao, X., et al. (2019). GLI1 overexpression promotes gastric cancer cell proliferation and migration and induces drug resistance by combining with the AKT-mTOR pathway. *Biomed. Pharmacother.* 111, 993–1004. doi: 10.1016/j.biopha.2019.01.018

Yap, T. A., Yan, L., Patnaik, A., Fearen, I., Olmos, D., Papadopoulos, K., et al. (2011). First-in-man clinical trial of the oral pan-AKT inhibitor MK-2206 in patients with advanced solid tumors. *J. Clin. Oncol.* 29, 4688–4695. doi: 10.1200/jco.2011.35.5263

Yeh, T. S., Wu, C. W., Hsu, K. W., Liao, W. J., Yang, M. C., Li, A. F., et al. (2009). The activated Notch1 signal pathway is associated with gastric cancer progression through cyclooxygenase-2. *Cancer Res.* 69, 5039–5048. doi: 10.1158/0008-5472.CAN-08-4021

Yeung, T. M., Gandhi, S. C., and Bodmer, W. F. (2011). Hypoxia and lineage specification of cell line-derived colorectal cancer stem cells. *Proc. Natl. Acad. Sci. U.S.A.* 108, 4382–4387. doi: 10.1073/pnas.1014519107

Yoon, C., Park, D. J., Schmidt, B., Thomas, N. J., Lee, H.-J., Kim, T. S., et al. (2014). CD44 expression denotes a subpopulation of gastric cancer cells in which hedgehog signaling promotes chemotherapy resistance. *Clin. Cancer Res.* 20, 3974–3988. doi: 10.1158/1078-0432.CCR-14-0011

Young, R. A. (2011). Control of the embryonic stem cell state. *Cell* 144, 940–954. doi: 10.1016/j.cell.2011.01.032

Yu, G., Wang, J., Chen, Y., Wang, X., Pan, J., Li, G., et al. (2009). Overexpression of phosphorylated mammalian target of rapamycin predicts lymph node metastasis and prognosis of chinese patients with gastric cancer. *Clin. Cancer Res.* 15, 1821–1829. doi: 10.1158/1078-0432.CCR-08-2138

Yu, H., Kortylewski, M., and Pardoll, D. (2007). Crosstalk between cancer and immune cells: role of STAT3 in the tumour microenvironment. *Nat. Rev. Immunol.* 7, 41–51. doi: 10.1038/nri1995

Yu, H., Pardoll, D., and Jove, R. (2009). STATs in cancer inflammation and immunity: a leading role for STAT3. *Nat. Rev. Cancer* 9, 798–809. doi: 10.1038/nrc2734

Yuan, X., Zhang, X., Zhang, W., Liang, W., Zhang, P., Shi, H., et al. (2016). SALL4 promotes gastric cancer progression through activating CD44 expression. *Oncogenesis* 5:e268. doi: 10.1038/oncsis.2016.69

Zhang, C., Li, C., He, F., Cai, Y., and Yang, H. (2011). Identification of CD44+CD24+ gastric cancer stem cells. *J. Cancer Res. Clin. Oncol.* 137, 1679–1686. doi: 10.1007/s00432-011-1038-5

Zhang, H., and Xue, Y. (2008). Wnt pathway is involved in advanced gastric carcinoma. *Hepatogastroenterology* 55, 1126–1130.

Zhang, H. L., Wang, P., Lu, M. Z., Zhang, S. D., and Zheng, L. (2019). c-Myc maintains the self-renewal and chemoresistance properties of colon cancer stem cells. *Oncol. Lett.* 17, 4487–4493. doi: 10.3892/ol.2019.10081

Zhang, J., Espinoza, L. A., Kinders, R. J., Lawrence, S. M., Pfister, T. D., Zhou, M., et al. (2013). NANOG modulates stemness in human colorectal cancer. *Oncogene* 32, 4397–4405. doi: 10.1038/onc.2012.461

Zhang, J., Tam, W. L., Tong, G. Q., Wu, Q., Chan, H. Y., Soh, B. S., et al. (2006). Sall4 modulates embryonic stem cell pluripotency and early embryonic development by the transcriptional regulation of Pou5f1. *Nat. Cell Biol.* 8, 1114–1123. doi: 10.1038/ncb1481

Zhang, L., Xu, Z., Xu, X., Zhang, B., Wu, H., Wang, M., et al. (2014). SALL4, a novel marker for human gastric carcinogenesis and metastasis. *Oncogene* 33, 5491–5500. doi: 10.1038/onc.2013.495

Zhang, N., Zhang, J., Wang, Z. W., Zha, L., and Huang, Z. (2012). Altered expression of Krüppel-like factor 4 and β-catenin in human gastric cancer. *Oncol. Lett.* 3, 1017–1022. doi: 10.3892/ol.2012.619

Zhang, S. S., Huang, Z. W., Li, L. X., Fu, J. J., and Xiao, B. (2016). Identification of CD200+ colorectal cancer stem cells and their gene expression profile. *Oncol. Rep.* 36, 2252–2260. doi: 10.3892/or.2016.5039

Zhang, X., Hua, R., Wang, X., Huang, M., Gan, L., Wu, Z., et al. (2016). Identification of stem-like cells and clinical significance of candidate stem cell markers in gastric cancer. *Oncotarget* 7, 9815–9831. doi: 10.18632/oncotarget.6890

Zhang, Y., Jin, Z., Zhou, H., Ou, X., Xu, Y., Li, H., et al. (2016). Suppression of prostate cancer progression by cancer cell stemness inhibitor napabucasin. *Cancer Med.* 5, 1251–1258. doi: 10.1002/cam4.675

Zhang, X., Hu, F., Li, G., Li, G., Yang, X., Liu, L., et al. (2018a). Human colorectal cancer-derived mesenchymal stem cells promote colorectal cancer progression through IL-6/JAK2/STAT3 signaling. *Cell Death Dis.* 9:25. doi: 10.1038/s41419-017-0176-3

Zhang, X., Yuan, X., Zhu, W., Qian, H., and Xu, W. (2015). SALL4: an emerging cancer biomarker and target. *Cancer Lett.* 357, 55–62. doi: 10.1016/j.canlet.2014.11.037

Zhang, X., Zhang, P., Shao, M., Zang, X., Zhang, J., Mao, F., et al. (2018b). SALL4 activates TGF-β/SMAD signaling pathway to induce EMT and promote gastric cancer metastasis. *Cancer Manag. Res.* 10, 4459–4470. doi: 10.2147/cmar.S177373

Zhang, Y., and Chen, H. (2011). Genistein attenuates WNT signaling by up-regulating sFRP2 in a human colon cancer cell line. *Exp. Biol. Med.* 236, 714–722. doi: 10.1258/ebm.2011.010347

Zhao, P., Li, Y., and Lu, Y. (2010). Aberrant expression of CD133 protein correlates with Ki-67 expression and is a prognostic marker in gastric adenocarcinoma. *BMC Cancer* 10:218. doi: 10.1186/1471-2407-10-218

Zhao, R., Liu, Z., Xu, W., Song, L., Ren, H., Ou, Y., et al. (2020). *Helicobacter* pylori infection leads to KLF4 inactivation in gastric cancer through a TET1-mediated DNA methylation mechanism. *Cancer Med.* 9, 2551–2563. doi: 10.1002/cam4.2892

Zhao, W., Li, Y., and Zhang, X. (2017). Stemness-related markers in cancer. *Cancer Transl. Med.* 3, 87–95. doi: 10.4103/ctm.ctm_69_16

Zhi, Q. M., Chen, X. H., Ji, J., Zhang, J. N., Li, J. F., Cai, Q., et al. (2011). Salinomycin can effectively kill ALDH(high) stem-like cells on gastric cancer. *Biomed. Pharmacother.* 65, 509–515. doi: 10.1016/j.biopha.2011.06.006

Zhou, Y., Xia, L., Wang, H., Oyang, L., Su, M., Liu, Q., et al. (2017). Cancer stem cells in progression of colorectal cancer. *Oncotarget* 9, 33403–33415. doi: 10.18632/oncotarget.23607

Conflict of Interest: The authors declare that the research was conducted in the absence of any commercial or financial relationships that could be construed as a potential conflict of interest.

frontiers in Cell and Developmental Biology

ORIGINAL RESEARCH
published: 09 July 2020
doi: 10.3389/fcell.2020.00471

Conditioned Medium From Azurin-Expressing Human Mesenchymal Stromal Cells Demonstrates Antitumor Activity Against Breast and Lung Cancer Cell Lines

Marília Silva, Gabriel Amaro Monteiro, Arsenio M. Fialho, Nuno Bernardes† and Cláudia Lobato da Silva*†*

iBB-Institute for Bioengineering and Biosciences, Department of Bioengineering, Instituto Superior Técnico, Universidade de Lisboa, Lisbon, Portugal

OPEN ACCESS

Edited by:
Erdal Karaoz, Istinye University, Turkey

Reviewed by:
Antonietta Rosa Silini, Fondazione Poliambulanza Istituto Ospedaliero, Italy
Lindolfo da Silva Meirelles, Universidade Luterana do Brazil, Brazil

***Correspondence:**
Nuno Bernardes
nuno.bernardes@tecnico.ulisboa.pt
Cláudia Lobato da Silva
claudia_lobato@tecnico.ulisboa.pt

† These authors have contributed equally to this work

Specialty section:
This article was submitted to Stem Cell Research, a section of the journal Frontiers in Cell and Developmental Biology

Received: *15 March 2020*
Accepted: *20 May 2020*
Published: *09 July 2020*

Citation:
Silva M, Monteiro GA, Fialho AM, Bernardes N and da Silva CL (2020) Conditioned Medium From Azurin-Expressing Human Mesenchymal Stromal Cells Demonstrates Antitumor Activity Against Breast and Lung Cancer Cell Lines. Front. Cell Dev. Biol. 8:471. doi: 10.3389/fcell.2020.00471

Recently, cell-based therapies have been explored as a strategy to enhance the specificity of anticancer therapeutic agents. In this perspective, human mesenchymal stromal cells (MSC) hold a promising future as cell delivery systems for anticancer proteins due to their unique biological features. In this study, we engineered human MSC to secrete a human codon-optimized version of azurin (hazu), a bacterial protein that has demonstrated anticancer activity toward different cancer models both *in vitro* and *in vivo*. To this end, microporation was used to deliver plasmid DNA encoding azurin into MSC derived from bone marrow (BM) and umbilical cord matrix (UCM), leading to expression and secretion of hazu to the conditioned medium (CM). Engineered hazu-MSC were shown to preserve tumor tropism toward breast (MCF-7) and lung (A549) cancer cell lines, comparable to non-modified MSC. Azurin was detected in the CM of transfected MSC and, upon treatment with hazu-MSC-CM, we observed a decrease in cancer cell proliferation, migration, and invasion, and an increase in cell death for both cancer cell lines. Moreover, expression of azurin caused no changes in MSC expression profile of cytokines relevant in the context of cancer progression, thus suggesting that the antitumoral effects induced by hazu-MSC secretome might be due to the presence of azurin independently. In conclusion, data shown herein indicate that MSC-produced azurin in a CM configuration elicits an anticancer effect.

Keywords: mesenchymal stromal cells, secretome, azurin, cancer, gene delivery

INTRODUCTION

Human mesenchymal stromal cells (MSC) are multipotent cells with the ability to modulate several biological mechanisms through paracrine activity (Hofer and Tuan, 2016), namely, limiting apoptosis (Gao et al., 2016) and inducing angiogenesis (Brewster et al., 2018; Mathew et al., 2019; Rifai et al., 2019), as well as to differentiate into a variety of cell lineages, including osteocytes,

adipocytes, and chondrocytes (Xie et al., 2013). Cells with these features hold a promising future for cell therapies and tissue engineering, by potentially replacing damaged tissues of mesodermal origin and promoting tissue regeneration,. As such, the number of clinical trials using MSC has been rising almost exponentially since 2004 (Murray and Péault, 2015), achieving a total of 916 studies in 2020 (data from clinicaltrials.gov/, accessed on February 29th, 2020, using the terms "mesenchymal stem cell OR mesenchymal stromal cell"), of which 269 have been completed to date. In addition, MSC show an intrinsic ability to specifically migrate toward pro-inflammatory microenvironments, such as tumor sites (Kim et al., 2016; Cao et al., 2018; Chulpanova et al., 2018). This phenomenon occurs through an intricate crosstalk of biochemical cues, and although the underlying mechanisms are still not fully elucidated in this process, it has been recognized that the C-XC chemokine receptor type 4 (CXCR4)–stromal cell-derived factor 1 (SDF1α) axis plays an important role (Song and Li, 2011; Bhoopathi et al., 2012; Ho et al., 2014). Taking advantage of their innate tropism for tumors, genetically engineered versions of MSC have been under preclinical and clinical development as cell delivery systems of several anticancer agents. One of the most commonly adopted approach is the enhancement of endogenous antitumor immunity by engineering MSC to produce antitumor cytokines or soluble factors such as β-interferon (Ahn et al., 2013; Dembinski et al., 2013; Chen et al., 2019), interleukin-2 (Mounayar et al., 2013; Zhao, 2013), interleukin-12 (Elzaouk et al., 2006; Jeong et al., 2015), interleukin-15 (Jing et al., 2014), INF-alpha (Ren et al., 2008), or CX3CL1 (Xin et al., 2007). Another approach is the use of MSC to deliver tumor cytotoxic agents such as TRAIL (TNF-α related apoptosis inducing ligand) (Grisendi et al., 2010; Loebinger et al., 2010; Deng et al., 2014; Yan et al., 2014; Xia et al., 2015; Rossignoli et al., 2019; Spano et al., 2019), osteoprotegerin (OPG) (Qiao et al., 2015), NK4 (Kanehira et al., 2007), and HGF (Zhu et al., 2009). The employment of MSC as gene-directed enzyme-producing vehicles, such as MSC expressing thymidine kinase of the Herpes simplex virus with ganciclovir as a prodrug (tkHSV-MSC/GCV system) (Matuskova et al., 2012) and MSC engineered to express fused yeast cytosine deaminase::uracil phosphoribosyl transferase (yCD::UPRT) with 5-fluorocytosine (5-FC) as a prodrug (yCD::UPRT-MSC/5FC system) (Ursula et al., 2019), has also demonstrated very promising results. Three first-in-human clinical trials assessing gastrointestinal cancer, lung cancer, and ovarian cancer are being conducted to investigate the efficacy of genetically modified MSC in cancer patients with results demonstrating safety and tolerability, and some preliminary signs of efficacy (von Einem et al., 2019).

Azurin, a small water-soluble (14-kDa) protein from the bacteria *Pseudomonas aeruginosa*, has been explored in what concerns its antitumoral capacity. Azurin is able to enter mammalian cells, preferentially cancer cells (Bizzarri et al., 2011; Bernardes et al., 2018), acting at the membrane level by increasing its permeability and attenuating proliferative signaling pathways (Bernardes et al., 2014, 2016). After internalization, azurin forms a complex with the tumor suppressor protein p53, stabilizing it, and increasing its concentration at the intracellular level, thereby inducing apoptosis (Yamada et al., 2004). Azurin is also described to be able to increase the effectiveness of conventional anticancer therapeutics such as doxorubicin and paclitaxel (Bernardes et al., 2018), and gefitinib or erlotinib (Bernardes et al., 2016). In addition, a peptide derived from this protein (named p28) also enhances the activity of DNA damaging chemotherapeutic agents (Yamada et al., 2016). Azurin and p28 have a complex mechanism of action targeting several independent signaling pathways relevant in tumor proliferation, while inducing reduced side effects *in vitro* and *in vivo* (Lulla et al., 2016). These features turn azurin/p28 distinct and promising relatively to other antitumor agents, which have a more limited range of action.

In the present study, we couple azurin's antitumoral effect to the tumor tropism ability of MSC, in a cell-based approach, by genetically engineering human MSC to produce and secrete azurin through non-viral methods. Though viral systems have demonstrated the highest gene transfer efficiencies in preclinical and clinical trials, non-viral vectors and gene transfer approaches are emerging as safer and effective alternatives. In this context, we employ a non-viral method, previously developed by our group, of human MSC transfection through microporation aiming at a high gene delivery efficiency, without compromising cell viability and recovery (Madeira et al., 2011).

When evaluating the role of naïve MSC in tumor progression/suppression, the majority of studies employ MSC isolated from the BM, the UCM, and the adipose tissue (AT) (Rahmatizadeh et al., 2019; Liang et al., 2020; Xia et al., 2020). Considering that MSC isolated from different tissue sources express different surface markers (Hass et al., 2011; Elahi et al., 2016), and may differ in what concerns differentiation potential (Rebelatto et al., 2008), the outcome from these studies may be dependent on the isolation source of MSC. Therefore, in the present study, all experiments were validated with MSC from two tissue sources, BM and UCM. Moreover, envisaging the translational potential of our approach, this study was performed under xenogeneic (xeno)-free culture conditions to avoid the batch-to-batch variations associated with the use of animal-derived products, allowing a better reproducibility and preventing contagious health risks from animal-derived viral agents, mycoplasma, and prions (Leong et al., 2016).

MATERIALS AND METHODS

Cell Lines and Cell Cultures

Cancer cell lines A549 (lung) and MCF-7 (breast) were obtained from ECACC (European Collection of Authenticated Cell Cultures) and cultured using high glucose Dulbecco's modified Eagles' medium (DMEM) supplemented with 10% of heat-inactivated fetal bovine serum (FBS) (Lonza), 100 IU/ml penicillin, 100 mg/ml streptomycin (PenStrep, Invitrogen), and passaged between 2 and 3 times per week, by chemical detachment with trypsin 0.05%.

Human MSC used in this study are part of the cell bank available at the Stem Cell Engineering Research Group (SCERG), Institute for Bioengineering and Biosciences at Instituto Superior Técnico (iBB-IST). MSC were previously

isolated/expanded according to protocols previously established at iBB-IST (Santos et al., 2009; Soure et al., 2016). Originally, human tissue samples were obtained from local hospitals under collaboration agreements with iBB-IST (bone marrow: Instituto Portuguˆes de Oncologia Francisco Gentil, Lisbon; umbilical cord: Hospital São Francisco Xavier, Lisbon, Centro Hospitalar Lisboa Ocidental, Lisbon). All human samples were obtained from healthy donors after written informed consent according to the Directive 2004/23/EC of the European Parliament and of the Council of 31 March 2004 on setting standards of quality and safety for the donation, procurement, testing, processing, preservation, storage, and distribution of human tissues and cells (Portuguese Law 22/2007, June 29), with the approval of the Ethics Committee of the respective clinical institution. Human MSC from the different tissue sources (BM and UCM) were kept cryopreserved in a liquid/vapor-phase nitrogen container. Upon thawing, cells were cultured in StemPro® Serum-free (SFM) medium and passaged two times per week, by chemical detachment with TrypLE™ Select (Gibco).

All cell lines were grown in a humidified atmosphere at 37°C with 5% CO_2 (Binder CO_2 incubator C150).

Construction of Azurin Recombinant Plasmid and Transfection Into Human MSC

Azurin coding sequence was obtained by gene synthesis following a codon optimization algorithm toward the human codon usage from the coding sequence from *P. aeruginosa* PAO1, to improve translation efficiency. Human codon optimized azurin (hazu) in fusion with the first 21 amino acids (aa) of the human tissue plasminogen activator (t-PA) (Qiu et al., 2000) was subcloned into a pVAX1-GFP vector by replacing the *GFP* gene, producing the recombinant pVAX-hazu plasmid. pVAX-GFP was constructed and produced as described elsewhere (Azzoni et al., 2007). The fidelity of the cloned sequence was evaluated by DNA sequencing. MSC were transfected with 10 μg of pVAX-hazu plasmid through microporation [Microporator MP100 (Neon/Invitrogen-Life Technologies)] according to Madeira et al. (2011); Sahin and Buitenhuis (2012). As a control, MSC were transfected with pVAX-GFP to assess the transfection efficiency. MSC conditioned media (CM) (MSC-CM) and cells were harvested at 72 and 96 h post-transfection. The expression and secretion of azurin were evaluated through Western blotting, and the percentage of GFP-positive cells was detected by flow cytometry (FACSCalibur, BD).

Western Blotting

MSC-CM were collected at 96 h, mixed with loading buffer (Tris–HCl 62.5 mM, pH 6.8, 2.5% SDS, 10% glycerol, 0.002% bromophenol blue, and 5% β-mercaptoethanol), and boiled at 95°C for 5 min. Denatured samples were run on 15% polyacrylamide gel and transferred onto nitrocellulose membranes (*Trans*-Blot Turbo, BioRad). The membranes were incubated overnight with 1:2000 dilution of specific custom-made primary anti-azurin antibody (SicGen) (Bernardes et al., 2013), 1:2000 anti-GFP (Santa Cruz Biotechnology), or 1:1000 anti-GAPDH (Santa Cruz Biotechnology). Following incubation, the membranes were washed with PBS–tween-20 (0.5%) and probed with 1:2000 secondary antibody (Santa Cruz Biotechnology) during 1 h by shaking at room temperature. Proteins were detected through the addition of ECL reagent (Pierce) as a substrate and exposed and captured the chemiluminescence by Fusion Solo (Vilber Lourmat) equipment. For the cleavage of N-linked oligosaccharides, 10 μg of total protein in MSC-derived conditioned medium (MSC-CM) was mixed with 1 μl of Glycoprotein Denaturating Buffer (10×) and H_2O, before boiling the sample for 10 min at 100°C. After briefly chilling on ice, 2 μl of GlycoBuffer (10×), 2 μl of 10% NP-40, and water were added to a final volume of 20 μl. Finally, 1 μl of PNGase F (New England Biolabs) was added and the mixture was incubated at 37°C for 1 h before analysis by Western blotting.

Cancer Cell Proliferation Assay

Presto Blue™ viability assay was used to determine proliferation of cancer cells upon treatment with MSC-CM. Cells were seeded on 96-well plates (Orange Scientific) at a density of 1×10^4 and 2×10^4 cells/well for MCF-7 and A549 cell lines, respectively. After 24 h, medium was exchanged with 100 μl of MSC-CM (keeping a baseline level of 50% cancer cells' culture media: 0%, 10%, 25%, and 50% MSC-CM). Afterward, Presto Blue Reagent (ThermoFisher) was added to each well and incubated at 37°C for 2 h. Fluorescence was determined at the following wavelengths: 540 nm excitation and 590 nm emission. Untreated cells were used as control, in order to determine the relative cell proliferation of treated cells.

Assessment of Cancer Cell Apoptosis

Cancer cell apoptosis was assessed using the Annexin V Apoptosis Detection kit (BD Sciences). Cells were plated on 6-well plates (Orange Scientific) at a density of 2×10^5 and 1.5×10^5 cells/well for MCF-7 and A549 cell lines, respectively. On the next day, medium was exchanged with MSC-CM (50% cancer cells' culture media/50% MSC-CM). After 24 h incubation, cells were harvested and stained for Annexin V and propidium iodide (PI) by flow cytometry.

Cancer Cell Invasion Assay

The ability of MSC to migrate toward tumor cells (tumor tropism) and cancer cell invasion was evaluated using CytoSelect™ 24-Well Cell Migration with 8 μm pore size, coated with Matrigel. For tumor tropism experiments, 1.5×10^5 lung (A549) and breast cancer (MCF-7) cells were cultured on 24-well plates and left overnight at 37°C and 5% CO_2. MSC (4×10^4) were incubated in the upper compartment of the culture chamber, placed on the wells, and left for 24 h at 37°C and 5% CO_2. For cancer cell invasiveness experiments, 1.5×10^5 A549 cells treated or untreated with MSC-CM were incubated in the upper compartment of the transwell, while culture medium (i.e., DMEM supplemented with 10% FBS) was added to the 24-well plates. Incubation was held at 37°C and 5% CO_2 for 24 h. Non-migrated cells were removed from the upper side of the chamber's filter with a cotton swab dipped

in PBS and chambers were washed with PBS. Migrated cells were fixed in cold methanol (4°C) for 10 min. The membrane was removed with a scalpel and placed in a microscope glass, and cells were stained with DAPI and counted under a microscope (Zeiss). In each condition, 10 independent fields were counted, and the average of these fields was considered as the mean number of migrated cells per condition. Results are presented as the fold change in the number of cells migrated in comparison with the control condition where no cancer cells were added.

Cancer Cell Migration Assay

A scratch assay was used to assess the migration of breast (MCF-7) and lung (A549) cancer cells *in vitro*, upon treatment with MSC-CM. Approximately 2×10^6 cells were seed in 2-well culture inserts (Ibidi), to ensure reproducibility within conditions, on 24-well dish and cultured in growth medium for 72 h until approximately 70–80% confluence. Inserts were removed, and cells were treated with 250 μl of MSC-CM (keeping the proportion 50% MSC-CM/50% cancer cells' culture medium). Cells were monitored over time by time-lapse recording and distance moved by the cells was determined by measuring the unoccupied scratch area (% of unoccupied area/h).

Cytokine Quantification by ELISA

The levels of IL6, TGF-β, SDF1-α, and VEGF were measured in 100 μl of MSC-CM collected at 96 h with a sandwich ELISA kit, according to the manufacturer's instructions (RayBiotech).

RESULTS

Human MSC Are Able to Express and Secrete Azurin Without Cell Viability Impairment

Bone marrow (BM)- and umbilical cord matrix (UCM)-derived MSC cultured under xenogeneic (xeno)-free conditions were transfected by microporation with plasmid DNA (pVAX-hazu) encoding for a human codon optimized version of azurin coding sequence containing on its N-terminal a secretory sequence leading to the secretion upon protein synthesis (Qiu et al., 2000). Codon optimization was used considering that azurin is from a bacterial source and its efficiency of translation in animal cells, such as MSC, could be reduced. In parallel, MSC were transfected with a control vector, containing a green fluorescence protein (GFP) sequence (pVAX-GFP).

Notably, azurin production has not induced alterations on MSC themselves, as we monitored cell viability over a 96-h period after cell microporation (**Figure 1A**). Non-transfected cells (control 1) displayed the highest cell number at day 2, 3, and 4, followed by cells microporated without DNA (control 2). Nevertheless, cells microporated with pVAX-GFP and pVAX-hazu entered the exponential growth phase with almost no differences between the groups. Flow cytometry demonstrated that 50 to 60% of the cell population was expressing GFP, 72 h post-transfection (**Figure 1B**), with a cellular recovery of 46% and a yield of transfection of 28% (comparable to 70, 40, and 30%, respectively, in Madeira et al., 2011). As negative controls, non-transfected cells (control 1) and microporated cells without DNA (control 2) were also evaluated.

After microporation, MSC were cultured for 96 h and the secreted azurin was detected in the CM by Western blotting (**Figure 1C**) (full membrane images are depicted in **Supplementary Material 1**). Specific bands around the expected MW of 15 kDa were observed only in the supernatants from MSC transfected with pVAX-hazu (hazu-MSC), which indicated that azurin was successfully expressed and released to the CM. However, it was possible to observe two bands corresponding to possible protein post-translational modifications. After treatment of MSC-derived CM (MSC-CM) with PNGase F (endoglycosidase that selectively removes N-glycans), only one band with more intensity was observed, which indicates that azurin is N-glycosylated in the CM of MSC-transfected cells (**Figure 1D**).

MSC Preserve Tumor Tropism After Microporation

Human MSC have been described to be intrinsically tropic to tumor sites (Kidd et al., 2009), which is a central feature to their potential role as delivery vehicles for anticancer agents in cancer therapy. In this study, the *in vitro* tumor tropism properties of bone marrow-derived MSC (BM MSC) (three donors) toward a breast cancer cell line (MCF-7) were evaluated by a transwell migration assay using CytoSelect chambers with 8-μm pores. Aiming at a better mimicry of the *in vivo* microenvironment, we studied the effect of physiological barriers like collagen type I and Matrigel™ as coatings on transwell chambers. Tumor cell lines were seeded on 24-well plates, and after 24 h, the upper chambers containing seeded MSC were added to each well at a MSC/tumor cells ratio = 1/4;. In the control condition, no tumor cells were added (the corresponding medium volume was added instead). Tumor cells triggered invasion of BM MSC as compared to the negative control, and the specificity of this process seems to be improved by the presence of Matrigel (**Figure 1E**).

Cell microporation and transgene expression could potentially induce changes in the physiological properties of MSC. Therefore, we compared the tumor tropism rate of un-modified MSC and hazu-MSC toward A549 cells (**Figure 1F**). As shown, the expression of azurin does not impact the homing ability of these cells, and these results are supported by the characterization of CXCR4 (**Supplementary Material 2**), a known chemokine receptor associated with the tumor tropism properties of MSC (21.2% expression in control MSC versus 23.2% expression in hazu-MSC, assessed by flow cytometry).

Cancer Cell Proliferation Decreases and Cell Death Increases Upon Treatment With hazu-MSC-CM

To investigate whether the secretome of azurin-producing MSC has an inhibitory effect on cancer cells' growth and proliferation, tumor cell lines A549 and MCF-7 were subjected to increasing concentrations of CM from hazu-MSC cultures, harvested 96 h

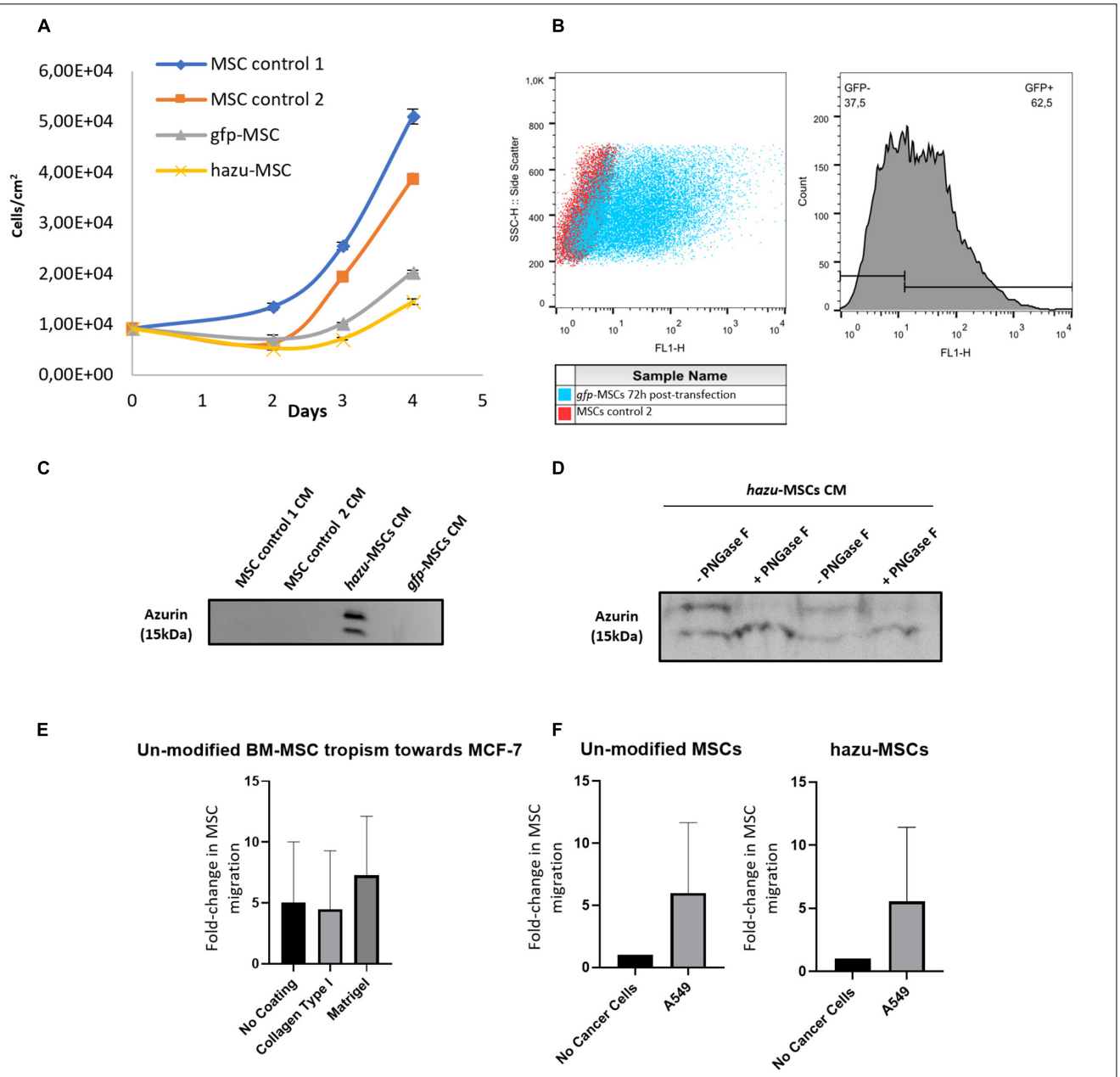

FIGURE 1 | Engineering of mesenchymal stem/stromal cells (MSC) to express azurin. **(A)** MSC number per square centimeter after microporation. MSC non-microporated (control 1) (blue line), MSC microporation control were transfected without the plasmid DNA (control 2) (orange line), gfp-MSC were microporated with pVAX-GFP (gray line), and hazu-MSC were microporated with pVAX-hazu (yellow line). A total of 9.23×10^3 cells per condition were initially microporated and counted at days 2, 3 and 4. Values are mean ± SD ($n = 3$). **(B)** Flow cytometry demonstrated that 50 to 60% of cell population was expressing GFP 72 h post-transfection. **(C)** Azurin is secreted by MSC to the conditioned media (CM) at 96 h after microporation. A representative image of Western blotting for one donor is depicted. **(D)** Ten micrograms of total protein from CM was incubated with PNGase F to remove *N*-linked oligosaccharides from glycoproteins. Western blotting image of MSC-CM from two independent donors is depicted. **(E)** Tumor tropism of un-modified bone marrow (BM)-derived MSC toward MCF-7 breast cancer cells. Results are presented as the fold change of migrated MSC toward tumor cells compared to negative control (migration toward culture media). **(F)** Comparison between tumor tropism rate of un-modified MSC and hazu-MSC toward A549. Results are presented as the fold change of migrated MSC toward tumor cells and the negative control (migration toward culture media).

post-microporation. Since MSC and cancer cells were cultured in different culture media (MSC in StemPro® MSC SFM XenoFree culture medium, whereas MCF-7 and A549 in DMEM high glucose supplemented with FBS), for this experiment, the concentration of MSC-CM was varied, while maintaining a baseline level of cancer cells' culture medium at 50%. Cytotoxicity and tumor cell proliferation were assessed by using PrestoBlue after 24 h treatment with MSC-CM (**Figure 2A**). The results

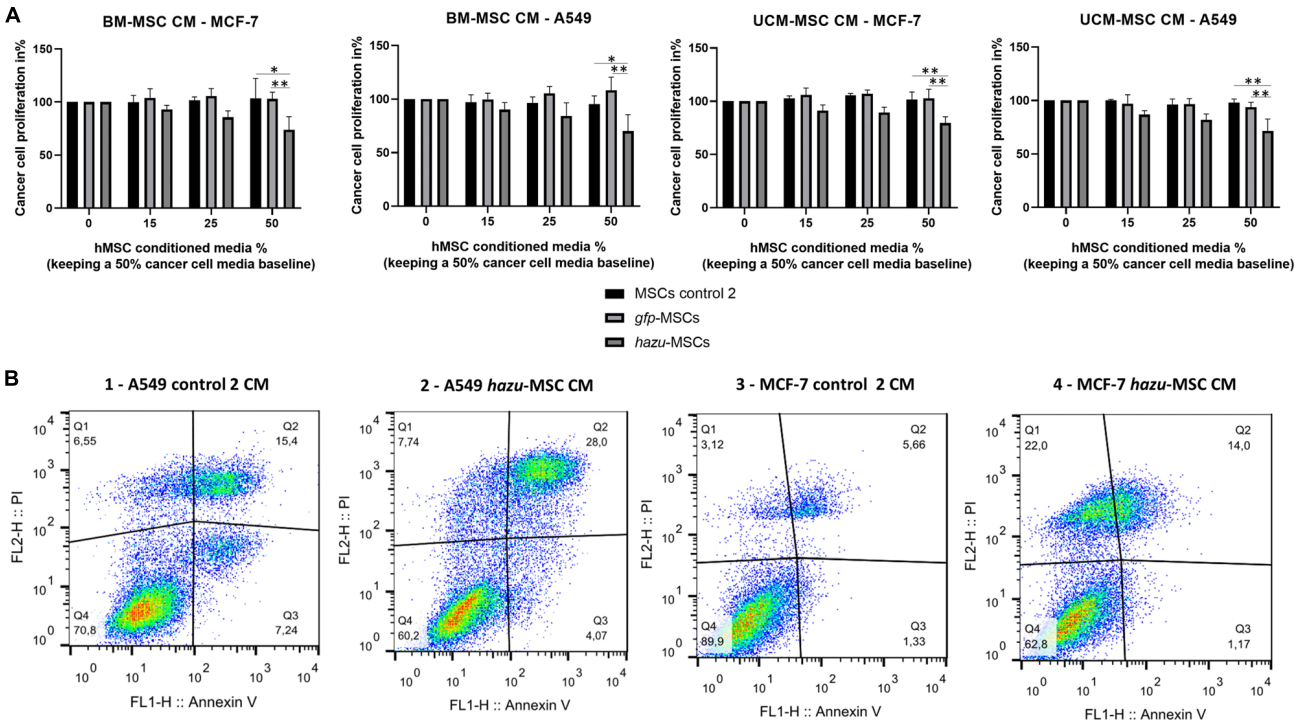

C

	A549 treated with:	Live Cells (%)	Dead Cells (%)	Ratio
BM-MSCs'	Control CM	71,8	20,1	1,8
	Azurin CM	61,1	36,1	
UCM-MSCs'	Control CM	69,2	26,4	1,3
	Azurin CM	62,1	34,3	

D

	MCF-7 treated with:	Live Cells (%)	Dead Cells (%)	Ratio
BM-MSCs'	Control CM	90,2	7,0	4,3
	Azurin CM	68,3	30,1	
UCM-MSCs'	Control CM	90,0	8,0	3,4
	Azurin CM	71,3	26,8	

FIGURE 2 | hazu-MSC CM inhibit cancer cell proliferation and induce cancer cell death *in vitro.* **(A)** Cytotoxicity and tumor cell viability were assessed by PrestoBlue in breast cancer (MCF-7) and lung cancer (A549) cell lines upon 24 h of exposition to conditioned media (CM) from MSC microporated with pVAX-hazu (hazu-MSC) (gray bars), pVAX-GFP (gfp-MSC) (light gray bars), or without DNA (microporation control 2) (black bars). MSC-CM was collected 96 h post-transfection. Due to differences in expansion media between cancer cells and MSC, MSC-CM concentration was variated (0–50%) while maintaining a level of cancer cells' culture media at 50%. Untreated cells were exposed to media without CM, and their proliferation rate was admitted as 100% (*p*-values compare % of proliferation between gfp-MSC or hazu-MSC with MSC control 2; $n = 4$). **(B)** Annexin V expression detection after treatment with hazu-MSC' CM, assessed by flow cytometry. Living cells are seen in the lower left quadrant, Annexin V (–)/ PI (–), [Q1]. The early apoptotic cells are shown in the lower right quadrant, Annexin V (+)/ PI (–), [Q2]. Advanced apoptotic or necrotic cells are seen in the upper right quadrant, Annexin V (+)/ PI (+), [Q3]. Annexin V (–)/ PI (+), [Q4] are cells in late necrosis or cellular debris. Panels 1 and 2 correspond to MCF-7 treated with control 2 MSC-CM and hazu-MSC-CM, respectively. Panels 3 and 4 correspond to A549 treated with control 2 MSC CM and hazu-MSC CM, respectively ($n = 2$). **(C)** Percentage of A549 live and dead cells based on flow cytometry results on annexin V expression, after treatment with MSC-CM and the ratio between dead cells treated with hazu-MSC' CM or control MSC' CM ($n = 1$). **(D)** Percentage of MCF-7 live and dead cells based on flow cytometry results on annexin V expression, after treatment with MSC-CM and the ratio between dead cells treated with hazu-MSC' CM or control MSC' CM ($n = 1$). Statistical differences are indicated with $^{*}p \leq 0.05$ and $^{**}p \leq 0.01$.

are presented in variation (%) of proliferation relatively to the control, where no MSC-CM was added (corresponding to 100% proliferation rate). The effect of hazu-MSC-CM seems to be inhibiting tumor cell proliferation, and this effect is more pronounced by increasing concentrations. On the other hand, CM retrieved from control MSC cause no change in the proliferation of both A549 and MCF-7 cell lines. The effect of hazu-MSC-CM induced an inhibition of 38.1% in A549 and an inhibition of 17.3% in MCF-7 with the highest concentration of CM (50% vol/vol). Moreover, we observed an average of 1.6- and 3.9-fold increase in the apoptotic levels of A549, assessed by flow cytometry (**Figures 2B,C**) and MCF-7 cells (**Figures 2B,D**), respectively, after treatment with hazu-MSC-CM when compared with the control CM.

Cancer Cell Migration and Invasion Decrease Upon Treatment With hazu-MSC-CM

The antitumoral effects of hazu-MSC-CM are also extended to the impairment of cancer cell invasion. These experiments were performed with indirect co-cultures, in a transwell migration assay, by culturing cancer cells treated and un-treated with MSC-CM in invasion chambers coated with Matrigel. Results are given in the percentage of cancer cell invasion in comparison to the control condition where cancer cells were treated with culture medium only (i.e., without MSC-CM). By analyzing the results, we can hypothesize that the naïve MSC' secretome by itself has an impact in reducing cancer cell invasion, and this effect is enhanced by the presence of azurin to a notorious extent (close to 20% invasive cells compared to control) (**Figure 3A**).

Cell migration in cancer cells is also affected by treatment with hazu-MSC-CM. Cell migration was estimated by means of a scratch assay and monitored by time-lapse microscopy. The distances of migrated cells were measured over several time points and the results show that treatment with CM from hazu-MSC induced a delay on cancer cell migration and repairment of the scratch area (**Figure 3B**). Twenty hours after treatment, the percentage of unoccupied area for A549 treated with hazu-MSC-CM was 23.4%, compared to 1.4% unoccupied area for A549 treated with CM from control 2 MSC. Regarding MCF-7, 32.8% was observed for cells treated with hazu-MSC-CM and 8.9% was observed for cells treated with CM from control 2 MSC.

Secretion of Cytokines Involved in Tumor Progression by Engineered MSC Quantified by ELISA

To get insights into the antitumoral effects induced by hazu-MSC-CM, namely, if these are due to a crosstalk between the induced azurin expression and the native secretome of MSC, we

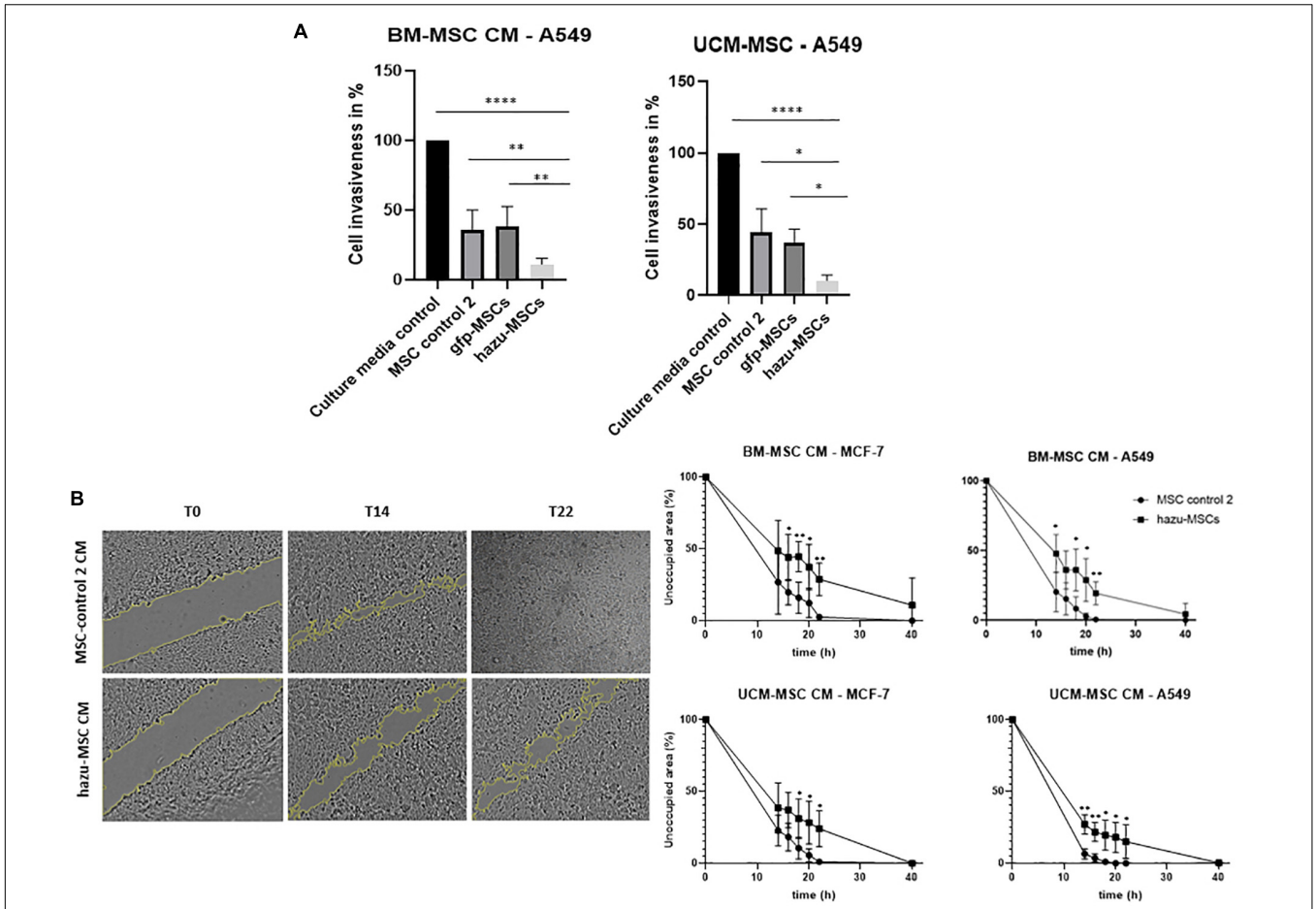

FIGURE 3 | Inhibition of cancer cell invasion and migration by hazu-MSC' CM *in vitro*. **(A)** A549 lung cancer cell invasion toward a chemoattractant (culture media supplemented with FBS) was evaluated in Matrigel invasion assays. Cells were treated with CM from gfp-MSC, hazu-MSC, MSC control 2, and cancer cell media (culture media control) during 24 h and migrated cells were quantified. Results are presented as the percentage of invasive cells compared to the control condition (p-values compare % of cancer cell invasiveness between hazu-MSC' CM treatment and the remaining treatment conditions; $n = 4$). **(B)** Cell migration was estimated by means of a scratch assay and monitored by time-lapse microscopy. A549 and MCF-7 were treated with control 2 MSC' CM or hazu-MSC' CM, and the distances of migrated cells were measured at several time points: 0, 14, 16, 18, 20, 22 and 40 h (p-values compare % of unoccupied area between A549 and MCF-7 treated with hazu-MSC' CM or MSC control 2 CM, at the same time point; $n = 4$). Statistical differences are indicated with $^{*}p \leq 0.05$, $^{**}p \leq 0.01$ and $^{****}p \leq 0.0001$.

evaluated the expression of four cytokines expressed by MSC that have been described to have a role in MSC interaction with cancer cells: inteuleukin-6 (IL6) (Kidd et al., 2009), vascular endothelial growth factor (VEGF) (Vera et al., 2019), stromal derived factor 1 alpha (SDF1-α) (Liu et al., 2010), and transforming growth factor beta (TGF-β) (Markell et al., 2010). To this end, we analyzed the concentration of these factors in MSC-CM by ELISA before and after microporation with pVAX-hazu and pVAX-GFP (**Figure 4**). The results are given in the relative fold change of cytokine expression relatively to MSC-CM in the control condition (control 2, i.e., MSC microporated without DNA). The microporation process seems to be inducing a general response in the expression of such cytokines, by decreasing their relative concentration. However, no significant differences were observed between the hazu-MSC-CM and gfp-MSC-CM, which might suggest that the effects observed in cancer regression can be due to the engineered expression of azurin independently.

DISCUSSION

One of the major challenges of developing more effective cancer therapies concerns the specific delivery of anticancer drugs to the tumor site. In this context, human MSC have been recently considered for cell-based therapies for cancer, due to their ability to migrate specifically and to incorporate within tumors, their low immunogenicity and the fact that these cells are relatively easy to isolate, culture, and manipulate (Xie et al., 2013; Hofer and Tuan, 2016; Gao et al., 2016; Brewster et al., 2018; Mathew et al., 2019; Rifai et al., 2019). Altogether, these features turn

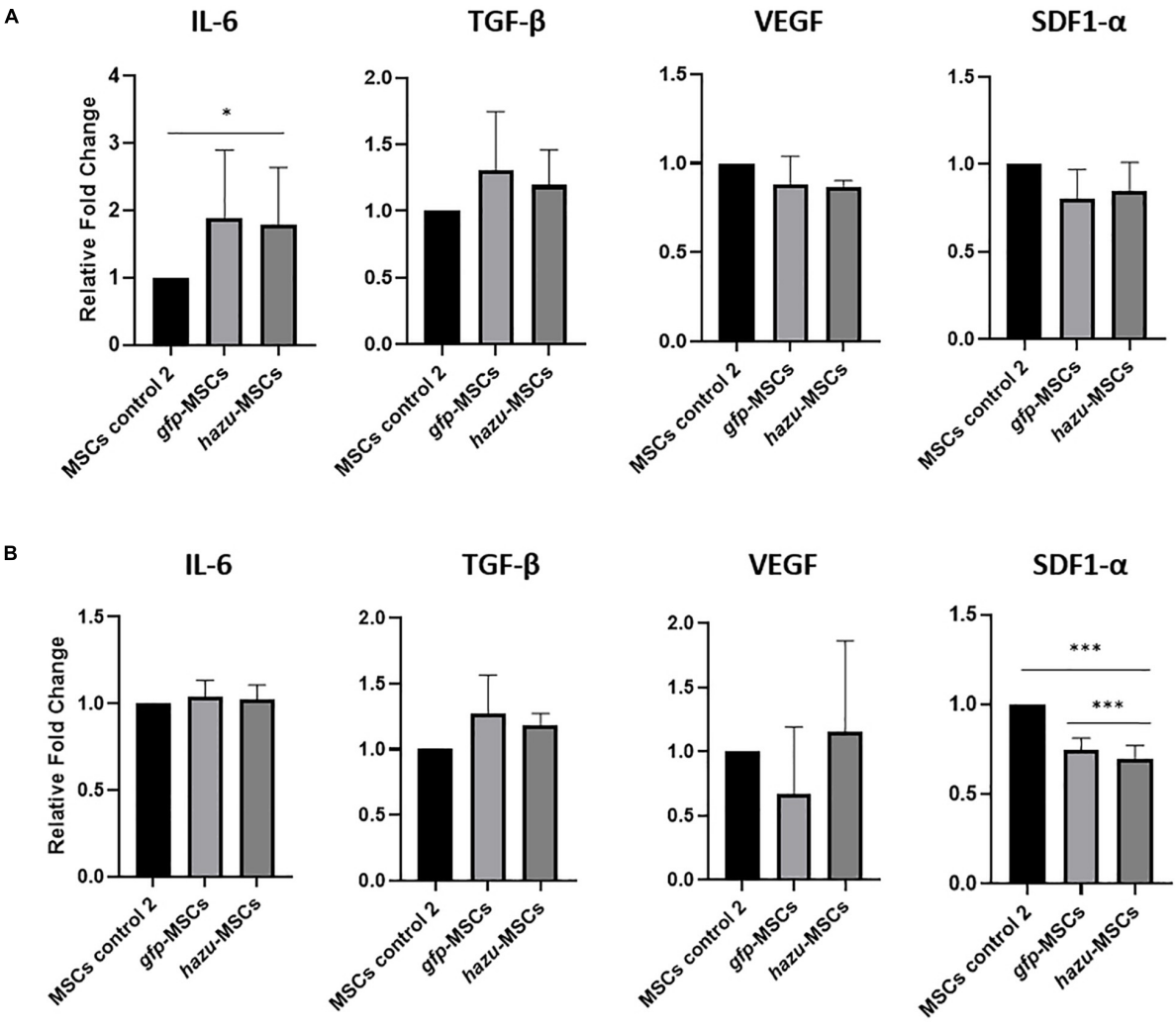

FIGURE 4 | Evaluation of MSC expression profile on cytokines relevant in cancer progression. The levels of inteuleukin-6 (IL6), vascular endothelial growth factor (VEGF), stromal derived factor 1 alpha (SDF1-α), and transforming growth factor beta (TGF-β) were analyzed by ELISA in MSC-CM before and after microporation with pVAX-hazu and pVAX-GFP. The results are given in the relative fold change of cytokine expression relatively to MSC-CM in the control condition (control 2) (p-values compare fold change between gfp-MSC and hazu-MSC conditions with MSC control 2; $n = 3$). **(A)** Cytokine expression profile in BM MSC-CM. **(B)** Cytokine expression profile in UCM MSC-CM. Statistical differences are indicated with $^{*}p \leq 0.05$ and $^{***}p \leq 0.001$.

MSC into exciting therapeutic candidates as drug delivery tools toward cancer. In the perspective of cell-based therapies, MSC do not only potentially solve the drug delivery specificity problem but also allow for the heightening of the drug compound's half-life in the organism, as well as a lower dosage and less repeated injections to potentially achieve meaningful responses (Elman et al., 2014).

Furthermore, MSC demonstrate a strong paracrine effect resulting from the high levels of bioactive molecules they secrete in response to their microenvironment. The panoply of factors produced by these cells is highly context dependent, being able to be modulated *in vitro*. For this reason, MSC's secretome, either in the format of CM or as purified extracellular vesicles (EVs), has been explored as a cell-free approach in several applications in regenerative medicine (Keshtkar et al., 2018; Eleuteri and Fierabracci, 2019). Despite the potential benefits of using MSC as a cell delivery system, studies have reported the supportive role of MSC in the progression of tumor density and metastasis, while others have shown antitumor effects both *in vitro* and in different models of cancer (Devarasetty et al., 2017; Liang et al., 2020; Xia et al., 2020). The conflicting data in the literature may hamper the establishment of cell therapies for cancer based on non-modified MSC since the therapeutic safety of such approach might be jeopardized (Rahmatizadeh et al., 2019).

The availability of genetic engineering tools may potentiate MSC as living factories of antitumoral proteins for cancer therapy. In this study, we genetically engineered human MSC, through non-viral methods, toward the production and secretion of the antitumoral protein azurin. Azurin, originally produced by *P. aeruginosa*, has a complex anticancer mechanism of action, targeting several independent pathways critical for tumor progression. These features allow a much broader action of azurin regarding the tumor types that it can target, while also supporting the prevention of tumor resistance (Bernardes et al., 2014, 2018, 2016). We engineered a recombinant plasmid containing the azurin coding sequence and an engineered secretory sequence that provides a signal for translocation of recombinant proteins into the lumen of the endoplasmic reticulum (ER), for transport through the ER and Golgi apparatus to the extracellular environment (Qiu et al., 2000). To the best of our knowledge, this study is the first to combine a stem cell-based approach to deliver a protein originated in bacteria for anticancer therapies.

In what concerns clinical trials studying the use of genetically engineered MSC as cell therapy for cancer, three first-in-human studies are being conducted. The phase I/II TREAT-ME trial (NCT02008539) assesses the safety and efficacy of autologous MSC genetically modified with a retroviral vector expressing tyrosine kinase and subsequent ganciclovir infusions in patients with gastrointestinal adenocarcinoma. The results known so far demonstrated safety and tolerability in treated patients, with preliminary signs of efficacy in terms of clinical stabilization of disease (von Einem et al., 2019). The TACTICAL trial (NCT03298763) assesses the safety and efficacy of allogeneic umbilical cord-derived MSC transduced with lentivirus to express TRAIL as a first-line therapy in conjunction with chemotherapy in patients with metastatic adenocarcinoma of the lung. Finally, a study employing MSC genetically modified with a plasmid vector to produce IFN-β (NCT02530047) assesses the safety and efficacy in patients with advanced ovarian cancer. Many other studies have recently reported engineered versions of MSC aimed to treat cancer at the preclinical level.

Over the last years, significant efforts have been made to address the limitations of MSC in early clinical trials, namely, by using genetic engineering tools to improve the therapeutic potential of these cells (Nowakowski et al., 2016). Despite the advantages of employing non-viral gene delivery methods, to date, the majority of conducted clinical trials based on genetically engineered MSC are relying on the use of viral methods. Although transduction efficiency is higher, issues regarding vectors safety and manufacturing have encouraged the implementation and optimization of non-viral based techniques such as microporation. The method used in this study is based on previous studies from our group (Madeira et al., 2011), aiming at a cell transfection with high efficiency without compromising cell viability and recovery. Regarding the percentage of GFP-positive cells, herein we obtained 60%, a cellular recovery of 46% and yield of transfection of 28% (70, 40, and 30%, respectively, in Madeira et al., 2011). hazu-MSC supernatants were collected at 96 h and azurin was detected by Western blotting. Besides the expected azurin, it was possible to observe a second band corresponding to a post-translationally modified protein, that was later identified as a glycosylated azurin after treatment with PNGase F. This brings us to hypothesize that the activity of this glycosylated form of azurin may differ from the native protein. Therefore, in future studies, it would be important to characterize this modified protein in terms of structure, functionality, and antitumoral activity. Although it is expected that MSC continue to secrete azurin for longer than 96 h, we anticipate that after culturing cells for such a long time period, their CM will be exhausted from key nutrients and MSC will likely secrete proteins and factors responding to metabolic stress, which makes the interpretation of the results difficult herein.

We tested the effect of hazu-MSC secretome in tumor progression by exposing MCF-7 and A549 cells to increasing concentrations of engineered MSC-derived CM. The plenitude of hazu-MSC produced factors inhibited 17.3 and 38.1% tumor proliferation in MCF-7 and A549, respectively, with the highest concentration of CM tested (50%, vol/vol) compared to MSC microporated with pVAX-GFP and MSC microporated with no DNA (control 2), where no inhibition was observed. In this experiment, we varied the concentration of MSC-CM, while maintaining a baseline level of cancer cells' culture medium at 50%. Thus, the effects observed in cancer proliferation are not associated with the medium change or the lack of FBS components. Along with a decrease in cancer cell proliferation, an increase in cancer cell apoptosis was observed. These results are in agreement with the anticancer properties of azurin, as previously mentioned (Yamada et al., 2004). Moreover, upon treatment with hazu-MSC-CM, a decrease in invasion through Matrigel for the A459 invasive cell line (Wang et al., 2017) and a decrease in cell migration were observed for both cancer cell lines. In previous work from our group, we demonstrated that bacterial produced azurin is able to interfere with pro-tumorigenic and proliferative signaling pathways FAK,

Src, and AKT, by attenuating the phosphorylation levels of these proteins in lung (Bernardes et al., 2016) and breast cancer cell lines (Bernardes et al., 2013). After treatment with azurin, besides a decrease of FAK and Src phosphorylation, we observed a 44–66% reduction of cancer cell invasion through Matrigel (Bernardes et al., 2013). In what concerns lung cancer cells, azurin was also associated with attenuated phosphorylation levels of Src Y416, Akt S473, and PI3K, which correlated to a 30% reduction in the invasive capacity of the cancer cells by around 30% (Bernardes et al., 2016). In this context, further studies should focus on the interaction between MSC-produced azurin and the activation of such signaling pathways.

MSC are emerging as promising anticancer agents, fundamentally due to their innate tropism toward proinflammatory environments, such as the tumor microenvironment in both primary and metastatic sites (Oieni et al., 2019). In this context, we demonstrated the migratory capacity of hazu-MSC toward MCF-7 and A549 cancer cell lines through indirect co-cultures. The results demonstrated no differences in the migratory potential of engineered when compared to unmodified cells. Furthermore, we evaluated the expression of four cytokines expressed by naïve MSC that play a pivotal role in the hallmarks of cancer progression in processes such as cancer cell proliferation, invasion, migration, angiogenesis, apoptosis, and development of metastases (Maskarinec et al., 2020). Microporation seems to be inducing an effect in the expression of such cytokines to a certain extent; however, we observed no significant differences between engineered MSC and naïve MSC, which may suggest that the results observed in cancer regression might be associated to the expression of azurin independently, rather than due to a crosstalk of azurin and the naïve MSC secretome.

The majority of the studies evaluating the effect of naïve MSC on tumor development employ MSC from the BM, the UCM, and the AT (Rahmatizadeh et al., 2019; Liang et al., 2020; Xia et al., 2020). When analyzing the outcome from these studies, it seems to be a conspicuous pattern of tumorigenicity, with BM MSC being more pro-tumorigenic and UCM MSC being more tumor suppressive. This pattern seems to be more pronounced when evaluating breast cancer, the most popular type of cancer tested with MSC cytotherapy (Christodoulou et al., 2018). For this reason, in the present study, all experiments were validated using MSC isolated from two different donors of two tissue sources, BM and UCM.

Although BM has been the main source for MSC isolation, the harvest of BM is a highly invasive procedure and the number, differentiation potential, and maximal life span of BM MSC decline with increasing age (Kern et al., 2006). In this regard, a significant advantage of the neonatal tissues, such as the UCM, as sources of MSC is that they are readily available, thus avoiding invasive procedures and ethical problems associated with adult tissues, and several studies have reported superior proliferative capacity, life span, and differentiation potential over BM MSC (Kern et al., 2006). Considering the ease of harvest, culture, and transfection of MSC, the use of autologous cells may be realistic. However, the number and quality of MSC differ from patient to patient, making the quantification of the therapeutic effect difficult to interpret. Therefore, the use of allogenic MSC from healthy donors would allow greater cell numbers of better characterized cells (Loebinger et al., 2009). Moreover, envisioning an MSC cell line that stably expresses the transgene could overcome some issues related to the translation of MSC cytotherapy to a clinical setting. Therefore, as ongoing work of our group, the establishment of a stable hazu-MSC cell line represents a more flexible system in terms of both manufacturing and therapeutic perspectives (cell-based product or cell-free approach based on CM).

CONCLUSION

In this study, we were able to engineer MSC from two different tissue sources (BM and UCM) to express and secrete a human codon optimized version of an antitumoral bacterial protein, secreting it into the extracellular environment. When testing the CM retrieved from hazu-MSC, we observed a decrease in cell proliferation, migration, and invasion of breast (MCF-7) and lung (A549) cancer cell lines. In addition, an increase in cell death was observed for both cell lines.

All in all, the results presented here add to the arsenal of cell-based therapies for cancer, using the natural tumor-targeting properties of MSC and the broad anticancer functional activity of azurin.

DATA AVAILABILITY STATEMENT

All datasets generated for this study are included in the article/**Supplementary Material**.

AUTHOR CONTRIBUTIONS

NB and CS conceived and designed the study. MS and NB performed the experiments. MS, NB, and CS wrote the manuscript. All authors critically read and approved the final manuscript.

FUNDING

Funding received by iBB-Institute for Bioengineering and Biosciences from the Portuguese Science and Technology Foundation (FCT) (UIDB/04565/2020) was acknowledged. FCT also provides MS with a Ph.D. grant SFRH/BD/128372/2017.

SUPPLEMENTARY MATERIAL

The Supplementary Material for this article can be found online at: https://www.frontiersin.org/articles/10.3389/fcell.2020.00471/full#supplementary-material

REFERENCES

Ahn, J. o, Lee, H. w, Seo, K. w, Kang, S. k, Ra, J. c, and Youn, H. y (2013). Anti-tumor effect of adipose tissue derived-mesenchymal stem cells expressing interferon-β and treatment with cisplatin in a xenograft mouse model for canine melanoma. *PLoS One* 8:e74897. doi: 10.1371/journal.pone.0074897

Azzoni, A. R., Ribeiro, S. C., Monteiro, G. A., and Prazeres, D. M. F. (2007). The impact of polyadenylation signals on plasmid nuclease-resistance and transgene expression. *J. Gene Med.* 9, 392–402. doi: 10.1002/jgm

Bernardes, N., Abreu, S., Carvalho, F. A., Fernandes, F., Santos, N. C., and Fialho, A. M. (2016). Modulation of membrane properties of lung cancer cells by azurin enhances the sensitivity to EGFR-targeted therapy and decreased b 1 integrin-mediated adhesion. *Cell Cycle* 15, 1415–1424. doi: 10.1080/15384101.2016.1172147

Bernardes, N., Garizo, A. R., Pinto, S. N., Caniço, B., Perdigão, C., Fernandes, F., et al. (2018). Azurin interaction with the lipid raft components ganglioside GM-1 and Caveolin-1 increases membrane fluidity and sensitivity to anti-cancer drugs. *Cell Cycle* 17, 1649–1666. doi: 10.1080/15384101.2018.1489178

Bernardes, N., Ribeiro, A. S., Abreu, S., Mota, B., Matos, R. G., Arraiano, C. M., et al. (2013). The bacterial protein azurin impairs invasion and FAK / Src signaling in P-cadherin-overexpressing breast cancer cell models. *PLoS One* 8:e69023. doi: 10.1371/journal.pone.0069023

Bernardes, N., Ribeiro, A. S., Abreu, S., Vieira, A. F., Carreto, L., Santos, M., et al. (2014). High-throughput molecular profiling of a P-cadherin overexpressing breast cancer model reveals new targets for the anti-cancer bacterial protein azurin. *Int. J. Biochem. Cell Biol.* 50, 1–9. doi: 10.1016/j.biocel.2014.01.023

Bhoopathi, P., Chetty, C., Gogineni, V. R., Gujrati, M., Dinh, D. H., Rao, J. S., et al. (2012). MMP-2 mediates mesenchymal stem cell tropism towards medulloblastoma tumors. *Gene Ther.* 18, 692–701. doi: 10.1038/gt.2011.14.MMP-2

Bizzarri, A. R., Santini, S., Coppari, E., Bucciantini, M., Agostino, S. D., and Cannistraro, S. (2011). Interaction of an anticancer peptide fragment of azurin with P53 and its isolated domains studied by atomic force spectroscopy. *Int. J. Nanomed.* 6, 3011–3019. doi: 10.2147/IJN.S26155

Brewster, L., Robinson, S., Wang, R., Griffiths, S., Li, H., Peister, A., et al. (2018). Expansion and angiogenic potential of mesenchymal stem cells from patients with critical limb ischemia. *J. Vasc. Surg.* 65, 826–838. doi: 10.1016/j.jvs.2015.02.061

Cao, M., Mao, J., Duan, X., Lu, L., Zhang, F., Lin, B., et al. (2018). *In vivo* tracking of the tropism of mesenchymal stem cells to malignant gliomas using reporter gene-based MR imaging. *Int. J. Cancer* 142, 1033–1046. doi: 10.1002/ijc.31113

Chen, X., Wang, K., Chen, S., and Chen, Y. (2019). Effects of mesenchymal stem cells harboring the interferon-β gene on A549 lung cancer in nude mice. *Pathol. Res. Pract.* 215, 586–593. doi: 10.1016/j.prp.2019.01.013

Christodoulou, I., Goulielmaki, M., Devetzi, M., Panagiotidis, M., and Koliakos, G. (2018). Mesenchymal stem cells in preclinical cancer cytotherapy: a systematic review. *Stem Cell Res. Ther.* 8, 1–38. doi: 10.1186/s13287-018-1078-8

Chulpanova, D. S., Kitaeva, K. V., Tazetdinova, L. G., James, V., Rizvanov, A. A., and Solovyeva, V. V. (2018). Application of mesenchymal stem cells for therapeutic agent delivery in anti-tumor treatment. *Front. Pharmacol.* 9:259. doi: 10.3389/fphar.2018.00259

Dembinski, J. L., Wilson, S. M., Spaeth, E. L., Studeny, M., Zompetta, C., Samudio, I., et al. (2013). Tumor stroma engraftment of gene-modified mesenchymal stem cells as anti-tumor therapy against ovarian cancer. *Cytotherapy* 15, 20–32.e2. doi: 10.1016/j.jcyt.2012.10.003

Deng, Q., Zhang, Z., Feng, X., Li, T., Liu, N., Lai, J., et al. (2014). TRAIL-secreting mesenchymal stem cells promote apoptosis in heat-shock-treated liver cancer cells and inhibit tumor growth in nude mice. *Br. Dent. J.* 217, 317–327. doi: 10.1038/gt.2013.88

Devarasetty, M., Wang, E., Soker, S., and Skardal, A. (2017). Mesenchymal stem cells support growth and organization of host- liver colorectal-tumor organoids and possibly resistance to chemotherapy. *Biofabrication* 9:021002. doi: 10.1088/1758-5090/aa7484

von Einem, J. C., Guenther, C., Volk, H. D., Grütz, G., Hirsch, D., Salat, C., et al. (2019). Treatment of advanced gastrointestinal cancer with genetically modified autologous mesenchymal stem cells: results from the phase 1/2 TREAT-ME-1 Trial. *Int. J. Cancer* 145, 1538–1546. doi: 10.1002/ijc.32230

Elahi, K. C., Klein, G., Avci-Adali, M., Sievert, K. D., Macneil, S., and Aicher, W. K. (2016). Human mesenchymal stromal cells from different sources diverge in their expression of cell surface proteins and display distinct differentiation patterns. *Stem Cells Int.* 2016:5646384. doi: 10.1155/2016/5646384

Eleuteri, S., and Fierabracci, A. (2019). Insights into the secretome of mesenchymal stem cells and its potential applications. *Int. J. Mol. Sci.* 20:4597. doi: 10.3390/ijms20184597

Elman, J. S., Murray, R. M., Wang, F., Shen, K., Gao, S., Conway, K. E., et al. (2014). Pharmacokinetics of natural and engineered secreted factors delivered by mesenchymal stromal cells. *PLoS One* 9:e89882. doi: 10.1371/journal.pone.0089882

Elzaouk, L., Moelling, K., and Pavlovic, J. (2006). Anti-tumor activity of mesenchymal stem cells producing IL-12 in a mouse melanoma model. *Exp. Dermatol.* 15, 865–874. doi: 10.1111/j.1600-0625.2006.00479.x

Gao, F., Chiu, S. M., Motan, D. A. L., Zhang, Z., Chen, L., Ji, H. L., et al. (2016). Mesenchymal stem cells and immunomodulation: current status and future prospects. *Cell Death Dis.* 7:e2062. doi: 10.1038/cddis.2015.327

Grisendi, G., Bussolari, R., Cafarelli, L., Petak, I., Rasini, V., Veronesi, E., et al. (2010). Adipose-derived mesenchymal stem cells as stable source of tumor necrosis factor-related apoptosis-inducing ligand delivery for cancer therapy. *Cancer Res.* 70, 3718–3729. doi: 10.1158/0008-5472.CAN-09-1865

Hass, R., Kasper, C., Böhm, S., and Jacobs, R. (2011). Different populations and sources of human mesenchymal stem cells (MSC): a comparison of adult and neonatal tissue-derived MSC. *Cell Commun. Signal.* 9:12. doi: 10.1186/1478-811X-9-12

Ho, I. A. W., Yulyana, Y., Sia, K. C., Newman, J. P., Guo, C. M., Hui, K. M., et al. (2014). Matrix metalloproteinase-1-mediated mesenchymal stem cell tumor tropism is dependent on crosstalk with stromal derived growth factor 1 / C-X-C chemokine receptor 4 axis. *FASEB J.* 28, 4359–4368. doi: 10.1096/fj.14-252551

Hofer, H. R., and Tuan, R. S. (2016). Secreted trophic factors of mesenchymal stem cells support neurovascular and musculoskeletal therapies. *Stem Cell Res. Ther.* 7, 1–14. doi: 10.1186/s13287-016-0394-0

Jeong, K., Lee, E., Kim, S. J., Yang, S., Sung, Y. C., and Seong, J. (2015). Irradiation-induced localization of IL-12-expressing mesenchymal stem cells to enhance the curative effect in murine metastatic hepatoma. *Int. J. Cancer* 137, 721–730. doi: 10.1002/ijc.29428

Jing, W., Chen, Y., Lu, L., Hu, X., Shao, C., Zhang, Y., et al. (2014). Human umbilical cord blood - derived mesenchymal stem cells producing il15 eradicate established pancreatic tumor in syngeneic mice human umbilical cord blood – derived mesenchymal stem cells producing il15 eradicate established pancreatic. *Mol. Cancer Ther.* 13, 2127–2137. doi: 10.1158/1535-7163.MCT-14-0175

Kanehira, M., Xin, H., Hoshino, K., Maemondo, M., Mizuguchi, H., Hayakawa, T., et al. (2007). Targeted delivery of NK4 to multiple lung tumors by bone marrow-derived mesenchymal stem cells. *Cancer Gene Ther.* 14, 894–903. doi: 10.1038/sj.cgt.7701079

Kern, S., Eichler, H., Stoeve, J., Klüter, H., and Bieback, K. (2006). Comparative analysis of mesenchymal stem cells from bone marrow, umbilical cord blood, or adipose tissue. *Stem Cells* 24, 1294–1301. doi: 10.1634/stemcells.2005-0342

Keshtkar, S., Azarpira, N., and Ghahremani, M. H. (2018). Mesenchymal stem cell-derived extracellular vesicles: novel frontiers in regenerative medicine. *Stem Cell Res. Ther.* 9:63. doi: 10.1186/s13287-018-0791-7

Kidd, S., Spaeth, E., Dembinski, J. L., Dietrich, M., Watson, K., Klopp, A., et al. (2009). Direct evidence of mesenchymal stem cell tropism for tumor and wounding microenvironments using *In vivo* bioluminescent imaging. *Stem Cells* 27, 2614–2623. doi: 10.1002/stem.187

Kim, S. M., Jeong, C. H., Woo, J. S., Ryu, C. H., Lee, J., and Jeun, S. (2016). *In vivo* near-infrared imaging for the tracking of systemically delivered mesenchymal stem cells: tropism for brain tumors and biodistribution. *Int. J. Nanomed.* 11, 13–23. doi: 10.2147/IJN.S97073

Leong, M. F., Lu, H. F., Lim, T. C., Du, C., Ma, N. K. L., and Wan, A. C. A. (2016). Electrospun polystyrene scaffolds as a synthetic substrate for xeno-free expansion and differentiation of human induced pluripotent stem cells. *Acta Biomater.* 46, 266–277. doi: 10.1016/j.actbio.2016.09.032

Liang, Y., Zhang, D., Li, L., Xin, T., Zhao, Y., and Ma, R. (2020). Exosomal MicroRNA-144 from bone marrow-derived mesenchymal stem cells inhibits

the progression of non-small cell lung cancer by targeting CCNE1 and CCNE2. *Stem Cell Res. Ther.* 11:87. doi: 10.1186/s13287-020-1580-7

Liu, B. Y., Soloviev, I., Chang, P., Lee, J., Huang, X., Zhong, C., et al. (2010). Stromal cell-derived factor-1/CXCL12 contributes to MMTV-Wnt1 tumor growth involving Gr1+CD11b+ cells. *PLoS One* 5:e8611. doi: 10.1371/journal.pone.0008611

Loebinger, M. R., Eddaoudi, A., Davies, D., and Janes, S. M. (2009). Mesenchymal stem cell delivery of TRAIL can eliminate metastatic cancer. *Cancer Res.* 69, 4134–4142. doi: 10.1158/0008-5472.CAN-08-4698

Loebinger, M. R., Sage, E. K., Davies, D., and Janes, S. M. (2010). TRAIL-expressing mesenchymal stem cells kill the putative cancer stem cell population. *Br. J. Cancer* 103, 1692–1697. doi: 10.1038/sj.bjc.6605952

Lulla, R. R., Goldman, S., Yamada, T., Beattie, C. W., Bressler, L., Pacini, M., et al. (2016). Phase 1 trial of P28 (NSC745104), a Non-HDM2-mediated peptide inhibitor of P53 ubiquitination in pediatric patients with recurrent or progressive central nervous system tumors: a pediatric brain tumor consortium study. *Neuro Oncol.* 18, 1319–1325. doi: 10.1093/neuonc/now047

Madeira, C., Ribeiro, S. C., Pinheiro, I. S. M., Martins, S. A. M., Andrade, P. Z., Silva, C. L., et al. (2011). Gene delivery to human bone marrow mesenchymal stem cells by microporation. *J. Biotechnol.* 151, 130–136. doi: 10.1016/j.jbiotec.2010.11.002

Markell, L. M., Hogan, K. A., Yuspa, S. H., and Glick, A. B. (2010). Transforming growth factor b 1 enhances tumor promotion in mouse skin carcinogenesis. *Carcinogenesis* 31, 1116–1123. doi: 10.1093/carcin/bgq041

Maskarinec, G., Ju, D., Shvetsov, Y. B., Horio, D., Chan, O., Loo, L. W. M., et al. (2020). Breast tumor tissue in Fl ammation but not lobular involution is associated with survival among breast cancer patients in the multiethnic cohort. *Cancer Epidemiol.* 65:101685. doi: 10.1016/j.canep.2020.101685

Mathew, A. S., Naik, C., Cahill, P. A., and Bhonde, R. R. (2019). Placental mesenchymal stromal cells as an alternative tool for therapeutic angiogenesis. *Cell. Mol. Life Sci.* 77, 253–265. doi: 10.1007/s00018-019-03268-1

Matuskova, M., Baranovicova, L., Kozovska, Z., Durinikova, E., Pastorakova, A., and Hunakova, L. (2012). Intrinsic properties of tumour cells have a key impact on the bystander effect mediated by genetically engineered mesenchymal stromal cells. *J. Gene Med.* 14, 776–787. doi: 10.1002/jgm

Mounayar, M., Magee, C. N., and Abdi, R. (2013). Immunomodulation by mesenchymal stem cells - a potential therapeutic strategy for type 1 diabetes. *Diabetes* 57, 1759–1767. doi: 10.1515/97831102983 07.309

Murray, I. R., and Péault, B. (2015). Q&A: mesenchymal stem cells – where do they come from and is it important? *BMC Biol.* 13:99. doi: 10.1186/s12915-015-0212-7

Nowakowski, A., Walczak, P., Lukomska, B., and Janowski, M. (2016). Genetic engineering of mesenchymal stem cells to induce their migration and survival. *Stem Cells Int.* 2016:4956063. doi: 10.1155/2016/4956063

Oieni, J., Levy, L., Khait, N. L., Yosef, L., Schoen, B., Fliman, M., et al. (2019). Nano-ghosts: biomimetic membranal vesicles, technology and characterization. *Methods* 1, 126–134. doi: 10.1016/j.ymeth.2019.11.013

Qiao, B., Shui, W., Cai, L., Guo, S., and Jiang, D. (2015). Human mesenchymal stem cells as delivery of osteoprotegerin gene: homing and therapeutic effect for osteosarcoma. *Drug Des. Dev. Ther.* 9, 969–976. doi: 10.2147/DDDT.S77116

Qiu, J., Liu, B., Tian, C., Pavlakis, G. N., and Yu, X. F. (2000). Enhancement of primary and secondary cellular immune responses against human immunodeficiency virus type 1 Gag by using DNA expression vectors that target gag antigen to the secretory pathway. *J. Virol.* 74, 5997–6005. doi: 10.1128/jvi.74.13.5997-6005.2000

Rahmatizadeh, F., Aziz, S. G., Khodadadi, K., and Ataei, M. L. (2019). Bidirectional and opposite effects of naïve mesenchymal stem cells on tumor growth and progression. *Tabriz Univ. Med. Sci.* 9, 539–558. doi: 10.15171/apb.2019.063

Rebelatto, C. K., Aguiar, A. M., Moretão, M. P., Senegaglia, A. C., Hansen, P., Barchiki, F., et al. (2008). Dissimilar differentiation of mesenchymal stem cells from bone marrow, umbilical cord blood, and adipose tissue. *Exp. Biol. Med.* 233, 901–913. doi: 10.3181/0712-rm-356

Ren, C., Kumar, S., Chanda, D., Chen, J., Mountz, J. D., and Ponnazhagan, S. (2008). Therapeutic potential of mesenchymal stem cells producing IFN- α in a mouse melanoma lung metastasis model. *Stem Cells* 26, 2332–2338. doi: 10.1634/stemcells.2008-0084.Therapeutic

Rifai, A., Nguyen, P., Bouland, N., Terryn, C., Kanagaratnam, L., Poitevin, G., et al. (2019). *In vivo* efficacy of endothelial growth medium stimulated mesenchymal stem cells derived from patients with critical limb ischemia. *J. Transl. Med.* 17:261. doi: 10.1186/s12967-019-2003-3

Rossignoli, F., Spano, C., Grisendi, G., Foppiani, E. M., Golinelli, G., Mastrolia, I., et al. (2019). MSC-delivered soluble TRAIl and paclitaxel as novel combinatory treatment for pancreatic adenocarcinoma. *Theranostics* 9, 436–448. doi: 10.7150/thno.27576

Sahin, A. O., and Buitenhuis, M. (2012). Molecular mechanisms underlying adhesion and migration of hematopoietic stem cells. *Cell Adh. Migr.* 6, 39–48. doi: 10.4161/cam.18975

Santos, F., Andrade, P. Z., Boura, J., Abecasis, M. M., da Silva, C. L., and Cabral, J. M. S. (2009). Ex vivo expansion of human mesenchymal stem cells: a more effective cell proliferation kinetics and metabolism under hypoxia. *J. Cell Physiol.* 223, 27–35. doi: 10.1002/jcp.21987

Song, C., and Li, G. (2011). CXCR4 and matrix metalloproteinase-2 are involved in mesenchymal stromal cell homing and engraftment to tumors. *Cytotherapy* 13, 549–561. doi: 10.3109/14653249.2010.542457

Soure, M., Fernandes-Platzgummer, A., Moreira, F., Lilaia, C., Liu, S., Ku, C., et al. (2016). Integrated culture platform based on a human platelet lysate supplement for the isolation and scalable manufacturing of umbilical cord matrix-derived mesenchymal stem / stromal cells. *J. Tissue Eng. Regener. Med.* 11, 1630–1640. doi: 10.1002/term

Spano, C., Grisendi, G., Golinelli, G., Rossignoli, F., Prapa, M., Bestagno, M., et al. (2019). Soluble TRAIL armed human MSC as gene therapy for pancreatic cancer. *Sci. Rep.* 9, 1–14. doi: 10.1038/s41598-018-37433-6

Ursula, A., Jana, J., Katarina, B., Petra, P., Martin, P., Pavel, P., et al. (2019). Prodrug suicide gene therapy for cancer targeted intracellular by mesenchymal stem cell exosomes. *Int. J. Cancer* 144, 897–908. doi: 10.1002/ijc.31792

Vera, N., Acuña-Gallardo, S., Grünenwald, F., Caceres-Verschae, A., Realini, O., Acuña, R., et al. (2019). Small extracellular vesicles released from ovarian cancer spheroids in response to cisplatin promote the pro-tumorigenic activity of mesenchymal stem cells. *Int. J. Mol. Sci.* 20:4972. doi: 10.3390/ijms20204972

Wang, Y., Wang, H., Pan, T., Li, L., Li, J., and Yang, H. (2017). STIM1 silencing inhibits the migration and invasion of A549 cells. *Mol. Med. Rep.* 14, 3283–3289. doi: 10.3892/mmr.2017.7010

Xia, C., Wang, T., Cheng, H., Dong, Y., Weng, Q., Sun, G., et al. (2020). Mesenchymal stem cells suppress leukemia via macrophage- mediated functional restoration of bone marrow microenvironment. *Leukemia*. doi: 10.1038/s41375-020-0775-3

Xia, L., Peng, R., Leng, W., Jia, R., Zeng, X., Yang, X., et al. (2015). TRAIL-expressing gingival-derived mesenchymal stem cells inhibit tumorigenesis of tongue squamous cell carcinoma. *J. Dent. Res.* 94, 219–228. doi: 10.1177/0022034514557815

Xie, L., Zhang, N., Marsano, A., Vunjak-Novakovic, G., Zhang, Y., and Lopez, M. J. (2013). *In vitro* mesenchymal trilineage differentiation and extracellular matrix production by adipose and bone marrow derived adult equine multipotent stromal cells on a collagen scaffold. *Stem Cell Rev. Rep.* 9, 858–872. doi: 10.1007/s12015-013-9456-1

Xin, H., Kanehira, M., Mizuguchi, H., Takao, H., Toshiaki, K., Nukiwa, T., et al. (2007). Targeted delivery of CX3CL1 to multiple lung tumors by mesenchymal stem cells. *Stem Cells* 25, 1618–1626. doi: 10.1634/stemcells.2006-0461

Yamada, T., Das Gupta, T. K., and Beattie, C. W. (2016). p28-Mediated activation of P53 in G2/M phase of the cell cycle enhances the efficacy of DNA damaging and antimitotic chemotherapy. *Cancer Res.* 76, 2354–2365. doi: 10.1158/0008-5472.CAN-15-2355

Yamada, T., Hiraoka, Y., Ikehata, M., Kimbara, K., Avner, B. S., Das Gupta, T. K., et al. (2004). Apoptosis or growth arrest: modulation of tumor suppressor P53 's specificity by bacterial redox protein azurin. *Proc. Natl. Acad. Sci. U.S.A.* 101, 4770–4775. doi: 10.1073/pnas.0400899101

Yan, C., Yang, M., Li, Z., Li, S., Hu, X., Fan, D., et al. (2014). Suppression of orthotopically implanted hepatocarcinoma in mice by umbilical cord-derived mesenchymal stem cells with STRAIL gene expression driven by AFP promoter. *Biomaterials* 35, 3035–3043. doi: 10.1016/j.biomaterials.2013.12.037

Zhao, R. C. (2013). *Essentials of Mesenchymal Stem Cell Biology and Its Clinical Translation*. Dordrecht: Springer Netherlands. doi: 10.1007/978-94-007-6716-4

Zhu, Y., Sun, Z., Han, Z., Liao, L., Wang, J., Bian, C., et al. (2009). Human mesenchymal stem cells inhibit cancer cell proliferation by secreting DKK-1. *Leukemia* 23, 925–933. doi: 10.1038/leu.2008.384

Conflict of Interest: The authors declare that the research was conducted in the absence of any commercial or financial relationships that could be construed as a potential conflict of interest.

frontiers in Cell and Developmental Biology

REVIEW
published: 22 July 2020
doi: 10.3389/fcell.2020.00612

Crosstalk Between the Hepatic and Hematopoietic Systems During Embryonic Development

Francisca Soares-da-Silva[1,2,3,4,5,6†], *Márcia Peixoto*[1,2,3,4,5,6†], *Ana Cumano*[4,5,6] *and Perpetua Pinto-do-Ó*[1,2,3*]

[1] *Instituto de Investigação e Inovação em Saúde, Universidade do Porto, Porto, Portugal,* [2] *Instituto Nacional de Engenharia Biomédica, Universidade do Porto, Porto, Portugal,* [3] *Instituto de Ciências Biomédicas Abel Salazar, Universidade do Porto, Porto, Portugal,* [4] *Lymphocytes and Immunity Unit, Immunology Department, Pasteur Institute, Paris, France,* [5] *INSERM U1223, Paris, France,* [6] *Université Paris Diderot, Sorbonne Paris Cité, Paris, France*

OPEN ACCESS

Edited by:
Joana Paiva Miranda, University of Lisbon, Portugal

Reviewed by:
Kenichi Miharada, Lund University, Sweden
Sandra Pinho, University of Illinois at Chicago, United States

***Correspondence:**
Perpetua Pinto-do-Ó
perpetua@ineb.up.pt

[†] *These authors have contributed equally to this work*

Specialty section:
This article was submitted to Stem Cell Research, a section of the journal Frontiers in Cell and Developmental Biology

Received: *21 April 2020*
Accepted: *19 June 2020*
Published: *22 July 2020*

Citation:
Soares-da-Silva F, Peixoto M, Cumano A and Pinto-do-Ó P (2020) Crosstalk Between the Hepatic and Hematopoietic Systems During Embryonic Development. Front. Cell Dev. Biol. 8:612. doi: 10.3389/fcell.2020.00612

Hematopoietic stem cells (HSCs) generated during embryonic development are able to maintain hematopoiesis for the lifetime, producing all mature blood lineages. HSC transplantation is a widely used cell therapy intervention in the treatment of hematologic, autoimmune and genetic disorders. Its use, however, is hampered by the inability to expand HSCs *ex vivo*, urging for a better understanding of the mechanisms regulating their physiological expansion. In the adult, HSCs reside in the bone marrow, in specific microenvironments that support stem cell maintenance and differentiation. Conversely, while developing, HSCs are transiently present in the fetal liver, the major hematopoietic site in the embryo, where they expand. Deeper insights on the dynamics of fetal liver composition along development, and on how these different cell types impact hematopoiesis, are needed. Both, the hematopoietic and hepatic fetal systems have been extensively studied, albeit independently. This review aims to explore their concurrent establishment and evaluate to what degree they may cross modulate their respective development. As insights on the molecular networks that govern physiological HSC expansion accumulate, it is foreseeable that strategies to enhance HSC proliferation will be improved.

Keywords: hematopoietic stem cells, fetal liver, fetal liver microenvironment, fetal hematopoiesis, hematopoietic stem cell expansion, hematopoietic stem cell niche, self-renewal, cytokine signaling

INTRODUCTION

In the adult organism, hematopoietic stem cells (HSCs) constitute a rare and largely quiescent cell population residing in the bone marrow (BM) (Cheshier et al., 1999). The current dogma states that HSCs self-renew to maintain their pool throughout life and reenter cell cycle in response to stress (Wilson et al., 2008). The balance between self-renewal and differentiation in adult BM has been extensively studied, with the identification of different cellular niches and molecular cues as important elements in HSC maintenance and differentiation – reviewed in Crane et al. (2017) and Pinho and Frenette (2019).

During ontogeny, HSCs undergo a high proliferative stage, expanding in the fetal liver (FL), one of the anatomical locations of embryonic hematopoiesis (Ema and Nakauchi, 2000). Therefore, it has long been assumed that the hepatic microenvironment may drive the proliferation of HSCs while sustaining their primary "stemness" hallmark (functional capacity to reconstitute the hematopoietic compartment of irradiated recipients). So far, however, limited information is available on an HSC supportive environment in the FL and the mechanisms conveying these functional properties remain elusive, hindering effective translation into clinical applications.

A thorough dissection of the architecture and cellular organization of the liver is critical to elucidate the nature of the hematopoietic FL niche and disclose the elements (soluble and/or cell-bound signals, cell-cell contact, cell-matrix interactions, physical properties, etc.) contributing for the regulation of HSCs. This review aims to discuss the role of the FL stroma (encompassing all non-hematopoietic FL cells) and explore the interplay of the two fetal systems – hepatic and hematopoietic – in mouse (or otherwise stated) and how they mutually influence their development.

THE EMERGENCE OF THE HEMATOPOIETIC SYSTEM DURING EMBRYOGENESIS

The adult hematopoietic system relies on a robust process whereby HSCs divide and differentiate generating all mature blood lineages. In physiological conditions, this process takes place in the BM in both humans and mice. Even though adult hematopoiesis occurs in the BM, this is merely the end-site of an otherwise thrilling journey through different anatomic locations (**Figure 1**).

The first hematopoietic cells emerge in the yolk sac (YS) in extra-embryonic structures named blood islands at around embryonic day (E) 7.5 in mice and 2–3 weeks post-conception (wpc) in humans (Bloom and Bartelmez, 1940; Palis et al., 1999). Primitive erythroid progenitors (EryP) generate primitive erythrocytes, large nucleated cells that express embryonic globins (Kingsley et al., 2006), which are found in circulation after the onset of cardiac contractions at E8.25 (∼3 wpc in humans) (Ji et al., 2003; Tavian et al., 1999) and oxygenate the developing embryo. Myeloid progenitors such as macrophage colony-forming cells or megakaryocyte colony-forming cells are also represented during early stages, concomitantly with EryP (Palis et al., 1999), suggesting that primitive hematopoiesis is limited to these three lineages.

Around 24 h later, at E8.5 (4–5 wpc in humans), a second wave of hematopoiesis initiates, with erythro-myeloid progenitors (EMPs) (Migliaccio et al., 1986; Bertrand et al., 2005b) emerging in the vascular plexus of the YS, in a process denominated endothelial to hematopoietic transition (EHT) (Frame et al., 2016; Kasaai et al., 2017). EMPs proliferate and differentiate in the YS into erythroid and myeloid cells but can also be identified in circulation and in the developing liver at later stages (E10.5) via surface expression of c-Kit, CD16/32 and low levels of CD45 (McGrath et al., 2015). These progenitors generate the first definitive erythrocytes, megakaryocytes, macrophages and other myeloid lineages such as neutrophils, granulocytes and mast cells, but lack HSC activity (Palis et al., 1999; McGrath et al., 2015). Although EMPs are a transient population at early stages of embryonic development, they generate different tissue-resident macrophages that, depending on the organ, can persist throughout adulthood (Gomez-Perdiguero et al., 2015), mast cells that are maintained until birth (Gentek et al., 2018), and are the major producers of erythrocytes throughout embryonic life (Soares-da-Silva et al., 2020, Preprint).

A third wave of hematopoiesis occurs between E9.5-E11 in mice (∼4 wpc in humans), with HSCs emergence in the aorta-gonads-mesonephros (AGM) region (Cumano et al., 1996; Medvinsky et al., 1996; Tavian et al., 1996) through EHT (Bertrand et al., 2010; Kissa and Herbomel, 2010). After generation, immature HSCs (imHSCs) undergo a maturation process as they migrate to the FL (Taoudi et al., 2008; Kieusseian et al., 2012) where they proliferate [expanding in numbers by >30-fold (Ema and Nakauchi, 2000)] and differentiate into all blood lineages: erythroid, myeloid and lymphoid. HSCs can be defined by their ability to provide long-term multilineage hematopoietic reconstitution (LTR) when transplanted to lethally irradiated mice (Morrison et al., 1995) and further repopulate secondary recipients. These cells can be found within the $Lin^{-}CD45^{+}Sca1^{+}c\text{-}Kit^{+}$ (LSK) compartment and be further divided according to their reconstitution ability in long-term (LSK $CD150^{+}CD48^{-}$ LT-HSC) or short-term (LSK $CD150^{-}CD48^{-}$ ST-HSC) reconstituting cells (Kim et al., 2006). Downstream progenitors of HSCs such as multipotent progenitors (MPPs), lympho-myeloid-primed progenitors (LMPPs), common lymphoid progenitors (CLPs) and common myeloid progenitors (CMPs) can also be found in FL and are responsible for the seeding of other hematopoietic organs such as the thymus (Ramond et al., 2014). Although adult and embryonic HSCs have similar lineage potentials, some lymphoid lineages are only produced during embryonic development, namely dendritic epidermal T cells (Ikuta et al., 1990), lymphoid tissue–inducer cells (Eberl et al., 2004), and a subset of IL-17-producer γδ T cells (Haas et al., 2012). Embryonic hematopoiesis also takes place in the placenta, starting at E10.5-E11 (∼6 wpc in humans) and declining at around E15.5 (Gekas et al., 2005; Ottersbach and Dzierzak, 2005; Robin et al., 2009). HSCs and other progenitors are also found in the fetal spleen after E15.5 (Christensen et al., 2004), even though without evidence for significant expansion and mostly differentiating into the macrophage lineage (Bertrand et al., 2006). At around E16.5 (∼10 wpc in humans) HSCs migrate to the BM, where they are maintained through adulthood (Charbord et al., 1996; Christensen et al., 2004). In the adult, BM HSCs are largely quiescent (Cheshier et al., 1999) and only divide to maintain the stem cell pool, while the replenishment of blood lineages appears to be guaranteed by downstream MPPs (Sun et al., 2014; Busch et al., 2015; Pei et al., 2017; Rodriguez-Fraticelli et al., 2018).

Thus, embryonic hematopoiesis is characterized by an overlap in time and space of three waves with distinct anatomical origins

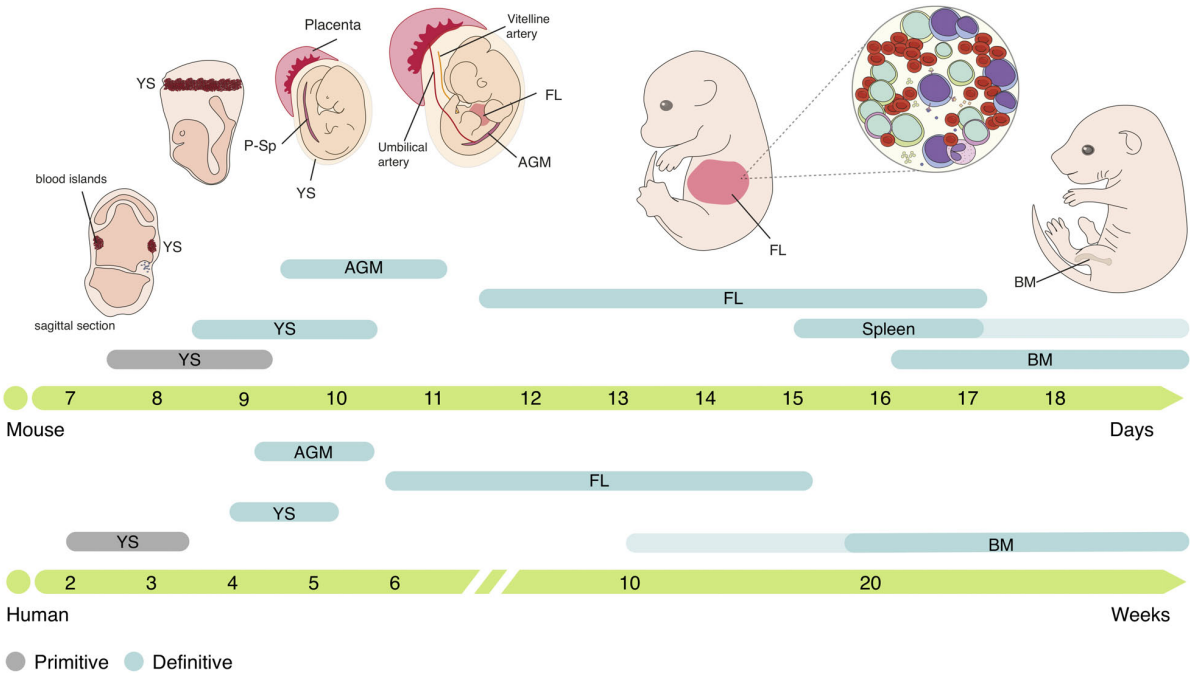

FIGURE 1 | Ontogeny of the hematopoietic system in mouse and human. Embryonic hematopoiesis is established in three distinct waves. The first hematopoietic cells emerge in YS blood islands, generating primitive erythrocytes, macrophages and megakaryocytes, constituting the primitive hematopoietic wave. The second hematopoietic wave initiates in the vascular plexus of the YS, generating EMPs that produce definitive erythrocytes, megakaryocytes, macrophages, neutrophils, granulocytes and mast cells, but lacks HSC activity. EMPs are the origin of tissue-resident macrophages that can persist throughout life. HSCs emerge in the AGM region and migrate to the FL, the major embryonic hematopoietic organ. In FL, HSCs expand and differentiate into all mature blood cell lineages. Small numbers of hematopoietic progenitors also colonize the fetal spleen and are still found few weeks after birth. Migration to the BM, where HSCs reside through adulthood, occurs as a continuous process and, in humans, can take several weeks. YS, yolk sac; P-Sp para-aortic splanchnopleura; FL, fetal liver; AGM, aorta-gonads-mesonephros; BM, bone marrow.

and lineage potential. All waves converge to the FL, the major hematopoietic organ during embryogenesis.

THE COLONIZATION OF THE FL BY THE HEMATOPOIETIC SYSTEM

Which Cells Are Present When Hematopoietic Progenitors Arrive?

As the embryo gastrulates and folds, endoderm envelops the YS ultimately forming a hollow structure, the primitive gut tube, subsequently patterned into foregut, midgut and hindgut regions. The foregut, located in the anterior endoderm, adjacent to the developing heart, generates the liver, alongside with the lungs, thyroid, and pancreas (Tremblay and Zaret, 2005). Embryonic liver development starts at around E8.5-E9 (∼4 wpc in humans) with the formation of the hepatic diverticulum, an extension of the ventral foregut epithelium that invades the septum transverse mesenchyme (STM) and forms a liver bud, by E9.5 (Severn, 1971; Wilson et al., 2006). The liver bud originates from a single-sheet of columnar endodermal epithelium with a gut morphology (**Figure 2A**), which then transitions to pseudostratified epithelial hepatoblasts (**Figure 2B**; Bort et al., 2006). At this stage, these cells are separated from the STM by a basement membrane rich in laminin and composed of other extracellular matrix (ECM) molecules, such as nidogen, type IV collagen, fibronectin, and heparan sulfate proteoglycan (Shiojiri and Sugiyama, 2004). A process of extensive hepatoblast proliferation follows, during which the cells outgrow the liver bud, disrupting the basement membrane, into the STM (**Figure 2C**; Douarin, 1975). The other constituents of the organ, sinusoidal endothelial cells (SECs), mesothelial, sub-mesothelial and hepatic stellate cells have a mesoderm origin (reviewed by Yang et al., 2019), as described below. Angioblasts or endothelial progenitor cells are found delimiting the basement membrane (**Figure 2A**), resembling a loose "necklace" of cells, and were shown to promote liver organogenesis. In Flk-$1^{-/-}$ mutant embryos, which lack endothelial cells, hepatic specification occurs, but proliferation and migration into the STM are impaired (Matsumoto et al., 2001). At E10.5–E11.0 (∼5–6 wpc in humans), hematopoietic cells colonize the FL that rapidly becomes the major fetal hematopoietic organ (Johnson and Moore, 1975; Migliaccio et al., 1986; Palis et al., 2001).

Hepatoblasts

Hepatoblasts are bipotent immature FL cells that differentiate into hepatocytes – the hepatic parenchyma main constituent – or cholangiocytes – the biliary epithelial cells. At the onset

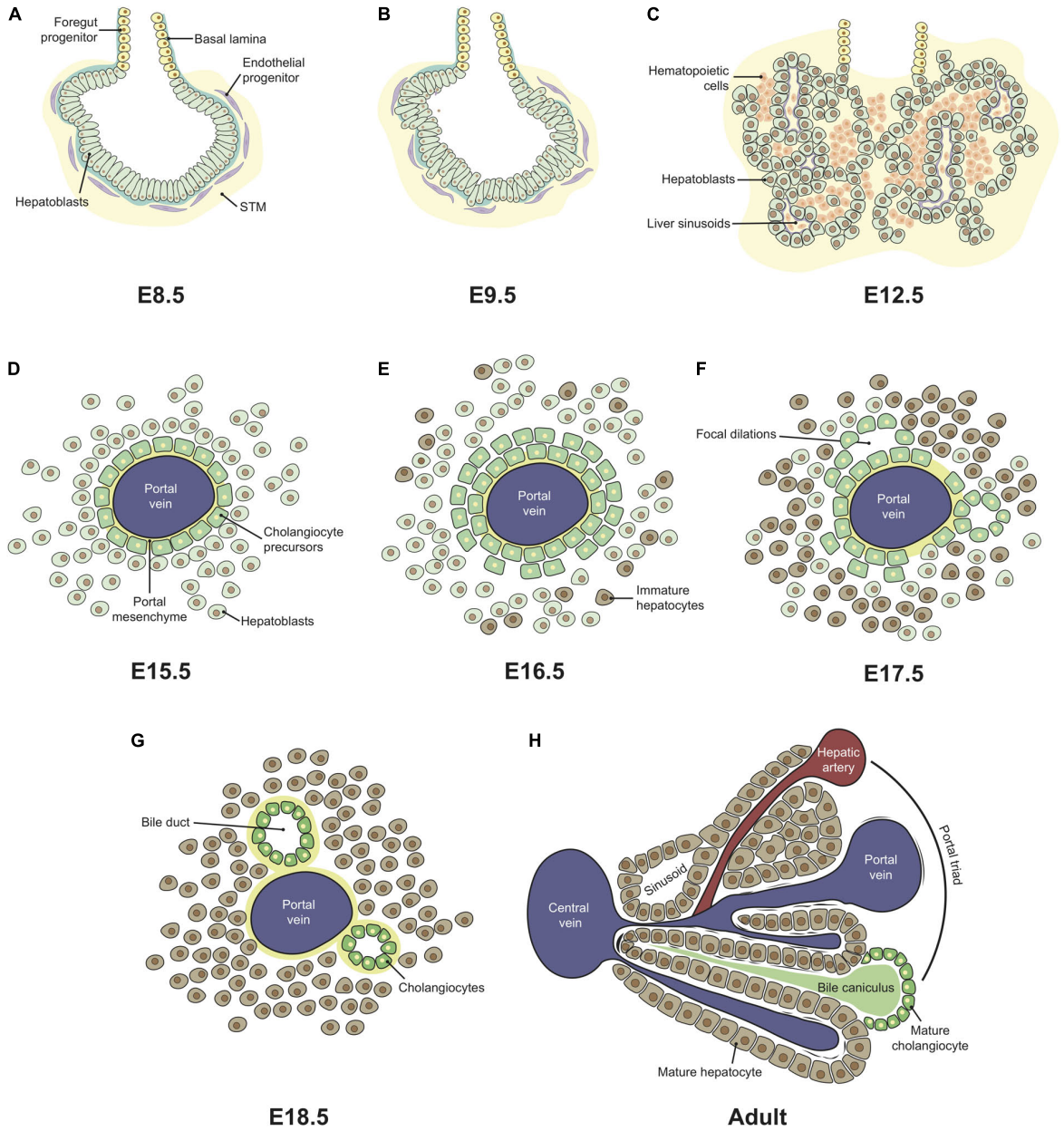

FIGURE 2 | Ontogeny of the fetal liver. Liver development is initiated with the formation of the hepatic diverticulum at E8.5 **(A)**. The single layer of columnar endodermal epithelial cells **(A)** thickens and transitions to a pseudostratified epithelium, followed by the delamination and migration of hepatoblasts into the STM, forming the liver bud by E9.5 **(B)**. Extensive hepatoblast proliferation follows, originating hepatic chords intermingled with the hepatic mesenchyme and surrounding the sinusoids, formed from pre-existing vitelline vessels. From E10.5, hematopoietic cells colonize the FL that rapidly becomes the major fetal hematopoietic organ up until E15.5 **(C)**. From E12.5-E15.5, the FL continues to enlarge, expanding both hematopoietic and hepatic compartments. Structural changes are only evident after hepatoblast-to-cholangiocyte specification occurs around the portal vessels, forming a monolayered ductal plate **(D)** that evolves into a bi-layer at E16.5 **(E)**. Focal dilations **(F)** evolve into bile duct structures in late gestation **(G)**. Portal triads characterize adult liver architecture where a hepatic artery, a portal vein and a bile duct form a complex structure, and a central vein, to which plates of hepatocytes lined by sinusoids converge **(H)**. This architecture is only recognizable few weeks after birth. STM, septum transversum mesenchyme.

of liver development, bipotent hepatoblasts express the liver-specific transcription factors (TFs) hematopoietically-expressed homeobox protein (HHEX) (Bogue et al., 2000), prospero homeobox protein 1 (PROX1) (Dudas et al., 2004), and co-express the hepatocytes' markers alpha-fetoprotein (AFP), albumin (ALB) (Cascio and Zaret, 1991), cytokeratin 18 (CK18) (Tanimizu et al., 2003), hepatocyte nuclear factor 4α (HNF4α) (Li et al., 2000) and cholangiocytes' markers such as cytokeratin 19 (CK19) (Tanimizu et al., 2004). Other typical hepatoblast markers are listed in **Table 1**.

TABLE 1 | Fetal liver non-hematopoietic compartment: cell types and associated markers.

Cell type	Gene expression	Markers used for isolation
Hepatoblasts	*Hhex, Prox1, Alb, Afp, Ck8, Ck18, Ck19, Met, Hnf6, Oc2, Hnf4a, Ttr, Foxm1, Foxa2, Tbx3, Dlk1, Lgr5, Epcam, Cdh1, Trgb1, Itga6, Liv2, Prom1, Anpep*	DLK1$^+$ (Tanimizu et al., 2003; Tan et al., 2017) E-Cadherin$^+$ (Nitou et al., 2002; Nierhoff et al., 2005) EpCAM$^+$DLK1$^+$ (Tanaka et al., 2009) Liv2$^+$CD31$^-$CD45$^-$Lgr5-eGFP$^+$ (Prior et al., 2018) Ter119$^-$CD45$^-$c-Kit$^-$CD49f$^+$CD29$^+$ (Suzuki et al., 2000) VCAM1$^+$ALCAM$^+$DLK1$^+$ (Tsuneto et al., 2013) Ter119$^-$CD45$^-$CD51$^+$VCAM1$^+$PDGFRα$^-$ (Brouard et al., 2017)
Hepatocytes	*Alb, Afp, Ttr, G6p, Apoa1, Apoh Por, Cps1*	–
Cholangiocytes	*Sox9, Hnf6, Oc2, Spp1, Ck19, Epcam, Krt7*	EpCAM$^+$ (Yang et al., 2017)
Endothelial cells	*Flk1, Flt1, Ve-cadh, Pecam1, Mcam, Tek, Tie, Lyve1, Kdr*	CD45$^-$Ter119$^-$CD31$^+$ (Khan et al., 2016) DLK1$^-$CD45$^-$Ter119$^-$CD31$^+$LYVE-1$^+$ and DLK1$^-$CD45$^-$Ter119$^-$CD31$^+$LYVE-1$^-$ (Tan et al., 2017)
Mesothelial cells	*Cytokeratin, Cd200, Gpm6a, Alcam, Gp38, Wt1, Podxl, Msln*	Flk1$^-$PODXL^{high} (Onitsuka et al., 2010)
Sub-mesothelial cells	*Alcam, Desmin, Nestin, p75tnr, Pdgfra, Wt1*	–
Hepatic stellate cells	*Vimentin, Acta2, Desmin, p75NTR, Foxf1, Lhx2, Hlx*	DLK1$^-$Ter119$^-$CD45$^-$CD31$^-$LYVE-1$^-$p75NTR$^+$ (Tan et al., 2017)
Pericytes	*NG2, Nestin, Vimentin, Acta2, Pdgfra, Pdgfrb, Dlk1, Itgav, Endoglin, Vcam, Mcam, Nr2f2*	Ter119$^-$CD45$^-$CD31$^-$Nestin$^+$NG2$^+$ (Khan et al., 2016) CD45$^-$CD56$^-$CD34$^-$CD146$^+$[1] (Gerlach et al., 2012)

[1] *Study performed in humans.*

Different markers have been used to isolate hepatoblasts, namely delta like non-canonical Notch ligand [DLK1 or preadipocyte factor 1 (Pref-1)] (Tanimizu et al., 2003), epithelial cadherin (E-cadherin) or CD324 (Nitou et al., 2002), epithelial cell adhesion molecule (EpCAM) or CD326 (Tanaka et al., 2009), and leucine-rich repeat-containing G-protein coupled receptor 5 (LGR5) (Prior et al., 2018). DLK1 is strongly expressed by hepatoblasts in the E10.5 liver bud and continues to be highly expressed until around E16.5, being significantly downregulated thereafter and absent in mature hepatocytes and cholangiocytes (Tanimizu et al., 2003; Tanaka et al., 2009). E-Cadherin, present at the onset of liver outgrowth, is downregulated by the time hepatoblasts migrate to the STM, disrupting the epithelial sheet, although it can be used as a hepatoblast-specific marker after E12.5 (Nitou et al., 2000; Margagliotti et al., 2007). Transient EpCAM expression labels newly formed hepatoblasts but is significantly reduced after E12, while expression after E16 specifically labels bile duct cells (Tanaka et al., 2009). Recently, combining multicolor clonal genetic lineage tracing, organoid cultures and analysis of single-cell RNA sequencing, LGR5 was shown to mark a subpopulation of *bonafide* bipotential hepatoblasts at E9.5–E10 as the origin of the hepatoblast pool (Prior et al., 2018).

Endothelial Cells

The main blood vessels in the adult liver are the portal and central veins and the hepatic artery. Up until birth, the hepatic artery is absent and embryonic circulation is sustained by a transient afferent vascular system, the extraembryonic umbilical and vitelline veins (Collardeau-Frachon and Scoazec, 2008). The portal vein arises early in the liver development, between E10.5–E12.5 in mouse (4–6 wpc in human) (Collardeau-Frachon and Scoazec, 2008; Swartley et al., 2016). The hepatic sinusoids are the first vessels to appear, by E10–E10.5, originating from the pre-existing vitelline vessels. The latter sprouts throughout the STM, by angiogenesis, receiving signals from the surrounding mesenchyme (**Figure 2C**; Swartley et al., 2016). Hepatoblasts were also identified as a positive stimulator of sinusoid morphogenesis and maturation (Takabe et al., 2012). Stabilin 2 (STAB-2) and lymphatic vessel endothelial hyaluronan receptor 1 (LYVE-1) (commonly used as a marker of lymphatics) – hyaluronan receptors – start to be expressed in SECs at E9.5 and E10.5, respectively, and continue to be expressed thereafter (Nonaka et al., 2007; Takabe et al., 2012). Of note, lymphatic vessels were only reported after birth (Swartley et al., 2016). At E9.5, endothelial cells located around the liver diverticulum (**Figure 2A**) express both CD31/PECAM-1 and Flk-1 (Sugiyama et al., 2010b). CD31 and Flk1 expression in SECs is strong in the early stages of liver development, but is downregulated with time. In adult livers, endothelial cells of portal and hepatic veins strongly express CD31, while it is absent or weakly detected in SECs (Sugiyama et al., 2010b; Takabe et al., 2012). Primitive SECs also strongly express Flk-1, contrarily to endothelial cells of portal and hepatic veins (Sugiyama et al., 2010b). During embryonic liver development, portal vessels express the arterial markers Ephrin-B2 and Neuropilin-1, but not the venous marker EphB4. This expression profile is inverted at the end of gestation, with the transition into a venular phenotype (Wang et al., 1998; Khan et al., 2016). Liver endothelial cells constitute a heterogeneous cellular compartment and different markers should be used for their identification according to vascular location and developmental stage.

Mesothelial and Sub-Mesothelial Cells

Mesothelial cells (MCs) compose a single epithelial layer (mesothelium) lining the liver parenchyma on the surface of lobes. From E12.5, MCs are characterized by the expression of cytokeratin, CD200, glycoprotein M6A (GPM6A), podoplanin (PDPN/Gp38), podocalyxin-like protein 1 (PODXL), and mesothelin (MSLN) (Lua and Asahina, 2016). PODXL is highly expressed in immature MCs, being downregulated during development, while MSLN is upregulated. MCs proliferate during liver development and remain quiescent after birth. Wilm's tumor-1 (WT1) is mainly expressed by MCs (Onitsuka et al., 2010). $WT1^{-/-}$ embryos show incomplete lobulation compared to control littermates at E13.5, reduced numbers of $Flk1^{-}PODXL^{high}$ MCs, $DLK1^{+}$ hepatoblasts, and total FL cells, suggesting that hepatic development was impaired due to defective MCs (Ijpenberg et al., 2007; Onitsuka et al., 2010). This is supported by the observation that fetal MCs express growth factors (PTN, MDK, and HGF) involved in hepatic development (Onitsuka et al., 2010).

Underneath the MC sheet lays a population of cells expressing Desmin, Nerve growth factor receptor (NGFR/p75NTR) and platelet-derived growth factor receptor α (PDGFRα/CD140a), associated with type IV collagen of the basal lamina, commonly referred as "sub-mesothelial cells" (sub-MC) or capsular fibroblasts. The expression of activated leukocyte cell adhesion molecule (ALCAM/CD166) and WT1 was also observed in MC and sub-MC around E11–E14 and, before that, in the STM by E9–E10 (Asahina et al., 2011; Lua and Asahina, 2016).

Hepatic Stellate Cells and/or Pericytes

Although the terms hepatic stellate cells and pericytes have been used by many authors as synonyms, it is not consensual they represent the same population. In adult liver, there is a population of perisinusoidal cells residing in the space of Disse between hepatocytes and SECs, that stores vitamin D lipids (Wake, 1971), and is a major player in liver fibrogenesis (Guyot et al., 2006). MesP1-expressing mesoderm has been considered its earliest ancestry, as it gives rise to the STM – the origin of the liver mesothelium and mesenchymal cells. Migration inward of MC and sub-MC from the liver surface is assumed to give rise to hepatic stellate cells and perivascular mesenchymal cells (Asahina, 2012). Hepatic stellate cells express Desmin, p75NTR, but not the MC markers ALCAM, WT1, and Gp38 (Asahina et al., 2010).

Gerlach et al. (2012) isolated $CD146^{+}CD45^{-}CD56^{-}CD34^{-}$ cells from fetal and adult human livers and identified them as pericytes, a distinct population from hepatic stellate cells. They showed that these cells express NG2 and vimentin, but not GFAP *in situ*, and are found around periportal but not pericentral blood vessels neither within the space of Disse. These cells exhibit high osteogenic and myogenic, but low adipogenic or chondrogenic differentiation potential, in *in vitro* differentiation assays. In mice, a population characterized by the expression of Nestin and NG2 was identified as periportal pericytes, which expresses mesenchymal markers and shows trilineage mesenchymal capacity *in vitro* (Khan et al., 2016).

Law of Attraction: What Brings Hematopoietic Progenitors to the Developing Liver?

Hematopoietic stem cells emerge from the dorsal aorta directly into circulation and can, therefore, be found in different locations (Cumano et al., 1996; Medvinsky et al., 1996). These cells can travel through the umbilical arteries to the placenta and return to the embryo through the umbilical veins. The umbilical veins drain directly into the liver by fusing with the intrahepatic vascular plexus of the vitelline veins, forming the hepatic sinus. Cells traveling in the right umbilical vein can bypass the liver directly to the vena cava through the *ductus venosus*, a structure only present during fetal development, and can be directed into other embryonic regions through the heart. The liver is also irrigated by the vitelline veins, which transport blood from the YS, and eventually mature to become the portal vein. Another route for newly formed HSCs is to travel from the dorsal aorta through the subcardinal vein to the liver or inferior cardinal vein to the heart. From the heart, circulating cells can reach the developing lungs or upper half of the body (Kiserud, 2005). However, it is in the developing FL that HSCs establish and remain until they migrate to the BM. Transplantation studies show that HSCs can also be found in the placenta (Gekas et al., 2005; Ottersbach and Dzierzak, 2005). The placenta of a mouse model lacking a functional circulatory system was shown to still harbor hematopoietic activity, suggesting that the placenta could generate *de novo* hematopoietic cells with multilineage potential (Rhodes et al., 2008), however, direct evidence for HSC emergence from the placenta is yet to attain.

Hematopoietic stem or progenitor cells (HSPCs) but also EMPs, colonize the FL after liver bud formation at E10.5 (Johnson and Moore, 1975; Palis et al., 2001). Distinct mechanisms of FL colonization have been proposed, mostly relying on cell adhesion-mediated processes and/or chemoattraction (cytokines, chemokine signaling, and growth factors) (**Figure 3**; Hayashi et al., 2019).

Several cell adhesion molecules have been identified in embryonic HSPCs, including integrins, selectins, cadherins, and others. Hematopoietic progenitors express vascular-endothelial cadherin (VE-Cadherin/CD144) as they emerge from the YS (in the case of EMPs) or AGM (in the case of HSCs) that is downregulated thereafter and undetectable in BM HSCs (Fraser et al., 2002; Taoudi et al., 2005). FL $CD34^{+}$ progenitors express higher levels of the integrins β1 (CD29), α2 (CD49b), and α5 (CD49e), similar levels of integrins α4 (CD49d) and α6 (CD49f), E- and P-selectins (CD62E and CD62P, respectively) and CD11b and CD11c molecules, but lower levels of integrin β2 (CD18), CD11a and CD44 than their adult BM equivalent (Roy and Verfaillie, 1999). Seminal studies showed that HSPCs lacking β1 integrin were unable to colonize the FL but were still present in the circulation and capable of generating all blood lineages, suggesting a role for integrin-mediated cell adhesion in FL colonization (Hirsch et al., 1996). Integrin receptors result from the dimerization of α and β subunits and analysis of the expression of the α chain partner of β1 integrin in LSK progenitors revealed integrins α4 and α6 as the most

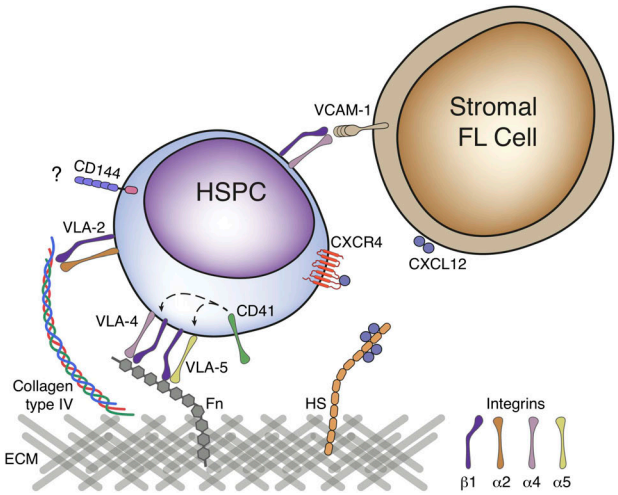

FIGURE 3 | Molecular mechanisms of fetal liver colonization. HSPC express a variety of cell adhesion molecules in their surface that can favor attachment to a specific location. β1 integrin is essential for colonization of FL by HSPC and can bind to the ECM components fibronectin and type IV collagen through dimerization with α4 and α5 or α2 integrins, respectively. VLA-4 and VLA-5 binding to fibronectin has been proposed to be modulated by CD41. VLA-4 (α4β1 integrin) can also mediate cell-cell interactions by binding with VCAM-1, expressed on the surface of FL stromal cells. Expression of the cadherin CD144 in HSCs as they emerge is assumed to play a role in the organ colonization, although no binding partner has been described in FL. CXCL12, a potent chemoattractant is expressed by FL stromal cells and binds to CXCR4, expressed on the surface of HSPC. CXCL12 gradients can be generated as this chemokine binds to proteoglycans in the ECM, namely to heparan sulfate (HS). HSPC, hematopoietic stem and progenitor cell; FL, fetal liver; ECM, extracellular matrix; VLA, very late antigen; Fn, fibronectin; HS, heparan sulfate.

predominant (Sugiyama et al., 2013). FL CD34$^+$ progenitors bind the ECM component fibronectin through the integrin receptors α4β1 and α5β1 (also known as VLA-4 and VLA-5) and this binding has been proposed to be modulated by the integrin α2b (GPIIb or CD41), also expressed in these cells (**Figure 3**; Roy and Verfaillie, 1999; Emambokus and Frampton, 2003). Other ECM components have been tested for adhesion of FL CD34$^+$ progenitors such as type I and type IV collagen and laminin, however, only type IV collagen promotes adherence at levels equivalent to that of fibronectin, through α2β1 integrin (VLA-2) (Roy and Verfaillie, 1999). In the FL, hepatoblasts (defined as DLK1$^+$ cells) are the major producers of ECM components, namely vitronectin and fibronectin (Sugiyama et al., 2013). Embryos lacking hepatoblasts can still form the liver bud but die between E10.5–E12.5 (Nishina et al., 1999). These FL show decreased expression of vitronectin and fibronectin that may play an important role in FL colonization by HSCs and YS EMPs, although this role has not been specifically assessed (Sugiyama et al., 2013). Integrins can also mediate cell-cell interactions. Cellular bound counterparts of VLA-4 include the vascular cell adhesion molecule-1 (VCAM-1/CD106), expressed by FL hepatoblasts (Sugiyama et al., 2010a).

Cytokine and chemokine signaling can also stand at the basis of FL colonization. The stromal cell-derived factor-1 (SDF-1), commonly known as CXC chemokine ligand 12 (CXCL12), acts through binding to its receptor CXCR4 present in HSPCs and has been extensively studied in the adult BM – reviewed in Yu and Scadden (2016); and Wei and Frenette (2018). CXCL12 expression is stabilized at the cell surface or in the surrounding ECM through proteoglycans binding, allowing the creation of chemokine gradients essential for cell migration (Schumann et al., 2010). In the FL, CXCL12 is expressed by DLK1$^+$ hepatoblasts (Chou and Lodish, 2010) and Nestin$^+$NG2$^+$ pericytes (Khan et al., 2016). The role of CXCL12 in FL colonization was analyzed using CXCL12$^{-/-}$ embryos. At early stages (E12.5–E14.5), the number of HSCs was similar in the FL of mutant animals and controls. By E16.5 FL HSCs were reduced by more than twofold and an abnormally high number was found in circulation. These observations indicate that CXCL12 is an important factor for retaining HSCs in FL, but not for its initial colonization (Ara et al., 2003).

Owing to the particular architecture of fetal circulation, FL is in an anatomically privileged location. Even if HSCs are traveling directly within the embryo through the subcardinal vein, or the umbilical veins after passing in the placenta, the FL is the first intraembryonic organ they encounter. Whether a passive retainment of circulating cells (e.g., through β1-integrin) occurs, or specific signals directly promote chemoattraction of HSPCs to FL is still unclear.

How Do the Hepatic and Hematopoietic Cell Types Organize During Development?

The structure of the FL changes dramatically during embryonic development. Crawford et al. (2010) extensively characterized the mouse developing hepatobiliary system from E9.5 to E18.5 creating a histology atlas. At initial stages (E10.5–E12.5), the liver is mainly constituted by a vascular plexus and migrating hepatoblasts that later form hepatic chords. At E11.5, the hepatic sinusoids are wide, which may favor the access and establishment of the newly generated hematopoietic progenitors. From E12.5 onward, the organization of the cells in the FL changes as the frequency of hematopoietic cells increases. At E13.5, the most frequent FL population are nucleated erythrocytes that, at early stages, are located throughout the liver parenchyma, in between the hepatic chords, but after E14.5 more mature enucleated erythroid cells are found within the vessels (Ayres-Silva et al., 2011). At this stage, megakaryocytes and erythroblastic islands, which consist of a central macrophage surrounded by erythroid cells, are also distinguishable in the liver parenchyma. These macrophages are responsible for the phagocytosis of the expelled nuclei during erythroid maturation (Bessis et al., 1978). Megakaryocytes are essential to thrombosis and hemostasis and may be determinant in an organ that is mostly constituted by erythroid cells. Moreover, the developing liver seems to provide a unique microenvironment for the expansion of megakaryocyte progenitors (Brouard et al., 2017).

From E13.5 to late gestation, no dramatic changes occur in the histology of the FL. Other hematopoietic cells such as B cell progenitors identified by Pax5 expression, can be found interspersed in the tissue by E12.5 and also forming perivascular aggregates by E18.5. Granulocytes are scattered throughout the tissue from E16.5 onward, concentrating/converging around central veins and in the periphery by E17.5, correlating with the presence of mesenchymal cells and suggesting a crosstalk between these distinct cell types (Ayres-Silva et al., 2011). By this time-point, as hematopoietic cells exit the organ and migrate to the BM, hepatoblasts and hepatocytes regain contact (Crawford et al., 2010).

Disclosure of HSCs distribution within the FL has been hindered by the multi-marker assessment required, i.e., Lin^-c-$Kit^+Sca1^+CD150^+CD48^-$, to phenotypically identify these cells. Hematopoietic progenitors (defined by c-Kit expression) are found in close association with $DLK1^+$ hepatoblasts at E14.5 (Sugiyama et al., 2013). Nevertheless, c-Kit^+ cells could mostly represent erythroid progenitors as they are the most frequent population at this stage (Soares-da-Silva et al., 2020, Preprint). Other approaches include the use of transgenic Ly6a-GFP (labeling $Sca1^+$ cells) mice, that together with Runx1 localized HSPCs at E11.5 in close contact with endothelial cells (Tamplin et al., 2015). HSCs, profiled as $CD150^+CD48^-Lin^-$, have been found in close association with $Nestin^+NG2^+$ pericytes surrounding the portal vessels (Khan et al., 2016). Although this characterization more closely identifies a potential HSC, FL studies using mouse models that directly label HSCs are still missing. Generation of a mouse with a single-color reporter driven by endogenous *Hoxb5* (*Hoxb5*–tri-mCherry), which expression in the BM is limited to LT-HSCs and *in situ* imaging evidenced the close proximity of LT-HSCs with VE-$Cadherin^+$ cells (Chen et al., 2016). Recently, another HSC-specific reporter line has been described, yet also only analyzed in the adult bone (Christodoulou et al., 2020).

THE INTERPLAY BETWEEN THE DEVELOPING HEPATIC-HEMATOPOIETIC TISSUES

How Does the FL Environment Modulate Hematopoiesis? A Role in Maturation, Expansion and Differentiation of HSCs?

Emerging imHSCs lack long-term reconstitution activity in conventional or $Rag2^{-/-}$ immunocompromised mice but can reconstitute NK-deficient $Rag2\gamma c^{-/-}$ animals (Cumano et al., 2001; Bertrand et al., 2005a). After co-culture with the OP9 BM stromal cell line in the presence of thrombopoietin (TPO) or with E10.5 FL rudiments, $CD31^+$c-Kit^+CD45^- imHSCs acquire an adult HSC phenotype (LSK $CD150^+CD48^-$) and develop LTR activity in $Rag2^{-/-}$ or conventional mice as they upregulate MHC class I molecules (Kieusseian et al., 2012). These experiments suggest that the FL provides the signals necessary for the maturation of newly formed HSCs. FL stroma also supports the differentiation of committed hematopoietic progenitors towards distinct lineages. Interleukine 7 (IL-7) promotes the survival and proliferation of lymphoid progenitors and controls the determination of the B cell lineage (Sudo et al., 1989; Peschon et al., 1994). In FL, IL-7 is produced by $VCAM1^+ALCAM^+DLK1^+$ hepatoblasts (Tsuneto et al., 2013) and controls the number of lymphoid progenitors that develop into the B-cell lineage by stabilizing the B-cell transcriptional signature (Berthault et al., 2017). For instance, erythropoietin (EPO) is produced by $DLK1^+$ hepatoblasts and is required for proliferation and terminal differentiation of erythroid progenitors (Sugiyama et al., 2011). Also, TPO expressing $Ter119^-CD45^-CD51^+VCAM1^+PDGFR\alpha^-$ FL hepatoblasts support the production of megakaryocytes from adult BM HSCs in a contact-dependent manner (Brouard et al., 2017). TPO is the main regulator of megakaryocyte differentiation and platelet production (Kaushansky, 1995; Eaton and de Sauvage, 1997) but has also been shown to promote survival and proliferation of BM HSPCs *in vitro* (Borge et al., 1996; Ku et al., 1996), the proliferation of fetal hematopoietic progenitors *in vivo* (Alexander et al., 1996) or expansion of BM HSCs following transplantation (Fox et al., 2002). Lack of TPO signaling causes decreased HSC function and numbers (Kimura et al., 1998; Solar et al., 1998), a consequence from the exit of a quiescent state (Nakamura et al., 2007; Qian et al., 2007), possibly leading to a premature exhaustion of the stem cell pool. The survival and proliferation effects of TPO are enhanced when used in combination with other early cytokines, namely FMS-like tyrosine kinase 3 ligand (FLT3L) and c-Kit ligand [KITL, also known as stem cell factor (SCF) or steel factor (SF)] both in murine and human adult BM cells (Ramsfjell et al., 1996; Borge et al., 1997). The highest levels of TPO in the adult are found in the liver (Lok et al., 1994). Systemic TPO produced by hepatocytes, but not by hematopoietic, osteoblast or BM mesenchymal stromal cells is required for BM HSC maintenance (Decker et al., 2018). It can be detected in FL as early as E10.5, having a strong impact on HSC expansion and survival in this organ (Petit-Cocault et al., 2007). Indeed, several cytokines/chemokines/growth factors are important for HSC proliferation, maintenance and survival, namely KITL, FLT3L, insulin growth factor (IGF), angiopoietin-3, angiopoietin-like 2, Wnt family growth factors, Ephrin2a, CSF1, EPO, CXCL12, and IL-6 – reviewed in Sauvageau et al. (2004). In FL, some of these cytokines are expressed by hepatoblasts or other stromal cells, such as stellate cells or pericytes (see **Table 2** and **Figure 4**; Charbord and Moore, 2005; Chou and Lodish, 2010; Khan et al., 2016; Tan et al., 2017).

The hypothesis that stem cells are regulated by their environment has been proposed by Schofield (1978) and postulates that stem cell properties are maintained by the surrounding cells designated "niche." Stromal regulation of hematopoiesis has been proposed by many and early studies of co-culture of hematopoietic progenitors with either FL fibroblast or epithelial-stromal cell lines showed erythroid and myeloid support (Tsai et al., 1986; Hata et al., 1993). More than 200 FL stromal cell lines have been developed and tested for maintenance or expansion of HSCs, however, only a few were able to maintain their repopulating activity

TABLE 2 | Cytokine signaling in fetal liver.

FL Supportive Stroma		Hematopoietic progenitors	
Pathway involved	**Expressing cell**	**Receptor**	**Effect**
KITL	DLK1$^+$ hepatoblasts (Chou and Lodish, 2010; Sugiyama et al., 2011) Nestin$^+$ cells (Khan et al., 2016) Stellate cells (Tan et al., 2017)	c-Kit (CD117) (Yarden et al., 1987)	BM HSC survival and self-renewal (Barker, 1994; Miller et al., 1997)
ANGPTL2	Nestin$^+$ cells (Khan et al., 2016)	PirB (Zheng et al., 2012)	BM HSC proliferation (Zhang et al., 2006)
ANGPTL3	DLK1$^+$ hepatoblasts (Chou and Lodish, 2010)	PirB (Zheng et al., 2012)	BM HSC maintenance (Zheng et al., 2011) BM HSC proliferation (Zhang et al., 2006)
FLT3L	Stellate cells (Tan et al., 2017)	Flt3 (CD135) (Matthews et al., 1991)	FL HSPC proliferation (Lyman et al., 1993)
TPO	DLK1$^+$ hepatoblasts (Chou and Lodish, 2010; Sugiyama et al., 2011; Brouard et al., 2017) Stellate cells (Tan et al., 2017)	MPL (TPO-R, CD110) (Vigon et al., 1992)	FL HSC survival and proliferation (Petit-Cocault et al., 2007) BM HSC quiescence (Nakamura et al., 2007; Qian et al., 2007)
CSF1	Stellate cells (Tan et al., 2017)	Csf-1 Receptor (Guilbert and Stanley, 1980)	Commitment to macrophage lineage (Rieger et al., 2009)
EPO	DLK1$^+$ hepatoblasts (Sugiyama et al., 2011) Stellate cells (Tan et al., 2017)	EPO receptor (Sawyer et al., 1987)	Proliferation and differentiation of FL erythroid progenitors (Lin et al., 1996)
CXCL12	Dlk1$^+$ hepatoblasts (Chou and Lodish, 2010) Nestin$^+$ cells (Khan et al., 2016) Stellate cells (Kubota et al., 2007)	CXCR4 (Bleul et al., 1996)	FL and FBM B-cell lymphopoiesis and FBM myelopoiesis (Nagasawa et al., 1996) BM HSC engraftment post-transplantation (Lai et al., 2014; McDermott et al., 2015) FL HSC retainment (Ara et al., 2003) BM HSC retainment (Sugiyama et al., 2006)
IL-7	VCAM1$^+$ALCAM$^+$DLK1$^+$ hepatoblasts (Tsuneto et al., 2013)	IL-7Rα (Park et al., 1990)	Lymphocyte expansion (Peschon et al., 1994)
IGF2	Dlk1$^+$ hepatoblasts (Chou and Lodish, 2010) Nestin$^+$ cells (Khan et al., 2016) Stellate cells (Tan et al., 2017)	IGF1-R (Rubin et al., 1983) IGF2-R (Morgan et al., 1987) Insulin receptor (House and Weidemann, 1970)	F L and BM HSC proliferation (Zhang and Lodish, 2004)

over a 3-week co-culture period (Wineman et al., 1996). The functional heterogeneity observed was not due to distinct cytokine production as all cell lines expressed similar cytokine profiles, including *Flt3l*, *Kitl*, *Tpo*, *Igf1*, *Il6*, *Il11*, leukemia inhibitory factor *(Lif)*, granulocyte-colony stimulating factor (G-CSF/*Csf3*), granulocyte/macrophage-colony stimulating factor (GM-CSF/*Csf2*), and transforming growth factor, beta 1 (*Tgfb1*). Importantly, the successful stromal cell lines have in common the expression of *Dlk1*, and overexpression of this factor is sufficient to enable hematopoietic support (Moore et al., 1997). Although these cell lines only maintain HSC potential and do not promote HSC expansion, some FL cells have been described to do so. Recent studies have addressed the role of specific FL populations *in vivo* or *in vitro*. It is the case of DLK1$^+$ hepatoblasts that are able to expand LT-HSC around 20-fold after a 3-week co-culture period (Chou et al., 2013). This expansion seems to be contact-dependent as DLK1$^+$ conditioned medium only allows expansion of ST-HSC and cells cultured in transwell inserts did not show the same expansion levels. Although promising, it is worth mentioning that these cultures were supplemented with KITL, TPO, and FLT3L and, therefore, it remains unclear which mechanisms underlie HSCs expansion in DLK1$^+$ cell co-cultures. Moreover, DLK1 knockdown in human hepatoblasts results in decreased hematopoietic support *in vitro* (Gerlach et al., 2019). The role of hepatoblasts *in vivo* has been difficult to assess as transgenic mice with hepatoblast deficiencies die between E10.5 and E12.5 and studies of liver development do not usually investigate the hematopoietic compartment (Nishina et al., 1999). DLK1 has been used to identify hepatoblasts but it is also expressed by the majority of Nestin$^+$ cells surrounding the portal vessels, a cell type that has been implicated as part of the FL niche (Tanimizu et al., 2003; Chou and Lodish, 2010; Chou et al., 2013; Khan et al., 2016). HSCs numbers are modestly reduced when Nestin$^+$NG2$^+$ pericytes are selectively eliminated and the remaining HSCs are less proliferative (Khan et al., 2016). So far, this is the only study that addresses the role of a specific cell type in HSC expansion and maintenance *in vivo*. Nestin$^+$ cells are the major producers of *Cxcl12* at E14.5 when compared to Nestin$^-$ cells, therefore, the reduction in FL HSCs could result from a defect in HSC expansion together with a displacement

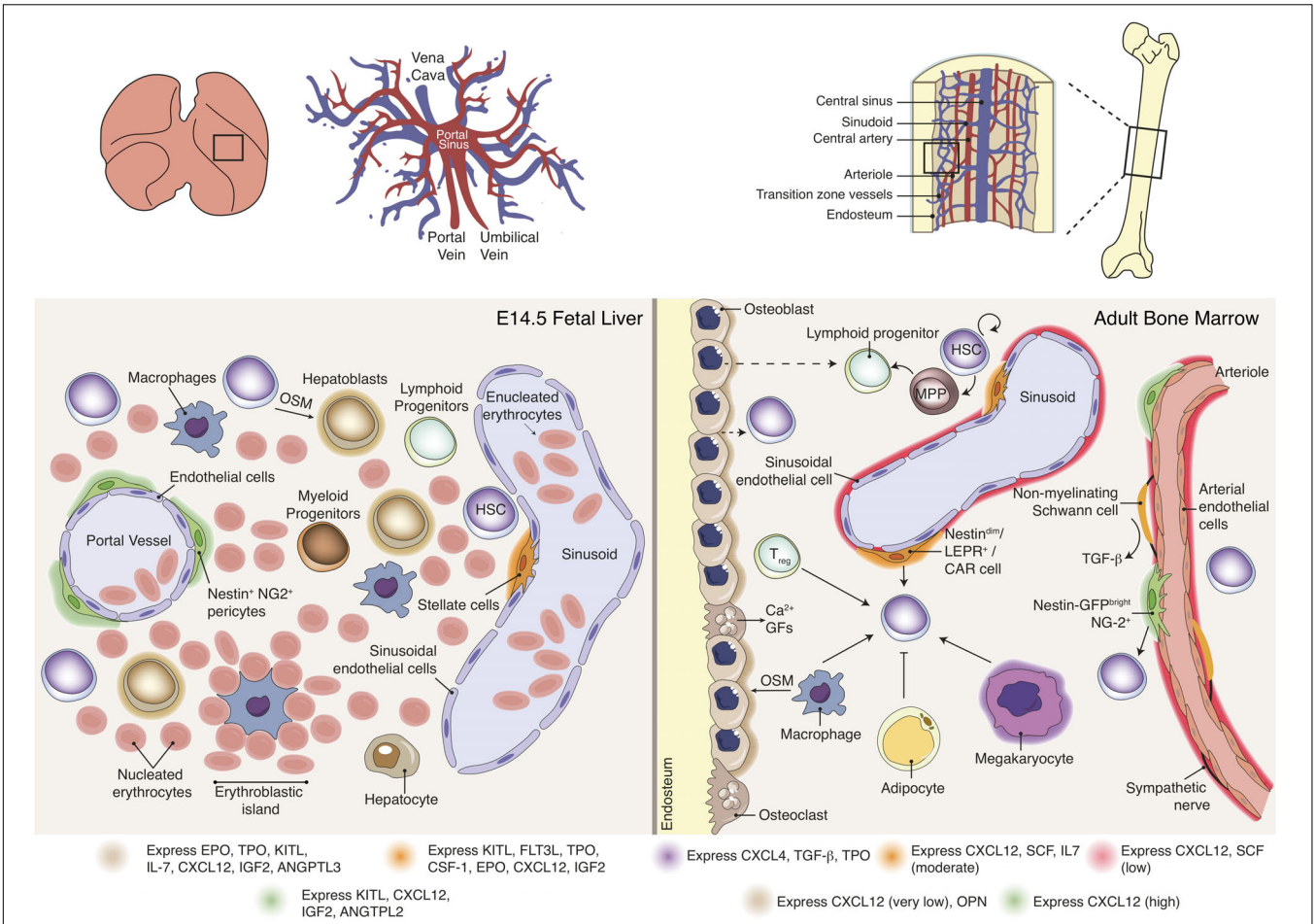

FIGURE 4 | Hematopoietic stem cell niche in fetal liver *versus* bone marrow. Distinct BM stromal cell populations have been described as modulators of HSC functions via expression of soluble and membrane-bound factors. Data available for FL stromal populations is scarce and consequently evidence for a direct role of stromal populations in HSC expansion or differentiation is not reported. The FL microenvironment includes cytokine-producing hepatoblasts, pericytes and stellate cells, together with high number of hematopoietic progenitors and distinct developmental stage erythroid cells. BM Nestin-GFP^{high}, NG2^{+} perisinusoidal cells and Nestin-GFP^{dim}, LepR^{+}, CAR sinusoidal cells are key regulators of HSC maintenance, contributing differentially for cytokine production. Macrophages, T_{reg} and megakaryocytes were also reported to contribute to HSC maintenance and mobilization. Sympathetic nerves regulate HSC mobilization through a tightly control of CXCL12 expression by stromal cells. Non-myelinating Schwann cells activate latent TGF-β into its active form, which may contribute for HSC maintenance. The role of osteoblasts in HSPC is still unclear. Adipocytes may negatively affect HSC maintenance.

of cells into circulation. Moreover, Nestin^{+} cells seem to be a transient population, important for HSC localization around the portal vessels during FL hematopoiesis but are no longer present postnatally, a stage at which HSCs migrate and reside in the BM. These cells have also been described in adult BM and ablation of Nestin^{+}NG2^{+} pericytes alters HSCs localization away from arterioles (Kunisaki et al., 2013). In the rat, fetal hepatic stellate cells were shown to express VCAM-1 and to secrete *Cxcl12* and hepatocyte growth factor *(Hgf)*, revealing a potential role for the hematopoietic and hepatic development (Kubota et al., 2007). Accordingly, mouse FL hepatic stellate cells (defined as p75NTR^{+}) express a range of hematopoietic cytokines, *Csf1*, *Igf2*, *Tpo*, *Kitl*, *Epo*, *Igf1*, *Il11*, *Flt3l* and Oncostatin M (*Osm*, involved in hepatic maturation) and were therefore proposed as potential niche components (Tan et al., 2017).

To date, researchers have undertaken a cell type-directed approach, however, it is conceivable that different FL populations play distinct roles in the maintenance and expansion of HSCs and act through cellular networks. Only an unsupervised analysis of the FL constituents as a whole will shed light on the part each cell type takes in the support of hematopoiesis.

The vascular labyrinthine of the placenta (where embryonic circulation meets maternal circulation) has also been proposed as a niche for HSC expansion (Gekas et al., 2005; Ottersbach and Dzierzak, 2005; Robin et al., 2009). Human placenta-derived stromal cell lines with pericyte characteristics were shown to support *in vitro* maintenance of cord blood (CB) hematopoietic progenitors and hematopoietic cells were found in close contact with pericytes/perivascular cells in the placenta by immunostaining (Robin et al., 2009). Taken together with what

has already been described for the FL (Khan et al., 2016), pericyte-like cells are likely to play a role on supporting hematopoiesis.

Can the Adult Liver Be a Hematopoietic Site?

Extramedullary hematopoiesis (EMH) is a process in which HSPCs leave their microenvironment in the BM and establish in distinct anatomical locations wherein they continue to produce mature blood cells. Although it is a physiologic process during embryonic development (YS, AGM, FL, and fetal spleen), in the adult it only occurs in pathological settings of BM failure, myelostimulation, tissue inflammation, or abnormal cytokine production (Johns and Christopher, 2012). EMH can occur sporadically in lymph nodes, spinal cord, kidneys, gastrointestinal tract, and lung (Chiu et al., 2015). It is interesting, however, that the predominant sites of EMH are shared between the embryo and the adult: the spleen and the liver. In fact, splenic or liver hematopoiesis can still be observed postnatally in many mammals but disappears before adulthood. Hematopoietic foci in the adult liver can be found within sinusoids and in close association with macrophages (Barberá-Guillem et al., 1989). BM HSPCs co-cultured with liver sinusoid endothelial cells (LSECs) were maintained for more than 6 weeks in cytokine supplemented media, demonstrating a putative niche role of endothelial cells in the adult liver (Cardier and Barberá-Guillem, 1997). An adherent layer of liver cells has been suggested to support megakaryopoiesis by the production of TPO and B lymphopoiesis by the production of *Il7* and *Flt3l* (Cardier and Dempsey, 1998; Wittig et al., 2010). Although endothelial cells have been reported to express TPO, this cytokine is mostly produced by the liver parenchyma (hepatocytes) (Nomura et al., 1997). In the adult, EPO is produced by the kidney, although hepatocytes can also support hepatic erythropoiesis in physiological or pathological conditions (Ploemacher and van Soest, 1977; Semenza et al., 1991; Eckardt et al., 1994; Weidemann and Johnson, 2009). In conclusion, under physiologic conditions, the liver harbors low numbers of HSPCs and supports extramedullary hematopoiesis (Taniguchi et al., 1996; Watanabe et al., 1996). Thus, it is conceivable that adult liver may keep some of its embryonic niche properties.

Is the Development of the FL and Hematopoietic Cells Symbiotic?

In mid-gestation, embryonic liver functions as a "bag" accommodating the expanding hematopoietic system before BM development. During the temporal window in which the organ is essentially a hematopoietic tissue – from E12.5 to E16.5 (∼6–18 wpc in humans) – and the ratio of non-hematopoietic cells/total liver cells is very low, the organ's architecture is far less complex than that of its adult counterpart. In the adult, hepatocytes are the main parenchymal cell type, organized in cords interspaced by an intricate vascular and biliary system (**Figure 2H**). Alongside with the massive migration of hematopoietic cells to the BM at E16.5 (Christensen et al., 2004), the liver tissue starts to mature – hepatocytes and cholangiocytes differentiate from hepatoblasts and cellular adhesion increases, creating tight hepatic parenchyma with dense hepatocyte cords (Crawford et al., 2010). Transcriptomic and proteomic analysis throughout FL development identified E15.5 as the time of onset of metabolic, detoxification and immune programs (Guo et al., 2009).

Hepatoblasts differentiate into hepatocytes starting at ∼E13.5 in mice and around 14 wpc in humans (Haruna et al., 1996; Yang et al., 2017). Single-cell transcriptomic studies along development (E10.5–E17.5) of hepatoblasts/hepatocytes/cholangiocytes (sorted based on the expression of DLK-1 and EpCAM) suggest that hepatoblast-to-hepatocyte lineage specification is the default process. Cholangiocyte specification occurs as early as E11.5 and is completed by E14.5 (Yang et al., 2017). Hepatoblasts fate decision is modulated by a gradient of Activin/TGF-β signaling, controlled by Onecut (OC) TFs (OC-1/HNF-6 and OC-2) (Clotman, 2005). Cholangiocyte-primed hepatoblasts appear in low numbers at E13.5 around the portal vein and portal sinus, forming a single-layered ductal plate at E15.5, that evolves to a double-layer by E16.5 (**Figures 2D,E**), characterized by CK19 and CK8 cytokeratins and β2 integrin (CD18) (Van Eyken et al., 1988; Tanimizu et al., 2009). At this stage, CK19 expression becomes specific to ductal plate cells (Van Eyken et al., 1988). Focal dilations between the two ductal plate cell layers give rise to the bile ducts (**Figures 2F,G**), whereas the remaining tissue progressively regresses (Clotman et al., 2002). This ductal plate remodeling involves tubulogenesis (Antoniou et al., 2009) and apoptosis (Terada and Nakanuma, 1995). Around birth, the portal mesenchyme encircles the cells of the ductal plate (Swartley et al., 2016). Hepatoblasts located away from the portal vein will gradually differentiate into hepatocytes and by E17 start to exhibit a characteristic polarized epithelial morphology disposed in hepatic cords alongside the bile canaliculi (Zorn, 2008). Because cholangiocyte differentiation occurs along the hilum-to-periphery axis, different maturation states can be observed at a given developmental time (Yang et al., 2017). Three-dimensional reconstructions of serial cross-sections/whole-mount immunostained FL and carbon ink injection have been used to disclose the morphogenesis of intrahepatic bile ducts (Vestentoft et al., 2011; Takashima et al., 2015; Tanimizu et al., 2016).

Kinoshita et al. (1999) showed that hematopoietic cells expand when cultured in a monolayer of primary fetal hepatic cells (in presence of hematopoietic cytokines) and that the addition of OSM suppresses *in vitro* hematopoiesis, by inducing the maturation of the hepatic cells. Since hematopoietic cells produce OSM, its expansion increases the local OSM concentration, consequently promoting hepatic development (Kamiya et al., 1999). It was hypothesized that a metabolically active liver no longer supports hematopoiesis (Miyajima et al., 2000). However, it is still not clear whether the displacement of the hematopoietic cells out of the FL facilitates liver maturation or if the changes in the microenvironment no longer support hematopoiesis.

Impaired hematopoiesis in *c-Myb* mutant (Mucenski et al., 1991) or $Ubc^{-/-}$ mice (Ryu et al., 2012) and abnormal erythropoiesis in *Rb*-deficient mice (Lee et al., 1992) also results in impaired liver growth. However, the

early embryonic lethality (at around E15) has hindered the analysis of the impact of the hematopoietic compartment in liver development.

The vasculature remodeling at the end of gestation was also correlated with the rapid loss of HSCs in the postnatal liver (Khan et al., 2016). After birth, the portal vein no longer receives blood from the vitelline vein, collecting the blood from the gut, draining it to the central vein and the hepatic artery arises. With the ligation of the umbilical inlet, the portal vessels acquire a vein phenotype and lose the periportal pericytes (Khan et al., 2016).

HEMATOPOIETIC EXIT FROM FL AND ESTABLISHMENT IN THE BM

What Makes the Hematopoietic System Move? How Is the BM Niche Established?

The BM is the ultimate destination of the hematopoietic system journey in the embryo, being the production hub for blood cells throughout life. LSK cell homing and colonization of mouse BM was reported at E15.5–E16.5, coinciding with the fetal bone marrow (FBM) vascularization (Gekas et al., 2005; Coşkun et al., 2014; Cao et al., 2019), although LT-HSC activity cannot be detected before E17.5 (Christensen et al., 2004). In mice, HSCs migrating out of the FL also seed the spleen, starting at E15.5, with HSC activity still being detected a few weeks after birth (Wolber et al., 2002; Christensen et al., 2004; Bertrand et al., 2006). In humans, although early colonization of fetal long bones was reported at ∼10 wpc (Charbord et al., 1996), the hematopoietic shift from the FL to the FBM occurs later, around 20 wpc (**Figure 1**).

Coşkun et al. (2014) showed that hematopoietic progenitor cells reside in the vascularized regions of fetal long bones, stage at which they are still proliferative. Previous work showed that in the BM, HSCs are cycling during the first 3 weeks after birth and become quiescent thereafter (Bowie et al., 2006). The shift to a quiescence state seems to be dependent on the cellular composition of the microenvironment (Coşkun et al., 2014). LSK cells isolated from *Osx*$^{-/-}$ FBM [that lack osteolineage cells (Nakashima et al., 2002) and some stromal populations (Mizoguchi et al., 2014)] form multi-lineage colonies *in vitro*, but fail to repopulate transplanted recipients (Mizoguchi et al., 2014). LSK cells exhibited dysregulated cell cycle progression and defective homing ability, suggesting that osteolineage and/or mesenchymal cells are necessary to establish and sustain BM LT-HSCs (Coşkun et al., 2014). Additionally, E15.5 CD105^{+}Thy1^{-} mesenchymal progenitors transplanted under the kidney capsule give rise to donor-derived chondrocytes and can create an ectopic niche with the recruitment of host-derived marrow and HSCs, evidencing the importance of endochondral ossification for HSC niche formation (Chan et al., 2009).

Osteopontin (OPN), also known as secreted phosphoprotein 1 (SPP1) has been suggested to be an important niche factor in BM. Its concentration in stromal cells is inversely correlated with HSC proliferation in the adult BM (Stier et al., 2005). The OPN dominant form thrombin-cleaved osteopontin (trOPN) is highly expressed in FBM (at the trabecular bone surface), but neglectable-to-none in the early-mid gestation FL (Cao et al., 2019). trOPN receptor α4β1 integrin is upregulated in fetal compared to adult HSCs. The differential concentration of the divalent metal cations, Ca^{2+}, Mg^{2+}, and Mn^{2+} between FL and FBM, being highly prevalent in the latter, was assumed to activate α4β1 in HSCs, possibly hindering their expansion in the BM (Cao et al., 2019).

CXCL12 expression in the vicinity of vascular endothelial cells in FBM supports the hematopoietic colonization of the organ (Nagasawa et al., 1996; Ara et al., 2003). HSCs isolated from CXCL12$^{-/-}$ embryos failed to colonize the BM in long-term repopulation assays whereas their migration ability could be rescued by enforced expression of CXCL12 under the control of vascular-specific Tie-2 regulatory sequences (Ara et al., 2003). Moreover, the CXCL12-mediated migration of HSPCs *in vitro* seems to be enhanced by the presence of KITL, indicating an additive effect, only found in fetal HSCs (Christensen et al., 2004). This suggests an important role of KITL for HSC seeding and homing during embryonic development.

CXCL12-GFP knock-in mice allowed the identification of CXCL12-abundant reticular (CAR) cells, a population with high expression of CXCL12, distributed near SECs and at a lower extent near the endosteum (Sugiyama et al., 2006). These cells show *in vitro* potential to differentiate into adipocytic and osteoblastic lineages (Omatsu et al., 2010). Specific markers have been identified for mesenchymal cells in BM. Leptin receptor (Lepr) is highly enriched in *Scf-GFP*-expressing perivascular stromal cells (Ding et al., 2012) and Lepr^{+} cells were shown to largely overlap with CAR cells (Zhou et al., 2014). A rare population of Nestin^{+} cells that contains all of the fibroblastic CFU (CFU-F) activity within the mouse BM, capable of generating mesenspheres (mesenchymal spheres) *in vitro*, multipotent and with self-renewal potential was identified as a mesenchymal stem cell (MSC) population (Méndez-Ferrer et al., 2010). Later, two different Nestin-GFP populations were discriminated based on the fluorescence intensity by microscopy. Rare quiescent *Nestin-GFP^{bright}* cells, positive for the pericyte marker NG2 and α-smooth muscle actin, are enriched for CFU-F activity and express *Cxcl12* and *Kitl*. These cells are located alongside arterioles, close to dormant HSCs (Kunisaki et al., 2013), and associated with sympathetic nerves, that regulate their CXCL12 expression through the β_3-adrenergic receptor (Méndez-Ferrer et al., 2010). *Nestin-GFP^{dim}* cells have a reticular shape, are mitotically active and line sinusoids, largely overlapping with Lepr^{+} cells (∼80%) (Kunisaki et al., 2013). Selective ablation of mouse Nestin^{+} cells (Méndez-Ferrer et al., 2010) or CAR cells (Omatsu et al., 2010) significantly impacts the maintenance of HSCs. The structural differences of the blood vessels and perivascular populations seem to be associated with heterogeneity in HSC function. Besides, the selective deletion of *Cxcl12* from arteriolar NG2^{+} cells, but not sinusoidal Lepr^{+} cells, significantly reduced the HSCs compartment in the BM and a similar effect was observed by deletion of *Kitl* in LepR^{+}; but not NG2^{+} cells, evidencing the differential contribution of

perivascular populations in the cytokine production (Asada et al., 2017). BM microenvironment is illustrated in **Figure 4**.

Nestin$^+$ cells can be prospectively isolated using PDGFRα and CD51 markers in the mouse and human fetal and adult BM (Pinho et al., 2013) and show MSC's properties and enrichment of *Cxcl12*, *Vcam1*, *Angpt1*, *Opn*, and *Scf* genes. Of note, in humans, these cells represent a small subset of CD146$^+$ cells (Pinho et al., 2013), the latter harboring all the CFU-F activity in BM (Sacchetti et al., 2007). Co-culture of human PDGFRα$^+$CD51$^+$ mesenspheres with human FBM CD34$^+$ cells in a serum-free, but cytokine supplemented (TPO, SCF, FLT3L) culture media can expand MPPs that engraft immunodeficient mice (Pinho et al., 2013).

In the FL, Nestin-GFP$^+$NG2$^+$ cells, associated with portal vessels, form a niche promoting HSC expansion during the FL development that is no longer found after birth. Concomitantly, the phenotype of the portal vessel transits from Neuropilin-1$^+$Ephrin-B2$^+$ arterial to EphB4$^+$ venular vessels (Khan et al., 2016). This role of Nestin$^+$NG2$^+$ cells in FL is opposite to that in BM, where Nestin$^+$NG2$^+$arteriolar pericytes were proposed to maintain HSC quiescent (Kunisaki et al., 2013).

UNRESOLVED QUESTIONS – *EX VIVO* EXPANSION OF HSCs

Hematopoietic stem cells are the only cells of the hematopoietic compartment with the potential to replenish all mature blood cells and to divide without triggering differentiation programs, a process known as self-renewal. The mechanisms conveying these properties have been under investigation over the last 60 years, however, to date, they remain poorly understood. The concept that specific BM niche/microenvironment components regulate the fate of HSCs has been proposed by many authors. Cordeiro Gomes et al. (2016) analyzed not only HSCs but also different hematopoietic progenitors and found both HSCs and MPPs locate near or in contact with the same mesenchymal progenitor CAR-cells, expressing CXCL12 and SCF, fundamental to maintain the HSC pool and IL-7 that acts as a short-range signal for lymphoid differentiation. These observations suggest that both maintenance and multilineage differentiation are locally regulated by the same niche (Cordeiro Gomes et al., 2016). In the FL, HSCs expand considerably and differentiate, producing different mature lineages. If a given stromal population is also involved in the regulation of both processes, by the expression of various cytokines, or different cell populations contribute with distinct cytokines is still unresolved.

Hematopoietic stem cell transplantation is a widely used cell therapy intervention in the treatment of hematologic, autoimmune and genetic disorders. However, this therapy is still associated with high mortality rates, mainly due to infection, graft-versus-host disease (GvHD) and organ dysfunction, urging the need for improvement (Tanaka et al., 2016). The most common source of HSCs for transplantation is the BM or mobilized circulating HSPCs. However, matching of major histocompatibility complex antigens is needed to avoid GvHD (Schuster et al., 2012; Walasek et al., 2012). CB can be successfully used as a source of partially mismatched HSCs, as it is readily available through CB banks and elicits low levels of GvHD. Low numbers of HSCs in CB and consequent absent or delayed reconstitution leads to post-transplantation infections, limiting the use of CB in adult patients (Ruggeri et al., 2014).

In vitro generation of HSCs would overcome some of the current clinical difficulties that transplantation faces, however, despite countless efforts to derive HSCs from pluripotent stem cell sources, generation of HSC *in vitro* has not yet been achieved – reviewed in Freire and Butler (2020). Another possibility to obtain higher numbers of HSCs would be to expand them *ex vivo* prior to transplantation. Distinct cytokine/growth factor cocktails have shown promising for expansion of HSCs, yet, limited success was reported in clinical studies due to a lack of LT-HSC expansion and rather proliferation of downstream progenitors together with undesirable stem cell differentiation – reviewed in Kumar and Geiger (2017) and Tajer et al. (2019). Cytokines currently used for *ex vivo* HSC expansion include KITL, TPO, IL-3, and FLT3L. *Kitl* and *Tpo* knockout mice show normal fetal development but reduced HSC numbers in the adult, suggesting that these cytokines are important for stem cell survival and proliferation in adulthood but might not be the drivers of HSC expansion during the embryonic period (Fujita et al., 1989; de Sauvage et al., 1996). There is growing evidence that the physical and mechanical properties of the microenvironment could impact on HSC decisions – reviewed in Kumar and Geiger (2017). A combination of cytokines with stroma derived ECM components – fibronectin and collagen – has shown encouraging results (Wohrer et al., 2014; Wilkinson et al., 2019). Moreover, culture of BM HSPCs in tropoelastin, the most elastic biomaterial known, induces a sixfold increase of LSK cells without supplementation with cytokines, suggesting that tropoelastin mediates a similar effect in survival and proliferation of LSK cells and its use could replace exogenous cytokines (Holst et al., 2010). Most cytokines studied have a role in HSC function in the BM, a site where HSC expansion does not occur in physiological conditions. The same cytokines have been found in FL stroma, but whether these are responsible for fetal HSC expansion is not known. Most likely, the FL expansion of newly generated HSCs results from intrinsic cellular properties together with a suitable microenvironment, physical cues included. Efforts have been made to replicate the embryonic microenvironment where HSCs expand, particularly by co-culture with FL hepatic or mesenchymal cells (Wineman et al., 1996; Chou and Lodish, 2010; Chou et al., 2013; Khan et al., 2016). Most strategies used so far focused on specific cell populations, either hepatoblasts or mesenchymal cells, but overlooked the possibility that distinct populations might need to interact. Only the co-culture of HSCs in a system where all the cytokine-expressing populations of the FL are present would reproduce the FL microenvironment. Such a system where hepatoblasts, endothelial and mesenchymal cells are cultured together in a 3D aggregate has already been devised, but no co-culture with hematopoietic cells has been attempted (Takebe et al., 2015). Liver cell culture models have been extensively developed for pharmacological and toxicological research or as a source for transplantation, to obtain an *in vitro* system that resembles a mature liver – reviewed in

Godoy et al. (2013), and for that reason are not suitable for recreating the FL niche environment.

Whereas the FL interactions between different cell types have been correlated with their contribution to the massive transient expansion of the hematopoietic system, other niche factors need to be addressed. Sigurdsson et al. (2016) reported the role of FL bile acids (BAs) as chemical chaperones, critical to sustain high protein production by expanding LT-HSCs without triggering endoplasmic reticulum (ER) stress. Inhibiting the biosynthesis of BAs *in vivo* resulted in reduced numbers of Lin^-, LSKs, and LSK $CD48^-CD150^+$ in the FL, with no apparent effect in the number of HSCs in the mother's BM (Sigurdsson et al., 2016). Comparison of FL and BM HSCs transcriptomes demonstrated that FL HSCs metabolism relies on oxygen-dependent pathways, which may be a requirement for extensive energy production during expansion. Contrary to BM HSCs, FL HSCs use oxidative phosphorylation (aside from glycolysis), have higher number of mitochondria and up regulate genes associated with antioxidant and DNA repair pathways, that are speculated to confer protection from reactive oxygen species-mediated (geno)toxicity (Manesia et al., 2015).

Exploring the complexity of HSC niches (cellular composition, cytokine and growth factors milieu, physical properties, oxygen availability, etc.) will improve into our understanding of HSC self-renewal capacity (recently reviewed by Wilkinson et al., 2020), that is currently insufficient to devise efficient strategies for HSC expansion *ex vivo*.

CONCLUDING REMARKS

Distinct studies have identified and characterized FL stromal populations that may contribute with specific cues, enabling the HSC expansion in this organ. Despite the efforts, the role of the FL microenvironment has not been directly shown. The possibility that HSCs proliferate exclusively due to intrinsic properties is however remote. Therefore, a model in which distinct populations cooperate is conceivable. An analysis that contemplates such complex multicellular networks has not been attempted. This review aimed to compile information on the cellular populations that could signal to HSCs during development, highlighting the advances and the unresolved questions in the field.

AUTHOR CONTRIBUTIONS

FS-d-S and MP: conceptualization and writing. AC: discussion and revision. PP-d-Ó: conceptualization and revision. All authors contributed to the article and approved the submitted version.

FUNDING

FS-d-S funded by FCT grants PD/BD/114128/2015 and POCI-0100145-FEDER-01638. MP funded by FCT grant SFRH/BD/143605/2019. AC financed by the Institut Pasteur, INSERM, ANR (grant Twothyme and EpiDev) and REVIVE Future Investment Program and Pasteur-Weizmann Foundation. PP-d-Ó financed by Portuguese funds through FCT/MCTES in the framework of the projects PTDC/MED-OUT/32656/2017, POCI-01-0145-FEDER-032656, and by – FCT – UIDB/04293/2020.

ACKNOWLEDGMENTS

We thank the members of PP-d-Ó and AC laboratories for critical discussions.

REFERENCES

Alexander, W. S., Roberts, A. W., Nicola, N. A., Li, R., and Metcalf, D. (1996). Deficiencies in progenitor cells of multiple hematopoietic lineages and defective megakaryocytopoiesis in mice lacking the thrombopoietic receptor c-Mpl. *Blood* 87, 2162–2170.

Antoniou, A., Raynaud, P., Cordi, S., Zong, Y., Tronche, F., Stanger, B. Z., et al. (2009). Intrahepatic bile ducts develop according to a new mode of tubulogenesis regulated by the transcription factor SOX9. *Gastroenterology* 136, 2325–2333. doi: 10.1053/j.gastro.2009.02.051

Ara, T., Tokoyoda, K., Sugiyama, T., Egawa, T., Kawabata, K., and Nagasawa, T. (2003). Long-term hematopoietic stem cells require stromal cell-derived factor-1 for colonizing bone marrow during ontogeny. *Immunity* 19, 257–267. doi: 10.1016/S1074-7613(03)00201-2

Asada, N., Kunisaki, Y., Pierce, H., Wang, Z., Fernandez, N. F., Birbrair, A., et al. (2017). Differential cytokine contributions of perivascular haematopoietic stem cell niches. *Nat. Cell Biol.* 19, 214–223. doi: 10.1038/ncb3475

Asahina, K. (2012). Hepatic stellate cell progenitor cells. *J. Gastroenterol. Hepatol.* 27(Suppl. 2), 80–84. doi: 10.1111/j.1440-1746.2011.07001.x

Asahina, K., Tsai, S. Y., Li, P., Ishii, M. Jr., and Henry, M. (2010). Mesenchymal origin of hepatic stellate cells, submesothelial cells, and perivascular mesenchymal cells during mouse liver development. *Hepatology* 49, 998–1011. doi: 10.1002/hep.22721.Mesenchymal

Asahina, K., Zhou, B., Pu, W. T., and Tsukamoto, H. (2011). Septum transversum-derived mesothelium gives rise to hepatic stellate cells and perivascular mesenchymal cells in developing mouse liver. *Hepatology* 53, 983–995. doi: 10.1002/hep.24119

Ayres-Silva, J. D. P., Manso, P. P. D. A., Madeira, M. R. D. C., Pelajo-Machado, M., and Lenzi, H. L. (2011). Sequential morphological characteristics of murine fetal liver hematopoietic microenvironment in Swiss Webster mice. *Cell Tissue Res.* 344, 455–469. doi: 10.1007/s00441-011-1170-1

Barberá-Guillem, E., Ayala, R., and Vidal-Vanaclocha, F. (1989). Differential location of hemopoietic colonies within liver acini of postnatal and phenylhydrazine-treated adult mice. *Hepatology* 9, 29–36. doi: 10.1002/hep.1840090106

Barker, J. E. (1994). Sl/Sld hematopoietic progenitors are deficient in situ. *Exp. Hematol.* 22, 174–177.

Berthault, C., Ramond, C., Burlen-Defranoux, O., Soubigou, G., Chea, S., Golub, R., et al. (2017). Asynchronous lineage priming determines commitment to T cell and B cell lineages in fetal liver. *Nat. Immunol.* 18, 1139–1149. doi: 10.1038/ni.3820

Bertrand, J., Chi, N. C., Santoso, B., Teng, S., Stainier, D. Y. R., and Traver, D. (2010). Haematopoietic stem cells derive directly from aortic endothelium during development. *Nature* 464, 108–111. doi: 10.1038/nature08738

Bertrand, J., Desanti, G. E., Lo-Man, R., Leclerc, C., Cumano, A., and Golub, R. (2006). Fetal spleen stroma drives macrophage commitment. *Development* 133, 3619–3628. doi: 10.1242/dev.02510

Bertrand, J., Giroux, S., Golub, R., Klaine, M., Jalil, A., Boucontet, L., et al. (2005a). Characterization of purified intraembryonic hematopoietic stem cells as a tool to define their site of origin. *Proc. Natl. Acad. Sci. U.S.A.* 102, 134–139. doi: 10.1073/pnas.0402270102

Bertrand, J., Jalil, A., Klaine, M., Jung, S., Cumano, A., and Godin, I. (2005b). Three pathways to mature macrophages in the early mouse yolk sac. *Blood* 106, 3004–3011. doi: 10.1182/blood-2005-02-0461

Bessis, M., Mize, C., and Prenant, M. (1978). Erythropoiesis: comparison of in vivo and in vitro amplification. *Blood Cells* 4, 155–174.

Bleul, C. C., Farzan, M., Choe, H., Parolin, C., Clark-Lewis, I., Sodroski, J., et al. (1996). The lymphocyte chemoattractant SDF-1 is a ligand for LESTR/fusin and blocks HIV-1 entry. *Nature* 382, 829–833. doi: 10.1038/382829a0

Bloom, W., and Bartelmez, G. W. (1940). Hematopoiesis in young human embryos. *Am. J. Anat.* 67, 21–53. doi: 10.1002/aja.1000670103

Bogue, C. W., Ganea, G. R., Sturm, E., Ianucci, R., and Jacobs, H. C. (2000). Hex expression suggests a role in the development and function of organs derived from foregut endoderm. *Dev. Dyn.* 219, 84–89.

Borge, O., Ramsfjell, V., Cui, L., and Jacobsen, S. E. (1997). Ability of early acting cytokines to directly promote survival and suppress apoptosis of human primitive CD34+CD38- bone marrow cells with multilineage potential at the single-cell level: key role of thrombopoietin. *Blood* 90, 2282–2292.

Borge, O., Ramsfjell, V., Veiby, O., Murphy, M., Lok, S., and Jacobsen, S. (1996). Thrombopoietin, but not erythropoietin promotes viability and inhibits apoptosis of multipotent murine hematopoietic progenitor cells in vitro. *Blood* 88, 2859–2870. doi: 10.1182/blood.V88.8.2859.bloodjournal8882859

Bort, R., Signore, M., Tremblay, K., Barbera, J. P. M., and Zaret, K. S. (2006). Hex homeobox gene controls the transition of the endoderm to a pseudostratified, cell emergent epithelium for liver bud development. *Dev. Biol.* 290, 44–56. doi: 10.1016/j.ydbio.2005.11.006

Bowie, M. B., McKnight, K. D., Kent, D. G., McCaffrey, L., Hoodless, P. A., and Eaves, C. J. (2006). Hematopoietic stem cells proliferate until after birth and show a reversible phase-specific engraftment defect. *J. Clin. Invest.* 116, 2808–2816. doi: 10.1172/JCI28310

Brouard, N., Jost, C., Matthias, N., Albrecht, C., Egard, S., Gandhi, P., et al. (2017). A unique microenvironment in the developing liver supports the expansion of megakaryocyte progenitors. *Blood Adv.* 1, 1854–1866. doi: 10.1182/bloodadvances.2016003541

Busch, K., Klapproth, K., Barile, M., Flossdorf, M., Holland-Letz, T., Schlenner, S. M., et al. (2015). Fundamental properties of unperturbed haematopoiesis from stem cells in vivo. *Nature* 518, 542–546. doi: 10.1038/nature14242

Cao, H., Cao, B., Heazlewood, C. K., Domingues, M., Sun, X., Debele, E., et al. (2019). Osteopontin is an important regulative component of the fetal bone marrow hematopoietic stem cell niche. *Cells* 8:985. doi: 10.3390/cells8090985

Cardier, J., and Barberá-Guillem, E. (1997). Extramedullary hematopoiesis in the adult mouse liver is associated with specific hepatic sinusoidal endothelial cells. *Hepatology* 26, 165–175. doi: 10.1002/hep.510260122

Cardier, J., and Dempsey, J. (1998). Thrombopoietin and its receptor, c-mpl, are constitutively expressed by mouse liver endothelial cells: evidence of thrombopoietin as a growth factor for liver endothelial cells. *Blood* 91, 923–929. doi: 10.1182/blood.V91.3.923

Cascio, S., and Zaret, K. S. (1991). Hepatocyte differentiation initiates during endodermal-mesenchymal interactions prior to liver formation. *Development* 113, 217–225.

Chan, C. K. F., Chen, C.-C., Luppen, C. A., Kim, J.-B., DeBoer, A. T., Wei, K., et al. (2009). Endochondral ossification is required for haematopoietic stem-cell niche formation. *Nature* 457, 490–494. doi: 10.1038/nature07547

Charbord, P., and Moore, K. A. (2005). Gene expression in stem cell-supporting stromal cell lines. *Ann. N. Y. Acad. Sci.* 1044, 159–167. doi: 10.1196/annals.1349.020

Charbord, P., Tavian, M., Humeau, L., and Peault, B. (1996). Early ontogeny of the human marrow from long bones: an immunohistochemical study of hematopoiesis and its microenvironment. *Blood* 87, 4109–4119. doi: 10.1182/blood.V87.10.4109.bloodjournal87104109

Chen, J. Y., Miyanishi, M., Wang, S. K., Yamazaki, S., Sinha, R., Kao, K. S., et al. (2016). Hoxb5 marks long-term haematopoietic stem cells and reveals a homogenous perivascular niche. *Nature* 530, 223–227. doi: 10.1038/nature16943

Cheshier, S. H., Morrison, S. J., Liao, X., and Weissman, I. L. (1999). In vivo proliferation and cell cycle kinetics of long-term self-renewing hematopoietic stem cells. *Proc. Natl. Acad. Sci. U.S.A.* 96, 3120–3125. doi: 10.1073/pnas.96.6.3120

Chiu, S.-C., Liu, H.-H., Chen, C.-L., Chen, P.-R., Liu, M.-C., Lin, S.-Z., et al. (2015). Extramedullary hematopoiesis (EMH) in laboratory animals: offering an insight into stem cell research. *Cell Transplant.* 24, 349–366. doi: 10.3727/096368915X686850

Chou, S., Flygare, J., and Lodish, H. F. (2013). Fetal hepatic progenitors support long-term expansion of hematopoietic stem cells. *Exp. Hematol.* 41, 479–490. doi: 10.1016/j.exphem.2013.02.003

Chou, S., and Lodish, H. F. (2010). Fetal liver hepatic progenitors are supportive stromal cells for hematopoietic stem cells. *Proc. Natl. Acad. Sci. U.S.A.* 107, 7799–7804. doi: 10.1073/pnas.1003586107

Christensen, J. L., Wright, D. E., Wagers, A. J., and Weissman, I. L. (2004). Circulation and chemotaxis of fetal hematopoietic stem cells. *PLoS Biol.* 2:e020075. doi: 10.1371/journal.pbio.0020075

Christodoulou, C., Spencer, J. A., Yeh, S.-C. A., Turcotte, R., Kokkaliaris, K. D., Panero, R., et al. (2020). Live-animal imaging of native haematopoietic stem and progenitor cells. *Nature* 578, 278–283. doi: 10.1038/s41586-020-1971-z

Clotman, F. (2005). Control of liver cell fate decision by a gradient of TGF signaling modulated by Onecut transcription factors. *Genes Dev.* 19, 1849–1854. doi: 10.1101/gad.340305

Clotman, F., Lannoy, V. J., Reber, M., Cereghini, S., Cassiman, D., Jacquemin, P., et al. (2002). The onecut transcription factor HNF6 is required for normal development of the biliary tract. *Development* 129, 1819–1828.

Collardeau-Frachon, S., and Scoazec, J. Y. (2008). Vascular development and differentiation during human liver organogenesis. *Anat. Rec.* 291, 614–627. doi: 10.1002/ar.20679

Cordeiro Gomes, A., Hara, T., Lim, V. Y., Herndler-Brandstetter, D., Nevius, E., Sugiyama, T., et al. (2016). Hematopoietic stem cell niches produce lineage-instructive signals to control multipotent progenitor differentiation. *Immunity* 45, 1219–1231. doi: 10.1016/j.immuni.2016.11.004

Coşkun, S., Chao, H., Vasavada, H., Heydari, K., Gonzales, N., Zhou, X., et al. (2014). Development of the fetal bone marrow niche and regulation of HSC quiescence and homing ability by emerging osteolineage cells. *Cell Rep.* 9, 581–590. doi: 10.1016/j.celrep.2014.09.013

Crane, G. M., Jeffery, E., and Morrison, S. J. (2017). Adult haematopoietic stem cell niches. *Nat. Rev. Immunol.* 17, 573–590. doi: 10.1038/nri.2017.53

Crawford, L. W., Foley, J. F., and Elmore, S. A. (2010). Histology atlas of the developing mouse hepatobiliary system with emphasis on embryonic days 9.5-18.5. *Toxicol. Pathol.* 38, 872–906. doi: 10.1177/0192623310374329

Cumano, A., Dieterlen-Lievre, F., and Godin, I. (1996). Lymphoid potential, probed before circulation in mouse, is restricted to caudal intraembryonic splanchnopleura. *Cell* 86, 907–916. doi: 10.1016/S0092-8674(00)80166-X

Cumano, A., Ferraz, J. C., Klaine, M., Di Santo, J. P., and Godin, I. (2001). Intraembryonic, but Not Yolk Sac hematopoietic precursors, isolated before circulation, provide long-term multilineage reconstitution. *Immunity* 15, 477–485. doi: 10.1016/S1074-7613(01)00190-X

de Sauvage, F. J., Carver-Moore, K., Luoh, S. M., Ryan, A., Dowd, M., Eaton, D. L., et al. (1996). Physiological regulation of early and late stages of megakaryocytopoiesis by thrombopoietin. *J. Exp. Med.* 183, 651–656. doi: 10.1084/jem.183.2.651

Decker, M., Leslie, J., Liu, Q., and Ding, L. (2018). Hepatic thrombopoietin is required for bone marrow hematopoietic stem cell maintenance. *Science* 360, 106–110. doi: 10.1126/science.aap8861

Ding, L., Saunders, T. L., Enikolopov, G., and Morrison, S. J. (2012). Endothelial and perivascular cells maintain haematopoietic stem cells. *Nature* 481, 457–462. doi: 10.1038/nature10783

Douarin, N. M. (1975). An experimental analysis of liver development. *Med. Biol.* 53, 427–455.

Dudas, J., Papoutsi, M., Hecht, M., Elmaouhoub, A., Saile, B., Christ, B., et al. (2004). The homeobox transcription factor Prox1 is highly conserved in embryonic hepatoblasts and in adult and transformed hepatocytes, but is absent

from bile duct epithelium. *Anat. Embryol.* 208, 359–366. doi: 10.1007/s00429-004-0403-4

Eaton, D. L., and de Sauvage, F. J. (1997). Thrombopoietin: the primary regulator of megakaryocytopoiesis and thrombopoiesis. *Exp. Hematol.* 25, 1–7.

Eberl, G., Marmon, S., Sunshine, M. J., Rennert, P. D., Choi, Y., and Littmann, D. R. (2004). An essential function for the nuclear receptor RORγt in the generation of fetal lymphoid tissue inducer cells. *Nat. Immunol.* 5, 64–73. doi: 10.1038/ni1022

Eckardt, K. U., Pugh, C. W., Meier, M., Tan, C. C., Ratcliffe, P. J., and Kurtz, A. (1994). Production of erythropoietin by liver cells in vivo and in vitro. *Ann. N. Y. Acad. Sci.* 718, 50–60. doi: 10.1111/j.1749-6632.1994.tb55703.x

Ema, H., and Nakauchi, H. (2000). Expansion of hematopoietic stem cells in the developing liver of a mouse embryo. *Blood* 95, 2284–2289.

Emambokus, N. R., and Frampton, J. (2003). The glycoprotein IIb molecule is expressed on early murine hematopoietic progenitors and regulates their numbers in sites of hematopoiesis. *Immunity* 19, 33–45. doi: 10.1016/S1074-7613(03)00173-0

Fox, N., Priestley, G., Papayannopoulou, T., and Kaushansky, K. (2002). Thrombopoietin expands hematopoietic stem cells after transplantation. *J. Clin. Invest.* 110, 389–394. doi: 10.1172/JCI15430

Frame, J. M., Fegan, K. H., Conway, S. J., McGrath, K. E., and Palis, J. (2016). Definitive hematopoiesis in the yolk sac emerges from wnt-responsive hemogenic endothelium independently of circulation and arterial identity. *Stem Cells* 34, 431–444. doi: 10.1002/stem.2213

Fraser, S. T., Ogawa, M., Yu, R. T., Nishikawa, S., Yoder, M. C., and Nishikawa, S. I. (2002). Definitive hematopoietic commitment within the embryonic vascular endothelial-cadherin+ population. *Exp. Hematol.* 30, 1070–1078. doi: 10.1016/S0301-472X(02)00887-1

Freire, A. G., and Butler, J. M. (2020). Blood making: learning what to put into the dish. *F1000Research* 9:38. doi: 10.12688/f1000research.21245.1

Fujita, J., Onoue, H., Ebi, Y., Nakayama, H., and Kanakura, Y. (1989). In vitro duplication and in vivo cure of mast-cell deficiency of Sl/Sld mutant mice by cloned 3T3 fibroblasts. *Proc. Natl. Acad. Sci. U.S.A.* 86, 2888–2891. doi: 10.1073/pnas.86.8.2888

Gekas, C., Dieterlen-Lièvre, F., Orkin, S. H., and Mikkola, H. K. A. (2005). The placenta is a niche for hematopoietic stem cells. *Dev. Cell* 8, 365–375. doi: 10.1016/j.devcel.2004.12.016

Gentek, R., Ghigo, C., Hoeffel, G., Bulle, M. J., Msallam, R., Gautier, G., et al. (2018). Hemogenic endothelial fate mapping reveals dual developmental origin of mast cells. *Immunity* 48, 1160–1171. doi: 10.1016/j.immuni.2018.04.025

Gerlach, J. C., Over, P., Turner, M. E., Thompson, R. L., Foka, H. G., Chen, W. C. W., et al. (2012). *Perivascular mesenchymal* progenitors in human fetal and adult liver. *Stem Cells Dev.* 21, 3258–3269. doi: 10.1089/scd.2012.0296

Gerlach, J. C., Thompson, R. L., Gridelli, B., and Schmelzer, E. (2019). Effects of delta-like noncanonical Notch ligand 1 expression of human fetal liver hepatoblasts on hematopoietic progenitors. *Stem Cells Intern.* 2019:7916275. doi: 10.1155/2019/7916275

Godoy, P., Hewitt, N. J., Albrecht, U., Andersen, M. E., Ansari, N., Bhattacharya, S., et al. (2013). Recent advances in 2D and 3D in vitro systems using primary hepatocytes, alternative hepatocyte sources and non-parenchymal liver cells and their use in investigating mechanisms of hepatotoxicity, cell signaling and ADME. *Arch. Toxicol.* 87:1315. doi: 10.1007/s00204-013-1078-5

Gomez-Perdiguero, E., Klapproth, K., Schulz, C., Busch, K., Azzoni, E., Crozet, L., et al. (2015). Tissue-resident macrophages originate from yolk-sac-derived erythro-myeloid progenitors. *Nature* 518, 547–551. doi: 10.1038/nature13989

Guilbert, L. J., and Stanley, E. R. (1980). Specific interaction of murine colony-stimulating factor with mononuclear phagocytic cells. *J. Cell Biol.* 85, 153–159. doi: 10.1083/jcb.85.1.153

Guo, Y., Zhang, X., Huang, J., Zeng, Y., Liu, W., Geng, C., et al. (2009). Relationships between hematopoiesis and hepatogenesis in the midtrimester fetal liver characterized by dynamic transcriptomic and proteomic profiles. *PLoS One* 4:e7641. doi: 10.1371/journal.pone.0007641

Guyot, C., Lepreux, S., Combe, C., Doudnikoff, E., Bioulac-Sage, P., Balabaud, C., et al. (2006). Hepatic fibrosis and cirrhosis: the (myo)fibroblastic cell subpopulations involved. *Intern. J. Biochem. Cell Biol.* 38, 135–151. doi: 10.1016/j.biocel.2005.08.021

Haas, J. D., Ravens, S., Düber, S., Sandrock, I., Oberdörfer, L., Kashani, E., et al. (2012). Development of interleukin-17-producing γδ T cells is restricted to a functional embryonic wave. *Immunity* 37, 48–59. doi: 10.1016/j.immuni.2012.06.003

Haruna, Y., Saito, K., Spaulding, S., Nalesnik, M. A., and Gerber, M. A. (1996). Identification of bipotential progenitor cells in human liver development. *Hepatology* 23, 476–481. doi: 10.1002/hep.510230312

Hata, M., Nanno, M., Doi, H., Satomi, S., Sakata, T., Suzuki, R., et al. (1993). Establishment of a hepatocytic epithelial cell line from the murine fetal liver capable of promoting hemopoietic cell proliferation. *J. Cell. Physiol.* 154, 381–392. doi: 10.1002/jcp.1041540222

Hayashi, Y., Sezaki, M., and Takizawa, H. (2019). Development of the hematopoietic system: Role of inflammatory factors. *Wil. Interdiscipl. Rev. Dev. Biol.* 8, 1–17. doi: 10.1002/wdev.341

Hirsch, E., Iglesias, A., Potocnik, A. J., Hartmann, U., and Fässler, R. (1996). Impaired migration but not differentiation of haematopoietic stem cells in the absence of β1 integrins. *Nature* 380, 171–175. doi: 10.1038/380171a0

Holst, J., Watson, S., Lord, M. S., Eamegdool, S. S., Bax, D. V., Nivison-Smith, L. B., et al. (2010). Substrate elasticity provides mechanical signals for the expansion of hemopoietic stem and progenitor cells. *Nat. Biotechnol.* 28, 1123–1128. doi: 10.1038/nbt.1687

House, P. D. R., and Weidemann, M. J. (1970). Characterization of an [125I]-Insulin binding plasma membrane fraction from rat liver. *Biochem. Biophys. Res. Commun.* 41, 541–548. doi: 10.1016/0006-291X(70)90046-X

Ijpenberg, A., Pérez-Pomares, J. M., Guadix, J. A., Carmona, R., Portillo-Sánchez, V., Macías, D., et al. (2007). Wt1 and retinoic acid signaling are essential for stellate cell development and liver morphogenesis. *Dev. Biol.* 312, 157–170. doi: 10.1016/j.ydbio.2007.09.014

Ikuta, K., Kina, T., MacNeil, I., Uchida, N., Peault, B., Chien, Y., et al. (1990). A developmental switch in thymic lymphocyte maturation potential occurs at the level of hematopoietic stem cells. *Cell* 62, 863–874. doi: 10.1016/0092-8674(90)90262-D

Ji, R. P., Phoon, C. K. L., Aristizábal, O., McGrath, K. E., Palis, J., and Turnbull, D. H. (2003). Onset of cardiac function during early mouse embryogenesis coincides with entry of primitive erythroblasts into the embryo proper. *Circ. Res.* 92, 133–135. doi: 10.1161/01.RES.0000056532.18710.C0

Johns, J. L., and Christopher, M. M. (2012). Extramedullary hematopoiesis: a new look at the underlying stem cell niche, theories of development, and occurrence in animals. *Vet. Pathol.* 49, 508–523. doi: 10.1177/0300985811432344

Johnson, G. R., and Moore, M. A. S. (1975). Role of stem cell migration in initiation of mouse foetal liver haemopoiesis. *Nature* 258, 726–728. doi: 10.1038/258726a0

Kamiya, A., Kinoshita, T., Ito, Y., Matsui, T., Morikawa, Y., Senba, E., et al. (1999). Fetal liver development requires a paracrine action of oncostatin M through the gp130 signal transducer. *EMBO J.* 18, 2127–2136. doi: 10.1093/emboj/18.8.2127

Kasaai, B., Caolo, V., Peacock, H. M., Lehoux, S., Gomez-Perdiguero, E., Luttun, A., et al. (2017). Erythro-myeloid progenitors can differentiate from endothelial cells and modulate embryonic vascular remodeling. *Sci. Rep.* 7, 25–28. doi: 10.1038/srep43817

Kaushansky, K. (1995). Thrombopoietin: the primary regulator of platelet production. *Blood* 86, 419–431. doi: 10.1182/blood.V86.2.419.bloodjournal862419

Khan, J., Mendelson, A., Kunisaki, Y., Birbrair, A., Kou, Y., Arnal-Estapé, A., et al. (2016). Fetal liver hematopoietic stem cell niches associate with portal vessels. *Science* 351, 176–180. doi: 10.1126/science.aad0084

Kieusseian, A., de la Grange, P. B., Burlen-Defranoux, O., Godin, I., and Cumano, A. (2012). Immature hematopoietic stem cells undergo maturation in the fetal liver. *Development* 139, 3521–3530. doi: 10.1242/dev.079210

Kim, I., He, S., Yilmaz, O. H., Kiel, M. J., Morrison, S. J., and Yilmaz, H. (2006). Enhanced purification of fetal liver hematopoietic stem cells using SLAM family receptors. *Blood* 108, 737–744. doi: 10.1182/blood-2005-10-4135

Kimura, S., Roberts, A. W., Metcalf, D., and Alexander, W. S. (1998). Hematopoietic stem cell deficiencies in mice lacking c-Mpl, the receptor for thrombopoietin. *Proc. Natl. Acad. Sci. U.S.A.* 95, 1195–1200. doi: 10.1073/pnas.95.3.1195

Kingsley, P. D., Malik, J., Emerson, R. L., Bushnell, T. P., McGrath, K. E., Bloedorn, L. A., et al. (2006). "Maturational" globin switching in primary primitive erythroid cells. *Blood* 107, 1665–1672. doi: 10.1182/blood-2005-08-3097

Kinoshita, T., Sekiguchi, T., Xu, M.-J., Ito, Y., Kamiya, A., Tsuji, K.-I., et al. (1999). Hepatic differentiation induced by oncostatin M attenuates fetal liver hematopoiesis. *Proc. Natl. Acad. Sci. U.S.A.* 96, 7265–7270. doi: 10.2177/jsci.21.supplement_215

Kiserud, T. (2005). Physiology of the fetal circulation. *Semin. Fet. Neonat. Med.* 10, 493–503. doi: 10.1016/j.siny.2005.08.007

Kissa, K., and Herbomel, P. (2010). Blood stem cells emerge from aortic endothelium by a novel type of cell transition. *Nature* 464, 112–115. doi: 10.1038/nature08761

Ku, H., Yonemura, Y., Kaushansky, K., and Ogawa, M. (1996). Thrombopoietin, the ligand for the Mpl receptor, synergizes with steel factor and other early acting cytokines in supporting proliferation of primitive hematopoietic progenitors of mice. *Blood* 87, 4544–4551.

Kubota, H., Yao, H., and Reid, L. M. (2007). Identification and characterization of vitamin a-storing cells in fetal liver: implications for functional importance of hepatic stellate cells in liver development and hematopoiesis. *Stem Cells* 25, 2339–2349. doi: 10.1634/stemcells.2006-0316

Kumar, S., and Geiger, H. (2017). HSC niche biology and hsc expansion Ex *Vivo*. *Trends Mol. Med.* 23, 799–819. doi: 10.1016/j.molmed.2017.07.003

Kunisaki, Y., Bruns, I., Scheiermann, C., Ahmed, J., Pinho, S., Zhang, D., et al. (2013). Arteriolar niches maintain haematopoietic stem cell quiescence. *Nature* 502, 637–643. doi: 10.1038/nature12612

Lai, C.-Y., Yamazaki, S., Okabe, M., Suzuki, S., Maeyama, Y., Iimura, Y., et al. (2014). Stage-specific roles for Cxcr4 signaling in murine hematopoietic stem/progenitor cells in the process of bone marrow repopulation. *Stem Cells* 32, 1929–1942. doi: 10.1002/stem.1670

Lee, E. Y.-H. P., Chang, C.-Y., Hu, N., Wang, Y.-C. J., Lai, C.-C., Herrup, K., et al. (1992). Mice deficient for Rb are nonviable and show defects in neurogenesis and haematopoiesis. *Nature* 359, 288–294. doi: 10.1038/359288a0

Li, J., Ning, G., and Duncan, S. A. (2000). Mammalian hepatocyte differentiation requires the transcription factor HNF-4alpha. *Genes Dev.* 14, 464–474. doi: 10.1128/MMBR.66.1.39-63.2002

Lin, C. S., Lim, S. K., D'Agati, V., and Costantini, F. (1996). Differential effects of an erythropoietin receptor gene disruption on primitive and definitive erythropoiesis. *Genes Dev.* 10, 154–164. doi: 10.1101/gad.10.2.154

Lok, S., Kaushansky, K., Holly, R. D., Kuijper, J. L., Lofton-Day, C. E., Oort, P. J., et al. (1994). Cloning and expression of murine thrombopoietin cDNA and stimulation of platelet production in vivo. *Nature* 369, 565–568. doi: 10.1038/369565a0

Lua, I., and Asahina, K. (2016). The role of mesothelial cells in liver development. *Injury Regener. Gut Liver* 10:166. doi: 10.5009/gnl15226

Lyman, S. D., James, L., Bos, T., Vanden de Vries, P., Brasel, K., Gliniak, B., et al. (1993). Molecular cloning of a ligand for the flt3flk-2 tyrosine kinase receptor: a proliferative factor for primitive hematopoietic cells. *Cell* 75, 1157–1167. doi: 10.1016/0092-8674(93)90325-K

Manesia, J. K., Xu, Z., Broekaert, D., Boon, R., van Vliet, A., Eelen, G., et al. (2015). Highly proliferative primitive fetal liver hematopoietic stem cells are fueled by oxidative metabolic pathways. *Stem Cell Res.* 15, 715–721. doi: 10.1016/j.scr.2015.11.001

Margagliotti, S., Clotman, F., Pierreux, C. E., Beaudry, J. B., Jacquemin, P., Rousseau, G. G., et al. (2007). The onecut transcription factors HNF-6/OC-1 and OC-2 regulate early liver expansion by controlling hepatoblast migration. *Dev. Biol.* 311, 579–589. doi: 10.1016/j.ydbio.2007.09.013

Matsumoto, K., Yoshitomi, H., Rossant, J., and Zaret, K. S. (2001). Liver organogenesis promoted by endothelial cells prior to vascular function. *Science* 294, 559–563. doi: 10.1126/science.1063889

Matthews, W., Jordan, C. T., Wiegand, G. W., Pardoll, D., and Lemischka, I. R. (1991). A receptor tyrosine kinase specific to hematopoietic stem and progenitor cell-enriched populations. *Cell* 65, 1143–1152. doi: 10.1016/0092-8674(91)90010-V

McDermott, D. H., Gao, J.-L., Liu, Q., Siwicki, M., Martens, C., Jacobs, P., et al. (2015). Chromothriptic cure of WHIM syndrome. *Cell* 160, 686–699. doi: 10.1016/j.cell.2015.01.014

McGrath, K. E., Frame, J. M., Fegan, K. H., Bowen, J. R., Conway, S. J., Catherman, S. C., et al. (2015). Distinct sources of hematopoietic progenitors emerge before HSCS and provide functional blood cells in the mammalian Embryo. *Cell Rep.* 11, 1892–1904. doi: 10.1016/j.celrep.2015.05.036

Medvinsky, A., Dzierzak, E., Ridgeway, T., and Hill, M. (1996). Definitive hematopoiesis is autonomously initiated by the AGM region. *Cell* 86, 897–906. doi: 10.1016/S0092-8674(00)80165-8

Méndez-Ferrer, S., Michurina, T. V., Ferraro, F., Mazloom, A. R., MacArthur, B. D., Lira, S. A., et al. (2010). Mesenchymal and haematopoietic stem cells form a unique bone marrow niche. *Nature* 466, 829–834. doi: 10.1038/nature09262

Migliaccio, G., Migliaccio, A. R., Petti, S., Mavilio, F., Russo, G., Lazzaro, D., et al. (1986). Human embryonic hemopoiesis. Kinetics of progenitors and precursors underlying the yolk sac-liver transition. *J. Clin. Invest.* 78, 51–60. doi: 10.1172/JCI112572

Miller, C. L., Rebel, V. I, Helgason, C. D., Lansdorp, D., and Eaves, C. J. (1997). Impaired steel factor responsiveness differentially affects the detection and long-term maintenance of fetal liver hematopoietic stem cells in vivo. *Blood* 89, 1214–1223. doi: 10.1182/blood.v89.4.1214

Miyajima, A., Kinoshita, T., Tanaka, M., Kamiya, A., Mukouyama, Y., and Hara, T. (2000). Role of oncostatin M in hematopoiesis and liver development. *Cytokine Growth. Factor. Rev.* 11, 177–183. doi: 10.1016/S1359-6101(00)00003-4

Mizoguchi, T., Pinho, S., Ahmed, J., Kunisaki, Y., Hanoun, M., Mendelson, A., et al. (2014). Osterix marks distinct waves of primitive and definitive stromal progenitors during bone marrow development. *Dev. Cell* 29, 340–349. doi: 10.1016/j.devcel.2014.03.013

Moore, K. A., Pytowski, B., Witte, L., Hicklin, D., and Lemischka, I. R. (1997). Hematopoietic activity of a stromal cell transmembrane protein containing epidermal growth factor-like repeat motifs. *Proc. Natl. Acad. Sci. U.S.A.* 94, 4011–4016. doi: 10.1073/pnas.94.8.4011

Morgan, D. O., Edman, J. C., Standring, D. N., Fried, V. A., Smith, M. C., Roth, R. A., et al. (1987). Insulin-like growth factor II receptor as a multifunctional binding protein. *Nature* 329, 301–307. doi: 10.1038/329301a0

Morrison, S. J., Hemmati, H. D., Wandycz, A. M., and Weissman, I. L. (1995). The purification and characterization of fetal liver hematopoietic stem cells. *Proc. Natl. Acad. Sci. U.S.A.* 92, 10302–10306. doi: 10.1073/pnas.92.22.10302

Mucenski, M. L., Mclain, K., Kier, A., Swerdlow, S. H., Schreiner, C. M., Miller, T. A., et al. (1991). A functional c-myb Gene is required for normal murine fetal hepatic hematopoiesis. *Cell* 65, 677–689.

Nagasawa, T., Hirota, S., Tachibana, K., Takakura, N., Nishikawa, S. I., Kitamura, Y., et al. (1996). Defects of B-cell lymphopoiesis and bone-marrow myelopoiesis in mice lacking the CXC chemokine PBSF/SDF-1. *Nature* 382, 635–638. doi: 10.1038/382635a0

Nakamura, Y., Hagiwara, T., Hosokawa, K., Iwasaki, H., Matsuoka, S., Takahashi, T., et al. (2007). Thrombopoietin/MPL signaling regulates hematopoietic stem cell quiescence and interaction with the osteoblastic niche. *Cell Stem Cell* 1, 685–697. doi: 10.1016/j.stem.2007.10.020

Nakashima, K., Zhou, X., Kunkel, G., Zhang, Z., Deng, J. M., Behringer, R. R., et al. (2002). The novel zinc finger-containing transcription factor osterix is required for osteoblast differentiation and bone formation. *Cell* 108, 17–29. doi: 10.1016/S0092-8674(01)00622-5

Nierhoff, D., Ogawa, A., Oertel, M., Chen, Y.-Q., and Shafritz, D. A. (2005). Purification and characterization of mouse fetal liver epithelial cells with high in vivo repopulation capacity. *Hepatology* 42, 130–139. doi: 10.1002/hep.20735

Nishina, H., Vaz, C., Billia, P., Nghiem, M., Sasaki, T., De la Pompa, J. L., et al. (1999). Defective liver formation and liver cell apoptosis in mice lacking the stress signaling kinase SEK1/MKK4. *Development* 126, 505–516.

Nitou, M., Ishikawa, K., and Shiojiri, N. (2000). Immunohistochemical analysis of development of desmin-positive hepatic stellate cells in mouse liver. *J. Anat.* 197, 635–646. doi: 10.1046/j.1469-7580.2000.19740635.x

Nitou, M., Sugiyama, Y., Ishikawa, K., and Shiojiri, N. (2002). Purification of fetal mouse hepatoblasts by magnetic beads coated with monoclonal anti-E-cadherin antibodies and their in vitro culture. *Exper. Cell Res.* 279, 330–343. doi: 10.1006/excr.2002.5615

Nomura, S., Ogami, K., Kawamura, K., Tsukamoto, I., Kudo, Y., Kanakura, Y., et al. (1997). Cellular localization of thrombopoietin mRNA in the liver by in situ hybridization. *Exp. Hematol.* 25, 565–572.

Nonaka, H., Tanaka, M., Suzuki, K., and Miyajima, A. (2007). Development of murine hepatic sinusoidal endothelial cells characterized by the expression of hyaluronan receptors. *Dev. Dyn.* 236, 2258–2267. doi: 10.1002/dvdy.21227

Omatsu, Y., Sugiyama, T., Kohara, H., Kondoh, G., Fujii, N., Kohno, K., et al. (2010). The essential functions of adipo-osteogenic progenitors as the hematopoietic stem and progenitor cell niche. *Immunity* 33, 387–399. doi: 10.1016/j.immuni.2010.08.017

Onitsuka, I., Tanaka, M., and Miyajima, A. (2010). Characterization and functional analyses of hepatic mesothelial cells in mouse liver development. *Gastroenterology* 138, 1525–1535. doi: 10.1053/j.gastro.2009.12.059

Ottersbach, K., and Dzierzak, E. (2005). The murine placenta contains hematopoietic stem cells within the vascular labyrinth region. *Dev. Cell* 8, 377–387. doi: 10.1016/j.devcel.2005.02.001

Palis, J., Chan, R. J., Koniski, A., Patel, R., Starr, M., and Yoder, M. C. (2001). Spatial and temporal emergence of high proliferative potential hematopoietic precursors during murine embryogenesis. *Proc. Natl. Acad. Sci. U.S.A.* 98, 4528–4533. doi: 10.1073/pnas.071002398

Palis, J., Robertson, S., Kennedy, M., Wall, C., and Keller, G. (1999). Development of erythroid and myeloid progenitors in the yolk sac and embryo proper of the mouse. *Development* 126, 5073–5084.

Park, L. S., Friend, D. J., Schmierer, A. E., Dower, S. K., and Namen, A. E. (1990). Murine interleukin 7 (IL-7) receptor: characterization on an IL-7-dependent Cell Line. *J. Exper. Med.* 171, 1073–1089. doi: 10.1084/jem.171.4.1073

Pei, W., Feyerabend, T. B., Rössler, J., Wang, X., Postrach, D., Busch, K., et al. (2017). Polylox barcoding reveals haematopoietic stem cell fates realized *in vivo*. *Nature* 548, 456–460. doi: 10.1038/nature23653

Peschon, J. J., Morrissey, P. J., Grabstein, K. H., Ramsdell, F. J., Maraskovsky, E., Gliniak, B. C., et al. (1994). Early lymphocyte expansion is severely impaired in interleukin 7 receptor-deficient mice. *J. Exp. Med.* 180, 1955–1960. doi: 10.1084/jem.180.5.1955

Petit-Cocault, L., Volle-Challier, C., Fleury, M., Peault, B., and Souyri, M. (2007). Dual role of Mpl receptor during the establishment of definitive hematopoiesis. *Development* 134, 3031–3040. doi: 10.1242/dev.001818

Pinho, S., and Frenette, P. S. (2019). Haematopoietic stem cell activity and interactions with the niche. *Nat. Rev. Mol. Cell Biol.* 20, 303–320. doi: 10.1038/s41580-019-0103-9

Pinho, S., Lacombe, J., Hanoun, M., Mizoguchi, T., Bruns, I., Kunisaki, Y., et al. (2013). PDGFRα and CD51 mark human Nestin+ sphere-forming mesenchymal stem cells capable of hematopoietic progenitor cell expansion. *J. Exper. Med.* 210, 1351–1367. doi: 10.1084/jem.20122252

Ploemacher, R. E., and van Soest, P. L. (1977). Morphological investigation on phenylhydrazine-induced erythropoiesis in the adult mouse liver. *Cell Tissue Res.* 178, 435–461. doi: 10.1007/bf00219567

Prior, N., Hindley, C. J., Rost, F., Esteban, E. M., Lau, W. W. Y., Göttgens, B., et al. (2018). Lgr5+ stem/progenitor cells reside at the apex of the embryonic hepatoblast pool. *bioRxiv* [Preprint]. doi: 10.1101/485870

Qian, H., Buza-Vidas, N., Hyland, C. D., Jensen, C. T., Antonchuk, J., Månsson, R., et al. (2007). Critical role of thrombopoietin in maintaining adult quiescent hematopoietic stem cells. *Cell Stem Cell* 1, 671–684. doi: 10.1016/j.stem.2007.10.008

Ramond, C., Berthault, C., Burlen-Defranoux, O., De Sousa, A. P., Guy-Grand, D., Vieira, P., et al. (2014). Two waves of distinct hematopoietic progenitor cells colonize the fetal thymus. *Nat. Immunol.* 15, 27–35. doi: 10.1038/ni.2782

Ramsfjell, V., Borge, O. J., Veiby, O. P., Cardier, J., Murphy, M. J., Lyman, S. D., et al. (1996). Thrombopoietin, but not erythropoietin, directly stimulates multilineage growth of primitive murine bone marrow progenitor cells in synergy with early acting cytokines: distinct interactions with the ligands for c-kit and FLT3. *Blood* 88, 4481–4492.

Rhodes, K. E., Gekas, C., Wang, Y., Lux, C. T., Francis, C. S., Chan, D. N., et al. (2008). The emergence of hematopoietic stem cells is initiated in the placental vasculature in the absence of circulation. *Cell Stem Cell* 2, 252–263. doi: 10.1016/j.stem.2008.01.001

Rieger, M. A., Hoppe, P. S., Smejkal, B. M., Eitelhuber, A. C., and Schroeder, T. (2009). Hematopoietic cytokines can instruct lineage choice. *Science* 325, 217–218. doi: 10.1126/science.1171461

Robin, C., Bollerot, K., Mendes, S., Haak, E., Crisan, M., Cerisoli, F., et al. (2009). Human placenta is a potent hematopoietic niche containing hematopoietic stem and progenitor cells throughout development. *Cell Stem Cell* 5, 385–395. doi: 10.1016/j.stem.2009.08.020

Rodriguez-Fraticelli, A. E., Wolock, S. L., Weinreb, C. S., Panero, R., Patel, S. H., Jankovic, M., et al. (2018). Clonal analysis of lineage fate in native haematopoiesis. *Nature* 553, 212–216. doi: 10.1038/nature25168

Roy, V., and Verfaillie, C. M. (1999). Expression and function of cell adhesion molecules on fetal liver, cord blood and bone marrow hematopoietic progenitors: implications for anatomical localization and developmental stage specific regulation of hematopoiesis. *Exp. Hematol.* 27, 302–312. doi: 10.1016/S0301-472X(98)00031-9

Rubin, J. B., Shia, M. A., and Pilch, P. F. (1983). Stimulation of tyrosine-specific phosphorylation in vitro by insulin-Like growth factor I. *Nature* 305, 438–440. doi: 10.1038/305438a0

Ruggeri, A., Labopin, M., Sormani, M. P., Sanz, G., Sanz, J., Volt, F., et al. (2014). Engraftment kinetics and graft failure after single umbilical cord blood transplantation using a myeloablative conditioning regimen. *Haematologica* 99, 1509–1515. doi: 10.3324/haematol.2014.109280

Ryu, K. Y., Park, H., Rossi, D. J., Weissman, I. L., and Kopito, R. R. (2012). Perturbation of the hematopoietic system during embryonic liver development due to disruption of polyubiquitin gene Ubc in mice. *PLoS One* 7:32956. doi: 10.1371/journal.pone.0032956

Sacchetti, B., Funari, A., Michienzi, S., Di Cesare, S., Piersanti, S., Saggio, I., et al. (2007). Self-renewing osteoprogenitors in bone marrow sinusoids can organize a hematopoietic microenvironment. *Cell* 131, 324–336. doi: 10.1016/j.cell.2007.08.025

Sauvageau, G., Iscove, N. N., and Humphries, R. K. (2004). In vitro and in vivo expansion of hematopoietic stem cells. *Oncogene* 23, 7223–7232. doi: 10.1038/sj.onc.1207942

Sawyer, S. T., Krantz, S. B., and Luna, J. (1987). Identification of the receptor for erythropoietin by cross-linking to Friend virus-infected erythroid cells. *Proc. Natl. Acad. Sci. U.S.A.* 84, 3690–3694. doi: 10.1073/pnas.84.11.3690

Schofield, R. (1978). The relationship between the spleen colony-forming cell and the haemopoietic stem cell. *Blood Cells* 4, 7–25.

Schumann, K., Lämmermann, T., Bruckner, M., Legler, D. F., Polleux, J., Spatz, J. P., et al. (2010). Immobilized chemokine fields and soluble chemokine gradients cooperatively shape migration patterns of dendritic cells. *Immunity* 32, 703–713. doi: 10.1016/j.immuni.2010.04.017

Schuster, J. A., Stupnikov, M. R., Ma, G., Liao, W., Lai, R., Ma, Y., et al. (2012). Expansion of hematopoietic stem cells for transplantation: current perspectives. *Exper. Hematol. Oncol.* 1:12. doi: 10.1186/2162-3619-1-12

Semenza, G. L., Koury, S. T., Nejfelt, M. K., Gearhart, J. D., and Antonarakis, S. E. (1991). Cell-type-specific and hypoxia-inducible expression of the human erythropoietin gene in transgenic mice. *Proc. Natl. Acad. Sci. U.S.A.* 88, 8725–8729. doi: 10.1073/pnas.88.19.8725

Severn, C. B. (1971). A morphological study of the development of the human liver. I. Development of the hepatic diverticulum. *Am. J. Anat.* 131, 133–158. doi: 10.1002/aja.1001310202

Shiojiri, N., and Sugiyama, Y. (2004). Immunolocalization of extracellular matrix components and integrins during mouse liver development. *Hepatology* 40, 346–355. doi: 10.1002/hep.20303

Sigurdsson, V., Takei, H., Soboleva, S., Radulovic, V., Galeev, R., and Siva, K. (2016). Bile acids protect expanding hematopoietic stem cells from unfolded protein stress in fetal liver short article bile acids protect expanding hematopoietic stem cells from unfolded protein stress in fetal liver. *Stem Cell* 18, 522–532. doi: 10.1016/j.stem.2016.01.002

Soares-da-Silva, F., Burlen-Defranoux, O., Elsaid, R., Iturri, L., Freyer, L., Sismeiro, O., et al. (2020). Yolk sac erythromyeloid progenitors sustain erythropoiesis throughout embryonic life. *bioRxiv* [Preprint]. doi: 10.1101/2020.02.27.968230

Solar, G. P., Kerr, W. G., Zeigler, F. C., Hess, D., Donahue, C., Sauvage, F. J., et al. (1998). Role of c-mpl in early hematopoiesis. *Blood* 92, 4–10.

Stier, S., Ko, Y., Forkert, R., Lutz, C., Neuhaus, T., Grunewald, E., et al. (2005). Osteopontin is a hematopoietic stem cell niche component that negatively regulates stem cell pool size. *J. Exper. Med.* 201, 1781–1791. doi: 10.1084/jem.20041992

Sudo, T., Ito, M., Ogawa, Y., Iizuka, M., Kodama, H., Kunisada, T., et al. (1989). Interleukin 7 production and function in stromal cell-dependent B cell development. *J. Exp. Med.* 170, 333–338. doi: 10.1084/jem.170.1.333

Sugiyama, D., Kulkeaw, K., and Mizuochi, C. (2013). TGF-beta-1 up-regulates extra-cellular matrix production in mouse hepatoblasts. *Mech. Dev.* 130, 195–206. doi: 10.1016/j.mod.2012.09.003

Sugiyama, D., Kulkeaw, K., Mizuochi, C., Horio, Y., and Okayama, S. (2011). Hepatoblasts comprise a niche for fetal liver erythropoiesis through cytokine production. *Biochem. Biophys. Res. Commun.* 410, 301–306. doi: 10.1016/j.bbrc.2011.05.137

Sugiyama, T., Kohara, H., Noda, M., and Nagasawa, T. (2006). Maintenance of the hematopoietic stem cell pool by CXCL12-CXCR4 chemokine signaling in bone marrow stromal cell niches. *Immunity* 25, 977–988. doi: 10.1016/j.immuni.2006.10.016

Sugiyama, Y., Koike, T., and Shiojiri, N. (2010a). Developmental changes of cell adhesion molecule expression in the fetal mouse liver. *Anat. Rec.* 293, 1698–1710. doi: 10.1002/ar.21204

Sugiyama, Y., Takabe, Y., Nakakura, T., Tanaka, S., Koike, T., and Shiojiri, N. (2010b). Sinusoid development and morphogenesis may be stimulated by VEGF-Flk-1 signaling during fetal mouse liver development. *Dev. Dyn.* 239, 386–397. doi: 10.1002/dvdy.22162

Sun, J., Ramos, A., Chapman, B., Johnnidis, J. B., Le, L., Ho, Y.-J., et al. (2014). Clonal dynamics of native haematopoiesis. *Nature* 514, 322–327. doi: 10.1038/nature13824

Suzuki, A., Zheng, Y. W., Kondo, R., Kusakabe, M., Takada, Y., Fukao, K., et al. (2000). Flow-cytometric separation and enrichment of hepatic progenitor cells in the developing mouse liver. *Hepatology* 32, 1230–1239. doi: 10.1053/jhep.2000.20349

Swartley, O. M., Foley, J. F., Livingston, D. P., Cullen, J. M., and Elmore, S. A. (2016). Histology atlas of the developing mouse hepatobiliary hemolymphatic vascular system with emphasis on embryonic days 11.5-18.5 and early postnatal development. *Toxicol. Pathol.* 44, 705–725. doi: 10.1177/0192623316630836

Tajer, P., Pike-Overzet, K., Arias, S., Havenga, M., and Staal, F. (2019). Ex vivo expansion of hematopoietic stem cells for therapeutic purposes: lessons from development and the niche. *Cells* 8:169. doi: 10.3390/cells8020169

Takabe, Y., Yagi, S., Koike, T., and Shiojiri, N. (2012). Immunomagnetic exclusion of E-cadherin-positive hepatoblasts in fetal mouse liver cell cultures impairs morphogenesis and gene expression of sinusoidal endothelial cells. *J. Anat.* 221, 229–239. doi: 10.1111/j.1469-7580.2012.01532.x

Takashima, Y., Terada, M., Kawabata, M., and Suzuki, A. (2015). Dynamic three-dimensional morphogenesis of intrahepatic bile ducts in mouse liver development. *Hepatology* 61, 1003–1011. doi: 10.1002/hep.27436

Takebe, T., Enomura, M., Yoshizawa, E., Kimura, M., Koike, H., Ueno, Y., et al. (2015). Vascularized and complex organ buds from diverse tissues via mesenchymal cell-driven condensation. *Cell Stem Cell* 16, 556–565. doi: 10.1016/j.stem.2015.03.004

Tamplin, O. J., Durand, E. M., Carr, L. A., Childs, S. J., Hagedorn, E. J., Li, P., et al. (2015). Hematopoietic stem cell arrival triggers dynamic remodeling of the perivascular niche. *Cell* 160, 241–252. doi: 10.1016/j.cell.2014.12.032

Tan, K. S., Kulkeaw, K., Nakanishi, Y., and Sugiyama, D. (2017). Expression of cytokine and extracellular matrix mRNAs in fetal hepatic stellate cells. *Genes Cells* 22, 836–844. doi: 10.1111/gtc.12517

Tanaka, M., Okabe, M., Suzuki, K., Kamiya, Y., Tsukahara, Y., Saito, S., et al. (2009). Mouse hepatoblasts at distinct developmental stages are characterized by expression of EpCAM and DLK1: drastic change of EpCAM expression during liver development. *Mech. Dev.* 126, 665–676. doi: 10.1016/j.mod.2009.06.939

Tanaka, Y., Kurosawa, S., Tajima, K., Tanaka, T., Ito, R., Inoue, Y., et al. (2016). Analysis of non-relapse mortality and causes of death over 15 years following allogeneic hematopoietic stem cell transplantation. *Bone Marrow Transplant.* 51, 553–559. doi: 10.1038/bmt.2015.330

Taniguchi, H., Toyoshima, T., Fukao, K., and Nakauchi, H. (1996). Presence of hematopoietic stem cells in the adult liver. *Nat. Med.* 2, 198–203. doi: 10.1038/nm0296-198

Tanimizu, N., Kaneko, K., Itoh, T., Ichinohe, N., Ishii, M., Mizuguchi, T., et al. (2016). Intrahepatic bile ducts are developed through formation of homogeneous continuous luminal network and its dynamic rearrangement in mice. *Hepatology* 64, 175–188. doi: 10.1002/hep.28521

Tanimizu, N., Miyajima, A., and Mostov, K. E. (2009). Liver progenitor cells fold up a cell monolayer into a double-layered structure during tubular morphogenesis. *Mol. Biol. Cell* 20, 2486–2494. doi: 10.1091/mbc.e08-02-0177

Tanimizu, N., Nishikawa, M., Saito, H., Tsujimura, T., and Miyajima, A. (2003). Isolation of hepatoblasts based on the expression of Dlk/Pref-1. *J. Cell Sci.* 116, 1775–1786. doi: 10.1242/jcs.00388

Tanimizu, N., Saito, H., Mostov, K., and Miyajima, A. (2004). Long-term culture of hepatic progenitors derived from mouse Dlk+ hepatoblasts. *J. Cell Sci.* 117, 6425–6434. doi: 10.1242/jcs.01572

Taoudi, S., Gonneau, C., Moore, K., Sheridan, J. M., Blackburn, C. C., Taylor, E., et al. (2008). Extensive hematopoietic stem cell generation in the AGM region via maturation of VE-Cadherin+CD45+ pre-definitive HSCs. *Cell Stem Cell* 3, 99–108. doi: 10.1016/j.stem.2008.06.004

Taoudi, S., Morrison, A. M., Inoue, H., Gribi, R., Ure, J., and Medvinsky, A. (2005). Progressive divergence of definitive haematopoietic stem cells from the endothelial compartment does not depend on contact with the foetal liver. *Development* 132, 4179–4191. doi: 10.1242/dev.01974

Tavian, M., Coulombel, L., Luton, D., Clemente, H. S., Dieterlen-Lièvre, F., and Péault, B. (1996). Aorta-associated CD34+ hematopoietic cells in the early human embryo. *Blood* 87, 67–72.

Tavian, M., Hallais, M. F., and Péault, B. (1999). Emergence of intraembryonic hematopoietic precursors in the pre-liver human embryo. *Development* 126, 793–803.

Terada, T., and Nakanuma, Y. (1995). Detection of apoptosis and expression of apoptosis-related proteins during human intrahepatic bile duct development. *Am. J. Pathol.* 146, 67–74.

Tremblay, K. D., and Zaret, K. S. (2005). Distinct populations of endoderm cells converge to generate the embryonic liver bud and ventral foregut tissues. *Dev. Biol.* 280, 87–99. doi: 10.1016/j.ydbio.2005.01.003

Tsai, S., Emerson, S. G., Sieff, C. A., and Nathan, D. G. (1986). Isolation of a human stromal cell strain secreting hemopoietic growth factors. *J. Cell. Physiol.* 127, 137–145. doi: 10.1002/jcp.1041270117

Tsuneto, M., Tokoyoda, K., Kajikhina, E., Hauser, A. E., Hara, T., Tani-ichi, S., et al. (2013). B-cell progenitors and precursors change their microenvironment in fetal liver during early development. *Stem Cells* 31, 2800–2812. doi: 10.1002/stem.1421

Van Eyken, P., Sciot, R., Callea, F., Steen, K., Van Der Moerman, P., and Desmet, V. J. (1988). The development of the intrahepatic bile ducts in man: a keratin-immunohistochemical study. *Hepatology* 8, 1586–1595. doi: 10.1002/hep.1840080619

Vestentoft, P. S., Jelnes, P., Hopkinson, B. M., Vainer, B., Møllgård, K., Quistorff, B., et al. (2011). Three-dimensional reconstructions of intrahepatic bile duct tubulogenesis in human liver. *BMC Dev. Biol.* 11:56. doi: 10.1186/1471-213X-11-56

Vigon, I., Mornon, J. P., Cocault, L., Mitjavila, M. T., Tambourin, P., Gisselbrecht, S., et al. (1992). Molecular cloning and characterization of MPL, the human homolog of the v- mpl oncogene: identification of a member of the hematopoietic growth factor receptor superfamily. *Proc. Natl. Acad. Sci. U.S.A.* 89, 5640–5644. doi: 10.1073/pnas.89.12.5640

Wake, K. (1971). "Sternzellen" in the liver: perisinusoidal cells with special reference to storage of vitamin A. *Am. J. Anat.* 132, 429–461. doi: 10.1002/aja.1001320404

Walasek, M. A., van Os, R., and de Haan, G. (2012). Hematopoietic stem cell expansion: challenges and opportunities. *Ann. N. Y. Acad. Sci.* 1266, 138–150. doi: 10.1111/j.1749-6632.2012.06549.x

Wang, H. U., Chen, Z. F., and Anderson, D. J. (1998). Molecular distinction and angiogenic interaction between embryonic arteries and veins revealed by ephrin-B2 and its receptor Eph-B4. *Cell* 93, 741–753. doi: 10.1016/S0092-8674(00)81436-1

Watanabe, H., Miyaji, C., Seki, S., and Abo, T. (1996). c-kit+ stem cells and thymocyte precursors in the livers of adult mice. *J. Exp. Med.* 184, 687–693. doi: 10.1084/jem.184.2.687

Wei, Q., and Frenette, P. S. (2018). Niches for hematopoietic stem cells and their progeny. *Immunity* 48, 632–648. doi: 10.1016/j.immuni.2018.03.024

Weidemann, A., and Johnson, R. S. (2009). Nonrenal regulation of EPO synthesis. *Kidney Int.* 75, 682–688. doi: 10.1038/ki.2008.687

Wilkinson, A. C., Igarashi, K. J., and Nakauchi, H. (2020). Haematopoietic stem cell self-renewal in vivo and ex vivo. *Nat. Rev. Genet.* 27, 273–278. doi: 10.1038/s41576-020-0241-0

Wilkinson, A. C., Ishida, R., Kikuchi, M., Sudo, K., Morita, M., Crisostomo, R. V., et al. (2019). Long-term ex vivo haematopoietic-stem-cell expansion allows nonconditioned transplantation. *Nature* 571, 117–121. doi: 10.1038/s41586-019-1244-x

Wilson, A., Laurenti, E., Oser, G., van der Wath, R. C., Blanco-Bose, W., Jaworski, M., et al. (2008). Hematopoietic stem cells reversibly switch from dormancy to self-renewal during homeostasis and repair. *Cell* 135, 1118–1129. doi: 10.1016/j.cell.2008.10.048

Wilson, W., Groat, C. S., and Leduc, E. H. (2006). Histogenesis of the liver. *Ann. N. Y. Acad. Sci.* 111, 8–24. doi: 10.1111/j.1749-6632.1963.tb36945.x

Wineman, J., Moore, K., Lemischka, I., and Müller-Sieburg, C. (1996). Functional heterogeneity of the hematopoietic microenvironment: rare stromal elements maintain long-term repopulating stem cells. *Blood* 87, 4082–4090.

Wittig, O., Paez-Cortez, J., and Cardier, J. E. (2010). Liver sinusoidal endothelial cells promote b lymphopoiesis from primitive hematopoietic cells. *Stem Cells Dev.* 19, 341–350. doi: 10.1089/scd.2009.0300

Wohrer, S., Knapp, D. J. H. F., Copley, M. R., Benz, C., Kent, D. G., Rowe, K., et al. (2014). Distinct stromal cell factor combinations can separately control hematopoietic stem cell survival, proliferation, and self-renewal. *Cell Rep.* 7, 1956–1967. doi: 10.1016/j.celrep.2014.05.014

Wolber, F. M., Leonard, E., Michael, S., Orschell-Traycoff, C. M., Yoder, M. C., and Srour, E. F. (2002). Roles of spleen and liver in development of the murine hematopoietic system. *Exp. Hematol.* 30, 1010–1019. doi: 10.1016/S0301-472X(02)00881-0

Yang, L., Li, L. C., Lamaoqiezhong, L., Wang, X., Wang, W. H., Wang, Y. C., et al. (2019). The contributions of mesoderm-derived cells in liver development. *Semin. Cell Dev. Biol.* 92, 63–76. doi: 10.1016/j.semcdb.2018.09.003

Yang, L., Wang, W. H., Qiu, W. L., Guo, Z., Bi, E., and Xu, C. R. (2017). A single-cell transcriptomic analysis reveals precise pathways and regulatory mechanisms underlying hepatoblast differentiation. *Hepatology* 66, 1387–1401. doi: 10.1002/hep.29353

Yarden, Y., Kuang, W. J., Yang-Feng, T., Coussens, L., Munemitsu, S., Dull, T. J., et al. (1987). Human proto-oncogene c-kit: a new cell surface receptor tyrosine kinase for an unidentified ligand. *EMBO J.* 6, 3341–3351. doi: 10.1002/j.1460-2075.1987.tb02655.x

Yu, V. W. C., and Scadden, D. T. (2016). Hematopoietic stem cell and its bone marrow niche. *Curr. Top. Dev. Biol.* 118, 21–44. doi: 10.1016/bs.ctdb.2016.01.009

Zhang, C. C., Kaba, M., Ge, G., Xie, K., Tong, W., Hug, C., et al. (2006). Angiopoietin-like proteins stimulate ex vivo expansion of hematopoietic stem cells. *Nat. Med.* 12, 240–245. doi: 10.1038/nm1342

Zhang, C. C., and Lodish, H. F. (2004). Insulin-like growth factor 2 expressed in a novel fetal liver cell population is a growth factor for hematopoietic stem cells. *Blood* 103, 2513–2521. doi: 10.1182/blood-2003-08-2955

Zheng, J., Huynh, H., Umikawa, M., Silvany, R., and Zhang, C. C. (2011). Angiopoietin-like protein 3 supports the activity of hematopoietic stem cells in the bone marrow niche. *Blood* 117, 470–479. doi: 10.1182/blood-2010-06-291716

Zheng, J., Umikawa, M., Cui, C., Li, J., Chen, X., Zhang, C. C. C., et al. (2012). Inhibitory receptors bind ANGPTLs and support blood stem cells and leukaemia development. *Nature* 485, 656–660. doi: 10.1038/nature11095

Zhou, B. O., Yue, R., Murphy, M. M., Peyer, J. G., and Morrison, S. J. (2014). Leptin-receptor-expressing mesenchymal stromal cells represent the main source of bone formed by adult bone marrow. *Cell Stem Cell* 15, 154–168. doi: 10.1016/j.stem.2014.06.008

Zorn, A. M. (2008). Liver development. *Stembook* 2, 1–26. doi: 10.3824/stembook.1.25.1

Conflict of Interest: The authors declare that the research was conducted in the absence of any commercial or financial relationships that could be construed as a potential conflict of interest.

frontiers in Cell and Developmental Biology

ORIGINAL RESEARCH
published: 22 September 2020
doi: 10.3389/fcell.2020.576592

Mitochondrial and Redox Modifications in Huntington Disease Induced Pluripotent Stem Cells Rescued by CRISPR/Cas9 CAGs Targeting

*Carla Lopes[1,2], Yang Tang[3,4], Sandra I. Anjo[1,5], Bruno Manadas[1], Isabel Onofre[1,2], Luís P. de Almeida[1,6], George Q. Daley[3,4,7,8], Thorsten M. Schlaeger[3,4] and Ana Cristina Carvalho Rego[1,5]**

[1] CNC-Center for Neuroscience and Cell Biology, University of Coimbra, Coimbra, Portugal, [2] IIIUC-Institute for Interdisciplinary Research, University of Coimbra, Coimbra, Portugal, [3] Division of Pediatric Hematology/Oncology, Children's Hospital Boston, Boston, MA, United States, [4] Harvard Stem Cell Institute, Boston, MA, United States, [5] Faculty of Medicine, University of Coimbra, Coimbra, Portugal, [6] Faculty of Pharmacy, University of Coimbra, Coimbra, Portugal, [7] Howard Hughes Medical Institute, Boston, MA, United States, [8] Department of Biological Chemistry and Molecular Pharmacology, Harvard Medical School, Boston, MA, United States

OPEN ACCESS

Edited by:
Susana Solá,
University of Lisbon, Portugal

Reviewed by:
Alessandro Prigione,
Heinrich Heine University, Germany
Dan Lindholm,
University of Helsinki, Finland

***Correspondence:**
Ana Cristina Carvalho Rego
acrego@cnc.uc.pt;
arego@fmed.uc.pt

Specialty section:
This article was submitted to Stem Cell Research, a section of the journal Frontiers in Cell and Developmental Biology

Received: 26 June 2020
Accepted: 27 August 2020
Published: 22 September 2020

Citation:
Lopes C, Tang Y, Anjo SI, Manadas B, Onofre I, de Almeida LP, Daley GQ, Schlaeger TM and Rego ACC (2020) Mitochondrial and Redox Modifications in Huntington Disease Induced Pluripotent Stem Cells Rescued by CRISPR/Cas9 CAGs Targeting. Front. Cell Dev. Biol. 8:576592. doi: 10.3389/fcell.2020.576592

Mitochondrial deregulation has gained increasing support as a pathological mechanism in Huntington's disease (HD), a genetic-based neurodegenerative disorder caused by CAG expansion in the *HTT* gene. In this study, we thoroughly investigated mitochondrial-based mechanisms in HD patient-derived iPSC (HD-iPSC) and differentiated neural stem cells (NSC) *versus* control cells, as well as in cells subjected to CRISPR/Cas9-CAG repeat deletion. We analyzed mitochondrial morphology, function and biogenesis, linked to exosomal release of mitochondrial components, glycolytic flux, ATP generation and cellular redox status. Mitochondria in HD cells exhibited round shape and fragmented morphology. Functionally, HD-iPSC and HD-NSC displayed lower mitochondrial respiration, exosomal release of cytochrome c, decreased ATP/ADP, reduced PGC-1α and complex III subunit expression and activity, and were highly dependent on glycolysis, supported by pyruvate dehydrogenase (PDH) inactivation. HD-iPSC and HD-NSC mitochondria showed ATP synthase reversal and increased calcium retention. Enhanced mitochondrial reactive oxygen species (ROS) were also observed in HD-iPSC and HD-NSC, along with decreased UCP2 mRNA levels. CRISPR/Cas9-CAG repeat deletion in HD-iPSC and derived HD-NSC ameliorated mitochondrial phenotypes. Data attests for intricate metabolic and mitochondrial dysfunction linked to transcriptional deregulation as early events in HD pathogenesis, which are alleviated following CAG deletion.

Keywords: induced pluripotent stem cells, huntington disease, mitochondrial dysfunction, neural stem cells, reactive oxygen species, transcriptional deregulation

Abbreviations: Ψm, mitochondrial transmembrane potential; AA, antimycin A; Ctr, control; ECAR, extracellular acidification rate; HD, huntington's disease; iPSC, induced pluripotent stem cells; mHTT, mutant huntingtin; MSN, medium spiny neurons; Nrf2, nuclear factor erythroid derived 2-related; NSC, neural stem cells; OCR, oxygen consumption rate; PDH, pyruvate dehydrogenase; PDK, pyruvate dehydrogenase kinases; PDP, PDH phosphatases; PGC1α, peroxisome proliferator-activated receptor-γ coactivator α; polyQ, expanded polyglutamine; Prx, peroxiredoxin; ROS, reactive oxygen species; SNP, single nucleotide polymorphisms; SOD, superoxide dismutase; TEM, transmission electron microscopy; TFAM, mitochondrial transcription factor.

INTRODUCTION

Huntington's disease is caused by CAG repeat expansion in the *HTT* gene, encoding for mHTT (No authors listed, 1993), with expanded polyglutamine (polyQ) stretch at the N-terminal. Symptoms include psychiatric disturbances, cognitive deficits and involuntary movements, correlated with a selective loss of striatal MSN and cortical atrophy (Roos, 2010). Neuropathological mechanisms described in HD include alterations in gene transcription, Ca^{2+} dyshomeostasis, metabolic and mitochondrial disturbances, and oxidative stress [reviewed in Gil and Rego (2008)]. Increased susceptibility of HD striatal cells to mitochondrial deregulation due to decreased Ca^{2+} handling, metabolic disturbances and mitochondrial ROS were previously documented by us (Oliveira et al., 2006; Ribeiro et al., 2014; Naia et al., 2017). Increasing evidence support that mitochondrial dysfunction occurs at HD early stages, e.g., as defined by proteomic analysis (McQuade et al., 2014); therefore, examining the mitochondrial processes that define the early stages of this complex human neurogenetic disease is of utmost importance.

Several groups have successfully generated HD patient-specific HD-iPSC that were differentiated into HD neural stem cells (HD-NSC) and neurons with striatal characteristics (Park et al., 2008; Zhang et al., 2010; Camnasio et al., 2012; Delli Carri et al., 2013; Mattis et al., 2015). Striatal-like MSN displayed altered electrophysiology, metabolism, cell adhesion and cell death for lines with long CAG, up to 180 repeats (Hd iPSC Consortium, 2012). Recently, the decreased bioenergetic capacity in HD-iPSC-derived striatal neurons was attributed to defects in glycolysis rather than mitochondrial defects, as it was reverted with pyruvate (Hd iPSC Consortium, 2020). Oxidative stress-related proteins, such as SOD1 (superoxide dismutase 1) and peroxiredoxin were also shown to be affected in HD-iPSC (Chae et al., 2012; Lu et al., 2014; Szlachcic et al., 2015).

The creation of isogenic lines in which expanded CAG was replaced by normal CAG repeat through homologous recombination (An et al., 2012), further enhanced by using CRISPR/Cas9 (An et al., 2014), has been also applied to HD. A 180 CAG iPSC was corrected using a CRISPR/Cas9 and piggyBac transposon-based approach, rescuing the phenotypic abnormalities (Xu et al., 2017). Another approach involved depletion of the *HTT* gene or allele-specific genome editing using Cas9 (Shin et al., 2016; Kolli et al., 2017; Monteys et al., 2017; Dabrowska et al., 2018), but none have specifically focused on mitochondrial-related abnormalities.

Here, we thoroughly investigated mitochondrial-based mechanisms in HD human iPSC and NSC early differentiated counterparts to identify mitochondrial abnormalities and altered metabolic pathways that may underlie neurodysfunction in HD and further investigated the influence of CAG repeat/exon 1 deletion in HD-iPSC using CRISPR/Cas9. Data indicate that mitochondrial dysfunction caused by deficient complex III and PDH activities are partially counterbalanced by glycolysis stimulation and leads to mitochondrial-driven ROS generation in early stages of differentiation in HD human cells. Importantly, these mitochondrial deficits are alleviated after the deletion of CAG expansion, reinforcing this strategy as an attractive HD therapy.

MATERIALS AND METHODS

HiPSC Culture and Differentiation

Heterozygous human iPSC designated HD4-iPSC (XY, passages 4–30) with an expanded allele (72 CAG repeats) and a normal (19 CAG repeats) was generated by Park et al. (2008), while control AMS4-iPSC (XY, passages 7–30) was generated and characterized by de Almeida and collaborators (Onofre et al., 2016). Cells were maintained on a layer of mitotically inactivated murine embryonic fibroblasts (MEFs) for a variable number of passages or allowed to grow under feeder-free conditions on Matrigel® and Geltrex®. Manual dissection was routinely used to passage the cells. MEFs were acquired from AMSBIO® expanded for 3 passages and inactivated with mitomycin C.

iPSC were cultured in DMEM/F12 supplemented with 20% KSR, 2 mM glutamine, 1 mM non-essential amino acids, 1% penicillin/streptomycin (100 units/mL penicillin and 100 μg/mL streptomycin), 100 μM 2-mercaptoethanol and 10 ng/ml recombinant human FGF2. Cultures were fed daily and passaged at least once-a-week. When cells were grown in matrigel, medium was conditioned for 24 h in MEFs and filtered. Neural differentiation was based on dual SMAD inhibition with SB431542 (Lefty/Activin/transforming growth factor beta – TGFβ inhibitor), dorsomorphin (bone morphogenetic protein – BMP inhibitor) and XAV-939 (β-catenin-transcription inhibitor and axin stabilizing agent) (Chambers et al., 2009; Delli Carri et al., 2013; Nicoleau et al., 2013). Colonies were grown on 6-well plates in matrigel until reaching 100% confluence. Neural induction medium consisted of 1:1 mixture of two base media, DMEM/F12 and Neurobasal, 1% N2 (100x), 2 mM L-glutamine, 100 μM non-essential amino acids, 100 μM 2-mercaptoethanol, 1% penicillin/streptomycin and 2% B-27 (50x). Neural induction occurred between day 0 and day 10–12. For day 0 to day 5, cells were maintained in KSR medium without FGF2 and incubated with 5 μM dorsomorphin, 10 μM SB431542 and 1 μM XAV-939. Medium was changed every day. From day 5 to day 10–12, the medium was gradually replaced by 75% KSR + 25% N2 medium, 50% KSR + 50% N2 medium until reaching 100% N2 medium plus 5 μM dorsomorphin, 10 μM SB431542 and 1 μM XAV939 (Chambers et al., 2009; Delli Carri et al., 2013; Nicoleau et al., 2013). Between days 10 and 12, fields full of rosettes became morphologically visible. To allow the cells to differentiate, cells were replated in matrigel coated 12-well plates. For detaching, 500 μl of 1X Accutase® was added in the plate and incubated at 37°C in 5% CO2, for 15–20 min. Accutase was diluted in DMEM/F12 medium pre-warmed at 37°C. Cells were collected and spun for 3 min at 1000 rpm, at room temperature (RT), and resuspended in 200 μl of media into a well of a 12-well plate. Cells were allowed to adhere for 30 min and then 300 μl N2 medium, supplemented

with 10 μM Y-27632, 10 ng/ml FGF2 and 10 ng/ml EGF, was added. Dishes were carefully transferred at 37°C and left overnight in a 5% CO_2 incubator. Cells were maintained in the same medium and passaged every 2–3 days for no more than 10 passages.

Karyotype Analysis

The karyotype was assessed on metaphasic chromosomal spreads after GTG-banding performed at Centre of Genomics and Biotechnology of the University of Trás-os-Montes and Alto Douro (CGB-UTAD), Portugal.

Transfection of CRISPR Into Human iPSC and PCR Characterization Following CRISPR Correction

Prior to transfection, hiPSC cells were exposed to 10 μM Y27632 for 1 h prior to collection, washed with PBS, dissociated into single cells using TryplE Select (4 min at 37°C), and washed with mTesR containing 10 μM Y27632. 1 million single-cell dissociated HD-iPSC were nucleofected with 10 μg dual sgRNA plasmid (sgRNA target sequences = GCCTCCGGGGACTGCCGTGC, gCAAACTC ACGGTCGGTGCAG) and 5 μg Cas9_GFP plasmid using the Lonza2D Nucleofector and the Amaxa Stem Cell Kit V (VCA-1003) with program B-016 as described previously (Burnight et al., 2017). Nucleofected cells were plated onto matrigel in a 12-well plate well using a 50:50 mix of fresh and iPSC conditioned mTesR medium with 10 μM Y27632. 44 h after transfection, the hiPSCs were again harvested with TryplE Select as before, and approximately 10,000 GFP+ cells sorted using a BD FACS Aria II (BSL2) were re-plated into a 6-well plate well in a 50:50 mix of fresh and iPSC conditioned mTesR medium with 10 μM Y27632 and grown in iPSC conditioned mTesR medium until colonies formed, after which the medium was switched to regular mTesR.

Each subclone was screened by genomic PCR. DNA was isolated by Qiagen DNeasy Blood and Tissue Kit according to the manufacturer's instructions. The loci of interest were amplified by PCR (GoTaq Green Kit) using 7% DMSO for HTT amplification and without DMSO for YAP1, and cycling conditions were 90 s at 95°C, 40 × (30 s at 94°C; 30 s at 65°C; 90 s at 72°C). Primers for HTT primers were: 5′ GAGTCCCTCAAGTCCTTCCAGCA 3′, 5′ GCCCAAACTCACGGTCGGT 3′ (Jacquet et al., 2015) and primers for YAP1 were: 5′ TGAGTGATTTAAGGGTGAAA AATG 3′, 5′ TCACCATGTCCCAGTTTCTG 3′. PCR products were separated by gel electrophoresis using 1% agarose gels. HTT locus Sanger sequencing was done using PCR primers 5′ CCTCACCCCATTACAGTCTCACCAC 3′ and 5′ CACCACTTTACTTGGCAACCAC 3′, the Takara Primestar GXL PCR kit, 7% DMSO, cycling conditions 35 × (10 s at 98°C, 120 s at 68°C), and sequencing primer 5′ CAAGGGAAGACCCAAGTGAG 3′. Potential off-target sites were identified using CasOffFinder (pmid: 24463181) and then ranked according to the number and location of mismatches using a Python script. All identified potential off-target sites featured at least 3 mismatches, including at least 1 within the PAM-proximal 12 nucleotides.

Transmission Electron Microscopy

For TEM, control and HD iPSC and NSC were collected and fixed with 2.5% glutaraldehyde in 0.1 M sodium cacodylate buffer and dehydrated in a graded ethanol series (70–100%). Following embedding in 2% molten agar, cell pellets were re-dehydrated in ethanol (30–100%), impregnated and included in Epoxy resin (Fluka Analytical). Ultrathin sections were mounted on copper grids and stained with lead citrate 0.2%, for 7 min. Observations were carried out on a FEI-Tec-nai G2 Spirit Bio Twin at 100 kV.

Mitochondrial Labeling and Immunocytochemistry

Mitochondrial morphology was examined with pDsRed2-Mito. Cells were plated in a 24-well plate until 70% confluence; then transfection was performed according to the indicated procedures for Lipofectamine™ 3000.

Cells were fixed with 4% Paraformaldehyde/PHEM (20 min, @RT), rehydrated with PBS/0.1% Triton X-100, blocked in 3% BSA/PBS (30 min) and incubated with primary antibody overnight at 4°C. Secondary antibodies and DAPI counterstain were applied for 1 h at room temperature. Primary antibodies are listed in Supplementary experimental procedures. Confocal analysis was performed on a Zeiss LSM 710 confocal system (Carl Zeiss Microscopy). For details see **Supplementary Data**.

Immunoblotting

Cells were lysed in lysis buffer with protease inhibitor cocktail. For the isolation of nuclear and cytoplasmic fractions a Nuclear/Cytosol Fractionation Kit (BioVision, Inc.) was used according to manufacturer's instructions. Protein lysates (25 μg) were denatured with SDS sample buffer at 95°C, for 5 min. Protein were loaded in 6% or 12% gel, subjected to SDS-PAGE and electrophoretically transferred onto polyvinylidene difluoride (PVDF) Hybond-P membranes. Immunoreactive bands were visualized with VersaDoc Imaging System (BioRad®, Hercules, CA, United States). For details see **Supplementary Data**.

DNA and RNA Extraction, cDNA and RT-qPCR

Genomic DNA was extracted using PureLink® Genomic DNA Kit and RNA with the PureZOL® RNA Isolation Reagent. The purified DNA and RNA was then quantified with NanoDropR spectrophotometer Reverse transcription was performed with iScript™ cDNA Synthesis Kit. Real-time PCR (qPCR) was performed with iQTM SYBR® Green Supermix on a CFX96 Touch™ Real-Time PCR Detection System. Q-PCR was performed according to manufacturer's protocol. Tubulin and 18S were used for internal reference gene. Expression values were calculated using the $2^{-\Delta\Delta Ct}$ method. All PCR samples were run in technical triplicates, and the average Ct-values were used for calculations. The primers pairs are shown in **Supplementary Data** (**Supplementary Table 2**).

Measurement of Adenine Nucleotides

In experiments aimed to inhibit glycolysis, the culture medium was replaced by DMEM with low glucose (2 mM) (GLUC) or supplemented with 17.5 mM 2-deoxy-D-glucose (2-DG). To inhibit mitochondrial ATP synthesis, 2 μg/ml oligomycin was added to glucose-containing medium or supplemented with 2-DG.

ATP, ADP, and AMP were measured by high-performance liquid chromatography (HPLC) following perchloric acid precipitation, as described previously (Stocchi et al., 1985). The chromatographic apparatus used was a Beckman-System Gold, consisting of a 126 Binary Pump Model and 166 Variable UV detector. Peak identity was determined by following the retention time of standards. Data normalized for total protein.

Pyruvate Dehydrogenase E1α Subunit Protein Levels and Serine Phosphorylation

PDH expression and phosphorylation were assessed using PDH Enzyme Activity Microplate Assay Kit from MitoSciences (Oregon, United States).

Mitochondrial Membrane Potential ($\Delta\Psi$m) and Intracellular Ca^{2+} Measurements in Cell Population

$\Delta\Psi$m was determined using the cationic fluorescent probe Rhodamine 123 (Rhod123). Briefly, iPSC were cultured in a 6-well plate and NSC in 96-well plate until reach confluence. For iPSC, detachment was required previously to incubation with the probes. Cells were incubated with accutase at 37°C in 5% CO2 for 15–20 min. Accutase was diluted in KSR medium pre-warmed at 37°C and left for 30 min to minimize the enzyme stress on cells. Then, iPSC were washed twice in Krebs medium, spunned and incubated at 37°C for 30 min with 8 μM Rhod123 and 1.5 μM Fura-2 acetoxy-methyl ester (Fura-2/AM). NSC were incubated in the 96-wells plates directly by following the same protocol, without enzymatic detach. After incubation, the basal fluorescence was taken in buffer with 8 μM Rhod123 during 5 min using a Microplate Spectrofluorometer Gemini EM (Molecular Devices, United States). Intracellular Ca^{2+} was measured with Fura-2/AM that has an excitation spectrum at 380 nm (calcium free) and 340 nm (calcium complex) (ratio 340/380) with emission at 540 nm. Oligomycin (2 μg/ml) and p-trifluoromethoxy carbonyl cyanide phenyl hydrazone (FCCP) (2 μM) (separately or together), were added to cells and the fluorescence was taken during another 5 min. Results were expressed as the difference between the increase in Rhod123 or Fura-2/AM fluorescence upon addition of oligomycin followed by FCCP or oligomycin plus FCCP and basal fluorescence values.

Mitochondrial Superoxide Anion and Hydrogen Peroxide

The rate of mitochondrial superoxide production was measured using the mitochondria-specific probe MitoSOX Red (Life Technologies). iPSC and NSC were incubated with 5 μM MitoSOX and analyzed on a Microplate Spectrofluorometer Gemini EM. Cells were treated acutely with the stressor compounds (1 μM AA). NSCs were cultured for 24 h at 37°C in 96-well assay plates prior analysis. For NSC, Mitochondria peroxy yellow 1 (MitoPY1) basal levels were measured for 10–15 min followed by an acute stimulus with 3 μM myxothiazol. To measure extracellular H_2O_2 production, the Amplex Red Hydrogen Peroxide/Peroxidase Assay Kit was used. Cells were loaded with 10 μM AmplexRed reagent and 0.5 U/mL Horseradish (HRP) peroxidase. Fluorescence was measure for a total time of 40 min. Resultant fluorescence was analyzed on a Microplate Spectrofluorometer Gemini EM. The results were calculated as RFU per 500.000 cells for iPSC or per mg of protein for NSC. For details see **Supplementary Data**.

Enzymatic Assays

For all enzymatic assays, cells were lysed and the resulting supernatant was used after protein quantification using the BioRad protein assay. SOD enzymatic activity was performed according to the SOD Assay Kit (Sigma-Aldrich). GPx and GRed activities and measurement of GSH and GSSG levels are detailed in **Supplementary Data**.

Mitochondrial Respiratory Chain Complexes Activities

The mitochondrial-enriched fractions obtained from iPSC and NSC were assayed for the activity of mitochondrial complexes (Cx) I–IV by spectrophotometry. Detailed description of preparation of mitochondrial fractions and mitochondrial complexes activities in **Supplementary Data**.

XF24 Extracellular Flux Analyzer

Mitochondrial respiration OCR, glycolysis ECAR and fatty acid oxidation measurements in iPSC and NSC was carried out using a Seahorse XF24 Extracellular Flux Analyzer (Seahorse Bioscience). Readings were normalized to the amount of protein and data analyzed using the Seahorse Wave software. Detailed description in **Supplementary Data**.

Data Analysis and Statistics

Results are the mean ± SEM of the indicated number of independent experiments in figure legends. *F* test was performed to analyze the interaction term, as described in figure legends. At least three independent assays were performed for each experimental condition. Statistical significance was analyzed using parametric and non-parametric tests, namely one-way ANOVA and two-way ANOVA, followed by Bonferroni *post hoc* test, Student's *t*-test for comparison between two Gaussian populations and Mann–Whitney and Kruskal–Wallis tests for non-Gaussian samples. $P < 0.05$ was considered significant.

RESULTS

HD-iPSC and Neural Differentiated HD-NSC Express Mutant HTT and Display Cell-Specific Protein Expression Patterns

NSC were generated from HD and control (Ctr) iPSC lines by a neural induction protocol for 12 days (**Figure 1A**; Delli Carri et al., 2013). HD-iPSC and HD-NSC express both normal and polyQ-expanded form of HTT (72 CAG) (Park et al., 2008; **Figure 1B**). iPSC pluripotency was confirmed by detection of OCT4 and SOX2 (**Figures 1B,C**). Successful differentiation into NSC was confirmed by the expression of SOX2 and nestin (**Figures 1D,E**). Furthermore, karyotyping and G-banding analysis showed that iPSC maintained a normal 46,XX karyotype (**Figure 1F**).

Abnormal Mitochondrial Morphology in HD-iPSC and HD-NSC

Mitochondrial fragmentation has been previously associated with HD pathogenesis (Song et al., 2011). Thus, we first studied the ultrastructural abnormalities of mitochondria by TEM. Mitochondria were characterized as round shape if the axis (a and b) were equal, or rod shape if there was a tubular elongated morphology with a major and minor axis (**Figures 2A,B**). Although mitochondrial round shape was predominant in iPSC and NSC, the percentage of mitochondria with rod shape was significantly reduced in HD-iPSC and HD-NSC, when compared to Ctr cells (**Figures 2A,C**). HD-iPSC also exhibited a higher number of mitochondria with undeveloped cristae (**Figure 2A**). Both HD-iPSC and HD-NSC exhibited significantly lower (∼41%) number of mitochondria and smaller mitochondrial area *per* cytoplasmatic area analyzed, as compared to control cells (**Figures 2D,E**), demonstrating that mitochondria were smaller and less abundant, two features of immature organelle morphology. Thus, reduced number of mitochondria that retain round-shape with underdeveloped cristae characterize both HD-iPSC and HD-NSC.

Next we analyzed mitochondrial morphometrics by immunocytochemistry using pDsRed2-Mito to label mitochondria (**Figures 2F,G**). In general, Ctr-iPSC and NSC mitochondria assumed a more perinuclear and compact localization, which was less evident in HD iPSC and HD-NSC. Additionally, we observed a decrease in OPA1 co-localization with mitochondria in HD-iPSC and HD-NSC (**Figures 2F,G**). Data suggest diminished fusion in HD cells, in accordance with round-shaped mitochondria in HD cells.

Extracellular Mitochondrial Components and Reduced Mitochondrial Respiratory Chain Activity in HD-iPSC and HD-NSC

Previously, multivesicles released from mesenchymal stem cells were reported to contain mitochondrial proteins and mtDNA (Phinney et al., 2015), suggesting that mitochondrial components can be secreted from cells in the form of extracellular vesicles, potentially affecting mitochondrial activity. In HD, several studies have demonstrated an imbalance toward fission events, leading to the accumulation of fragmented and damaged mitochondria (Cherubini et al., 2015, 2020). Considering the mitochondrial fragmentation observed in HD-iPSC and NSC we hypothesize that cells could shuttle mitochondrial proteins in exosomes. Therefore, exosomes were isolated from iPSC media (isolation of exosomes described in **Supplementary Data**) and analyzed by NanoSight and TEM demonstrating predominant cup-shaped membrane vesicles of ∼150 nm in diameter (**Supplementary Figures S1A–C**); similar results were observed for exosomes derived from NSC (not shown). Mass spectrometry analysis (described in **Supplementary Data**) showed that 31% of the proteomic content was common between iPSC and NSC (**Supplementary Figure S1D**). Several proteins are differentially released in exosomes from HD when compared to Ctr cells, with an enrichment in mitochondrial related functions and the presence of mitochondrial proteins in HD exosomes (**Supplementary Figures S1E,F**). In HD-iPSC, a 2-fold increase in proteins involved in apoptotic pathway (namely cytochrome C; $p = 0.057$) and ATP synthesis was observed, whilst in HD-NSC exosomal content included mitochondrial proteins involved in metabolic processes, namely ATP synthesis and TCA cycle (**Supplementary Figure S1F**). Increased exosomal release of metabolic-related proteins suggest a process by which mitochondria become dysfunctional.

Therefore, we measured the OCR and the ECAR (**Figures 3A–D**). HD-iPSC (**Figure 3A**) and HD-NSC (**Figure 3B**) showed a significant decrease in basal respiration compared to Ctr cells. Oligomycin was used to determine ATP-linked OCR followed by FCCP to induce maximal respiratory capacity. Both parameters were slightly lower, whereas the proton leak was slightly higher ($p = 0.06$) in HD *versus* Ctr iPSC (**Figure 3A**). HD-iPSC also showed significantly reduced spare respiratory capacity (**Figure 3A**). Following neural differentiation, a marked decrease in basal OCR was observed in HD-NSC (**Figure 3B**). Other OXPHOS components, namely ATP-linked OCR, maximal respiratory capacity, proton leakage and spare respiratory capacity were significantly decreased in HD-NSC, when compared to Ctr-NSC (**Figure 3B**), evidencing reduced OXPHOS. These data suggest that HD mitochondria are less dependent on OXPHOS than control mitochondria and have lower biometabolic reserve in conditions of increased ATP demand.

Another energy production pathway is glycolysis. HD-iPSC have higher ECAR basal levels and glycolytic capacity, determined after glucose addition, indicating that HD cells rely more on glycolysis for energy production when compared to Ctr-iPSC (**Figure 3C**). HD-NSC also showed augmented basal proton production. After sequential addition of glucose to fuel glycolysis, an increase of 278% in ECAR was observed for HD-NSC, while for Ctr-NSC the increase was of 257% (**Figure 3D**). Indeed, HD-NSC exhibited increased dependence on glycolysis (**Figure 3D**). Accordingly, reduced OCR/ECAR ratio was observed in HD-iPSC and HD-NSC, supporting the decreased predominance of OXPHOS over glycolysis. After neural differentiation, OXPHOS and glycolysis decline as described previously (Birket et al., 2011).

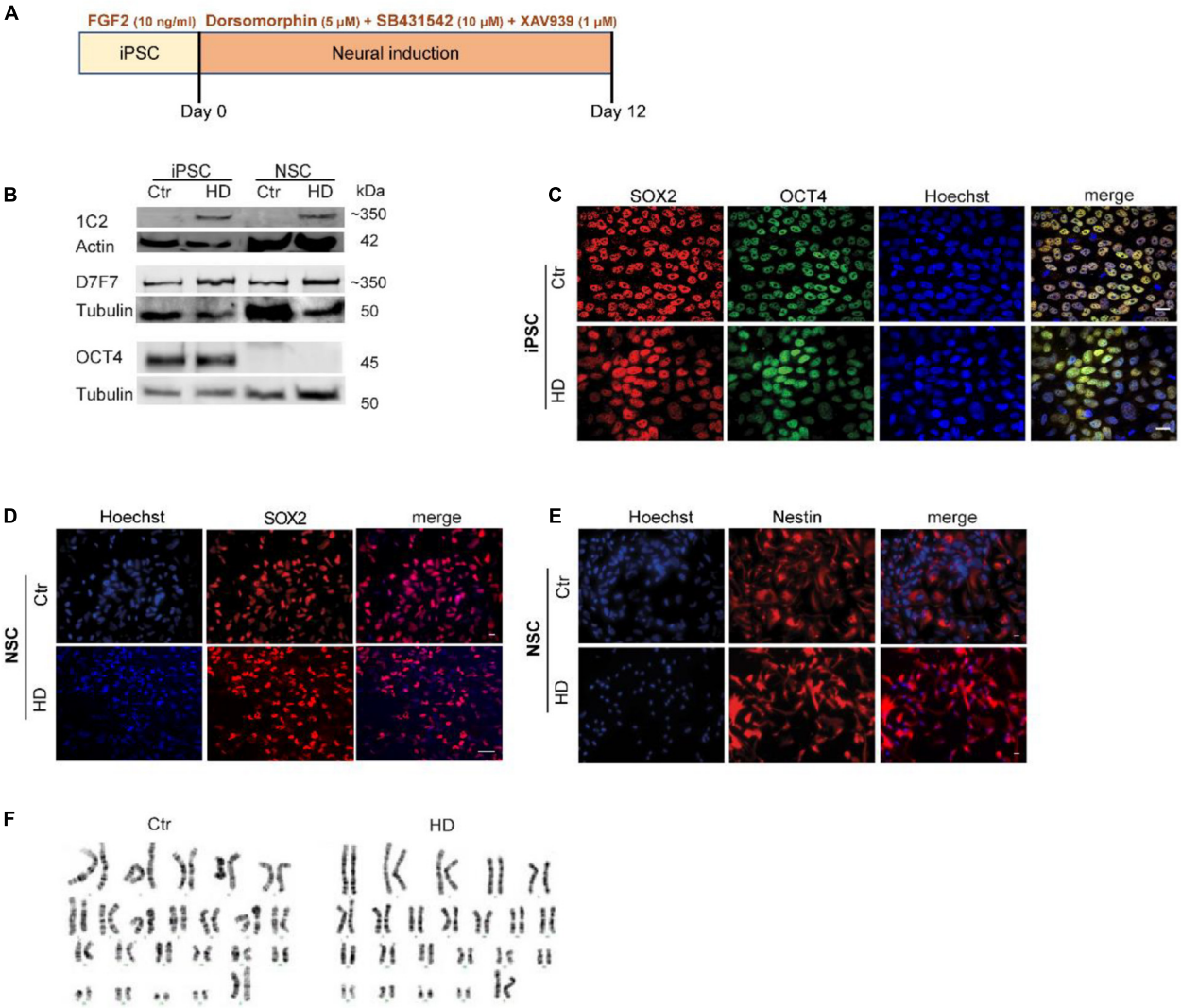

FIGURE 1 | Characterization of HD and Control-iPSC and NSC Lines. **(A)** Scheme of neural differentiation protocol based on dual SMAD inhibition. **(B)** Western blots of HTT protein expression in iPSC and iPSC-derived NSC with the HTT antibody 1C2 (polyglutamine stretch) and D7F7 (residues surrounding Pro1220) demonstrate normal and mutant HTT expression, respectively. The pluripotency marker OCT4 is shown in iPSC only. **(C)** Expression of pluripotency markers OCT4 and SOX2 in iPSC. **(D,E)** Expression of neural stem cell markers SOX2 and Nestin, respectively. Scale bar (in panel **C,E**) indicates 50 μm. **(F)** Karyotyping and g-band analysis show that iPSC lines have a normal 46,XX karyotype.

Data suggest that HD iPSC and NSC rely less on mitochondrial respiration and largely produce energy by glycolysis.

Changes in Mitochondrial Transmembrane Potential and Calcium Dyshomeostasis in HD-iPSC and HD-NSC

Mitochondria not only regulate energy production, but also govern intracellular Ca^{2+} levels driven by the Ψm [for review, Demaurex et al. (2009)]. Thus, we estimated Ψm in HD-iPSC and HD-NSC by assessing their ability to retain rhodamine123. Exposure of HD-iPSC and HD-NSC to oligomycin and FCCP together, in order to achieve complete mitochondrial depolarization, caused a higher release of the probe when compared to Ctr cells, consistent with highly hyperpolarized mitochondria (**Figure 3E**).

Because hyperpolarized mitochondria may result from reversal of ATP synthase under conditions of inhibition of mitochondrial complex(es), we incubated oligomycin and FCCP at different time points. Results were consistent with oligomycin-evoked depolarization, which occurred in both HD and Ctr iPSC and differentiated counterparts, but was significantly more evident in HD-iPSC (**Figure 3F**) and HD-NSC (**Figure 3G**), when compared to control cells, indicating enhanced ATP synthase reversal in HD cells. In HD-iPSC oligomycin induced almost maximal release of the probe indicating that Ψm was largely secured through ATP synthase reversal.

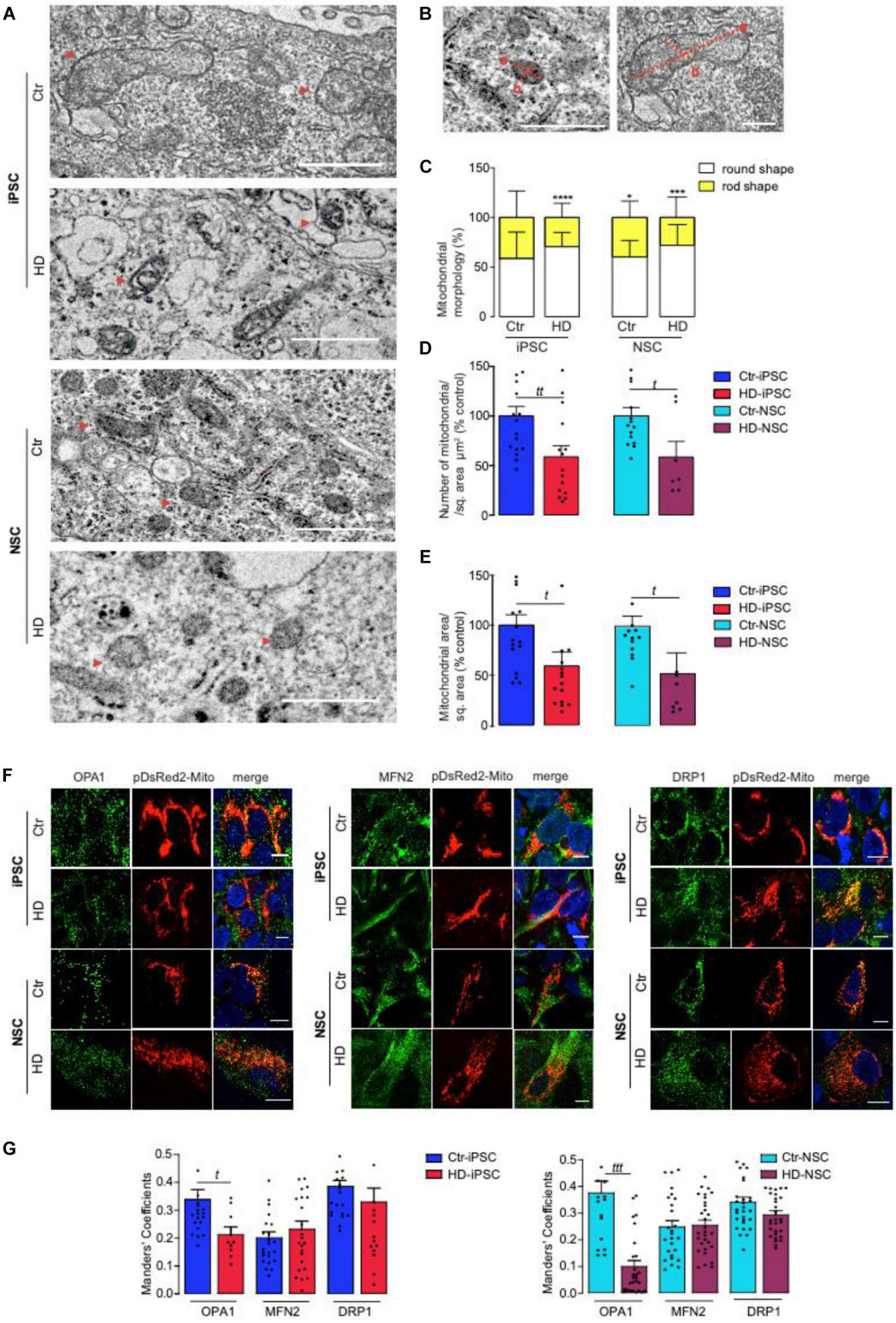

FIGURE 2 | Mitochondrial Ultrastructure and Dynamics Abnormalities in HD and Control iPSC and NSC. **(A)** TEM analysis of mitochondrial morphology, size and number in control vs HD iPSC and NSC (red arrowheads point to some mitochondria). **(B–E)** Analysis of TEM images was made using JACoP ImageJ. Mitochondria were quantified as round shape when equal perpendicular axis is present (a,b) and with rod shape if one axis is longer (a > b) and normalized with cytoplasmatic area in each random field. Mitochondria number per region of interest (ROI) and mitochondria area (π.a.b) per region of interest (ROI) were analyzed. The evaluations

(Continued)

FIGURE 2 | Continued
were made in 18 random fields with the same magnification. Scale bar indicates 2000 nm. The results are expressed as the mean ± S.E.M. Statistical significance was determined using two-way ANOVA and Bonferroni multiple comparisons test. A significant effect of mitochondrial morphology (a,b) over genotype was observed [$F(1,106) = 58.64$, $p < 0.0001$]. ****$p < 0.0001$; ***$p < 0.001$; *$p < 0.05$. Student's *t*-test: *t* $p < 0.05$, *tt* $p < 0.01$. **(F,G)** Immunocytofluorescence analysis of mitochondrial proteins OPA1, MFN2 (fusion) and DRP1 (fission) molecules in pDsRed2-Mito transfected cells. Images were photographed at ×63. The quantification of the images was performed on Z-stacks using JACoP ImageJ plugin. Scale bar of 10 μm. Values for three independent biological replicates, data presented as mean ± SEM. Student's *t*-test *t*: $p < 0.05$; *ttt* $p < 0.001$.

Association between altered Ca^{2+} mitochondrial handling and Ψm abnormalities has been described in several studies, with mHTT showing a close interaction with mitochondria (Panov et al., 2002), although such interaction has not been unequivocally shown in HD-NSC (**Supplementary Figure S2**). Basal intracellular Ca^{2+} levels were slightly, but significantly, increased in HD-iPSC, but decreased upon differentiation into HD-NSC (**Figure 3H**). We assessed mitochondrial Ca^{2+} handling by challenging the cells with oligomycin plus FCCP to cause Ψm collapse. HD-iPSC mitochondria retained more Ca^{2+}, compared to Ctr cells (**Figure 3I**), which could be related with higher Ψm (**Figure 3E**). Notably, the capacity to accumulate Ca^{2+} within the organelle was largely decreased in HD-NSC when compared to HD-iPSC (**Figure 3I**).

Altered Mitochondrial Biogenesis and Complex III Activity in HD-iPSC and HD-NSC

Peroxisome proliferator-activated receptor-γ coactivator α is a key component of mitochondrial biogenesis, which promotes expression of Mitochondrial Transcription Factor A (TFAM), involved in the synthesis of mitochondrial respiratory chain components. A pronounced reduction in PGC-1α mRNA levels was observed in both HD-iPSC and HD-NSC, whilst TFAM mRNA levels were decreased in HD-iPSC only, when compared to the respective control cells (**Figures 4A,B**).

To assess the influence of these results on mitochondrial function we measured the activities of mitochondrial complexes I to IV. We found that only Cx I + III activity was significantly reduced in HD-iPSC, mainly resulting from changes in the activity of Cx-III (**Figure 4C**). Concordantly, Cx-III activity was significantly decreased in HD-NSC (**Figure 4D**), while activity of citrate synthase was unchanged (**Figure 4E**). We further analyzed the mRNA levels of three genes encoding for Cx-III subunits: nuclear-encoded CYC1 and UQCR10 and mitochondrial-encoded MT-CYB; and mitochondrial-encoded ND1 for Cx-I and COX3 for Cx IV. Data revealed a reduction in the mRNA levels of Cx-III nuclear- and mitochondrial-encoded subunits, and an apparent compensatory increase in mRNA levels of Cx-I ND1 subunit in HD-iPSC, compared to Ctr cells (**Figure 4F**). In the case of HD-NSC, decreased Cx-III activity could not be attributed to changes in expression of these selected subunits, although we cannot exclude that other Cx-III subunits are affected. Interestingly, Cx-III CYC1, UQCR10 and MT-CYB subunits mRNA levels were increased in HD-NSC when compared to the pluripotent/undifferentiated counterparts (HD-iPSC), although reduced expression of Cx-I ND1 and Cx-IV COX3 subunits was observed in neural differentiated HD-NSC (**Figure 4F**).

The lower dependence on OXPHOS, accompanied by glycolysis stimulation in both HD-iPSC and HD-NSC is consistent with a decrease in mRNA levels of transcription factors involved in mitochondrial biogenesis and Cx-III (for HD-iPSC) subunits, leading to reduced enzymatic activity.

Energetic Imbalance in HD-iPSC and HD-NSC

To examine the changes in bioenergetics in HD *versus* Ctr undifferentiated iPSC and differentiated NSC, we measured the levels of adenine nucleotides (ATP, ADP and AMP) before and after modulation of glycolytic and mitochondrial metabolic fluxes. Significantly lower levels of cellular ATP (**Figure 5A**) and ATP/ADP (not shown) were detected in HD-iPSC and HD-NSC, when compared to Ctr cells. In HD-iPSC decreased ATP was not counterbalanced by ADP or AMP (**Figure 5A**), suggesting the metabolic conversion into other metabolites that are part of the purine metabolic pathway. When adding oligomycin to the media, in the presence of glucose, to inhibit ATP synthase and stimulate the glycolytic flux (**Figure 5B**), a decrease in ATP levels was observed mainly in Ctr-iPSC (by 60%), compared to non-treated cells, confirming that Ctr-iPSC relies more on OXPHOS for ATP production than HD-iPSC (oligomycin repressed ATP levels by 36%); however, no changes occurred in NSC. After glycolysis inhibition with 2-DG all cells suffered a decrease in ATP levels, when compared to untreated cells, but HD-iPSC cells were more affected; addition of 2-DG markedly decreased ATP levels by 67% in HD-iPSC, and about 50% in Ctr-iPSC; in HD and Ctr NSC ATP decreased by 51% and 46%, respectively, (**Figures 5A,C**). Inhibiting both glycolysis and mitochondrial ATP generation with 2-DG plus oligomycin completed reduced ATP and ADP levels, elevating cellular AMP levels in Ctr- iPSC and NSC, and HD-iPSC, but not in HD-NSC (**Figure 5D**), suggesting severe metabolic defect.

Enhanced Phosphorylation of E1 Subunit of Pyruvate Dehydrogenase Complex in HD-iPSC and HD-NSC

Because inhibition of PDH complex might contribute for decreased mitochondrial function in HD cells (Ferreira et al., 2011), we analyzed whether mitochondrial pyruvate metabolism through the PDH complex might be affected in HD iPSC and NSC. Phosphorylation of PDHE1α by PDK 1–4 causes PDH inhibition, while dephosphorylation by PDP 1–2 promotes its activation. The protein levels of PDHE1α

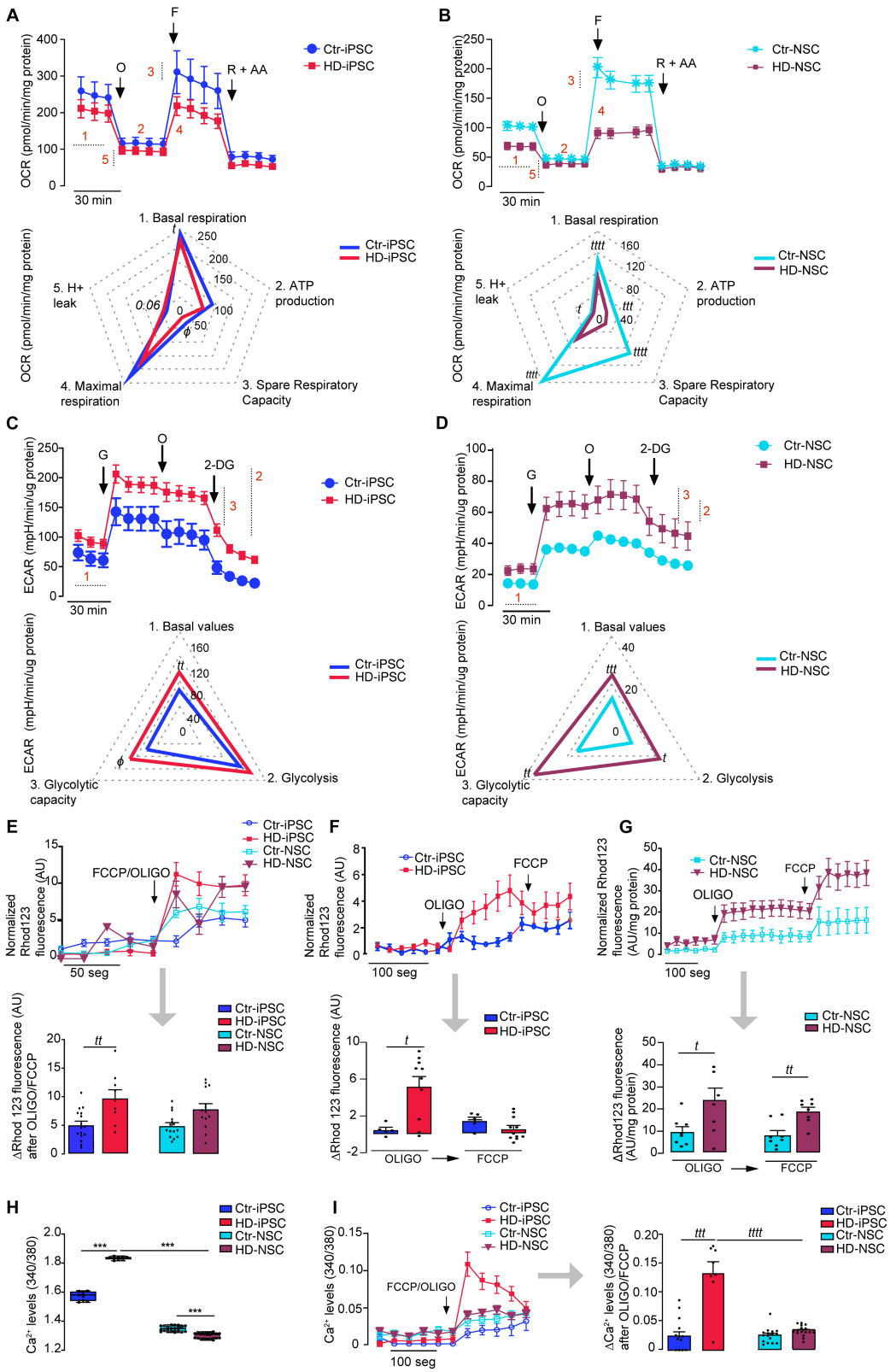

FIGURE 3 | HD Promotes Glycolysis Stimulation and Abnormal High Mitochondrial Membrane Potential Plus Altered Calcium Homeostasis. **(A,B)** For analysis of mitochondrial OCR, inhibitors were injected sequentially: 1 μM oligomycin (O), 1 μM FCCP (F), 1 μM rotenone and 1 μM AA (R + A). OCR graphs shown on top and

(Continued)

FIGURE 3 | Continued
spider plots on the bottom: (1) basal respiration; (2) oxygen consumed for ATP generation through the complex V; (3) Spare respiratory capacity; (4) maximal respiration capacity; (5) passive proton leakage across the mitochondrial inner membrane. Values for mean ± S.E.M of at least three independent experiments. Student's *t*-test: $t\ p < 0.05$; $tttt\ p < 0.0001$ or Mann–Whitney U test: $\phi < 0.05$. **(C,D)** Analysis of ECAR. ECAR graphs shown on top and spider plots on the bottom: (1) Basal ECAR; (2) Glycolysis; (3) Glycolytic capacity. The results are expressed as the mean ± S.E.M of at least three independent experiments. Student's *t*-test: $t\ p < 0.05$; $tt\ p < 0.01$, $ttt\ p < 0.001$ or Mann–Whitney U test: $\phi < 0.05$. **(E–G)** Representative traces of mitochondrial membrane potential measured with the fluorescent lipophilic cationic probe Rhod123. Cells were exposed to 2 μg/ml oligomycin and 2 μM FCCP together or to 2 μg/ml oligomycin followed by 2 μM of FCCP. The bar graphs correspond to the variation of the fluorescence values; values for three independent experiments; Student's *t*-test: $t\ p < 0.05$; $tt\ p < 0.01$. **(H,I)** Mitochondrial calcium release following exposure to oligomicyn plus FCCP and representative traces (as previous). The results are expressed as the mean ± S.E.M. from three independent experiments. Student's *t*-test: ($t\ p < 0.05$; $tt\ p < 0.01$; $ttt\ p < 0.001$; $tttt\ p < 0.0001$) and one-way ANOVA, followed by Bonferroni *post hoc* test $^{***}p < 0.001$.

subunit were significantly increased in HD-iPSC (**Figure 5E**) but decreased after neural differentiation (**Figure 5H**). High levels of phosphorylated PDHE1α (Ser 232, 293 and 300) were found in both HD iPSC and NSC, underlying PDH partial inactivation (**Figures 5F,I**). We also measured PDK1 and PDP1 mRNA levels. Only PDK1 can phosphorylate all 3 serines (Korotchkina and Patel, 2001) and an increase in gene expression for PDK1 was previously detected in stem cells (Varum et al., 2011), while PDP1 can dephosphorylate all three sites with similar preference (Rardin et al., 2009). PDK1 mRNA levels were upregulated in HD-iPSC, whereas PDP1 mRNA levels were downregulated (**Figure 5G**), correlating with enhanced PDHE1 phosphorylation. In HD-NSC, PDK1 levels were also increased (**Figure 5J**), although in a less extent when compared to HD-iPSC (**Figure 5G**). Contrarily to iPSC, HD-NSC displayed slightly augmented PDP1 mRNA levels (**Figure 5J**), which may explain the relative reduction in all Ser phosphorylation in NSC (**Figure 5I**).

These data indicate that, apart from decreased Cx-III activity, dysfunctional mitochondrial metabolism is due to PDH complex inactivation in undifferentiated HD iPSC and NSC.

HD-iPSC and HD-NSC Exhibit Increased Levels of Mitochondrial and Cellular ROS and Dysregulation of Antioxidant Response

Because inhibition of Cx-III is linked to electron leakage at the mitochondrial respiratory chain and increased production of $O_2^{\cdot -}$, we further determined the levels of mitochondrial ROS in HD iPSC and NSC. Both HD cells exhibited higher basal levels of mitochondrial $O_2^{\cdot -}$ (**Figure 6A**) as well as increased production of ROS after addition of AA (**Figure 6B**). Likewise, HD-iPSC produced increased levels of cellular H_2O_2 under basal conditions, which were exacerbated after pre-incubation with oxidant stimulus (**Figure 6C**).

Considering that ROS production is influenced by the activity of endogenous antioxidant enzymes, and $O_2^{\cdot -}$ dismutation is the main source of H_2O_2, we evaluated the activity of SOD1 and SOD2, as both may co-exist in mitochondria. Apart from a significant increase in SOD2 activity in HD cells upon neural differentiation (**Figure 6D**), which may partially counterbalance the enhanced production of mitochondrial $O_2^{\cdot -}$, no other significant differences were detected in SODs levels (including acetyl-SOD2 at Lys68) (2A-B) or total SOD activity (not shown).

Another mechanism involved in attenuating ROS production and metabolism regulation is mediated by the protein UCP2. Lower UCP2 levels facilitate ROS accumulation, which seems to contribute for differentiation into certain lineages (Zhang et al., 2011). Our results show a pronounced downregulation of UCP2 mRNA levels in HD-NSC compared to controls ($p = 0.07$) (**Figure 6E**), supporting mitochondrial-driven oxidative stress.

Increased levels of ROS can induce the activation of the Nrf2, a transcription factor that regulates the antioxidant response by activating phase II detoxification enzymes, which are described to be compromised in HD NSC (Quinti et al., 2017). In our results, HD-NSC only showed significantly higher levels of Nrf2 mRNA when compared to HD-iPSC and Ctr-NSC (**Figure 6F**); an increase in P(Ser40)Nrf2 in cytoplasm was observed in HD-iPSC (**Supplementary Figure S3C**), supporting the increase in ROS levels. To further study the impact of Nrf2/ARE pathway on antioxidant gene expression we analyzed GCLc and HO-1 transcripts (**Figures 6G,H**), the latter supporting GSH synthesis. GCLc mRNA levels were significantly upregulated in HD-iPSC and, interestingly, a pronounced reduction was observed after differentiation (**Figure 6G**). HD-iPSC had higher levels of GSH (**Supplementary Figure S3D**), suggesting that glutathione system is important for the maintenance of the redox state.

CRISPR/Cas9-Targeted Deletion of Exon-1/CAG Repeats Reverses HD-Related Phenotypic Abnormalities

We employed a CRISPR/Cas9 excision strategy to remove the expansion of CAG repeats in exon 1 of the HTT gene. We designed a pair of HTT sgRNAs for excision with S. pyogenes Cas9 to specifically excise the repeat-containing exon 1 fragment (**Figure 7A**). The sgRNA pair was expressed from a plasmid containing two human Pol III U6 promoter driven sgRNA expression cassettes. The sgRNA plasmid and a Cas9-GFP expression plasmid (pCas9_GFP, a gift from Kiran Musunuru, Addgene #44719) were co-transfected into hiPSCs as described previously (Burnight et al., 2017). The transfected cells were sorted 2 days later to enrich for Cas9-GFP high-expressing cells followed by single-cell plating, colony picking, expansion, and analysis. Targeted clones were identified by PCR (**Figure 7B**). Additionally, karyotyping and G-banding analysis showed that CRISPR targeted cells maintained a normal 46,XX karyotype (**Figure 7C**). Sanger sequencing confirmed the precise excision of the region between the two expected Cas9-induced double-strand

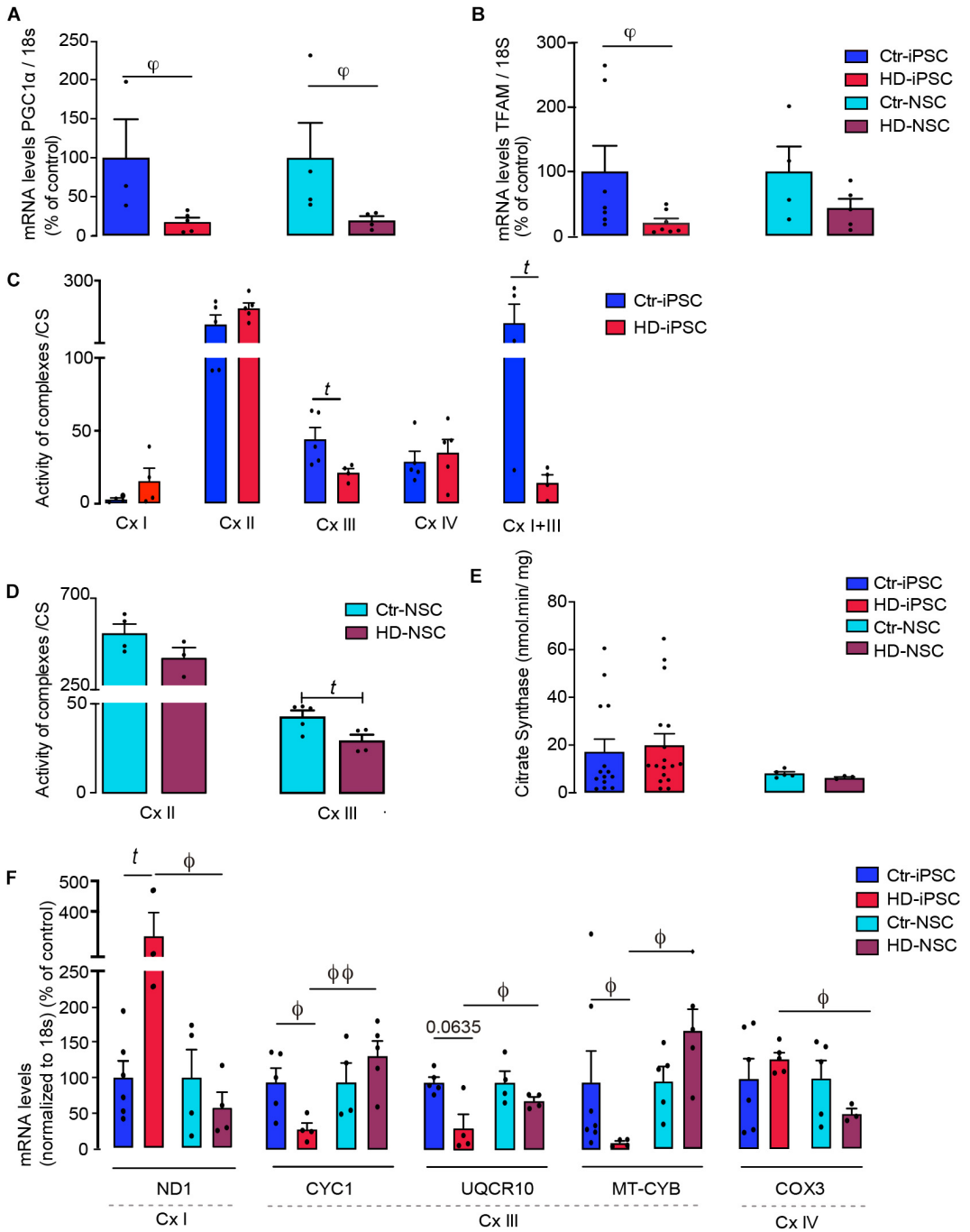

FIGURE 4 | PGC-1α/TFAM Mediates Downregulation of Mitochondrial and Nuclear-Encoded Subunit Transcripts and Compromises Complex III Activity in HD. **(A,B)** mRNA levels of PGC-1α and TFAM normalized to 18S; values for five independent biological replicates shown as mean ± SEM; Kruskal–Wallis H test: $\varphi < 0.05$, $\varphi\varphi < 0.01$. **(C–E)** Mitochondrial respiratory chain complexes (Cx) and citrate synthase (CS) activities determined in mitochondrial fractions of iPSC and NSC; values for five independent biological replicates shown as mean ± SEM; Student's *t*-test: *t* $p < 0.05$. **(F,G)** mRNA levels of cytochrome c1 (CYC1), ubiquinol-cytochrome C reductase, complex III subunit X (UQCR10) and mitochondrial-encoded cytochrome B (MT-CYB); mitochondrial-encoded NADH:ubiquinone oxidoreductase core subunit 1 (ND1) and mitochondrial-encoded cytochrome C oxidase III (COX3), normalized to 18S. Values are the mean ± S.E.M. of five independent experiments, normalized for protein content and citrate synthase activity. Student's *t*-test: *t* $p < 0.05$, Mann–Whitney U test $\phi < 0.05$, $\phi\phi < 0.01$.

breaks (**Figure 7D**). Potential off-target sites were identified using CasOffFinder. Consistent with published observations according to which off-target mutations at such sites are exceedingly rare (pmid: 25425480, 24996165, 26212079, 24996167) we did not find any *de novo* mutations among the four tested most-likely off-target sites (genomic DNA PCR product Sanger sequencing

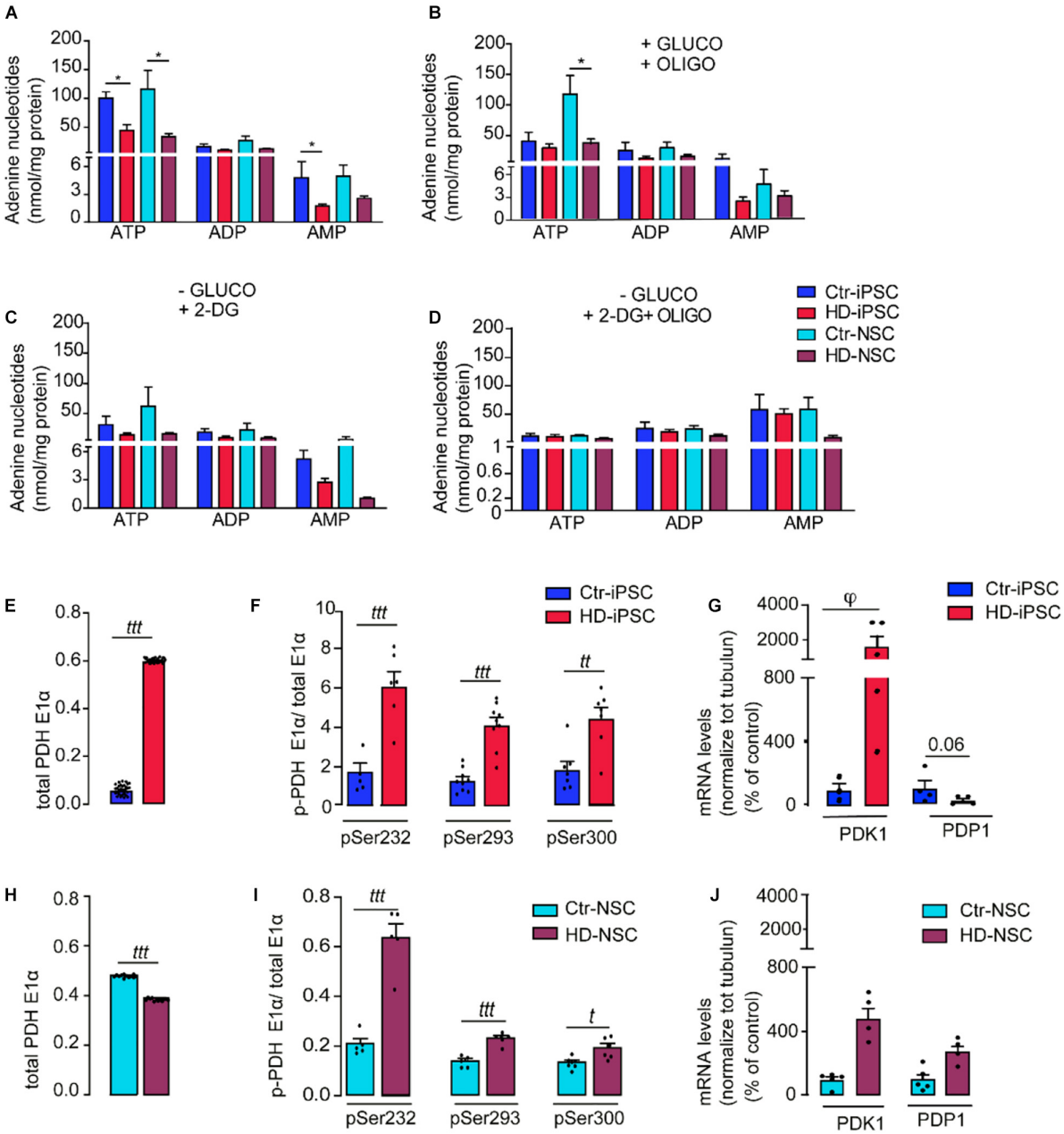

FIGURE 5 | Energetic Imbalance in HD-iPSC and NSC. **(A)** The cell lysates were assayed for ATP, ADP, and AMP by separation in a reverse-phase HPLC. The results are expressed as the mean ± S.E.M of at least three independent samples; $^{*}p < 0.05$ determined by one-way ANOVA and Bonferroni's multiple comparisons test. **(B–D)** iPSC and NSC were challenged with 2 μg/ml oligomycin (OLIGO), or media depleted in glucose (-GLUCO) and supplemented with 2-DG or 2-DG plus 2 μg/ml oligomycin, for 2 h. Two way ANOVA analyses followed by Bonferroni's multiple comparisons test revealed that there is a significant effect of treatment on ATP levels [$F(4,74) = 8.76$, $p < 0.0001$]. The results are expressed as the mean ± S.E.M of at least three independent samples; $^{*}p < 0.05$; **(E,H)** Determination of total PDH levels in iPSC and NSC. **(F,I)** Quantification of the activity levels of phospho-PDH (Ser 232, 293, 300 of the E1-α subunit). Two way ANOVA analysis revealed that there is a significant effect of genotype on levels of phospho-PDH in iPSC [$F(1,44) = 98.96$, $p < 0.001$] and in NSC [$F(2,26) = 32.58$, $p < 0.0001$]. The results are expressed as the mean ± S.E.M of at least three independent samples. Student's *t*-test: *ttt* $p < 0.001$; *tt* $p < 0.001$. **(G,J)** mRNA levels of PDK1 and PDP1 in iPSC and NSC; results are expressed as the mean ± S.E.M of at least three independent samples. Kruskal–Wallis H test $\varphi < 0.05$.

data shown for the highest-scoring off-target loci of the 5′ and 3′ HTT sgRNAs) (**Supplementary Figure S4**). Successful deletion of the CAG expansion was verified by western blotting using antibodies for polyglutamine stretch (1C2) and HTT (residues surrounding Pro1220) (**Figure 7E**). We then examined the pluripotency characteristics of the excised iPSC (eHD-iPSC) showing a positive staining for OCT4 and SOX2, and for Nestin after differentiation into NSC (eHD-NSC) (**Figure 7F**).

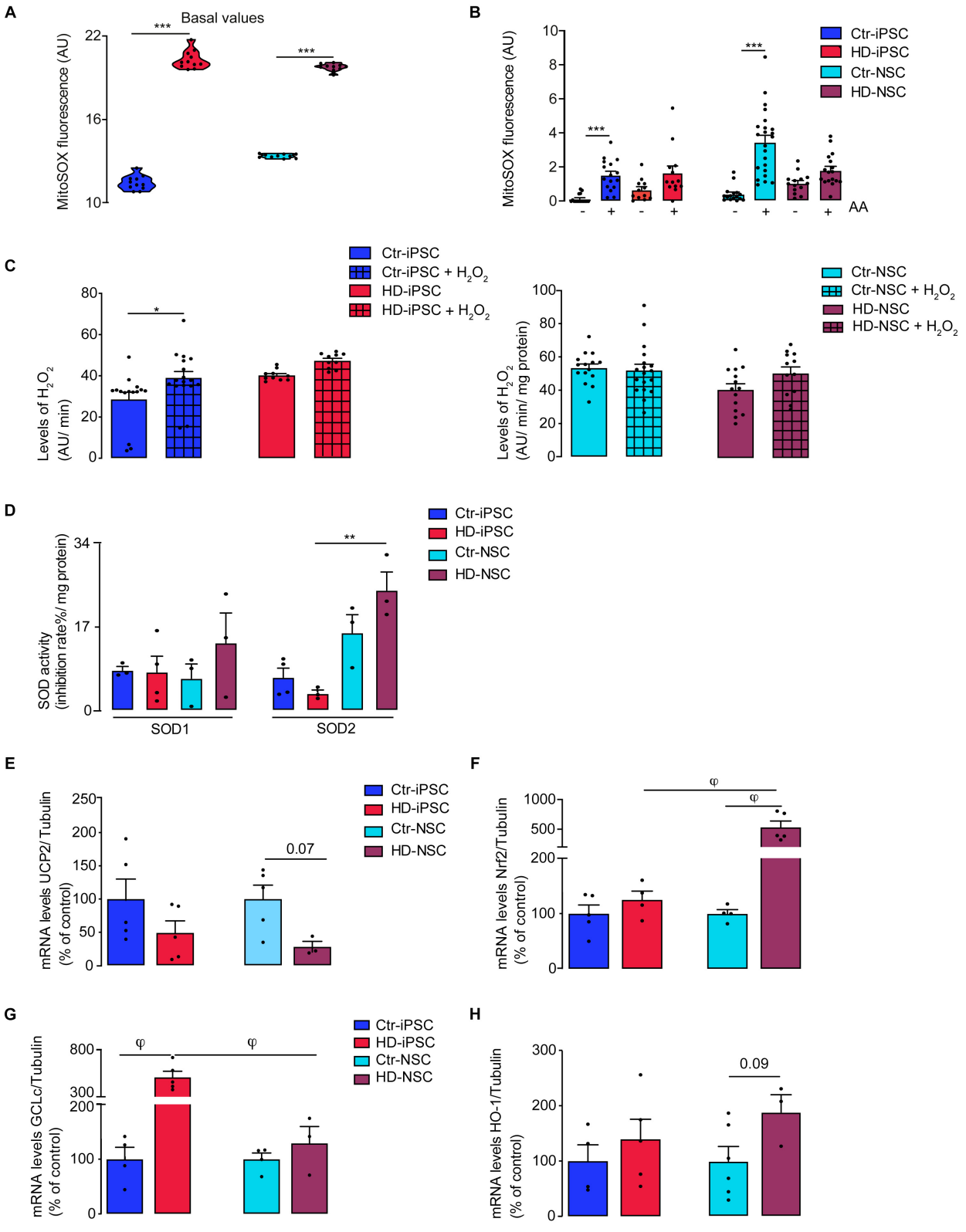

FIGURE 6 | Increased Vulnerability to Oxidative Stress in HD Cells Associated to a Reduced Antioxidant Response. **(A,B)** Basal levels of mitochondrial $O_2^{\bullet -}$ and generation of $O2^{-}$ after acute exposure to 1 μM AA in iPSC and NSC; *n* = 3 independent biological replicates; values shown as median with interquartile range for A

(Continued)

FIGURE 6 | Continued
and or mean ± SEM for B; ***$p < 0.001$, one way ANOVA and Bonferroni's multiple comparisons test. **(C)** Detection of extracellular hydrogen peroxide by AmplexRed assay in iPSC and NSC; $n = 3$ independent biological replicates; values shown as mean ± SEM; one-way ANOVA and Bonferroni's multiple comparisons test *$p < 0.05$. **(D)** Superoxide dismutase (SOD) activity were determined in iPSC and NSC. $n = 3$ independent biological replicates; values shown as mean ± SEM; one-way ANOVA **$p < 0.01$. **(E–H)** mRNA expression of UCP2, Nrf2, GCLc and HO-1 normalized to tubulin. Results are the mean ± SEM of at least 3 independent samples. Kruskal-Wallis H test $\varphi < 0.05$.

Next, we sought to establish whether CAG deletion results in reversal of previously observed HD key metabolic phenotypes, namely mitochondrial respiration, mitochondrial driven H_2O_2 production and expression of genes related to mitochondrial biogenesis or bioenergetics. We found that CAG excision results in improved basal respiration (**Figure 7G**) and a significant reduction of mitochondrial ROS levels in eHD-NSC (**Figure 7H**). Furthermore, while no changes were observed in PGC-1α or TFAM mRNA levels (**Figure 7I**), involved in mitochondrial biogenesis, in eHD-iPSC or eHD-NSC, a significant increase in mRNA levels of complex III subunits (CYC1, UQCR10 and MT-CYB) was observed in eHD-iPSC (**Figure 7J**), supporting the rescue in mitochondrial function.

DISCUSSION

In this study, we observed that early differentiated human HD iPSC and NSC exhibit intricate features of mitochondrial and metabolic impairment linked to decreased activities of complex III and PDH complex, reduced oxygen consumption and mitochondrial ATP production, with the organelle exhibiting enhanced production of mitochondrial-driven ROS and a fragmented morphology. Of relevance, altered mRNA levels of nuclear-encoded complex III subunits and PDK *versus* PDH phosphatase endorse inhibitory effects on respiratory chain complex III and PDH. These changes were accompanied by hyperpolarized mitochondria that retained more calcium and by glycolysis stimulation to partially compensate the cellular bioenergetic demand imposed by mHTT expression. A link between nuclear morphology and enhanced store-operated calcium channels activity was described in HD iPSCs-derived neurons, supporting the previous findings of calcium transport deregulation in HD models (Nekrasov et al., 2016).

Mitochondrial fission and fusion proteins regulate morphology, function, integrity and topographic distribution of mitochondria. Indeed, HD models exhibit altered expression of DRP1, Fis1, OPA1 and MFN1/2 proteins (Song et al., 2011; Shirendeb et al., 2012). Concordantly, we showed abnormal mitochondrial dynamics in HD iPSC and NSC, in which the organelle assumes a spherical morphology (Facucho-Oliveira et al., 2007; Prigione et al., 2010; Zhang et al., 2011; Kelly et al., 2013) and lower mitochondrial levels of OPA1 in HD-iPSC and NSC, which may underlie altered mitochondrial morphology (Chen et al., 2016).

Our result is supported by the observation that mHtt reduced the expression of OPA1 mRNA in R6/2 mice and *postmortem* HD patient's brains (Shirendeb et al., 2011; Hering et al., 2017). The interaction of mHTT with DRP1 increases its GTPase activity resulting in fragmented mitochondria. Consequently, Drp1/Fis1-mediated mitochondrial fission has been described as a major player in the progression of HD (Guo et al., 2013; Joshi et al., 2019). In our study the levels of DRP1 were similar to controls, suggesting that its upregulation could be associated to late-stage HD progression (Shirendeb et al., 2011).

Alongside, we observed alterations in mitochondrial respiration and bioenergetics in HD iPSC and NSC, as described in higher CAG length cell lines (Hd iPSC Consortium, 2012). These findings are in agreement with reduced gene expression of two nuclear-encoded and one mitochondrial-encoded subunits of mitochondrial Cx-III (CYC1, UQCR10 and MT-CYB) and Cx-III activity in human HD-iPSC. Importantly, we observed that exosomes can package mitochondrial proteins (e.g., cytochrome c), which increased release from HD cells might constitute a mechanism that relates with decreased Cx-III subunit expression and activity; although its physiological relevance is still unclear, exosomal release of mitochondrial components may constitute a cell survival mechanism in response to oxidative stress and mitochondrial dysfunction (Phinney et al., 2015).

Different lines of evidence indicate that in iPSC Ψm appears to be maintained by glycolytic ATP, used for maintaining the hydrolase activity of complex V (ATP synthase) and the higher Ψm. Consistently, previous studies showed that ATP synthase can be reversed in iPSC, hydrolyzing glycolytic ATP to maintain the Ψm and mitochondria in a less functional state resorting to the inhibition of respiratory chain complex(es) (Cho et al., 2006; Nicholls, 2006; Zhang et al., 2011; Lorenz et al., 2017; Ghosh et al., 2020). Here, we show that this is exacerbated in HD iPSC and NSC as displayed by mitochondrial hyperpolarized status. In a recent study, NSC expressing *HTT* exon 1 with expanded 71 and 122 CAG repeats displayed impaired activities of complex I and II + III, increased retention of TMRM, suggesting hyperpolarized mitochondria, associated to altered morphology (Ghosh et al., 2020). Importantly these findings highlight that exon 1 *HTT* fragments are sufficient to cause mitochondrial dysfunction in a CAG number dependent manner supporting its role in the pathogenesis of HD.

A key metabolic regulator favoring glycolysis *versus* OXPHOS involves the PDH complex (Varum et al., 2011). hESC express high levels of hexokinase2 (localizing to the outer mitochondrial membrane) and have an inactive PDH complex. Also, mRNA levels of PDK1,3 declined significantly during neuronal differentiation, whereas PDP1 mRNA levels increased, favoring PDH activity in neurons (Zheng et al., 2016). Here we show that PDH E1α subunit significantly increased in HD-iPSC, but serines 232, 293 and 300 residues were highly phosphorylated in both HD iPSC and NSC, indicating decreased activity of this enzymatic complex; indeed, PDK1 mRNA levels were

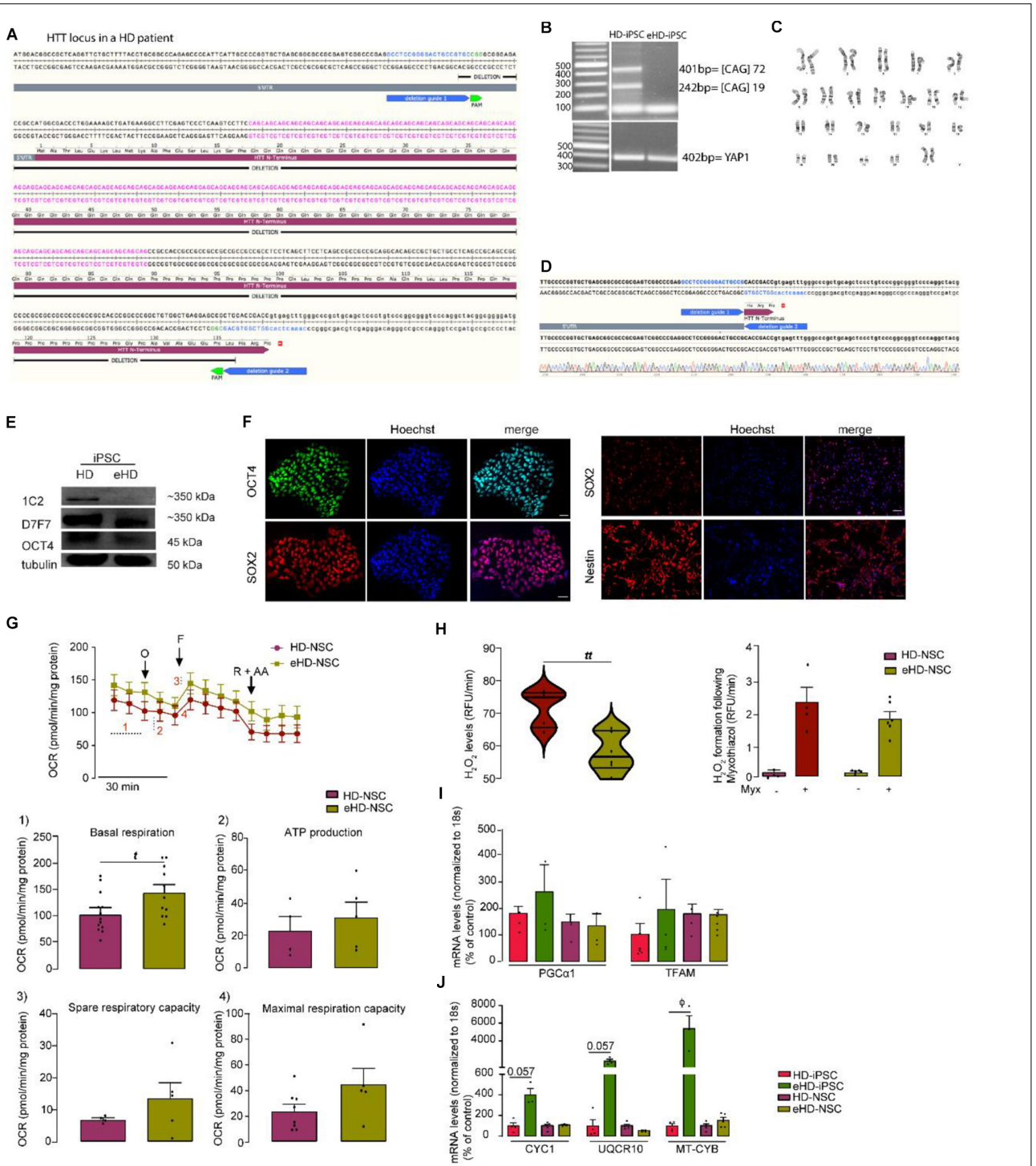

FIGURE 7 | CRISPR/Cas9-mediated Deletion of the polyQ-encoding Region in HTT Gene in HD-iPSC Reverses the Phenotypic Abnormalities. **(A)** Schematic overview of mutant HTT cutting strategy. **(B)** Overview of a PCR for a successfully targeted iPSC clone. **(C)** Karyotype analysis of corrected HD-iPSC. **(D)** Sanger sequencing performed for the PCR bands cut from the gel. **(E)** Expression of normal HTT is maintained in iPSC, as defined using HTT antibody 1C2 (polyglutamine stretch) and D7F7 (residues surrounding Pro1220). **(F)** The CAG deleted iPSC maintains pluripotency as shown by positive immunostaining for the pluripotency marker OCT4 and the potential to differentiate into NSC by positive immunostaining for Nestin. **(G)** Measures of mitochondrial respiration in HD-NSC and isogenic control (. **(H)** Basal levels of mitochondrial H_2O_2 and generation of H_2O_2 after acute exposure to 3 μM myxothiazol (Myx) in control, HD and CAG deleted NSC; values are the median with interquartile range (violin plot) or mean ± SEM (bar graph) of at least three independent samples. *tt* $p < 0.01$; Student *t*-test. **(I,J)** mRNA levels of PGC-1α and TFAM, cytochrome c1 (CYC1), ubiquinol-cytochrome C reductase, complex III subunit X (UQCR10) and mitochondrial-encoded cytochrome B (MT-CYB) for HD-iPSC and NSC and CAG deleted controls; values for four independent biological replicates shown as mean ± SEM; ϕ < 0.05, Mann–Whitney U test.

upregulated and PDP1 downregulated in HD iPSC, consistent with enhanced PDHE1α phosphorylation, as identified in distinct HD models and patient's brain tissue (Sorbi et al., 1983; Ferreira et al., 2011; Naia et al., 2017). Indeed, several studies reported, in human iPSC and differentiated cell, mitochondrial dysfunction and metabolic deficits attributed to mHTT (An et al., 2012; Hd iPSC Consortium, 2012, 2017, 2020; Xu et al., 2017; Ghosh et al., 2020) but to our knowledge PDH activity was not assessed. Our results point to decreased PDH activity as an early event in HD pathophysiology.

Antioxidant genes such as UCP2 are expected to be upregulated in iPSC and reduced UCP2 expression facilitates ROS accumulation in hiPSC and hESC (Zhang et al., 2011). Consistently, we observed a decrease in UCP2 mRNA levels in HD-iPSC (67%), suggesting that UCP2 can assume an important role in endogenous ROS management, prompting HD-iPSC susceptibility to mitochondrial dysfunction associated with increased ROS production. A rise in mitochondrial $O_2^{\cdot -}$ levels was consistent with Cx-III inhibition. Previous studies described increased cell death in striatal-like neurons differentiated from HD-iPSC lines in response to toxic stressors, (Hd iPSC Consortium, 2012) and increased generation of mitochondrial ROS in HD mouse striatal cells (Ribeiro et al., 2014). Moreover, proteomic analysis in the same 72 CAG HD-iPSC used in this work showed that antioxidant enzymes, such as SOD1 or peroxiredoxin (Prx) were downregulated or up-regulated, respectively, (Chae et al., 2012). While we observed mitochondrial abnormalities, other researchers reported the absence of mitochondrial dysfunction, claiming that bioenergetic deficits and ROS production are not decisive factors in HD pathology in the pre-symptomatic stage despite recognizing the involvement at later stages of the disease (Hamilton et al., 2020). The reason for this discrepancy is not clear but could be attributed to differences in cell culture and/or methodologies.

A question arising from this work is the variability of the iPSC genetic background, which may result in inaccurate interpretation of disease phenotypes *in vitro*. Several approaches have been described to block mHTT expression and therefore clarify the role of CAG expansion on disease phenotype and potential use as therapeutic strategy. In this work, we demonstrate that CRISPR-Cas9-mediated excision of exon 1 fragment-containing CAG repeats in HD-iPSC (eHD-iPSC) can reverse phenotypic alterations found in HD iPSC and NSC, including deficits in mitochondrial respiration, ROS production and mitochondrial gene-related expression further demonstrating that HD-associated mitochondrial and metabolic impairments are associated to the HD genotype and not to variability of the iPSC genetic background, reprograming or differentiation protocols.

Genetic correction of HD-iPSC using CRISPR/Cas9-assisted techniques was previously achieved showing rescuing effects (An et al., 2014; Xu et al., 2017), but not thoroughly with a focus on mitochondria as in the present work. Cellular abnormalities including mitochondrial deficits, low levels of BDNF, altered cadherin and TGF-β signaling, impaired neural rosette formation and increased susceptibility to growth factor withdrawal were rescued in corrected isogenic HD lines (An et al., 2014; Xu et al., 2017). Other approaches used non-allele selective suppression or SNP-based approach to efficiently disrupt exogenous/endogenous WT/mutant *HTT* gene, being associated with decreased mHTT aggregation (Shin et al., 2016; Kolli et al., 2017; Monteys et al., 2017; Yang et al., 2017). These and our results support gene-silencing approaches such as the recently reported intrathecal administration of antisense oligonucleotide designed to inhibit *HTT* transcripts, which resulted in dose-dependent reduction in mHTT levels in human HD carriers (Tabrizi et al., 2019); it will be relevant to examine whether these novel gene silencing approaches also impact on mitochondrial function and redox activity in HD patient's cells, along with major HD-related symptoms.

CONCLUSION

In summary, our study shows in large detail mitochondrial impairment that could be attributed to reduced mitochondrial biogenesis and decreased CxIII and PDK1 levels, causing metabolic imbalance, and enhanced mitochondrial generation of ROS, linked to round shape mitochondrial morphology in early stages of undifferentiation, in human HD iPSC, which were mostly replicated in iPSC-derived NSC expressing mHTT. Of relevance, CAG repeat excision in the mutant *HTT* gene ameliorated relevant mitochondrial-associated phenotypes, including the expression of mitochondrial and nuclear-encoded Cx-III subunits, demonstrating a positive impact of CAG correction strategies on early onset HD phenotypes related with mitochondrial deregulation (Figure S5_Graphical abstract).

DATA AVAILABILITY STATEMENT

The raw data supporting the conclusions of this article will be made available by the authors, without undue reservation.

ETHICS STATEMENT

There are no ethical concerns since both heterozygous (19/72 CAG repeats) human HD and control iPSC have been previously generated, at GD (Harvard Medical School, Boston, MA, United States) and LA (University of Coimbra, Coimbra, Portugal) labs, respectively (Park et al., 2008; Onofre et al., 2016); HD-NSC and control NSC, as well as CRISPR/Cas9 iPSC and NSC corrected lines were obtained from original iPSC.

AUTHOR CONTRIBUTIONS

CL and ACR were responsible for the experimental design, data interpretation and writing of the manuscript. CL performed and analyzed most of the experiments and prepared the initial draft of the manuscript. YT and TS were responsible for CRISPR/Cas9 correction and assay design. SA and BM performed the MS analysis. ACR supervised the study and provided funds. All co-authors reviewed and edited the manuscript.

FUNDING

This study was supported by the 'FLAD Life Science 2020' prize, funded by 'Fundação Luso-Americana para o Desenvolvimento' (FLAD), Portugal. The work was also financed by the European Regional Development Fund (ERDF), through the Centro 2020 Regional Operational Programme under project CENTRO-01-0145-FEDER-000012- HealthyAging2020, and through COMPETE 2020-Operational Programme for Competitiveness and Internationalization and Portuguese national funds via FCT–Fundação para a Ciência e a Tecnologia, under projects POCI-01-0145-FEDER-007440, POCI-01-0145-FEDER-029621, POCI-01-0145-FEDER-016428 (ref.: SAICTPAC/0010/2015), POCI-01-0145-FEDER-30943 (ref.: PTDC/MEC-PSQ/30943/2017), PTDC/MED-NEU/27946/2017; by The National Mass Spectrometry Network (RNEM) under the contract POCI-01-0145-FEDER-402-022125 (ref. ROTEIRO/0028/2013), UID/NEU/04539/2019 and UIDB/04539/2020.

ACKNOWLEDGMENTS

We thank Dr. Mónica Zuzarte for electron microscopy images and to Dr. Henrique Girão and Teresa Ribeiro-Rodrigues for NTA analysis and useful discussions.

SUPPLEMENTARY MATERIAL

The Supplementary Material for this article can be found online at: https://www.frontiersin.org/articles/10.3389/fcell.2020.576592/full#supplementary-material

REFERENCES

An, M. C., O'Brien, R. N., Zhang, N., Patra, B. N., De La Cruz, M., Ray, A., et al. (2014). Polyglutamine disease modeling: epitope based screen for homologous recombination using CRISPR/Cas9 system. *PLoS Curr.* 6. doi: 10.1371/currents.hd.0242d2e7ad72225efa72f6964589369a

An, M. C., Zhang, N., Scott, G., Montoro, D., Wittkop, T., Mooney, S., et al. (2012). Genetic correction of Huntington's disease phenotypes in induced pluripotent stem cells [Research Support, N.I.H., Extramural Research Support, Non-U.S. Gov't]. *Cell. Stem Cell* 11, 253–263. doi: 10.1016/j.stem.2012.04.026

Birket, M. J., Orr, A. L., Gerencser, A. A., Madden, D. T., Vitelli, C., Swistowski, A., et al. (2011). A reduction in ATP demand and mitochondrial activity with neural differentiation of human embryonic stem cells. *J. Cell Sci.* 124(Pt. 3), 348–358. doi: 10.1242/jcs.072272

Burnight, E. R., Gupta, M., Wiley, L. A., Anfinson, K. R., Tran, A., Triboulet, R., et al. (2017). Using CRISPR-Cas9 to generate gene-corrected autologous iPSCs for the treatment of inherited retinal degeneration. *Mol. Ther.* 25, 1999–2013. doi: 10.1016/j.ymthe.2017.05.015

Camnasio, S., Delli Carri, A., Lombardo, A., Grad, I., Mariotti, C., Castucci, A., et al. (2012). The first reported generation of several induced pluripotent stem cell lines from homozygous and heterozygous Huntington's disease patients demonstrates mutation related enhanced lysosomal activity [Research Support, Non-U.S. Gov't]. *Neurobiol. Dis.* 46, 41–51. doi: 10.1016/j.nbd.2011.12.042

Chae, J. I., Kim, D. W., Lee, N., Jeon, Y. J., Jeon, I., Kwon, J., et al. (2012). Quantitative proteomic analysis of induced pluripotent stem cells derived from a human Huntington's disease patient [Research Support, Non-U.S. Gov't]. *Biochem. J.* 446, 359–371. doi: 10.1042/BJ20111495

Chambers, S. M., Fasano, C. A., Papapetrou, E. P., Tomishima, M., Sadelain, M., and Studer, L. (2009). Highly efficient neural conversion of human ES and iPS cells by dual inhibition of SMAD signaling [Research Support, N.I.H., ExtramuralResearch Support, Non-U. S. Gov't]. *Nat. Biotechnol.* 27, 275–280. doi: 10.1038/nbt.1529

Chen, J., Riazifar, H., Guan, M. X., and Huang, T. (2016). Modeling autosomal dominant optic atrophy using induced pluripotent stem cells and identifying potential therapeutic targets. *Stem Cell Res. Ther.* 7:2. doi: 10.1186/s13287-015-0264-1

Cherubini, M., Lopez-Molina, L., and Gines, S. (2020). Mitochondrial fission in Huntington's disease mouse striatum disrupts ER-mitochondria contacts leading to disturbances in Ca. *Neurobiol. Dis.* 136:104741. doi: 10.1016/j.nbd.2020.104741

Cherubini, M., Puigdellívol, M., Alberch, J., and Ginés, S. (2015). Cdk5-mediated mitochondrial fission: A key player in dopaminergic toxicity in Huntington's disease. *Biochim. Biophys. Acta* 1852(10 Pt. A), 2145–2160. doi: 10.1016/j.bbadis.2015.06.025

Cho, Y. M., Kwon, S., Pak, Y. K., Seol, H. W., Choi, Y. M., Park, J., et al. (2006). Dynamic changes in mitochondrial biogenesis and antioxidant enzymes during the spontaneous differentiation of human embryonic stem cells [Research Support, Non-U.S. Gov't]. *Biochem. Biophys. Res. Commun.* 348, 1472–1478. doi: 10.1016/j.bbrc.2006.08.020

Dabrowska, M., Juzwa, W., Krzyzosiak, W. J., and Olejniczak, M. (2018). Precise Excision of the CAG Tract from the Huntingtin Gene by Cas9 Nickases. *Front. Neurosci.* 12:75. doi: 10.3389/fnins.2018.00075

Delli Carri, A., Onorati, M., Castiglioni, V., Faedo, A., Camnasio, S., Toselli, M., et al. (2013). Human pluripotent stem cell differentiation into authentic striatal projection neurons [Research Support, Non-U.S. Gov't]. *Stem Cell Rev.* 9, 461–474. doi: 10.1007/s12015-013-9441-8

Demaurex, N., Poburko, D., and Frieden, M. (2009). Regulation of plasma membrane calcium fluxes by mitochondria [Research Support, Non-U.S. *Gov't Review]. Biochim. Biophys. Acta* 1787, 1383–1394. doi: 10.1016/j.bbabio.2008.12.012

Facucho-Oliveira, J. M., Alderson, J., Spikings, E. C., Egginton, S., and St John, J. C. (2007). Mitochondrial DNA replication during differentiation of murine embryonic stem cells [Research Support, Non-U.S. Gov't]. *J. Cell Sci.* 120(Pt. 22), 4025–4034. doi: 10.1242/jcs.016972

Ferreira, I. L., Cunha-Oliveira, T., Nascimento, M. V., Ribeiro, M., Proenca, M. T., Januario, C., et al. (2011). Bioenergetic dysfunction in Huntington's disease human cybrids [Research Support. Non-U.S. Gov't]. *Exp. Neurol.* 231, 127–134. doi: 10.1016/j.expneurol.2011.05.024

Ghosh, R., Wood-Kaczmar, A., Dobson, L., Smith, E. J., Sirinathsinghji, E. C., Kriston-Vizi, J., et al. (2020). Expression of mutant exon 1 huntingtin fragments in human neural stem cells and neurons causes inclusion formation and mitochondrial dysfunction. *FASEB J.* 34, 8139–8154. doi: 10.1096/fj.201902277RR

Gil, J. M., and Rego, A. C. (2008). Mechanisms of neurodegeneration in Huntington's disease [Research Support, Non-U.S. *Gov't Review]. Eur. J. Neurosci.* 27, 2803–2820. doi: 10.1111/j.1460-9568.2008.06310.x

Guo, X., Disatnik, M. H., Monbureau, M., Shamloo, M., Mochly-Rosen, D., and Qi, X. (2013). Inhibition of mitochondrial fragmentation diminishes Huntington's disease-associated neurodegeneration. *J. Clin. Invest.* 123, 5371–5388. doi: 10.1172/JCI70911

Hamilton, J., Brustovetsky, T., Sridhar, A., Pan, Y., Cummins, T. R., Meyer, J. S., et al. (2020). Energy metabolism and mitochondrial superoxide anion production in pre-symptomatic striatal neurons derived from human-induced pluripotent stem cells expressing mutant huntingtin. *Mol. Neurobiol.* 57, 668–684. doi: 10.1007/s12035-019-01734-2

Hd iPSC Consortium (2012). Induced pluripotent stem cells from patients with Huntington's disease show CAG-repeat-expansion-associated phenotypes [Research Support, N.I.*H., Extramural Research Support, Non-U.S. Gov't]. Cell. Stem Cell* 11, 264–278. doi: 10.1016/j.stem.2012.04.027

Hd iPSC Consortium (2017). Developmental alterations in Huntington's disease neural cells and pharmacological rescue in cells and mice. *Nat. Neurosci.* 20, 648–660. doi: 10.1038/nn.4532

Hd iPSC Consortium (2020). Bioenergetic deficits in Huntington's disease iPSC-derived neural cells and rescue with glycolytic metabolites. *Hum. Mol. Genet.* 29, 1757–1771. doi: 10.1093/hmg/ddy430

Hering, T., Kojer, K., Birth, N., Hallitsch, J., Taanman, J. W., and Orth, M. (2017). Mitochondrial cristae remodelling is associated with disrupted OPA1 oligomerisation in the Huntington's disease R6/2 fragment model. *Exp. Neurol.* 288, 167–175. doi: 10.1016/j.expneurol.2016.10.017

Jacquet, L., Neueder, A., Földes, G., Karagiannis, P., Hobbs, C., Jolinon, N., et al. (2015). Three huntington's disease specific mutation-carrying human embryonic stem cell lines have stable number of cag repeats upon *in vitro* differentiation into cardiomyocytes. *PLoS One* 10:e0126860. doi: 10.1371/journal.pone.0126860

Joshi, A. U., Ebert, A. E., Haileselassie, B., and Mochly-Rosen, D. (2019). Drp1/Fis1-mediated mitochondrial fragmentation leads to lysosomal dysfunction in cardiac models of Huntington's disease. *J. Mol. Cell Cardiol.* 127, 125–133. doi: 10.1016/j.yjmcc.2018.12.004

Kelly, R. D., Sumer, H., McKenzie, M., Facucho-Oliveira, J., Trounce, I. A., Verma, P. J., et al. (2013). The effects of nuclear reprogramming on mitochondrial DNA replication. *Stem Cell Rev.* 9, 1–15. doi: 10.1007/s12015-011-9318-7

Kolli, N., Lu, M., Maiti, P., Rossignol, J., and Dunbar, G. L. (2017). CRISPR-Cas9 Mediated Gene-Silencing of the Mutant Huntingtin Gene in an In Vitro Model of Huntington's Disease. *Int. J. Mol. Sci.* 18:754. doi: 10.3390/ijms18040754

Korotchkina, L. G., and Patel, M. S. (2001). Site specificity of four pyruvate dehydrogenase kinase isoenzymes toward the three phosphorylation sites of human pyruvate dehydrogenase. *J. Biol. Chem.* 276, 37223–37229. doi: 10.1074/jbc.M103069200

Lorenz, C., Lesimple, P., Bukowiecki, R., Zink, A., Inak, G., Mlody, B., et al. (2017). Human iPSC-derived neural progenitors are an effective drug discovery model for neurological mtDNA disorders. *Cell Stem Cell* 20, 659.e9-674.e9. doi: 10.1016/j.stem.2016.12.013

Lu, X. H., Mattis, V. B., Wang, N., Al-Ramahi, I., van den Berg, N., Fratantoni, S. A., et al. (2014). Targeting ATM ameliorates mutant Huntingtin toxicity in cell and animal models of Huntington's disease. *Sci. Transl. Med.* 6:268ra178. doi: 10.1126/scitranslmed.3010523

Mattis, V. B., Tom, C., Akimov, S., Saeedian, J., Ostergaard, M. E., Southwell, A. L., et al. (2015). HD iPSC-derived neural progenitors accumulate in culture and are susceptible to BDNF withdrawal due to glutamate toxicity [Research Support, N.I.H., Extramural Research Support, Non-U.S. Gov't]. *Hum. Mol. Genet.* 24, 3257–3271. doi: 10.1093/hmg/ddv080

McQuade, L. R., Balachandran, A., Scott, H. A., Khaira, S., Baker, M. S., and Schmidt, U. (2014). Proteomics of Huntington's disease-affected human embryonic stem cells reveals an evolving pathology involving mitochondrial dysfunction and metabolic disturbances. *J. Proteome Res.* 13, 5648–5659. doi: 10.1021/pr500649m

Monteys, A. M., Ebanks, S. A., Keiser, M. S., and Davidson, B. L. (2017). CRISPR/Cas9 Editing of the mutant huntingtin allele in vitro and in vivo. *Mol. Ther.* 25, 12–23. doi: 10.1016/j.ymthe.2016.11.010

Naia, L., Cunha-Oliveira, T., Rodrigues, J., Rosenstock, T. R., Oliveira, A., Ribeiro, M., et al. (2017). Histone deacetylase inhibitors protect against pyruvate dehydrogenase dysfunction in huntington's disease. *J. Neurosci.* 37, 2776–2794. doi: 10.1523/JNEUROSCI.2006-14.2016

Nekrasov, E. D., Vigont, V. A., Klyushnikov, S. A., Lebedeva, O. S., Vassina, E. M., Bogomazova, A. N., et al. (2016). Manifestation of Huntington's disease pathology in human induced pluripotent stem cell-derived neurons. *Mol. Neurodegener.* 11:27. doi: 10.1186/s13024-016-0092-5

Nicholls, D. G. (2006). Simultaneous monitoring of ionophore- and inhibitor-mediated plasma and mitochondrial membrane potential changes in cultured neurons [Research Support, N.I.H., Extramural]. *J. Biol. Chem.* 281, 14864–14874. doi: 10.1074/jbc.M510916200

Nicoleau, C., Varela, C., Bonnefond, C., Maury, Y., Bugi, A., Aubry, L., et al. (2013). Embryonic stem cells neural differentiation qualifies the role of Wnt/beta-Catenin signals in human telencephalic specification and regionalization [Research Support. Non-U.S. Gov't]. *Stem Cells* 31, 1763–1774. doi: 10.1002/stem.1462

No authors listed (1993). A novel gene containing a trinucleotide repeat that is expanded and unstable on Huntington's disease chromosomes. The huntington's disease collaborative research group. *Cell* 72, 971–983. doi: 10.1016/0092-8674(93)90585-e

Oliveira, J. M., Chen, S., Almeida, S., Riley, R., Gonçalves, J., Oliveira, C. R., et al. (2006). Mitochondrial-dependent Ca2+ handling in Huntington's disease striatal cells: effect of histone deacetylase inhibitors. *J Neurosci* 26, 11174–11186. doi: 10.1523/jneurosci.3004-06.2006

Onofre, I., Mendonca, N., Lopes, S., Nobre, R., de Melo, J. B., Carreira, I. M., et al. (2016). Fibroblasts of Machado Joseph disease patients reveal autophagy impairment. *Sci. Rep.* 6:28220.

Panov, A. V., Gutekunst, C. A., Leavitt, B. R., Hayden, M. R., Burke, J. R., Strittmatter, W. J., et al. (2002). Early mitochondrial calcium defects in Huntington's disease are a direct effect of polyglutamines. *Nat. Neurosci.* 5, 731–736. doi: 10.1038/nn884

Park, I. H., Arora, N., Huo, H., Maherali, N., Ahfeldt, T., Shimamura, A., et al. (2008). Disease-specific induced pluripotent stem cells. *Cell* 134, 877–886.

Phinney, D. G., Di Giuseppe, M., Njah, J., Sala, E., Shiva, S., St Croix, C. M., et al. (2015). Mesenchymal stem cells use extracellular vesicles to outsource mitophagy and shuttle microRNAs. *Nat. Commun.* 6:8472.

Prigione, A., Fauler, B., Lurz, R., Lehrach, H., and Adjaye, J. (2010). The senescence-related mitochondrial/oxidative stress pathway is repressed in human induced pluripotent stem cells [Research Support, Non-U.S. Gov't]. *Stem Cells* 28, 721–733. doi: 10.1002/stem.404

Quinti, L., Dayalan Naidu, S., Trager, U., Chen, X., Kegel-Gleason, K., Lleres, D., et al. (2017). KEAP1-modifying small molecule reveals muted NRF2 signaling responses in neural stem cells from Huntington's disease patients. *Proc. Natl. Acad. Sci. U.S.A.* 114, E4676–E4685. doi: 10.1073/pnas.1614943114

Rardin, M. J., Wiley, S. E., Naviaux, R. K., Murphy, A. N., and Dixon, J. E. (2009). Monitoring phosphorylation of the pyruvate dehydrogenase complex. *Anal. Biochem.* 389, 157–164. doi: 10.1016/j.ab.2009.03.040

Ribeiro, M., Rosenstock, T. R., Oliveira, A. M., Oliveira, C. R., and Rego, A. C. (2014). Insulin and IGF-1 improve mitochondrial function in a PI-3K/Akt-dependent manner and reduce mitochondrial generation of reactive oxygen species in Huntington's disease knock-in striatal cells [Research Support, Non-U.S. Gov't]. *Free Radic. Biol. Med.* 74, 129–144. doi: 10.1016/j.freeradbiomed.2014.06.023

Roos, R. A. (2010). Huntington's disease: a clinical review. *Orphanet J. Rare Dis.* 5:40. doi: 10.1186/1750-1172-5-40

Shin, J. W., Kim, K. H., Chao, M. J., Atwal, R. S., Gillis, T., MacDonald, M. E., et al. (2016). Permanent inactivation of Huntington's disease mutation by personalized allele-specific CRISPR/Cas9. *Hum. Mol. Genet.* 25, 4566–4576. doi: 10.1093/hmg/ddw286

Shirendeb, U., Reddy, A. P., Manczak, M., Calkins, M. J., Mao, P., Tagle, D. A., et al. (2011). Abnormal mitochondrial dynamics, mitochondrial loss and mutant huntingtin oligomers in Huntington's disease: implications for selective neuronal damage. *Hum. Mol. Genet.* 20, 1438–1455. doi: 10.1093/hmg/ddr024

Shirendeb, U. P., Calkins, M. J., Manczak, M., Anekonda, V., Dufour, B., McBride, J. L., et al. (2012). Mutant huntingtin's interaction with mitochondrial protein Drp1 impairs mitochondrial biogenesis and causes defective axonal transport and synaptic degeneration in Huntington's disease [Research Support, N.I.H., Extramural Research Support, Non-U.S. Gov't]. *Hum. Mol. Genet.* 21, 406–420. doi: 10.1093/hmg/ddr475

Song, W., Chen, J., Petrilli, A., Liot, G., Klinglmayr, E., Zhou, Y., et al. (2011). Mutant huntingtin binds the mitochondrial fission GTPase dynamin-related protein-1 and increases its enzymatic activity. *Nat. Med.* 17, 377–382. doi: 10.1038/nm.2313

Sorbi, S., Bird, E. D., and Blass, J. P. (1983). Decreased pyruvate dehydrogenase complex activity in Huntington and Alzheimer brain. *Ann. Neurol.* 13, 72–78. doi: 10.1002/ana.410130116

Stocchi, V., Magnani, M., Cucchiarini, L., Novelli, G., and Dallapiccola, B. (1985). Red blood cell adenine nucleotides abnormalities in Down syndrome. *Am. J. Med. Genet.* 20, 131–135. doi: 10.1002/ajmg.1320200116

Szlachcic, W. J., Switonski, P. M., Krzyzosiak, W. J., Figlerowicz, M., and Figiel, M. (2015). Huntington disease iPSCs show early molecular changes in intracellular signaling, the expression of oxidative stress proteins and the p53 pathway. *Dis. Model Mech.* 8, 1047–1057. doi: 10.1242/dmm.019406

Tabrizi, S. J., Leavitt, B. R., Landwehrmeyer, G. B., Wild, E. J., Saft, C., Barker, R. A., et al. (2019). Targeting huntingtin expression in patients with Huntington's disease. *N. Engl. J. Med.* 380, 2307–2316. doi: 10.1056/NEJMoa1900907

Varum, S., Rodrigues, A. S., Moura, M. B., Momcilovic, O., Easley, C. A. T., Ramalho-Santos, J., et al. (2011). Energy metabolism in human pluripotent stem cells and their differentiated counterparts [Research Support, N.I.H., Extramural Research Support, Non-U.S. Gov't]. *PLoS One* 6:e20914. doi: 10.1371/journal.pone.0020914

Xu, X., Tay, Y., Sim, B., Yoon, S. I., Huang, Y., Ooi, J., et al. (2017). Reversal of phenotypic abnormalities by CRISPR/Cas9-mediated gene correction in huntington disease patient-derived induced pluripotent stem cells. *Stem Cell Rep.* 8, 619–633. doi: 10.1016/j.stemcr.2017.01.022

Yang, S., Chang, R., Yang, H., Zhao, T., Hong, Y., Kong, H. E., et al. (2017). CRISPR/Cas9-mediated gene editing ameliorates neurotoxicity in mouse model of Huntington's disease. *J. Clin. Invest.* 127, 2719–2724. doi: 10.1172/JCI92087

Zhang, J., Khvorostov, I., Hong, J. S., Oktay, Y., Vergnes, L., Nuebel, E., et al. (2011). UCP2 regulates energy metabolism and differentiation potential of human pluripotent stem cells [Research Support, N.I.H., Extramural Research Support, Non-U.S. Gov't]. *EMBO J.* 30, 4860–4873. doi: 10.1038/emboj.2011.401

Zhang, N., An, M. C., Montoro, D., and Ellerby, L. M. (2010). Characterization of human Huntington's disease cell model from induced pluripotent stem cells. *PLoS Curr.* 2:RRN1193. doi: 10.1371/currents.RRN1193

Zheng, X., Boyer, L., Jin, M., Mertens, J., Kim, Y., Ma, L., et al. (2016). Metabolic reprogramming during neuronal differentiation from aerobic glycolysis to neuronal oxidative phosphorylation. *eLife* 5, e13374. doi: 10.7554/eLife.13374

Conflict of Interest: The authors declare that the research was conducted in the absence of any commercial or financial relationships that could be construed as a potential conflict of interest.

frontiers in Cell and Developmental Biology

PERSPECTIVE
published: 17 November 2020
doi: 10.3389/fcell.2020.605274

A Bird's Eye View on the Origin of Aortic Hemogenic Endothelial Cells

Pedro Seco[1], *Gabriel G. Martins*[2,3], *António Jacinto*[1] *and Ana Teresa Tavares*[1]*

[1] iNOVA4Health, CEDOC, NOVA Medical School, Universidade Nova de Lisboa, Lisbon, Portugal, [2] Instituto Gulbenkian de Ciência, Oeiras, Portugal, [3] Faculdade de Ciências, Universidade de Lisboa, Lisbon, Portugal

During early embryogenesis, the hemogenic endothelium of the developing dorsal aorta is the main source of definitive hematopoietic stem cells (HSCs), which will generate all blood cell lineages of the adult organism. The hemogenic endothelial cells (HECs) of the dorsal aorta are known to arise from the splanchnic lateral plate mesoderm. However, the specific cell lineages and developmental paths that give rise to aortic HECs are still unclear. Over the past half a century, the scientific debate on the origin of aortic HECs and HSCs has largely focused on two potential and apparently alternative birthplaces, the extraembryonic yolk sac blood islands and the intraembryonic splanchnic mesoderm. However, as we argue, both yolk sac blood islands and aortic HECs may have a common hemangioblastic origin. Further insight into aortic HEC development is being gained from fate-mapping studies that address the identity of progenitor cell lineages, rather than their physical location within the developing embryo. In this perspective article, we discuss the current knowledge on the origin of aortic HECs with a particular focus on the evidence provided by studies in the avian embryo, a model that pioneered the field of developmental hematopoiesis.

Keywords: hemogenic endothelium, hemangioblast, dorsal aorta, yolk sac, avian embryo, lineage-tracing

OPEN ACCESS

Edited by:
Susana Solá,
University of Lisbon, Portugal

Reviewed by:
Valerie Kouskoff,
The University of Manchester, United Kingdom
Eirini Trompouki,
Max Planck Institute for Immunobiology and Epigenetics, Germany
Thierry Jaffredo,
Centre National de la Recherche Scientifique (CNRS), France

***Correspondence:**
Ana Teresa Tavares
anateresa.tavares@nms.unl.pt

Specialty section:
This article was submitted to Stem Cell Research, a section of the journal Frontiers in Cell and Developmental Biology

Received: *11 September 2020*
Accepted: *28 October 2020*
Published: *17 November 2020*

Citation:
Seco P, Martins GG, Jacinto A and Tavares AT (2020) A Bird's Eye View on the Origin of Aortic Hemogenic Endothelial Cells. Front. Cell Dev. Biol. 8:605274. doi: 10.3389/fcell.2020.605274

INTRODUCTION

Hemogenic endothelial cells (HECs) are specialized vascular endothelial cells with the potential to give rise to hematopoietic stem/progenitor cells (HSPC) during vertebrate embryogenesis (Jaffredo et al., 1998; Zovein et al., 2008; Gritz and Hirschi, 2016). During this differentiation process, known as endothelial-to-hematopoietic transition (EHT), HECs gradually round up, separate from their neighboring cells and bud off from the endothelium (Eilken et al., 2009; Lancrin et al., 2009; Bertrand et al., 2010; Boisset et al., 2010; Kissa and Herbomel, 2010; Lam et al., 2010; Ottersbach, 2019; **Figure 1A**). Depending on developmental stage and location, HECs differentiate into HSPC populations with different hematopoietic potential. In mammalian and avian embryos, the first HECs are observed in the yolk sac blood islands and give rise to erythro-myeloid progenitors (EMPs) (Li et al., 2005; McGrath et al., 2015; Frame et al., 2016) and lymphoid progenitors (Yoshimoto et al., 2011, 2012). In addition, HECs located in the endocardium only generate EMPs (Nakano et al., 2013), whereas those in the head arteries and vitelline/umbilical arteries generate both EMPs and definitive hematopoietic stem cells (HSCs), the founders of adult hematopoietic cells (De Bruijn et al., 2000; Zovein et al., 2010; Li et al., 2012). Yet, HSC-producing HECs reside

mainly in the ventral wall of the dorsal aorta in all vertebrate embryos studied to date (Medvinsky and Dzierzak, 1996; Jaffredo et al., 1998; Ciau-Uitz et al., 2000; Oberlin et al., 2002; Zovein et al., 2008; Bertrand et al., 2010). Recent studies suggest that aortic HECs retain a dual potential for differentiation into endothelial or hematopoietic cells (Hou et al., 2020), which may be driven toward a hemogenic fate by local cues that promote their detachment from the endothelium and cell cycle re-entry (Yue et al., 2012; Zhang et al., 2014; Canu et al., 2020).

In contrast to their clear developmental fate, the origin of aortic HECs and HSCs remains a matter of active debate. The enduring question is whether aortic HECs arise from extraembryonic yolk sac-derived progenitors that migrate into the developing aorta or from local intraembryonic progenitors, with experimental evidence supporting both possibilities (reviewed in Medvinsky et al., 2011; Wittamer and Bertrand, 2020). The seemingly contradictory results may be explained by the use of different models, time frames and methods. Namely, the evaluation of HSC differentiation potential in *in vitro* culture and transplantation assays was used to verify the presence of HSC precursor cells in different embryonic tissues. Data from these studies mostly support an intraembryonic origin for aortic HECs (Medvinsky and Dzierzak, 1996; Cumano et al., 2001; Yvernogeau and Robin, 2017). However, differentiation potentials may not reflect the original developmental fate of the explanted cell populations, which is largely influenced by their natural microenvironment and commitment status. Alternatively, the origin of aortic HECs has been more accurately investigated using fate-mapping and live imaging methods. In particular, lineage-tracing experiments using tamoxifen-inducible mouse models have indicated that yolk sac-derived cells migrate into the embryo and give rise to aortic HECs (Samokhvalov et al., 2007; Tanaka et al., 2014). However, conclusions from these studies may be compromised by the persistence of tamoxifen in the system and consequent labeling of intraembryonic cells (Senserrich et al., 2018). In addition to mouse models, fate-mapping studies in avian embryos have also greatly contributed to the discussion. For more than a century, observations in avian embryo models have led to major fundamental discoveries in the field of hematopoietic development (Le Douarin and Dieterlen-Lièvre, 2013; Jaffredo and Yvernogeau, 2014). After a brief description of yolk sac and dorsal aorta development, this perspective article will review and discuss the experimental evidence in chick and quail embryos that provided key insight into the origin of aortic HECs and vastly enriched our understanding of hematopoietic development.

YOLK SAC AND DORSAL AORTA DEVELOPMENT IN THE AVIAN EMBRYO

To better interpret the evidence supporting each of the two proposed sites of origin of aortic HECs, the yolk sac blood islands (extraembryonic) and the prospective ventral dorsal aorta (intraembryonic), it is important to understand when and how these tissues develop. Both the yolk sac blood islands and the ventral endothelium of the dorsal aorta derive from the splanchnic lateral plate mesoderm, which, together with the endoderm, forms the splanchnopleure (Prummel et al., 2020). During gastrulation, these mesodermal cells arise from median-posterior sections of the primitive streak, with the posterior region giving rise to more lateral (extraembryonic) tissues (Psychoyos and Stern, 1996). In addition to their common mesodermal origin, the developmental paths of the yolk sac and dorsal aorta are closely coordinated in time and space, thus ensuring the proper establishment of embryonic blood circulation.

The yolk sac blood islands give rise to the extraembryonic vascular network and to the first hematopoietic cells of the developing embryo (Sabin, 1920). These structures are formed by a subpopulation of mesodermal-derived cells known as hemangioblasts, the precursors of both endothelial and hematopoietic cell lineages (Sabin, 1920; Murray, 1932). In the chick embryo, hemangioblasts arise in the yolk sac at Hamburger and Hamilton (HH) stage 5–6 (Hamburger and Hamilton, 1992), where they aggregate into blood islands at stage HH7–8 and start to differentiate into endothelial and hematopoietic cells at stage HH9–10 (Nagai et al., 2018). It is currently thought that these hematopoietic cells originate from two types of hemangioblast-derived progenitors: primitive hematopoietic cells derive from hemogenic angioblasts, whereas EMPs derive from hemogenic endothelial cells (Lacaud and Kouskoff, 2017). Proximal blood islands differentiate only into endothelial cells that will form a connecting network between the extraembryonic vasculature and the intraembryonic vascular plexus (Coffin and Poole, 1988; Nagai et al., 2018). At stages HH9 to HH11, this vascular plexus is contiguous with the developing endocardium (anterior region) and dorsal aorta (posterior region) and will later give rise the vitelline veins and arteries (le Noble et al., 2004).

The dorsal aorta is not only the first and largest intraembryonic blood vessel, but also an important site of secondary hematopoiesis (reviewed in Medvinsky et al., 2011). In avian embryos, paired dorsal aortae arise at stage HH8 as bilateral longitudinal cords of endothelial precursor cells (or angioblasts), which are derived from the splanchnic mesoderm (Poole and Coffin, 1989; Pardanaud et al., 1996). At stage HH9, angioblasts start to coalesce and remodel into two endothelial vessels. A few hours later (stage HH10), the two vessels move toward the ventral midline, where they will fuse into a single tube (stage HH13) (Pardanaud et al., 1987; Coffin and Poole, 1988). During these stages, somite-derived endothelial cells are integrated into the dorsal region (roof) of the dorsal aorta and gradually displace the splanchnic mesoderm-derived endothelial cells to the ventral region (floor), which is where HECs arise (Pardanaud et al., 1996; Jaffredo et al., 2013). In the caudal region of the embryo, the dorsal aorta elongates posteriorly and becomes attached to the intraembryonic vascular plexus, thus forming a connection with the extraembryonic vascular network (Pardanaud et al., 1987; Coffin and Poole, 1988). Circulating blood cells can be seen in the dorsal aorta by stage HH12 (early day 2 of development), shortly after heartbeat onset at stage HH10–11 (Hogers et al., 1995). From then on, blood circulation between the yolk sac and the embryo body is established, which

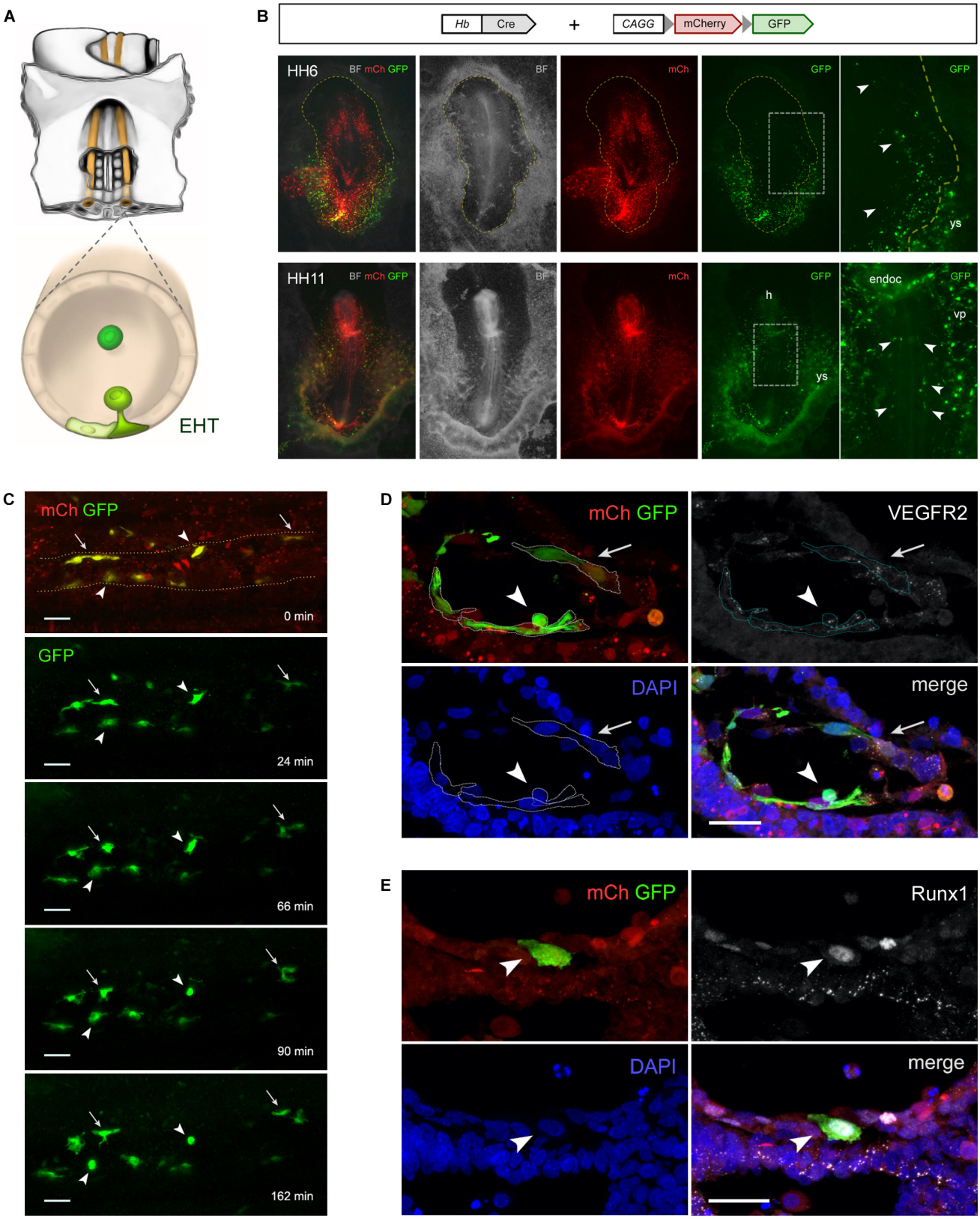

FIGURE 1 | Continued

FIGURE 1 | Hemangioblasts give rise to aortic hemogenic endothelial cells in the chick embryo. **(A)** Illustration of the central region of a stage HH11 chick embryo (ventral side up) highlighting the paired dorsal aortae (orange) and the hemogenic endothelial cells (HECs; green) localized in the aortic floor that differentiate into hematopoietic stem/progenitor cells via an endothelial-to-hematopoietic transition (EHT). **(B–E)** Hb-Cre and pCAGG-LoxP-mCherry-LoxP-GFP plasmids were used to analyze the progeny of chick hemangioblasts. Chick embryos were electroporated *ex ovo* at stage HH3 using an Intracel TSS20 electroporator, incubated until stage HH13 in New culture (New, 1955) or until stage HH16 in MC culture (Nagai et al., 2011), and imaged either as whole mounts using a Zeiss SteREO Lumar stereomicroscope **(B)** and a Prairie Multiphoton system **(C)**, or in immunolabeled cryosections using a Zeiss LSM710 confocal microscope **(D,E)**. **(B)** While mCherry (mCh) is ubiquitously expressed in all electroporated cells, GFP expression is specifically detected in hemangioblasts and their progeny. mCh expression in GFP+ cells may result from the presence of unrecombined copies of the reporter construct and/or persistent mCh transcripts and protein. At stage HH6 (n = 36; top), GFP+ hemangioblasts are found in both the yolk sac (ys) and the intraembryonic region (arrowhead; dashed yellow line outlines the embryo). At stage HH11 (n = 52; bottom), GFP+ hemangioblast-derived cells are found in the yolk sac (ys), head region (h), endocardium (endoc), intraembryonic vascular plexus (vp) and dorsal aorta (arrowheads). **(C)** Time-lapse images of electroporated HH11–12 chick embryo showing the dynamics of GFP+ hemangioblast-derived cells in the dorsal aorta endothelium (n = 3; see Video S1 and legend). During the imaging period (168 min), two GFP+ HECs undergo EHT (arrowheads), whereas other GFP+ cells remain as endothelial cells (arrows). **(D,E)** Transverse sections through the dorsal aortae of electroporated chick embryos immunolabeled with primary antibodies against GFP (Roche, 11814460001; Invitrogen, A11122; green), VEGFR2 (gift from Anne Eichmann; Eichmann et al., 1997; n = 5; **D**; HH13; white) or Runx1 (Abcam, ab92336; n = 6; **E**; HH16; white), and secondary antibodies with Alexa Fluor 488 (Invitrogen, A11001 and A11008) or Alexa Fluor 647 (Jackson ImmunoResearch, 715-605-151 and 711-605-152). Cell nuclei were labeled with DAPI (Sigma-Aldrich; blue). Electroporated cells are identified by mCh fluorescence (red). **(D)** GFP+ cells co-express VEGFR2, a marker of endothelial cells, and exhibit either a HEC morphology (arrowhead) or a typical endothelial cell shape (arrow). **(E)** Prior to emergence from the aortic floor, a GFP+ cell can be identified as a HEC by Runx1 expression (arrowhead), a marker of endothelial cells with hemogenic potential. BF, brightfield; n, number of embryos.

makes it impossible to determine if aortic HECs that may arise hereafter have an extra- or intraembryonic origin.

TRACING THE ORIGIN OF AVIAN AORTIC HECs

Since aortic HECs arise prior to the establishment of circulation, their progenitor cells are thought to either migrate into the presumptive ventral aorta region from the adjacent yolk sac (extraembryonic origin) or develop *in situ* within the presumptive dorsal aorta region (intraembryonic origin) (Medvinsky et al., 2011; Wittamer and Bertrand, 2020). Both hypotheses have gathered support over the years from fate-mapping studies using classical grafting techniques as well as more recent genetic and time-lapse imaging methods in electroporated or transgenic avian embryos.

Early experimental studies addressed the origin of definitive HSCs before the identification of aortic HECs as their progenitor cells (Cormier and Dieterlen-Lièvre, 1988; Jaffredo et al., 1998). The colonization of developing hematopoietic organs by yolk sac-derived HSCs was initially suggested by studies using parabiotic chick embryos (Moore and Owen, 1965). Yet, these experiments evaluated only the contribution of circulating cells (at 6–8 days of development), suggesting that embryo-derived HSCs might be already present in the yolk sac. The intraembryonic origin of HSCs was originally proposed in a series of classical grafting studies using avian yolk sac chimeras (reviewed in Jaffredo and Yvernogeau, 2014). The first experimental evidence came from analyzing chimeras of quail embryo bodies grafted onto chick yolk sacs before circulation is established. In most chimeras, the dorsal aorta (Dieterlen-Lièvre and Martin, 1981), spleen and thymus (Dieterlen-Lièvre, 1975) contained exclusively quail cells, thus indicating that the adult hematopoietic system was derived from the embryo proper and not from the yolk sac. The same conclusion was reached in studies of homospecific yolk sac chimeras from different-sex or allogeneic chick embryos (Lassila et al., 1978, 1982; Martin et al., 1978; Beaupain et al., 1979). Nonetheless, since the earliest stage of grafting was HH9 (Dieterlen-Lièvre, 1975; Lassila et al., 1978; Beaupain et al., 1979; Dieterlen-Lièvre and Martin, 1981), the possibility exists that yolk sac-derived angioblasts (or hemangioblasts) have colonized the presumptive dorsal aorta region before this stage.

The hypothesis that hemangioblasts give rise to aortic endothelial cells is supported by evidence showing that dorsal aorta-forming angioblasts express the hemangioblast and endothelial/blood marker Tal1/Scl (Drake et al., 1997) and that extraembryonic cells migrate to and contribute to the dorsal aorta endothelium (Sato et al., 2010; Tanaka et al., 2014; Eliades et al., 2016). However, as mentioned earlier, developmental cell fate is best addressed with *in vivo* lineage-tracing and time-lapse imaging methods, which first require the identification of a lineage-specific marker capable of labeling a particular cell population and its progeny (Stern and Fraser, 2001). Indeed, we have identified a hemangioblast enhancer (Hb) that is able to specifically activate the expression of a reporter gene (eGFP) in chick embryo hemangioblasts as they ingress through the posterior primitive streak at stages HH3 to HH6 (Teixeira et al., 2011). The Hb-eGFP reporter was used to study the dynamics of blood island morphogenesis in live imaging assays (Teixeira et al., 2011), and to isolate and characterize the gene expression profile of chick embryo hemangioblasts (Serrado Marques et al., 2018). Moreover, Zamir et al. (2017) used this reporter to show that a subpopulation of Hb-eGFP+ hemangioblasts gives rise to hemogenic angioblasts that can be found in both the extraembryonic yolk sac and intraembryonic lateral plate mesoderm at stage HH7, and that contribute to the hemogenic endothelium of the dorsal aorta. However, although eGFP RNA and protein stability may enable the detection of Hb-eGFP+ hemangioblast-derived cells, lineage-tracing analysis is required to accurately identify the progeny of hemangioblasts.

In order to label and trace the hemangioblast lineage, we took advantage of a Cre-Lox system in which a plasmid containing the hemangioblast enhancer driving Cre recombinase expression (Hb-Cre) and the conditional reporter plasmid pCAGG-LoxP-mCherry-LoxP-GFP are co-electroporated into chick embryos (stage HH3), as previously reported for neuronal lineages (Avraham et al., 2009). In this system, cells that express Cre

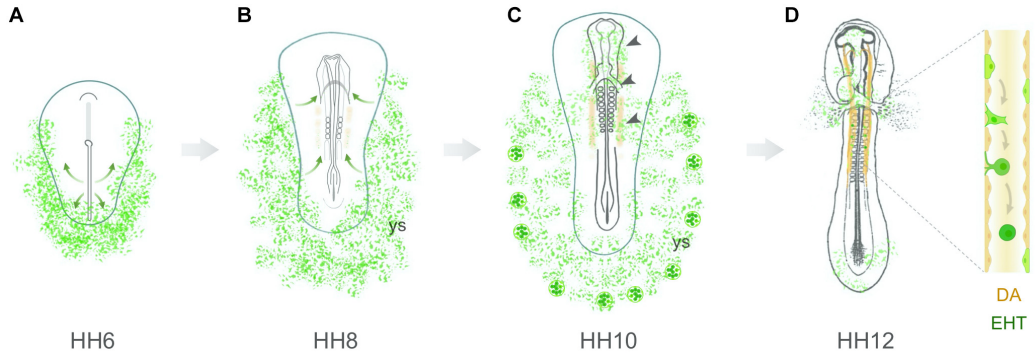

FIGURE 2 | Hemangioblastic origin of aortic hemogenic endothelial cells in the early chick embryo. **(A)** Hemangioblasts arise from lateral plate mesodermal cells that ingress through the posterior region of the primitive streak. At stage HH6, these cells are located in the lateral and posterior regions of the embryo, both in the yolk sac and intraembryonic region. **(B)** At stage HH7–8, hemangioblasts aggregate to form blood islands within the yolk sac (ys). Concomitantly, a subpopulation of hemangioblast-derived cells (or angioblasts) starts to migrate toward the presumptive paired dorsal aortae (orange). **(C)** At stage HH10, yolk sac hemangioblasts have already started to differentiate into endothelial and hematopoietic cells in the distal blood islands. Inside the embryo, hemangioblast-derived cells are found in the head region, endocardium, vascular plexus and dorsal aortae (arrowheads). **(D)** At stages HH11–12, hemangioblast-derived HECs are detected in the dorsal aortae (DA), where they undergo an endothelial-to-hematopoietic transition (EHT).

under the control of the Hb enhancer will recombine out the floxed mCherry sequence and activate GFP expression, enabling the identification of hemangioblasts as well as their progeny. We observed that GFP+ cells are present in both the yolk sac and intraembryonic lateral plate mesoderm at early stages (**Figure 1B**, top), which supports the existence of a subpopulation of intraembryonic hemangioblasts. At later stages, GFP+ hemangioblast-derived cells are detected in the yolk sac blood islands, head region, endocardium, intraembryonic vascular plexus and dorsal aorta (**Figure 1B**, bottom). Using time-lapse multiphoton microscopy imaging of electroporated chick embryos, we observed that some GFP+ cells in the dorsal aorta undergo EHT at stages HH11–12 (**Supplementary Video S1** and **Figure 1C**). GFP+ cells in the aortic endothelium display either a flat endothelial morphology or HEC features, as seen also in cross-sections of the dorsal aorta labeled for VEGFR2, a marker of endothelial cells (Eichmann et al., 1993; **Figure 1D**), and for Runx1, a marker of HECs (Jaffredo et al., 2005; **Figure 1E**). Of note, Runx1 expression is also detected in some mCherry+GFP- cells, suggesting that hemangioblasts are not the exclusive source of aortic hemogenic endothelium. Taken together, these observations indicate that hemangioblast-derived hemogenic angioblasts give rise to a subpopulation of aortic HECs in the chick embryo. However, further experiments are required to reveal the hematopoietic potential of hemangioblast-derived aortic HECs. Our findings are consistent with lineage-tracing experiments in the mouse embryo showing that extraembryonic Runx1+ hemogenic angioblasts migrate into the intraembryonic region prior to circulation and contribute to the dorsal aorta hemogenic endothelium (Tanaka et al., 2014). It is therefore, conceivable that both yolk sac blood islands and aortic HECs originate from hemangioblasts.

In summary, recent evidence suggests that hemangioblasts colonize the presumptive dorsal aorta region (stages HH7–8), contribute to the developing aortic endothelium (stages HH9–10) and give rise to aortic HECs (stage HH11 onwards; **Figure 2**). Yet, it remains to be determined if these hemangioblasts are originally located in the intraembryonic splanchnic mesoderm (as shown in **Figure 1B**, top; Zamir et al., 2017) or if they migrate medially from the yolk sac at stages HH7–8. In any case, this early population of aortic HECs progenitors would be reasonably considered to have an intraembryonic origin in grafting studies of yolk sac chimeras established at stage HH9 and later. In conclusion, aortic HECs are likely to originate from multiple sources that combine hemangioblasts and other splanchnic mesoderm-derived hemogenic progenitors.

Further evidence supporting a hemangioblastic origin for aortic HECs was provided by studies in *Xenopus* embryos. Lineage tracing and co-expression analysis of endothelial and blood markers demonstrated that HSC-producing aortic HECs arise from hematovascular progenitors known as adult or definitive hemangioblasts (Walmsley et al., 2002; Ciau-Uitz et al., 2013). Definitive hemangioblasts arise from lateral plate mesodermal cells that express Tal1/Scl and lie close to the somites. These features are also typical of aortic HEC precursors in zebrafish, chick and mouse, suggesting that definitive hemangioblasts may indeed exist in all vertebrates (reviewed in Ciau-Uitz and Patient, 2016). Furthermore, converging evidence has come from *in vitro* differentiation studies of human embryonic stem cells and induced pluripotent stem cells, which show that definitive HSCs-producing HECs can be derived from hemangioblastic progenitors (reviewed in Chen et al., 2015). Ultimately, this information can be used to develop hemangioblast-based differentiation protocols for the *in vitro* generation of transplantable HSCs.

CONCLUDING REMARKS

The hemogenic endothelium of the developing dorsal aorta is considered to be the major site of HSC production in the early

embryo. As such, aortic HECs have been the subject of extensive research on many of their biological aspects, such as molecular signature, differentiation potential and developmental origin. For over 40 years, the extra- vs. intraembryonic origin of HSCs and aortic HECs has been the focus of numerous studies, for which the avian embryo was a pioneer model. However, classical grafting experiments in avian embryos need to be reinterpreted in light of recent lineage-tracing evidence demonstrating that hemangioblasts give rise to aortic HECs at early developmental stages. This finding is particularly relevant in the context of *in vitro* differentiation of pluripotent stem cells into HSCs for clinical applications.

DATA AVAILABILITY STATEMENT

The original contributions presented in the study are included in the article/**Supplementary Material**, further inquiries can be directed to the corresponding author.

ETHICS STATEMENT

Ethical review and approval was not required for the animal study because all experimental procedures were performed in chicken embryos with less than 3 days of development, which are not considered experimental animal subjects according to the Portuguese Law (Decree-Law 113/2013) and European Guidelines (Directive 2010/63/EU).

AUTHOR CONTRIBUTIONS

PS performed the experiments and contributed to the manuscript writing. GM helped with the research design, image acquisition, and data analysis. AJ contributed to the data interpretation and scientific discussion. AT designed and performed the experiments, analyzed and interpreted the data, and wrote the manuscript. All authors contributed to manuscript revision and approved the final version.

FUNDING

This work was supported by the FCT – Fundação para a Ciência e a Tecnologia, I.P. (PTDC/BTM-SAL/29377/2017) and iNOVA4Health (UID/Multi/04462/2019). The Advanced Imaging Facility of the Instituto Gulbenkian de Ciência was supported by national Portuguese funding co-financed by the Lisboa Regional Operational Programme (Lisboa 2020), under the Portugal 2020 Partnership Agreement, through the European Regional Development Fund (FEDER) and FCT (PPBI-POCI-01-0145-FEDER-022122). AT was funded by the FCT in the context of a program contract under "Norma Transitória" (DL57/2016 of 29 August, as amended by DL57/2017 of 19 July).

ACKNOWLEDGMENTS

We are grateful to Natacha Arede, Vera Teixeira, Ana Farinho, and Telmo Pereira for technical assistance, Ofélia Carvalho for critically revising the manuscript, Anne Eichmann for kindly providing the avian VEGFR2 antibody and Avihu Klar for kindly providing plasmid constructs.

SUPPLEMENTARY MATERIAL

The Supplementary Material for this article can be found online at: https://www.frontiersin.org/articles/10.3389/fcell.2020.605274/full#supplementary-material

Supplementary Video 1 | Hemangioblast-derived hemogenic endothelial cells are detected in the chick embryo dorsal aorta. Time-lapse movie of a stage HH11–12 live chick embryo in New culture electroporated at stage HH3 with Hb-Cre and pCAGG-LoxP-mCherry-LoxP-GFP reporter constructs showing a portion of the dorsal aorta (still frames in **Figure 1C**). The anterior side is to the left. Brightfield images were acquired on a Zeiss SteREO Lumar stereomicroscope (initial frames). Time-lapse 4D stacks were acquired on a Prairie Multiphoton system equipped with GaAsP detectors mounted on an Olympus BX61 microscope equipped with a 10× 0.3NA objective, and the datasets were processed and 3D reconstructed using Fiji (ImageJ) and Imaris software (Bitplane). Red represents mCherry, and green, GFP expression. Arrowheads point at two GFP+ hemogenic endothelial cells that round up and emerge from the aortic wall. Arrows point at GFP+ cells that maintain an endothelial morphology. Time is indicated in minutes in the lower right corner.

REFERENCES

Avraham, O., Hadas, Y., Vald, L., Zisman, S., Schejter, A., Visel, A., et al. (2009). Transcriptional control of axonal guidance and sorting in dorsal interneurons by the Lim-HD proteins Lhx9 and Lhx1. *Neural Dev.* 4:21. doi: 10.1186/1749-8104-4-21

Beaupain, D., Martin, C., and Dieterlen-Lièvre, F. (1979). Are developmental hemoglobin changes related to the origin of stem cells and site of erythropoiesis? *Blood* 53, 212–225. doi: 10.1182/blood.V53.2.212.212

Bertrand, J. Y., Chi, N. C., Santoso, B., Teng, S., Stainier, D. Y. R., and Traver, D. (2010). Haematopoietic stem cells derive directly from aortic endothelium during development. *Nature* 464, 108–111. doi: 10.1038/nature08738

Boisset, J. C., Van Cappellen, W., Andrieu-Soler, C., Galjart, N., Dzierzak, E., and Robin, C. (2010). In vivo imaging of haematopoietic cells emerging from the mouse aortic endothelium. *Nature* 464, 116–120. doi: 10.1038/nature08764

Canu, G., Athanasiadis, E., Grandy, R. A., Garcia-Bernardo, J., Strzelecka, P. M., Vallier, L., et al. (2020). Analysis of endothelial-to-haematopoietic transition at the single cell level identifies cell cycle regulation as a driver of differentiation. *Genome Biol.* 21:157. doi: 10.1186/s13059-020-02058-4

Chen, T., Wang, F., Wu, M., and Wang, Z. Z. (2015). Development of hematopoietic stem and progenitor cells from human pluripotent stem cells. *J. Cell. Biochem.* 116, 1179–1189. doi: 10.1002/jcb.25097

Ciau-Uitz, A., and Patient, R. (2016). The embryonic origins and genetic programming of emerging haematopoietic stem cells. *FEBS Lett.* 590, 4002–4015. doi: 10.1002/1873-3468.12363

Ciau-Uitz, A., Pinheiro, P., Kirmizitas, A., Zuo, J., and Patient, R. (2013). VEGFA-dependent and -independent pathways synergise to drive Scl expression and initiate programming of the blood stem cell lineage in *Xenopus*. *Development* 140, 2632–2642. doi: 10.1242/dev.090829

Ciau-Uitz, A., Walmsley, M., and Patient, R. (2000). Distinct origins of adult and embryonic blood in *Xenopus*. *Cell* 102, 787–796. doi: 10.1016/S0092-8674(00)00067-2

Coffin, J. D., and Poole, T. J. (1988). Embryonic vascular development: immunohistochemical identification of the origin and subsequent morphogenesis of the major vessel primordia in quail embryos. *Development* 102, 735–748.

Cormier, F., and Dieterlen-Lièvre, F. (1988). The wall of the chick embryo aorta harbours M-CFC, G-CFC, GM-CFC and BFU-E. *Development* 102, 279–285.

Cumano, A., Ferraz, J. C., Klaine, M., Di Santo, J. P., and Godin, I. (2001). Intraembryonic, but not yolk sac hematopoietic precursors, isolated before circulation, provide long-term multilineage reconstitution. *Immunity* 15, 477–485. doi: 10.1016/S1074-7613(01)00190-X

De Bruijn, M. F. T. R., Speck, N. A., Peeters, M. C. E., and Dzierzak, E. (2000). Definitive hematopoietic stem cells first develop within the major arterial regions of the mouse embryo. *EMBO J.* 19, 2465–2474. doi: 10.1093/emboj/19.11.2465

Dieterlen-Lièvre, F. (1975). On the origin of haemopoietic stem cells in the avian embryo: an experimental approach. *J. Embryol. Exp. Morphol.* 33, 607–619.

Dieterlen-Lièvre, F., and Martin, C. (1981). Diffuse intraembryonic hemopoiesis in normal and chimeric avian development. *Dev. Biol.* 88, 180–191. doi: 10.1016/0012-1606(81)90228-1

Drake, C. J., Brandt, S. J., Trusk, T. C., and Little, C. D. (1997). TAL1/SCL is expressed in endothelial progenitor cells/angioblasts and defines a dorsal-to-ventral gradient of vasculogenesis. *Dev. Biol.* 192, 17–30. doi: 10.1006/dbio.1997.8751

Eichmann, A., Corbel, C., Nataf, V., Vaigot, P., Bréant, C., and Le Douarin, N. M. (1997). Ligand-dependent development of the endothelial and hemopoietic lineages from embryonic mesodermal cells expressing vascular endothelial growth factor receptor 2. *Proc. Natl. Acad. Sci. U.S.A.* 94, 5141–5146. doi: 10.1073/pnas.94.10.5141

Eichmann, A., Marcelle, C., Bréant, C., and Le Douarin, N. M. (1993). Two molecules related to the VEGF receptor are expressed in early endothelial cells during avian embryonic development. *Mech. Dev.* 42, 33–48. doi: 10.1016/0925-4773(93)90096-G

Eilken, H. M., Nishikawa, S. I., and Schroeder, T. (2009). Continuous single-cell imaging of blood generation from haemogenic endothelium. *Nature* 457, 896–900. doi: 10.1038/nature07760

Eliades, A., Wareing, S., Marinopoulou, E., Fadlullah, M. Z. H., Patel, R., Grabarek, J. B., et al. (2016). The hemogenic competence of endothelial progenitors is restricted by Runx1 silencing during embryonic development. *Cell Rep.* 15, 2185–2199. doi: 10.1016/j.celrep.2016.05.001

Frame, J. M., Fegan, K. H., Conway, S. J., McGrath, K. E., and Palis, J. (2016). Definitive hematopoiesis in the yolk sac emerges from Wnt-responsive hemogenic endothelium independently of circulation and arterial identity. *Stem Cells* 34, 431–444. doi: 10.1002/stem.2213

Gritz, E., and Hirschi, K. K. (2016). Specification and function of hemogenic endothelium during embryogenesis. *Cell. Mol. Life Sci.* 73, 1547–1567. doi: 10.1007/s00018-016-2134-0

Hamburger, V., and Hamilton, H. L. (1992). A series of normal stages in the development of the chick embryo. 1951. *Dev. Dyn.* 195, 231–272. doi: 10.1002/aja.1001950404

Hogers, B., DeRuiter, M. C., Baasten, A. M. J., Gittenberger-de Groot, A. C., and Poelmann, R. E. (1995). Intracardiac blood flow patterns related to the yolk sac circulation of the chick embryo. *Circ. Res.* 76, 871–877. doi: 10.1161/01.RES.76.5.871

Hou, S., Li, Z., Zheng, X., Gao, Y., Dong, J., Ni, Y., et al. (2020). Embryonic endothelial evolution towards first hematopoietic stem cells revealed by single-cell transcriptomic and functional analyses. *Cell Res.* 30, 376–392. doi: 10.1038/s41422-020-0300-2

Jaffredo, T., Bollerot, K., Sugiyama, D., Gautier, R., and Drevon, C. (2005). Tracing the hemangioblast during embryogenesis: developmental relationships between endothelial and hematopoietic cells. *Int. J. Dev. Biol.* 49, 269–277. doi: 10.1387/ijdb.041948tj

Jaffredo, T., Lempereur, A., Richard, C., Bollerot, K., Gautier, R., Canto, P. Y., et al. (2013). Dorso-ventral contributions in the formation of the embryonic aorta and the control of aortic hematopoiesis. *Blood Cells, Mol. Dis.* 51, 232–238. doi: 10.1016/j.bcmd.2013.07.004

Jaffredo, T., Rodolphe, G., Eichmann, A., and Dieterlen-Lièvre, F. (1998). Intraaortic hemopoietic cells are derived from endothelial cells during ontogeny. *Trends Cardiovasc. Med.* 125, 4575–4583.

Jaffredo, T., and Yvernogeau, L. (2014). How the avian model has pioneered the field of hematopoietic development. *Exp. Hematol.* 42, 661–668. doi: 10.1016/j.exphem.2014.05.009

Kissa, K., and Herbomel, P. (2010). Blood stem cells emerge from aortic endothelium by a novel type of cell transition. *Nature* 464, 112–115. doi: 10.1038/nature08761

Lacaud, G., and Kouskoff, V. (2017). Hemangioblast, hemogenic endothelium, and primitive versus definitive hematopoiesis. *Exp. Hematol.* 49, 19–24. doi: 10.1016/j.exphem.2016.12.009

Lam, E. Y. N., Hall, C. J., Crosier, P. S., Crosier, K. E., and Flores, M. V. (2010). Live imaging of Runx1 expression in the dorsal aorta tracks the emergence of blood progenitors from endothelial cells. *Blood* 116, 909–914. doi: 10.1182/blood-2010-01-264382

Lancrin, C., Sroczynska, P., Stephenson, C., Allen, T., Kouskoff, V., and Lacaud, G. (2009). The haemangioblast generates haematopoietic cells through a haemogenic endothelium stage. *Nature* 457, 892–895. doi: 10.1038/nature07679

Lassila, O., Eskola, J., Toivanen, P., Martin, C., and Dieterlen-Lièvre, F. (1978). The origin of lymphoid stem cells studied in chick yolk sac-embryo chimaeras. *Nature* 272, 353–354. doi: 10.1038/272353a0

Lassila, O., Martin, C., Toivanen, P., and Dieterlen-Lièvre, F. (1982). Erythropoiesis and lymphopoiesis in the chick yolk-sac-embryo chimeras: contribution of yolk sac and intraembryonic stem cells. *Blood* 59, 377–381. doi: 10.1182/blood.V59.2.377.377

Le Douarin, N. M., and Dieterlen-Lièvre, F. (2013). How studies on the avian embryo have opened new avenues in the understanding of development: a view about the neural and hematopoietic systems. *Dev. Growth Differ.* 55, 1–14. doi: 10.1111/dgd.12015

le Noble, F., Moyon, D., Pardanaud, L., Yuan, L., Djonov, V., Matthijsen, R., et al. (2004). Flow regulates arterial-venous differentiation in the chick embryo yolk sac. *Development* 131, 361–375. doi: 10.1242/dev.00929

Li, W., Ferkowicz, M. J., Johnson, S. A., Shelley, W. C., and Yoder, M. C. (2005). Endothelial cells in the early murine yolk sac give rise to CD41-expressing hematopoietic cells. *Stem Cells Dev.* 14, 44–54. doi: 10.1089/scd.2005.14.44

Li, Z., Lan, Y., He, W., Chen, D., Wang, J., Zhou, F., et al. (2012). Mouse embryonic head as a site for hematopoietic stem cell development. *Cell Stem Cell* 11, 663–675. doi: 10.1016/j.stem.2012.07.004

Martin, C., Beaupain, D., and Dieterlen-Lièvre, F. (1978). Developmental relationships between vitelline and intra-embryonic haemopoiesis studied in avian 'yolk sac chimaeras'. *Cell Differ.* 7, 115–130. doi: 10.1016/0045-6039(78)90012-X

McGrath, K. E., Frame, J. M., Fegan, K. H., Bowen, J. R., Conway, S. J., Catherman, S. C., et al. (2015). Distinct sources of hematopoietic progenitors emerge before HSCs and provide functional blood cells in the mammalian embryo. *Cell Rep.* 11, 1892–1904. doi: 10.1016/j.celrep.2015.05.036

Medvinsky, A., and Dzierzak, E. (1996). Definitive hematopoiesis is autonomously initiated by the AGM region. *Cell* 86, 897–906. doi: 10.1016/S0092-8674(00)80165-8

Medvinsky, A., Rybtsov, S., and Taoudi, S. (2011). Embryonic origin of the adult hematopoietic system: advances and questions. *Development* 138, 1017–1031. doi: 10.1242/dev.040998

Moore, M., and Owen, J. (1965). Chromosome marker studies on the development of the haemopoietic system in the chick embryo. *Nature* 208:956. doi: 10.1038/208956a0

Murray, P. D. F. (1932). The development in vitro of the blood of the early chick embryo. *Proc. R. Soc. Lond. Ser. B Contain. Pap. Biol.* 111, 497–521. doi: 10.1098/rspb.1932.0070

Nagai, H., Lin, M. C., and Sheng, G. (2011). A modified cornish pasty method for ex ovo culture of the chick embryo. *Genesis* 49, 46–52. doi: 10.1002/dvg.20690

Nagai, H., Shin, M., Weng, W., Nakazawa, F., Jakt, L. M., Alev, C., et al. (2018). Early hematopoietic and vascular development in the chick. *Int. J. Dev. Biol.* 62, 137–144. doi: 10.1387/ijdb.170291gs

Nakano, H., Liu, X., Arshi, A., Nakashima, Y., van Handel, B., Sasidharan, R., et al. (2013). Haemogenic endocardium contributes to transient definitive haematopoiesis. *Nat. Commun.* 4:1564. doi: 10.1038/ncomms2569

New, D. A. T. (1955). A new technique for the cultivation of the chick embryo in vitro. *Development* 3, 326–331.

Oberlin, E., Tavian, M., Blazsek, I., and Péault, B. (2002). Blood-forming potential of vascular endothelium in the human embryo. *Development* 129, 4147–4157.

Ottersbach, K. (2019). Endothelial-to-haematopoietic transition: an update on the process of making blood. *Biochem. Soc. Trans.* 47, 591–601. doi: 10.1042/BST20180320

Pardanaud, L., Altmann, C., Kitos, P., Dieterlen-Lièvre, F., and Buck, C. A. (1987). Vasculogenesis in the early quail blastodisc as studied with a monoclonal antibody recognizing endothelial cells. *Development* 100, 339–349.

Pardanaud, L., Luton, D., Prigent, M., Bourcheix, L. M., Catala, M., and Dieterlen-Lièvre, F. (1996). Two distinct endothelial lineages in ontogeny, one of them related to hemopoiesis. *Development* 122, 1363–1371.

Poole, T. J., and Coffin, J. D. (1989). Vasculogenesis and angiogenesis: two distinct morphogenetic mechanisms establish embryonic vascular pattern. *J. Exp. Zool.* 251, 224–231. doi: 10.1002/jez.1402510210

Prummel, K. D., Nieuwenhuize, S., and Mosimann, C. (2020). The lateral plate mesoderm. *Development* 147:dev175059. doi: 10.1242/dev.175059

Psychoyos, D., and Stern, C. D. (1996). Fates and migratory routes of primitive streak cells in the chick embryo. *Development* 122, 1523–1534.

Sabin, F. (1920). Studies on the origins of blood-vessels and of red blood-corpuscles as seen in the living blastoderm of chicks during the second day of development. *Contrib. Embryol.* 36, 213–262.

Samokhvalov, I. M., Samokhvalova, N. I., and Nishikawa, S. I. (2007). Cell tracing shows the contribution of the yolk sac to adult haematopoiesis. *Nature* 446, 1056–1061. doi: 10.1038/nature05725

Sato, Y., Poynter, G., Huss, D., Filla, M. B., Czirok, A., Rongish, B. J., et al. (2010). Dynamic analysis of vascular morphogenesis using transgenic quail embryos. *PLoS One* 5:e12674. doi: 10.1371/journal.pone.0012674

Senserrich, J., Batsivari, A., Rybtsov, S., Gordon-Keylock, S., Souilhol, C., Buchholz, F., et al. (2018). Analysis of Runx1 using induced gene ablation reveals its essential role in pre-liver HSC development and limitations of an in vivo approach. *Stem Cell Rep.* 11, 784–794. doi: 10.1016/j.stemcr.2018.08.004

Serrado Marques, J., Teixeira, V., Jacinto, A., and Tavares, A. (2018). Identification of novel hemangioblast genes in the early chick embryo. *Cells* 7:9. doi: 10.3390/cells7020009

Stern, C. D., and Fraser, S. E. (2001). Tracing the lineage of tracing cell lineages. *Nat. Cell Biol.* 3, E216–E218. doi: 10.1038/ncb0901-e216

Tanaka, Y., Sanchez, V., Takata, N., Yokomizo, T., Yamanaka, Y., Kataoka, H., et al. (2014). Circulation-independent differentiation pathway from extraembryonic mesoderm toward hematopoietic stem cells via hemogenic angioblasts. *Cell Rep.* 8, 31–39. doi: 10.1016/j.celrep.2014.05.055

Teixeira, V., Arede, N., Gardner, R., Rodríguez-Leán, J., and Tavares, A. T. (2011). Targeting the hemangioblast with a novel cell type-specific enhancer. *BMC Dev. Biol.* 11:76. doi: 10.1186/1471-213X-11-76

Walmsley, M., Ciau-Uitz, A., and Patient, R. (2002). Adult and embryonic blood and endothelium derive from distinct precursor populations which are differentially programmed by BMP in *Xenopus*. *Development* 129, 5683–5695. doi: 10.1242/dev.00169

Wittamer, V., and Bertrand, J. Y. (2020). Yolk sac hematopoiesis: does it contribute to the adult hematopoietic system?. *Cell. Mol. Life Sci.* 77, 4081–4091. doi: 10.1007/s00018-020-03527-6

Yoshimoto, M., Montecino-Rodriguez, E., Ferkowicz, M. J., Porayette, P., Shelley, W. C., Conway, S. J., et al. (2011). Embryonic day 9 yolk sac and intra-embryonic hemogenic endothelium independently generate a B-1 and marginal zone progenitor lacking B-2 potential. *Proc. Natl. Acad. Sci. U.S.A.* 108, 1468–1473. doi: 10.1073/pnas.1015841108

Yoshimoto, M., Porayette, P., Glosson, N. L., Conway, S. J., Carlesso, N., Cardoso, A. A., et al. (2012). Autonomous murine T-cell progenitor production in the extra-embryonic yolk sac before HSC emergence. *Blood* 119, 5706–5714. doi: 10.1182/blood-2011-12-397489

Yue, R., Li, H., Liu, H., Li, Y., Wei, B., Gao, G., et al. (2012). Thrombin receptor regulates hematopoiesis and endothelial-to-hematopoietic transition. *Dev. Cell* 22, 1092–1100. doi: 10.1016/j.devcel.2012.01.025

Yvernogeau, L., and Robin, C. (2017). Restricted intra-embryonic origin of bona fide hematopoietic stem cells in the chicken. *Development* 144, 2352–2363. doi: 10.1242/dev.151613

Zamir, L., Singh, R., Nathan, E., Patrick, R., Yifa, O., Yahalom-Ronen, Y., et al. (2017). Nkx2.5 marks angioblasts that contribute to hemogenic endothelium of the endocardium and dorsal aorta. *eLife* 6:e20994. doi: 10.7554/eLife.20994

Zhang, C., Lv, J., He, Q., Wang, S., Gao, Y., Meng, A., et al. (2014). Inhibition of endothelial ERK signalling by Smad1/5 is essential for haematopoietic stem cell emergence. *Nat. Commun.* 5:3431. doi: 10.1038/ncomms4431

Zovein, A. C., Hofmann, J. J., Lynch, M., French, W. J., Turlo, K. A., Yang, Y., et al. (2008). Fate tracing reveals the endothelial origin of hematopoietic stem cells. *Cell Stem Cell* 3, 625–636. doi: 10.1016/j.stem.2008.09.018

Zovein, A. C., Turlo, K. A., Ponec, R. M., Lynch, M. R., Chen, K. C., Hofmann, J. J., et al. (2010). Vascular remodeling of the vitelline artery initiates extravascular emergence of hematopoietic clusters. *Blood* 116, 3435–3444. doi: 10.1182/blood-2010-04-279497

Conflict of Interest: The authors declare that the research was conducted in the absence of any commercial or financial relationships that could be construed as a potential conflict of interest.

frontiers in Cell and Developmental Biology

REVIEW
published: 19 November 2020
doi: 10.3389/fcell.2020.602647

Mesenchymal Stem Cells (MSCs) as a Potential Therapeutic Strategy in COVID-19 Patients: Literature Research

*André Coelho[1], Rui Damásio Alvites[2,3], Mariana Vieira Branquinho[2,3], Susana G. Guerreiro[4,5,6] and Ana Colette Maurício[2,3]**

[1] Biotecnologia Medicinal, Escola Superior de Saúde do Porto, Instituto Politécnico do Porto, Porto, Portugal, [2] Departamento de Clínicas Veterinárias, Instituto de Ciências Biomédicas de Abel Salazar, Universidade do Porto, Porto, Portugal, [3] Centro de Estudos de Ciência Animal, Instituto de Ciências, Tecnologias e Agroambiente da Universidade do Porto, Porto, Portugal, [4] Departamento de Biomedicina, Faculdade de Medicina, Universidade do Porto, Porto, Portugal, [5] Instituto de Investigação e Inovação em Saúde (I3S), Universidade do Porto, Porto, Portugal, [6] Instituto de Patologia e Imunologia Molecular da Universidade do Porto, Porto, Portugal

In 2019, an outbreak of an unknown coronavirus – SARS-CoV-2 – responsible for COVID-19 disease, was first reported in China, and evolved into a pandemic of huge dimensions and raised serious concerns for global health. The number of critical cases continues to increase dramatically, while vaccines and specific treatments are not yet available. There are several strategies currently being studied for the treatment of adverse symptoms of COVID-19, that encompass Acute Lung Injury (ALI)/Acute Respiratory Distress Syndrome (ARDS), extensive pulmonary inflammation, cytokine storm, and pulmonary edema, due to virus-induced pneumonia. Mesenchymal stem cells (MSCs) are at the origin of new revolutionary treatments, which may come to be applied in such as Regenerative Medicine, Immunotherapy, Tissue Engineering, and Cell and Molecular Biology due to immunomodulation and anti-inflammatory activity. MSCs have already been studied with positive outcomes for other lung pathologies, thus representing and being identified as an important opportunity for the treatment of COVID-19. It has recently been shown that these cells allow hopeful and effective therapies for serious or critical COVID-19, minimizing its adverse symptoms. In this study we will analyze the MSCs, their origin, differentiation, and therapeutic potential, making a bridge with the COVID-19 disease and its characteristics, as a potential therapeutic strategy but also reporting recent studies where these cell-based therapies were used for the treatment of COVID-19 patients.

Keywords: cell-based therapies, secretome, mesenchymal stem cells, coronavirus, SARS-CoV-2

OPEN ACCESS

Edited by:
Susana Solá, University of Lisbon, Portugal

Reviewed by:
Bruce Alan Bunnell, University of North Texas Health Science Center, United States
Robert Chunhua Zhao, Peking Union Medical College Hospital (CAMS), China

****Correspondence:***
Ana Colette Maurício
acmauricio@icbas.up.pt;
ana.colette@hotmail.com

Specialty section:
This article was submitted to Stem Cell Research, a section of the journal Frontiers in Cell and Developmental Biology

Received: *03 September 2020*
Accepted: *30 October 2020*
Published: *19 November 2020*

Citation:
Coelho A, Alvites RD, Branquinho MV, Guerreiro SG and Maurício AC (2020) Mesenchymal Stem Cells (MSCs) as a Potential Therapeutic Strategy in COVID-19 Patients: Literature Research. Front. Cell Dev. Biol. 8:602647. doi: 10.3389/fcell.2020.602647

Abbreviations: AF, amniotic fluid; ALI, acute lung injury; ARSD, acute respiratory distress syndrome; AT, adipose tissue; AT-MSCs, adipose tissue mesenchymal stem cells; BM, bone marrow; BM-MSCs, bone marrow mesenchymal stem cells; CFU-F, colony forming unit-fibroblast; DP, dental pulp; DP-MSCs, dental pulp mesenchymal stem cells; EVs, extracellular vesicles; GM-CSF, granulocyte-macrophage colony-stimulating factor; HGF, hepatocyte growth factor; ISCT, The International Society for Cellular Therapy; MERS, middle east respiratory syndrome; MHC, major histocompatibility complex; MSCs, mesenchymal stem cells; OM-MSCs, olfactory mucosa mesenchymal stem/stromal cells; SARS, Severe Acute Respiratory Syndrome; TMPRSS2, transmembrane protease serine-2; UCB, umbilical cord blood; UCB-MSCs, umbilical cord blood mesenchymal stem cells; UCT, umbilical cord tissue; UC-MSCs, umbilical cord mesenchymal stem cells; WJ, Wharton's Jelly; WJ-MSCs, Wharton's Jelly mesenchymal stem cells.

INTRODUCTION

Since the end of 2019 that a series of unexplained cases of pneumonia caused by an unknown virus were reported in Wuhan, China. The research began and on 12 January 2020, when the World Health Organization (WHO) identified the newly discovered virus as the "2019 Novel Coronavirus" (2019-nCoV), formally naming the infection as Coronavirus Disease 2019 – COVID-19 – on 30 January. On the same day, the International Committee on Taxonomy of Viruses identified the 2019-nCoV as a Severe Acute Respiratory Syndrome 2 – SARS-CoV-2 (Sun et al., 2020b). First outbreak reported in China, this disease quickly spread to all continents mainly due to international flights, becoming a pandemic recognize by the WHO since January 2020, affecting nowadays 213 countries and territories, with more than 11 million active cases and more than half a million deaths, representing a serious global public health emergency (**Table 1**) (Worldometer, 2020).

SARS-CoV-2 is characterized as a coronavirus, belonging to the cluster of β−coronavirus. COVID-19 appears as the third zoonotic disease caused by this type of virus, after Severe Acute Respiratory Syndrome (SARS) and the Middle East Respiratory Syndrome (MERS). The first cases identified as COVID-19 were related to the Huanan seafood market, since environmental samples were collected from the seafood market, and consequently, it is believed that SARS-CoV-2 mutated and an intermediate host that infected the patient zero in the market allowed the interspecies transmission to humans (Li et al., 2020b). Although it has not been possible to determine with certainty whether a particular specie carries the SARS-CoV-2, studies demonstrated that SARS−CoV−2 was a chimeric virus that originated from a bat coronavirus and another one of undetermined origin. As a well-known natural reservoir for α-coronavirus and β-coronavirus, bats are carriers of distinct SARS-like-CoVs (Sun et al., 2020a). Therefore, various researches reinforced the hypothesis that the transmission chain originated from animals (bats) to humans.

Structure and Mechanism of SARS-CoV-2

Coronaviruses, or Orthocoronavirinae, are enveloped, positive, single−stranded large RNA viruses that researchers previously thought that transmitted disease only to animals until the world witnessed the SARS epidemic outbreak caused by SARS-CoV in 2002. Currently are known 7 CoVs (SARS-CoV-2 included) responsible for causing human respiratory illnesses, although only SARS-CoV-2, MERS-CoV, and SARS-CoV have been associated with outbreaks with high infection rate and high mortality (Li et al., 2020a). Coronavirus dimensions can vary from 26 to 32 kb in length, 60–140 nm in diameter, with peptameric spiky projections on its external surface, looking as crown like spikes under the electron microscopy (Madabhavi et al., 2020). The spike protein is mainly responsible for the occurrence of cell tropism and inter-species transmission, since it allows the virus to bind to a cell receptor and its subsequent penetration into the cell through its membrane. Researchers discovered that angiotensin−converting enzyme 2 (ACE-2) is the receptor for SARS−CoV−2 (Madabhavi et al., 2020; Sun et al., 2020a) in healthy human lung, being expressed on alveolar epithelial cells type I and II. The attachment of SARS−CoV−2 to ACE-2 leads to an elevation of the expression of ACE-2, that can trigger injures on alveolar cells. Sequentially, these lesions can promote severe systemic reactions and culminate in death. ACE-2 is expressed in other tissues such as the kidney, liver, heart and other organs, this expression being the reason behind critical patients suffering not only from respiratory complications, but multiple organ dysfunction as well (Sun et al., 2020b). The nasal epithelium was found the first site of infection but also in transmission among patients, with symptomatic but also asymptomatic clinical spectrum (Xiao et al., 2020). Like it is observed in other SARS-CoV infections, the S protein of SARS-CoV-2 is able to bind the ACE-2 which allows the cell entering catalyzed by transmembrane protease serine-2 (TMPRSS2) protease mostly in type II alveolar cells in the pulmonary parenchyma but also other target cells that express ACE-2 (Spike, 2010).

Epidemiological Characteristics of COVID-19

As of October 6, 2020, the total number of confirmed cases was 35,736,102, including 1,046,546 deaths in all five continents, and a total of 26,894,740 recovered patients (Worldometer, 2020), nowadays a second vague of infection is being observed worldwide (**Table 1**). All ages are vulnerable to this lethal virus infection, and its transmission is made in the course of coughing and sneezing, through infected droplets by infected patients, able to spread about 1–2 m and deposit on surfaces. One of the main factors of the high rate of transmission of this virus is the fact that can also occur from asymptomatic people before the start of symptoms. The incubation period varies from 2 to 14 days. The first studies about COVID-19 transmission profile revealed that the basic reproductive number (R0) of 2019-nCoV is positioned between 1.4 and 3.9 (Bulut and Kato, 2020). Researchers also noticed a 3.25:1 ratio of male to female deaths, a fact probably related to the higher numbers of ACE-2 receptors present in male alveoli. The age range of deaths by COVID-19 was 70 years or older, although the deaths of younger age groups are now increasing. Findings made so far indicate that the progression of the disease is faster in older individuals, especially on those who have comorbidities, than in the young (Sun et al., 2020b).

COVID-19 can be clinically divided in five groups: asymptomatic, mild, moderate, severe, and critical. The symptoms of these categories vary, with asymptomatic having no symptoms with a positive SARS-CoV-2 PCR test. The mild group manifests itself through signs such as fever, myalgia, cough, fatigue, sore throat, and sneezing, runny nose without evolution to pneumonia, basically signs of acute upper respiratory tract infection. More aggressive symptoms such as fever, cough and pneumonia with no indication of shortness of breath or hypoxemia should be included in the moderate group. The severe group includes cases of rapid

TABLE 1 | Total confirmed cases, total deaths, and total cases per 1M population of the 10 countries most affected by COVID-19, and the data from Portugal for comparison (Data consulted on October 10 at worldometers.info/coronavirus) (Worldometer, 2020).

Country	Total Cases	Total Deaths	Total cases/1M pop
United States	7,895,738	218,685	23,816
India	6,979,423	107,450	5,044
Brazil	5,057,190	149,692	23,746
Russia	1,285,084	22,454	8,805
Colombia	894,300	27,495	17,525
Spain	890,367	32,929	19,041
Argentina	871,468	23,225	19,234
Peru	843,355	33,158	25,482
Mexico	809,751	83,507	6,262
France	691,977	32,583	11,567
Portugal (49th)	83,928	2,062	8,238

evolution (in most cases in 1 week), where oxygen saturation below 92% promotes signs of central cyanosis, dyspnea and other symptoms of hypoxemia. Finally, the critical patients present acute ARDS or respiratory failure with multiple organ dysfunction, requiring mechanical ventilation and life support (Bulut and Kato, 2020). The main pathologic traits for COVID-19 patients in the severe or critical groups include the development of extensive pulmonary edema, pulmonary inflammation, diffuse alveolar damage with cellular fibromyxoid exudates, hyaline membrane formation and hypoxemia. Even though the pathologic alterations are similar to ALI/ARDS, also witnessed in MERS and SARS coronavirus infections, more serious phenomena of inflammatory cytokine storm, severe inflammatory exudation, milder pulmonary fibrosis and consolidation, pulmonary edema and serious inflammatory exudation were observed in severe or critical COVID-19 (Liu et al., 2020). The severe and critical patients will have long-term health impact of COVID-19. Taken all together, MSCs-based therapy seems to be a possible strategy for patients' treatment and rehabilitation, mostly what concerns pulmonary parenchyma regeneration.

Prevention and Treatment of COVID-19

At the date of October 2020, there is not yet a vaccine against COVID-19 available. The vaccine is considered as an effective prophylactic strategy for control and prevention, and is being researched and developed in about 90 institutions worldwide. The knowledge of the structure of the SARS-COV-2 spike protein (S) should enable rapid evaluation and further studies to optimize vaccination strategies. Several possible treatments are also being studied, some of them were already considered ineffective for COVID-19, such as chloroquine and hydroxychloroquine. The multiple treatment strategies include antiviral agents like Remdesivir designed for Ebola treatment, drugs routinely used to treat autoimmune diseases and malaria which drew attention for their potential as broad-spectrum antiviral drugs; corticosteroids to suppress lung inflammation; several immunotherapies; convalescent plasmas transfusion. Finally, new therapies like blocking agents that present affinity to bind to ACE2 receptor and the use of cell-based approaches such as MSCs, have been studied and tested as potential approaches (Zhai et al., 2020).

The currently available treatment to COVID-19 depends basically on the patients' immune system. COVID-19 can trigger a destroying immune overreaction, contributing to the worsening of the disease. When the immune system is activated in a reactive way, the physiological mechanisms of containment of the virus trigger the production and release of several inflammatory mediators, resulting in a severe cascade of cytokines. This mechanism can culminate in injuries to several organs, followed by acute cardiac injury, edema, ARDS, changes in gas exchange, secondary opportunistic infections, multi-organ failure and death. That said, preventing or attenuating the development of the cytokine cascade seems to be the way forward in the treatment of COVID-19 infected patients (Atluri et al., 2020). On the other hand, until an effective treatment is established, the management of the pandemic essentially involves the control of infections and the community transmission of the virus. The set of strategies should include ensuring early diagnosis with effective data sharing, isolation of the infected, maintenance of social orders, quarantine, the fidelity of disseminated information, and supportive treatments. For individuals, protective measures like the improvement of personal hygiene measures, the use of protective barriers such as masks, visors and gloves and the guarantee of good ventilation in closed spaces, can effectively reduce the transmission of the virus (Madabhavi et al., 2020). In summary, COVID-19 is an unprecedented challenge for clinicians because of the high transmission rate (Sun et al., 2020a), making the number of cases classified as severe increasing markedly worldwide while effective and precise treatments are still absent. Efforts are being made in a global perspective to find solutions or treatments (Zhai et al., 2020).

Cell-based therapies, particularly those involving MSCs or their extracellular vesicles (EVs) and secretome, have recently started to be used in the treatment of COVID-19 respiratory disease (Khoury et al., 2020). MSCs are non-hematopoietic, multipotent cells, able to differentiate into the three dermal lineages, and are present in tissues of different sources, ranging from fetal to many adult tissues. Due to their proven benefits when used in Regenerative Medicine, MSCs are good options for use as cell-based therapies in regenerating and replacing injured tissues and organs, but their potential goes way beyond that, with multiple therapeutic utilities and positive outcomes with immunomodulatory and anti-inflammatory properties in neurodegenerative, autoimmune, and cardiovascular diseases (Ullah et al., 2015; Li and Hua, 2017; Denton et al., 2018; Shammaa et al., 2020). While lodged in the lungs, the MSCs can balance the inflammatory response and release mediators including antimicrobial peptides, angiogenic growth factors, and EVs (Khoury et al., 2020), presenting MSCs as an valuable option to be used to treat COVID-19. As a matter of fact, MSCs present immunomodulatory capacity, so, it is observed their ability to prevent and attenuate the cytokine storm, reducing the morbidity and mortality. This literature review aims at discussing MSCs as a strategy for the medical approach of

severe or critical COVID-19 patients and further understanding the impact of MSCs origin and *in vitro* culture conditioning methods, as well as their characterization, on their therapeutic potential and clinical significance toward COVID-19 disease. Recent clinical trials outcomes, with use of MSCs for COVID-19 will be analyzed. It seems that expanded umbilical cord mesenchymal stem cells (UC-MSCs) may be the most efficient possible treatment available, associated to supportive therapies, for severe clinical cases (Atluri et al., 2020; Xiao et al., 2020).

ORIGINS, DEVELOPMENT AND CLINICAL APPLICATIONS OF MESENCHYMAL STEM CELLS (MSCs)

Origins, Discovery and Brief Historical Context of MSCs

Friedenstein was one of the pioneers in the study of stem cells and the identification of multipotential stromal precursor cells. Based on his 1960s and 1970s discoveries, it was shown that mouse bone marrow (BM), like other blood-forming organs, contained clonogenic progenitor cells that, once in culture, could originate fibroblasts and other mesodermal cells. He also understood that these cells were precursors of cartilage and bone-forming cells but did not belong to the hematopoietic cell lineage (Frieedenstein et al., 1968). From BM, Friedenstein was also able to isolate adherent cells identical to fibroblasts that grew rapidly *in vitro* and were able to form clonogenic colonies called colony forming unit-fibroblast [CFU-F]. Cells isolated from CFU-F had the additional ability to differentiate into chondrocytes, osteocytes, osteoblasts and adipocytes *in vitro* (Friedenstein et al., 1974). Arnold Caplan later called these cells "Mesenchymal Stem Cells," establishing similarities with stem cells originating from mesodermal tissues at the embryonic level, having been able to promote their growth from adult tissues (Caplan, 2009). Haynesworth et al. (1992b) was able to grow and expand BM-MSCs from the iliac crest's BM collected in human donors, revealing the human BM's ability to produce cells with the potential to grow in culture and with osteogenic capacity. SH-2 and SH-3 were identified as specific cell surface antigens on MSCs by the same group (Haynesworth et al., 1992a). Subsequently, Barry et al. (2001) established CD105 and CD73 as ligands corresponding to SH-2 and SH-3.

In the next years, massive interest in MSCs studies was established and, even though BM was exploited as the source organ of MSCs in the first place, quickly adult adipose tissue (AT) was established as a main niche of MSCs, demonstrating an equally interesting multipotency *ex vivo* (Gomez-Salazar et al., 2020). The rapid interest that fell on MSCs, associated with their demonstrated clinical relevance and some controversy associated with the characteristics and nomenclature attributed, raised the need to establish an official and more restricted definition for these cells. The International Society for Cellular Therapy (ISCT) in 2006 (Dominici et al., 2006), established the parameters that were established as the four minimum criteria that should be used to define cells as MSCs, which were quickly accepted by the scientific community: (i) be plastic adherent; (ii) expression of CD105, CD90, and CD73 cell surface antigens; (iii) no expression of CD45, CD19, CD14 CD11b, CD34, CD79a, and HLA-DR cell surface antigens; (vi) Capacity to differentiate into adipocytes, chondrocytes and osteoblasts. MSCs have been frequently re-baptized with various names such as "Mesenchymal Progenitor Cells," "Multipotent Adult Progenitor Cells" or "Multipotent Adult Stem Cells" that diverged only vaguely from the original definition. Other denomination such as "Multipotential Stromal Cells" or "Mesenchymal Stromal Cells," even fitting in the MSCs acronym, are based on radical differences in terms of biologic meaning (Gomez-Salazar et al., 2020). It is true that MSCs share several characteristics with stem cells, but some of their elements related to permanent cell lineage repletion *in vivo* do not allow them to be considered as "true stem cells" and require the use of a different denomination. More recently, one work has established MSCs as natural precursors for adventitial cells, perivascular fibroblasts and pericytes, pointing to a stromal origin for MSCs (Crisan et al., 2008). Although more recently the 2006 ISCT guidelines have advised the use of the term "Multipotent Mesenchymal Stromal Cells," the original term "Mesenchymal Stem Cells" continues to be mostly used. Finally, to highlight the fact that the therapeutic action of these cells may be primarily related with releasing growth factors and cytokines, Arnold Caplan supported the use of the term "Medicinal Signaling Cells" (Caplan, 2017). To simplify, to make everything uniform, and facilitate bibliographic research, the term "Mesenchymal Stem Cell" remains the most commonly used name. Recent findings demonstrate that MSCs can be isolated from any mesenchymal tissue or niche that manifests regenerative capacity, and that these cells have basic Stem Cell capabilities such as clonogenic potential, self-renewal, and ability to regenerate tissues *in vivo* and multi-lineage differentiation capacity. Some MSCs that are cultured *in vitro* lack specific identifying markers (Lanza et al., 2009), so the variable expression level of these markers could probably arise from differences between species, tissue sources, and culture conditions that we will discuss in this review. MSCs represent an important tool in the development of new possible therapies with applications in regenerative medicine, immunotherapy, tissue engineering, and cell and molecular biology with almost 10,000 papers published in the last 40 years [search, in the PUBMED.gov search engine, by the term *"(Mesenchymal stem cell) OR (MSCs),"* on 08/31/2020] and hundreds of clinical trials made over the years, with more than 500 active trials currently (**Figure 1**) (research, in the ClinicalTrials.gov database, under the terms "*MSCs,*" on 08/31/2020).

Sources, Isolation, and Cultivation of MSCs

Stem cells can be categorized considering their profile of differentiation and source within the human body. Discovered originally in the BM, this type of cells is still recognized as the more promising for clinical application and research, although some alternative sources including AT, birth-derived tissues,

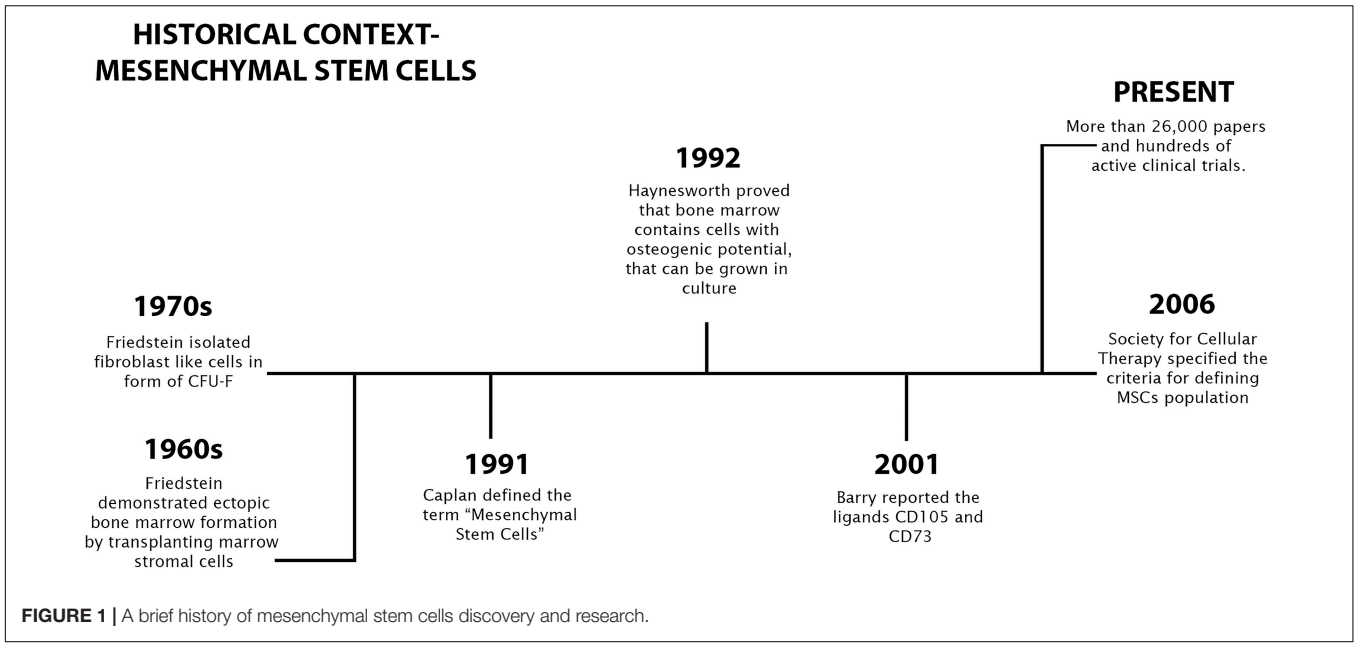

FIGURE 1 | A brief history of mesenchymal stem cells discovery and research.

amniotic fluid (AF) and placenta, dental pulp (DP), olfactory tissues, synovium and synovial fluid, endometrium, muscle, and peripheral blood — have since been identified, as we can see in **Figure 2** (Berebichez-Fridman and Montero-Olvera, 2018).

In theory, MSCs can be isolated from almost any tissue in the human body. Despite this, it is necessary to consider some practical limitations, such as the associated difficulty, the degree of invasion of the collection method and the characteristics of the donor himself. Parameters such as tissue source, isolation technique and the culture medium used can alter the properties of the collected human MSCs. MSCs can differentiate in the neuroectodermic and endoderm lines, in addition to the already known capacity for mesodermal lineage differentiation (Mushahary et al., 2018). The developmental origin of mesenchymal tissues, including not only mesoderm but also the cranial neural crest, may be the explanation for this ability. It is important to note that recently it was demonstrated that MSCs are mostly derived from the neural crest and neuroepithelium, even though traditionally it was considered the mesodermal origin (Uccelli et al., 2008). Embryonic Stem Cells (ESCs) are totipotent because they can form both embryonic and extraembryonic structures. Moreover, ESCs can proliferate indefinitely under specific culture conditions and retain the capacity to differentiate into cell types from the three embryonic germ layers. On the other hand, adult stem cells are undifferentiated multipotent stem cells obtained from adult individuals and differentiate into the cell types that constitute their respective source tissue (Uccelli et al., 2008; Berebichez-Fridman and Montero-Olvera, 2018).

Bone Marrow

The procedure to obtain BM-MSCs is a highly invasive and can result in pain or infection, making the selection of other sources, like peripheral blood or surgical remnants such as AT, preferable (Berebichez-Fridman et al., 2017). The cell yield, longevity, and potential for differentiation decrease with donor age (Choudhery et al., 2014). About 0.01 and 0.001% of the total nucleated cells isolated from BM aspirates are MSCs (Salem and Thiemermann, 2010). Besides that, these cells continue to be widely used, as they can be effortlessly isolated from a small quantities of aspirate and have a short culture time, being able to double 40 times its numbers in about 8–10 weeks of culture (Salem and Thiemermann, 2010). In terms of differentiation, BM-MSCs have an advantage when compared to other sources, with high multi-lineage differentiation and proliferation capacity. This type of stem cell is the most widely investigated, with active studies in arterial hypertension, ischemic heart failure, digestive system, treatment of spinal cord injuries, among others, and therefore is considered to be the gold standard (Choudhery et al., 2014).

Adipose Tissue

Adipose tissue is the second most reputable source of MSCs, with an estimated 98–100% cell viability. The morphological, phenotypical, and functional characteristics of AT-MSCs are similar to BM-MSCs (Choudhery et al., 2014). Besides their stability in long-term cell cultures, AT-MSCs can expand effectively *in vitro* and possess high multi-lineage differentiation potential. AT is a more advantageous autologous niche of MSCs for tissue engineering than BM (Choudhery et al., 2014). Its main advantage as a MSCs source is convenience, as human AT is usually abundant throughout the body and is easily accessible through liposuction procedures.

Birth-Derived Tissues

Currently, umbilical cord blood (UCB) is accepted as a source of hematopoietic stem cells, but also of MSCs and the abundance of UCB, availability of donors, facility of acquisition, and reliability of sample collection are relevant advantages

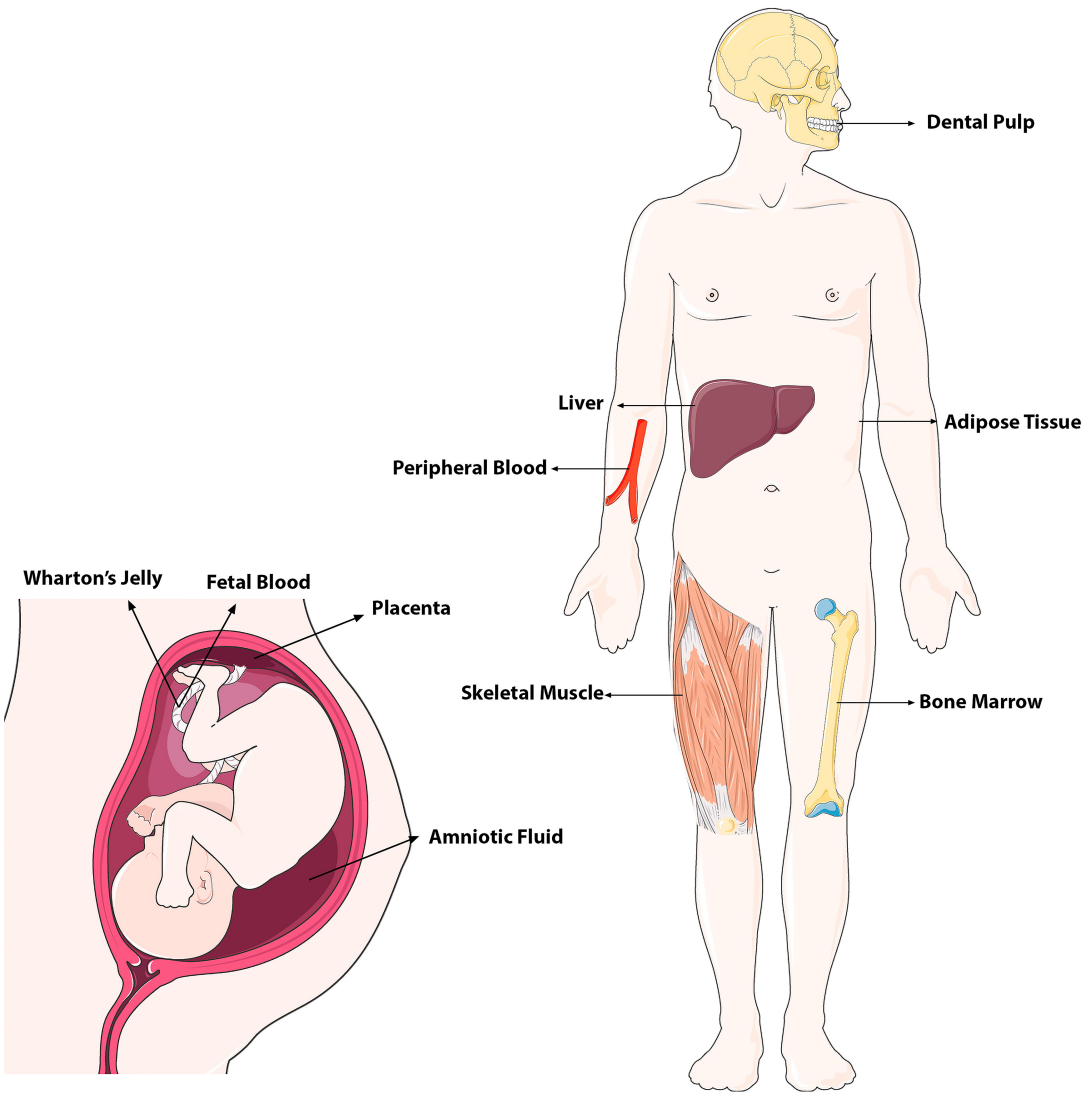

FIGURE 2 | Adult and fetal tissue sources (niches) of MSCs in the body (modified from Servier Medical Art, licensed under a Creative Common Attribution 3.0 Generic Licence. https://smart.servier.com/).

(Berebichez-Fridman and Montero-Olvera, 2018). UCB-MSCs are more immature than other types of adult stem cells, and do not evoke a strong immune rejection response in an allogeneic recipient. UCB-MSCs can be cryopreserved in vast quantities for later cultivation and research, but also for the treatment of hematologic pathologies, and possess osteogenic, chondrogenic, adipogenic, and myogenic differentiation potential. Lately, Wharton's Jelly (WJ) has gained attention as an excellent source of MSCs, as these MSCs present immuno-privileged and immunomodulatory phenotype (Caseiro et al., 2015).

Amniotic Fluid and Placenta

The phenotype of cultured cells collected from AF is similar to that of BM-MSCs. Cultured cells obtained from this source can differentiate into mesenchymal lineages, with a high self-renewal capacity and a doubling time of 36 h, maintaining a normal karyotype even at late passages. Placenta-derived MSCs also express embryonic stem cell markers and can differentiate into mesenchymal as well as hepatic, pancreatic, and neuronal lineages (Spitzhorn et al., 2017).

Mobilized Peripheral Blood

Peripheral blood stem cells may be mobilized from healthy donors using granulocyte-macrophage colony-stimulating factor (GM-CSF). The underlying mechanism involves several adhesion molecules that facilitate the binding of stem cells to BM and their disruption allows for their release into the circulation. A large volume of blood and, therefore, a higher quantity of MSCs can be collected compared to BM-MSCs (Pouryazdanpanah et al., 2018).

Synovium and Synovial Fluid

In humans, cartilage and synovium originate from a common pool of cells during synovial joint development. Synovia-derived MSCs are far superior to cells derived from the skeletal muscle and AT, as determined by their *in vitro* expandability, differentiation potential, and epitope profiles (Berebichez-Fridman and Montero-Olvera, 2018). Their superior chondrogenic and proliferation potential has been reported by several groups, making these cells fair candidates for cell therapy applications, particularly regarding osteoarticular disorders (Branquinho et al., 2012).

Dental Pulp

DP-derived MSCs specialize in odontoblasts, which produce dentin. These cells are obtained from pulp tissue and the periodontal ligament, and are extracted by an enzymatic digestive process or explant method. DP-MSCs are easy to cryopreserve and, similarly to AT-MSCs, possess immunomodulatory properties. In addition to differentiating into osteo/chondroblasts and adipocytes, DP-MSCs can also differentiate into neuronal lineages (Caseiro et al., 2019).

Olfactory Tissues

The *lamina propria* of the olfactory mucosa is the niche for olfactory mucosa mesenchymal stem/stromal cells (OM-MSCs) that are derived from the neural crest. Different works involving OM-MSCs revealed its fibroblastic-like cytomorphology, development of low density colonies, the plastic-adhesion, the expression of expected surface markers and also the capacity for differentiation, not only the classic tri-differentiation but also other pathways such as neuroglial and myogenic (Alvites et al., 2020a). Its secretome has also started to be analyzed, and it was possible to identify several bioactive molecules with pro-regenerative and immunomodulatory functions (Ge et al., 2016). The clinical use of these cells can be advantageous due to their anatomical location, easily accessible, and also to their wide distribution in the nasal cavity. Additionally, previous studies have already shown that OM-MSCs can be maintained in culture for extended periods without chromosomal or tumorigenic changes being observed. This capacity, affected by the donor's age, seems to be related with some inhibiting of apoptotic activity and conservation of telomeric activity (Alvites et al., 2020a). OM-MSCs have already been isolated from the olfactory mucosa of several species (Veron et al., 2018), including humans (Delorme et al., 2010), and their therapeutic effectiveness has also been tested with promising results in neurodegenerative diseases of the central nervous system, peripheral nerve injuries, autoimmune diseases and even myocardial tissue injuries (Alvites et al., 2020b).

Isolation and Cultivation

Mesenchymal stem cells are plastic-adherent cell populations, isolated through procedures involving tissue mincing, enzymatic digestion, and cell growth on a plastic surface. The two main procedures are the enzymatic and explant protocols (Mushahary et al., 2018). In the explant method, one of the earliest techniques applied, the tissue is rinsed with a saline solution and mechanically split into smaller fragments. Fragments are further placed on a culture dish and covered in adequate culture medium. After some days in culture, MSCs start outgrowing from the explants' limits, and as they reach total confluence, explants can be carefully detached. The enzymatic method entails a more complex protocol. After rinsing with a saline solution and mechanical splitting into smaller fragments, identically to the first steps on the explant method, the tissue is incubated with an enzymatic solution. As a result, singe cells or aggregates are released and remain suspended in the enzymatic solution. After centrifugation for elimination of the enzymatic solution, the cell pellet is re-suspended in adequate culture medium and seeded in culture dishes. MSCs therapeutic potential toward a specific tissue regeneration lies not only on the MSCs tissue of origin, but also on their potential *itself* and on their secretion potential of bio-factors with pharmacological properties, the so called secretome. MSCs protocols between groups regarding isolation, culture conditions and characterization varies immensely, impairing the reproductivity of results between different research groups. A critical parameter when considering MSCs is the cell potential toward regeneration. It has been reported to be influenced by cell passage number/age, and cryopreservation/defrosting cycle-related injury (Rendra et al., 2020). An improved therapeutic efficacy of MSCs is greatly influenced by optimized culture condition protocols (Alvites et al., 2020a).

Characterization and Phenotype of MSCs

As previously mentioned, in 2006 the ISCT proposed four minimum criteria to characterize cells as MSCs for research purposes (Dominici et al., 2006): be plastic-adherent in standard culture conditions (Dominici et al., 2006). Second, the MSC population must express CD105 (known as endoglin, first known as SH-2), CD73 (known as ecto 5' nucleotidase, first identified as SH-3), and CD90 (also known as Thy-1), and lack expression of CD45 (pan-leukocyte marker), CD34 (hematopoietic progenitors and endothelial cells marker), CD14 or CD11b (expressed on monocytes and macrophages), CD79a or CD19 (markers of B cells) and HLA class II. Lastly, MSCs most be able to differentiate into three different lineages: osteoblasts, adipocytes and chondroblasts. It's crucial to know that these identifying criteria should not be confused by no means and does not represent adequate criteria and characteristics for MSCs used therapeutically and in clinical studies because the proposal is meant only to describe identifying criteria for research purposes. The homogeneity of these characteristics is relative as different MSCs population express different surface markers, an understandable feature, as MSCs present plasticity, a dynamic capacity to adapt and vary over time to different conditions. Different antigen sets are applied from different research groups, to characterize these cells, with different outcomes, thus, no specific marker was identified as to uniquely characterize MSCs. MSCs can differentiate into different cell types when an array of differentiation factors is used to mimic osteogenic, chondrogenic, or adipogenic *in vitro*

microenvironment, for instance. Standardized procedures for culture conditions and MSCs characterization still remains a major challenge. Although the official criteria speak of tri-differentiation, it has long been known that MSCs can follow multiple types of differentiation and that is also a factor in the discussion of these criteria, with some studies suggesting the addition of other criteria factors for MSCs characterization. Some research groups suggest that to profile MSCs we must observe key parameters like CFU-F efficiency, MSC isolation, multilineage differentiation, immunomodulation, telomere length, trophic factor quantification, cumulative growth, and surface phenotype (Samsonraj et al., 2017). However, the ISCT guidelines are still the recommended criteria for the isolation and characterization of MSCs and are precise enough to combine the majority of the today existing knowledge, recognizing that future research, along with scientific breakthroughs, will probably lead to optimization of the criteria (Greif et al., 2020; Kurenkova et al., 2020).

Multipotency Analysis of MSCs

Considering MSCs are an interesting source for autologous transplantation and analysis of their cellular and molecular pathway has been performed, as well as the niche changes, as to assess on the cytokines, chemokines and other bioactive factors role in the differentiation potential of these cells (Alvites et al., 2020b). MSCs present a great differentiation potential toward mesenchymal lineages. Under specific *in vitro* inducing conditions, they can differentiate into adipogenic, osteogenic, or chondrogenic lineage. Differentiation can be induced *in vitro*, when seeding MSCs in specific differentiation supplemented media, as shown in **Figure 3**.

Regarding differentiation into the adipogenic lineage, supplementation includes dexamethasone, indomethacin, insulin, and isobutylmethylxanthine. As for the chondrogenic lineage, the cells can be cultured in Dulbecco's modified Eagle's medium supplemented with insulin, transferrin, selenium, linoleic acid, selenium acid, pyruvate, ascorbic phosphate, dexamethasone, and TGF-β III, and optionally IGF-1 and bone morphogenetic proteins-2. The osteogeneic lineage differentiation includes supplementation with of ascorbic acid, β-glycerophosphate, and dexamethasone (Mushahary et al., 2018). The differentiation into these three lineages is evaluated as for the presence of fat droplets (adipogenesis), proteoglycans and type II collagen synthesis (chondrogenesis), or mineralization of calcium deposits and increase in alkaline phosphatase expression (osteogenesis) (Sami et al., 2016). MSCs can differentiate into other lineages, such as the neurogenic, myogenic, tenogenic, and others as it was previously reported by several research groups (Branquinho et al., 2012; Ge et al., 2016). For instance, a process defined as *mesengenesis* has been reported by Caplan (1994), where MSCs originated myoblasts, ligaments, tendons and other cell types (Sami et al., 2016). Ever since, MSCs have been reported to originate cells from the heart, peripheral blood, cord blood, muscle, AT, lung, trabecular bone, intestine, kidney, liver, pancreas, synovium, skin, and even in the brain (Mushahary et al., 2018), being described as multipotent cells that representing a promising source for Regenerative Medicine.

Clinical Significance of MSCs Therapy

The discovery of MSCs and their properties has increased the interest in deepening knowledge over their therapeutic features. MSCs are an excellent candidate for cell therapy since they are easily accessible – tissue collection and isolation are relatively simple, and proliferate *in vitro*. MSCs are easily preserved, maintaining their potential, and clinical trials have been showing promising results (Andrzejewska et al., 2019). Firstly studied because of their potential in Regenerative Medicine, other mechanisms of action have been studied and investigated in different areas like immunomodulation and inflammatory process, as well as the paracrine effects of MSC secretome (Caseiro et al., 2019). The attention is now focused on the secretome and EVs as candidates to explain the therapeutic effects of MSCs (An et al., 2020; d'Angelo et al., 2020; Varderidou-Minasian and Lorenowicz, 2020).

Mesenchymal stem cells therapeutic potential toward restauration of tissue function is associated with three different, but complementary, mechanisms. "Homing" is the term used to describe their aptitude to migrate toward the lesion site, due to chemotactic mechanisms, mediated by integrins and selectins. The second mechanisms, as described before, is the multi-lineage differentiation capacity, promoting cell engraftment and tissue regeneration (Caplan and Dennis, 2006). The third mechanism entails the secretion of bioactive factors, modulating both local and systemic physiological processes (Biju and Jack, 2013). In animal models, there are several registered successful clinical trials with promising results in several different tissues like myocardial, renal, hepatic, neuronal, among others (Shammaa et al., 2020). Therefore, the regenerative properties of MSCs are the main feature studied, with a focus on degenerative conditions that are widely exploited. The most recent approaches in regenerative medicine employ *scaffolds* (Pedrosa et al., 2017; Vizoso et al., 2017) or MSC engineering on both genetic and architectural levels (Shammaa et al., 2020).

Apart from their tissue regeneration potential, MSCs have been described as modulators of the immune system, attenuating tissue impairment due to inflammatory processes. The modulation of the immune system by the MSCs is mediated by the secretion of soluble factors and direct contact with immune cells. Studies have reported MSCs interaction and suppression of immune cells, native and adaptive (Alvites et al., 2020a). MSCs also induce regulatory T cells and suppress self-reactive T-effector responses (Pedrosa et al., 2017). The ability to modulate the immune system by cell contact has been investigated, and it is specially of benefit when considering autoimmune conditions and neurodegenerative disorders (Shammaa et al., 2020).

Secretome and Conditioned Media as a New Therapeutic Strategy

The secretome is defined as substances, factors/molecules secreted by the cells to the extracellular matrix, a promising mechanism considering regenerative cell based-therapies and cellular mechanisms. The secretome includes soluble proteins, free nuclei acids, lipids, EVs among others. The use of cell-free

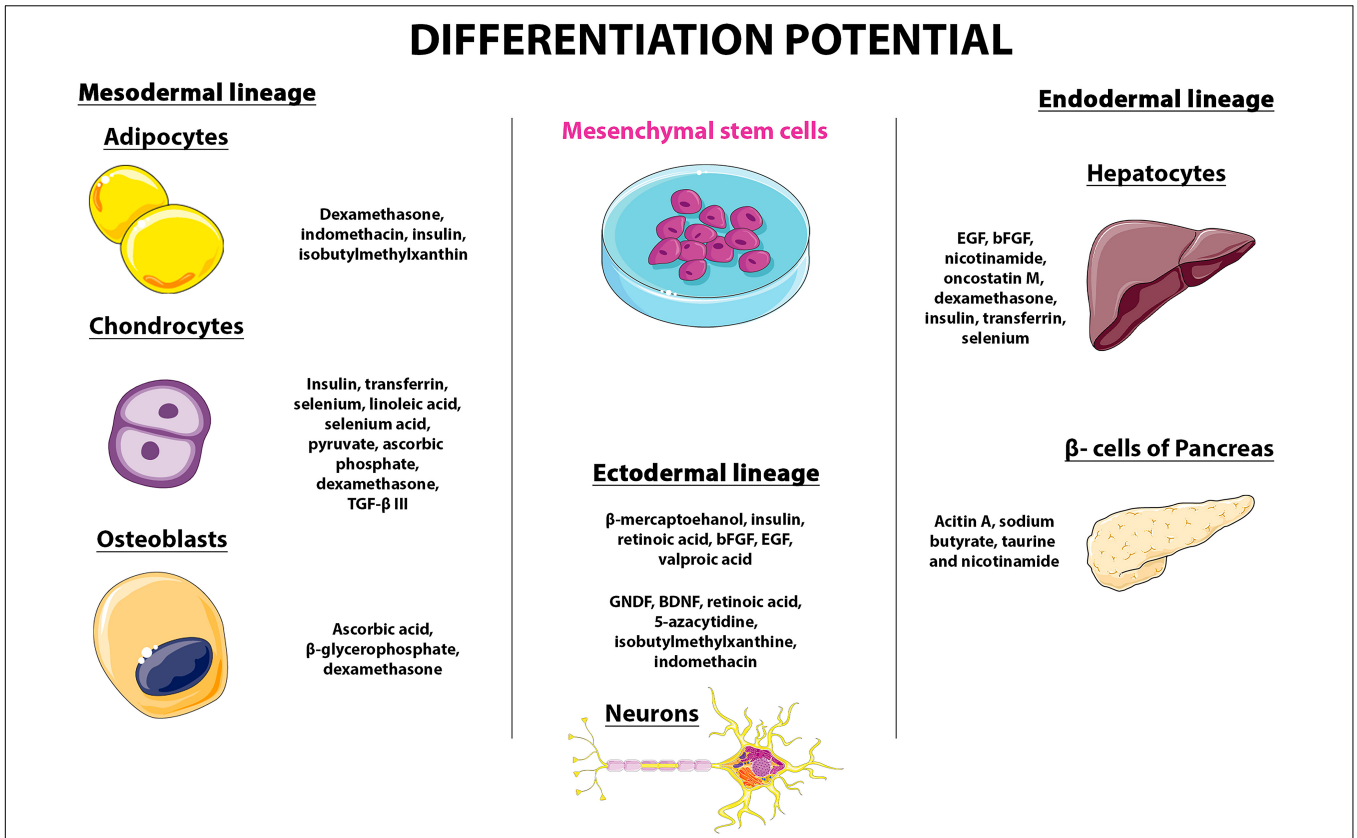

FIGURE 3 | Differentiation potential and the mesengenic process (modified from Servier Medical Art, licensed under a Creative Common Attribution 3.0 Generic Licence. https://smart.servier.com/).

therapies, using, for example, the conditioned media as a source of MSCs' secretome, reveals several benefits such as safety, once that the application of the secretome resolves potential impairments as immune compatibility, tumorigenicity, emboli formation and the transmission of infections. It has other advantages like the storage without potentially toxic cryoprotectors, it is more economic and the time of expansion and maintenance can be considerably reduced. MSCs' secretome has diverse mechanisms and great potential in immunomodulation, anti-apoptotic activity, wound healing and tissue repair, neuroprotective effect, angiogenesis regulation, antimicrobial effect, and antitumor effect (Caseiro et al., 2019; Alvites et al., 2020a). EVs, elements of the MSCs secretome, deserve a specific mention due to the recently accelerated studies of its clinical applications. EVs are exosomes, microvesicles and apoptotic bodies, that transport biologically active molecules and genetic information to target cells, thus affecting their potential and function (Trohatou and Roubelakis, 2017).

MSCs AS A POTENTIAL THERAPY FOR COVID-19

According to the WHO, the control of COVID-19 has mainly directed on infection prevention, case detection, and monitoring, since the currently approved treatments are of support and not directly envisioning the cure of the pathology. Although vaccines are being developed in order to reduce the infection rate of COVID-19, a developing demand to cure the increasing number of patients who develop pneumonia and other critical symptoms is emerging. That's where MSCs can have a crucial role, by minimizing the symptoms of COVID-19 and giving a chance to the patient immune system to act against the virus and promote the pulmonary parenchyma regeneration (WHO, 2020).

As previously reported, the most clinical used MSCs are the ones obtained from the autologous BM. The other MSCs available for clinical application are the ones from the adipose tissue, umbilical cord tissue and blood, amniotic membrane and dental pulp (Atluri et al., 2020). According to recent publications and by consulting the site www.clinicaltrials.gov, the umbilical cord is the most adequate source for MSCs, for several reasons: (i) high concentration of MSCs, (ii) UC-MSCs can be obtained during or after birth, by non-invasive techniques, (iii) the Wharton-jelly is considered a by-product, and several high quality samples are cryopreserved around the world in public and private high-regulated banks; (iv) UC-MSCs present faster doubling times, since these cells are closer to embryonic-stem-cells (ESCs) when compared to bone-marrow or adipose tissue MSCs; (v) on the other

hand the UC-MSCs are safer than ESCs because are not tumorigenic; (vi) can be used as an allogenic treatment since these cells are immunoevasive and express low levels of major histocompatibility complex (MHC) class 1 molecules and no MHC class II (Caseiro et al., 2015, 2019). The intravenous administration is the selected route for the treatment with UC-MSCs, since most of the infused UC-MSCs will be trapped in the lungs, the most affected organ in COVID-19 patients (Wang et al., 2020).

As an important cell population, MSCs have the potential to conduct to very promising outcomes, when considered for the treatment of lung disease. The regulation of the immune system in the lung, by these cells, entails modulation of activation and effector function of immune cells, suppressing of infiltrated cells and diminishing edema (Liu et al., 2020). MSCs have been reported to efficiently cure ALI/ARDS, principally by paracrine mechanisms based on the action of EVs, such as microvesicles and exosomes (Chan et al., 2015). *In vitro* studies reported that UC-MSC demonstrated therapeutic efficacy on mice with ALI induced by influenza A (H5N1) virus. Researchers confirmed that UC-MSCs presented effective results for the restoration of damaged alveolar fluid clearance and protein permeability of influenza A infected alveolar epithelial cells (Fujita et al., 2018). Clinical studies made in patients with Influenza H7N9 virus, which presented symptoms such as ARDS, lung failure, and fulminant pneumonia, showed that MSCs are a promising choice for treating virus-induced pneumonia. Based on informed consent, 44 patients with H7N9 induced ARDS were included as the control group, while 17 patients with H7N9 induced ARDS served as the experimental group, injected with allogeneic menstrual blood-derived MSCs. The transplantation of MSCs significantly lowered the mortality rate compared with the control group, with no adverse effects. The results suggest MSCs improved the survival rate. Once Influenza A and COVID-19 share analogous symptoms (such as ARDS and lung failure) and similar multi-organ dysfunction, along with the positive results of *in vitro* tests and clinical studies, MSCs-based therapy are considered a promising therapeutic alternative for treating COVID-19 (Khatri et al., 2018).

MSCs as a Treatment for COVID-19

To date, there is limited published information regarding COVID-19 disease and the potential efficacy of MSCs, although MSCs efficacy in influenza lung infections has been recently reported. MSCs can affect the performance of immune cells, both adaptive and innate, and therefore, MSCs therapy can theoretically inhibit the over-triggering of the immune system and promoting endogenous repair following SARS-CoV-2 infection. Several countries have begun clinical studies on MSCs therapies, and some positive results have been published. A study reported from China, on a 65-year-old female patient with a critical condition of COVID-19 presented promising outcomes after 21 days of treatment with UCB-MSCs. Initially, the patient showed neutrophil increase and lymphocyte decreased, and was treated with several antiviral drugs, while being subjected to non-invasive mechanical ventilation. As the vital signs deteriorated, the patient received 3 doses of single UCB-MSCs solution. The vital signs improved after the second MSCs administration as other symptoms gradually disappeared. Following, the patient was removed from the ventilator, with a normal number of immune system blood cells. The results suggested UCB-MSCs to be an alternative and effective treatment option for patients suffering with COVID-19, alone or in combination with other existing therapies (Chen et al., 2020). A different group in China of 7 patients with COVID-19 were selected, one with critical diagnosis, 4 with severe diagnosis, and 2 showing moderate symptoms. Three additional patients with severe diagnoses were chosen as placebo control. All patients presented pyrexia, breath impairment, and thus low oxygenation rates, and pneumonia. As the patients' health status was aggravating, 1 million MSCs per kilogram body weight were administered. Patients were kept on observation during 2 weeks recovery period. Mitigation of the symptoms was observed 2–4 days after treatment, along with a decrease in pneumonia infiltration, with no apparent adverse effects. This study as the one previously described, demonstrated MSCs intravenous infusion as a safe and efficient therapeutic alternative for treating COVID-19 patients (Golchin et al., 2020). As mention before, as the immune system is over-triggered it leads to a cytokine storm. The cytokine storm is one of the worst consequences of the disease with the production of inflammatory cytokine accompanied by a weak interferon response. Notably, SARS-CoV-2 triggers pathogenic Th1 cells into secreting pro-inflammatory cytokines, as GM-CSF and interleukin-6 (IL-6). Furthermore GM-CSF activates CD14+CD16+ inflammatory monocytes into producing extensively IL-6, TNF-α. Thus, The COVID-19 consequent cytokine-storm constitutes on a large expression of IL-6 and TNF-α, but recent investigations also showed that high levels of IFN-y, interleukin (IL)- 1β, 2, 4, 6, 8, 10, 17, induced protein 10 (IP10), monocyte chemoattractant protein-1 (MCP-1), are also significantly elevated in patients with severe COVID-19 (Hu et al., 2020). Both studies presented before, included patients with those characteristics. However, the immunomodulation capacity of MSCs was the key to the promising results obtained and transplantation of MSCs also presented excellent outcomes. Suppressing over-triggering of the immune system and enhancing of the endogenous microenvironment repair capacity are some of the potential of MSCs therapies. Their particular immunomodulation potential results in reduced concentration levels in pro-inflammatory cytokines and chemokines in the patients' serum. MSCs regulatory capacity also includes increased dendritic cells migrating to the injured tissue, as well as a minor migration of mononuclear/macrophages migration to the lesion site, resulting in a decrease of the levels of reactive C-protein (a biomarker for inflammation), a rise in oxygen saturation and improvement of lymphopenia (low level of lymphocytes in the blood). Moreover, the increase of IL-10 modulated the immune system and Vascular Endothelial Growth Factor (VEGF) also promoted angiogenesis conducting to lung repair. MSCs can release VEGF but also hepatocyte growth factor (HGF), which are able to stabilize endothelial barrier function by restoring pulmonary capillary permeability. By inhibiting pulmonary

vascular endothelial cell apoptosis, enhancing the recovery of VE cadherin, and reducing pro-inflammatory factors, MSCs control inflammation and protect the lung endothelial barrier (Wang et al., 2020). In both studies intravenous infusion was applied, and it seems to be the most beneficial route of administration due to the fact that, some MSCs concentrate in the lung tissue, after intravenous infusion. Intuitively, this should likely be beneficial and enhance the pulmonary microenvironment recovery, protecting alveolar epithelial cells, preventing fibrotic tissue formation, thus improving pulmonary function (Bulut and Kato, 2020; Madabhavi et al., 2020). Those clinical trials also investigated if SARS-CoV-2 could infect the MSCs used, through the ACE-2 receptor widely distributed on human cells, but the MSCs that were initially negative, remained ACE-2 negative and free from COVID-19. The positive results of those two studies are thought to be related to immunomodulatory properties of MSCs as well as MSCs differentiation potential that can avoid lung tissue impairment, by blocking the cytokine storm and by promoting regenerative and reconstructive processes on the affected tissue. Furthermore, MSCs secretion of paracrine factors, and their interaction with immune cells, leads to immunomodulation and a robust anti-inflammatory activity (Chan et al., 2015).

Future Challenges and Perspectives

Given the urgent need to find out an effective treatment, there are 3567 active clinical trials concerning COVID-19 at the date of October 1, 2020, involving several different approaches, several mechanisms of action, biomolecules and drugs. Knowing the potential of MSCs, and based on positive results already obtained, several clinical trials using MSCs have already began or are outlined to start shortly. Searching the words "COVID-19" and "Mesenchymal Stem Cells" is possible to identify 62 active trials. Of the 62 trials, 16 are located in the American continent, 9 are located in Europe, 11 in East Asia, and the other 26 are distributed over the remaining continents. Considering the different origins of MSCs, 17 of the clinical trials use UC-MSCs, 9 assays use AT-MSCs, 6 use BM-MCs, 5 use WJ-MSCs, 2 use DP-MSCs, 1 uses OM-MSCs, 1 uses MSCs derived exosomes, and 21 clinical trials do not specify concretely the source, or use more than one. Notably, 57 of the clinical trials are in Phase 1 or Phase 2, research phases to describe and collect preliminary data on the drug performance in people suffering with the disease, and 3 clinical trials are already in Phase 3, a phase of research that collects information on the pharmaceutical safety and effectiveness, analyzing diverse populations, dosages and application of the drug combined with others (research, in the ClinicalTrials.gov database, under the terms "MSCs," on 10/1/2020).

CONCLUSION

The current pandemic we are facing, that has not yet shown signs of weakening, is one of the great scourges of recent years and considering the need for mitigation, envisioning at keeping mortality rates low, there is an urgent need to discover effective mechanisms of prevention and therapies. Global efforts are focused on research and development of new therapies, testing different approaches, where MSCs based-therapies standing out. Regarding the pathogenesis of the SARS-CoV-2, several groups reported an initial recognition of the ACE-2 receptor. These are cell-membrane receptors, widely distributed, and particularly in alveolar cells. In addition to the mild symptoms as fever, cough, muscular soreness, expectoration, and dyspnea, COVID-19 can trigger an immune system overreaction, causing a cytokine storm followed by edema, inefficient gas exchange, ARDS, cardiac impairment, and secondary infection that can lead to death. The currently available cure of the COVID-19 disease is mainly dependent on the immune system function of the patient, therefore, avoiding cytokine overproduction may be decisive to recovery of SARS-CoV-2 patients. Current evidence suggests that therapies applying MSCs and MSCs secretome/EVs are a safe and an efficient approach for treating patients suffering from COVID-19 induced pneumonia, with the possibility to reverse severe critical disease with high potency, without the occurrence of severe adverse events. The immunomodulatory properties of MSCs can prevent lung tissue impairment by inhibiting pro-inflammatory cytokines overproduction and by promoting regeneration of the damaged tissue, as MSCs secrete a variety of paracrine factors, responsible for their immunomodulation and anti-inflammatory properties. Stem cell therapy, especially MSCs can potentially be an ideal therapy or be part of a combination of therapies to treat COVID-19 patients, nonetheless, since the number of patients who underwent this kind of treatment is still restricted, more studies with larger samples are needed to validate this therapeutic option, to comprehend the SARS-CoV-2 mechanism of action and to optimize this therapeutic option, by applying randomized studies promoting safety and efficacy of MSCs application on COVID-19 disease.

AUTHOR CONTRIBUTIONS

All authors listed have made a substantial, direct and intellectual contribution to the work, and approved it for publication.

FUNDING

This research was supported by COMPETE 2020, from ANI – Projetos ID&T Empresas em Copromoção, by the project "insitu.Biomas – Reinvent biomanufacturing systems by using an usability approach for *in situ* clinic temporary implants fabrication" with the reference POCI-01-0247-FEDER-017771, by the project "Print-on-Organs – Engineering bioinks and processes for direct printing on organs" with the reference POCI-01-0247-FEDER-033877, and by the project "Bone2Move – Development of '*in vivo*' experimental techniques and modeling methodologies for the evaluation of 4D scaffolds for bone defect in sheep model: an integrative research approach" with the reference POCI-01-0145-FEDER-031146.

REFERENCES

Alvites, R. D., Branquinho, M. V., Caseiro, A. R., Amorim, I., Santos Pedrosa, S., Rêma, A., et al. (2020a). Rat Olfactory Mucosa Mesenchymal Stem/Stromal Cells (OM-MSCs): A Characterization Study. *Int. J. Cell Biol.* 2020:2938258. doi: 10.1155/2020/2938258

Alvites, R. D., Branquinho, M. V., Caseiro, A. R., Pedrosa, S. S., Luís, A. L., Geuna, S., et al. (2020b). *Biomaterials and Cellular Systems at the Forefront of Peripheral Nerve Regeneration. Peripheral Nerves-Injuries, Disorders and Treatment*. London: IntechOpen.

An, T., Chen, Y., Tu, Y., and Lin, P. (2020). Mesenchymal Stromal Cell-Derived Extracellular Vesicles in the Treatment of Diabetic Foot Ulcers: Application and Challenges. *Stem Cell Rev. Rep.* 2020, 1–10. doi: 10.1007/s12015-020-10014-9

Andrzejewska, A., Lukomska, B., and Janowski, M. (2019). Concise Review: Mesenchymal Stem Cells: From Roots to Boost. *Stem Cells* 37, 855–864. doi: 10.1002/stem.3016

Atluri, S., Manchikanti, L., and Hirsch, J. A. (2020). Expanded umbilical cord mesenchymal stem cells (UC-MSCs) as a therapeutic strategy in managing critically ill COVID-19 patients: the case for compassionate use. *Pain Physician* 23, E71–E83.

Barry, F., Boynton, R., Murphy, M., and Zaia, J. (2001). The SH-3 and SH-4 antibodies recognize distinct epitopes on CD73 from human mesenchymal stem cells. *Biochem. Biophys. Res. Commun.* 289, 519–524. doi: 10.1006/bbrc.2001.6013

Berebichez-Fridman, R., and Montero-Olvera, P. R. (2018). Sources and clinical applications of mesenchymal stem cells state-of-the-art review. *Sultan Qaboos Univ. Med. J.* 18, 264–277e. doi: 10.18295/squmj.2018.18.03.002

Berebichez-Fridman, R., Gómez-García, R., Granados-Montiel, J., Berebichez-Fastlicht, E., Olivos-Meza, A., Granados, J., et al. (2017). The Holy Grail of Orthopedic Surgery: Mesenchymal Stem Cells - Their Current Uses and Potential Applications. *Stem Cells Int.* 2017:2638305. doi: 10.1155/2017/2638305

Biju, P., and Jack, M. M. (2013). Mesenchymal Stem Cells as Therapeutics. *Annu. Rev. Biomed. Eng.* 23, 1–7. doi: 10.1038/jid.2014.371

Branquinho, M., Pedrosa, S. S., and Maurício, R. D. A. A. C. (2012). "Synovia-Derived Mesenchymal Stem Cell Application in Musculoskeletal Injuries: A Review,". in *Tissue Regeneration*. ed. H. Kaoud (London: Intech). doi: 10.1016/j.colsurfa.2011.12.014

Bulut, C., and Kato, Y. (2020). Epidemiology of covid-19. *Turk. J. Med. Sci.* 50, 563–570. doi: 10.3906/sag-2004-172

Caplan, A. I. (1994). The mesengenic process. *Clinics in Plastic Surgery* 21, 429–435. doi: 10.1016/S0094-1298(20)31020-8

Caplan, A. I. (2009). "Mesenchymal Stem Cells," in *Essentials of Stem Cell Biology*. eds R. Lanza, E. D. Thomas, B. Hogan, R. A. Pedersen, D Melton, J. A. Thomson et al. (Amsterdam: Elsevier), 243–248. doi: 10.1016/B978-0-12-374729-7.00029-9

Caplan, A. I. (2017). Mesenchymal stem cells: Time to change the name! *Stem Cells Transl. Med.* 6, 1445–1451. doi: 10.1002/sctm.17-0051

Caplan, A. I., and Dennis, J. E. (2006). Mesenchymal stem cells as trophic mediators. *J. Cell. Biochem.* 98, 1076–1084. doi: 10.1002/jcb.20886

Caseiro, A. R., Pedrosa, S. S., Ivanova, G., Branquinho, M. V., Almeida, A., Faria, F., et al. (2019). Mesenchymal Stem/ Stromal Cells metabolomic and bioactive factors profiles: A comparative analysis on the umbilical cord and dental pulp derived Stem/ Stromal Cells secretome. *PLoS One* 14, 1–33. doi: 10.1371/journal.pone.0221378

Caseiro, A. R., Pereira, T., Ribeiro, J., Amorim, I., Faria, F., Bártolo, P. J., et al. (2015). Neuro-muscular regeneration using scaffolds with mesenchymal stem cells (MSCs) isolated from human umbilical cord Wharton's jelly: Functional and morphological analysis using rat sciatic nerve neurotmesis injury model. *Procedia Engine.* 110, 106–113. doi: 10.1016/j.proeng.2015.07.016

Chan, J. F. W., Choi, G. K. Y., Tsang, A. K. L., Tee, K. M., Lam, H. Y., Yip, C. C. Y., et al. (2015). Development and evaluation of novel real-time reverse transcription-PCR assays with locked nucleic acid probes targeting leader sequences of human-pathogenic coronaviruses. *J. Clin. Microbiol.* 53, 2722–2726. doi: 10.1128/JCM.01224-15

Chen, J., Hu, C., Chen, L., Tang, L., Zhu, Y., Xu, X., et al. (2020). Clinical study of mesenchymal stem cell treating acute respiratory distress sy drome induced by epidemic Influenza A (H7N9) infection, a hint for COVID-1 treatment. *Engineering* 2020:eng.2020.02.006. doi: 10.1016/j.eng.2020.02.006

Choudhery, M. S., Badowski, M., Muise, A., Pierce, J., and Harris, D. T. (2014). Donor age negatively impacts adipose tissue-derived mesenchymal stem cell expansion and differentiation. *J. Transl. Med.* 12, 1–14. doi: 10.1186/1479-5876-12-8

Crisan, M., Yap, S., Casteilla, L., Chen, C. W., Corselli, M., Park, T. S., et al. (2008). A Perivascular Origin for Mesenchymal Stem Cells in Multiple Human Organs. *Cell Stem Cell* 3, 301–313. doi: 10.1016/j.stem.2008.07.003

d'Angelo, M., Cimini, A., and Castelli, V. (2020). Insights into the Effects of Mesenchymal Stem Cell-Derived Secretome in Parkinson's Disease. *Int. J. Mol. Sci.* 21:5241. doi: 10.3390/ijms21155241

Delorme, B., Nivet, E., Gaillard, J., Häupl, T., Ringe, J., Devèze, A., et al. (2010). The human nose harbors a niche of olfactory ectomesenchymal stem cells displaying neurogenic and osteogenic properties. *Stem Cells Dev.* 19, 853–866. doi: 10.1089/scd.2009.0267

Denton, A. E., Roberts, E. W., and Fearon, D. T. (2018). Stromal cells in the tumor microenvironment. *Adv. Exp. Med. Biol.* 1060, 99–114. doi: 10.1007/978-3-319-78127-3

Dominici, M., Le Blanc, K., Mueller, I., Slaper-Cortenbach, I., Marini, F. C., Krause, D. S., et al. (2006). Minimal criteria for defining multipotent mesenchymal stromal cells. The International Society for Cellular Therapy position statement. *Cytotherapy* 8, 315–317. doi: 10.1080/14653240600855905

Friedenstein, A. J., Chailakhyan, R. K., Latsinik, N. V., Panasyvk, A. F., and Keiliss-Borok, I. V. (1974). Stromal cells responsible for transferring the microenvironment of the hemopoietic tissues: Cloning in vitro and retransplantation in vivo. *Transplantation* 17, 331–340. doi: 10.1097/00007890-197404000-00001

Frieedenstein, A., Petrakova, K., Kurolesova, A., and Frolova, G. (1968). Hetrotopic of bone marrow. Analysis of precursor cells for osteogenic and hematopoetic tissue. *Transplantacion* 6:230.

Fujita, Y., Kadota, T., Araya, J., Ochiya, T., and Kuwano, K. (2018). Clinical Application of Mesenchymal Stem Cell-Derived Extracellular Vesicle-Based Therapeutics for Inflammatory Lung Diseases. *J. Clin. Med.* 7:355. doi: 10.3390/jcm7100355

Ge, L., Jiang, M., Duan, D., Wang, Z., Qi, L., Teng, X., et al. (2016). Secretome of olfactory mucosa mesenchymal stem cell, a multiple potential stem cell. *Stem Cells Int.* 2016:1243659. doi: 10.1155/2016/1243659

Golchin, A., Seyedjafari, E., and Ardeshirylajimi, A. (2020). Mesenchymal Stem Cell Therapy for COVID-19: Present or Future. *Stem Cell Rev. Rep.* 16, 427–433. doi: 10.1007/s12015-020-09973-w

Gomez-Salazar, M., Gonzalez-Galofre, Z. N., Casamitjana, J., Crisan, M., James, A. W., and Péault, B. (2020). Five Decades Later, Are Mesenchymal Stem Cells Still Relevant? *Front. Bioengine. Biotechnol.* 8:148. doi: 10.3389/fbioe.2020.00148

Greif, D. N., Kouroupis, D., Murdock, C. J., Griswold, A. J., Kaplan, L. D., Best, T. M., et al. (2020). Infrapatellar Fat Pad/Synovium Complex in Early-Stage Knee Osteoarthritis: Potential New Target and Source of Therapeutic Mesenchymal Stem/Stromal Cells. *Front. Bioengine. Biotechnol.* 8:860.doi: 10.3389/fbioe.2020.00860

Haynesworth, S. E., Barer, M. A., and Caplan, A. I. (1992a). Cell surface antigens on human marrow-derived mesenchymal cells are detected by monoclonal antibodies. *Bone* 13, 69–80. doi: 10.1016/8756-3282(92)90363-2

Haynesworth, S. E., Goshima, J., Goldberg, V. M., and Caplan, A. I. (1992b). Characterization of cells with osteogenic potential from human marrow. *Bone* 13, 81–88. doi: 10.1016/8756-3282(92)90364-3

Hu, B., Huang, S., and Yin, L. (2020). The cytokine storm and COVID−19. *J. Med. Virol.* 2, 0–2. doi: 10.1002/jmv.26232

Khatri, M., Richardson, L. A., and Meulia, T. (2018). Mesenchymal stem cell-derived extracellular vesicles attenuate influenza virus-induced acute lung injury in a pig model. *Stem Cell Res. Ther.* 9, 1–13. doi: 10.1186/s13287-018-0774-8

Khoury, M., Cuenca, J., Cruz, F. F., Figueroa, F. E., Rocco, P. R. M., and Weiss, D. J. (2020). Current Status of Cell-Based Therapies for Respiratory Virus Infections: Applicability to COVID-19. *Eur. Respir. J.* 55:2000858. doi: 10.1183/13993003.00858-2020

Kurenkova, A. D., Medvedeva, E. V., Newton, P. T., and Chagin, A. S. (2020). Niches for Skeletal Stem Cells of Mesenchymal Origin. *Front. Cell Dev. Biol.* 8:592. doi: 10.3389/fcell.2020.00592

Lanza, R., Gearhart, J., Hogan, B., Melton, D., Pedersen, R., Thomas, E. D., et al. (2009). *Essentials of Stem Cell Biology*. Amsterdam: Elsevier. doi: 10.1016/C2009-0-00078-6

Li, C., Zhao, C., Bao, J., Tang, B., Wang, Y., and Gu, B. (2020a). Laboratory Diagnosis of Coronavirus Disease-2019 (COVID-19). *Clin. Chimica Acta* 510, 35–46. doi: 10.1016/j.cca.2020.06.045

Li, N., and Hua, J. (2017). Interactions between mesenchymal stem cells and the immune system. *Cell. Mol. Life Sci.* 74, 2345–2360. doi: 10.1007/s00018-017-2473-5

Li, Q., Guan, X., Wu, P., Wang, X., Zhou, L., Tong, Y., et al. (2020b). Early transmission dynamics in Wuhan. China, of novel coronavirus-infected pneumonia. *N. Engl. J. Med.* 382, 1199–1207. doi: 10.1056/NEJMoa2001316

Liu, S., Peng, D., Qiu, H., Yang, K., Fu, Z., and Zou, L. (2020). Mesenchymal stem cells as a potential therapy for COVID-19. *Stem Cell Res. Ther.* 11, 8–11. doi: 10.1186/s13287-020-01678-8

Madabhavi, I., Sarkar, M., and Kadakol, N. (2020). CoviD-19: A review. *Monaldi Arch. Chest Dis.* 90, 248–258. doi: 10.4081/monaldi.2020.1298

Mushahary, D., Spittler, A., Kasper, C., Weber, V., and Charwat, V. (2018). Isolation, cultivation, and characterization of human mesenchymal stem cells. *Cytometry Part A* 93, 19–31. doi: 10.1002/cyto.a.23242

Pedrosa, S. S., Caseiro, A. R., Santos, J. D., and Maurício, A. C. (2017). Scaffolds for peripheral nerve regeneration, the importance of in vitro and in vivo studies for the development of cell-based therapies and biomaterials: state of the art. *Scaffolds Tissue Engine.* 9:179. doi: 10.5772/intechopen.69540

Pouryazdanpanah, N., Dabiri, S., Derakhshani, A., Vahidi, R., and Farsinejad, A. (2018). Peripheral blood-derived mesenchymal stem cells: Growth factor-free isolation, molecular characterization and differentiation. *Iran. J. Pathol.* 13, 461–466.

Rendra, E., Scaccia, E., and Biebac, K. (2020). Recent advances in understanding mesenchymal stromal cells. *F1000Research* 9, 1–9. doi: 10.12688/f1000research.21862.1

Salem, H. K., and Thiemermann, C. (2010). Mesenchymal stromal cells: Current understanding and clinical status. *Stem Cells* 28, 585–596. doi: 10.1002/stem.269

Sami, G. A., Devendra, K., and Agrawal, P. D. (2016). Key Transcription Factors in the Differentiation of Mesenchymal Stem Cells. *Physiol. Behav.* 176, 139–148. doi: 10.1016/j.physbeh.2017.03.040

Samsonraj, R. M., Raghunath, M., Nurcombe, V., Hui, J. H., van Wijnen, A. J., and Cool, S. M. (2017). Concise Review: Multifaceted Characterization of Human Mesenchymal Stem Cells for Use in Regenerative Medicine. *Stem Cells Transl. Med.* 6, 2173–2185. doi: 10.1002/sctm.17-0129

Shammaa, R., El-Kadiry, A. E. H., Abusarah, J., and Rafei, M. (2020). Mesenchymal Stem Cells Beyond Regenerative Medicine. *Front. Cell Dev. Biol.* 8, 1–17. doi: 10.3389/fcell.2020.00072

Spike, R. S. C. (2010). Efficient Activation of the Severe Acute. *J. Virol.* 84:12658.

Spitzhorn, L. S., Rahman, M. S., Schwindt, L., Ho, H. T., Wruck, W., Bohndorf, M., et al. (2017). Isolation and molecular characterization of amniotic fluid-derived mesenchymal stem cells obtained from caesarean sections. *Stem Cells Int.* 2017:5932706. doi: 10.1155/2017/5932706

Sun, J., He, W-T., Wang, L., Lai, A., Ji, X., Zhai, X., et al. (2020a). COVID-19 : Epidemiology. Evolution, and Cross-Disciplinary Perspectives. *Trends Mol. Med.* 26:13. doi: 10.1016/j.molmed.2020.02.008

Sun, P., Lu, X., Xu, C., Sun, W., and Pan, B. (2020b). Understanding of COVID−19 based on current evidence. *J. Med. Virol.* 92, 548–551. doi: 10.1002/jmv.25722

Trohatou, O., and Roubelakis, M. G. (2017). Mesenchymal Stem/Stromal Cells in Regenerative Medicine: Past. Present, and Future. *Cell. Reprog.* 19, 217–224. doi: 10.1089/cell.2016.0062

Uccelli, A., Moretta, L., and Pistoia, V. (2008). Mesenchymal stem cells in health and disease. *Nat. Rev. Immunol.* 8, 726–736. doi: 10.1038/nri2395

Ullah, I., Subbarao, R. B., and Rho, G. J. (2015). Human mesenchymal stem cells - Current trends and future prospective. *Biosci. Rep.* 35:e00191. doi: 10.1042/BSR20150025

Varderidou-Minasian, S., and Lorenowicz, M. J. (2020). Mesenchymal stromal/stem cell-derived extracellular vesicles in tissue repair: challenges and opportunities. *Theranostics* 10:5979. doi: 10.7150/thno.40122

Veron, A. D., Bienboire-Frosini, C., Feron, F., Codecasa, E., Deveze, A., Royer, D., et al. (2018). Isolation and characterization of olfactory ecto-mesenchymal stem cells from eight mammalian genera. *BMC Vet. Res.* 14, 1–11. doi: 10.1186/s12917-018-1342-2

Vizoso, F. J., Eiro, N., Cid, S., Schneider, J., and Perez-Fernandez, R. (2017). Mesenchymal stem cell secretome: Toward cell-free therapeutic strategies in regenerative medicine. *Int. J. Mol. Sci.* 18:1852. doi: 10.3390/ijms18091852

Wang, J., Jiang, M., Chen, X., and Montaner, L. J. Cytokine storm, and leukocyte changes in mild versus severe SARS-CoV-2 infection: Review of. (2020)COVID-19 patients in China and emerging pathogenesis and therapy concepts. *J. Leukocyte Biol.* 108, 17–41. doi: 10.1002/jlb.3covr0520-272r

WHO (2020). *Coronavirus disease (COVID-19) advice for the public*. Geneva: World Health Organization.

Worldometer (2020). *Coronavirus Cases*. China: National Health Commission.

Xiao, K., Hou, F., Huang, X., Li, B., Qian, Z. R., and Xie, L. (2020). Mesenchymal stem cells: current clinical progress in ARDS and COVID-19. *Stem Cell Res. Ther.* 11, 1–7.

Zhai, P., Ding, Y., Wu, X., Long, J., Zhong, Y., and Li, Y. (2020). The epidemiology, diagnosis and treatment of COVID-19. *Int. J. Antimicrob. Agents* 55:13. doi: 10.1016/j.ijantimicag.2020.105955

Conflict of Interest: The authors declare that the research was conducted in the absence of any commercial or financial relationships that could be construed as a potential conflict of interest.

frontiers in Cell and Developmental Biology

ORIGINAL RESEARCH
published: 10 December 2020
doi: 10.3389/fcell.2020.610427

Modeling Rett Syndrome With Human Patient-Specific Forebrain Organoids

*Ana Rita Gomes[1,2], Tiago G. Fernandes[1], Sandra H. Vaz[2,3], Teresa P. Silva[1,2], Evguenia P. Bekman[1,2,4], Sara Xapelli[2,3], Sofia Duarte[5], Mehrnaz Ghazvini[6], Joost Gribnau[7], Alysson R. Muotri[8,9,10,11,12], Cleber A. Trujillo[8,9,10], Ana M. Sebastião[2,3], Joaquim M. S. Cabral[1] and Maria Margarida Diogo[1]**

[1] Department of Bioengineering and iBB-Institute for Bioengineering and Biosciences, Instituto Superior Técnico, Universidade de Lisboa, Lisboa, Portugal, [2] Instituto de Medicina Molecular João Lobo Antunes, Faculdade de Medicina, Universidade de Lisboa, Lisboa, Portugal, [3] Instituto de Farmacologia e Neurociências, Faculdade de Medicina, Universidade de Lisboa, Lisboa, Portugal, [4] The Discoveries Centre for Regenerative and Precision Medicine (Lisbon Campus), Instituto Superior Técnico, Universidade de Lisboa, Lisboa, Portugal, [5] Department of Pediatric Neurology, Centro Hospitalar Universitário de Lisboa Central, Lisbon, Portugal, [6] Erasmus MC iPS Facility, Erasmus Medical Center, University Medical Center, Rotterdam, Netherlands, [7] Department of Developmental Biology, Erasmus Medical Center, University Medical Center, Rotterdam, Netherlands, [8] Department of Pediatrics, School of Medicine, University of California, San Diego, La Jolla, CA, United States, [9] Rady Children's Hospital San Diego, School of Medicine, University of California, San Diego, La Jolla, CA, United States, [10] Department of Cellular and Molecular Medicine, School of Medicine, University of California, San Diego, La Jolla, CA, United States, [11] Kavli Institute for Brain and Mind, University of California, San Diego, La Jolla, CA, United States, [12] Center for Academic Research and Training in Anthropogeny, La Jolla, CA, United States

OPEN ACCESS

Edited by:
Joana Paiva Miranda, University of Lisbon, Portugal

Reviewed by:
Zhiping P. Pang, Rutgers, The State University of New Jersey, United States
Dan Lindholm, University of Helsinki, Finland

***Correspondence:**
Maria Margarida Diogo
margarida.diogo@tecnico.ulisboa.pt

Specialty section:
This article was submitted to Stem Cell Research, a section of the journal Frontiers in Cell and Developmental Biology

Received: *25 September 2020*
Accepted: *23 November 2020*
Published: *10 December 2020*

Citation:
Gomes AR, Fernandes TG, Vaz SH, Silva TP, Bekman EP, Xapelli S, Duarte S, Ghazvini M, Gribnau J, Muotri AR, Trujillo CA, Sebastião AM, Cabral JMS and Diogo MM (2020) Modeling Rett Syndrome With Human Patient-Specific Forebrain Organoids. Front. Cell Dev. Biol. 8:610427. doi: 10.3389/fcell.2020.610427

Engineering brain organoids from human induced pluripotent stem cells (hiPSCs) is a powerful tool for modeling brain development and neurological disorders. Rett syndrome (RTT), a rare neurodevelopmental disorder, can greatly benefit from this technology, since it affects multiple neuronal subtypes in forebrain sub-regions. We have established dorsal and ventral forebrain organoids from control and RTT patient-specific hiPSCs recapitulating 3D organization and functional network complexity. Our data revealed a premature development of the deep-cortical layer, associated to the formation of TBR1 and CTIP2 neurons, and a lower expression of neural progenitor/proliferative cells in female RTT dorsal organoids. Moreover, calcium imaging and electrophysiology analysis demonstrated functional defects of RTT neurons. Additionally, assembly of RTT dorsal and ventral organoids revealed impairments of interneuron's migration. Overall, our models provide a better understanding of RTT during early stages of neural development, demonstrating a great potential for personalized diagnosis and drug screening.

Keywords: human induced pluripotent stem cells, organoids, forebrain, Rett syndrome, disease modeling, neurodevelopmental disorders

INTRODUCTION

Rett syndrome (RTT) is a severe neurological disorder that affects brain development and function in approximately 1 in 10.000 live births, and it is caused by mutations in the gene encoding for methyl-CpG-binding protein 2 (MeCP2). *MeCP2* mutations in females lead to developmental regression after 6–18 months after birth, with a range of neurodevelopmental defects, including loss of speech, acquired movement skills and severe cognitive impairment after an apparently normal

development. Less frequent, *MeCP2* mutations in males usually lead to wide spectrum of symptoms, from mild mental retardations to severe congenital encephalopathies and death within the first 2 years of age (Chahrour and Zoghbi, 2007). The range of RTT phenotypes is large and varies according to the mutations, with missense and nonsense mutations accounting for the majority, while small C-terminal deletions and complex rearrangements are less frequent (Chahrour and Zoghbi, 2007). The *MeCP2* gene is localized on the X-chromosome, which causes the disease to be presented in females in a mosaic pattern, with some cells expressing the wild-type *MeCP2* allele and others the mutant (Ananiev et al., 2011).

Rett syndrome has been studied using post-mortem samples of human brain (Colantuoni et al., 2001), as well as transgenic mouse models (Chen et al., 2001). However, the onset of neurological symptoms in mice can be less severe (Veeraragavan et al., 2016) and does not fully recapitulate the phenotypic aspects of human RTT. Recently, RTT was modeled using neural cells differentiated from patient-specific hiPSCs with *MeCP2*-mutant neurons exhibiting impaired maturation, including the presence of fewer synapses, smaller soma size, altered calcium signaling, functional defects in firing activity and excitatory/inhibitory (E/I) imbalance (Marchetto et al., 2010; Ananiev et al., 2011; Fernandes et al., 2015; Tang et al., 2016). However, in the majority of these studies, neural differentiation was performed in 2D adherent monolayer, which provides a simplistic recapitulation of the human cortex development. As a recent innovation in the stem cell field, organoid techniques provide unique platforms to model brain development and neurological disorders (Lancaster et al., 2013). 3D cerebral organoids derived from hiPSCs were recently used for RTT modeling, reveling a decrease in neurite growth, neurite coalescence, and soma size of interneurons (Xiang et al., 2020), in addition to impaired neurogenesis and neural progenitor's migration deficits (Mellios et al., 2017). However, in cerebral organoids all the regions of the brain are co-generated together, which causes the differentiation process to be poorly controlled and non-region specific (Qian et al., 2016). To overcome these limitations, it is possible to generate independently distinct organoids recapitulating the dorsal and ventral regions of the forebrain (Bagley et al., 2017). *In vivo*, the dorsal forebrain contains the majority of excitatory glutamatergic pyramidal neurons, whereas some evidences in the literature claim that inhibitory *g*-aminobutyric acid (GABA)-producing interneurons are originated in the ventral region, integrating the dorsal cortical circuit upon migration. Ultimately, forebrain multilineage assembloids can be patterned to contain a dorsal–ventral axis and then used to recapitulate human interneuron migration (Bagley et al., 2017; Xiang et al., 2017; Sloan et al., 2018).

In this study, we generated dorsal, ventral and assembled 3D forebrain organoids from RTT patient-derived hiPSCs and their isogenic pair (IC), as well as from several healthy control hiPSCs. These *in vitro* humanized models were used for studying RTT-derived molecular, structural and functional alterations. Intriguingly, our findings suggest that neural progenitors in dorsal organoids derived from RTT female hiPSCs undergo a premature transition into early born neurons, yielding neurons with functional deficits. Our results also propose impairments in the formation of medial ganglionic eminence (MGE) progenitors in ventral organoids, which seems to impact negatively on interneuron's migration process. Overall, these human *in vitro* 3D models of RTT recapitulate previously reported hallmarks of the disease while providing new clues for the molecular mechanisms involved in this syndrome.

MATERIALS AND METHODS

hiPSC Lines and Maintenance

We used four healthy-control hiPSCs lines and two hiPSCs lines derived from patients with RTT-associated mutations. The healthy-control hiPSC lines were **F002.1A.13** [46, XX cell line derived from a health donor by TCLab (Tecnologias Celulares para Aplicação Médica, Unipessoal, Lda.)], reprogrammed using a standard protocol by Takahashi et al. (2007); **Gibco® iPSC6.2** (46, XY human Episomal cell line, from a healthy donor) and **iPS-DF6-9-9T.B** (46, XY cell line, reprogrammed from foreskin fibroblasts, collected from healthy donors, using defined factors, in the Laboratory of Dr. James Thomson, at University of Wisconsin, and provided by WiCell Bank). All the previous healthy hiPSCs-controls were purchased under MTAs. The RTT cell lines were **EMC25i/WT-R/F7** (46, XX cell line, derived from a healthy donor); **EMC24i/R2 (C6)** [46, XX cell line of a RTT patient with mutation at *MECP2* (R255X), a nonsense mutation on C to T transitions at hypermutable CpG sites within the gene] and **EMC24i/R2 (C5)** (the respective isogenic cell line). The last three cell lines were derived by reprogramming skin fibroblasts ensuring data protection issues. Human skin punch biopsy samples (3 mm) were collected using a standard technique. The protocol was established with the Paediatric Surgery Department at Centro Hospitalar de Lisboa Norte (CHLN) to collect skin samples during minor surgeries. Biopsy tissue was expanded at Instituto de Medicina Molecular, Lisboa. Hospital Sant Joan de Déu (HSJD) and CHLN Ethic Committees approved the study and written informed consent was obtained from patient's legal guardians. Then, the reprogramming of fibroblasts was performed at the iPSC Facility, Erasmus Medical Center, Rotterdam, using engineered color-coded lentiviral vectors (Varga et al., 2016). Moreover, a **RTT male cell line was also used, Rett Male: Q83X** (46, XY cell line, derived from fibroblasts of a RTT male patient with a mutation at the amino acid residue 83 from glutamine to a premature stop codon, resulting in truncation and degradation of the MeCP2 protein). This cell line was donated by Alysson Muotri Lab at UCSD, United States, under an MTA. These cells were reprogrammed with retroviral reprogramming vectors (Sox2, Oct4, c-Myc, and Klf4) (Takahashi and Yamanaka, 2006), and provided by University of California, San Diego Campus and approved by the institutional review boards at Salk Institute for Biological Studies and University of California, San Diego, as well as Pennsylvania State University (Marchetto et al., 2010).

All the hiPSCs lines were cultured on Matrigel™ (Corning)-coated plates with either Essential 8™ Medium (Thermofisher Scientific) or mTeSR™1 Plus Medium (StemCell Technologies).

Medium was changed according to the respective procedures. Cells were passaged every 3–4 days (at approximately 85% of cell confluence) using 0.5 mM EDTA dissociation buffer (Thermofisher Scientific). Before starting the differentiation process, two to three passages were performed.

3D Induction of Dorsal and Ventral Forebrain Organoids

Before starting the ventral and dorsal neural induction protocols, the hiPSC were incubated with ROCK inhibitor (ROCKi, Y-27632, 10 μM, StemCell Technologies) for 30 min at 37°C and then treated with accutase (Sigma) for 5 min at 37°C. After dissociation, cells were seeded on microwell plates (AggreWell^{TM}800, StemCell Technologies) according to the manufacturer's instructions. The cell density used was 1.5 × 10^6 cells/well in 1.5 mL/well of E8^{TM} or mTeSR^{TM}1 Plus supplemented with 10 μM ROCKi. The entire expansion medium was changed after 24 h, without ROCKi supplementation. Usually after 2–3 days, when the aggregates attained a diameter of 250–300 μm, the medium was half-changed to induction medium, and this day was defined as day 0. The neural induction medium used was N2B27, composed by 50% of DMEM/F12/N2 (DMEM-F12, (Thermofisher Scientific) supplemented with 1% (v/v) N2 (Thermofisher Scientific), 1.6 g/L Glucose (Sigma), 1% (v/v) PenStrep, and 20 μg/mL Insulin (Sigma) and 50% of Neurobasal/B27 [Neurobasal medium (Thermofisher Scientific) supplemented with 2% (v/v) B27(-Vitamin A)-supplement (Thermofisher Scientific), 2 mM L-glutamine (Thermofisher Scientific) and 1% (v/v) PenStrep]. For the dorsal forebrain patterning, the previously described medium was supplemented with 2 μM Dorsomorphine (Sigma) and 2 μM A83-01 (Tocris) until day 5, with half-medium changed at days 0, 3 and 5. For the ventral patterned aggregates, the medium was supplemented with 10 μM SB-431542 (SB) (Sigma) and 100 nM LDN-193189 (LDN) (Stemgent). At day 5, cell aggregates (around 300 aggregates per each well of the microwell plate used) were collected from the microwell plates and seeded in an Ultra-Low attachment 6-well plate (Corning). At day 7, half of the medium was changed for both dorsal and ventral patterning. In dorsal patterning cultures, the medium was supplemented with 1 μM CHIR99021 (Stemgent), 10 μM SB-431542 (Sigma) and 10 μg/ml Heparin (Sigma) and ventral patterning culture medium was supplemented with 2.5 μM IWP2 (Stemgent), 100 nM SAG (Millipore) and 10 μg/ml Heparin (Sigma). When required, on day 13, the assembly of one dorsal with one ventral organoid was performed inside a 96-TC Plate, Suspension, C (Sarstedt) and after 24 h the fused organoid was transferred into an Ultra-Low attachment 24-well plate.

Maintenance and Maturation of Dorsal, Ventral and Fused Organoids

On day 13, the medium was half-changed to N2B27 (+Vitamin A) without any small molecule supplementation and was maintained in the presence of this medium until day 41. This medium was replaced every 2/3 days. On day 41 of differentiation, the organoids were cultured in BrainPhys^{TM} Neuronal Medium (StemCell Technologies), supplemented with NeuroCult^{TM} SM1 Neuronal Supplement (StemCell Technologies), N2 Supplement-A (StemCell Technologies), Recombinant Human Brain Derived Neurotrophic Factor (BDNF, PeproTech, 20 ng/mL), Recombinant Human Glial-Derived Neurotrophic Factor (GDNF, PeproTech, 20 ng/mL), dibutyryl cAMP (1 mM, Sigma), and ascorbic acid (200 nM, Sigma). One third of the total volume was replaced every 2–3 days.

Tissue Preparation and Immunostaining

Organoids replated in coverslips were fixed in 4% (w/v) PFA (Sigma) for 20 min at 4°C, followed by washing in phosphate buffered saline (PBS, 0.1M). Whole 3D organoids were fixed in 4% PFA for 30 min at 4°C, with agitation, followed by washing in PBS 0.1M and overnight incubation in 15% (w/v) sucrose at 4°C. Then, they were embedded in 7.5% gelatin/15% sucrose and isopenthane (Sigma) was subsequently used for freezing at −80°C. A cryostat-microtome (Leica CM3050S, Leica Microsystems) was used to prepare organoid sections with approximately 12 μm thickness and collected on Superfrost^{TM} Microscope Slides (Thermo Scientific) (stored at −20°C). Organoid sections were de-gelatinized in PBS at 37°C for 45 min and then analyzed by immunohistochemistry. Organoid sections and cells plated on coverslips were then incubated in 0.1 M Glycine (Millipore) for 10 min at room temperature (RT), permeabilized with 0.1% Triton X-100 (Sigma) for 10 min at RT, and blocked with 10% fetal bovine serum (FBS, Thermofisher Scientific) in TBST [20 mM Tris-HCl pH 8.0, 150 mM NaCl, 0.05% (v/v) Tween-20, Sigma] for 1 h at RT. Then, primary antibodies were diluted in blocking solution and incubated overnight at 4°C. After three washing steps with TBST, secondary antibodies were incubated for 45 min at RT. For phalloidin staining, cells were incubated with Alexa Fluor® 488 Phalloidin during 30 min (1:50 in PBS, Thermofisher Scientific). For GFP staining, cryosections were incubated with anti-GFP polyclonal IgG, Alexa Fluor®–488. Nuclear counterstaining was performed using 4′,6-diamidino-2-phenylindole (DAPI, 1.5 μg/mL; Sigma). After drying, sections and coverslips were mounted in Mowiol (Sigma). Fluorescence images were acquired using Zeiss LSM 710 Confocal Laser Point-Scanning Microscopes and images were processed in ZEN 2.3 blue edition software (Zeiss).

Flow Cytometry

Samples were collected with accutase (Sigma) for 5 min at 37°C and then stored in 2% w/v PFA (Sigma). Samples were centrifuged at 1000 rpm for 5 min and washed twice with PBS. Samples for KI67 analyzes were also collected with accutase, and then fixed drop by drop with 70% (v/v) ethanol (−20°C) with vortex. Samples were stored at −20°C, being then centrifuged at 1000 rpm for 10 min and washed twice with PBS. The Eppendorf tubes were coated with 1% v/v bovine serum albumin (BSA; Thermofisher Scientific) solution in PBS for 15 min. For intracellular staining, cell were resuspended in 3% (v/v) normal goat serum (NGS, Sigma), at approximately 1 × 10^6 cells per condition. The cell suspension was centrifuged again at 1000 rpm for 3 min. The cell membrane was then permeabilized using a

solution 1:1 of 3% (v/v) NGS and 1% (v/v) saponin (Sigma) for 15 min, at RT. After washing three times with 1% (v/v) NGS, cells were resuspended in primary antibody solution (in 3% NGS) and incubated for 1 h at room temperature. Cells were then washed three times with 1% NGS, and incubated for 30 min in the dark with the secondary antibody (in 3% NGS) and 300 μL were transferred to a FACS (flow cytometry) tube. For surface staining, cells were resuspended in primary antibody diluted in 10% (v/v) FBS in PBS, at approximately 0.5×10^6 cells per condition, and incubated for 30 min at RT. Finally, cells were washed with PBS and resuspended in 10% (v/v) FBS in PBS and incubated with secondary antibodies for 15 min, at room temperature. After another washing step, cells were resuspended in PBS and 300 μL were transferred to a flow cytometry tube. Flow cytometry was performed using a FACSCalibur™ flow cytometer (by Becton Dickinson) and the data acquisition was performed with the Cell Quest software (Becton Dickinson). A minimum of 10,000 events were analyzed for each sample. The data analysis was performed using Flowing Software 2.0. As negative controls, unstained samples and samples stained with only the secondary antibody were used, without showing relevant differences between them. The gate was selected to contain less than 1% of false positives (i.e., 1% of the negative control samples). Primary antibodies used for flow cytometry were SSEA-4-PE (Miltenyi Biotec, 1:10) for surface staining and OCT4 (Invitrogen, 1:300) and KI67 (BD, 1:100) for intracellular staining. Secondary antibodies used were goat anti-mouse IgG Alexa Fluor – 488 (Invitrogen, 1:300) and anti-mouse IgG-PE (1:300, Miltenyi Biotec).

Quantitative Real Time (qRT)-PCR

At different time points of differentiation, RNA samples were extracted by using High Pure RNA Isolation Kit (Roche) and converted into complementary cDNA with Transcriptor High Fidelity cDNA Synthesis Kit (Roche). Real-time quantitative PCR (qPCR) was performed using the StepOne™ or the ViiA™ 7 RT-PCR Systems (Applied BioSystems). Taqman® Gene Expression Assays (20X, Applied Biosystems) were selected for *NANOG*, *PAX6*, *TBR1, DLX2, NKX2.1, LHX6, FOXG1* and *GAPDH*. *DLL1*, *HES5*, *PARVALBUMIN (PV)*, *VGLUT1* and *GAPDH* analysis were performed using the SYBR Green Master Mix (Nzytech). The results were analyzed with the StepOne™ or the QuantStudio™ RT-PCR Software. All PCR reactions were done in duplicate or triplicate and then normalized to the housekeeping gene *GAPDH*. The fold change was calculated using the $2^{\Delta Ct}$ method and in some graphical results it was calculated relatively to the control condition levels obtained. The representative heatmaps were generated using the web tool Clustvis (Metsalu and Vilo, 2015).

RNA *in situ* Hybridization

The probes were generated by using a template cDNA, amplified by PCR, with the reverse primers containing the T7 site: *DLL1*-fw (TGTGCCTCAAGCACTACCAG) rv(+T7) (TA ATACGACTCACTATAGGGATGCTGCTCATCACATCCAG);

HES5-fw (ACGCAGATGAAGCTGCTGTA) rv(+T7) (TA ATACGACTCACTATAGGGGGCCCTGAAGAAAGTCCTCT).

The PCR products were gel-purified using the NZYGelpure kit (NZYTech) and used for reverse transcription with T7 polymerase (Agilent Technologies), DIG-dNTPs (Sigma), and RNase inhibitor. The RNA was precipitated with EtOH and $NaOAC_3$ at 20°C overnight, centrifuged 30 min at 13.000 *g*, and then washed with 70% EtOH, dried, and resuspended in nuclease-free H_2O with 10mM of EDTA (stored at 20°C until use).

The organoids were fixed in 4% PFA (w/v) during 1 h at 4°C. Fresh cryosections (12 μm) were incubated with 10 nM FISH probes, overnight, at 65°C in hybridization buffer, containing 1x salts, 10% dextran sulfate, 1 mg/mL rRNA, 1x Denhardt's and 50% of deionized formamide (Sigma). After hybridization, the cells were washed twice, for 30 min at 65°C, using a washing buffer [10% formamide (Sigma) in 2 × SSC] and then washed at RT with TBST. The slices were then blocked using TBST with 2% (v/v) blocking reagent (Roche) and 20% (v/v) heat inactivated sheep serum (Sigma) for 1h at RT. The slices were then stained with antibody anti-DIG (Abcam) diluted into TBST, 2% (v/v) blocking reagent, 1% sheep serum and left to incubate overnight, at 4°C. After incubation, slices were washed four times with TBST. Afterward, organoid slices were incubated twice during 10 min in 0.4M NaCl, Tris 0.1M (pH8). The incubation was then performed with Fast-red tablets substrate (Sigma) diluted in 0.4M NaCl, Tris 0.1M (pH8) for 1–3 h in the dark until the visible spots appear, and then the reaction was stopped with PTW [PBS + 0.1% (v/v) Tween-20]. Immunofluorescence staining was then performed. Images were acquired using Zeiss LSM 710 Confocal Laser Point-Scanning Microscopes and processed in ZEN 2.3 blue edition software (Zeiss).

Single Cell Calcium Imaging (SCCI)

The organoids used in calcium imaging recordings were first dissociated gently with accutase, 4–5 days before the recordings, and replated into matrigel-coated 8-well chambers Lab-TekTM Chamber Slide (ThermoFisher Scientific). Before the experiments, cells were loaded with 5 μM Fura-2 AM (Invitrogen) in Krebs solution (132 mM NaCl, 4 mM KCl, 1.4 mM MgCl2, 2.5 mM $CaCl_2$, 6 mM glucose, 10 mM HEPES, pH 7.4) for 45 min at 37°C in an incubator with 5% CO_2 and 95% atmospheric air (Silva et al., 2020). Cells were washed in Krebs solution and then mounted on an inverted microscope with epifluorescence optics (Axiovert 135TV, Zeiss). Cells were continuously perfused with Krebs solution and stimulated by applying high-potassium Krebs solution (containing 50 mM KCl, isosmotic substitution with NaCl) or 100 μM histamine. The time course of SCCI experiments was the following: 300 s baseline, stimulation with KCl from 300 to 420 s, KCl washout from 420 to 600 s, stimulation with histamine from 600 to 720 s and histamine washout from 720 to 900 s recordings. Following that, Histamine/KCl ratios were calculated using the corresponding peak values given by normalized ratios of fluorescence at 340/380 nm from image pairs acquired every 200 ms by exciting the cells at 340 and 380 nm. Mature neurons typically depict ratios below 0.8 (Agasse et al., 2008; Bernardino et al., 2013). Excitation wavelengths were changed through a high-speed switcher (Lambda DG4, Sutter Instrument, Novato, CA, United States). The emission fluorescence was recorded

at 510 nm by a cooled CCD camera (Photometrics CoolSNAP fx). Images were processed and analyzed using the software MetaFluor (Universal Imaging, West Chester, PA, United States). Regions of interest were defined randomly and manually over the cell profile.

Patch-Clamp Recordings

Organoids were first dissociated gently with accutase, 4–5 days before the recordings, and replated into glass coverslips previously coated with matrigel. Whole-cell patch-clamp recordings were visualized with an upright microscope (Zeiss Axioskop 2FS) equipped with differential interference contrast optics using a Zeiss AxioCam MRm camera and a x40 IR-Achroplan objective. During recordings, cells were continuously superfused with artificial cerebrospinal fluid (aCSF) containing 124 mM NaCl, 3 mM KCl, 1.2 mM $NaH2PO_4$, 25 mM $NaHCO_3$, 2 mM $CaCl_2$, 1 mM $MgSO_4$, and 10 mM glucose, which was continuously gassed with $95\%O_2/5\%CO_2$. Recordings were performed at room temperature in current-clamp or voltage-clamp mode [holding potential (Vh) = −70 mV] with an Axopatch 200B (Axon Instruments) amplifier (Dias et al., 2014). The step-and-hold stimulation protocol included 11 steps of 500 ms long depolarization pulses. The first injection current was −25 pA and the subsequent ones increased progressively until 225 pA.

Action potential activity was recorded using patch pipettes (4–9 MΩ resistance) pulled from borosilicate glass capillaries (1.5 mm outer diameter, 0.86 mm inner diameter, Harvard Apparatus, Holliston, MA, United States) with a PC-10 Puller (Narishige Group, London, United Kingdom) filled with an internal solution containing 125 mM K-gluconate, 11 mM KCl, 0.1 mM CaCl2, 2 mM MgCl2, 1 mM EGTA, 10 mM HEPES, 2 mM MgATP, 0.3 mM NaGTP, and 10 mM phosphocreatine, pH 7.3, adjusted with 1 M NaOH, 280–290 mOsm. Acquired signals were filtered using an in-built, 2-kHz, three-pole Bessel filter, and data were digitized at 5 kHz under control of the pCLAMP 11 software programs (Molecular Devices, San José, CA, United States). The junction potential was not compensated for, and offset potentials were nulled before gigaseal formation. The resting membrane potential was measured immediately after establishing whole cell configuration and the junction potential of the electrode was considered (−12 mV). Firing patterns of neurons were determined in current-clamp mode immediately after achieving whole-cell configuration by a series of hyperpolarizing and depolarizing steps of current injection (1 s). In the voltage-clamp mode, spontaneous miniature postsynaptic currents were recorded in a CSF solution during 5 min. Analysis of the amplitude and half-peak within were performed off line using the Clampfit 11 software. AP velocity (dV/dt) in a train of AP firing near threshold was represented from the first derivate of the first AP generated.

Lentiviral Transfection for Derivation of GFP$^+$ hiPSCs Lines

HEK 293T cells were used for lentiviral production, followed by concentration by ultra-centrifugation. Briefly, a second generation packaging system composed of three plasmids (transfer vector with expression construct LV-GFP, the packaging plasmid psPAX2, and the envelope protein expression plasmid pMD2.G – pMD2.G, a gift from Didier Trono (Addgene plasmid # 12259[1]; RRID: Addgene_12259), was mixed in a ratio of 2:1:1 in DMEM (Thermofisher Scientific) and Fugene6 transfection reagent (Roche) and 293T cells were transfected during 4 h to overnight. The supernatant from the transfected plate was collected every 24 h in serum-free conditions and concentrated by ultracentrifugation (Beckman XL-90) at 90.000 rpm for 2 h at 4°C. The concentrated viral solution was passed through a 0.45 μm low-protein binding filter and aliquots were used to transfect the hiPSCs lines. The cell lines F002.1A.13, Gibco® iPSC6.2 and EMC24i/R2 (C6) were successfully transfected, by first incubating the cells in a 24-well plate during 30 min at 37°C with E8 medium, 10 μM ROCKi and 5 μg/mL of Polybreme (Sigma). Then, LV-GFP previously dissolved in E8 was added dropwise and the cells were incubated during 1 h30 min. Culture medium was then changed daily. After cell growth and expansion, FACS sorting of GFP$^+$ cells was performed using BD FACSAria^{TM} III (BD Biosciences-US) in order to obtain pure populations.

Statistical Analysis

The data were expressed as mean of ± standard error of mean (SEM) from at least three independent n experimental replicates/differentiations, as n number of organoids analyzed or n neurons (SCCI and patch-clamp recordings). Mean differences between control cell lines and RTT lines were evaluated by two-tailed unpaired and non-parametric *t*-test. Statistical processing was performed using Microsoft Excel and GraphPad Prism Software. Statistical significance level was set for (*) *p*-values < 0.05; (**) *p*-values < 0.01; (***) *p*-values < 0.001. The statistical details of experiments are also present in the figure legends.

Data Availability

The authors declare that all raw data presented in all the figures of the manuscripts that support the findings of this study are available from the corresponding author upon request.

RESULTS

MeCP2:R255X Dorsal Forebrain Organoids Reveal Premature Formation of Cortical Plate Neurons

Glutamatergic pyramidal neurons arise mainly from progenitors in the dorsal region of the forebrain (the pallium), specifically from radial glial cells (RGs), found in the VZ, and from outer radial glial cells (oRGs) and intermediate progenitors (IPs), found in the subventricular zone (SVZ) (Lui et al., 2011). For modeling RTT-derived alterations in the process of neurogenesis in the dorsal forebrain, we engineered organoids

[1]http://n2t.net/addgene:12259

resembling this brain region. Dorsal organoids were generated from four distinct female and male healthy control hiPSCs and two patient-specific RTT hiPSC lines (female MeCP2:R255X and male MeCP2:Q83X). It is known that, in females, random inactivation of the X-chromosome occurs during development (Balachandar et al., 2016). Therefore, as *MeCP2* gene is located in the long arm of the X chromosome, RTT female patients are characterized by the presence of somatic mosaicism. Since female hiPSCs retain an inactive X-chromosome in a non-random pattern (Tchieu et al., 2010), it was possible to obtain an isogenic control (IC-MeCP2:R255X) from a distinct clone isolated upon reprogramming of the mosaic female cell line (**Supplementary Figure 1.1A**). Upon differentiation, IC cells exhibited only the non-mutated *MeCP2* active X-chromosome. The presence/absence of the mutations was confirmed by Sanger sequencing of gDNA and cDNA (**Supplementary Figure 1.1B**). The pluripotent phenotype of the IC and female and male RTT hiPSC lines was confirmed by flow cytometry (**Supplementary Figure 1.1C**).

The dorsal forebrain organoids were generated according to the dual-SMAD inhibition protocol and cultured until day 41 by adapting previously described methodologies (Qian et al., 2016) (**Figure 1A**). As an important modification, hiPSCs were cultured in Aggrewell^{TM} 800 plates during the 5 days of neural induction (Miranda et al., 2015, 2016, 2018). This strategy allowed the generation of size-controlled aggregates, with a narrow size-distribution (diameter 250–300 μm) (**Supplementary Figure 1.1D**), allowing a more homogeneous feeding of soluble factors across the aggregate. At day 13 of dorsal induction, histological analysis of organoid cryosections, revealed the presence of cells expressing the forebrain specific progenitor marker OTX1/2 in all dorsal organoids (see **Supplementary Figure 1.1E**). Moreover, the formation of SOX2$^+$/NCAD$^+$ neural rosette-like structures, resembling the neural tube, was also observed (see **Supplementary Figure 1.1F**). All dorsal organoids revealed the presence of SOX2+ progenitor cells, resembling the proliferative regions of the human VZ. In addition, the rosette structures exhibited the cadherins junction marker N-CAD, located at the luminal side (see **Supplementary Figure 1.1F**).

To further confirm the dorsal identity of these organoids, we examined the mRNA expression levels of dorsal, ventral and pluripotency markers at day 41 of differentiation by qRT-PCR (**Figures 1B,C**). Expression of *FOXG1* was observed in all organoids, confirming their forebrain identity. The ventral layer markers, *DLX2, NKX2.1* and *LHX6*, and the pluripotency marker *NANOG*, were almost undetectable. It was also detected a high expression of the neural progenitor dorsal-cortical marker *PAX6*, and of *TBR1*, a marker typically expressed in neurons of deep cortical layer VI (Hevner et al., 2001). No significant differences were found when comparing the mRNA levels of the male-RTT organoids with the ones of the control organoids. For this reason, we focused our subsequent analyzes on the RTT female cell line, the respective IC and the healthy-controls. Interestingly, female RTT dorsal organoids exhibited a statistically significant higher expression of *TBR1* (see **Figure 1Ei**) when compared with the IC and healthy-control dorsal organoids, and a statistically significant lower expression of *PAX6* (see **Supplementary Figure 1.2A**) when compared to the healthy-control organoids. A specific oRG cells marker, HOPX, was used to verify the presence of a prominent oRGC-like population (Qian et al., 2016). On **Supplementary Figure 1.2B**, by immunocytochemistry, it was possible to observe the presence of that progenitor layer, which is characteristic of human cortical development. However, a narrower expression pattern was detected for the Rett female cell line organoids in comparison to control organoids. Moreover, immunocytochemistry analysis of organoid sections showed that control organoids developed a well-defined TBR2$^+$ IP cell region, confirming the presence of a SVZ layer, an important hallmark of human cerebral cortex development. Conversely, female RTT dorsal organoids lacked SVZ formation, as observed by the absence of TBR2$^+$/SOX2$^+$ cells (**Supplementary Figure 1.2C**). In line with this observation, quantification of the number of TBR2$^+$ cell nuclei confirmed the presence of these progenitor cells in healthy-control (16 ± 4%) and IC (18 ± 2%) organoids and the almost complete absence of these cells in female RTT organoids (**Supplementary Figure 1.2D**). We further detected that TBR1 was mainly expressed superficially to the progenitor SOX2$^+$ VZ-like layer (**Figure 1D**). Importantly, TBR1 protein was expressed in a higher percentage of cells in the female RTT organoids (41 ± 5%), when compared with the healthy-control (21 ± 3%) and with the IC (22 ± 4%) organoids (**Figure 1Eii**). Furthermore, RTT female organoids exhibited the presence of CTIP2$^+$ cells, indicating the specification of a deep cortical plate layer, which at this time-point is not yet observed in healthy-control and IC organoids (**Figure 1D**).

Overall, dorsal forebrain organoids derived from the RTT mutant female hiPSCs revealed a higher expression and premature formation of newborn deep-layer cortical neurons, in parallel with a depletion of IP cells and a decrease in the number of oRG cells. These results suggest that for the hiPSC lines exhibiting the MeCP2:R255X mutation, molecular and structural alterations start to occur early in development, during the process of formation of cortical layers in dorsal forebrain consistent with a premature neuronal differentiation process.

Premature Differentiation in MeCP2:R255X Dorsal Organoids

Considering the imbalance in the neurogenesis process revealed by the female RTT dorsal forebrain organoids, we next questioned which neurodevelopmental processes could be responsible and/or affected by this phenomenon. Quantitative analysis of the thickness of the early born TUJ1$^+$ neuronal layer (schematic view in **Figure 2A**), localized above the SOX2$^+$ VZ layer apical region, revealed a significant increase in RTT female organoids (39.03 ± 3.35 μm) in comparison with healthy-control (27.71 ± 2.87 μm) and IC organoids (24.22 ± 2.10 μm) (**Figures 2B,C**). Moreover, flow cytometry analysis revealed a significantly lower percentage of KI67$^+$ proliferative cells in female RTT dorsal organoids (24 ± 1%) in comparison with the control (37 ± 4%) and the IC organoids (35 ± 8%) (**Figure 2E** and **Supplementary Figure 2C**). In agreement with these results,

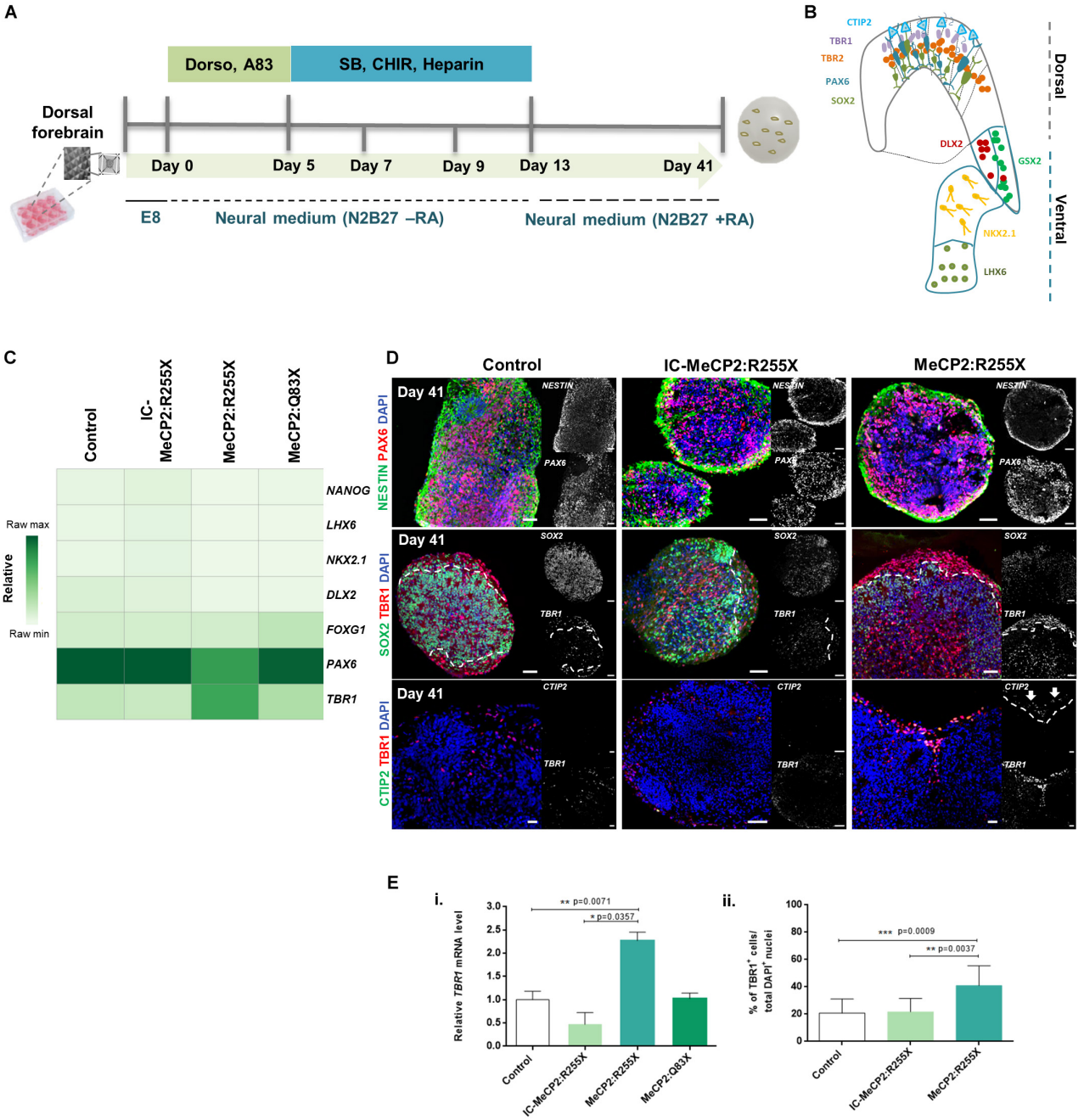

FIGURE 1 | Dorsal forebrain organoids derived from RTT-specific hiPSCs reveal a premature formation of the cortical plate. **(A)** Schematic overview of the protocol for dorsal forebrain organoid development until day 41 of differentiation. **(B)** Schematic overview of the two forebrain regions of the mammalian cortex presenting the characteristic markers/populations for dorsal and ventral regions. **(C)** Transcriptional profile of dorsal forebrain organoids at day 41 of differentiation. Quantitative RT-PCR analysis of the pluripotency marker *NANOG*, the forebrain ventral characteristic markers *LHX6, NKX2.1* and *DLX2*, the generic forebrain marker *FOXG1* and the dorsal characteristic markers *PAX6* and *TBR1*. All values were normalized and relative to *GAPDH*. Raw minimum (min) and raw maximum (max) values were taken as a reference for heatmap representation. (n = independent experiments. Control $n = 10$; IC $n = 5$; MeCP2:R255X $n = 4$; MeCP2:Q83X $n = 4$). **(D)** Immunofluorescence characterization of dorsal organoids at day 41. Representative images of dorsal organoid sections were stained against PAX6, NESTIN and SOX2 (neural progenitor markers), TBR1 (marker for new-born neurons of the deep cortical layer VI), and CTIP2 (marker for neurons of deep cortical layer V). Scale bars, 50 μm. **(E) (i)** Relative mRNA levels of *TBR1* on dorsal organoids at day 41 of differentiation already represented on the heatmap **(C)**. mRNA levels relative to *GAPDH* and normalized to control condition. n = independent experiments; Control $n = 10$; WT-MeCP2:R255X $n = 5$; MeCP2:R255X $n = 4$; MeCP2:Q83X $n = 4$. For all graphics depicted, Student's t-test (two-tailed) statistics, was applied $^{*}p < 0.05$, $^{**}p < 0.01$, $^{***}p < 0.001$; error bars represent SEM. **(ii)** Immunocytochemistry quantification of the percentage (%) of cells expressing TBR1 normalized to the total number of cells stained with DAPI. TBR1: Control $n = 3$ (12 organoids); IC-MeCP2:R255X $n = 3$ (8 organoids); MeCP2:R255X $n = 3$ (10 organoids). n = independent experiments. For all graphics depicted, Student's t-test (two-tailed) statistics, was applied $^{*}p < 0.05$, $^{**}p < 0.01$, $^{***}p < 0.001$; error bars represent SEM.

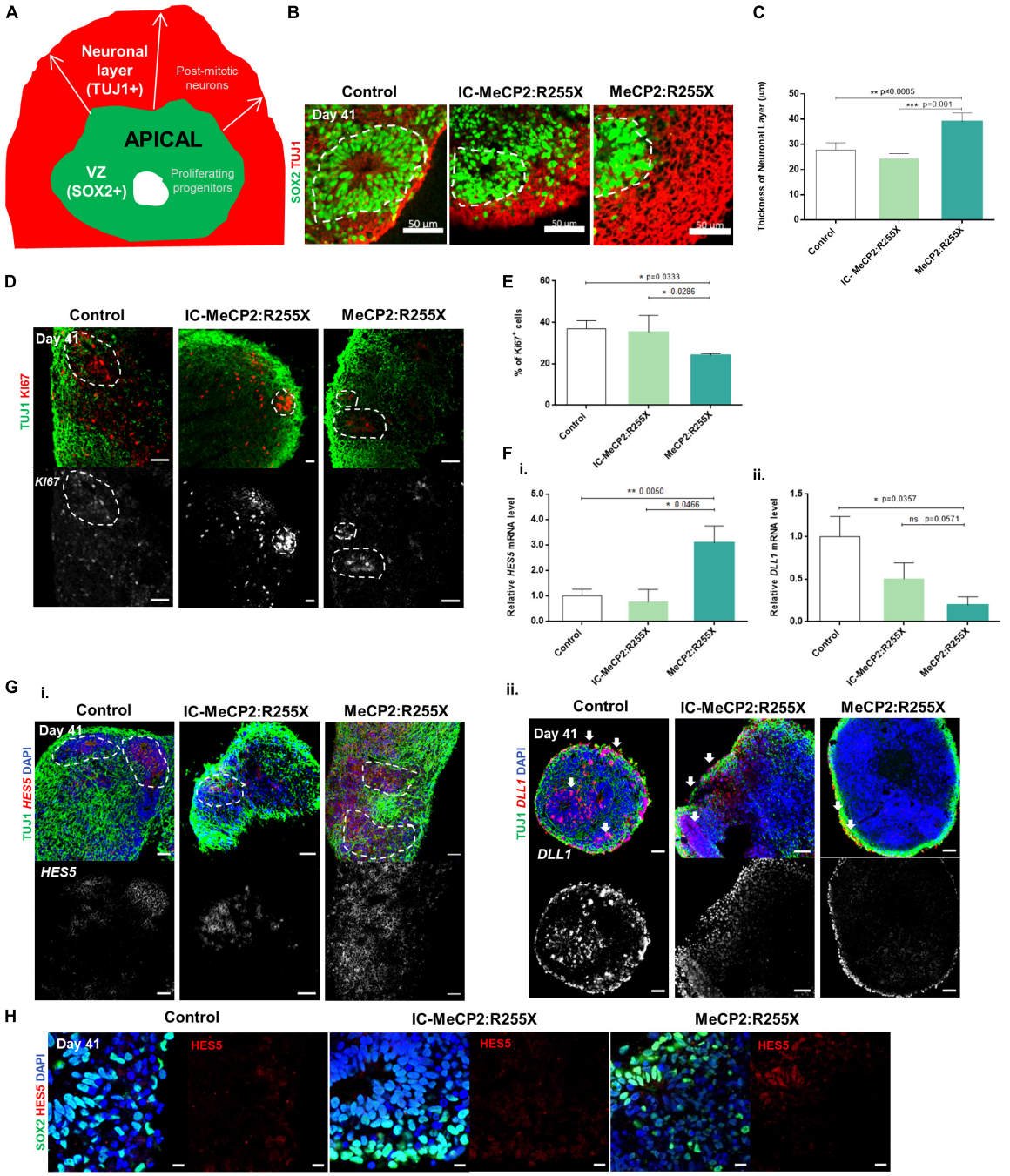

FIGURE 2 | Altered proliferation pattern and dynamics of expression of Notch signaling operands *HES5* and *DLL1* during differentiation of RTT female patient-derived dorsal organoids. **(A)** Schematic representation of SOX2^{+} ventricular zone (VZ) and TUJ1^{+} neuronal layer measurement in cortical structures. For each cortical structure, three measurements were taken for the post-mitotic neuronal zone. **(B)** Representative images of the VZ delineated by white dashes and the neuronal layer containing TUJ1^{+} cells at day 41. Scale bars, 50 µm. **(C)** Mean value of the thicknesses of the neuronal zone layer (µm). Three measurements were performed for each zone in each structure. (n = independent experiments; healthy control: $n = 10$ and 19 cortical structures from at least 10 individual organoids; IC-MeCP2:R255X: $n = 5$ and 14 cortical structures from at least 10 individual organoids; MeCP2:R255X: $n = 4$ and 25 cortical structures from at least 10 individual organoids). **(D)** Representative immunofluorescence images of KI67 proliferative marker and TUJ1^{+} neuronal marker at day 41. Scale bars, 50 µm. **(E)** Quantification of the% of KI67^{+} cells as determined by flow cytometry analysis. **(F)** qRT-PCR analysis of the expression of **(i)** the Notch target and the transcription repressor of proneuronal genes *HES5* (days 41) and **(ii)** the Notch ligand *DLL1* (day 41). mRNA levels relative to *GAPDH* and normalized to the control condition. (n = independent experiments; WT: $n = 6$; IC-MeCP2:R255X: $n = 4$; MeCP2:R255X: $n = 3$). **(G)** Representative images of *in situ* hybridization of **(i)** *HES5* and **(ii)** *DLL1* as RNA probes and their co-localization with TUJ1 performed by Immunofluorescence. Scale bars, 50 µm. **(H)** Representative immunofluorescence images of HES5 staining and the co-localization with the progenitor marker SOX2. Scale bars, 10 µm. For all graphics depicted, Student's t-test (two-tailed) statistics, was applied $^{*}p < 0.05$, $^{**}p < 0.01$, $^{***}p < 0.001$; error bars represent SEM.

histological sections of dorsal organoids revealed the presence of KI67$^+$ cells in control and IC organoids, mainly located near the apical surface of VZ-area, whereas a lower number of these cells were observed in RTT organoids (**Figure 2D**). We also examined cell death by apoptosis as a potential mechanism for the undetectable IP cell pool in female RTT organoids by quantifying the cells expressing cleaved (active) caspase-3 (CAS3). However, this analysis revealed the presence of rare apoptotic cells, at day 41, for all the organoids (**Supplementary Figures 2A,B**). Altogether, these results suggest a possible imbalance in the generation of differentiating neurons in RTT organoids, with premature exhaustion of proliferating progenitor pool and increase in the number of newborn neurons.

Notch signaling regulates the generation and maintenance of several cell types, including cells from the SVZ, outer SVZ and cortical plate (Kageyama et al., 2008). To elucidate the molecular mechanisms by which MeCP2:R255X mutation may influence the premature transition toward neuronal differentiation, we examined mRNA levels at day 41 of the Notch ligand Deltalike1 (*DLL1*) and of the Hes family basic helix-loop-helix factor 5 (*HES5*), a direct downstream target of Notch. The levels of *HES5* mRNA were found significantly increased for the female RTT dorsal organoids when compared with the healthy-controls, and increased in comparison to the IC organoids (**Figure 2Fi**). On the other hand, it was observed a significant decrease in the expression of *DLL1* in MeCP2:R255X organoids (**Figure 2Fii**). The premature formation of post-mitotic neurons can be related with the dynamics of gene expression of Notch operands that regulates, both cell-autonomously and cell-non-autonomously, the time-transitions of progenitor cells into differentiated neural cells (Kageyama et al., 2008). Thus, for better understanding the levels of gene expression of Notch signaling ligands and targets, we performed *in situ* hybridizations at day 41, co-localized with immunostaining for TUJ1$^+$ neurons and SOX2$^+$ progenitors. In healthy-controls and IC organoids the expression of the Notch ligand *DLL1* is observed in the TUJ1$^+$ neuronal cell layer, and also in scattered progenitors (**Figure 2Gii**). On the other hand, in female RTT organoids, *DLL1* expression is reduced, being expressed exclusively in TUJ1$^+$ post-mitotic neurons (**Figure 2Gii**). Furthermore, *HES5* expression is found only in PAX6$^+$ progenitor cells (**Supplementary Figure 2D**), and not in the post-mitotic TUJ1$^+$ neurons (**Figure 2Gi**), as it would be expected. Moreover, the expression of the HES5 protein is also higher in the female RTT organoids when compared with controls (**Figure 2H**). Altogether, these results suggest a possible deregulation of the Notch signaling in MeCP2:R255X organoids, during the stage of deep cortical layer formation.

MeCP2:R255X Neurons Exhibit Altered Intracellular Calcium Dynamics and Functional Neural Network

The functionality of mature neurons derived from dorsal organoids, generated from healthy-controls, IC and RTT female hiPSC lines, was characterized using single cell calcium imaging (SCCI) and whole-cell patch-clamp analysis (Silva et al., 2020). SCCI analysis was used for functional discrimination of the organoid populations in terms of expression/sensitivity of voltage sensitive calcium channels (VSCC) and for testing their responsiveness to depolarization. Functional recordings of SCCI were performed at days 44–47 and at days 64–67, during which time cultures were maintained in serum-free BrainPhys^{TM} medium (Satir et al., 2020) (**Supplementary Figure 3A**). Dorsal organoids were preloaded with the calcium indicator Fura-2AM on the day of the experiment. Cells were then exposed to 50 mM of KCL, which in excitable cells, like neurons, leads to the opening of VSCCs and a massive influx of calcium, followed by stimulation with Histamine, which leads to an increase in intracellular calcium concentration in stem/progenitor cells due to the activation of H1 receptor (Molina-Hernández and Velasco, 2008). **Figure 3A** shows representative peaks of SCCI for replated organoids obtained during KCL and Histamine stimulation. Histamine/KCl ratios for mature neurons are typically below 0.8 (Agasse et al., 2008; Bernardino et al., 2013). Between days 44–47, female RTT organoids contained 74 $\pm$ 7% of cells behaving like neurons, while the mean percentage of neurons present in healthy-controls and IC organoids was 48 $\pm$ 7% and 48 $\pm$ 8%, respectively. At later time points, between days 64 and 67, an expected maturation was observed in healthy-controls and IC organoids, with 62 $\pm$ 11% and 57 $\pm$ 8% of cells presenting a neuron-like response, respectively (**Figure 3B**). However, MeCP2:R255X organoids displayed a significant decrease in the percentage of cells with neuron-like response in comparison with days 44–47 of differentiation, and also in comparison with control organoids. Immunostaining analysis revealed that, on days 44–47, female RTT organoids exhibited denser TUJ1$^+$ neuronal networks compared with IC and healthy controls and on days 64–67, MeCP2:R255X neurons showed punctate MAP2 staining (**Figure 3A**). Nevertheless, from days 44–47 to 64–67, this culture showed a significant increase of cells not responsive to KCL neither to Histamine (**Figure 3C**). Thus, altogether, these results indicate that prematurely differentiated MeCP2:R255X neurons might not be able to complete their functional maturation.

Functional maturation of dorsal organoids was also assessed by whole-cell patch-clamp, at days 44–47. For the healthy-control organoids, a total of 8 cells were analyzed, with 50% of the cells being able to respond to a continuous current injection, demonstrating a typical repetitive neuronal firing action potential (AP) (**Figures 3D,E**). For the IC organoids, from a total of 9 cells analyzed, 88% presented a typical firing AP. However, for the MeCP2:R255X organoids, from a total of 11 cells, 45% exhibited an atypical firing AP, with a decreased firing frequency (**Supplementary Figure 3Bi**) and with most of the neurons presenting an abortive-like AP (**Figures 3D,E**). Overall, the majority of control neurons exhibited more mature AP firing properties, presenting a faster and consistent AP velocity near threshold (dV/dt), while MeCP2:R255X neurons were more immature, presenting a reduced AP velocity (**Figure 3G**).

Additionally, from the analysis of spiking cells, a significant reduction in AP amplitude was observed for MeCP2:R255X organoids when compared with IC, and also when compared with the healthy-control neurons (**Figure 3Fi**). As shown in **Figure 3Fii**, the half-peak width of female RTT neurons was

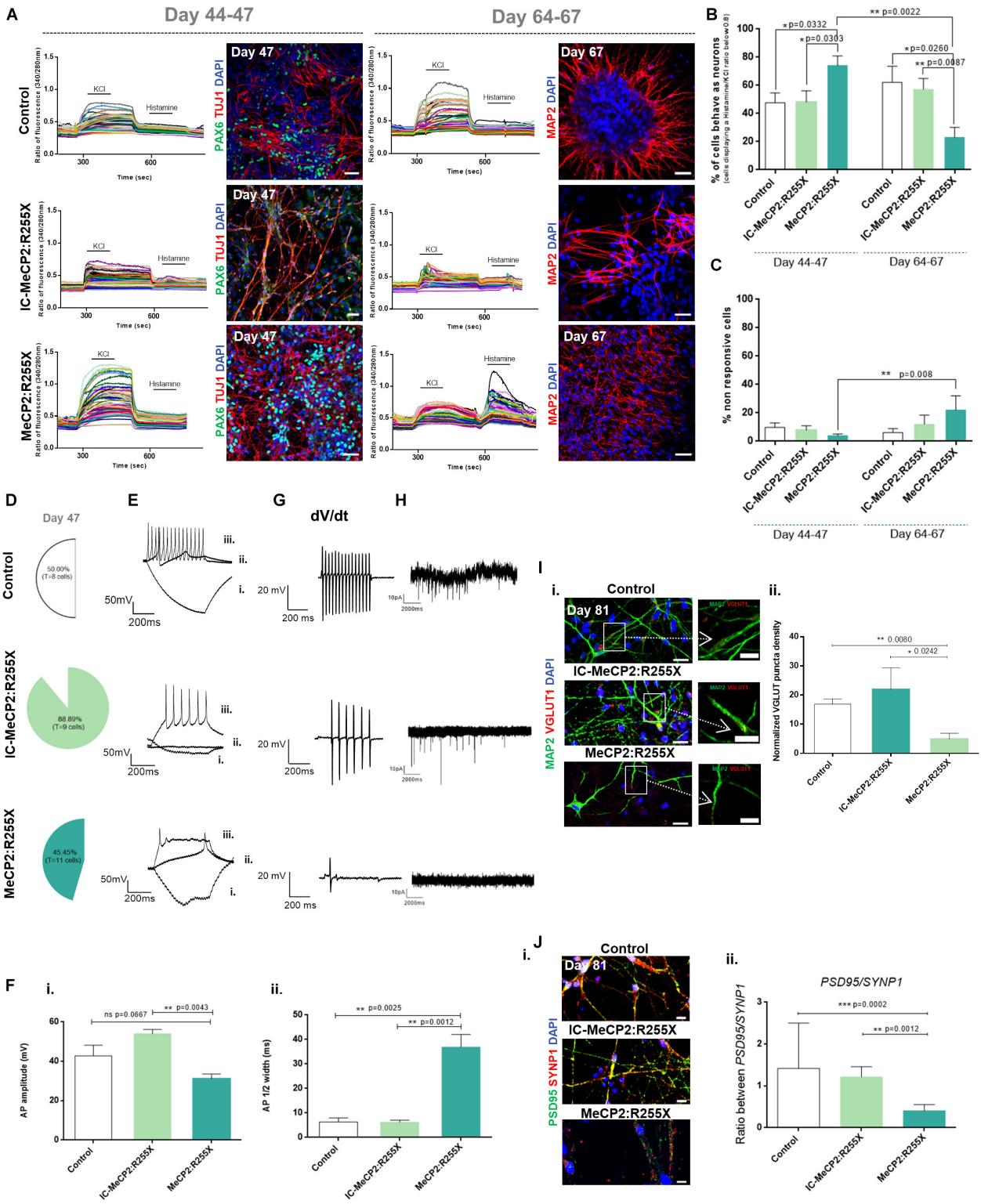

FIGURE 3 | Functional analysis of dorsal forebrain organoids during maturation. **(A–C)** Single cell calcium imaging (SCCI) of dorsal organoids. **(A)** Representative fluorescence ratio profiles (left) of individual cells on days 44–47 and 64–67. Representative immunofluorescence images (right) for the neural progenitor marker PAX6 and for the new-born neuronal marker TUJ1 on days 44–47 and for the mature neuronal marker MAP2 on days 64–67. Immunofluorescence analysis was performed by using the cultures previously analyzed by SCCI. Scale bar 50 μm; **(B)** Percentage of cells displaying a Histamine/KCl ratio below 0.8, which is indicative of the% of cells functionally behaving like neurons. **(C)** Percentage of cells that neither respond to histamine neither to KCL. Total number of cells analyzed

(Continued)

FIGURE 3 | Continued
(n = independent experiments): Control: $n = 6$ with 618 cells analyzed at day 44–47 and 407 cells analyzed at days 64–67; IC-MeCP2:R255X: $n = 4$ with 358 cells analyzed at days 44–47 and 271 cells analyzed at days 64–67; MeCP2:R255X: $n = 3$ with 461 cells analyzed at day 44–47 and 415 analyzed at days 64–67. **(D–G)** Patch-clamp recordings of single cells at day 47. **(D)** Percentage of cells depicting at least one firing action potential (AP). **(E)** Representative traces of firing responses evoked under current-clamp mode by injection of a 500 ms current pulse [–25 **(i)** to +275 pA in 25-pA increments **(ii,iii)** from an initial holding potential (Vh) of –70 mV]. Scale bars correspond to 50 pA and 200 ms. **(F) (i)** AP amplitudes measured from the first AP depicted; **(ii)** Half-peak width measured from the first AP depicted. **(G)** Representative views of the AP velocity firing near threshold (dV/dt). Scale bars correspond to 20 pA and 200 ms. **(H)** Representative recordings of spontaneous postsynaptic currents. Scale bars correspond to 10 pA and 2000 ms. **(I) (i)** Representative immunofluorescence images of 4–5 days-old replated organoid cultures stained for VGLUT1 and MAP2. Scale bar 20 μm. Representative amplification of neurons showing VGLUT1 puncta on MAP2 neurites. Scale bar 10 μm. **(ii)** Normalized density of VGLUT1 pre-synaptic puncta. n = independent experiments; Control: $n = 7$; IC-MeCP2:R255X: $n = 4$; MeCP2:R255X: $n = 6$. **(J) (i)** Immunofluorescence images of PSD95 and SYNP1. The overlap between PSD95 and SYNP1 (yellow) indicate sites of synaptogenesis. Scale bar 10 μm. **(ii)** PSD95/SYNP1 ratio measured from immunofluorescence images. For all graphics depicted, Student's t-test (two-tailed) statistics was applied: $^{*}p < 0.05$, $^{**}p < 0.01$, $^{***}p < 0.001$; error bars represent SEM.

significantly larger when compared with that of the control neurons. In spiking cells, the resting membrane potential values were similar for all the neuronal cells analyzed (**Supplementary Figure 3Bii**). At later time points of maturation, by day 81, healthy-control neurons presented an increase in spiking activity, whereas for the MeCP2:R255X neurons, none of the 8 cells analyzed presented firing AP (see **Supplementary Figures 3C,D**). Moreover, spontaneous currents, which provide an indication of the presence of functional neurotransmitter receptors, were also recorded. The representative traces indicate the absence of synaptic transmission for MeCP2:R255X organoids and the establishment of some neuronal functional connections for both the control and the IC-derived neurons (**Figure 3H**).

Neurons from dorsal organoids were also characterized concerning the expressing of characteristic markers of mature neurons. A higher mRNA expression of the vesicular glutamate transporter marker VGLUT1 was observed at day 81 in MeCP2:R255X organoids when compared with all control neurons (**Supplementary Figure 3E**), with VGLUT1 puncta being observed in MAP2+ dendrites (**Figure 3Ii**). However, a reduction in the density of VGLUT1 puncta was observed in MeCP2:R255X organoids when compared with control and IC organoids (**Figure 3Iii**).

Furthermore, cells were stained for the pre-synaptic protein synapsin-1, SYNP1, and the post-synaptic-protein PSD95 and the PSD95/SYNP1 ratio was found to be significantly lower for RTT organoids, which could indicate a decreased synaptic density (**Figure 3Jii**). Additionally, the co-localization of these two indicators of mature excitatory synapses was observed in healthy-control and IC organoids but not in female RTT neurons (**Figure 3Ji**). Interestingly, we observed the presence of $GFAP^{+}$ astrocytes in close association with neurons in all the dorsal organoids at day 81 (**Supplementary Figure 3F**).

$Ca2^{+}$ diffusion and synaptic transmission have been correlated with spine morphology, which changes during developmental maturation (Risher et al., 2014). As MeCP2 has been proved to be essential for dendritic spine formation, the spine head width and neck length of neurons in dorsal organoids were measured at days 47 and 67. The proportion of mushroom and stubby spines, which increases with spine complexity and maturation, was found to decrease along the differentiation for the female RTT organoids, which instead presented an increase in the number of filopodia and long thin spine types. Conversely, an increased number of more mature branched spines were observed in all control neurons (see **Supplementary Figures 3G,H**).

Taken together, these results indicate that healthy-control and IC dorsal organoids supported the generation of functional neurons, by establishing neuronal connectivity, while MeCP2:R255X organoids present defects in neuronal maturation.

Impaired Interneuron Migration in RTT Forebrain Organoids

Ventral cortical organoids were generated from all hiPSC lines and cultured until day 81 (**Figure 4A**). Neural induction was performed by dual-SMAD inhibition followed by activation of the sonic hedgehog (SHH)-signaling pathway, as previously described (Bagley et al., 2017). The ventral identity of organoids was assessed by qRT-PCR analysis at day 41 (**Figure 4B**). The mRNA expression of typical dorsal markers, *TBR1* and *PAX6,* and of the pluripotency marker *NANOG* was almost undetectable. The ventral marker *DLX2* was expressed at low levels, accompanied with high expression of the forebrain marker *FOXG1* (**Figure 4B**). qRT-PCR was also used to characterize the expression of the different interneuron progenitor's subtypes that are produced in specific subregions of the ganglionic eminence (GE) zone of the ventral forebrain (Gelman et al., 2012). *NKX2.1*, which is expressed in the MGE (Sandberg et al., 2016) and from which several ventral interneuron subtypes are generated, was found highly expressed in our ventral organoids. The mRNA levels of *LHX6*, expressed in a sub-region of MGE that also originates ventral interneuron subtypes, was also found increased in ventral organoids, with no significant differences being found between controls and RTT organoids (**Figure 4B**). Importantly, at day 41, RTT cells showed a significant decrease in mRNA levels for the *NKX2.1* gene when compared with the healthy control cells, and a tendency for a decreased expression of this marker in comparison with the IC organoids (**Supplementary Figure 4A**). Again, no significant differences were observed between male ventral RTT organoids and the respective healthy controls, so we decided to proceed with a detailed analysis for the RTT female cell line.

MGE-derived post-mitotic interneurons migrate toward the dorsal cortex region, integrating into an appropriate

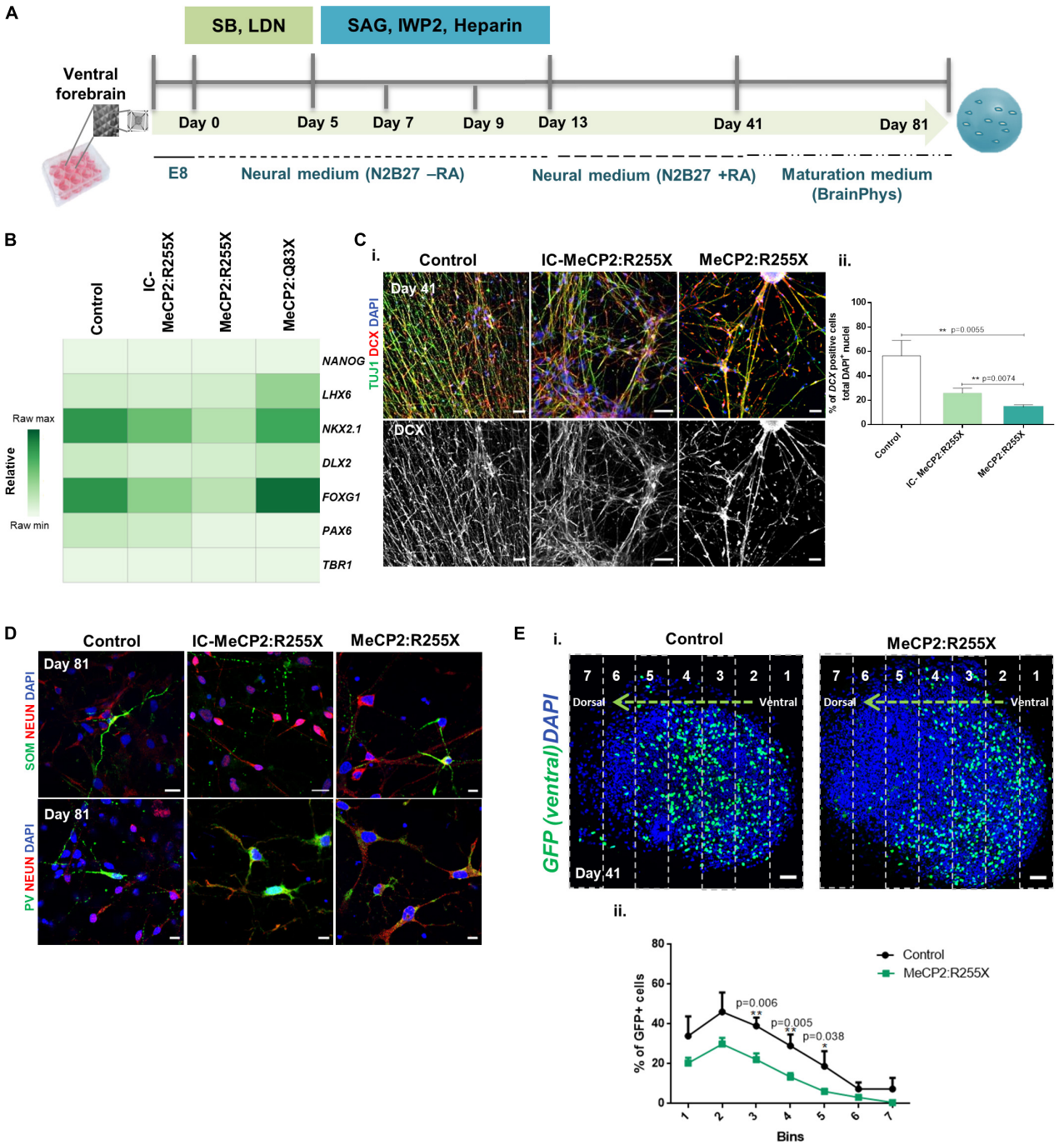

FIGURE 4 | Ventral and fused forebrain organoids derived from the female patient-specific RTT hiPSC line reveal impairments in cell migration. **(A)** Schematic overview of the protocol for ventral patterning of hiPSCs until day 81 of culture. **(B)** Transcription profile of ventral forebrain organoids at day 41 of differentiation. Quantitative RT-PCR analysis for the pluripotency marker *NANOG*, the forebrain ventral markers *LHX6, NKX2.1* and *DLX2*, the generic forebrain marker *FOXG1* and the dorsal markers *PAX6* and *TBR1*. All values were normalized to *GAPDH*. Raw minimum (min) and raw maximum (max) values were taken as a reference for the heatmap representation. *n* = independent experiments; Control: *n* = 11; IC-MeCP2:R255X: *n* = 4; MeCP2:R255X: *n* = 4; MeCP2:Q83X: *n* = 5. **(C) (i)** Immunofluorescence images of replated ventral organoids stained for DCX and TUJ1 (images used for DCX count). Scale bar 50 μm **(ii)** Percentage of DCX^+ immature migrating interneurons relative to total $DAPI^+$ nuclei. *n* = independent experiments; Control: *n* = 3 (5 images); IC-MeCP2:R255X: *n* = 3 (9 images); MeCP2:R255X: *n* = 3 (11 images). **(D)** Immunofluorescence staining of replated ventral organoids for markers of MGE-derived GABAergic neurons, PV and SOM, with the mature neuronal marker NEUN. Scale bar 10 μm. **(E) (i)** Fused organoids (GFP^- dorsal organoids fused with GFP^+ ventral organoids) stained with DAPI. Images were divided into 7 segments, the % of GFP^+ cells was analyzed in each segment and normalized to the $DAPI^+$ nuclei. Scale bar 50 μm **(ii)** Migration distance for GFP^+ cells in MeCP2:R255X derived-fused organoids. Control (9 organoids); MeCP2:R255X (9 organoids). For all graphics depicted, Student's *t*-test (two-tailed) statistics, was applied $^*p < 0.05$, $^{**}p < 0.01$; error bars represent SEM.

neuronal circuit (Zimmer-bensch, 2018). To investigate potential alterations to this process in female RTT ventral organoids, the expression of DCX, a marker for immature migrating interneurons, was quantified at day 41. Interestingly, the expression levels for DCX were significantly decreased in the ventral female RTT organoids, when compared with all control organoids (**Figures 4Ci,ii**). It is also known that the large majority of neurons produced in the MGE region express parvalbumin (PV) and somatostatin (SOM) (Gelman et al., 2012). The presence of SOM^+ and PV^+ interneurons at day 81 was indeed detected in all our ventral organoids (**Figure 4D**). The possible alteration in the generation of *NKX2.1*$^+$ interneuron progenitors and the observed DCX decrease could consequently induce changes in the interneuron migratory dynamics. To evaluate this hypothesis, we employed a more complex system, obtained by assembling organoids of dorsal and ventral forebrain identities (Bagley et al., 2017; Xiang et al., 2017) (**Supplementary Figure 4B**). Upon characterization of the fused organoids at day 41, we found the same molecular alterations previously observed in independently generated dorsal and ventral organoids regarding the expression of *TBR1* and *NKX2.1* (see **Supplementary Figures 4Ci,ii**). To follow the process of interneuron migration, the MECP2:R255X and two control cell lines were induced to express GFP by lentiviral transfection. To test whether interneurons from the ventral region could migrate, the ventral patterning protocol using the GFP^+ reporter line and the dorsal patterning protocol using the GFP^- cell line were employed. The assembly of both organoid types was then performed at day 13, with merged organoids being observed already by day 14 (**Supplementary Figure 4D**). Finally, we analyzed migrating GFP^+ cells at day 41 in organoid cryosections. Interestingly, it could be observed that the GFP^+ ventral cells in MECP2:R255X fused organoids migrated shorter distances than GFP^+ cells from healthy-control hiPSCs (**Figures 4Ei,ii**). These fused organoids derived from the controls and MECP2:R255X lines were later characterized, at day 81, by immunostaining. It was found that they contained cells expressing MAP2 and the astrocyte marker GFAP (**Supplementary Figure 4Ei**), as well as the mature glutamatergic pyramidal neuronal marker VGLUT1 and the GABAergic interneuron marker VGAT (**Supplementary Figure 4Eii**.).

DISCUSSION

Herein, hiPSCs derived from RTT patients were used to model the development of the human forebrain by using region-specific and assembled forebrain organoids. Several aspects were studied, including the formation of the neuroepithelial layers, their intrinsic cellular diversity and the neuronal network functionality. In contrast with the majority of MeCP2 gene-KO mice and hiPSCs-based RTT models, we developed 3D models presenting phenotypical characteristics of RTT caused by the female MeCP2:R255X mutation and the male MeCP2:Q83X mutation, present in the human population.

First, we developed organoids exhibiting the main molecular developing features of the dorsal forebrain domain. MeCP2:R255X dorsal organoids displayed an increase in gene and protein expression for the TBR1 marker, present in glutamatergic post-mitotic neurons in the cortical subplate (Englund et al., 2005). Our data also indicate a lack of $TBR2^+$ IPs in these organoids that might be caused by the increased levels of TBR1. In fact, TBR2 downregulation occurs upon upregulation of TBR1, and upon formation of early born neurons that migrate through the inner zone into the cortical plate (Englund et al., 2005). Importantly, mouse models showing *TBR2* downregulation have been associated to microcephaly (Arnold et al., 2008), with the decreased brain volume accompanied by increased neuronal density, a feature also reported in RTT patients (Schanen et al., 2004) and RTT mouse models (Chen et al., 2001). Consistently, our results show a clear correlation between the formation of the early post-mitotic cortical deeper layers and an increase in neuronal layer thickness, and a decrease of $KI67^+$ proliferative cells. Additionally, a decreased expression of PAX6 mRNA and a lower number of $HOPX^+$ oRG cells observed could be a possible evidence of the imbalance between neuronal differentiation and maintenance of the progenitor pool.

Our RTT male dorsal organoids did not reveal the same initial phenotypic alterations observed in the female ones, further demonstrating the potential capacity of our models to highlight mutation-dependent alterations in the differentiation/proliferation equilibrium.

In line with our findings, Li et al. (2014) found that mutant-*MeCP2* serine 421 phosphorylation in progenitor cells, isolated from adult mouse hippocampus, displayed an imbalance between proliferation and neuronal differentiation, and that this imbalance was mediated by alterations of the Notch signaling pathway (Li et al., 2014). Moreover, *Edri et al.* verified that neurons populating the cortical deep layers are generated from RG progenitors in a Notch-dependent manner. It was also shown that early progenitor stages require Notch activation to generate early appearing neurons (Edri et al., 2015). Our data shows that the premature appearance of deep cortical neurons observed in MeCP2:R255X dorsal organoids is associated to *HES5* overexpression, which points to the hypothesis that the observed premature differentiation may be a consequence of alterations of the Notch regulatory mechanism. In fact, Notch ligands, effectors and pro-neuronal genes are expressed in an oscillatory, dynamic and site-specific manner in the developing mammalian nervous system (Kobayashi and Kageyama, 2010; Kageyama, 2011). In line with our observations, Bansod et al. (2017) demonstrated that *Hes5*-overexpression in mice induced the early shift from deep to superficial layer neurogenesis and regulated the timing of neurogenesis. As an alternative hypothesis, a regulatory mechanism known as lateral inhibition, which is responsible for the proper maintenance of the pool of neural progenitors during neurogenesis, may be altered. Under normal circumstances, the newborn neurons express the Notch ligand *DLL1*, activating the Notch signaling in the neighboring cells, thus inhibiting their neuronal differentiation (Kageyama et al., 2008). However, when this pathway is deregulated, neural progenitors prematurely differentiate into early born

neurons. As the mRNA levels of the Notch ligand *DLL1* were decreased in our RTT female organoids, the premature formation of post-mitotic neurons in these organoids could indicate a deregulation of Notch signaling pathway, more precisely the mechanistic process of lateral inhibition. In fact, the previously mentioned report from Li et al. (2014) also demonstrated that phosphor-mutant MeCP2 protein has altered promoter occupancy at the promoters of *DLL1*, decreasing the levels of transcription of this Notch ligand (Li et al., 2014). Future studies should be performed to confirm our hypothesis of alterations of the Notch signaling lateral inhibition pathway driven by the MeCP2:R255X mutation.

We also studied the impact of mutated *MeCP2* in regulating neural function and activity in dorsal forebrain organoids namely by performing SSCI and patch-clamp analysis. Organoid slices have been commonly used by others (Xiang et al., 2017) for this type of studies namely because this method allows the preservation of the original cell to cell interactions and the maintenance of the 3D organization in the selected part of the slice. However, in the case of our approach, the 3D organoids were dissociated and replated 4–5 days before the analysis because we believe that analyzing networks without dense cell overlaps is a more accurate way to perform the recording and the analysis of both calcium imaging and patch-clamp experiments. Since the organoid forming cells were capable of re-establishing the self-organized neuronal networks upon replating, we believe that this approach allows this functional analysis to capture the interactions between the cells that were previously composing the entire 3D organoid, both neurons and progenitor cells. In addition to SSCI and patch-clamp analysis, also immune quantifications of pre- and pos-synaptic markers, as well as dendritic spines characterization, were performed by replating of the 3D organoids, thus keeping all the manipulation procedures for functional-related analysis and the respective results consistent.

Single cell calcium imaging performed at days 44–47 of differentiation of RTT female dorsal organoids corroborate the previously raised hypothesis of premature development of newborn neurons. Later in differentiation, SCCI analysis showed an increased percentage of cells that do not respond to KCl or histamine stimulation, suggesting a decrease in the percentage of cells presenting a neuronal-like profile along the maturation process. This is consistent with previous studies showing *MeCP2*-mutant neurons with altered calcium signaling (Chen et al., 2003; Marchetto et al., 2010), associated to an impairment in the expression/sensitivity of VSCC and consequently to a defective neuronal responsiveness to depolarization (Gandaglia et al., 2019).

The capacity of human cortical neurons to generate repetitive AP upon a current depolarization was not detected before 20 gestational weeks (GW), whereas single AP firing was present as early as 16 GW (Moore et al., 2009). We observed that neurons in our control dorsal organoids presented features of maturation, exhibiting electrophysiological activity. Conversely, the prematurely formed neurons in MeCP2:R255X dorsal organoids, at day 47, exhibit slow activity, with decreased firing properties. This was demonstrated by the appearance of one single AP firing in almost all of the analyzed cells, by the broad AP half width of the first AP, by the decreased AP amplitude and by the reduced AP velocity (dV/dt) in a train of AP firing near threshold. APs are generated by special types of voltage-gated ion channels embedded in the plasma membrane, such as voltage-gated potassium and sodium channels (Johnson et al., 2007; Weick, 2016; Silva et al., 2020). Thus, our results observed in APs generated by MeCP2:R255X neurons may potentially indicate the presence of fewer release sites or less release probability. Our results are aligned with other studies previously published in the literature. In fact, electrophysiological recordings of RTT hiPSCs-derived neurons had already exhibited immature spike characteristics (Marchetto et al., 2010). Moreover, a different study analyzing RTT neurons showed dysfunction in AP generation and voltage-gated Na^+ currents (Djuric et al., 2016). Nevertheless, for the exact determination of potential alterations of neuronal membrane ion channels, in the future both sodium and potassium current injections measurements must be performed. As another demonstration of an altered electrophysiological profile, synaptic transmission, which requires the existence of functional neurotransmitter receptors, was also affected in our RTT female organoids, as determined by analysis of spontaneous synaptic currents, suggesting the existence of impairments in neuronal maturation and synaptic connection.

Later in maturation, at day 81, no AP was detected in dorsal MeCP2:R255X neurons. In agreement with this result, our analyses also demonstrated a decrease in VGLUT1 puncta, a specific protein of glutamatergic neurons responsible for loading glutamate into synaptic vesicles. In contradiction with these results, an increase in mRNA levels of *VGLUT1* was detected, which could be potentially related with a homeostatic compensation for the differential number of pre- and post-synaptic structures observed. In fact, previous studies using postmortem samples of RTT female patients demonstrated differential temporal distributions in glutamate levels in the forebrain (Lane et al., 1999). In agreement with our VGLUT1 puncta analysis, other studies using MECP2-mutated neurons derived from hiPSCs (Marchetto et al., 2010) or neurons lacking MECP2 derived from mice (Chao et al., 2007), also revealed a decrease in VGLUT1 puncta and consequently a decrease in functional synaptic densities.

As an additional functional characterization, we analyzed the dendritic spine morphology, as they are known to present a reduced density in RTT patients (Armstrong, 1995; Zhou et al., 2006). Accordingly, we observed a reduction of the number of mushroom and stubby-shaped spines in our RTT neurons, already reported for other RTT models (Chapleau et al., 2009).

Overall, our RTT female organoids revealed functional immaturity/impairments, excitatory imbalance and regression in spine morphology. This can be potentially explained by the premature formation of early post-mitotic neurons that possibly lack the spatial-temporal cues needed for a proper maturation. Moreover, together with other studies reported in the literature (Blue et al., 1999; Marchetto et al., 2010), our results suggest an apparent role of MeCP2 in regulating

glutamatergic synapse formation, synaptic function and neuronal maturation features.

Upon ventral patterning of RTT hiPSCs, we observed a significant decrease in the expression of the MGE domain characteristic marker, *NKX2.1,* in RTT female ventral organoids. MGE domain is composed of progenitor cells that originate GABAergic interneuron subtypes. Thus, this result is consistent with previous studies using *MeCP2*-mutant mice in which GABA-releasing neurons showed reduced inhibitory neurotransmitter capacity, being responsible for RTT symptoms such as repetitive behaviors and impaired motor coordination (Chao et al., 2010). During neurodevelopment, interneurons formed in MGE begin a migratory process to populate the dorsal pallium, by performing a tangential migration followed by integration into neural circuits, undergoing activity-dependent maturation (Gelman et al., 2012). A study from Sandberg et al. (2016) demonstrated that the combinatorial binding of *NKX2.1* and *LHX6* promotes the transcriptional activation of genes expressed in cortical migrating interneurons (Sandberg et al., 2016), influencing the process of interneuron migration. Moreover, *Nkx2.1* mutant-mice demonstrated deficits in the MGE migration (Anderson et al., 2001). Consistently, we also found a decrease of DCX expression for ventral MECP2:R255X organoids. In fact, previous studies in *DCX*-KO-mouse models demonstrated that this microtubule-associated protein is crucial for radial migration of interneurons (Liu et al., 2007), affecting their number and distribution (Kappeler et al., 2006). In a more recent study using 3D organoids and monolayer RTT-derived *MeCP2*-knockdown hiPSCs, it was also observed a decrease in DCX expression, and consequently defects in neurogenesis and neuronal differentiation (Mellios et al., 2017).

Taking together these alterations of the molecular and functional profile of interneurons, we decided to develop a more appropriate model to study their migration process by assembling ventral and dorsal organoids (Bagley et al., 2017; Xiang et al., 2017; Sloan et al., 2018). By using this model we observed that neurons traveled a shorter distance during their migration process when using female RTT fused organoids and we also observed a decreased percentage of GFP^+ ventral cells integrating into the dorsal part of the assembloid at early stages of development. So far, no other studies were yet performed regarding interneuron migration in the context of RTT. However, it is known that migratory interneurons integrate into neural dorsal circuits, contributing to the E/I balance (Gelman et al., 2012), whose disturbance has been previously reported for RTT (Chao et al., 2010). It is known that neuron-specific K^+ – Cl^- co-transporter 2 (KCC2) is a critical downstream gene target of *MeCP2*, being responsible for neuronal network formation, maturation delay and perturbations of GABAergic neurotransmission (Tang et al., 2016; Ruffolo et al., 2020). It was also proved that signaling molecules such as GABA neurotransmitter, influenced neuronal progenitor proliferation and embryonic neuron migration (Wang et al., 2003). In the future, our fused organoid model may be treated with the active peptide fragment of Insulin-like Growth Factor 1 (IGF-1) (Tropea et al., 2009), in order to study the possible rescue of neuronal migration and network integration delays, and consequently the rescue of functional GABA deficits. Additionally, efforts should be made to further identify which specific subtypes of interneurons are affected. The disequilibrium between excitation and inhibition (E/I) in RTT could be a consequence of both glutamatergic neurotransmission deregulation and GABAergic neurotransmission defects. Our fused forebrain organoids, resembling neural organization, differentiation and network formation of both dorsal and ventral regions, and containing both GABAergic and glutamatergic neuronal sub-types, could be intensively used for the study of the nature and mode of action of the local signals responsible for the (E/I) disequilibrium of different RTT patients.

CONCLUSION

Our model highlights the impact of MeCP2 mutations in different stages and brain regions during forebrain development. We have observed previously described aspects of the disease, particularly for later stages, which have been reported for both hiPSC-derived cells and animal models, suggesting the relevance of our platform for this type of studies. However, the model also demonstrates that different mutations are associated to distinct phenotype characteristics, as revealed by the results obtained with two different RTT cell lines. Importantly, our model revealed early developmental alterations in one female RTT-derived cell line, which have not been revealed before using other models, probably because our platform provides an improved recapitulation of the initial stages of cortical layer formation. Overall, we were able to show that our RTT forebrain organoid models can greatly help toward a better understanding of the pathophysiology of RTT in a patient-specific context, and for further testing of potential candidate drugs or other therapeutic strategies in RTT patient-specific organoids. An added value of our investigation relies on the fact that all the significant differences observed are based on comparisons performed between two hiPSC lines with the same genetic background (isogenic pair). In the future, our conclusions must be confirmed by extending our work to studies with other cell lines of the same patient and additional cell lines from other patients carrying the same mutation. Nevertheless, we truly believe that our results are reliable and that our work at this stage is already a valuable and innovative contribution to the field.

DATA AVAILABILITY STATEMENT

The raw data supporting the conclusions of this article will be made available by the authors, without undue reservation.

AUTHOR CONTRIBUTIONS

All the authors contributed to design research. AG performed the hiPSCs expansion and differentiation cultures and cell culture characterization. TF and TS assisted with cell culture maintenance, growth and characterization. TF assisted with flow cytometry experiments. EB assisted with *in situ* hybridization

and sequencing. SV, SX, and AS contributed for the design of functional experiments. AG and SV performed the single cell calcium imaging and patch-clamp experiments. SD derived the female RTT hiPSCs lines. AG and MD wrote the manuscript. All authors contributed to the article and approved the submitted version.

FUNDING

Funding received from Fundação para a Ciência e a Tecnologia (FCT), Portugal, through iBB, Institute for Bioengineering and Biosciences (UIDB/04565/2020) and from Programa Operacional Regional de Lisboa 2020 (Project No. 007317). AG was supported by FCT (PD/BD/128373/2017).

ACKNOWLEDGMENTS

We acknowledge the members of the iMM bioimaging facility for helping with confocal microscopy and with the FACS sorting and Simão Rocha (IMM), for sharing two plasmids for the lentiviral production and for helping with cell line sequencing. We acknowledge Cleber Trujillo and Alysson R. Muotri and UCSD's for providing the Rett syndrome male hiPSCs cell line – Q83X. We are grateful to Didier Tronon for providing the plasmid pMD2.G (Addgene plasmid # 12259; http://n2t.net/addgene:12259; RRID:Addgene_12259). We also acknowledge financial support from Fundação para a Ciência e a Tecnologia (FCT), Portugal, through iBB, Institute for Bioengineering and Biosciences (UIDB/04565/2020) and from Programa Operacional Regional de Lisboa 2020 (Project No. 007317). AG was supported by FCT (PD/BD/128373/2017).

SUPPLEMENTARY MATERIAL

The Supplementary Material for this article can be found online at: https://www.frontiersin.org/articles/10.3389/fcell.2020.610427/full#supplementary-material

REFERENCES

Agasse, F., Bernardino, L., Silva, B., Ferreira, R., Grade, S., and Malva, J. O. (2008). Response to histamine allows the functional identification of neuronal progenitors, neurons, astrocytes, and immature cells in subventricular zone cell cultures. *Rejuvenation Res.* 11, 187–200. doi: 10.1089/rej.2007.0600

Ananiev, G., Williams, E. C., Li, H., and Chang, Q. (2011). Isogenic Pairs of Wild Type and Mutant Induced Pluripotent Stem Cell (iPSC) Lines from Rett Syndrome Patients as In Vitro Disease Model. *PLoS One* 6:e25255. doi: 10.1371/journal.pone.0025255

Anderson, S. A., Marín, O., Horn, C., Jennings, K., and Rubenstein, J. L. R. (2001). Distinct cortical migrations from the medial and lateral ganglionic eminences. *Development* 128, 353–363.

Armstrong, M. D. D., (1995). Selective Dendritic Alterations in the Cortex of Rett Syndrome. *J. Neuropathol. Exp. Neurol.* 54, 195–201. doi: 10.1097/00005072-199503000-00006

Arnold, S. J., Huang, G., Cheung, A. F. P., Era, T., Nishikawa, S., Bikoff, E. K., et al. (2008). The T-box transcription factor Eomes Tbr2 regulates neurogenesis in the cortical subventricular zone. *Genes Dev.* 22, 2479–2484. doi: 10.1101/gad.475408

Bagley, J. A., Reumann, D., Bian, S., Lévi-strauss, J., and Knoblich, J. A. (2017). Fused cerebral organoids model interactions between brain regions. *Nat. Methods* 14, 743–751. doi: 10.1038/nmeth.4304

Balachandar, V., Dhivya, V., Gomathi, M., Mohanadevi, S., and Geetha, B. (2016). A review of Rett syndrome (RTT) with induced pluripotent stem cells. *Stem Cell Investig.* 52, 1–15.

Bansod, S., Kageyama, R., and Ohtsuka, T. (2017). Hes5 regulates the transition timing of neurogenesis and gliogenesis in mammalian neocortical development. *Co. Biol.* 144, 3156–3167. doi: 10.1242/dev.147256

Bernardino, L., Santos, T., Schitine, C., Reis, R. A. D. M., Ribeiro, F. F., Valero, J., et al. (2013). Activation of Type 1 Cannabinoid Receptor (CB1R) Promotes Neurogenesis in Murine Subventricular Zone Cell Cultures. *PLoS One* 8:e63529.doi: 10.1371/journal.pone.0063529

Blue, M. E., Naidu, S., and Johnston, M. V. (1999). Altered Development of Glutamate and GABA Receptors in the Basal Ganglia of Girls with Rett Syndrome. *Exp. Neurol.* 352, 345–352. doi: 10.1006/exnr.1999.7030

Chahrour, M., and Zoghbi, H. Y. (2007). Review The Story of Rett Syndrome: From Clinic to Neurobiology. *Neuron* 56, 422–437. doi: 10.1016/j.neuron.2007.10.001

Chao, H., Chen, H., Samaco, R. C., Xue, M., Chahrour, M., Yoo, J., et al. (2010). Dysfunction in GABA signalling mediates autism-like stereotypies and Rett syndrome phenotypes. *Nature* 468, 263–269. doi: 10.1038/nature09582

Chao, H., Zoghbi, H. Y., and Rosenmund, C. (2007). MeCP2 Controls Excitatory Synaptic Strength by Regulating Glutamatergic Synapse Number. *Neuron* 56, 58–65. doi: 10.1016/j.neuron.2007.08.018

Chapleau, C. A., Calfa, G. D., Lane, M. C., Albertson, A. J., Larimore, J. L., Kudo, S., et al. (2009). Dendritic spine pathologies in hippocampal pyramidal neurons from Rett syndrome brain and after expression of Rett-associated MECP2 mutations. *Neurobiol. Dis.* 35, 219–233. doi: 10.1016/j.nbd.2009.05.001

Chen, R. Z., Akbarian, S., Tudor, M., and Jaenisch, R. (2001). Deficiency of methyl-CpG binding protein-2 in CNS neurons results in a Rett-like phenotype in mice. *Nature* 27, 327–331. doi: 10.1038/85906

Chen, W. G., Chang, Q., Lin, Y., Meissner, A., West, A. E., Griffith, E. C., et al. (2003). Derepression of BDNF Transcription Involves Calcium-Dependent Phosphorylation of MeCP2. *Science* 302, 885–890. doi: 10.1126/science.1086446

Colantuoni, C., Jeon, O., Hyder, K., Chenchik, A., Khimani, A. H., Narayanan, V., et al. (2001). Gene Expression Profiling in Postmortem Rett Syndrome Brain: Differential Gene Expression and Patient Classification. *Neurobiol Dis.* 865, 847–865. doi: 10.1006/nbdi.2001.0428

Dias, R. B., Rombo, D. M., and Sebastião, A. M. (2014). Homeostatic plasticity induced by brief activity deprivation enhances long-term potentiation in the mature rat hippocampus. *J. Neurophysiol.* 112, 3012–3022. doi: 10.1152/jn.00058.2014

Djuric, U., Cheung, A. Y. L., Zhang, W., Mok, R. S., Piekna, A., Hendry, J. A., et al. (2016). MECP2e1 isoform mutation affects the form and function od neurons from Rett syndrome patient iPS cells. *Neurobiol. Dis.* 76, 37–45. doi: 10.1016/j.nbd.2015.01.001

Edri, R., Yaffe, Y., Ziller, M. J., Mutukula, N., Volkman, R., David, E., et al. (2015). Analysing human neural stem cell ontogeny by consecutive isolation of Notch active neural progenitors. *Nat. Commun.* 6:6500. doi: 10.1038/ncomms7500

Englund, C., Fink, A., Lau, C., Pham, D., Daza, R. A. M., Bulfone, A., et al. (2005). Pax6, Tbr2, and Tbr1 Are Expressed Sequentially by Radial Glia, Intermediate Progenitor Cells, and Postmitotic Neurons in Developing Neocortex. *J. Neurosci.* 25, 247–251. doi: 10.1523/jneurosci.2899-04.2005

Fernandes, T. G., Duarte, S. T., Ghazvini, M., Gaspar, C., and Santos, D. C. (2015). Neural commitment of human pluripotent stem cells under defined conditions recapitulates neural development and generates patient-specific neural cells. *Biotechnol. J.* 10, 1578–1588. doi: 10.1002/biot.201400751

Gandaglia, A., Brivio, E., Carli, S., Palmieri, M., Bedogni, F., Stefanelli, G., et al. (2019). A Novel Mecp2 Y120D Knock-in Model Displays Similar Behavioral Traits But Distinct Molecular Features Compared to the Mecp2 -Null Mouse Implying Precision Medicine for the Treatment of Rett Syndrome. *Mol. Neurobiol.* 56, 4838–4854. doi: 10.1007/s12035-018-1412-2

Gelman, D. M., Marín, O., and Rubenstein, J. L. R. (2012). The Generation of Cortical Interneurons. *Jasper's Basic Mech. Epilepsies* 4, 1–17.

Hevner, R. F., Shi, L., Justice, N., Hsueh, Y., Sheng, M., Smiga, S., et al. (2001). Tbr1 Regulates Differentiation of the Preplate and Layer 6. *Neuron* 29, 353–366. doi: 10.1016/s0896-6273(01)00211-2

Johnson, M. A., Weick, J. P., Pearce, R. A., and Zhang, S. (2007). Functional Neural Development from Human Embryonic Stem Cells: Accelerated Synaptic Activity via Astrocyte Coculture. *J. Neurosci.* 27, 3069–3077. doi: 10.1523/jneurosci.4562-06.2007

Kageyama, R. (2011). Dynamic expression of Notch signaling genes in neural stem/progenitor cells. *Front. Neurosci.* 5, 1–7. doi: 10.1007/978-4-431-54496-8_1

Kageyama, R., Ohtsuka, T., Shimojo, H., and Imayoshi, I. (2008). Dynamic Notch signaling in neural progenitor cells and a revised view of lateral inhibition. *Nat. Neurosci.* 11, 1247–1251. doi: 10.1038/nn.2208

Kappeler, C., Saillour, Y., Baudoin, J., and Francis, F. (2006). Branching and nucleokinesis defects in migrating interneurons derived from doublecortin knockout mice. *Hum. Mol. Genet.* 15, 1387–1400. doi: 10.1093/hmg/ddl062

Kobayashi, T., and Kageyama, R. (2010). Hes1 regulates embryonic stem cell differentiation by suppressing Notch signaling. *Genes Cells* 15, 689–698. doi: 10.1111/j.1365-2443.2010.01413.x

Lancaster, M. A., Renner, M., Martin, C., Wenzel, D., Bicknell, L. S., Hurles, M. E., et al. (2013). Cerebral organoids model human brain development and microcephaly. *Nature* 501, 373–379. doi: 10.1038/nature12517

Lane, J. B., Hetherington, H., Percy, A. K., and Jullie, W. (1999). Rett Syndrome: H Spectroscopic Imaging at 4 .1 Tesla. *J. Child Neurol.* 14, 524–528. doi: 10.1177/088307389901400808

Li, H., Zhong, X., Chau, K. F., Santistevan, N. J., Guo, W., Kong, G., et al. (2014). Cell cycle-linked MeCP2 phosphorylation modulates adult neurogenesis involving the Notch signalling pathway. *Nat. Commun.* 5, 1–9. doi: 10.1038/ncomms6601

Liu, J. S., Antypa, M., Rakic, S., Walsh, C. A., and Parnavelas, J. G. (2007). Both Doublecortin and Doublecortin-Like Kinase Play a Role in Cortical Interneuron Migration. *J. Neurosci.* 27, 3875–3883. doi: 10.1523/jneurosci.4530-06.2007

Lui, J. H., Hansen, D. V., and Kriegstein, A. R. (2011). Review Development and Evolution of the Human Neocortex. *Cell* 146, 18–36. doi: 10.1016/j.cell.2011.06.030

Marchetto, M. C. N., Carromeu, C., Acab, A., Yu, D., Yeo, G. W., Mu, Y., et al. (2010). A Model for Neural Development and Treatment of Rett Syndrome Using Human Induced Pluripotent Stem Cells. *Cell* 143, 527–539. doi: 10.1016/j.cell.2010.10.016

Mellios, N., Feldman, D. A., Sheridan, S. D., Ip, J. P. K., Kwok, S., Amoah, S. K., et al. (2017). MeCP2-regulated miRNAs control early human neurogenesis through differential effects on ERK and AKT signaling. *Mol. Psychiatr.* 23, 1051–1065. doi: 10.1038/mp.2017.86

Metsalu, T., and Vilo, J. (2015). ClustVis: a web tool for visualizing clustering of multivariate data using Principal Component Analysis and heatmap. *Nucleic Acids Res.* 43, W566–W570. doi: 10.1093/nar/gkv468

Miranda, C. C., Fernandes, T. G., Pinto, S. N., and Prieto, M. (2018). A scale out approach towards neural induction of human induced pluripotent stem cells for neurodevelopmental toxicity studies. *Toxicol. Lett.* 294, 51–60. doi: 10.1016/j.toxlet.2018.05.018

Miranda, C., Fernandes, T. G., and Pascoal, J. (2015). Spatial and temporal control of cell aggregation efficiently directs human pluripotent stem cells towards neural commitment. *Biotechnol. J.* 10, 1612–1624. doi: 10.1002/biot.201400846

Miranda, C., Fernandes, T. G., Diogo, M., and Cabral, J. M. S. (2016). Scaling Up a Chemically-Defined Aggregate-Based Suspension Culture System for Neural Commitment of Human Pluripotent Stem Cells. *Biotechnol. J.* 11, 1628–1638. doi: 10.1002/biot.201600446

Molina-Hernández, A., and Velasco, I. (2008). Histamine induces neural stem cell proliferation and neuronal differentiation by activation of distinct histamine receptors. *J. Neurochem.* 106, 706–717. doi: 10.1111/j.1471-4159.2008.05424.x

Moore, A. R., Filipovic, R., Mo, Z., Rasband, N., Zecevic, N., and Antic, S. D. (2009). Electrical Excitability of Early Neurons in the Human Cerebral Cortex during the Second Trimester of Gestation. *Cereb. Cortex* 19, 1795–1805. doi: 10.1093/cercor/bhn206

Qian, X., Nguyen, H. N., Song, M. M., Hadiono, C., Ogden, S. C., Hammack, C., et al. (2016). Brain-Region-Specific Organoids Using Mini- bioreactors for Modeling ZIKV Exposure Brain-Region-Specific Organoids Using Mini-bioreactors for Modeling ZIKV Exposure. *Cell* 165, 1–17.

Risher, W. C., Ustunkaya, T., Alvarado, J. S., and Eroglu, C. (2014). Rapid Golgi Analysis Method for Efficient and Unbiased Classification of Dendritic Spines. *PLoS One* 9:e107591. doi: 10.1371/journal.pone.0107591

Ruffolo, G., Cifelli, P., Miranda-Lourenço, C., De Felice, E., Limatola, C., Sebastião, A. M., et al. (2020). Rare Diseases of Neurodevelopment: Maintain the Mystery or Use a Dazzling Tool for Investigation? The Case of Rett Syndrome. *Neuroscience* 439, 146–152. doi: 10.1016/j.neuroscience.2019.06.015

Sandberg, M., Flandin, P., Silberberg, S., Visel, A., Nord, A. S., Rubenstein, J. L. R., et al. (2016). Transcriptional Networks Controlled by NKX2-1 in the Development of Forebrain GABAergic Neurons Article Transcriptional Networks Controlled by NKX2-1 in the Development of Forebrain GABAergic Neurons. *Neuron* 91, 1260–1275. doi: 10.1016/j.neuron.2016.08.020

Satir, T. M., Nazir, F. H., Vizlin-Hodzic, D., Hardselius, E., Blennow, K., Wray, S., et al. (2020). Accelerated neuronal and synaptic maturation by BrainPhys medium increases Aβ secretion and alters Aβ peptide ratios from iPSC-derived cortical neurons. *Sci. Rep.* 10, 1–17. doi: 10.1038/s41598-020-57516-7

Schanen, C., Houwink, E. J. F., Dorrani, N., Lane, J., Everett, R., Feng, A., et al. (2004). Phenotypic Manifestations of MECP2 Mutations in Classical and Atypical Rett Syndrome. *Am. J. Med. Genet.* 126A, 129–140. doi: 10.1002/ajmg.a.20571

Silva, T. P., Bekman, E. P., Fernandes, T. G., Vaz, S. H., Rodrigues, C. A. V., Diogo, M. M., et al. (2020). Maturation of Human Pluripotent Stem Cell-Derived Cerebellar Neurons in the Absence of Co-culture. *Front. Bioeng. Biotechnol.* 8:1–17. doi: 10.3389/fbioe.2020.00070

Sloan, S. A., Andersen, J., Pa, A. M., Birey, F., and Pa, S. P. (2018). Generation and assembly of human brain region – specific three-dimensional cultures. *Nat. Protoc.* 13, 2062–2085. doi: 10.1038/s41596-018-0032-7

Takahashi, K., and Yamanaka, S. (2006). Induction of Pluripotent Stem Cells from Mouse Embryonic and Adult Fibroblast Cultures by Defined Factors. *Cell* 126, 663–676. doi: 10.1016/j.cell.2006.07.024

Takahashi, K., Tanabe, K., Ohnuki, M., Narita, M., Ichisaka, T., Tomoda, K., et al. (2007). Induction of Pluripotent Stem Cells from Adult Human Fibroblasts by Defined Factors. *Cell* 131, 861–872. doi: 10.1016/j.cell.2007.11.019

Tang, X., Kim, J., Zhou, L., Wengert, E., Zhang, L., Wu, Z., et al. (2016). KCC2 rescues functional deficits in human neurons derived from patients with Rett syndrome. *PNAS* 113, 751–756. doi: 10.1073/pnas.1524013113

Tchieu, J., Kuoy, E., Chin, M. H., Trinh, H., Patterson, M., Sean, P., et al. (2010). Female human iPS cells retain inactive X-chromosome. *Cell Stem Cell* 7, 329–342. doi: 10.1016/j.stem.2010.06.024

Tropea, D., Giacometti, E., Wilson, N. R., Beard, C., McCurry, C., Dong, D. F., et al. (2009). Partial reversal of Rett Syndrome-like symptoms in MeCP2 mutant mice. *Proc. Natl. Acad. Sci. U. S. A.* 106, 2029–2034. doi: 10.1073/pnas.0812394106

Varga, E., Nemes, C., Kovács, E., Bock, I., Varga, N., Fehér, A., et al. (2016). Generation of human induced pluripotent stem cell (iPSC) line from an unaffected female carrier of Mucopolysaccharidosis type II (MPS II) disorder. *Stem Cell Res.* 17, 514–516. doi: 10.1016/j.scr.2016.09.035

Veeraragavan, S., Wan, Y., Connolly, D. R., Hamilton, S. M., Ward, C. S., Soriano, S., et al. (2016). Loss of MeCP2 in the rat models regression, impaired sociability and transcriptional deficits of Rett syndrome. *Hum. Mol. Genet.* 25, 3284–3302. doi: 10.1093/hmg/ddw178

Wang, D. D., Krueger, D. D., and Bordey, A. (2003). GABA depolarizes neuronal progenitors of the postnatal subventricular zone via GABAA receptor activation. *J. Physiol.* 550, 785–800. doi: 10.1113/jphysiol.2003.042572

Weick, J. P. (2016). Functional Properties of Human Stem Cell-Derived Neurons in Health and Disease. *Stem Cells Int.* 2016:4190438. doi: 10.1155/2016/4190438

Xiang, Y., Tanaka, Y., Patterson, B., Hwang, S. M., Hysolli, E., Cakir, B., et al. (2020). Dysregulation of BRD4 Function Underlies the Functional Abnormalities of MeCP2 Mutant Neurons. *Mol. Cell* 79, 84.e–98.e. doi: 10.1016/j.molcel.2020.05.016

Xiang, Y., Tanaka, Y., Patterson, B., Lee, S., Weissman, S. M., Park, I., et al. (2017). Fusion of Regionally Specified hPSC-Derived Organoids Models Human Brain Development and Interneuron Migration Resource Fusion of Regionally Specified hPSC-Derived Organoids Models Human Brain Development. *Cell Stem Cell* 21,1–16.

Zhou, Z., Hong, E. J., Cohen, S., Zhao, W., Ho, H. H., Schmidt, L., et al. (2006). Brain-Specific Phosphorylation of MeCP2 Regulates Activity-Dependent Bdnf Transcription, Dendritic Growth, and Spine Maturation. *Neuron* 52, 255–269. doi: 10.1016/j.neuron.2006.09.037

Zimmer-bensch, G. (2018). Diverse facets of cortical interneuron migration regulation - implications of neuronal activity and epigenetics. *Brain Res.* 1700, 160–169. doi: 10.1016/j.brainres.2018.09.001

Conflict of Interest: The authors declare that the research was conducted in the absence of any commercial or financial relationships that could be construed as a potential conflict of interest.

The handling editor declared a shared affiliation with several of the authors, AG, TF, SV, TS, EB, SX, SD, AS, JC, and MD, at the time of review.

frontiers in Cell and Developmental Biology

REVIEW
published: 12 January 2021
doi: 10.3389/fcell.2020.621644

Bearing My Heart: The Role of Extracellular Matrix on Cardiac Development, Homeostasis, and Injury Response

*Ana Catarina Silva[1,2,3], Cassilda Pereira[1,2], Ana Catarina R. G. Fonseca[1,2], Perpétua Pinto-do-Ó[1,2,4] and Diana S. Nascimento[1,2,4]**

[1] i3S – Instituto de Investigação e Inovação em Saúde, Universidade do Porto, Porto, Portugal, [2] INEB – Instituto Nacional de Engenharia Biomédica, Universidade do Porto, Porto, Portugal, [3] Gladstone Institutes, San Francisco, CA, United States, [4] ICBAS – Instituto de Ciências Biomédicas Abel Salazar, Universidade do Porto, Porto, Portugal

The extracellular matrix (ECM) is an essential component of the heart that imparts fundamental cellular processes during organ development and homeostasis. Most cardiovascular diseases involve severe remodeling of the ECM, culminating in the formation of fibrotic tissue that is deleterious to organ function. Treatment schemes effective at managing fibrosis and promoting physiological ECM repair are not yet in reach. Of note, the composition of the cardiac ECM changes significantly in a short period after birth, concurrent with the loss of the regenerative capacity of the heart. This highlights the importance of understanding ECM composition and function headed for the development of more efficient therapies. In this review, we explore the impact of ECM alterations, throughout heart ontogeny and disease, on cardiac cells and debate available approaches to deeper insights on cell–ECM interactions, toward the design of new regenerative therapies.

Keywords: heart, extracellular matrix, cardiac ontogeny, cardiovascular diseases, decellularization, fibrosis, regeneration

OPEN ACCESS

Edited by:
Susana Solá, University of Lisbon, Portugal

Reviewed by:
Katherine Yutzey, Cincinnati Children's Hospital Medical Center, United States
Manvendra K. Singh, Duke-NUS Medical School, Singapore

***Correspondence:**
Diana S. Nascimento
dsn@ineb.up.pt

Specialty section:
This article was submitted to Stem Cell Research, a section of the journal Frontiers in Cell and Developmental Biology

Received: *26 October 2020*
Accepted: *07 December 2020*
Published: *12 January 2021*

Citation:
Silva AC, Pereira C, Fonseca ACRG, Pinto-do-Ó P and Nascimento DS (2021) Bearing My Heart: The Role of Extracellular Matrix on Cardiac Development, Homeostasis, and Injury Response. Front. Cell Dev. Biol. 8:621644. doi: 10.3389/fcell.2020.621644

INTRODUCTION

The heart is one of the least regenerative organ systems in mammals, which partially explains the high mortality and morbidity rates of cardiovascular diseases (Virani et al., 2020). Long considered a post-mitotic organ and well-illustrated by deficient myocardium renewal capacity, it is nowadays known to retain cardiomyocyte turnover throughout life (Beltrami et al., 2001; Bergmann et al., 2009; Bergmann and Jovinge, 2014; Lázár et al., 2017) although at levels incompatible with the restoration of tissue function in disease or after injury (Porrello et al., 2011). For example,

Abbreviations: ADAMTs, A disintegrin and metalloproteinase with thrombospondin repeats; AV, Atrioventricular; BMP, Bone morphogenetic protein; cFB, Cardiac fibroblasts; ECM, Extracellular matrix; EndoMT, Endocardial-to-mesenchymal transition; EMT, Epithelial-to-mesenchymal transition; E, Embryonic day; FN, Fibronectin; FSTL1, Follistatin-like 1; GAGs, Glycosaminoglycans; HA, Hyaluronic acid; LOX, Lysyl oxidase; MI, Myocardial infarction; miRNAs, MicroRNAs; MMPs, Matrix metalloproteinases; NCCs, Neural crest cells; P, Postnatal day; SDS, Sodium dodecyl sulfate; SPARC, Secreted protein acidic and cysteine rich; TAZ, Transcriptional coactivator WWTR1; Tbx18, T-box transcription factor 18; Tcf21, Transcription factor 21; TGF-β, Transforming growth factor β; TNC, Tenascin-C; TSP, Thrombospondin; YAP, Yes-associated protein; Wnt, Wingless-related integration site; Wt1, Wilms' tumor 1; 3D, Three-dimensional.

cardiomyocytes lost after myocardial infarction (MI) are not replaced by new muscle, and instead, nonfunctional fibrotic tissue is deposited in the affected region (replacement fibrosis).

Effective regeneration of the mammalian heart is observed only during fetal–neonatal stages and requires triggering the proliferation of preexisting cardiomyocytes (Robledo, 1956; Herdrich et al., 2010; Porrello et al., 2011; Uygur and Lee, 2016; Sampaio-Pinto et al., 2018). This regenerative capacity falls abruptly in the first days after birth, which coincides with the final phase of cardiomyocyte maturation and concomitant cessation of proliferative activity (Quaini et al., 2002; Porrello et al., 2011; Notari et al., 2018; Sampaio-Pinto et al., 2018; Ye et al., 2018; Zhu et al., 2018). Despite this time limitation, the neonatal regenerative capacity has been widely dissected toward identification of pro-regenerative mechanisms. However, most studies are yet centered on the cellular compartment of the heart, overlooking the role of the extracellular matrix (ECM) in this response (Bassat et al., 2017).

Herein, the relevance of the ECM for healthy and diseased hearts and the importance of addressing the ECM for new cutting-edge regenerative therapies will be revisited and discussed.

CARDIAC ECM

The ECM constitutes a complex network of fibrillary (fibrillar collagens) and non-fibrillary (composed by the basement membrane, proteoglycans, and glycoproteins) components within the extracellular space that have both signaling and structural functions (Chute et al., 2019). New proteomic approaches have revealed that 90% of cardiac ECM is composed of 10 different proteins, from which serum albumin, collagens (collagens I, III, and IV), non-collagenous glycoproteins [fibronectin (FN) and laminin], proteoglycans, glucosaminoglycans (GAGs), and elastins are the most common (Lindsey et al., 2018). The fibrillar collagenous matrix comprises essentially type I (over 80%) and type III (over 10%) collagens (Weber, 1989) anchored to the myocardial cell basement membranes through collagen type IV and FN (Bashey et al., 1992; McCurdy et al., 2010). In addition, ECM works as a reservoir of anchored growth factors, cytokines, chemokines, proteases [e.g., matrix metallopeptidases (MMPs)], proteases inhibitors [e.g., tissue inhibitors of metalloproteinases (TIMPs)], and noncoding RNAs such as microRNAs (miRNAs) (Hynes, 2009; Jourdan-Lesaux et al., 2010; Fan et al., 2014).

Spatially, ECM is organized into two main regions, the basement membrane/pericellular matrix and interstitial matrix. The basement membrane/pericellular matrix constitutes a tissue specialized network of ECM molecules that involve each cell, promoting cell polarity and function (e.g., differentiation and migration) via cell surface receptors, such as integrins, through an outside–in signaling (Corda et al., 2000; LeBleu et al., 2007; Valiente-Alandi et al., 2016). This ECM compartment is mainly composed of FN, collagen IV, laminin, procollagens, hyaluronic acid (HA), and proteoglycans (Chang et al., 2016). As for the interstitial matrix, ECM molecules, such as collagens I and III, granting structural and mechanical support to the tissue, are main constituents.

The cell modulatory nature of the extracellular microenvironment results from a continuous remodeling of ECM composition and structural rearrangement, but also by the formation of bioactive peptides, known as matrikines, via enzymatic degradation of the ECM macromolecules (Maquart et al., 1999, 2005). These alterations affect cell function but also promote ECM remodeling in a feedback loop. ECM remodeling occurs in waves, a consequence of the tight control between synthesis and degradation, and generates active extracellular niches that regulate different cellular responses, namely, proliferation, migration, cell fate decisions, and even cell death. Cardiac fibroblasts (cFBs) are majorly responsible for ECM production and remodeling under homeostatic and pathological conditions, but other cells also contribute to the synthesis of ECM, particularly to the basement membrane, such as endothelial cells, smooth muscle cells, and cardiomyocytes (Aggeler, 1988; Pelouch et al., 1993; Corda et al., 2000; Anderson and Hinds, 2012; Bax et al., 2019).

Several transmembrane cell surface molecules such as CD44 and integrins, among others, mediate the bidirectional communication between cells and their environment (Valiente-Alandi et al., 2016). Integrin-mediated adhesions are the most frequent and well-described cell–ECM interactions (Howard and Baudino, 2014). Integrins are a large family of transmembrane receptors composed by α and β subunits and splice variants with different ligand specificities that undergo several conformational changes that impact integrin–ECM affinity (Ross, 2004; Askari et al., 2009). The integrin subunits expressed on cardiomyocytes throughout heart development and their ECM ligands have been extensively reviewed elsewhere (Ross, 2004). Integrin receptors interact directly or indirectly with different molecules, such as focal adhesion kinases, and with actin cytoskeleton filaments that, upon activation, trigger several signaling cascades regulating cellular processes (Askari et al., 2009). ECM–integrin–cytoskeleton linkage also mediates mechanotransduction signaling (Sun et al., 2016; Jansen et al., 2017). The mechanism that links integrin signaling with well-recognized mechanotransduction pathways, e.g., YAP/TAZ [Yes-associated protein (YAP) and transcriptional coactivator with PDZ-binding motif (TAZ)], is not completely understood, but the possibility of a direct correlation between integrins and YAP/TAZ signaling has recently emerged (Elbediwy et al., 2016; Chakraborty et al., 2017; Sabra et al., 2017; Martino et al., 2018). Integrins and actin filaments have been demonstrated to interact directly or indirectly with protein adaptors, such as vinculin, talin, and α-actinin (Schwartz, 2010). Indeed, transduction of mechanical changes observed on intracellular (formation of stress fibers) and extracellular spaces (ECM stiffness) is an important regulator of cardiomyocyte behavior through the regulation of the expression of mechanosensitive genes such *egr-1*, *iex-1*, and *c-fos* (Engler et al., 2008; Jaalouk and Lammerding, 2009; Martino et al., 2018).

Heart morphogenesis, maturation, and pathophysiology result from intrinsic factors related to the cellular transcriptional landscape, but also extrinsic cues from the ECM. Comprehension

of ECM dynamics and cell modulatory properties is crucial for the establishment of *in vitro* culture systems that recapitulate *in vivo*-like microenvironments, but also for development of more effective heart therapies.

ROLE OF ECM IN CARDIAC ONTOGENY

Embryonic and Fetal Heart

Throughout heart development, the ECM supports a tight spatiotemporal regulation of different cellular processes and progresses from a high hydrated gel rich in morphogenic molecules to a structurally defined collagen network poor in morphogens.

At E7.5, myocardial precursors, also known as primary and secondary heart fields, migrate to the midline of the embryo forming the heart tube (**Figure 1**, cardiac crescent). A primitive heart ECM derived from endoderm, mainly composed by chondroitin sulfate, collagens I and IV, laminin, fibulin, fibrillin, and FN, orchestrates the migration of these precursors (Little and Rongish, 1995; Lockhart et al., 2011). Among these molecules, FN promotes the migration of myocardial precursors toward the embryo midline by temporal modulation of cell adhesion and polarity. Consequently, FN mutation leads to aberrant formation of the heart such as cardia bifida, resulting in embryonic lethality (Linask and Lash, 1988; George et al., 1993; Trinh and Stainier, 2004; Mittal et al., 2013).

At E8.0, the heart has a tubular shape and is composed of two cell layers—the myocardium (outer layer) and the endocardium (inner layer)—separated by an amorphous matrix-denominated cardiac jelly (**Figure 1**, heart tube). The cardiac jelly consists of a network of ECM molecules enriched in HA; collagens I, III, and IV; laminin; FN; fibrillin; perlecan; fibulin-1; and thrombospondin (TSP) (Little and Rongish, 1995; Männer and Yelbuz, 2019). The heart expands by the contribution of second heart field (SHF) cells and undergoes a series of looping events at E8.5 (**Figure 1**, looping heart). Although mechanisms behind heart looping are not completely understood, HA is one of the most abundant molecules in the cardiac jelly. While the removal of HA by enzymatic degradation does not affect heart looping progression, the absence of HA leads to extensive alterations in heart tissue hemodynamics (Baldwin et al., 1994; Grandoch et al., 2018; Petz et al., 2019). In addition, ECM has a determinant function on the morphogenesis of specific heart substructures such as trabeculae, valve formation, atrial and ventricular septation, and outflow tract remodeling.

Myocardial Trabeculation and Compaction

Trabeculae formation is initiated at day E8.0 of mouse development with the sprouting of the endocardium toward the myocardium. At this stage, the myocardium is multilayered and presents a compact and discontinued (clusters) layer of cardiomyocytes (premature trabeculae cardiomyocytes). At E8.5, endocardial sprouting develops through the cardiac jelly, forming distinct columns that anchor with the compact myocardium—the endocardium touchdowns. Endocardial ridges are formed between the touchdowns, creating domes enriched in HA and FN, and clusters of cardiomyocytes, forming the trabecular units. The cardiomyocytes at the trabecular units organize in a radial disposition and grow in a radial fashion (trabecular extension), peaking around E14.5, concurrent with a progressive reduction of ECM content. Endocardial sprouting and touchdown are regulated by Notch signaling by promoting the expression of several ECM proteases, such as *Adamts1*, *Mmp2*, and *Hyal2* (**Table 1**; Del Monte-Nieto et al., 2018). The abrogation or overexpression of NOTCH1 signaling has been demonstrated to cause ventricular dysplasia and trabecular defects or ventricular hypertrabeculation, respectively (Grego-Bessa et al., 2007; Chen et al., 2013; Zhao et al., 2014; D'Amato et al., 2016). On the other hand, neuregulin-1 signaling, a downstream target of Notch, promotes the synthesis of ECM components necessary for trabecular growth (**Table 1**; Passer et al., 2016; Del Monte-Nieto et al., 2018). Thus, trabeculation of the heart is a process dependent not only on ECM synthesis but also on spatial and temporal regulation of ECM degradation (Stankunas et al., 2008; Lockhart et al., 2011; Del Monte-Nieto et al., 2018). Myocardial trabeculation and compaction are two fundamental processes for proper cardiac chamber maturation. Both processes depend on Notch signaling and entail the degradation of the cardiac jelly for proper heart morphogenesis (Sandireddy et al., 2019). In particular, ventricular compaction has been demonstrated to be regulated by other molecules, such as *Slc39a8* zinc transporter and Sema3E/plexinD1 signaling, which positively regulates several ECM proteases from the ADAMTS family (*Adamts1,5,7,17*) (**Table 1**; Lin et al., 2018; Sandireddy et al., 2019). ADAMTS9 has been also pointed as essential to myocardial compaction by promoting versican degradation as demonstrated by ADAMTS9 haploinsufficient mice that develop abnormal projections and a "spongy" ventricular wall, resembling human hearts with left ventricular non-compaction congenital cardiomyopathy (**Table 1**; Kern et al., 2010; Lockhart et al., 2011; Sarma, 2011).

Atrioventricular and Outflow Tract Cushions

Atrioventricular (AV) and outflow tract cushions form by the differentiation of the local endocardium that, around E9.5, undergoes endocardial-to-mesenchymal transition (EndoMT), invading the neighboring cardiac jelly deposits (**Figure 1**, looping heart). The cardiac cushion ECM is enriched in HA and proteoglycans (versicans V0 and V1, perlecan, and glypicans) which confer these regions the consistency of a hydrated gel (Baldwin et al., 1994; Lockhart et al., 2011). Other ECM components are also identified on these acellular structures such as FN, collagens, laminin, nephronectin, tenascin-C (TNC), vitronectin, fibulin-1, fibulin-2, fibrillin, and enzymes (chondroitin-6-*O*-sulfotransferase-1 and chondroitin-6-*O*-sulfotransferase-14) (Patra et al., 2011). The content of HA in cardiac cushions is crucial for correct valve formation. Both the impairment and overproduction of HA result in valve malformations and the development of congenital defects (Baldwin et al., 1994; Petz et al., 2019). Bone morphogenic protein (BMP) and transforming growth factor β (TGF-β) signaling are major regulators of heart morphogenesis in mice and avians, including AV septation by modulating cardiac cushion ECM

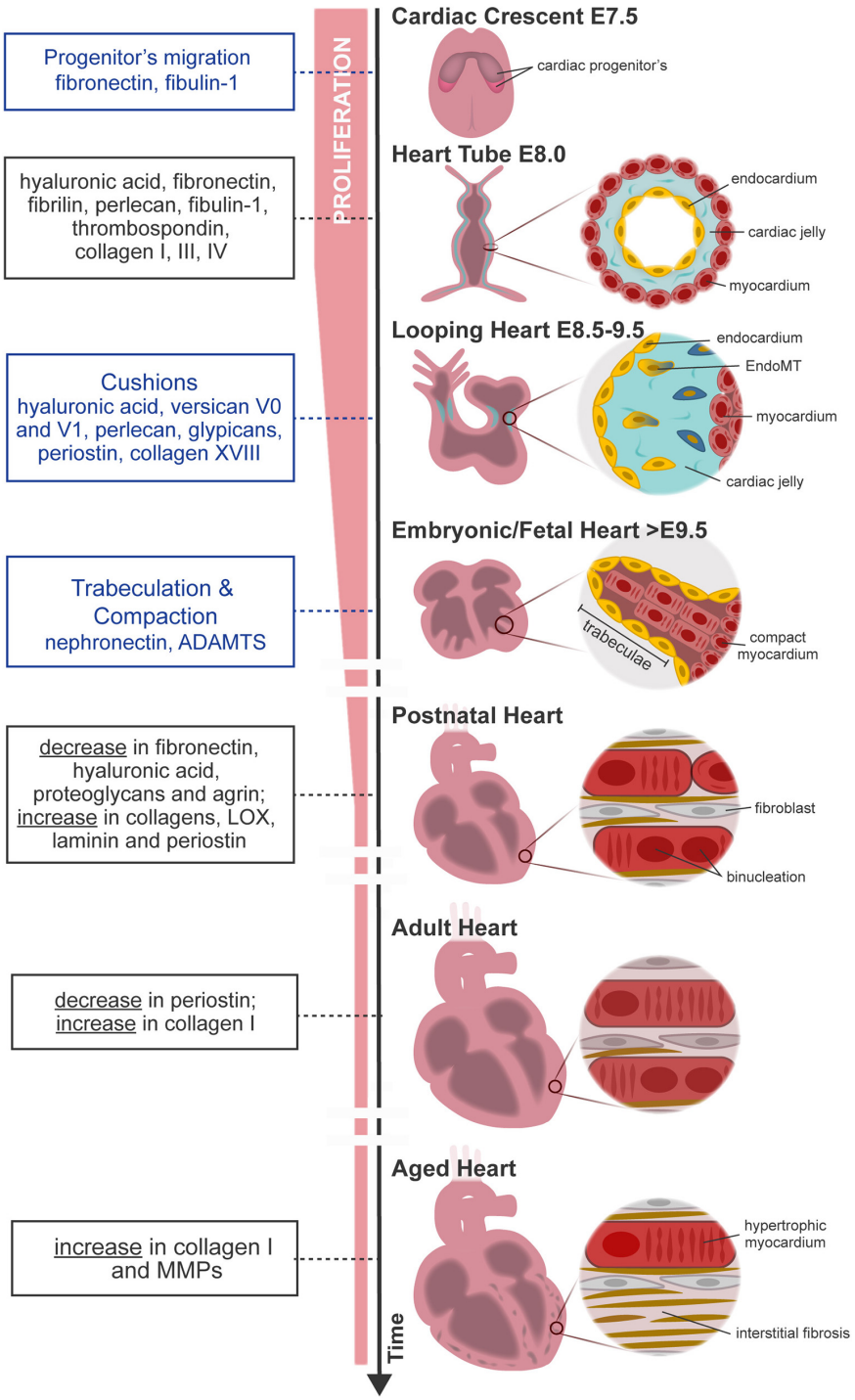

FIGURE 1 | Overview of mouse heart development, maturation, and aging. FN from primitive ECM paves the way for the migration of cardiac progenitor cells **(cardiac crescent)** to the embryo midline. Upon fusion, cardiac progenitor cells form the **heart tube**. The latter is constituted by two cell layers—the myocardium (outer layer) and the endocardium (inner layer)—separated by an amorphous matrix known as the cardiac jelly. The heart starts looping **(looping heart)** toward the formation of a four-chambered organ. In parallel, endocardial cells invade the cardiac cushion, that is, an extensive accumulation of cardiac jelly at primitive valve structures, and undergo EndoMT, forming valve tissue cells. The heart evolves, and the size of the myocardium increases while cardiomyocytes proliferate and mature at the compact and trabecular layers, respectively. Compaction and trabeculation are regulated by the transient expression of nephronectin and by the enzymatic degradation of the versican promoted by ADAMTs **(fetal heart)**. After birth, the ECM undergoes extensive remodeling characterized by a decrease in hyaluronic acid, FN, and proteoglycans. At the same time, cardiomyocytes cease proliferation and finalize maturation, acquiring robust sarcomeres and a rod-shaped morphology **(postnatal–adult heart)**. Aging contributes to functional impairment by the loss of cardiomyocytes and formation of fibrotic tissue **(aged heart)**. Blue box, specific morphological events regulated by the ECM; black box, variations on ECM composition throughout ontogeny.

TABLE 1 | Summary table of the signaling pathways that regulate ECM dynamics and associated cell function.

Heart ontogeny/disease	Heart structures	Signaling pathways	ECM remodeling	Cellular impact	References
Embryonic/fetal heart development	Trabeculae	Neuregulin 1	ECM synthesis: • HA • Fibronectin	Polarized cardiomyocyte division	Passer et al., 2016; Del Monte-Nieto et al., 2018
		Notch 1	ECM proteolysis: • ADAMTS1 • MMP2 • HYAL2		Del Monte-Nieto et al., 2018
	Myocardial compaction	Notch 1 Slc39a8 Sema3E/plexinD1	ECM proteolysis: • ADAMTS1,5,7,9,17 • MMP2 • HYAL2		Del Monte-Nieto et al., 2018; Lin et al., 2018; Sandireddy et al., 2019
	Atrioventricular and valve cushions	BMP2	ECM synthesis: • HA • Versican	Cardiac cushion mesenchyme migration	Inai et al., 2013
		BMP4 (inhibition)*	Nephronectin ECM reduced proteolysis: • HAS2	Restriction of atrioventricular channel differentiation and cardiac jelly swelling	Patra et al., 2011
		TGF-β3	ECM synthesis: • Periostin • Collagen 1	Differentiation of the cushion mesenchyme into fibroblasts	Norris et al., 2009
	Outflow tract remodeling	SMAD4	ECM proteolysis: • MT1-MMP	NCC migration	Jia et al., 2007
	Myocardium	β1-integrin*	Fibronectin	Cardiomyocyte proliferation	Ieda et al., 2009
		YAP/TAZ* ERK*	Soft ECM Agrin		Snider et al., 2008; von Gise et al., 2012; Bassat et al., 2017
Postnatal–adult heart	Myocardium	YAP/TAZ downregulation*	Stiff ECM	Inhibition of cardiomyocyte differentiation	von Gise et al., 2012
Adult heart ischemia	Epicardium, myocardium	TGF-β/Smad3 Hippo downregulation	ECM synthesis: • Periostin • Collagen 1	Epicardial cells EMT into fibroblast-like cells Fibroblast activation (myofibroblasts)	Liu et al., 2015; Piersma et al., 2015; Travers et al., 2016; Ramjee et al., 2017

**ECM downstream signaling pathways.*

composition, cellular invasion, and differentiation (Ma et al., 2005; Jiao et al., 2006; Prados et al., 2018). Specifically, BMP2 signaling has been implicated in HA and versican production by the chick cardiac cushion mesenchyme promoting its migration *in vitro* (Inai et al., 2013). On the other hand, studies in zebrafish suggested that nephronectin, an ECM component of the cardiac cushions, inhibits BMP4-Has2 signaling restricting AV channel differentiation and cardiac jelly swelling (Patra et al., 2011). TGF-β3 signaling further contributes to the AV valve maturation in mice by promoting the differentiation of the cushion mesenchyme into fibroblasts through the expression of periostin and collagen I production (**Table 1**; Norris et al., 2009; Lockhart et al., 2011). Periostin-knockout mice (Kii et al., 2006) and Peri^{lacZ}-null mice (Rios et al., 2005) exhibit both valve and septal defects (Snider et al., 2008; Lockhart et al., 2011). Collagen XVIII, a non-fibrillar form of collagen, is also expressed during early AV cushion development (Carvalhaes et al., 2006). Col18a1 knockdown leads to thickening of the endothelial basement membrane surrounding the AV valves (Utriainen et al., 2004; Lockhart et al., 2011) with no compromise of the heart function, despite causing hydrocephalus and decreased kidney filtration capacity (Utriainen et al., 2004; Hamano et al., 2010). While periostin and collagen XVIII can be detected in early heart development in the AV and outflow tract cushions and throughout the ventricular wall, as the heart matures, they become confined to specific areas, namely, the valves (Lockhart et al., 2011; González-González and Alonso, 2018).

Outflow Tract Development and Remodeling

Outflow tract development is a process that results from the remodeling of the vasculature and the migration of distinct cell types, endothelial/endocardial cells and cardiac neural crest cells (NCCs). Endocardial cells undergo epithelial-to-mesenchymal transition (EMT), invading the ECM-enriched cardiac cushions with the NCCs migrating to the nascent aortopulmonary septum and outflow tract cushion (Jiang et al., 2000). Smad signaling has been shown to impact NCC migration by regulating several vasculature/remodeling [e.g., *Id(1–4)*] and ECM organization-related (e.g., MMPs) genes in mice (Jia et al., 2007; Moskowitz et al., 2011). Specifically, *Smad4* inactivation in NCCs induce

a reduction of *Id* gene expression, which negatively impacts ECM proteinase MT1–MMP expression. Similar observations were reported upon *Id1/Id3* inactivation studies. The reduction of MT1–MMP expression affects migration of NCCs, as it translates in accumulation of ECM along the route of OFT caudal movement (**Table 1**; Jia et al., 2007).

Cardiomyocyte proliferation during fetal development is responsive to the surrounding embedding ECM. Ieda et al. (2009) demonstrated that ECM secreted by embryonic cFB at E12.5 favors cardiomyocyte proliferation more than adult ECM. ECM molecules secreted by embryonic cFB such as FN, TNC, hyaluronan, and proteoglycan link protein 1 have been shown to promote different cellular responses. Thus, while FN favored cardiomyocyte proliferation via β1-integrin signaling, hyaluronan enhanced cell adhesion in an integrin-independent manner (**Table 1**; Ieda et al., 2009). A similar mitogenic effect of FN has also been reported by Williams et al. (2014) while culturing cardiomyocytes on tissue culture plates coated with enzymatically digested fetal (E18–E19) heart tissue-derived ECM.

Even though the ECM qualitatively remains the same until birth, alterations of ECM molecule abundance and arrangement within the myocardium are observed. For example, laminin networks evolve from a punctuated patch-like deposition in the fetal heart (E11.5–E15) to a more extensive deposition in the developing basal membrane of cardiomyocytes in the neonatal heart and then to a contiguous layer along the basal membrane in the adult heart (Price et al., 1992; Yang et al., 2015). Laminin modulates cell adhesion by interacting with cell receptors such as integrins and forming a transmembrane link to the cytoskeleton via dystroglycan and dystrophin (Henry and Campbell, 1996; Okada et al., 2016). Deficiency on laminin expression results in muscular dystrophies and dilated cardiomyopathy at birth or early childhood, associated with metabolic deficiencies (Cox and Kunkel, 1997; Oliviéro et al., 2000; Yap et al., 2019).

The relevance of the ECM in heart development has been recently strengthened by the generation of three-dimensional (3D) mouse heart organoids *in vitro* in the presence of the laminin–entactin (LN/ET) complex and exogenous fibroblast growth factor 4 (FGF4). These organoids formed from self-organizing embryoid bodies, resulting in structures with atrium- and ventricle-like contractile structures (Lee et al., 2020).

Postnatal Heart

After birth, the heart undergoes severe alterations at the cellular and extracellular levels to adapt to physiological requirements of the growing body. The ECM is largely remodeled, involving a decline in the abundance of ECM molecules serving as morphogenic cues such as FN, HA, and proteoglycans, along with a concomitant increase in structural molecules, such as collagens I and III and laminin (Kim et al., 1999; Ieda et al., 2009; Williams et al., 2014). These alterations result in a more structured ECM that confines each cardiomyocyte individually, resembling a honeycomb-like organization (**Figure 1**; Robinson et al., 1988; Pelouch et al., 1993). These alterations coincide with the timing when the regenerative capacity of the heart ceases. Hence, one can argue that alterations at the ECM may be involved in the transition from a regenerative period to a reparative period. In agreement with this perspective, P1 but not P7 cardiac ECM fragments are able to stimulate cell cycle activity of neonatal cardiomyocytes. An elegant study by Notari et al. (2018) demonstrated that pharmacological inhibition of lysyl oxidase (LOX), an ECM cross-linking enzyme using 3-aminopropionitrile, a LOX inhibitor previously described to reduce lung ECM stiffness in newborn mice (Mammoto et al., 2013), could rescue the regenerative capacity of P3 hearts. Similar evidences were observed *in vitro*, wherein Yahalom-Ronen et al. (2015) demonstrated that culture of neonatal cardiomyocytes in rigid surfaces leads to enhanced myofibrillar organization and facilitates karyokinesis. Conversely, compliant surfaces promoted cardiomyocyte rounding, sarcomere disorganization, and cytokinesis. These findings demonstrate that the increase in ECM stiffness around birth might dictate the transition from a regenerative period to a reparative period, strengthening the relevance of the regulatory role of ECM mechanical properties.

YAP is a downstream effector of the Hippo pathway, a well-conserved mechanotransduction pathway on mammals with an important role during embryo development in the regulation of proper organ size. In the heart, YAP/TAZ activity has been mainly implicated in embryonic heart development, in postnatal growth, and in response to injury by promoting cardiomyocyte proliferation through the activation of cell cycle-related genes, such as *Ccna2*, *Ccnb1*, *Cdc2*, *Aurka*, *Aurkb*, and *Cdc25b* (von Gise et al., 2012; Xin et al., 2013; Mosqueira et al., 2014; Singh et al., 2016). The decline of cardiomyocyte proliferation observed post birth seems to correlate with a reduction in YAP expression and increase of YAP phosphorylation (inactivation) observed with aging (**Table 1**; von Gise et al., 2012). Deletion of *Yap* in the heart hampers neonatal regeneration at P2 and elicits a fibrotic response similar to what is observed in older animals. In fact, overexpression of a constitutively active form of YAP in the heart of 4-week-old mice enhances cardiac function after MI. These studies collectively show that biomechanical alterations at the ECM around birth may influence cardiomyocyte cycling activity and subsequently impact the regenerative capacity of the heart.

Aging Heart

Cellular aging is characterized by an accumulation of defective molecules and organelles at the cytoplasm and decline of reparative mechanisms. Thus, with age, cardiomyocytes accumulate dysfunctional mitochondria, oxidized proteins such as advanced glycation end products (AGE), and lipofuscin particles, denoted as "cellular garbage" (Kilhovd et al., 1999; Terman et al., 2008). These age-related alterations are progressively deleterious, resulting in a decrease in the number of cardiomyocytes and subsequent pathological hypertrophy of the remaining cardiomyocytes, inflammation, and gradual development of cardiac fibrosis (Bernhard and Laufer, 2008).

Heterochronic parabiosis studies suggest the participation of the extracellular milieu on cardiomyocyte aging by demonstrating that systemic factors impact age-related cardiomyocyte hypertrophy (Loffredo et al., 2013). Hypertrophic cardiomyocytes have a higher demand on oxygen and energy, creating a low-oxygen environment with consequent free radical production and cellular damage, as reviewed in

Meschiari et al. (2017). To compensate for the progressive cardiomyocyte loss, the ECM content increases, in particular collagen I (**Figure 1**; Bernhard and Laufer, 2008; Spadaccio et al., 2015; Horn and Trafford, 2016; Meschiari et al., 2017). Along with the increased collagen deposition and cross-linking, the ECM degradation capacity also augments through the production of MMPs, predominantly MMP9 (Meschiari et al., 2017). Increased MMP activity also attenuates angiogenic activity, contributing to the formation of a deleterious hypoxic environment (Yabluchanskiy et al., 2014).

The excessive accumulation of ECM and imbalance on ECM degradation lead to tissue scarring and cardiac dysfunction. Interstitial fibrosis has a detrimental effect on myocardial function by interfering with cardiomyocyte electrical coupling. The latter is characterized by an accumulation of collagen that separates cardiomyocytes, expediting the emergence of arrhythmogenic events and, in worst cases, sudden cardiac death (Stein et al., 2008; Nguyen et al., 2014).

ECM IN DISEASE/FIBROTIC HEART

Contrary to the regenerative response observed in neonates, the adult heart responds to an insult largely through the development of cardiac fibrosis. While at the start of the reparative process some ECM molecules secreted are similar to those seen in the regenerative response [e.g., FN (Konstandin et al., 2013) and TNC (Kasprzycka et al., 2015)], once cardiomyocytes have exited the cell cycle, upregulation of these ECM constituents is no longer enough, by itself, to induce proliferation. The result is the net accumulation of a collagen-rich ECM in the myocardium and subsequent formation of a stiff scar (Ieda et al., 2009; Hortells et al., 2019). Differences in cell surface receptor expression during development may influence cell response to injury and explain the shift from regeneration to repair. Integrin subunits, for example, are known to vary temporally, by cell type and with disease (Israeli-Rosenberg et al., 2014). A unique integrin profile can be observed in myocytes vs. fibroblasts or endothelial cells, in fetal vs. neonatal or adult myocytes, and in normal vs. pathological hearts (e.g., normal vs. failing or post-MI tissue). In cardiomyocytes, the integrin heterodimers most highly expressed are α1β1, α5β1, and α7β1, predominantly collagen-, FN-, and laminin-binding receptors, respectively (Israeli-Rosenberg et al., 2014). While the α5 subunit is prevalent in fetal and neonatal cardiomyocytes, α7 replaces α5 at the onset of postnatal development and becomes the main subunit detected in mature adult cardiomyocytes (Brancaccio et al., 1998; Israeli-Rosenberg et al., 2014).

Cardiac Fibrosis as a Response to Injury

Cardiac fibrosis can be reactive, in response to chronic stress (such as inflammation, pressure overload, and aging) without involving cardiomyocyte death, or reparative, when replacing lost cardiomyocytes as observed during MI (Kong et al., 2014). Several other conditions can result in progressive cardiac fibrosis such as hypertrophic cardiomyopathy, toxic insults (e.g., alcohol and anthracyclines), and metabolic disturbances such as diabetes and obesity, as reviewed in Kong et al. (2014). Regardless of the pathological trigger, excessive fibrosis in the myocardium may have a variety of deleterious consequences (Berk et al., 2007). In fact, clinical evidence correlates adverse outcomes in patients with heart failure with increased and stiffer cardiac ECM. Patients with heart failure with preserved ejection fraction (HFpEF) show an expansion of the interstitial ECM network, associated with coronary microvascular rarefaction and inflammatory activation, as reviewed by Paulus and Tschöpe (2013) and Mohammed et al. (2015).

The fibrotic remodeling of the heart results from the relative contribution of several cell types either by directly producing matrix proteins (fibroblasts) or by indirectly secreting fibrogenic mediators (macrophages, mast cells, lymphocytes, cardiomyocytes, and vascular cells). Common to all conditions associated with cardiac fibrosis, fibroblast transdifferentiation into secretory and contractile myofibroblasts is a key event that drives the fibrotic response (Kong et al., 2014).

Epicardium as the Major Source of ECM-Producing Cells

Lineage tracing studies revealed that the prominent source of cFBs, including those activated as response following injury, is a subset of cells originating from the embryonic epicardium (Russell et al., 2011; Zhou et al., 2011, 2012; van Wijk et al., 2012). These cells undergo EMT and migrate into the myocardial wall (Zhou et al., 2008; Ali et al., 2014; Moore-Morris et al., 2014; Hortells et al., 2019; Quijada et al., 2020) as reveled by basic helix–loop–helix (bHLH) transcription factor 21 (Tcf21) (Acharya et al., 2012), T-box transcription factor 18 (Tbx18) (Cai et al., 2008), and Wilms' tumor 1 (Wt1) (Zhou et al., 2008) reporter mouse lines (Pérez-Pomares et al., 2002; Braitsch et al., 2012; Greulich et al., 2012; Braitsch and Yutzey, 2013). These transcription factors repress genes encoding epithelial adhesion molecules (E-cadherin, claudins, and occludens) and the activation of mesenchymal genes (N-cadherin, collagens, and FN) necessary for ECM production and cell migration (Lamouille et al., 2014; Quijada et al., 2020). This transdifferentiation process is also relying on TGF-β, BMP, Wingless-related integration site (Wnt), and retinoic acid (RA) signaling, reviewed in detail elsewhere (von Gise and Pu, 2012; Braitsch and Yutzey, 2013).

After development, the epicardium becomes relatively dormant; however, despite the differences in duration of regeneration and the nature of the specific injury insult, reactivation of embryonic epicardial potential is conserved in zebrafish and neonatal mouse heart regeneration (Lepilina et al., 2006; Jopling et al., 2010; Kikuchi et al., 2010, 2011b; Chablais et al., 2011; González-Rosa et al., 2011, 2012; Porrello et al., 2011; Schnabel et al., 2011; Wang et al., 2011; González-Rosa and Mercader, 2012; Mercer et al., 2013). Similarly, studies using mouse models of cardiovascular disease and human diseased hearts show that the regulatory programs that promote the cFB lineage development are reactivated in the adult cardiac fibrotic response (Zhou et al., 2011; Braitsch et al., 2013). Although full recapitulation of the embryonic program has not been definitively established, several observations point toward at

least some degree of epicardial involvement post injury (Lepilina et al., 2006; Kikuchi et al., 2010, 2011b; González-Rosa et al., 2011, 2012; Porrello et al., 2011; Schnabel et al., 2011; Wang et al., 2011; Jesty et al., 2012; Smits and Riley, 2014).

This way, Tcf21, Tbx18, and Wt1 serve as markers of both developmental and injury-induced epicardial-derived fibroblasts in zebrafish and mammalian adult hearts (Kikuchi et al., 2011a; Braitsch et al., 2013; Ali et al., 2014; Moore-Morris et al., 2014; Kanisicak et al., 2016). Resident cardiac mouse fibroblasts labeled with Col1a1-GFP, PDGFRα, and Tcf21 transgenic alleles display the ability to proliferate after injury and give rise to a majority of cells in the fibrotic scar (Acharya et al., 2012; Kanisicak et al., 2016). Myofibroblasts, labeled by periostin, emerge from Tcf21 lineage-traced epicardium-derived fibroblasts when mice are subjected to MI or left ventricle pressure overload and are a major source of ECM (Kanisicak et al., 2016; Fu et al., 2018).

The epicardium responds to ischemic injury (e.g., MI) through major signaling pathways. Among them, TGF-β/Smad3 is the key intracellular pathway promoting cell activation, namely, fibroblasts, and fibrogenesis (Travers et al., 2016; **Table 1**). Wnt signaling is activated by the expression of Wnt1 by epicardial cells upon ischemia reperfusion damage *in vivo*, in a mouse model, and *in vitro*, epicardial cells undergo EMT and adopt a fibroblast-like phenotype when treated with Wnt1 (Duan et al., 2012). Crossing $WT1^{Cre}$ with $\beta catenin^{flox/flox}$ mice specifically abrogated Wnt signaling in epicardial cells, and as a result, there were minimal expansion of the epicardium post ischemia reperfusion injury and reduced collagen deposition in the subepicardium (Duan et al., 2012). Hippo signaling, which normally keeps cFBs in the resting state, is inactivated after cardiac injury, resulting in spontaneous transition toward a myofibroblast state that favors fibrosis and remodeling (Liu et al., 2015; Piersma et al., 2015; Ramjee et al., 2017; Johansen and Molkentin, 2019). Also involved in the postnatal epicardial response to the ischemic stress is Notch signaling, by modulating the differentiation of profibrotic myofibroblasts and thus counteracting the effects of the profibrotic TGF-β (Ali et al., 2014; Nistri et al., 2017).

ECM Dynamics in Cardiac Fibrosis

Following cardiomyocyte death, subjacent to cardiac insult, dynamic changes in the composition of the ECM act as regulators of the cellular responses leading to cardiac repair (Dobaczewski et al., 2010). The repair process can be divided into three overlapping phases: an inflammatory phase, a proliferative phase, and a maturation phase (**Figure 2**). At the extracellular space, four key events occur during repair, namely, the degradation of the interstitial matrix, production and resolution of the provisional ECM, and lastly, scar formation.

The death of cardiomyocytes after MI triggers an inflammatory reaction through the release of inflammatory mediators (cytokines and chemokines) that leads to the recruitment of leukocytes and neutrophil activation, revised in detail by Ong et al. (2018). Inflammation increases vascular permeability, resulting in extravasation of plasma proteins like fibrin, fibrinogen, and FN, and increases MMP expression and activity, leading to degradation of the interstitial matrix generating bioactive fragments (matrikines) that contribute to the activation of the inflammatory cascades. Consequent formation of a fibrin- and FN-based matrix network formed from the extravasated plasma proteins, known as provisional ECM, enriched with growth factors (PDGF, FGF, VEGF, and TGF families) and inflammatory cytokines secreted by various cell types, serves as a highly permeable conduit for infiltrating inflammatory cells (Dobaczewski et al., 2006; Bujak et al., 2008; Saxena et al., 2013; Takawale et al., 2015; Barker and Engler, 2017; Frangogiannis, 2017). Fibroblasts and other resident cells can adhere to this matrix, enabling fibroblast migration and inducing fibroblast proliferation and transdifferentiation to start the repair of the damaged areas (Serini et al., 1998; Rybarczyk et al., 2003; Chistiakov et al., 2016). Fibroblasts in the provisional ECM secrete other ECM molecules, such as proteoglycans, hyaluronan, and versican, that stabilize this provisional matrix (Wight and Potter-Perigo, 2011). Clearance of dead cells and ECM debris by phagocytes induces the release of anti-inflammatory mediators necessary for the resolution of the inflammatory phase, marking the transition to the proliferative phase. At this point, the ECM is enriched with matricellular proteins that modulate cellular phenotype, activate proteases and growth factors, and impinge on signaling cascades (Murphy-Ullrich and Sage, 2014). During the proliferative phase, growth factors secreted by mononuclear cells and macrophages activate myofibroblast-mediated deposition of large amounts of structural ECM proteins. The provisional matrix is degraded, and cellular FN is secreted primarily by fibroblasts and macrophages. Cellular FN containing extra domain A together with TGF-β and mechanical tension were required for myofibroblast transdifferentiation (Hinz et al., 2007; Shu and Lovicu, 2017). ECM structural proteins are then deposited to preserve the integrity of the myocardial wall (Zymek et al., 2006; Nielsen et al., 2019). While most matricellular proteins are rare or absent in the healthy myocardium, they are highly upregulated following cardiac injury. These proteins do not play a structural role but modulate cell function, promote matrix assembly, and protect the myocardium from adverse remodeling, as reviewed in Frangogiannis (2017). They include TSPs, TNC and TNX, osteopontin (OPN), secreted protein acidic and cysteine rich (SPARC), periostin, osteoglycin, and members of the cellular communication network factor (CCN) family (Dobaczewski et al., 2010; Kong et al., 2014). Recently, a different role of myofibroblasts has been described, as these cells were found capable of engulfing dead cells and acquiring an anti-inflammatory phenotype. The findings show that myofibroblasts cooperate with infiltrating macrophages to remove dead cells, raising the hypothesis that myofibroblast-mediated engulfment may itself activate the production of ECM proteins independently of macrophages (Nakaya et al., 2017).

Some studies suggest that the end of the proliferative phase and beginning of the maturation phase are marked by apoptosis of the majority of the myofibroblasts—to eliminate the granulation tissue cells from the infarcted area—however, the mechanism behind this proapoptotic process has not been fully investigated (Zhao et al., 2004; Xue and Jackson, 2015). The collagen content increases, and the upregulation of enzymes such as LOX induces collagen cross-linking (Al-U'datt et al., 2019).

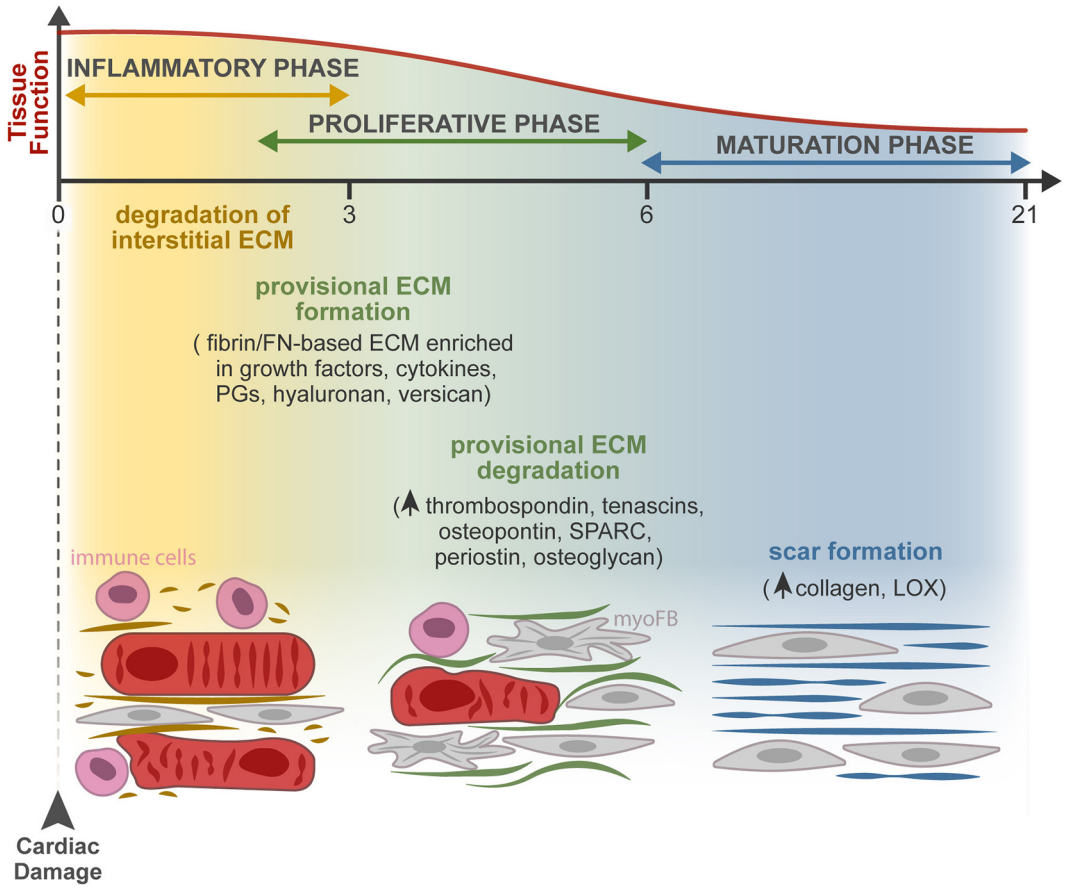

FIGURE 2 | ECM dynamics during tissue repair after MI. Progressive changes in the composition of the ECM occur during the three overlapping phases of the injury response: inflammatory, proliferative, and maturation phases. At the extracellular space, the main remodeling events encompass the degradation of the interstitial matrix (dark yellow lines), production and resolution of the provisional ECM (green lines), and lastly, scar formation (blue lines). Firstly, the release of inflammatory mediators by dead cells leads to the recruitment of leukocytes and neutrophil activation (pink cells) and increases vascular permeability and MMP expression and activity. The latter degrades the interstitial matrix (yellow), generating bioactive fragments (matrikines) that contribute to the inflammatory cascade. From the extravasated plasma proteins, a fibrin- and FN-based matrix network is formed (provisional ECM, green). This transient ECM is rich in growth factors and inflammatory cytokines and serves as a highly permeable conduit for cells. Fibroblasts (gray cells) adhere to this matrix, initiate the repair of the damaged area through proliferation and differentiation in myofibroblasts (myoFBs), and secrete different ECM molecules, such as proteoglycans (PGs), hyaluronan, and versican, that stabilize this provisional ECM. During the proliferative phase, myoFBs deposit large amounts of structural ECM proteins, mostly collagens, to preserve the integrity of the myocardial wall, and the provisional matrix is degraded. As the maturation phase initiates, the collagen content increases, and enzymes such as LOX are upregulated, inducing collagen cross-linking and the formation of a rigid scar.

Therefore, a rigid scar is formed without contractility and relaxation capacity, ultimately leading to heart stiffening, electrical signaling impairment, and consequent heart failure (Miragoli et al., 2007; Richardson et al., 2015; Murtha et al., 2017). The existence of endogenous mechanisms that restrain the matricellular signals to protect the myocardium from progressive fibrosis, when a mature ECM environment is formed, remains to be explored.

ECM MODULATION

Despite the advances on the role of the ECM in cardiac pathophysiology, the mechanisms that drive the feedback communication between ECM remodeling and cell response are not fully elucidated due to their intricate nature. Hence, the establishment of *ex vivo* model systems replicating the native myocardium is central to address further fundamental mechanistic questions.

Decellularization as a Methodology to Deconstruct ECM Composition, Structure, and Bioactivity

First, insights on the relevance of cell–ECM cross talk in the heart came forth through the observation of two-dimensional (2D) immunostainings of tissue sections and the analysis of pathophysiological alterations resultant of mutations in ECM-related genes or perturbations in related signaling pathways. The development of decellularization methodologies facilitated

further structural (Silva et al., 2016) and proteomic analyses (e.g., mass spectrometry) of the extracellular contents (Mayorca-Guiliani et al., 2017) by providing ECM protein enrichment as a result of the cellular content removal (cellular "noise") (de Castro Bras et al., 2013; Naba et al., 2015; Silva et al., 2016). Decellularization separates tissue ECM by the removal of cells and their associated material. This is achieved by applying, alone or in combination, chemical (buffers and detergents), enzymatic (trypsin and DNase), and physical (agitation and sonication) agents delivered using different techniques (perfusion, immersion, and agitation) (Beacham et al., 2007; Ott et al., 2008; Badylak et al., 2011; Crapo et al., 2011; Gillies et al., 2011; **Figure 3**). Ultimately, the central goal of decellularization is to obtain a balance between clearance of cellular materials and the retention of a close-to-native ECM.

Sodium dodecyl sulfate (SDS) is the most common detergent used for cardiac tissue decellularization. SDS concentration and duration of exposure affects greatly the preservation and integrity of the ECM. High SDS concentrations induce protein denaturation, collagen fibril disruption, and removal of GAGs (Gilbert et al., 2006; Crapo et al., 2011). In contrast, low SDS concentrations have been shown to preserve important ECM features, such as coil structures identified on fetal mouse heart ECM (Silva et al., 2016). Hence, reliable comparisons of different ECM microenvironments require the use of similar preparation methods. A versatile decellularization protocol working efficiently on distinct organs and also on the same tissue but on different ontogenetic stages (young and adult tissues) or health status has been recently reported (Silva et al., 2016, 2019; Garlikova et al., 2017; Pinto et al., 2017). This approach mitigates differences resultant from the application of distinct decellularization protocols, allowing fair comparisons on ECM composition and functional alterations across tissues, age, and normalcy vs. disease status (Perestrelo et al., 2020).

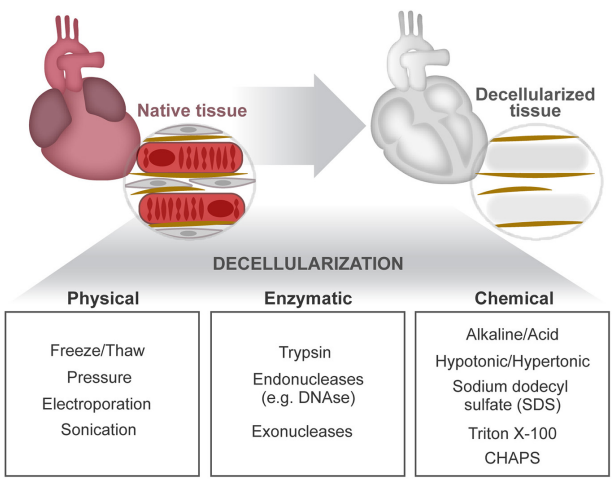

FIGURE 3 | Cardiac decellularization. Decellularization aims to remove the cellular compartment of a tissue, while preserving the composition and architectural arrangement of the ECM. This can be achieved by combined application of physical, enzymatic, and chemical treatments.

Decellularization can be performed on tissues/organs or on cells cultured *in vitro* as monolayers or aggregates (Beacham et al., 2007; Nair et al., 2008). The latter *in vitro* models facilitate manipulation of ECM-related genes (e.g., gene knockdown) to expose the role of specific ECM molecules (Ott et al., 2008; Williams et al., 2014; Silva et al., 2016; Pinto et al., 2017). For instance, Kong et al. (2018) using different approaches, including CRISPR/Cas9-mediated knockout of hyaluronan synthase 2 (the enzyme necessary to produce hyaluronan), found that hyaluronan inhibits vascular calcification involving BMP2 signaling. Despite being straightforwardly obtained and manipulated, *in vitro*-derived ECM misses to recreate the native organ ECM complexity. To the contrary, tissue-derived ECM often preserves native biochemical and mechanical properties, constituting an attractive alternative for studying the impact of ECM on complex scenarios such as age, disease, and injury as well as for therapeutic applications in regenerative medicine. Decellularized tissues were readily translated into the clinic as surgical scaffolds since ECM molecules are highly preserved across species, permitting the application of allogenic and xenogenic tissue-derived ECM. These applications demonstrated low immunogenicity while promoting specific cell functions (Wicha et al., 1982; Badylak, 2004; Gilbert et al., 2006; Crapo et al., 2011; Svystonyuk et al., 2020). Decellularization methodologies have evolved toward whole-organ decellularization by improvements such as the delivery of decellularization agents through the vasculature (perfusion) which promotes clearance of cellular remnants *in situ* (Ott et al., 2008; Badylak et al., 2011). Nevertheless, tissue-derived ECM holds limitations related both to batch-to-batch variability and to contaminants remaining after ineffective cell removal.

The development of decellularization methods opened new avenues to a more detailed assessment of tissue-derived ECM and of *in vitro* ECM–cell interactions. This will ultimately lead the way to the development of ECM-based therapies.

Cardiac ECM-Based Strategies for Regeneration and Repair

Excessive ECM, common to several cardiac pathologies, is an obstacle for normal organ function (Richardson et al., 2015), and clinical therapeutic strategies to control cardiac fibrosis are still on the horizon (Tzahor and Poss, 2017).

Previously reported ECM-derived therapies for MI encompass: (i) the delivery of decellularized cardiac ECM (Johnson et al., 2014; Wang et al., 2019), (ii) scaffolds functionalized with ECM-derived proteins or peptides (Zhang et al., 2019), and (iii) biomaterials that mimic the ECM (Youngblood et al., 2018; Yuan et al., 2019) and that are able to deliver soluble cytokines/growth factors (Rufaihah et al., 2017), miRNAs (Bheri and Davis, 2019), or cells (Chakravarti et al., 2018).

Cardiac-derived ECM, obtained by decellularization, has the benefit of conserving the organ-specific ECM architecture and composition and ensuing retention of biochemical cues that favor recellularization (Kc et al., 2019) and has shown promising results in animal models (Wainwright et al., 2012;

Sarig et al., 2016; Wang et al., 2016) and for human applications (Rego et al., 2019). However, decellularized matrices still pose many technical challenges that need to be addressed to meet clinical standards (Kc et al., 2019). Unfortunately and due to the complex composition of tissue-derived ECM, most authors do not attempt to discriminate which ECM factors or properties (e.g., architecture and stiffness) contribute to the observed beneficial effect.

Our growing knowledge on cardiac ECM function paves the way for new and promising therapeutic targets that can not only repair the injured heart but also induce cardiac regeneration. Recently, peptides generated from the degradation of ECM proteins have gained increasing attention for therapeutic application as increasing evidence supports that these molecules regulate various processes during cardiac repair and homeostasis (Ricard-Blum and Vallet, 2019). For example, p1158/p1159, the products of MMP2- and MMP9-mediated degradation of type I collagen, has been shown to promote angiogenesis and to reduce scar formation after MI (Lindsey et al., 2015). Canstatin, the product of MMP2-mediated degradation of type IV collagen, has been shown to regulate cardiomyocyte calcium channel activity (Imoto et al., 2018) and to reduce hypoxia-induced cardiomyocyte apoptosis (Okada et al., 2016). Tumstatin, the product of MMP9-mediated degradation of type IV collagen, protects cardiomyocytes against reactive oxygen species (ROS)-induced apoptosis (Yasuda et al., 2017), and on the other hand, endostatin, a cleaved fragment of type XVIII collagen, increases the proliferation and migration of myofibroblasts (Sugiyama et al., 2018).

The extracellular proteins from the SPARC family have important roles in cellular adhesion, migration, and proliferation modulating ECM processing and the TGF-β signaling (Bradshaw, 2012). Follistatin-like 1 (FSTL1), for instance, a member of this family, is a BMP4 antagonist that can improve heart function after MI (Altekoester and Harvey, 2015) and abrogates aldosterone-induced cardiac myocyte hypertrophy (Tanaka et al., 2016). However, only recombinant FSTL1 produced in bacteria or epicardium-derived, but not myocardium-derived, FSTL1 activates cardiomyocyte proliferation and cardiac regeneration (Wei et al., 2015). This appears to relate with the glycosylation of FSTL1 since a single replacement of asparagine with glutamine in the N-glycosylation site at position 180 of human FSTL1, hampering glycosylation at this position, was enough to activate cardiomyocyte proliferation and limit cardiac remodeling post MI, following the delivery of this modified FSTL1 mRNA to the mouse myocardium (Magadum et al., 2018).

Another relevant function of the ECM is to work as a reservoir of bioactive molecules, namely, miRNAs. The latter are also able to modulate cardiomyocyte proliferation and cardiac repair (Katz et al., 2016). For example, miR-17–miR-92, miR-199a, miR-214, miR-222, miR-302–miR-367, and miR-590 can promote

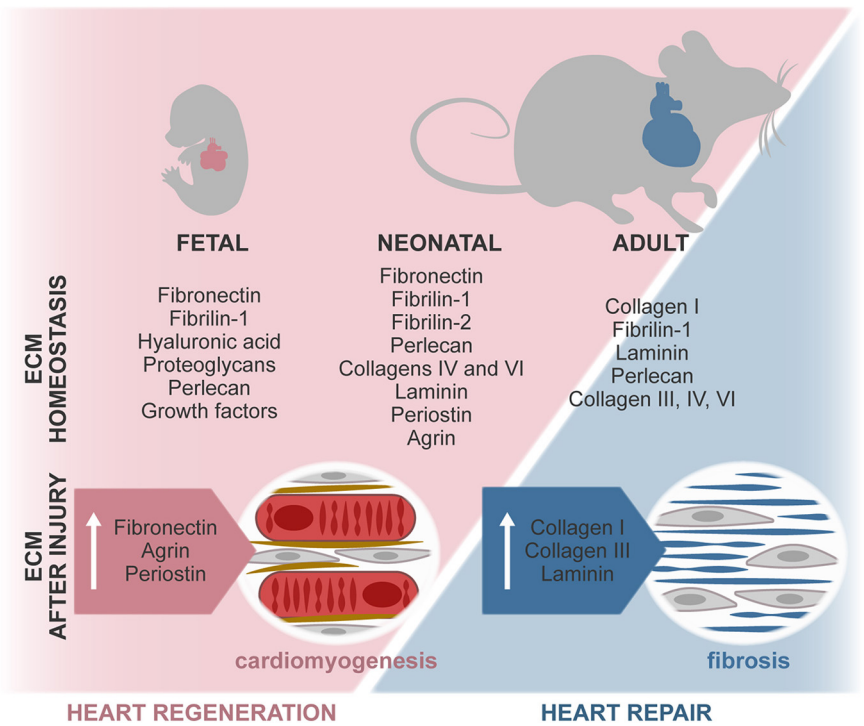

FIGURE 4 | ECM composition during regenerative (fetal/neonate) and reparative (adult) stages. The composition of the ECM changes around birth, resulting in a stiffer and less regenerative environment. In the fetal–neonatal heart, agrin and periostin stimulate cardiomyocyte proliferation and neovascularization, thus promoting regeneration of the tissue. During adult heart repair, increased expression of fetal-associated ECM is observed, namely, through the expression of FN and hyaluronan. However, this reactivation of the fetal program is incomplete, and adult cardiomyocytes are unable to proliferate, resulting in the formation of a collagen-rich scar.

cardiomyocyte proliferation and cardiac regeneration, whereas miR-15 family miRNAs inhibit cardiomyocyte proliferation and cardiac repair (Hashimoto et al., 2018; Deshmukh et al., 2019).

An emergent area in cardiac ECM for therapeutic purposes is the exploitation of young ECM as a source of regenerative targets as different findings support that severe changes in the ECM and in fibroblasts may dictate the loss of cardiac regenerative capacity after birth (Notari et al., 2018; Hortells et al., 2019). In fact, neonatal cardiac ECM improves myocardial function *in vivo*, reduces MI-induced fibrosis, and promotes angiogenesis and endothelial cell activity while the adult counterpart showed no beneficial effect (Wang et al., 2019). Consistently, the dystrophin complex protein agrin, whose expression in the heart decreases from P1 to P7, is an important regulator of cardiomyocyte division during the transient neonatal regenerative period (Bassat et al., 2017). Conditional deletion of *Agrn* in the cardiac mesoderm promoted maturation and reduced cell cycle activity of cardiomyocytes and impaired cardiac regeneration at P1 (Bassat et al., 2017). Bassat et al. (2017) also showed that intramyocardial administration of recombinant agrin after MI in a mouse model promotes moderate cardiomyocyte cell cycle reentry and proliferation on the healthy heart near the injury, leading to a significant reduction of the scar area 35 days after MI and improved cardiac function, when compared with the control. In an *in vitro* setting, agrin promoted proliferation and delayed maturation of induced pluripotent stem cell-derived cardiomyocytes (iPSC-CM) through Dag1, extracellular signal-regulated kinase (ERK), and YAP signaling. Another example of an ECM-associated protein highly expressed in the postnatal heart and barely detectable in the adult heart is periostin (Snider et al., 2008). The latter promotes cardiac regeneration by switching differentiated cardiomyocytes into cycling cells, improving cardiac function after MI (Kühn et al., 2007). However, whereas periostin-knockout mice showed impaired regeneration and abundant fibrosis following MI at P1 (Chen et al., 2017), no effect was reported for periostin knockout or overexpression on cardiomyocyte proliferation after MI in adult mice (Lorts et al., 2009). In fact, periostin also regulates cardiac fibrogenesis as targeted ablation of fibroblasts expressing periostin precludes adverse cardiac remodeling (Kaur et al., 2016). This exemplifies how the pleiotropic effect of different ECM proteins may complicate their direct application for therapeutic purposes.

CONCLUSION

Regulation of heart formation, homeostasis, and response to injury derives from intricate interactions between cells and their extracellular microenvironment. A misbalance on the expression of ECM and ECM-related molecules often leads to congenital malformations and development of disease. Although *in vitro* studies have exposed the relevance of several microenvironmental features, the dynamics of the complex 3D ECM network throughout life and its effect on cardiac cells remain largely elusive. Recently, different studies revealed that ECM-associated factors promote neonatal heart regeneration and that changes on ECM stiffness may limit this capacity to the first days after birth (**Figure 4**). These evidences, together with *in vitro* studies showing the beneficial properties of young ECM on cardiac cells, support that tissue engineering and regenerative medicine strategies aimed at promoting cardiac regeneration could benefit from mimicking the fetal–neonatal extracellular environment.

AUTHOR CONTRIBUTIONS

All authors designed, drafted, and revised the manuscript.

FUNDING

This work was funded by the European Regional Development Fund (ERDF) through COMPETE 2020, Portugal 2020, and by the FCT (Fundação para a Ciência e Tecnologia) (POCI-01-0145-FEDER-030985) and by the FCT/Ministério da Ciência, Tecnologia e Inovação in the framework of individual funding (CEECINST/00091/2018) to DN.

REFERENCES

Acharya, A., Baek, S. T., Huang, G., Eskiocak, B., Goetsch, S., Sung, C. Y., et al. (2012). The bHLH transcription factor Tcf21 is required for lineage-specific EMT of cardiac fibroblast progenitors. *Development* 139, 2139–2149. doi: 10.1242/dev.079970

Aggeler, J. (1988). Three-dimensional organization of the extracellular matrix secreted by cultured rat smooth muscle cells. *Vitro Cell Dev. Biol.* 24, 633–638.

Ali, S. R., Ranjbarvaziri, S., Talkhabi, M., Zhao, P., Subat, A., Hojjat, A., et al. (2014). Developmental heterogeneity of cardiac fibroblasts does not predict pathological proliferation and activation. *Circ. Res.* 115, 625–635. doi: 10.1161/CIRCRESAHA.115.303794

Altekoester, A. K., and Harvey, R. P. (2015). Bioengineered FSTL1 patches restore cardiac function following myocardial infarction. *Trends Mol. Med.* 21, 731–733. doi: 10.1016/j.molmed.2015.10.006

Al-U'datt, D., Allen, B. G., and Nattel, S. (2019). Role of the lysyl oxidase enzyme family in cardiac function and disease. *Cardiovasc. Res.* 115, 1820–1837. doi: 10.1093/cvr/cvz176

Anderson, D. E., and Hinds, M. T. (2012). Extracellular matrix production and regulation in micropatterned endothelial cells. *Biochem. Biophys. Res. Commun.* 427, 159–164. doi: 10.1016/j.bbrc.2012.09.034

Askari, J. A., Buckley, P. A., Mould, A. P., and Humphries, M. J. (2009). Linking integrin conformation to function. *J. Cell Sci.* 122, 165–170. doi: 10.1242/jcs.018556

Badylak, S. F. (2004). Xenogeneic extracellular matrix as a scaffold for tissue reconstruction. *Transpl. Immunol.* 12, 367–377. doi: 10.1016/j.trim.2003.12.016

Badylak, S. F., Taylor, D., and Uygun, K. (2011). Whole-organ tissue engineering: decellularization and recellularization of three-dimensional matrix scaffolds. *Annu. Rev. Biomed. Eng.* 13, 27–53. doi: 10.1146/annurev-bioeng-071910-124743

Baldwin, H. S., Lloyd, T. R., and Solursh, M. (1994). Hyaluronate degradation affects ventricular function of the early postlooped embryonic rat heart in situ. *Circ. Res.* 74, 244–252.

Barker, T. H., and Engler, A. J. (2017). The provisional matrix: setting the stage for tissue repair outcomes. *Matrix Biol.* 60–61, 1–4. doi: 10.1016/j.matbio.2017.04.003

Bashey, R. I., Martinez-Hernandez, A., and Jimenez, S. A. (1992). Isolation, characterization, and localization of cardiac collagen type VI. Associations with other extracellular matrix components. *Circ. Res.* 70, 1006–1017. doi: 10.1161/01.res.70.5.1006

Bassat, E., Mutlak, Y. E., Genzelinakh, A., Shadrin, I. Y., Baruch Umansky, K., Yifa, O., et al. (2017). The extracellular matrix protein agrin promotes heart regeneration in mice. *Nature* 547, 179–184. doi: 10.1038/nature22978

Bax, N. A. M., Duim, S. N., Kruithof, B. P. T., Smits, A. M., Bouten, C. V. C., and Goumans, M. J. (2019). In vivo and in vitro approaches reveal novel insight into the ability of epicardium-derived cells to create their own extracellular environment. *Front. Cardiovasc. Med.* 6:81. doi: 10.3389/fcvm.2019.00081

Beacham, D. A., Amatangelo, M. D., and Cukierman, E. (2007). Preparation of extracellular matrices produced by cultured and primary fibroblasts. *Curr. Protoc. Cell Biol. Chapt.* 10:Unit1019. doi: 10.1002/0471143030.cb1009s33

Beltrami, A. P., Urbanek, K., Kajstura, J., Yan, S.-M., Finato, N., Bussani, R., et al. (2001). Evidence that human cardiac myocytes divide after myocardial infarction. *N. Engl. J. Med.* 344, 1750–1757. doi: 10.1056/nejm200106073442303

Bergmann, O., Bhardwaj, R. D., Bernard, S., Zdunek, S., Barnabe-Heider, F., Walsh, S., et al. (2009). Evidence for cardiomyocyte renewal in humans. *Science* 324, 98–102.

Bergmann, O., and Jovinge, S. (2014). Cardiac regeneration in vivo: mending the heart from within? *Stem Cell Res.* 13(3 Part B), 523–531. doi: 10.1016/j.scr.2014.07.002

Berk, B. C., Fujiwara, K., and Lehoux, S. (2007). ECM remodeling in hypertensive heart disease. *J. Clin. Invest.* 117, 568–575. doi: 10.1172/jci31044

Bernhard, D., and Laufer, G. (2008). The aging cardiomyocyte: a mini-review. *Gerontology* 54, 24–31. doi: 10.1159/000113503

Bheri, S., and Davis, M. E. (2019). Nanoparticle-hydrogel system for post-myocardial infarction delivery of MicroRNA. *ACS Nano.* 13, 9702–9706. doi: 10.1021/acsnano.9b05716

Bradshaw, A. D. (2012). Diverse biological functions of the SPARC family of proteins. *Int. J. Biochem. Cell Biol.* 44, 480–488. doi: 10.1016/j.biocel.2011.12.021

Braitsch, C. M., Combs, M. D., Quaggin, S. E., and Yutzey, K. E. (2012). Pod1/Tcf21 is regulated by retinoic acid signaling and inhibits differentiation of epicardium-derived cells into smooth muscle in the developing heart. *Dev. Biol.* 368, 345–357. doi: 10.1016/j.ydbio.2012.06.002

Braitsch, C. M., Kanisicak, O., van Berlo, J. H., Molkentin, J. D., and Yutzey, K. E. (2013). Differential expression of embryonic epicardial progenitor markers and localization of cardiac fibrosis in adult ischemic injury and hypertensive heart disease. *J. Mol. Cell Cardiol.* 65, 108–119. doi: 10.1016/j.yjmcc.2013.10.005

Braitsch, C. M., and Yutzey, K. E. (2013). Transcriptional control of cell lineage development in epicardium-derived cells. *J. Dev. Biol.* 1, 92–111. doi: 10.3390/jdb1020092

Brancaccio, M., Cabodi, S., Belkin, A. M., Collo, G., Koteliansky, V. E., Tomatis, D., et al. (1998). Differential onset of expression of alpha 7 and beta 1D integrins during mouse heart and skeletal muscle development. *Cell Adhes. Commun.* 5, 193–205. doi: 10.3109/15419069809040291

Bujak, M., Dobaczewski, M., Chatila, K., Mendoza, L. H., Li, N., Reddy, A., et al. (2008). Interleukin-1 receptor type I signaling critically regulates infarct healing and cardiac remodeling. *Am. J. Pathol.* 173, 57–67. doi: 10.2353/ajpath.2008.070974

Cai, C.-L., Martin, J. C., Sun, Y., Cui, L., Wang, L., Ouyang, K., et al. (2008). A myocardial lineage derives from Tbx18 epicardial cells. *Nature* 454, 104–108. doi: 10.1038/nature06969

Carvalhaes, L. S., Gervásio, O. L., Guatimosim, C., Heljasvaara, R., Sormunen, R., Pihlajaniemi, T., et al. (2006). Collagen XVIII/endostatin is associated with the epithelial-mesenchymal transformation in the atrioventricular valves during cardiac development. *Dev. Dyn.* 235, 132–142. doi: 10.1002/dvdy.20556

Chablais, F., Veit, J., Rainer, G., and Jaźwińska, A. (2011). The zebrafish heart regenerates after cryoinjury-induced myocardial infarction. *BMC Dev. Biol.* 11:21. doi: 10.1186/1471-213x-11-21

Chakraborty, S., Njah, K., Pobbati, A. V., Lim, Y. B., Raju, A., Lakshmanan, M., et al. (2017). Agrin as a mechanotransduction signal regulating yap through the hippo pathway. *Cell Rep.* 18, 2464–2479. doi: 10.1016/j.celrep.2017.02.041

Chakravarti, A. R., Pacelli, S., Alam, P., Bagchi, S., Modaresi, S., Czirok, A., et al. (2018). Pre-conditioning stem cells in a biomimetic environment for enhanced cardiac tissue repair: in vitro and in vivo analysis. *Cell Mol. Bioeng.* 11, 321–336. doi: 10.1007/s12195-018-0543-x

Chang, C. W., Dalgliesh, A. J., López, J. E., and Griffiths, L. G. (2016). Cardiac extracellular matrix proteomics: challenges, techniques, and clinical implications. *Proteom. Clin. Appl.* 10, 39–50. doi: 10.1002/prca.201500030

Chen, H., Zhang, W., Sun, X., Yoshimoto, M., Chen, Z., Zhu, W., et al. (2013). Fkbp1a controls ventricular myocardium trabeculation and compaction by regulating endocardial Notch1 activity. *Development* 140, 1946–1957. doi: 10.1242/dev.089920

Chen, Z., Xie, J., Hao, H., Lin, H., Wang, L., Zhang, Y., et al. (2017). Ablation of periostin inhibits post-infarction myocardial regeneration in neonatal mice mediated by the phosphatidylinositol 3 kinase/glycogen synthase kinase 3β/cyclin D1 signalling pathway. *Cardiovasc. Res.* 113, 620–632. doi: 10.1093/cvr/cvx001

Chistiakov, D. A., Orekhov, A. N., and Bobryshev, Y. V. (2016). The role of cardiac fibroblasts in post-myocardial heart tissue repair. *Exp. Mol. Pathol.* 101, 231–240. doi: 10.1016/j.yexmp.2016.09.002

Chute, M., Aujla, P., Jana, S., and Kassiri, Z. (2019). The Non-fibrillar side of fibrosis: contribution of the basement membrane, proteoglycans, and glycoproteins to myocardial fibrosis. *J. Cardiovasc. Dev. Dis.* 6:35. doi: 10.3390/jcdd6040035

Corda, S., Samuel, J. L., and Rappaport, L. (2000). Extracellular matrix and growth factors during heart growth. *Heart Fail. Rev.* 5, 119–130. doi: 10.1023/A:1009806403194

Cox, G. F., and Kunkel, L. M. (1997). Dystrophies and heart disease. *Curr. Opin. Cardiol.* 12, 329–343.

Crapo, P. M., Gilbert, T. W., and Badylak, S. F. (2011). An overview of tissue and whole organ decellularization processes. *Biomaterials* 32, 3233–3243. doi: 10.1016/j.biomaterials.2011.01.057

D'Amato, G., Luxan, G., del Monte-Nieto, G., Martinez-Poveda, B., Torroja, C., Walter, W., et al. (2016). Sequential Notch activation regulates ventricular chamber development. *Nat. Cell Biol.* 18, 7–20. doi: 10.1038/ncb3280

de Castro Bras, L. E., Ramirez, T. A., DeLeon-Pennell, K. Y., Chiao, Y. A., Ma, Y., Dai, Q., et al. (2013). Texas 3-step decellularization protocol: looking at the cardiac extracellular matrix. *J. Proteom.* 86, 43–52. doi: 10.1016/j.jprot.2013.05.004

Del Monte-Nieto, G., Ramialison, M., Adam, A. A. S., Wu, B., Aharonov, A., D'Uva, G., et al. (2018). Control of cardiac jelly dynamics by NOTCH1 and NRG1 defines the building plan for trabeculation. *Nature* 557, 439–445. doi: 10.1038/s41586-018-0110-116

Deshmukh, V., Wang, J., and Martin, J. F. (2019). Leading progress in heart regeneration and repair. *Curr. Opin. Cell Biol.* 61, 79–85. doi: 10.1016/j.ceb.2019.07.005

Dobaczewski, M., Bujak, M., Zymek, P., Ren, G., Entman, M. L., and Frangogiannis, N. G. (2006). Extracellular matrix remodeling in canine and mouse myocardial infarcts. *Cell Tissue Res.* 324, 475–488. doi: 10.1007/s00441-005-0144-146

Dobaczewski, M., Gonzalez-Quesada, C., and Frangogiannis, N. G. (2010). The extracellular matrix as a modulator of the inflammatory and reparative response following myocardial infarction. *J. Mol. Cell Cardiol.* 48, 504–511. doi: 10.1016/j.yjmcc.2009.07.015

Duan, J., Gherghe, C., Liu, D., Hamlett, E., Srikantha, L., Rodgers, L., et al. (2012). Wnt1/βcatenin injury response activates the epicardium and cardiac fibroblasts to promote cardiac repair. *EMBO J.* 31, 429–442. doi: 10.1038/emboj.2011.418

Elbediwy, A., Vincent-Mistiaen, Z. I., Spencer-Dene, B., Stone, R. K., Boeing, S., Wculek, S. K., et al. (2016). Integrin signalling regulates YAP and TAZ to control skin homeostasis. *Development* 143, 1674–1687. doi: 10.1242/dev.133728

Engler, A. J., Carag-Krieger, C., Johnson, C. P., Raab, M., Tang, H.-Y., Speicher, D. W., et al. (2008). Embryonic cardiomyocytes beat best on a matrix with heart-like elasticity: scar-like rigidity inhibits beating. *J. Cell Sci.* 121:3794. doi: 10.1242/jcs.029678

Fan, D., Creemers, E. E., and Kassiri, Z. (2014). Matrix as an interstitial transport system. *Circ. Res.* 114, 889–902. doi: 10.1161/CIRCRESAHA.114.302335

Frangogiannis, N. G. (2017). The extracellular matrix in myocardial injury, repair, and remodeling. *J. Clin. Invest.* 127, 1600–1612. doi: 10.1172/JCI87491

Fu, X., Khalil, H., Kanisicak, O., Boyer, J. G., Vagnozzi, R. J., Maliken, B. D., et al. (2018). Specialized fibroblast differentiated states underlie scar formation in the infarcted mouse heart. *J. Clin. Invest.* 128, 2127–2143. doi: 10.1172/jci98215

Garlikova, Z., Silva, A. C., Rabata, A., Potesil, D., Ihnatova, I., Dumkova, J., et al. (2017). Generation of a close-to-native In Vitro system to study lung cells-extracellular matrix crosstalk. *Tissue Eng. Part C Methods* 24, 1–13. doi: 10.1089/ten.tec.2017.0283

George, E. L., Georges-Labouesse, E. N., Patel-King, R. S., Rayburn, H., and Hynes, R. O. (1993). Defects in mesoderm, neural tube and vascular development in mouse embryos lacking fibronectin. *Development* 119, 1079–1091.

Gilbert, T. W., Sellaro, T. L., and Badylak, S. F. (2006). Decellularization of tissues and organs. *Biomaterials* 27, 3675–3683.

Gillies, A. R., Smith, L. R., Lieber, R. L., and Varghese, S. (2011). Method for Decellularizing skeletal muscle without detergents or proteolytic enzymes. *Tissue Eng. Part C Methods* 17, 383–389. doi: 10.1089/ten.tec.2010.0438

González-González, L., and Alonso, J. (2018). Periostin: a matricellular protein with multiple functions in cancer development and progression. *Front. Oncol.* 8:225. doi: 10.3389/fonc.2018.00225

González-Rosa, J. M., Martín, V., Peralta, M., Torres, M., and Mercader, N. (2011). Extensive scar formation and regression during heart regeneration after cryoinjury in zebrafish. *Development* 138, 1663–1674. doi: 10.1242/dev.060897

González-Rosa, J. M., and Mercader, N. (2012). Cryoinjury as a myocardial infarction model for the study of cardiac regeneration in the zebrafish. *Nat. Protoc.* 7, 782–788. doi: 10.1038/nprot.2012.025

González-Rosa, J. M., Peralta, M., and Mercader, N. (2012). Pan-epicardial lineage tracing reveals that epicardium derived cells give rise to myofibroblasts and perivascular cells during zebrafish heart regeneration. *Dev. Biol.* 370, 173–186. doi: 10.1016/j.ydbio.2012.07.007

Grandoch, M., Bollyky, P. L., and Fischer, J. W. (2018). Hyaluronan: a master switch between vascular homeostasis and inflammation. *Circ. Res.* 122, 1341–1343. doi: 10.1161/CIRCRESAHA.118.312522

Grego-Bessa, J., Luna-Zurita, L., del Monte, G., Bolós, V., Melgar, P., Arandilla, A., et al. (2007). Notch signaling is essential for ventricular chamber development. *Dev. Cell* 12, 415–429. doi: 10.1016/j.devcel.2006.12.011

Greulich, F., Farin, H. F., Schuster-Gossler, K., and Kispert, A. (2012). Tbx18 function in epicardial development. *Cardiovasc. Res.* 96, 476–483. doi: 10.1093/cvr/cvs277

Hamano, Y., Okude, T., Shirai, R., Sato, I., Kimura, R., Ogawa, M., et al. (2010). Lack of collagen XVIII/endostatin exacerbates immune-mediated glomerulonephritis. *J. Am. Soc. Nephrol.* 21, 1445–1455. doi: 10.1681/ASN.2009050492

Hashimoto, H., Olson, E. N., and Bassel-Duby, R. (2018). Therapeutic approaches for cardiac regeneration and repair. *Nat. Rev. Cardiol.* 15, 585–600. doi: 10.1038/s41569-018-0036-36

Henry, M. D., and Campbell, K. P. (1996). Dystroglycan: an extracellular matrix receptor linked to the cytoskeleton. *Curr. Opin. Cell Biol.* 8, 625–631. doi: 10.1016/s0955-0674(96)80103-80107

Herdrich, B. J., Danzer, E., Davey, M. G., Allukian, M., Englefield, V., Gorman, J. H., et al. (2010). Regenerative healing following foetal myocardial infarction. *Eur. J. Cardiothorac. Surg.* 38, 691–698. doi: 10.1016/j.ejcts.2010.03.049

Hinz, B., Phan, S. H., Thannickal, V. J., Galli, A., Bochaton-Piallat, M. L., and Gabbiani, G. (2007). The myofibroblast: one function, multiple origins. *Am. J. Pathol.* 170, 1807–1816. doi: 10.2353/ajpath.2007.070112

Horn, M. A., and Trafford, A. W. (2016). Aging and the cardiac collagen matrix: novel mediators of fibrotic remodelling. *J. Mol. Cell Cardiol.* 93, 175–185. doi: 10.1016/j.yjmcc.2015.11.005

Hortells, L., Johansen, A. K. Z., and Yutzey, K. E. (2019). Cardiac fibroblasts and the extracellular matrix in regenerative and nonregenerative hearts. *J. Cardiovasc. Dev. Dis.* 6:29. doi: 10.3390/jcdd6030029

Howard, C. M., and Baudino, T. A. (2014). Dynamic cell-cell and cell-ECM interactions in the heart. *J. Mol. Cell Cardiol.* 70, 19–26. doi: 10.1016/j.yjmcc.2013.10.006

Hynes, R. O. (2009). The extracellular matrix: not just pretty fibrils. *Science* 326, 1216–1219. doi: 10.1126/science.1176009

Ieda, M., Tsuchihashi, T., Ivey, K. N., Ross, R. S., Hong, T. T., Shaw, R. M., et al. (2009). Cardiac fibroblasts regulate myocardial proliferation through beta1 integrin signaling. *Dev. Cell* 16, 233–244. doi: 10.1016/j.devcel.2008.12.007

Imoto, K., Hirakawa, M., Okada, M., and Yamawaki, H. (2018). Canstatin modulates L-type calcium channel activity in rat ventricular cardiomyocytes. *Biochem. Biophys. Res. Commun.* 499, 954–959. doi: 10.1016/j.bbrc.2018.04.026

Inai, K., Burnside, J. L., Hoffman, S., Toole, B. P., and Sugi, Y. (2013). BMP-2 induces versican and hyaluronan that contribute to post-EMT AV cushion cell migration. *PLoS One* 8:e77593. doi: 10.1371/journal.pone.0077593

Israeli-Rosenberg, S., Manso, A. M., Okada, H., and Ross, R. S. (2014). Integrins and integrin-associated proteins in the cardiac myocyte. *Circ. Res.* 114, 572–586. doi: 10.1161/circresaha.114.301275

Jaalouk, D. E., and Lammerding, J. (2009). Mechanotransduction gone awry. *Nat. Rev. Mol. Cell Biol.* 10, 63–73. doi: 10.1038/nrm2597

Jansen, K. A., Atherton, P., and Ballestrem, C. (2017). Mechanotransduction at the cell-matrix interface. *Semin. Cell Dev. Biol.* 71, 75–83.

Jesty, S. A., Steffey, M. A., Lee, F. K., Breitbach, M., Hesse, M., Reining, S., et al. (2012). c-kit+ precursors support postinfarction myogenesis in the neonatal, but not adult, heart. *Proc. Natl. Acad. Sci. U.S.A.* 109, 13380–13385. doi: 10.1073/pnas.1208114109

Jia, Q., McDill, B. W., Li, S.-Z., Deng, C., Chang, C.-P., and Chen, F. (2007). Smad signaling in the neural crest regulates cardiac outflow tract remodeling through cell autonomous and non-cell autonomous effects. *Dev. Biol.* 311, 172–184. doi: 10.1016/j.ydbio.2007.08.044

Jiang, X., Rowitch, D. H., Soriano, P., McMahon, A. P., and Sucov, H. M. (2000). Fate of the mammalian cardiac neural crest. *Development* 127, 1607–1616.

Jiao, K., Langworthy, M., Batts, L., Brown, C. B., Moses, H. L., and Baldwin, H. S. (2006). Tgfβ signaling is required for atrioventricular cushion mesenchyme remodeling during in vivo cardiac development. *Development* 133, 4585–4593. doi: 10.1242/dev.02597

Johansen, A. K. Z., and Molkentin, J. D. (2019). Hippo signaling does it again: arbitrating cardiac fibroblast identity and activation. *Genes Dev.* 33, 1457–1459. doi: 10.1101/gad.332791.119

Johnson, T. D., Braden, R. L., and Christman, K. L. (2014). Injectable ECM scaffolds for cardiac repair. *Methods Mol. Biol.* 1181, 109–120. doi: 10.1007/978-1-4939-1047-2_10

Jopling, C., Sleep, E., Raya, M., Martí, M., Raya, A., and Izpisúa Belmonte, J. C. (2010). Zebrafish heart regeneration occurs by cardiomyocyte dedifferentiation and proliferation. *Nature* 464, 606–609. doi: 10.1038/nature08899

Jourdan-Lesaux, C., Zhang, J., and Lindsey, M. L. (2010). Extracellular matrix roles during cardiac repair. *Life Sci.* 87, 391–400. doi: 10.1016/j.lfs.2010.07.010

Kanisicak, O., Khalil, H., Ivey, M. J., Karch, J., Maliken, B. D., Correll, R. N., et al. (2016). Genetic lineage tracing defines myofibroblast origin and function in the injured heart. *Nat. Commun.* 7:12260. doi: 10.1038/ncomms12260

Kasprzycka, M., Hammarström, C., and Haraldsen, G. (2015). Tenascins in fibrotic disorders-from bench to bedside. *Cell Adhes. Migrat.* 9, 83–89. doi: 10.4161/19336918.2014.994901

Katz, M. G., Fargnoli, A. S., Kendle, A. P., Hajjar, R. J., and Bridges, C. R. (2016). The role of microRNAs in cardiac development and regenerative capacity. *Am. J. Physiol. Heart Circ. Physiol.* 310, H528–H541. doi: 10.1152/ajpheart.00181.2015

Kaur, H., Takefuji, M., Ngai, C. Y., Carvalho, J., Bayer, J., Wietelmann, A., et al. (2016). Targeted ablation of periostin-expressing activated fibroblasts prevents adverse cardiac remodeling in mice. *Circ. Res.* 118, 1906–1917. doi: 10.1161/circresaha.116.308643

Kc, P., Hong, Y., and Zhang, G. (2019). Cardiac tissue-derived extracellular matrix scaffolds for myocardial repair: advantages and challenges. *Regen. Biomater.* 6, 185–199. doi: 10.1093/rb/rbz017

Kern, C. B., Wessels, A., McGarity, J., Dixon, L. J., Alston, E., Argraves, W. S., et al. (2010). Reduced versican cleavage due to Adamts9 haploinsufficiency is associated with cardiac and aortic anomalies. *Matrix Biol.* 29, 304–316. doi: 10.1016/j.matbio.2010.01.005

Kii, I., Amizuka, N., Minqi, L., Kitajima, S., Saga, Y., and Kudo, A. (2006). Periostin is an extracellular matrix protein required for eruption of incisors in mice. *Biochem. Biophys. Res. Commun.* 342, 766–772. doi: 10.1016/j.bbrc.2006.02.016

Kikuchi, K., Gupta, V., Wang, J., Holdway, J. E., Wills, A. A., Fang, Y., et al. (2011a). *tcf21*$^{+}$ epicardial cells adopt non-myocardial fates during zebrafish heart development and regeneration. *Development* 138, 2895–2902. doi: 10.1242/dev.067041

Kikuchi, K., Holdway, J. E., Major, R. J., Blum, N., Dahn, R. D., Begemann, G., et al. (2011b). Retinoic acid production by endocardium and epicardium is an

injury response essential for zebrafish heart regeneration. *Dev. Cell* 20, 397–404. doi: 10.1016/j.devcel.2011.01.010

Kikuchi, K., Holdway, J. E., Werdich, A. A., Anderson, R. M., Fang, Y., Egnaczyk, G. F., et al. (2010). Primary contribution to zebrafish heart regeneration by gata4(+) cardiomyocytes. *Nature* 464, 601–605. doi: 10.1038/nature08804

Kilhovd, B. K., Berg, T. J., Birkeland, K. I., Thorsby, P., and Hanssen, K. F. (1999). Serum levels of advanced glycation end products are increased in patients with type 2 diabetes and coronary heart disease. *Diabetes Care* 22, 1543–1548. doi: 10.2337/diacare.22.9.1543

Kim, H., Yoon, C. S., Kim, H., and Rah, B. (1999). Expression of extracellular matrix components fibronectin and laminin in the human fetal heart. *Cell Struct. Funct.* 24, 19–26.

Kong, P., Christia, P., and Frangogiannis, N. G. (2014). The pathogenesis of cardiac fibrosis. *Cell Mol. Life. Sci.* 71, 549–574. doi: 10.1007/s00018-013-1349-1346

Kong, Y., Liang, Q., Chen, Y., Yang, P., Liu, X., Li, Y., et al. (2018). Hyaluronan negatively regulates vascular calcification involving BMP2 signaling. *Lab. Invest.* 98, 1320–1332. doi: 10.1038/s41374-018-0076-x

Konstandin, M. H., Toko, H., Gastelum, G. M., Quijada, P., Torre, A. D. L., Quintana, M., et al. (2013). Fibronectin is essential for reparative cardiac progenitor cell response after myocardial infarction. *Circ. Res.* 113, 115–125. doi: 10.1161/CIRCRESAHA.113.301152

Kühn, B., del Monte, F., Hajjar, R. J., Chang, Y. S., Lebeche, D., Arab, S., et al. (2007). Periostin induces proliferation of differentiated cardiomyocytes and promotes cardiac repair. *Nat. Med.* 13, 962–969. doi: 10.1038/nm1619

Lamouille, S., Xu, J., and Derynck, R. (2014). Molecular mechanisms of epithelial-mesenchymal transition. *Nat. Rev. Mol. Cell Biol.* 15, 178–196. doi: 10.1038/nrm3758

Lázár, E., Sadek, H. A., and Bergmann, O. (2017). Cardiomyocyte renewal in the human heart: insights from the fall-out. *Eur. Heart J.* 38, 2333–2342. doi: 10.1093/eurheartj/ehx343

LeBleu, V. S., Macdonald, B., and Kalluri, R. (2007). Structure and function of basement membranes. *Exp. Biol. Med.* 232, 1121–1129. doi: 10.3181/0703-MR-72

Lee, J., Sutani, A., Kaneko, R., Takeuchi, J., Sasano, T., Kohda, T., et al. (2020). In vitro generation of functional murine heart organoids via FGF4 and extracellular matrix. *Nat. Commun.* 11:4283. doi: 10.1038/s41467-020-18031-5

Lepilina, A., Coon, A. N., Kikuchi, K., Holdway, J. E., Roberts, R. W., Burns, C. G., et al. (2006). A dynamic epicardial injury response supports progenitor cell activity during zebrafish heart regeneration. *Cell* 127, 607–619. doi: 10.1016/j.cell.2006.08.052

Lin, W., Li, D., Cheng, L., Li, L., Liu, F., Hand, N. J., et al. (2018). Zinc transporter Slc39a8 is essential for cardiac ventricular compaction. *J. Clin. Invest.* 128, 826–833. doi: 10.1172/jci96993

Linask, K. K., and Lash, J. W. (1988). A role for fibronectin in the migration of avian precardiac cells. I. Dose-dependent effects of fibronectin antibody. *Dev. Biol.* 129, 315–323.

Lindsey, M. L., Iyer, R. P., Zamilpa, R., Yabluchanskiy, A., DeLeon-Pennell, K. Y., Hall, M. E., et al. (2015). A novel collagen Matricryptin reduces left ventricular dilation post-myocardial infarction by promoting scar formation and angiogenesis. *J. Am. Coll. Cardiol.* 66, 1364–1374. doi: 10.1016/j.jacc.2015.07.035

Lindsey, M. L., Jung, M., Hall, M. E., and DeLeon-Pennell, K. Y. (2018). Proteomic analysis of the cardiac extracellular matrix: clinical research applications. *Expert Rev. Proteom.* 15, 105–112. doi: 10.1080/14789450.2018.1421947

Little, C. D., and Rongish, B. J. (1995). The extracellular matrix during heart development. *Experientia* 51, 873–882. doi: 10.1007/bf01921738

Liu, F., Lagares, D., Choi, K. M., Stopfer, L., Marinkoviæ, A., Vrbanac, V., et al. (2015). Mechanosignaling through YAP and TAZ drives fibroblast activation and fibrosis. *Am. J. Physiol. Lung Cell. Mol. Physiol.* 308, L344–L357. doi: 10.1152/ajplung.00300.2014

Lockhart, M., Wirrig, E., Phelps, A., and Wessels, A. (2011). Extracellular matrix and heart development. *Birth Defect. Res. A Clin. Mol. Teratol.* 91, 535–550. doi: 10.1002/bdra.20810

Loffredo, F. S., Steinhauser, M. L., Jay, S. M., Gannon, J., Pancoast, J. R., Yalamanchi, P., et al. (2013). Growth differentiation factor 11 is a circulating factor that reverses age-related cardiac hypertrophy. *Cell* 153, 828–839. doi: 10.1016/j.cell.2013.04.015

Lorts, A., Schwanekamp, J. A., Elrod, J. W., Sargent, M. A., and Molkentin, J. D. (2009). Genetic manipulation of periostin expression in the heart does not affect myocyte content, cell cycle activity, or cardiac repair. *Circ. Res.* 104, e1–e7. doi: 10.1161/CIRCRESAHA.108.188649

Ma, L., Lu, M. F., Schwartz, R. J., and Martin, J. F. (2005). Bmp2 is essential for cardiac cushion epithelial-mesenchymal transition and myocardial patterning. *Development* 132, 5601–5611. doi: 10.1242/dev.02156

Magadum, A., Singh, N., Kurian, A. A., Sharkar, M. T. K., Chepurko, E., and Zangi, L. (2018). Ablation of a Single N-Glycosylation site in human FSTL 1 induces cardiomyocyte proliferation and cardiac regeneration. *Mol. Ther. Nucleic Acids* 13, 133–143. doi: 10.1016/j.omtn.2018.08.021

Mammoto, T., Jiang, E., Jiang, A., and Mammoto, A. (2013). Extracellular matrix structure and tissue stiffness control postnatal lung development through the lipoprotein receptor-related protein 5/Tie2 signaling system. *Am. J. Respir. Cell Mol. Biol.* 49, 1009–1018. doi: 10.1165/rcmb.2013-0147OC

Männer, J., and Yelbuz, T. M. (2019). Functional morphology of the cardiac jelly in the tubular heart of vertebrate embryos. *J. Cardiovasc. Dev. Dis.* 6:12. doi: 10.3390/jcdd6010012

Maquart, F. X., Bellon, G., Pasco, S., and Monboisse, J. C. (2005). Matrikines in the regulation of extracellular matrix degradation. *Biochimie* 87, 353–360. doi: 10.1016/j.biochi.2004.10.006

Maquart, F. X., Simeon, A., Pasco, S., and Monboisse, J. C. (1999). Regulation of cell activity by the extracellular matrix: the concept of matrikines. *J. Soc. Biol.* 193, 423–428.

Martino, F., Perestrelo, A. R., Vinarskı, V., Pagliari, S., and Forte, G. (2018). Cellular mechanotransduction: from tension to function. *Front. Physiol.* 9:824. doi: 10.3389/fphys.2018.00824

Mayorca-Guiliani, A. E., Madsen, C. D., Cox, T. R., Horton, E. R., Venning, F. A., and Erler, J. T. (2017). ISDoT: in situ decellularization of tissues for high-resolution imaging and proteomic analysis of native extracellular matrix. *Nat. Med.* 23, 890–898. doi: 10.1038/nm.4352

McCurdy, S., Baicu, C. F., Heymans, S., and Bradshaw, A. D. (2010). Cardiac extracellular matrix remodeling: fibrillar collagens and secreted protein acidic and rich in Cysteine (SPARC). *J. Mol. Cell Cardiol.* 48, 544–549. doi: 10.1016/j.yjmcc.2009.06.018

Mercer, S. E., Odelberg, S. J., and Simon, H. G. (2013). A dynamic spatiotemporal extracellular matrix facilitates epicardial-mediated vertebrate heart regeneration. *Dev. Biol.* 382, 457–469. doi: 10.1016/j.ydbio.2013.08.002

Meschiari, C. A., Ero, O. K., Pan, H., Finkel, T., and Lindsey, M. L. (2017). The impact of aging on cardiac extracellular matrix. *Geroscience* 39, 7–18. doi: 10.1007/s11357-017-9959-9959

Miragoli, M., Salvarani, N., and Rohr, S. (2007). Myofibroblasts induce ectopic activity in cardiac tissue. *Circ. Res.* 101, 755–758. doi: 10.1161/CIRCRESAHA.107.160549

Mittal, A., Pulina, M., Hou, S.-Y., and Astrof, S. (2013). Fibronectin and integrin alpha 5 play requisite roles in cardiac morphogenesis. *Dev. Biol.* 381, 73–82. doi: 10.1016/j.ydbio.2013.06.010

Mohammed, S. F., Hussain, S., Mirzoyev, S. A., Edwards, W. D., Maleszewski, J. J., and Redfield, M. M. (2015). Coronary microvascular rarefaction and myocardial fibrosis in heart failure with preserved ejection fraction. *Circulation* 131, 550–559. doi: 10.1161/CIRCULATIONAHA.114.009625

Moore-Morris, T., Guimarães-Camboa, N., Banerjee, I., Zambon, A. C., Kisseleva, T., Velayoudon, A., et al. (2014). Resident fibroblast lineages mediate pressure overload-induced cardiac fibrosis. *J. Clin. Invest.* 124, 2921–2934. doi: 10.1172/JCI74783

Moskowitz, I. P., Wang, J., Peterson, M. A., Pu, W. T., Mackinnon, A. C., Oxburgh, L., et al. (2011). Transcription factor genes Smad4 and Gata4 cooperatively regulate cardiac valve development. *Proc. Natl. Acad. Sci. U.S.A.* 108, 4006–4011. doi: 10.1073/pnas.1019025108

Mosqueira, D., Pagliari, S., Uto, K., Ebara, M., Romanazzo, S., Escobedo-Lucea, C., et al. (2014). Hippo pathway effectors control cardiac progenitor cell fate by acting as dynamic sensors of substrate mechanics and nanostructure. *ACS Nano* 8, 2033–2047. doi: 10.1021/nn4058984

Murphy-Ullrich, J. E., and Sage, E. H. (2014). Revisiting the matricellular concept. *Matrix Biol.* 37, 1–14. doi: 10.1016/j.matbio.2014.07.005

Murtha, L. A., Schuliga, M. J., Mabotuwana, N. S., Hardy, S. A., Waters, D. W., Burgess, J. K., et al. (2017). The processes and mechanisms of cardiac and pulmonary fibrosis. *Front. Physiol.* 8:777. doi: 10.3389/fphys.2017.00777

Naba, A., Clauser, K. R., and Hynes, R. O. (2015). Enrichment of extracellular matrix proteins from tissues and digestion into peptides for mass spectrometry analysis. *J. Vis. Exp.* 2015:e53057. doi: 10.3791/53057

Nair, R., Shukla, S., and McDevitt, T. C. (2008). Acellular matrices derived from differentiating embryonic stem cells. *J. Biomed. Mater. Res. A* 87, 1075–1085. doi: 10.1002/jbm.a.31851

Nakaya, M., Watari, K., Tajima, M., Nakaya, T., Matsuda, S., Ohara, H., et al. (2017). Cardiac myofibroblast engulfment of dead cells facilitates recovery after myocardial infarction. *J. Clin. Invest.* 127, 383–401. doi: 10.1172/JCI83822

Nguyen, T. P., Qu, Z., and Weiss, J. N. (2014). Cardiac fibrosis and arrhythmogenesis: the road to repair is paved with perils. *J. Mol. Cell Cardiol.* 0, 83–91. doi: 10.1016/j.yjmcc.2013.10.018

Nielsen, S. H., Mouton, A. J., DeLeon-Pennell, K. Y., Genovese, F., Karsdal, M., and Lindsey, M. L. (2019). Understanding cardiac extracellular matrix remodeling to develop biomarkers of myocardial infarction outcomes. *Matrix Biol.* 75–76, 43–57. doi: 10.1016/j.matbio.2017.12.001

Nistri, S., Sassoli, C., and Bani, D. (2017). Notch signaling in ischemic damage and fibrosis: evidence and clues from the heart. *Front. Pharmacol.* 8:187. doi: 10.3389/fphar.2017.00187

Norris, R. A., Potts, J. D., Yost, M. J., Junor, L., Brooks, T., Tan, H., et al. (2009). Periostin promotes a fibroblastic lineage pathway in atrioventricular valve progenitor cells. *Dev. Dyn.* 238, 1052–1063. doi: 10.1002/dvdy.21933

Notari, M., Ventura-Rubio, A., Bedford-Guaus, S. J., Jorba, I., Mulero, L., Navajas, D., et al. (2018). The local microenvironment limits the regenerative potential of the mouse neonatal heart. *Sci. Adv.* 4:eaao5553. doi: 10.1126/sciadv.aao5553

Okada, M., Morioka, S., Kanazawa, H., and Yamawaki, H. (2016). Canstatin inhibits isoproterenol-induced apoptosis through preserving mitochondrial morphology in differentiated H9c2 cardiomyoblasts. *Apoptosis* 21, 887–895. doi: 10.1007/s10495-016-1262-1261

Oliviéro, P., Chassagne, C., Salichon, N., Corbier, A., Hamon, G., Marotte, F., et al. (2000). Expression of laminin α2 chain during normal and pathological growth of myocardium in rat and human. *Cardiovasc. Res.* 46, 346–355. doi: 10.1016/s0008-6363(00)00034-31

Ong, S.-B., Hernández-Reséndiz, S., Crespo-Avilan, G. E., Mukhametshina, R. T., Kwek, X.-Y., Cabrera-Fuentes, H. A., et al. (2018). Inflammation following acute myocardial infarction: multiple players, dynamic roles, and novel therapeutic opportunities. *Pharmacol. Therap.* 186, 73–87. doi: 10.1016/j.pharmthera.2018.01.001

Ott, H. C., Matthiesen, T. S., Goh, S. K., Black, L. D., Kren, S. M., Netoff, T. I., et al. (2008). Perfusion-decellularized matrix: using nature's platform to engineer a bioartificial heart. *Nat. Med.* 14, 213–221. doi: 10.1038/nm1684

Passer, D., van de Vrugt, A., Atmanli, A., and Domian, I. J. (2016). Atypical protein Kinase C-dependent polarized cell division is required for myocardial Trabeculation. *Cell Rep.* 14, 1662–1672. doi: 10.1016/j.celrep.2016.01.030

Patra, C., Diehl, F., Ferrazzi, F., van Amerongen, M. J., Novoyatleva, T., Schaefer, L., et al. (2011). Nephronectin regulates atrioventricular canal differentiation via Bmp4-Has2 signaling in zebrafish. *Development* 138, 4499–4509. doi: 10.1242/dev.067454

Paulus, W. J., and Tschöpe, C. (2013). A novel paradigm for heart failure with preserved ejection fraction: comorbidities drive myocardial dysfunction and remodeling through coronary microvascular endothelial inflammation. *J. Am. Coll. Cardiol.* 62, 263–271. doi: 10.1016/j.jacc.2013.02.092

Pelouch, V., Dixon, I. M., Golfman, L., Beamish, R. E., and Dhalla, N. S. (1993). Role of extracellular matrix proteins in heart function. *Mol. Cell. Biochem.* 129, 101–120.

Perestrelo, A. R., Silva, A. C., Cruz, J. O.-D. L., Martino, F., Horvath, V., Caluori, G., et al. (2020). Multiscale analysis of extracellular matrix remodeling in the failing heart. *Circ. Res.* doi: 10.1161/CIRCRESAHA.120.317685

Pérez-Pomares, J. M., Phelps, A., Sedmerova, M., Carmona, R., González-Iriarte, M., Muñoz-Chápuli, R., et al. (2002). Experimental studies on the spatiotemporal expression of WT1 and RALDH2 in the embryonic avian heart: a model for the regulation of myocardial and valvuloseptal development by epicardially derived cells (EPDCs). *Dev. Biol.* 247, 307–326. doi: 10.1006/dbio.2002.0706

Petz, A., Grandoch, M., Gorski, D. J., Abrams, M., Piroth, M., Schneckmann, R., et al. (2019). Cardiac hyaluronan synthesis is critically involved in the cardiac macrophage response and promotes healing after ischemia reperfusion injury. *Circ. Res.* 124, 1433–1447. doi: 10.1161/CIRCRESAHA.118.313285

Piersma, B., de Rond, S., Werker, P. M., Boo, S., Hinz, B., van Beuge, M. M., et al. (2015). YAP1 is a driver of myofibroblast differentiation in normal and diseased fibroblasts. *Am. J. Pathol.* 185, 3326–3337. doi: 10.1016/j.ajpath.2015.08.011

Pinto, M. L., Rios, E., Silva, A. C., Neves, S. C., Caires, H. R., Pinto, A. T., et al. (2017). Decellularized human colorectal cancer matrices polarize macrophages towards an anti-inflammatory phenotype promoting cancer cell invasion via CCL18. *Biomaterials* 124, 211–224. doi: 10.1016/j.biomaterials.2017.02.004

Porrello, E. R., Mahmoud, A. I., Simpson, E., Hill, J. A., Richardson, J. A., Olson, E. N., et al. (2011). Transient regenerative potential of the neonatal mouse heart. *Science* 331, 1078–1080. doi: 10.1126/science.1200708

Prados, B., Gomez-Apinaniz, P., Papoutsi, T., Luxan, G., Zaffran, S., Perez-Pomares, J. M., et al. (2018). Myocardial Bmp2 gain causes ectopic EMT and promotes cardiomyocyte proliferation and immaturity. *Cell Death Dis.* 9:399. doi: 10.1038/s41419-018-0442-z

Price, R. L., Nakagawa, M., Terracio, L., and Borg, T. K. (1992). Ultrastructural localization of laminin on in vivo embryonic, neonatal, and adult rat cardiac myocytes and in early rat embryos raised in whole-embryo culture. *J. Histochem. Cytochem.* 40, 1373–1381. doi: 10.1177/40.9.1506674

Quaini, F., Urbanek, K., Beltrami, A. P., Finato, N., Beltrami, C. A., Nadal-Ginard, B., et al. (2002). Chimerism of the transplanted heart. *New Engl. J. Med.* 346, 5–15. doi: 10.1056/NEJMoa012081

Quijada, P., Trembley, M. A., and Small, E. M. (2020). The role of the epicardium during heart development and repair. *Circ. Res.* 126, 377–394. doi: 10.1161/CIRCRESAHA.119.315857

Ramjee, V., Li, D., Manderfield, L. J., Liu, F., Engleka, K. A., Aghajanian, H., et al. (2017). Epicardial YAP/TAZ orchestrate an immunosuppressive response following myocardial infarction. *J. Clin. Invest.* 127, 899–911. doi: 10.1172/jci88759

Rego, A., Cheung, P. C., Harris, W. J., Brady, K. M., Newman, J., and Still, R. (2019). Pericardial closure with extracellular matrix scaffold following cardiac surgery associated with a reduction of postoperative complications and 30-day hospital readmissions. *J. Cardiothorac. Surg.* 14:61. doi: 10.1186/s13019-019-0871-875

Ricard-Blum, S., and Vallet, S. D. (2019). Fragments generated upon extracellular matrix remodeling: biological regulators and potential drugs. *Matrix Biol.* 75–76, 170–189. doi: 10.1016/j.matbio.2017.11.005

Richardson, W. J., Clarke, S. A., Quinn, T. A., and Holmes, J. W. (2015). Physiological implications of myocardial scar structure. *Compr. Physiol.* 5, 1877–1909. doi: 10.1002/cphy.c140067

Rios, H., Koushik, S. V., Wang, H., Wang, J., Zhou, H.-M., Lindsley, A., et al. (2005). periostin null mice exhibit dwarfism, incisor enamel defects, and an early-onset periodontal disease-like phenotype. *Mol. Cell. Biol.* 25, 11131–11144. doi: 10.1128/MCB.25.24.11131-11144.2005

Robinson, T. F., Cohen-Gould, L., Factor, S. M., Eghbali, M., and Blumenfeld, O. O. (1988). Structure and function of connective tissue in cardiac muscle: collagen types I and III in endomysial struts and pericellular fibers. *Scann. Microsc.* 2, 1005–1015.

Robledo, M. (1956). Myocardial regeneration in young rats. *Am. J. Pathol.* 32, 1215–1239.

Ross, R. S. (2004). Molecular and mechanical synergy: cross-talk between integrins and growth factor receptors. *Cardiovasc. Res.* 63, 381–390. doi: 10.1016/j.cardiores.2004.04.027

Rufaihah, A. J., Johari, N. A., Vaibavi, S. R., Plotkin, M., Di Thien, D. T., Kofidis, T., et al. (2017). Dual delivery of VEGF and ANG-1 in ischemic hearts using an injectable hydrogel. *Acta Biomater.* 48, 58–67. doi: 10.1016/j.actbio.2016.10.013

Russell, J. L., Goetsch, S. C., Gaiano, N. R., Hill, J. A., Olson, E. N., and Schneider, J. W. (2011). A dynamic notch injury response activates epicardium and contributes to fibrosis repair. *Circ. Res.* 108, 51–59. doi: 10.1161/circresaha.110.233262

Rybarczyk, B. J., Lawrence, S. O., and Simpson-Haidaris, P. J. (2003). Matrix-fibrinogen enhances wound closure by increasing both cell proliferation and migration. *Blood* 102, 4035–4043. doi: 10.1182/blood-2003-03-0822

Sabra, H., Brunner, M., Mandati, V., Wehrle-Haller, B., Lallemand, D., Ribba, A. S., et al. (2017). beta1 integrin-dependent Rac/group I PAK signaling mediates YAP activation of Yes-associated protein 1 (YAP1) via NF2/merlin. *J. Biol. Chem.* 292, 19179–19197. doi: 10.1074/jbc.M117.808063

Sampaio-Pinto, V., Rodrigues, S. C., Laundos, T. L., Silva, E. D., Vasques-Nóvoa, F., Silva, A. C., et al. (2018). Neonatal apex resection triggers Cardiomyocyte

proliferation, neovascularization and functional recovery despite local fibrosis. *Stem Cell Rep.* 10, 860–874. doi: 10.1016/j.stemcr.2018.01.042

Sandireddy, R., Cibi, D. M., Gupta, P., Singh, A., Tee, N., Uemura, A., et al. (2019). Semaphorin 3E/PlexinD1 signaling is required for cardiac ventricular compaction. *JCI Insight.* 4:e125908. doi: 10.1172/jci.insight.125908

Sarig, U., Sarig, H., de-Berardinis, E., Chaw, S. Y., Nguyen, E. B., Ramanujam, V. S., et al. (2016). Natural myocardial ECM patch drives cardiac progenitor based restoration even after scarring. *Acta Biomater.* 44, 209–220. doi: 10.1016/j.actbio.2016.08.031

Sarma, R. J. (2011). *Genetic Diagnoses*. Hauppauge, NY: Nova Science Publishers.

Saxena, A., Chen, W., Su, Y., Rai, V., Uche, O. U., Li, N., et al. (2013). IL-1 induces proinflammatory leukocyte infiltration and regulates fibroblast phenotype in the infarcted myocardium. *J. Immunol.* 191:4838. doi: 10.4049/jimmunol.1300725

Schnabel, K., Wu, C. C., Kurth, T., and Weidinger, G. (2011). Regeneration of cryoinjury induced necrotic heart lesions in zebrafish is associated with epicardial activation and cardiomyocyte proliferation. *PLoS One* 6:e18503. doi: 10.1371/journal.pone.0018503

Schwartz, M. A. (2010). Integrins and extracellular matrix in mechanotransduction. *Cold Spring Harb. Perspect. Biol.* 2:a005066. doi: 10.1101/cshperspect.a005066

Serini, G., Bochaton-Piallat, M. L., Ropraz, P., Geinoz, A., Borsi, L., Zardi, L., et al. (1998). The fibronectin domain ED-A is crucial for myofibroblastic phenotype induction by transforming growth factor-beta1. *J. Cell Biol.* 142, 873–881. doi: 10.1083/jcb.142.3.873

Shu, D. Y., and Lovicu, F. J. (2017). Myofibroblast transdifferentiation: the dark force in ocular wound healing and fibrosis. *Prog. Retin. Eye Res.* 60, 44–65. doi: 10.1016/j.preteyeres.2017.08.001

Silva, A. C., Oliveira, M. J., McDevitt, T. C., Barbosa, M. A., Nascimento, D. S., and Pinto-do-Ó, P. (2019). Comparable decellularization of fetal and adult cardiac tissue explants as 3D-like platforms for in vitro studies. *J. Vis. Exp.* 145:e56924. doi: 10.3791/56924

Silva, A. C., Rodrigues, S. C., Caldeira, J., Nunes, A. M., Sampaio-Pinto, V., Resende, T. P., et al. (2016). Three-dimensional scaffolds of fetal decellularized hearts exhibit enhanced potential to support cardiac cells in comparison to the adult. *Biomaterials* 104, 52–64. doi: 10.1016/j.biomaterials.2016.06.062

Singh, A., Ramesh, S., Cibi, D. M., Yun, L. S., Li, J., Li, L., et al. (2016). Hippo signaling mediators Yap and Taz are required in the epicardium for coronary vasculature development. *Cell Rep.* 15, 1384–1393. doi: 10.1016/j.celrep.2016.04.027

Smits, A. M., and Riley, P. R. (2014). Epicardium-derived heart repair. *J. Dev. Biol.* 2, 84–100. doi: 10.3390/jdb2020084

Snider, P., Hinton, R. B., Moreno-Rodriguez, R. A., Wang, J., Rogers, R., Lindsley, A., et al. (2008). Periostin is required for maturation and extracellular matrix stabilization of noncardiomyocyte lineages of the heart. *Circ. Res.* 102, 752–760. doi: 10.1161/circresaha.107.159517

Spadaccio, C., Rainer, A., Mozetic, P., Trombetta, M., Dion, R. A., Barbato, R., et al. (2015). The role of extracellular matrix in age-related conduction disorders: a forgotten player? *J. Geriatr. Cardiol.* 12, 76–82. doi: 10.11909/j.issn.1671-5411.2015.01.009

Stankunas, K., Hang, C. T., Tsun, Z. Y., Chen, H., Lee, N. V., Wu, J. I., et al. (2008). Endocardial Brg1 represses ADAMTS1 to maintain the microenvironment for myocardial morphogenesis. *Dev. Cell* 14, 298–311. doi: 10.1016/j.devcel.2007.11.018

Stein, M., Noorman, M., van Veen, T. A. B., Herold, E., Engelen, M. A., Boulaksil, M., et al. (2008). Dominant arrhythmia vulnerability of the right ventricle in senescent mice. *Heart Rhythm.* 5, 438–448. doi: 10.1016/j.hrthm.2007.10.033

Sugiyama, A., Hirano, Y., Okada, M., and Yamawaki, H. (2018). Endostatin stimulates proliferation and migration of Myofibroblasts isolated from myocardial infarction model rats. *Int. J. Mol. Sci.* 19:741. doi: 10.3390/ijms19030741

Sun, Z., Guo, S. S., and Fässler, R. (2016). Integrin-mediated mechanotransduction. *J. Cell Biol.* 215, 445–456. doi: 10.1083/jcb.201609037

Svystonyuk, D. A., Mewhort, H. E. M., Hassanabad, A. F., Heydari, B., Mikami, Y., Turnbull, J. D., et al. (2020). Acellular bioscaffolds redirect cardiac fibroblasts and promote functional tissue repair in rodents and humans with myocardial injury. *Sci. Rep.* 10:9459. doi: 10.1038/s41598-020-66327-66329

Takawale, A., Sakamuri, S. S., and Kassiri, Z. (2015). Extracellular matrix communication and turnover in cardiac physiology and pathology. *Compr. Physiol.* 5, 687–719. doi: 10.1002/cphy.c140045

Tanaka, K., Valero-Munoz, M., Wilson, R. M., Essick, E. E., Fowler, C. T., Nakamura, K., et al. (2016). Follistatin like 1 regulates hypertrophy in heart failure with preserved ejection fraction. *JACC Basic Transl. Sci.* 1, 207–221. doi: 10.1016/j.jacbts.2016.04.002

Terman, A., Kurz, T., Gustafsson, B., and Brunk, U. T. (2008). The involvement of lysosomes in myocardial aging and disease. *Curr. Cardiol. Rev.* 4, 107–115. doi: 10.2174/157340308784245801

Travers, J. G., Kamal, F. A., Robbins, J., Yutzey, K. E., and Blaxall, B. C. (2016). Cardiac fibrosis: the fibroblast awakens. *Circ. Res.* 118, 1021–1040. doi: 10.1161/circresaha.115.306565

Trinh, L. A., and Stainier, D. Y. (2004). Fibronectin regulates epithelial organization during myocardial migration in zebrafish. *Dev. Cell* 6, 371–382.

Tzahor, E., and Poss, K. D. (2017). Cardiac regeneration strategies: staying young at heart. *Science* 356, 1035–1039. doi: 10.1126/science.aam5894

Utriainen, A., Sormunen, R., Kettunen, M., Carvalhaes, L. S., Sajanti, E., Eklund, L., et al. (2004). Structurally altered basement membranes and hydrocephalus in a type XVIII collagen deficient mouse line. *Hum. Mol. Genet.* 13, 2089–2099. doi: 10.1093/hmg/ddh213

Uygur, A., and Lee, R. T. (2016). Mechanisms of cardiac regeneration. *Dev. Cell* 36, 362–374. doi: 10.1016/j.devcel.2016.01.018

Valiente-Alandi, I., Schafer, A. E., and Blaxall, B. C. (2016). Extracellular matrix-mediated cellular communication in the heart. *J. Mol. Cell Cardiol.* 91, 228–237. doi: 10.1016/j.yjmcc.2016.01.011

van Wijk, B., Gunst, Q. D., Moorman, A. F., and van den Hoff, M. J. (2012). Cardiac regeneration from activated epicardium. *PLoS One* 7:e44692. doi: 10.1371/journal.pone.0044692

Virani, S. S., Alonso, A., Benjamin, E. J., Bittencourt, M. S., Callaway, C. W., Carson, A. P., et al. (2020). Heart disease and stroke statistics-2020 Update: a report from the American Heart Association. *Circulation* 141, e139–e596. doi: 10.1161/CIR.0000000000000757

von Gise, A., Lin, Z., Schlegelmilch, K., Honor, L. B., Pan, G. M., Buck, J. N., et al. (2012). YAP1, the nuclear target of Hippo signaling, stimulates heart growth through cardiomyocyte proliferation but not hypertrophy. *Proc. Natl. Acad. Sci. U.S.A.* 109, 2394–2399. doi: 10.1073/pnas.1116136109

von Gise, A., and Pu, W. T. (2012). Endocardial and epicardial epithelial to mesenchymal transitions in heart development and disease. *Circ. Res.* 110, 1628–1645. doi: 10.1161/circresaha.111.259960

Wainwright, J. M., Hashizume, R., Fujimoto, K. L., Remlinger, N. T., Pesyna, C., Wagner, W. R., et al. (2012). Right ventricular outflow tract repair with a cardiac biologic scaffold. *Cells Tissues Organs* 195, 159–170. doi: 10.1159/000331400

Wang, J., Panáková, D., Kikuchi, K., Holdway, J. E., Gemberling, M., Burris, J. S., et al. (2011). The regenerative capacity of zebrafish reverses cardiac failure caused by genetic cardiomyocyte depletion. *Development* 138, 3421–3430. doi: 10.1242/dev.068601

Wang, Q., Yang, H., Bai, A., Jiang, W., Li, X., Wang, X., et al. (2016). Functional engineered human cardiac patches prepared from nature's platform improve heart function after acute myocardial infarction. *Biomaterials* 105, 52–65. doi: 10.1016/j.biomaterials.2016.07.035

Wang, Z., Long, D. W., Huang, Y., Chen, W. C. W., Kim, K., and Wang, Y. (2019). Decellularized neonatal cardiac extracellular matrix prevents widespread ventricular remodeling in adult mammals after myocardial infarction. *Acta Biomater.* 87, 140–151. doi: 10.1016/j.actbio.2019.01.062

Weber, K. T. (1989). Cardiac interstitium in health and disease: the fibrillar collagen network. *J. Am. Coll. Cardiol.* 13, 1637–1652. doi: 10.1016/0735-1097(89)90360-90364

Wei, K., Serpooshan, V., Hurtado, C., Diez-Cunado, M., Zhao, M., Maruyama, S., et al. (2015). Epicardial FSTL1 reconstitution regenerates the adult mammalian heart. *Nature* 525, 479–485. doi: 10.1038/nature15372

Wicha, M. S., Lowrie, G., Kohn, E., Bagavandoss, P., and Mahn, T. (1982). Extracellular matrix promotes mammary epithelial growth and differentiation in vitro. *Proc. Natl. Acad. Sci. U.S.A.* 79, 3213–3217.

Wight, T. N., and Potter-Perigo, S. (2011). The extracellular matrix: an active or passive player in fibrosis? *Am. J. Physiol. Gastrointest. Liver Physiol.* 301, G950–G955. doi: 10.1152/ajpgi.00132.2011

Williams, C., Quinn, K. P., Georgakoudi, I., and Black, L. D. III (2014). Young developmental age cardiac extracellular matrix promotes the expansion of neonatal cardiomyocytes in vitro. *Acta Biomater.* 10, 194–204. doi: 10.1016/j.actbio.2013.08.037

Xin, M., Kim, Y., Sutherland, L. B., Murakami, M., Qi, X., McAnally, J., et al. (2013). Hippo pathway effector Yap promotes cardiac regeneration. *Proc. Natl. Acad. Sci. U.S.A.* 110, 13839–13844. doi: 10.1073/pnas.1313192110

Xue, M., and Jackson, C. J. (2015). Extracellular matrix reorganization during wound healing and its impact on abnormal scarring. *Adv. Wound Care* 4, 119–136. doi: 10.1089/wound.2013.0485

Yabluchanskiy, A., Ma, Y., Chiao, Y. A., Lopez, E. F., Voorhees, A. P., Toba, H., et al. (2014). Cardiac aging is initiated by matrix metalloproteinase-9-mediated endothelial dysfunction. *Am. J. Physiol. Heart Circ. Physiol.* 306, H1398–H1407. doi: 10.1152/ajpheart.00090.2014

Yahalom-Ronen, Y., Rajchman, D., Sarig, R., Geiger, B., and Tzahor, E. (2015). Reduced matrix rigidity promotes neonatal cardiomyocyte dedifferentiation, proliferation and clonal expansion. *eLife* 4:e07455. doi: 10.7554/eLife.07455

Yang, H., Borg, T. K., Liu, H., and Gao, B. Z. (2015). Interactive relationship between basement-membrane development and sarcomerogenesis in single cardiomyocytes. *Exp. Cell Res.* 330, 222–232. doi: 10.1016/j.yexcr.2014.08.020

Yap, L., Tay, H. G., Nguyen, M. T. X., Tjin, M. S., and Tryggvason, K. (2019). Laminins in cellular differentiation. *Trends Cell Biol.* 29, 987–1000. doi: 10.1016/j.tcb.2019.10.001

Yasuda, J., Okada, M., and Yamawaki, H. (2017). T3 peptide, an active fragment of tumstatin, inhibits H_2O_2-induced apoptosis in H9c2 cardiomyoblasts. *Eur. J. Pharmacol.* 807, 64–70. doi: 10.1016/j.ejphar.2017.04.032

Ye, L., D'Agostino, G., Loo, S. J., Wang, C. X., Su, L. P., Tan, S. H., et al. (2018). Early regenerative capacity in the porcine heart. *Circulation* 138, 2798–2808. doi: 10.1161/CIRCULATIONAHA.117.031542

Youngblood, R. L., Truong, N. F., Segura, T., and Shea, L. D. (2018). It's all in the delivery: designing hydrogels for cell and non-viral gene therapies. *Mol. Ther.* 26, 2087–2106. doi: 10.1016/j.ymthe.2018.07.022

Yuan, Z., Tsou, Y. H., Zhang, X. Q., Huang, S., Yang, Y., Gao, M., et al. (2019). Injectable citrate-based hydrogel as an angiogenic biomaterial improves cardiac repair after myocardial infarction. *ACS Appl. Mater. Interf.* 11, 38429–38439. doi: 10.1021/acsami.9b12043

Zhang, Y., Zhu, D., Wei, Y., Wu, Y., Cui, W., Liuqin, L., et al. (2019). A collagen hydrogel loaded with HDAC7-derived peptide promotes the regeneration of infarcted myocardium with functional improvement in a rodent model. *Acta Biomater.* 86, 223–234. doi: 10.1016/j.actbio.2019.01.022

Zhao, C., Guo, H., Li, J., Myint, T., Pittman, W., Yang, L., et al. (2014). Numb family proteins are essential for cardiac morphogenesis and progenitor differentiation. *Development* 141, 281–295. doi: 10.1242/dev.093690

Zhao, W., Lu, L., Chen, S. S., and Sun, Y. (2004). Temporal and spatial characteristics of apoptosis in the infarcted rat heart. *Biochem. Biophys. Res. Commun.* 325, 605–611. doi: 10.1016/j.bbrc.2004.10.064

Zhou, B., Honor, L. B., He, H., Ma, Q., Oh, J. H., Butterfield, C., et al. (2011). Adult mouse epicardium modulates myocardial injury by secreting paracrine factors. *J. Clin. Invest.* 121, 1894–1904. doi: 10.1172/jci45529

Zhou, B., Honor, L. B., Ma, Q., Oh, J.-H., Lin, R.-Z., Melero-Martin, J. M., et al. (2012). Thymosin beta 4 treatment after myocardial infarction does not reprogram epicardial cells into cardiomyocytes. *J. Mol. Cell Cardiol.* 52, 43–47. doi: 10.1016/j.yjmcc.2011.08.020

Zhou, B., Ma, Q., Rajagopal, S., Wu, S. M., Domian, I., Rivera-Feliciano, J., et al. (2008). Epicardial progenitors contribute to the cardiomyocyte lineage in the developing heart. *Nature* 454, 109–113. doi: 10.1038/nature07060

Zhu, W., Zhang, E., Zhao, M., Chong, Z., Fan, C., Tang, Y., et al. (2018). Regenerative potential of neonatal porcine hearts. *Circulation* 138, 2809–2816. doi: 10.1161/CIRCULATIONAHA.118.034886

Zymek, P., Bujak, M., Chatila, K., Cieslak, A., Thakker, G., Entman, M. L., et al. (2006). The role of platelet-derived growth factor signaling in healing myocardial infarcts. *J. Am. Coll. Cardiol.* 48, 2315–2323. doi: 10.1016/j.jacc.2006.07.060

Conflict of Interest: The authors declare that the research was conducted in the absence of any commercial or financial relationships that could be construed as a potential conflict of interest.

frontiers in Cell and Developmental Biology

ORIGINAL RESEARCH
published: 28 January 2021
doi: 10.3389/fcell.2020.596819

Mitochondrial Dynamics in the *Drosophila* Ovary Regulates Germ Stem Cell Number, Cell Fate, and Female Fertility

Marcia Garcez[1,2†], *Joana Branco-Santos*[1†], *Patricia C. Gracio*[1] *and Catarina C. F. Homem*[1*]

[1] *iNOVA4Health, CEDOC, NOVA Medical School, NMS, Universidade Nova de Lisboa, Lisbon, Portugal,* [2] *Graduate Program in Areas of Basic and Applied Biology (GABBA), Universidade do Porto, Porto, Portugal*

OPEN ACCESS

Edited by:
Susana Solá, University of Lisbon, Portugal

Reviewed by:
Yuan Wang, Michigan State University, United States
Maria Fernanda Forni, Yale University, United States

***Correspondence:**
Catarina C. F. Homem
catarina.homem@nms.unl.pt

[†] *These authors have contributed equally to this work*

Specialty section:
This article was submitted to Stem Cell Research, a section of the journal Frontiers in Cell and Developmental Biology

Received: *20 August 2020*
Accepted: *30 November 2020*
Published: *28 January 2021*

Citation:
Garcez M, Branco-Santos J, Gracio PC and Homem CCF (2021) Mitochondrial Dynamics in the Drosophila Ovary Regulates Germ Stem Cell Number, Cell Fate, and Female Fertility. Front. Cell Dev. Biol. 8:596819. doi: 10.3389/fcell.2020.596819

The fate and proliferative capacity of stem cells have been shown to strongly depend on their metabolic state. Mitochondria are the powerhouses of the cell being responsible for energy production *via* oxidative phosphorylation (OxPhos) as well as for several other metabolic pathways. Mitochondrial activity strongly depends on their structural organization, with their size and shape being regulated by mitochondrial fusion and fission, a process known as mitochondrial dynamics. However, the significance of mitochondrial dynamics in the regulation of stem cell metabolism and fate remains elusive. Here, we characterize the role of mitochondria morphology in female germ stem cells (GSCs) and in their more differentiated lineage. Mitochondria are particularly important in the female GSC lineage. Not only do they provide these cells with their energy requirements to generate the oocyte but they are also the only mitochondria pool to be inherited by the offspring. We show that the undifferentiated GSCs predominantly have fissed mitochondria, whereas more differentiated germ cells have more fused mitochondria. By reducing the levels of mitochondrial dynamics regulators, we show that both fused and fissed mitochondria are required for the maintenance of a stable GSC pool. Surprisingly, we found that disrupting mitochondrial dynamics in the germline also strongly affects nurse cells morphology, impairing egg chamber development and female fertility. Interestingly, reducing the levels of key enzymes in the Tricarboxylic Acid Cycle (TCA), known to cause OxPhos reduction, also affects GSC number. This defect in GSC self-renewal capacity indicates that at least basal levels of TCA/OxPhos are required in GSCs. Our findings show that mitochondrial dynamics is essential for female GSC maintenance and female fertility, and that mitochondria fusion and fission events are dynamically regulated during GSC differentiation, possibly to modulate their metabolic profile.

Keywords: mitochondrial dynamics, germ stem cell, oxidative phosphorylation, differentiation, oogenesis, fertility, *Drosophila melanogaster*

INTRODUCTION

Metabolic plasticity, in particular the balance between glycolysis and oxidative phosphorylation (OxPhos), has been shown to regulate cell fate both in stem cells and in their differentiated lineages, across several models (Tsogtbaatar et al., 2020). High glycolytic flux and low mitochondria content have been observed in stem cells, whereas more specialized cells rely mainly on OxPhos to meet their metabolic demands and have higher numbers of mitochondria (Rafalski et al., 2012). Mitochondria are central organelles in metabolism regulation, with several key metabolic pathways, such as the Tricarboxylic Acid Cycle (TCA), lipid beta oxidation, and OxPhos, occurring in these organelles. Mitochondria are also important regulators of Ca^{2+} homeostasis and apoptosis among other processes (Nunnari and Suomalainen, 2012). Mitochondria function is tightly linked to their morphology that is modulated through events of fusion and fission between their inner and outer membranes, a process known as mitochondrial dynamics. While predominance of fission events is associated with smaller and more punctate mitochondria, shifting the balance toward fusion leads to larger and more aggregated mitochondria (Spurlock et al., 2020). These changes in mitochondria morphology occur rapidly in response to changes in metabolic requirements or external signals (Zhang et al., 2018).

However, it is not clear how stem cell fate and specific metabolic profiles are associated with mitochondria morphology. To address this question, we took advantage of the well-characterized ovarian germ stem cell (GSC) lineage in *Drosophila*. Female GSCs are located in a simple anatomical structure known as germarium and are among a few of the stem cells present in adult tissues. GSCs can be reliably identified, and their lineages well-characterized and easily traced. This, together with the large availability of genetic tools for their manipulation, makes them one of the best models to study stem cell biology.

Mitochondria in female GSCs are of particular importance because, in addition to their role in metabolic regulation, these cells provide the only pool of mitochondria that will be inherited by the progeny, since male mitochondrial DNA (mtDNA) is eliminated during spermatogenesis (DeLuca and O'Farrell, 2012). Mitochondrial dynamics plays an important role in ensuring the quality of mitochondria to be inherited by the progeny. While fusion events enable mixing of matrix components between mitochondria, promoting their homogenization and a healthy mitochondria pool (Chan, 2012), mitochondrial fission was shown to be crucial for selection of mitochondria without deleterious mtDNA (Lieber et al., 2019). Although male mitochondria do not contribute to progeny, mitochondrial dynamics has been shown to be important in the early stages of spermatogenesis, with disruptions in this mechanism causing defects in GSC number or spermatogenesis arrest (Demarco et al., 2019; Varuzhanyan et al., 2019).

Previous studies of *Drosophila* female GSCs showed that mitochondria morphology changes during GSC lineage differentiation (Cox and Spradling, 2003), suggesting that mitochondrial dynamics may play an important role in fate regulation. It has also been shown that female GSCs have reduced mitochondrial membrane potential (Wang et al., 2019) and reduced levels of electron transport chain (ETC) proteins (Kai et al., 2005) when compared with more differentiated germ cells. These results suggest that mitochondria play an unimportant role in GSCs, and that they only become important for the increase in OxPhos that occurs with differentiation. Despite these observations suggesting that the metabolic profile of GSC lineages correlates with their fate and potency, it is still not known if mitochondria play a role in GSCs. Furthermore, it is not clear if there is a functional link between mitochondria morphology and the fate of GSC lineages.

To address the role of mitochondrial dynamics in female GSCs, we interfered with mitochondrial fission and fusion mechanisms in the female germline of *Drosophila* to determine how lineages are affected. Each ovariole contains two to three GSCs located at the tip of the germarium, in a protected microenvironment or niche (**Figures 1A,A′**). GSCs are connected to niche cells, the cap cells, and are characterized by the presence of the spectrosome (**Figure 1A′**, region 1). GSCs divide to produce one daughter cell through self-renewal and another daughter cell that is no longer directly connected to cap cells and therefore initiates differentiation, the cystoblast. The cystoblast undergoes four subsequent mitotic divisions with incomplete cytokinesis to generate a cyst of 16 interconnected cells. Cyst differentiation is accompanied by the differentiation of the spectrosome into the fusome, a germline-specific organelle of communication. This cyst is then completely encapsulated by follicle cells (**Figure 1A′**, regions 2a and 2b), and one cell in this 16-cell cyst is specified as the oocyte, whereas the remaining 15 cells become nurse cells (**Figure 1A′**, region 3). The surrounding nurse cells support oocyte growth that continues developing in sequentially more mature follicles until a fully developed egg is formed at the posterior end of the ovariole (**Figure 1A**).

Here, we have characterized mitochondria morphology in GSCs and in their early differentiated lineage in the *Drosophila* germarium. We have also knocked down the regulators of fusion, Mitochondrial Assembly Regulatory Factor (Marf or mitofusin) and Optic Atrophy 1 (Opa1), as well as the regulator of fission Dynamin-related protein 1 (Drp1) in female GSCs, and analyzed how their depletion affects GSC number and lineage. Our results show that the undifferentiated GSCs predominantly have sparse and punctate mitochondria, whereas more differentiated germ cells show more aggregated mitochondria, suggesting more fusion. Dysregulation of mitochondrial dynamics in GSCs, by interfering with fusion or fission mechanisms, leads to a loss of GSCs and causes a severe reduction in female fecundity. In addition, depletion of mitochondrial dynamics regulators in GSCs tends to increase mitochondrial membrane potential that correlates with GSC loss and defects in germline development in a mechanism independent of reactive oxygen species (ROS). Interestingly, reducing the levels of key enzymes in the TCA cycle also leads to a reduction in the number of GSCs, suggesting that mitochondrial dynamics may be required for TCA/OxPhos and, thus, GSC maintenance. Surprisingly, we found that impairment of mitochondrial dynamics strongly affects egg chamber structural organization, ultimately causing arrest of egg chamber development at late stages and consequently reduced oogenesis. Overall, our results show that mitochondria, and specifically TCA/OxPhos metabolism, play an essential role in

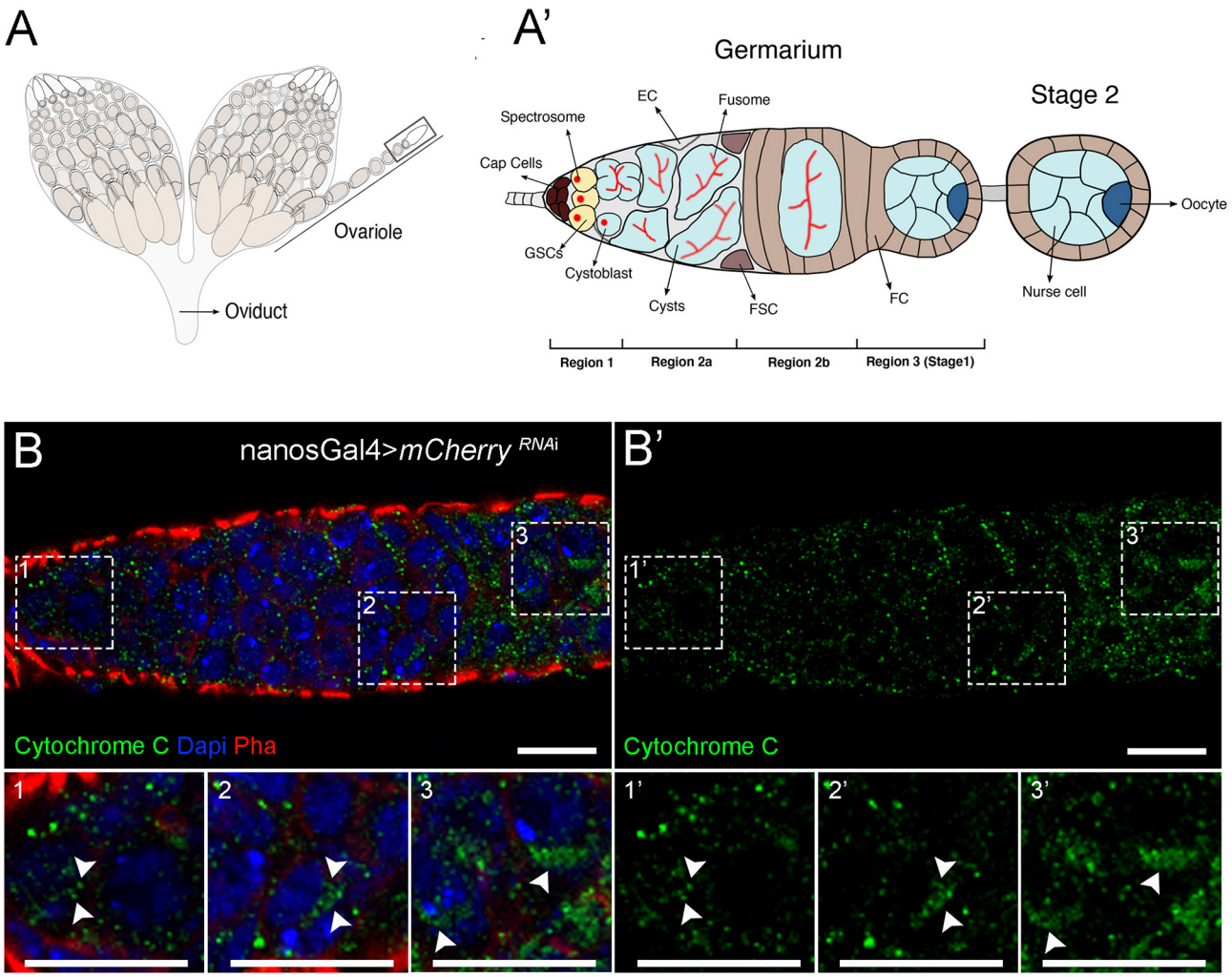

FIGURE 1 | Mitochondria undergo changes in morphology during cellular differentiation in the adult germarium. **(A)** Schematic representation of *Drosophila* ovaries illustrating the different stages of egg formation in the ovarioles. **(A′)** Enlarged view of the germarium. The germarium is located at the most anterior part of the ovariole (black box outlined in **A**). At the most anterior tip of the germarium (region 1) reside the germ stem cells (GSCs). GSCs are connected to niche cells, the cap cells, and are characterized by the presence of round spectrosomes. GSCs divide to self-renew and form one cystoblast that occupies a more posterior position and is not in direct contact with cap cells. The cystoblast starts differentiation and divides to give rise to cysts (region 2a); this process is accompanied by the differentiation of the spectrosome into an elongated structure, the fusome. In region 2b, the cysts are encapsulated by follicle cells (FC), and in region 3, 1 out of the 16 cyst cells is specified as the oocyte (dark blue cell at the posterior side of the cyst), whereas the remaining 15 cells become nurse cells, supportive cells that will aid in oocyte development into one mature egg. Escort cells (ECs) and follicle stem cells (FSCs) are also represented. **(B)** Representative images of a control germarium (expressing *mCherry*^{RNAi} driven by *nos*Gal4) showing staining for mitochondria in the different developmental regions. Mitochondria labeled by Cytochrome *c* staining are visualized in green **(B′)**. GSCs mostly display punctate and fragmented mitochondria (1 and 1′) that progressively aggregate during cyst differentiation (2–3 and 2′-3′), suggesting more fusion. Fissed and fused mitochondria in regions 1 (1 and 1′), 2b (2 and 2′), and 3 (3 and 3′) of the germarium are identified with arrowheads in zoomed areas (dashed white squares). Nuclei are labeled with DAPI (blue), and F-actin is labeled with Phalloidin (Pha, red). Scale bars represent 10 μm.

the maintenance of GSCs contradicting the notion that these are mostly required in differentiated cells. Additionally, our work uncovers a novel role for mitochondrial dynamics in the regulation of egg chamber development and female fertility.

MATERIALS AND METHODS

Fly Husbandry and Stocks

Flies were raised and maintained on standard cornmeal medium at 25°C in 12 h light/dark cycle, unless otherwise stated. To identify mitochondrial regulators that impact GSC number, we analyzed UAS-RNAi lines targeting genes mediating mitochondrial fission (*Drp1*) and fusion (*Marf* and *Opa1*) and genes encoding key mitochondrial metabolic enzymes (*Scsalpha1* and *alpha-KGDHC*). The RNAi stocks were obtained from the Bloomington *Drosophila* Stock Center (BDSC) or the Vienna *Drosophila* Resource Center (VDRC) and included the following strains: UAS-*Drp1*^{RNAi} (strains BL51483, BL67160, v44156), UAS-*Marf*^{RNAi} (strains BL55189, BL67158, v40478, v105261), UAS-*Opa1*^{RNAi} (strains BL32358, BL67159, v106290),

UAS-*Scsalpha1*^{RNAi} (CG1065, v107164), and UAS-*CG5214*^{RNAi}, referred in text as UAS-*alpha-KGDHC*^{RNAi} (v108403). The *nanos*Gal4 line (BL25751) was used to drive the expression of UAS-RNAi transgenes specifically in germ cells. In all experiments, UAS-*mCherry* ^{RNAi} (BL35758) was used as a control. Genotypes and sources are detailed in **Supplementary Table 1**.

Dissection of Adult *Drosophila* Ovaries

For RNAi-mediated knockdown experiments, crosses of *nanos*Gal4 females with males from RNAi lines were set up. Newly eclosed F1 females were kept in yeast-enriched food for 16 h at 25°C to allow proper ovary maturation. Ovaries were dissected in Schneider's *Drosophila* medium (Gibco) at room temperature as previously described (Gates et al., 2009). Briefly, 5–10 adult flies per genotype were anesthetized with CO_2, and ovaries were isolated with the aid of forceps. Ovarioles were partially individualized before fixation to facilitate permeabilization.

Immunostaining and Confocal Microscopy

Ovaries were fixed in 4% paraformaldehyde for 20 min at room temperature and washed 3× with PBST (0.1% Triton X-100 in 1× PBS). Ovaries were blocked using 1% normal goat serum (Jackson Immunoresearch) in 0.1% PBST for at least 20 min at room temperature and incubated overnight at 4°C with primary antibodies (listed below) diluted in blocking solution. Afterwards, ovaries were washed 3×, blocked for 20 min, and incubated for 2 h at room temperature with secondary antibodies (listed below), Alexa Fluor 568 Phalloidin (1:500; Invitrogen) and DAPI (1:1,000; Sigma-Aldrich). Ovaries were then manipulated in 1× PBS using micro dissecting needles (Fine Science Tools) for ovariole individualization and mounted in Aqua-Poly/Mount (Polysciences, Inc.). Images were acquired using a Zeiss LSM880 confocal microscope (Zeiss).

The following primary antibodies were used: mouse monoclonal anti-Hts 1B1 [1:5; Developmental Studies Hybridoma Bank, University of Iowa (DSHB)], rat monoclonal anti-Vasa (1:50; DSHB), and rabbit anti-Cytochrome *c* (1:100; Cell Signaling Technology). The following secondary antibodies (1:1,000; Invitrogen) were used: Alexa Fluor 647-conjugated goat anti-mouse, Alexa Fluor 488-conjugated goat anti-rat, and Alexa Fluor 488-conjugated goat anti-rabbit.

TMRM and MitoTracker Analysis

To investigate mitochondrial activity, we used a combination of two fluorescent dyes: MitoTracker Deep Red (Life Sciences), to determine the localization of mitochondria, and TMRM [tetramethylrhodamine methyl ester, perchlorate (Biotium)], an indicator of mitochondrial membrane potential. Ovaries were dissected as described above and incubated for 30 min with MitoTracker (500 nM) in Schneider's Drosophila medium at room temperature. Half-way through MitoTracker incubation, TMRM (100 nM) dye was added (15 min incubation period). Ovaries were washed 3× and mounted in PBS. Images of live germaria were acquired immediately after mounting using a Zeiss LSM880 confocal microscope (Zeiss).

ROS Analysis

Dihydroethidium (DHE) staining was used to probe the levels of ROS. Ovaries were dissected as described above and incubated for 10 min with DHE (30 μM; Life Technologies) and DAPI (1 μg/ml; Sigma-Aldrich) in Schneider's Drosophila medium at room temperature. This was followed by a quick fixation for 5 min in 4% paraformaldehyde after which ovaries were washed once in PBS and mounted in Aqua-Poly/Mount. Germaria were immediately imaged in a Zeiss LSM880 confocal microscope (Zeiss).

Quantification and Statistical Analysis

All images were analyzed and prepared for publication using the Fiji software (Schindelin et al., 2012).

GSC Quantification

Cells were considered GSCs only when the following characteristics were observed: (1) presence of a rounded spectrosome (labeled by anti-Hts antibody) and (2) physical contact with their niche cells in region 1 of the germarium. The average number of GSCs and the corresponding standard deviations (SDs) were calculated for at least 16 germaria per genotype.

Statistical analysis was performed using Prism 6 (GraphPad Software Inc., La Jolla, CA, USA). All data are represented as mean ± SD of at least three independent experiments. Statistical significance of difference to control was calculated using Student's *t*-test and considered significant when $P < 0.05$. Statistically significant differences are depicted as follows: $^{*}P < 0.05$, $^{**}P < 0.01$, $^{***}P < 0.001$, and $^{****}P < 0.0001$. # indicates $P < 0.10$ and represents a relevant trend of decrease in GSC number. Non-significant (n.s.) differences are $P > 0.10$.

TMRM/MitoTracker Quantification

To quantify the average ratio between TMRM and MitoTracker, region 1 of the germarium was delineated using the freehand tool in Fiji, and the mean intensities of TMRM and MitoTracker were measured. TMRM/MitoTracker ratios were calculated by dividing the mean intensity value of TMRM by the one of MitoTracker. Ratiometric images were generated by dividing the TMRM channel by the one of MitoTracker using the Image Calculator in Fiji. The resulting image was pseudo-colored using Rainbow RGB, and a calibration bar was included to facilitate image interpretation. Ratiometric images representative of each genotype are presented. These are in line with the average values of TMRM/MitoTracker ratios calculated for region 1. Statistical analysis was done using Student's *t*-test. Statistically significant differences are depicted as follows: $^{*}P < 0.05$. # indicates $P < 0.10$ and represents a relevant trend. Data are represented as mean ± SD.

Quantification of DHE Labeling

ROS assessment was based on the quantification of nuclear DHE, since when oxidized DHE converts to ethidium, which intercalates within DNA and is therefore within the nucleus (Carter et al., 1994). For cells in region 1 of the germarium with observable nuclear DHE inclusion, the areas of nuclear

DHE were delineated using the freehand tool in Fiji, and the mean intensity of fluorescence was measured. Similarly, three sample measurements of the cytoplasmic region surrounding the nucleus were taken and averaged to obtain the cytoplasmic level of DHE. The mean intensity of nuclear DHE level was normalized by the cytoplasmic intensity to account for staining variability. Statistical significance of differences *vs.* control was calculated using *Dunn*'s multiple comparisons. Non-significant (n.s.) differences are when $P > 0.10$. Data are represented as mean ± SD.

Fecundity Assays

To evaluate egg production, w^{1118} males were crossed to female virgins expressing UAS-$Drp1^{RNAi}$ (v44156), UAS-$Opa1^{RNAi}$ (v106290), UAS-$Marf^{RNAi}$ (v40478), UAS-$Scsalpha1^{RNAi}$ (CG1065, v107164), and UAS-$CG5214^{RNAi}$ (referred in text as UAS-*alpha-KGDHC*^{RNAi}, v108403) or UAS-$mCherry^{RNAi}$ (BL35758) under the control of *nanos*Gal4. Flies were allowed to courtship and mate for 36 h at 25°C prior to egg counting. Three independent crosses were set up per condition, and flies were kept on fresh laying pots with apple juice agar plates enriched with yeast paste to stimulate egg laying during 3 consecutive days. Agar plates were replaced 3× per day at 3 h interval (plates from overnight periods were discarded). At the end of the day, eggs and female flies were counted. Fecundity was calculated as the number of laid eggs per female per hour.

qPCR Analysis

Brains from L3 wandering larvae expressing UAS-$Scsalpha1^{RNAi}$ (v107164) or UAS-$mCherry^{RNAi}$ (BL35758) driven by actin-GAL4 were dissected in Schneider's Drosophila medium. mRNA was isolated using TRIzol™ LS Reagent (Invitrogen) and treated with TURBO DNA-free™ Kit (Invitrogen™). cDNA was prepared using the RevertAid First Strand cDNA Synthesis Kit (Thermo Scientific™). The following primers were used for amplification:

Scsalpha1: GACATGGTGAAGGTGAAGCA and GATGCC GATCTTGCACTGT.
Act5C: GATAATGATGATGGTGTGCAGG and AGTGGT GGAAGTTTGGAGTG.

qPCRs were done using GoTaq qPCR Master mix (Promega) on a LightCycler 96 (Roche). Expression of *Scsalpha1* was normalized to *Act5C*, and relative levels were calculated vs. control ($mCherry^{RNAi}$) using the $2^{(-\Delta\Delta Ct)}$ method (Livak and Schmittgen, 2001). All measurements were done with technical triplicates.

RESULTS

Mitochondrial Dynamics Is an Important Regulator of Female GSCs

To clarify the role of mitochondrial dynamics in the female GSC lineage, we started by characterizing mitochondria morphology in GSCs and in their differentiated lineage in the germarium. To analyze mitochondrial morphology, we used an antibody against Cytochrome *c*, a mitochondrial protein present in the intermembrane space of these organelles, commonly used as a mitochondrial marker (Schägger, 2002). Consistently to what had been previously documented by electron microscopy (EM) (Mahowald and Strassheim, 1970; Carpenter, 1975; Cox and Spradling, 2003), we found that GSCs in region 1 have predominantly small punctate mitochondria (**Figure 1B**, close-up#1), and that mitochondria progressively become more aggregated in regions 2b and 3 consistent with an increase in mitochondria fusion (**Figure 1B**, close-up#2 and close-up#3, respectively). This increase in mitochondria fusion along cell differentiation suggests that mitochondrial dynamics may play a role in regulating cell fate.

In *Drosophila*, there are two regulators of mitochondria fusion, *Marf* or *mitofusin* that regulates mitochondrial outer-membrane fusion and *Opa1* that mediates fusion of the inner membrane of mitochondria (Pernas and Scorrano, 2016). Mitochondrial fission is mediated by *Drp1* that is recruited to the mitochondrial outer membrane and constricts mitochondria until organelle division occurs (Pernas and Scorrano, 2016). In order to test the hypothesis that mitochondrial dynamics is important for cell fate regulation in the germline, we interfered with both mitochondria fusion and fission regulators and asked whether this affects GSCs. We individually knocked down *Drp1*, *Marf*, or *Opa1* in germ cells by expressing UAS-RNAi transgenes under the control of *nanos*Gal4 (*nos*Gal4). The UAS/Gal4 system is a method for directing the expression of a genetic element of interest to a specific tissue (Brand and Perrimon, 1993). The Gal4 protein, derived from yeast, serves as a transcriptional activator that binds and activates the upstream activating sequence (UAS), driving the expression of the genetic element under the control of UAS. To induce knockdown, we expressed UAS-dsRNA targeting the genes of interest and simultaneously expressed Gal4 under the control of the *nanos* promotor, which is specifically expressed in the germline.

Because there are several RNAi lines available to target each of the mitochondrial dynamics regulatory genes, with variable efficiencies reported (Rai et al., 2014; Sandoval et al., 2014; Deng et al., 2016; Wang et al., 2016; Demarco and Jones, 2019; Demarco et al., 2019; Amartuvshin et al., 2020), we initially analyzed all lines for a possible phenotype in GSCs. While control germaria consistently have 2 or 3 GSCs (**Figures 2A,E**), 2 out of the 3 RNAi lines used for *Drp1* abrogation show a significant reduction in GSCs, with some germaria having no GSCs present (**Figures 2B,E**). Knockdown of the outer-membrane fusion regulator *Marf* also leads to a decrease in GSCs number, with 2 out of 4 RNAi lines showing a significant reduction and 2 lines showing a relevant trend toward a decrease (**Figures 2C,E**). Consistently, downregulation of the inner-membrane fusion regulator *Opa1* significantly reduces GSCs number in 2 out of 3 RNAi lines tested, with some germaria having no GSCs present (**Figures 2D,E**). Thus, knockdown of mitochondrial dynamics regulators with independent RNAi lines consistently leads to a reduction in GSC numbers, validating the observed phenotypes (see **Supplementary Table 2** for detailed characterization). For further analysis of each of these genes, we selected the RNAi line that shows the strongest phenotype and that had been previously validated: $Marf^{RNAi}$ v40478 (Trevisan

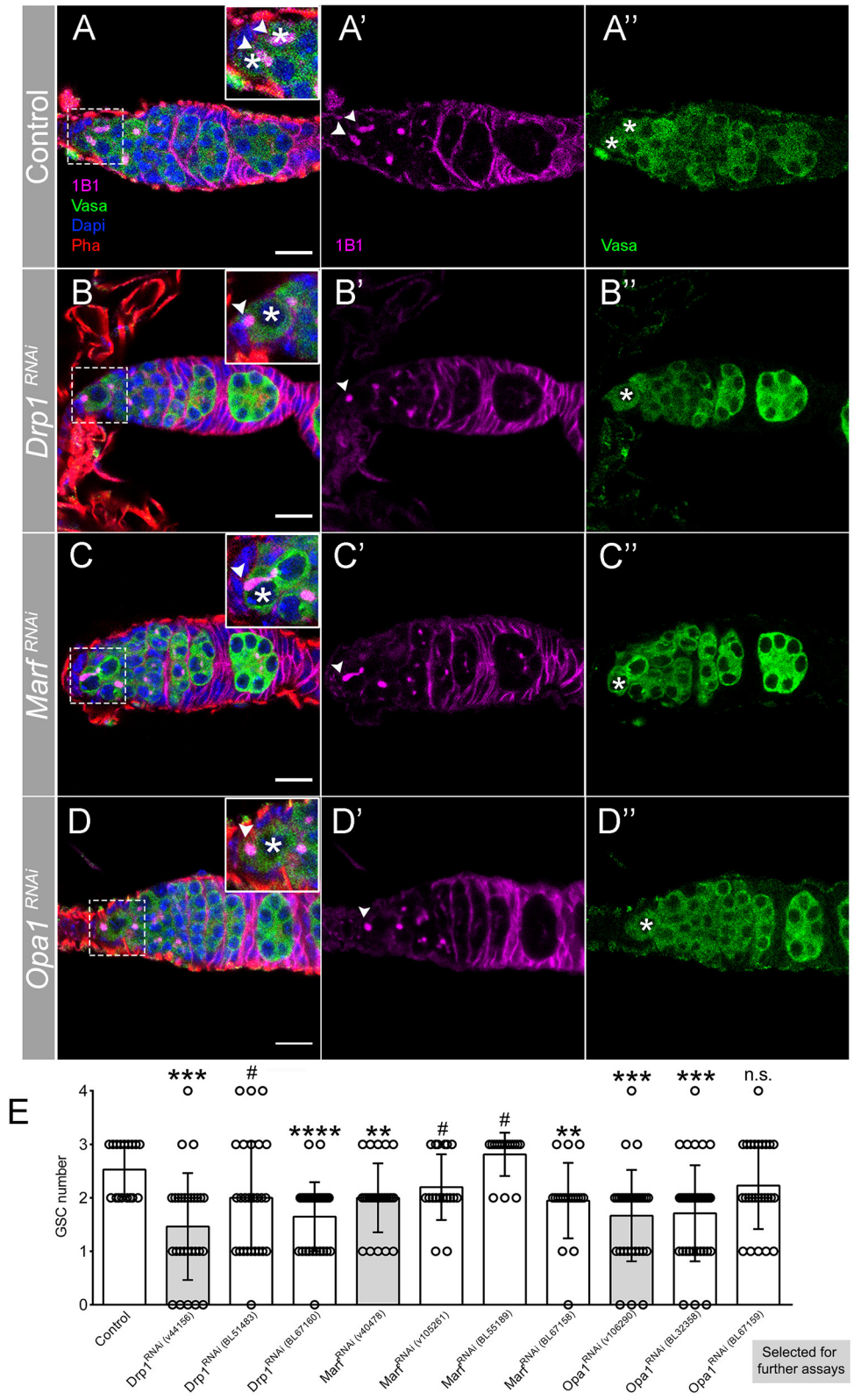

FIGURE 2 | Regulators of mitochondrial fission and fusion are essential for GSC maintenance. **(A–D)** Representative images of adult *Drosophila* germaria expressing RNAi transgenes against *mCherry* (control), *Drp1*, *Marf*, and *Opa1* by *nos*Gal4. Germ cells are labeled with Vasa antibody (green), and GSCs are marked by the

(Continued)

FIGURE 2 | presence of Hts-labeled spectrosome (1B1, pink). The dashed white squares highlight GSCs, marked by asterisks. Arrowheads point to spectrosome of GSCs that are in contact with niche cells. Control germaria typically have 2–3 GSCs **(A–A″,E)**. Depletion of mitochondrial fission regulator *Drp1* **(B–B″,E)** or mitochondrial fusion regulators *Marf* **(C–C″,E)** and *Opa1* **(D–D″,E)** significantly decreases GSC number. Images shown are representative of Drp1^{RNAi} (v44156), Marf^{RNAi} (v40478), and Opa1^{RNAi} (v106290) germaria. Nuclei and F-actin are labeled with DAPI (blue) and Phalloidin (Pha, red), respectively. Scale bars represent 10 μm. **(E)** Quantification of the average number of GSCs (±SD) per germarium expressing the indicated RNAi lines in GSCs (*nos*Gal4). Gray bars indicate the RNAi lines used in the following analyses for each of the mitochondrial dynamics regulators. Statistical significance *vs.* control was calculated using simple sample *t*-test. $^{**}P < 0.01$; $^{***}P < 0.001$; $^{****}P < 0.0001$; $^{\#}P < 0.10$; n.s., non-significant.

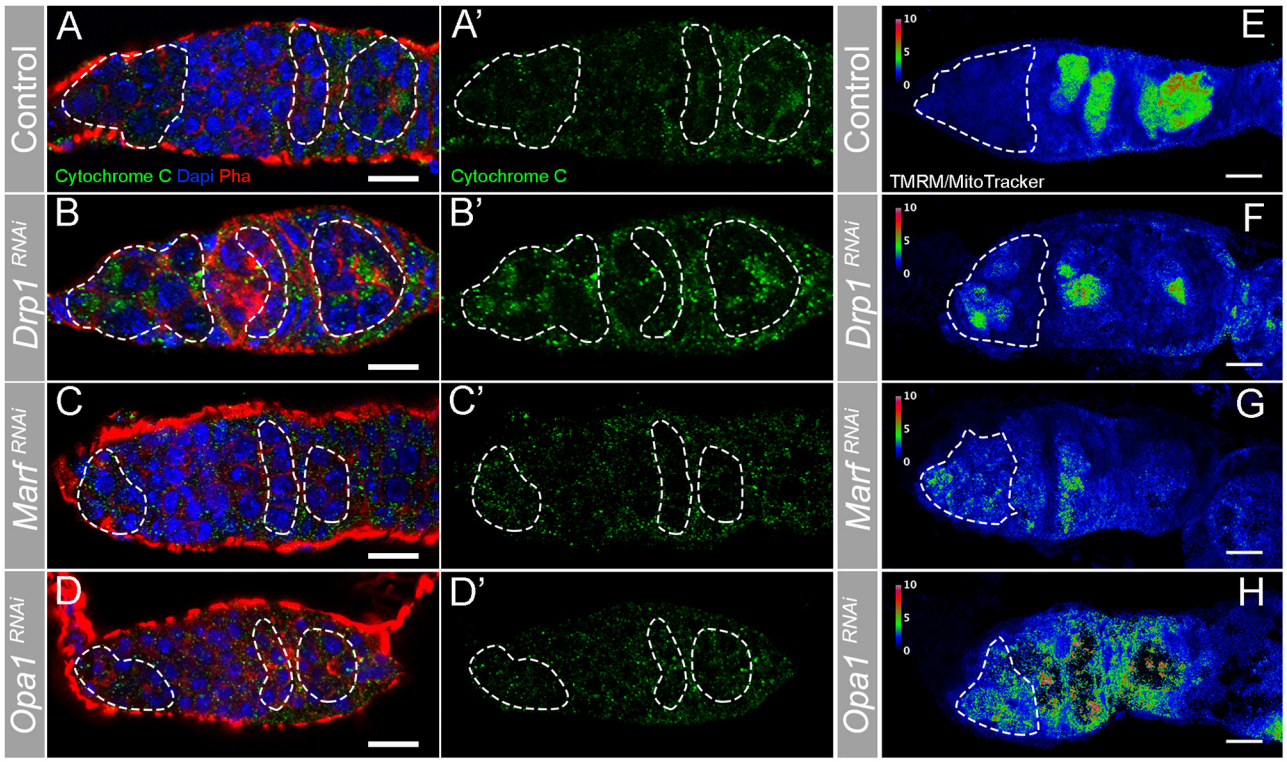

FIGURE 3 | RNAi of *Drp1*, *Marf*, or *Opa1* disrupts mitochondria morphology in the germarium increasing mitochondrial membrane potential in GSCs. **(A–H)** Representative images of germaria expressing *mCherry*^{RNAi}, *Drp1*^{RNAi}, *Marf*^{RNAi}, and *Opa1*^{RNAi} driven by *nos*Gal4. **(A–D)** Mitochondria are labeled by Cytochrome *c* antibody (green). Outlines are indicative of the areas where GSCs (in region 1) and their lineage (in regions 2b and 3) are found to facilitate visual comparison. **(A,A′)** In control germaria, fissed mitochondria are visible in GSCs (region 1), whereas differentiating cysts (regions 2b–3) have progressively more aggregated mitochondria suggesting a higher fusion-to-fission ratio. **(B,B′)** *Drp1*^{RNAi} causes hyperfusion of mitochondria in both GSCs (region 1) and differentiating cysts (regions 2b–3). **(C,C′,D,D′)** RNAi of *Marf* or *Opa1* in germ cells leads to a decrease of fused/aggregated mitochondria in regions 2b–3. Nuclei and F-actin are labeled with DAPI (blue) and Phalloidin (Pha, red), respectively. **(E–H)** Ratiometric images of germaria stained with TMRM (indicator of mitochondrial membrane potential) and MitoTracker (indicator of mitochondrial mass). The ratio of TMRM to MitoTracker intensity was calculated in Fiji, and a pseudo-colored image was generated using the rainbow RGB gradient. Outlines indicate region 1, where GSCs are localized. **(E)** Control GSCs have small TMRM/MitoTracker values, indicating low mitochondrial membrane potential. GSCs expressing *Drp1*^{RNAi} **(F)**, *Marf*^{RNAi} **(G)**, or *Opa1*^{RNAi} **(H)** have higher TMRM/MitoTracker ratios than control, indicating that depletion of fission or fusion increases mitochondrial membrane potential. Scale bars represent 10 μm.

et al., 2018; ∼80% knockdown), *Opa1*^{RNAi} v106290 (Rai et al., 2014; ∼70% knockdown), and *Drp1*^{RNAi} v44156 (Trevisan et al., 2018; ∼70% knockdown, same dsRNA).

To confirm that depleting regulators of mitochondrial dynamics through RNAi successfully modulates mitochondria morphology, we characterized mitochondria morphology in *Drp1*^{RNAi}, *Marf*^{RNAi}, and *Opa1*^{RNAi} germaria (**Figure 3**). Compared with control (**Figures 3A,A′**), germaria expressing *Drp1*^{RNAi} show more mitochondria aggregates in region 1, where GSCs are located, as well as in regions 2b and 3 (**Figures 3B,B′**). This increase in fused-like mitochondria is consistent with a decrease in mitochondrial fission events caused by depletion of fission regulator *Drp1*. In contrast, RNAi of either *Marf* (**Figures 3C,C′**) or *Opa1* (**Figures 3D,D′**) causes a reduction of mitochondria aggregation in regions 2b and 3. The decrease in mitochondria aggregation is again consistent with a reduction in fusion events upon depletion of fusion regulators. These results show that interfering with *Drp1*, *Marf*, and *Opa1* efficiently disrupts mitochondrial dynamics and morphology.

The results showing that interfering with either mitochondria fusion or fission leads to a decrease in GSC number were surprising. One hypothesis to explain these results is that mitochondrial activity might be equally disrupted in both conditions. To test this idea, we measured the mitochondrial inner membrane potential, generated by the ETC complexes. Mitochondria membrane potential is used for the production of ATP being therefore an indicator of mitochondrial respiration (reviewed in Iannetti et al., 2019). Mitochondrial inner membrane potential was measured as the ratio of TMRM (an established indicator of mitochondrial membrane potential) to MitoTracker Deep Red (a marker of mitochondrial mass) (Zhang et al., 2019). This analysis revealed that in control germaria, mitochondria in region 1 have low levels of mitochondrial membrane potential that then increase along germline differentiation (**Figure 3E**, region 1 outlined), consistent with what has been previously described (Wang et al., 2019). In contrast, in germaria expressing $Drp1^{RNAi}$ or $Opa1^{RNAi}$, although variable, mitochondria present in region 1 show increased membrane potential when compared with control (**Figures 3E–H**, **Supplementary Figure 1A**). Despite not causing such a strong effect, $Marf^{RNAi}$ also trends in the same direction with a fraction of the knocked down germaria presenting higher TMRM/MitoTracker values than the control (**Figures 3E,G**, **Supplementary Figure 1A**). Interestingly, the change in mitochondrial membrane potential nicely correlates with the severity of the phenotypes observed regarding GSC number. Germaria expressing either $Drp1^{RNAi}$ or $Opa1^{RNAi}$ have, on average, one GSC with several germaria presenting no GSCs, whereas $Marf^{RNAi}$ expressing germaria have on average two GSCs (**Figure 2E**). These results suggest that interfering with mitochondrial dynamics regulators in GSCs is not unspecifically disrupting mitochondria viability, and that GSCs have all the required components for the effective usage and regulation of their mitochondria. These experiments also reveal that interfering with fusion or fission can lead to increased mitochondrial membrane potential in GSCs, indicating that there is no straightforward connection between mitochondrial dynamics and activity in this context.

Since mitochondria are important sources of ROS, dysregulation of mitochondrial dynamics could also be affecting GSCs by the generation of detrimental ROS levels. Indeed, it was shown that interfering with mitochondrial fission increases the levels of ROS in the *Drosophila* testis (Demarco and Jones, 2019). To evaluate if ROS levels are increased upon knockdown of *Drp1*, *Marf*, or *Opa1* in GSCs, we used DHE staining, a commonly used method for ROS detection. This analysis has, however, revealed that depletion of any of these genes does not cause a significant change of ROS levels when compared with control ($mCherry^{RNAi}$) (**Supplementary Figure 1B**).

Taken together, our data show that interfering with mitochondrial dynamics, both fusion and fission, compromises GSC pool maintenance leading to a reduction in GSC number. Interestingly, although we found that, in wild-type conditions, germ cells located in region 1 of the germarium have predominantly fissed mitochondria, disruption of fusion mechanisms results in a loss of GSCs, indicating that fusion events play an unexpectedly important role at this stage. Analysis of mitochondrial membrane potential confirmed that mitochondria in wild-type GSCs have low membrane potential that increases along germline differentiation. Altering mitochondrial dynamics in either way leads to increased membrane potential in a fraction of the analyzed germaria, a phenomenon never observed in control germaria. Interestingly, interfering with mitochondrial dynamics in GSCs does not cause a change in the levels of ROS.

Defective Mitochondrial Dynamics Compromises Ovariole Development and Leads to Reduced Fecundity

GSC polarized division is responsible for their self-renewal and for the formation of a daughter cell that is further away from the stem cell niche, the cystoblast that will divide several times. Hence, progressively more differentiated cells are located further away from GSCs. This results in an ovariole with undifferentiated cells at the most anterior tip, in the germarium, and more differentiated egg chambers at the most posterior side culminating with a fully developed egg (**Figure 1**). By individually knocking down *Drp1*, *Marf*, or *Opa1* in germ cells, we found that these ovarioles are shorter than control (**Figures 4A–D**), with later/more differentiated egg chambers being absent in most cases. We found that egg chamber development arrests by vitellogenic stage 8/9 and very rarely egg chambers progress to form a mature egg. Additionally, the egg chambers that are formed in these abnormal ovarioles have obvious morphological defects (**Figures 4A–H**).

A closer analysis of egg chambers in ovarioles where either RNAi targeting *Drp1*, *Marf*, or *Opa1* is expressed in the germline revealed that defects in egg chamber morphology are visible from very early on, with nurse cell sizes within the same egg chamber being abnormally variable (**Figures 4E–H**). Interestingly, in $Drp1^{RNAi}$, $Marf^{RNAi}$, and $Opa1^{RNAi}$ egg chambers, the oocyte can be identified by the typical accumulation of F-actin (**Figures 4E–H**, yellow dashed line), indicating that the oocyte is specified and correctly positioned at the posterior side of stage 3/4 egg chambers. Surprisingly, as egg chamber development progresses, the asymmetries in nurse cell sizes become more obvious. Very large cells with enlarged nuclei can be observed, usually accompanied by the presence of abnormally small nurse cells with small nuclei (**Figures 4E′–H′**, dotted lines). The presence of nurse cells with large nuclei was very surprising and could potentially be a result of nuclei fusion events. However, in egg chambers with large cells/nuclei, we can identify a total of 16 nuclei (15 nurse cells and 1 oocyte, data not shown), therefore discarding the hypothesis of nuclear fusion. In some cases, multinucleated nurse cells can be observed (**Figures 4E″,F″**), indicating defects in membrane stability. In addition, a variety of DNA structure-related defects are also visible (**Figures 4E″–H‴**), with some nuclei appearing to be broken with small DNA fragments (DAPI positive) being separated from the nucleus (**Figures 4G″,H″,F‴,G‴**). In several cases, these smaller fragments are quite distant from the nucleus being observed close to cell membranes (**Figure 4F‴**) or in ring

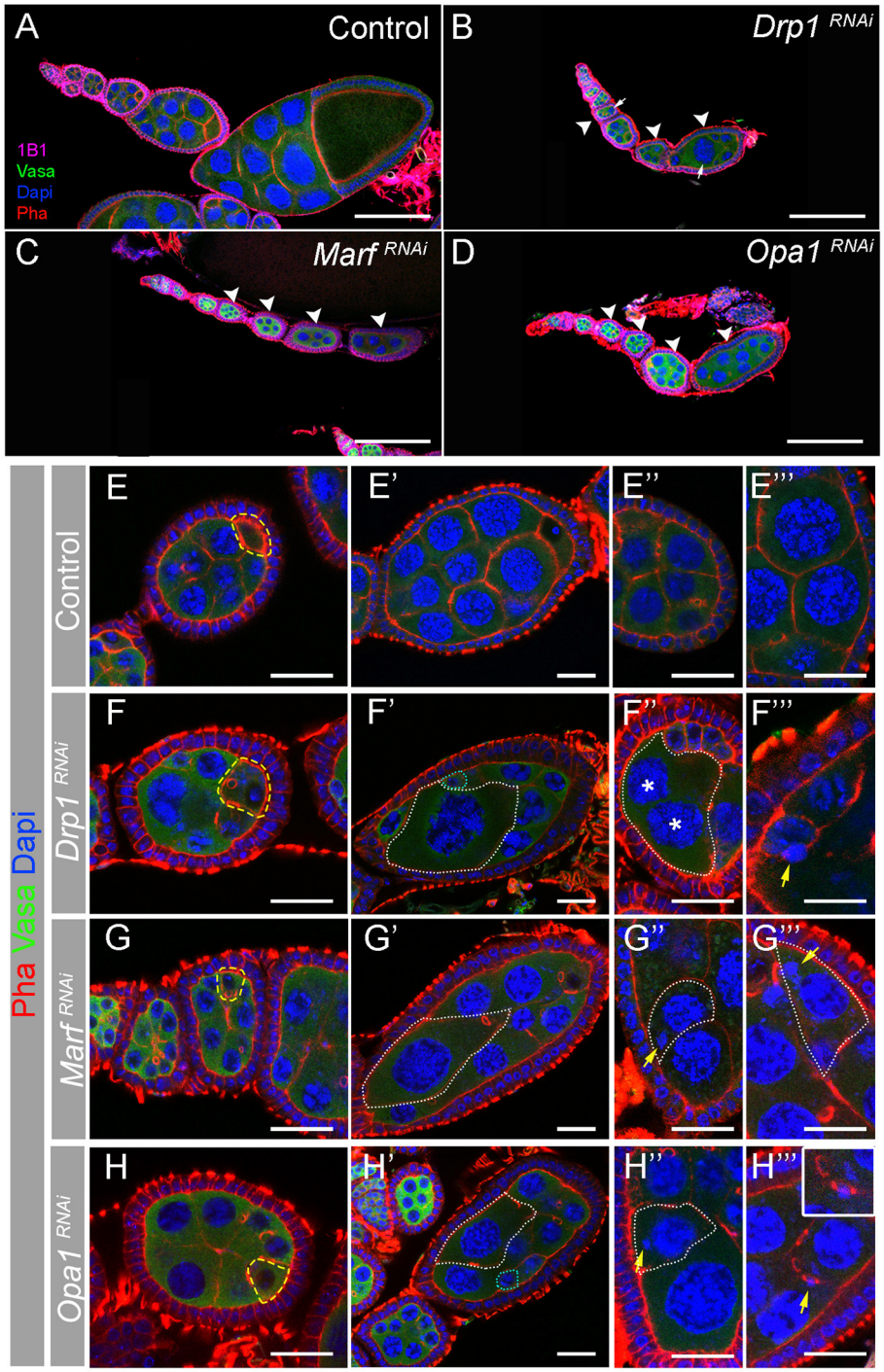

FIGURE 4 | Depletion of *Drp1*, *Marf*, or *Opa1* induces multiple egg chamber defects. **(A–D)** Representative images of ovarioles from indicated RNAi driven by *nos*Gal4. Germ cells are marked with Vasa antibody (green). Fusomes are labeled with Hts (1B1, pink). Nuclei and F-actin are labeled by DAPI (blue) and Phalloidin (Pha, red), respectively. Scale bars represent 100 μm. Control (*mCherry*^{RNAi}) ovariole **(A)** with a germarium in its anterior tip and a series of egg chambers progressively older. *Drp1*^{RNAi} **(B)**, *Marf*^{RNAi} **(C)**, or *Opa1*^{RNAi} **(D)** egg chambers degenerate before entering vitellogenic stages 8 and 9. When disrupting mitochondrial dynamics, egg chambers lose their normal structural organization presenting multiple defects in nurse cells morphology (arrowheads). **(E–H)** Several egg chamber defects are observed when mitochondrial dynamics regulators are knocked down. Abnormal egg chambers **(F–H)** are typically detected from egg chamber stage 3 or 4. Oocytes seem to be correctly specified based on the accumulation of F-actin in the posterior tip of egg chambers (outlined by dashed yellow line). **(E′-H′)** Egg chambers are severely disorganized in *Drp1*^{RNAi}, *Marf*^{RNAi}, and *Opa1*^{RNAi}. Nurse cells show uneven cytoplasmic and nuclear size (white dashed lines). **(E″–H″, E‴–H‴)** Magnified areas show the variety of defects observed in abnormal egg chambers: multinucleated cells (**F″**, cell membrane is outlined by white line, and nuclei are labeled by asterisks) and DNA mislocalized in the cytoplasm **(G″,G‴,H″)**, in contact with cell membranes **(F‴)** or with ring canals (**H‴**, see magnified area). Scale bars represent 20 μm.

canals (**Figure 4H‴**). These findings suggest a functional link between mitochondrial dynamics and nurse cell morphology and may indicate a novel role of mitochondrial dynamics in nurse cell structure regulation.

So far, we have established that mitochondrial dynamics is critical for the maintenance of GSC pool and correct egg chamber development in ovarioles. Next, we explored the physiological impact of mitochondrial dynamics on reproduction. Each female has two ovaries, composed by multiple ovarioles where the mature eggs are formed (**Figure 1A**). To determine how the defects in GSC number and egg chamber development, caused by deficient mitochondrial dynamics, affect female fertility, we started by analyzing ovarian morphology. Individual depletion of *Drp1*, *Marf*, or *Opa1* causes a dramatic reduction in ovary size (**Figures 5A–D**) with more differentiated egg chambers being mostly absent. We therefore asked whether these defects in ovaries could impact female fecundity. Indeed, the decrease in ovary size is consistent with a dramatic reduction in the number of eggs laid per female (**Figure 5E**). Interestingly, a closer analysis of the few eggs laid by females where *Drp1*, *Marf*, or *Opa1* is knocked down in germ cells revealed that these eggs have defective dorsal appendages with dorsal appendages' fusion being observed. Whereas two dorsolateral appendages are observed in control eggs, a single broad appendage is observed in $Drp1^{RNAi}$ and $Marf^{RNAi}$ (**Figure 5F**). Compared with control, eggs expressing *Drp1*, *Marf*, or *Opa1* RNAi have also smaller length to width ratio (**Figure 5G**), which translates into rounder eggs. These defects in the eggshell are an indication of defective egg chamber and oocyte development (Osterfield et al., 2017), which is consistent with the multiple defects observed in *Drp1*-, *Marf* -, or *Opa1*-depleted ovarioles (**Figure 4**).

These results show that mitochondrial dynamics in the female germline is not only essential for GSC regulation but is also essential during germline differentiation being required for the correct development of egg chambers, structural maintenance of nurse cells, egg formation, and ultimately female fertility.

Downregulation of TCA Cycle Enzymes in GSCs Mimics the Phenotype Caused by Disruption of Mitochondrial Dynamics

Having identified mitochondrial dynamics as an important process in several stages of ovarian germ cell lineage development, we sought to further explore by which mechanism mitochondrial morphology could be playing a role.

It is known that during stem cell differentiation, OxPhos metabolism is favored over glycolysis (Rafalski et al., 2012). Since it has been shown that mitochondria morphology may be connected to energy metabolism in stem cells (Fang et al., 2016; Seo et al., 2020), we hypothesized that the changes in mitochondrial dynamics that occurs along germ cell lineage differentiation in the germarium could be necessary for the balance between glycolysis and OxPhos and therefore cell fate. In order to test this hypothesis, we depleted Succinyl-coenzyme A synthetase α subunit 1 [referred to as *scsalpha1*; UAS-$scsalpha1^{RNAi}$ (v107164); knockdown ∼90% validated by qPCR, this study] and E2 member of alpha-Ketoglutarate Dehydrogenase complex (referred to as *alpha-KGDHC*; UAS-$alpha\text{-}KGDH^{RNAi}$ (v108403) as in Homem et al., 2014) in germ cells (*nos*Gal4). These are key regulatory enzymes of the TCA cycle whose activity levels were shown to be directly correlated with OxPhos (Tretter and Adam-Vizi, 2000; Phillips et al., 2009; Homem et al., 2014). Interestingly, RNAi-mediated depletion of both enzymes leads to a decrease in the GSC pool (**Figures 6A–D**), mimicking the phenotype caused by $Drp1^{RNAi}$, $Marf^{RNAi}$, and $Opa1^{RNAi}$ (see **Supplementary Table 2** for detailed characterization).

However, contrary to knockdown of mitochondrial dynamics regulators, *scsalpha1*- and *alpha-KGDHC*-depleted ovarioles have normal egg chamber morphology with correct nurse cell organization and oocyte formation. These results indicate that mitochondrial dynamics may have an OxPhos-dependent role in GSCs and additional OxPhos-independent roles in nurse cells. Interestingly, while in ovarioles of control and $scsalpha1^{RNAi}$ an average of eight distinct developmental stages are visible (**Figures 7A,B**), ovarioles of $alpha\text{-}KGDHC^{RNAi}$ consistently present fewer chambers (only 3 or 4 stages), thus being considerably shorter (**Figure 7C**). This phenotype indicates delayed formation of novel egg chambers, possibly due to slower GSC division timings or lower survival of differentiated cystoblasts in $alpha\text{-}KGDHC^{RNAi}$. Consistently, expression of $alpha\text{-}KGDHC^{RNAi}$ in GSCs causes a significant reduction in the number of laid eggs, reducing female fecundity (**Figure 7D**). Interestingly, knockdown of *scsalpha1* in the germline is not sufficient to decrease female fecundity, suggesting that solely a reduction in GSC number without defects in ovariole development is not sufficient to compromise fecundity (**Figure 7D**). Both the ovaries and the eggs laid by $alpha\text{-}KGDHC^{RNAi}$ or $scsalpha1^{RNAi}$ females are morphologically indistinguishable from control (**Supplementary Figures 2A,B**), again confirming that interfering with TCA cycle alone is not sufficient to mimic the nurse cell defects caused by $Drp1^{RNAi}$, $Marf^{RNAi}$, and $Opa1^{RNAi}$.

Together, these results surprisingly suggest that at least basal levels of TCA/OxPhos are required for the formation or maintenance of a stable GSC pool. Additionally, reducing TCA cycle enzyme levels in germ cells does not block germ cell differentiation in the germarium, although $alpha\text{-}KGDHC^{RNAi}$ affects the pace of egg chamber formation. Contrary to depletion of fusion/fission regulators, knocking down TCA cycle enzymes does not lead to defects in nurse cell morphology, suggesting that the observed defects in older egg chambers are not only related to abnormal OxPhos levels.

DISCUSSION

Our work has revealed that both mitochondrial fusion and fission are required for the maintenance of the female GSC pool in *Drosophila* (**Figure 8**). Although GSCs predominantly have small, punctate mitochondria, we show that mitochondrial fusion is required in GSCs, indicating that the balance between fusion and fission also plays a functional role at this undifferentiated stage. The predominance of fissed mitochondria in GSCs and

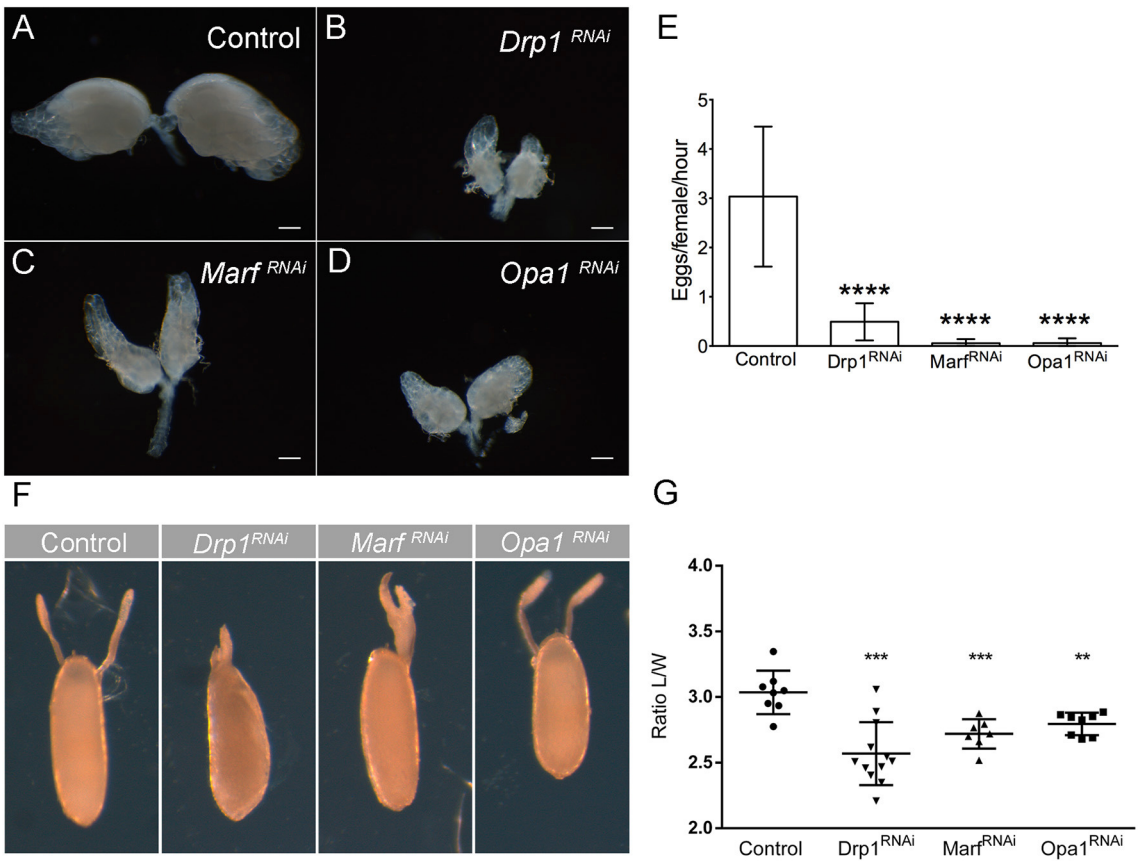

FIGURE 5 | Knockdown of *Drp1*, *Marf*, or *Opa1* in GSCs leads to reduced fecundity. **(A–D)** Ovaries of 1-day-old female virgins expressing $Drp1^{RNAi}$, $Marf^{RNAi}$, or $Opa1^{RNAi}$ in the germline by *nos*Gal4. **(A)** Bright-field images of whole ovaries of control ($mCherry^{RNAi}$) females show normal ovary development and formation of mature eggs. **(B–D)** $Drp1^{RNAi}$, $Marf^{RNAi}$, or $Opa1^{RNAi}$ females have tiny ovaries containing mainly germaria-like structures and generally lacking mature eggs. Scale bars represent 200 μm. **(E)** Quantification of the average number of eggs laid (±SD), per hour post-mating per female of the indicated genotype when crossed to wild-type males. Quantification revealed a significant decrease in fecundity of *Drp1*-, *Marf*-, and *Opa1*-knockdown females when compared with control ($mCherry^{RNAi}$). **(F)** Representative images of dorsal appendage defects in eggs produced by females of the indicated genotypes. **(G)** Ratio Length/Width (L/W) (average ± SD) of the produced eggs. Eggs laid by *Drp1*-, *Marf*-, and *Opa1*-knockdown females show smaller L/W ratio indicating abnormal egg morphology. Statistical significance of differences compared with control was calculated using simple sample *t*-test. $^{**}P < 0.01$; $^{***}P < 0.001$; $^{****}P < 0.0001$.

in region 1 of the germarium reported here is consistent with what has been observed in EM studies (Cox and Spradling, 2003). However, since stem cells are reported to mainly depend on glycolysis, to have low mitochondrial content and predominantly fissed mitochondria, our finding that mitochondria fusion events are an essential requirement in female GSCs is unexpected.

A closer analysis of mitochondrial activity revealed that GSCs normally have low mitochondrial membrane potential that increases with germline differentiation, consistently to what has been previously described (Wang et al., 2019). Interestingly, in a fraction of germaria depleted for either fusion or fission regulators, we observe the appearance of mitochondria with high levels of mitochondrial inner membrane potential that are never observed in the control situation. Notably, the phenotypes caused by $Opa1^{RNAi}$, the regulator of inner mitochondrial fusion, are stronger than those originated by $Marf^{RNAi}$, the regulator of outer-membrane fusion. Since *Opa1* has additional roles, other than fusion, being also important for mitochondria cristae shape and for maintaining ETC supercomplexes in the mitochondria cristae, this may explain the different outcomes (Cogliati et al., 2013). These results confirm that GSCs have functional mitochondria since a change in mitochondrial dynamics is capable of increasing mitochondrial activity. An increase in mitochondrial membrane potential could favor the formation of ROS; however, we did not find obvious evidence that GSC loss phenotypes are mediated by ROS. At first sight, these results might seem contradictory, but these bring to the spotlight the fact that, so far, no straightforward connection has been established between mitochondrial dynamics and bioenergetics, reported to depend on the cell type and context (reviewed in Liesa and Shirihai, 2013). Additionally, these results also support the notion that a fine balance between mitochondria fusion and fission is required to maintain a stable mitochondrial inner membrane potential and ensure healthy cell functions (Vazquez-Martin et al., 2012; Khacho et al., 2016; Luchsinger et al., 2016). Therefore, our data can

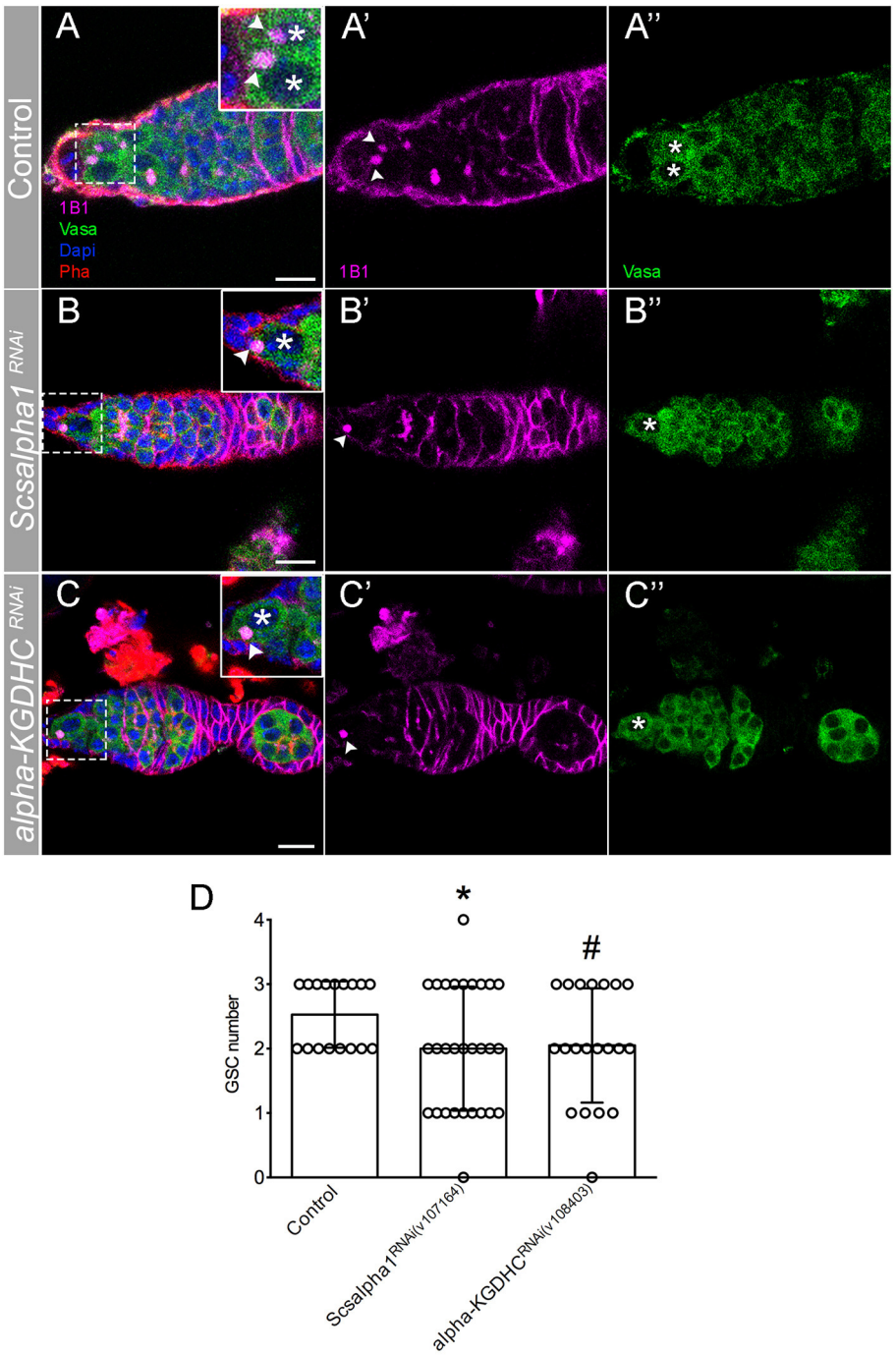

FIGURE 6 | RNAi of TCA cycle enzymes leads to GSC loss. **(A–C)** Representative images of adult *Drosophila* germaria expressing *mCherry*^{RNAi} (control) **(A–A″)**, *Scsalpha1*^{RNAi} **(B–B″)**, or *alpha-KGDHC*^{RNAi} **(C–C″)** in the germline (*nos*Gal4). *Scsalpha1*^{RNAi} leads to a significant loss of GSCs. Despite not statistically significantly, *alpha-KGDHC*^{RNAi} also affects GSCs number. Spherical spectrosome (1B1, pink) identifies GSCs. Germ cells are labeled by Vasa antibody (green), nuclei by DAPI (blue), and F-actin by Phalloidin (Pha, red). Scale bars represent 10 μm. **(D)** Quantification of the average number of GSCs per germarium (±SD). Statistical significance of differences compared with control was calculated using simple sample *t*-test. $^{*}P < 0.05$; $^{\#}P < 0.10$.

contribute to the understanding of how the normal balance of mitochondrial dynamics is important for fate regulation and how its unbalance affects both mitochondria morphology, activity, and ultimately GSCs.

Even though the mechanism is unclear, mitochondria morphology is known to strongly impact the cell metabolic state, and several studies report fused mitochondria being associated with OxPhos metabolism (Rafalski et al., 2012; Mishra and

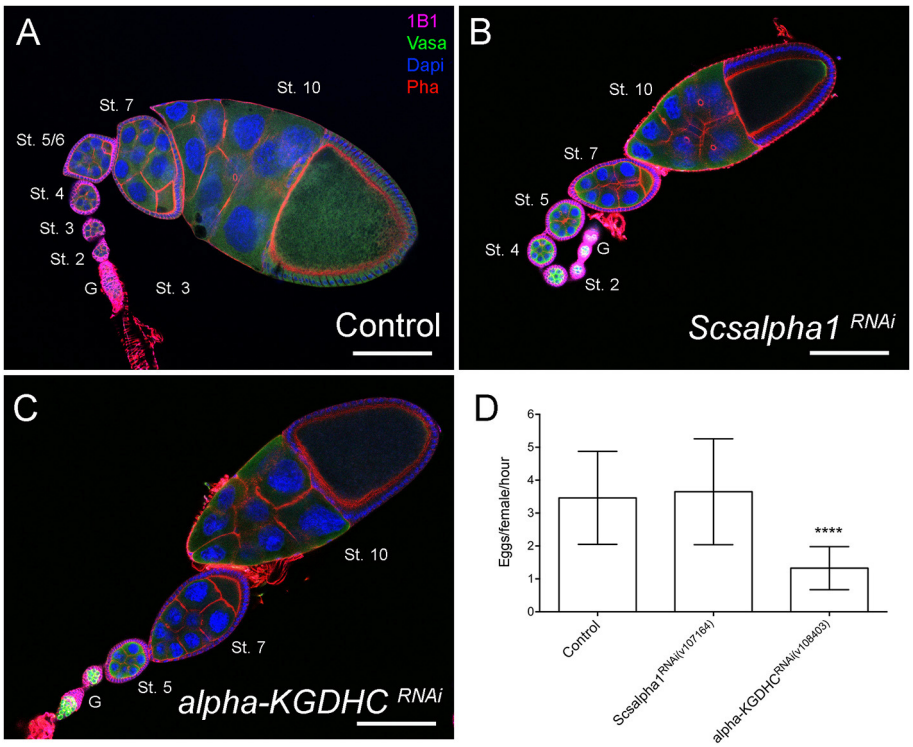

FIGURE 7 | Downregulation of essential TCA cycle enzymes in the germline does not affect egg chamber morphology. **(A–C)** Representative images of ovarioles of indicated genotypes. Ovarioles of *Scsalpha1*^{RNAi} **(B)** or *alpha-KGDHC*^{RNAi} **(C)** show no obvious defects in egg chamber morphology compared with control (*mCherry*^{RNAi}) **(A)**. Ovarioles of *alpha-KGDHC*^{RNAi} **(C)** present a reduced number of developing egg chambers comparing with control **(A)** or *scsalpha1*^{RNAi} **(B)**. Developmental stages of egg chambers are indicated (St.). Scale bars represent 100 μm. **(D)** Quantification of the average number of eggs laid (±SD) per hour post-mating, per female of the indicated genotype when crossed to wild-type males. Consistently, females expressing *alpha-KGDHC*^{RNAi} show decreased fertility. Statistical significance of differences compared with control was calculated using simple sample *t*-test. ****$P < 0.0001$.

Chan, 2016). The critical importance of fine tuning the levels of OxPhos and glycolysis for the regulation of stem cell fate could explain why mitochondrial dynamics may be fundamental in GSCs. Consistent with this hypothesis, we found that depletion of essential enzymes in the TCA cycle (*Scsalpha1* or *alpha-KGDHC*) also causes GSC loss, hence mimicking the defects caused by disrupting mitochondrial dynamics. Previous studies reported that GSCs express at low levels several members of the ETC (Kai et al., 2005) and have minor levels of mitochondrial respiration (Wang et al., 2019). Nevertheless, our results show that albeit at a minimal level, a functional TCA cycle, and probably OxPhos, is required in GSCs. This is in line with the currently accepted view that although stem cells primarily depend on glycolysis, these cells also require basal levels of OxPhos metabolism (Ito and Suda, 2014; Folmes and Terzic, 2016; Tsogtbaatar et al., 2020). Consistently, it has also been reported that human pluripotent stem cells possess functional respiratory complexes and are capable of consuming O_2 at maximum capacity (Zhang et al., 2011), and that mouse pluripotent cells (mPSCs) require a certain degree of OxPhos to establish the primordial GSC identity (Bothun and Woods, 2020). Alternatively, one could argue that TCA cycle enzymes might play an additional unknown functional role in mitochondria maturation. However, this is unlikely since defects in mitochondria maturation do not cause GSC loss (Teixeira et al., 2015). Furthermore, mitochondria fusion is also known to be crucial for mitochondria quality control (Chan, 2012), allowing mixing of mitochondrial content to dilute damages, so our findings could reflect an accumulation of damaged mitochondria due to reduced fusion events, culminating in GSCs loss. Importantly, our results are consistent with what was recently observed in the male germline (Demarco et al., 2019) where depletion of mitochondrial fusion in GSCs results in GSC loss, suggesting that the requirement for basal levels of mitochondrial fusion is a common feature of *Drosophila* GSCs. Another noteworthy study showed that mitochondria fission regulator *Drp1* is also involved in aging-dependent GSC loss with an increase in fragmented mitochondria being associated with aged female GSC (Amartuvshin et al., 2020). This suggests that mitochondrial fusion is required for maintenance of female GSCs also during aging.

The work described here also shows that besides being important for GSC maintenance, mitochondrial dynamics is essential at later stages during germline differentiation. We found that impairment of mitochondrial fission or fusion leads to abnormal egg chambers with multiple defects in nurse cell morphology, culminating in the arrest of egg chamber development around vitellogenic stage 8/9. These defects in

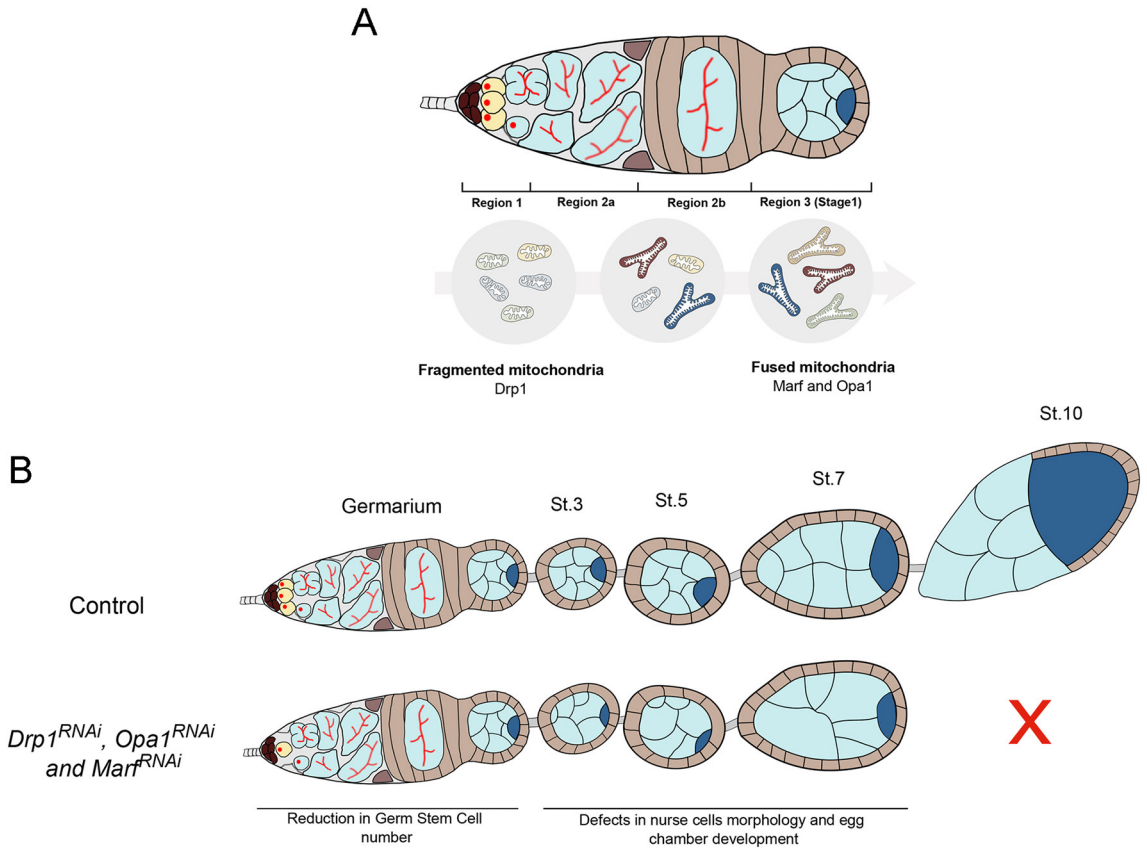

FIGURE 8 | Mitochondrial dynamics is critical for *Drosophila* GSC maintenance and oogenesis. **(A)** GSCs in germarium region 1 have predominantly fragmented mitochondria. Throughout germ cell differentiation, mitochondria become more aggregated, indicative of increased fusion. These differential mitochondria morphologies along GSC lineage progression are regulated by fission regulator *Drp1* and fusion regulators *Marf* and *Opa1*. **(B)** Disruption of mitochondrial dynamics, by depletion of fission or fusion regulators in germ cells, causes defective mitochondria morphologies and GSC loss. Defective mitochondrial dynamics in the germline also causes severe defects in egg chambers that contain morphologically abnormal nurse cells and arrest their development before vitellogenic stages. Together, these defects in mitochondrial dynamics in the germline compromise egg chamber formation ultimately resulting in abnormal egg morphologies and reduced female fecundity.

egg chambers at later stages were surprising, and this novel role for mitochondrial dynamics in nurse cell regulation is worth further exploration. One hypothesis is that abnormal fusion/fission events in the germline lead to defects in cyst formation and to defective oocyte specification. In the female germline, all differentiating cells are connected by ring canals and therefore exist in a syncytium. Once the oocyte is selected among the 16 cyst cells, all remaining 15 cells become nurse cells and transfer their mitochondria through ring canals into the oocyte to support its development (Cox and Spradling, 2003). Interestingly, a closer analysis of the previously published EM images of mitochondria in region 3 at the dumping stage (Cox and Spradling, 2003) shows that mitochondria are elongated and therefore predominantly fused, while crossing ring canals into the oocyte. Thus, abnormal mitochondria morphology could compromise mitochondria transfer, leading to a poorly developed oocyte that cannot progress further in oogenesis. In particular, we reported abnormal egg chambers showing obvious defects in nurse cell morphology, including the presence of highly variable cell and nuclei sizes, multinucleated cells, and also several DNA-related defects. Mitochondria are well-known sources of ROS as well as important regulators of intracellular calcium (Ca^{2+}). Since ROS and Ca^{2+} levels play an important role in the regulation of actin cytoskeleton dynamics (Xu and Chisholm, 2014; Prudent et al., 2016; Hunter et al., 2018), impairment of mitochondria could explain the observed defects. Moreover, it was recently shown that mitochondrial fission modulator *Drp1* regulates F-actin dynamics during wound closure in the *Drosophila* epithelia (Ponte et al., 2020). In future studies, it would be interesting to test whether F-actin modulators are dysregulated and whether their impairment would result in similar egg chamber defects. On the other hand or in parallel, mitochondrial defects could lead to abnormal ROS levels, since mitochondrial-ROS production is highly dependent on organelle morphology (Galloway et al., 2012). High levels of ROS can lead to cellular oxidative stress and consequently to damages

in DNA, lipids, and proteins (Rowe et al., 2008). Thus, the DNA defects observed in developing egg chamber upon *Drp1*, *Marf*, and *Opa1* downregulation in germ cells could possibly be explained by ROS-induced DNA damage and impaired DNA damage response (Srinivas et al., 2019). However, this is unlikely as we did not observe increased ROS levels in GSCs knocked down for mitochondrial dynamics regulators.

Reducing mitochondrial dynamics in germ cells ultimately results in reduced fecundity with the few eggs that are formed presenting an abnormal morphology. The morphology of the eggs and dorsal appendages directly results from late egg chamber shape, with eggshell components being secreted by follicle cells, which tightly surround the oocyte, mimicking its shape. Follicle cells are also responsible for the formation of the dorsal appendages or respiratory filaments, located at the dorsal-anterior end of the eggshell (Osterfield et al., 2017). Therefore, incorrect egg morphology indicates that egg chambers and oocyte did not develop as normal. Consistently, mitochondria morphology was also found to be important for proper oocyte development in mice, highlighting the critical role of mitochondria in oogenesis (Udagawa et al., 2014; Liu et al., 2016; Carvalho et al., 2020). Strikingly, decreasing the levels of OxPhos/TCA cycle enzymes in germ cells does not cause the same defects in late egg chamber development, nor in nurse cell morphology. These results indicate that the morphological defects in nurse cells observed when interfering with mitochondrial dynamics are not solely dependent on OxPhos. However, RNAi-mediated depletion of *alpha-KGDHC*, an enzyme of the TCA cycle, in germ cells leads to smaller ovarioles with the average ovariole presenting fewer developmental stages (3/4 stages vs. ∼8 stages in control) and reduced fecundity. This phenotype could be caused by slower cycling of GSCs or lower survival of differentiated cystoblasts, which would then lead to sporadic formation and development of novel egg chambers. In combination these results suggest that, in GSCs, at least one of the roles of mitochondria is to maintain basal levels of TCA/OxPhos. Notwithstanding, in later stages of germline development, mitochondrial dynamics seem to play additional roles. This is consistent with the far-reaching influence of mitochondrial membrane potential, which is required not only for OxPhos but also for calcium storage, lipogenesis, activation of ROS and hypoxia-inducible factor (HIF), biogenesis of iron–sulfur clusters (ISCs), and mitochondrial protein import, among others (Picard et al., 2016).

Overall, our work highlights the importance of mitochondrial dynamics in the *Drosophila* female germline and the major impact of compromised fusion/fission events in oogenesis and consequently on fly fertility. We show that GSC number is regulated by both mitochondrial dynamics and TCA/OxPhos metabolism, suggesting that these two processes function together in these undifferentiated cells. Our results also reveal an OxPhos-independent role for mitochondrial dynamics in the regulation of nurse cell and egg chamber morphology, suggesting that mitochondria fusion and fission events play a broader role in oogenesis.

DATA AVAILABILITY STATEMENT

The original contributions presented in the study are included in the article/**Supplementary Material**, further inquiries can be directed to the corresponding author.

AUTHOR CONTRIBUTIONS

MG designed and performed experiments, data analysis, design of data analysis, figure assembly, and wrote the manuscript. JB-S designed and performed experiments, data analysis, design of data analysis, and figure assembly. PG performed experiments, data analysis, and manuscript editing. CH did conceptual design of the study, designed experiments, data analysis, assisted figure assembly, and wrote the manuscript. All authors contributed to the article and approved the submitted version.

FUNDING

This project has received funding from the European Research Council (ERC) under the European Union's Horizon 2020 research and innovation program (H2020-ERC-2017-STG-GA 759853-StemCellHabitat), Wellcome Trust and Howard Hughes Medical Institute (HHMI-208581/Z/17/Z-Metabolic Reg SC fate), EMBO Installation grant (H2020-EMBO-3311/2017/G2017), and by Fundação para a Ciência e Tecnologia (IF/01265/2014/CP1252/CT0004 and PD/BD/128003/2016 to MG).

ACKNOWLEDGMENTS

We would like to thank Rita Teodoro for critical reading of the manuscript. We thank Telmo Pereira from the Microscopy Facility at CEDOC for technical support; the Fly Facility at CEDOC; CONGENTO: consortium for genetically tractable organisms (LISBOA-01-0145-FEDER-022170); the Vienna Drosophila Resource Center and Bloomington Drosophila Stock Center (NIH P40OD018537) for stocks used in this study; the Developmental Studies Hybridoma Bank, created by the NICHD of the NIH and maintained at The University of Iowa, Department of Biology, Iowa City, IA 52242.

SUPPLEMENTARY MATERIAL

The Supplementary Material for this article can be found online at: https://www.frontiersin.org/articles/10.3389/fcell.2020.596819/full#supplementary-material

REFERENCES

Amartuvshin, O., Lin, C., Hsu, S., Kao, S., Chen, A., Tang, W., et al. (2020). Aging shifts mitochondrial dynamics toward fission to promote germline stem cell loss. *Aging Cell* 19:e13191. doi: 10.1111/acel.13191

Bothun, A. M., and Woods, D. C. (2020). Inherent mitochondrial activity influences specification of the germ line in pluripotent stem cells. *Heliyon* 6:e03651. doi: 10.1016/j.heliyon.2020.e03651

Brand, A. H., and Perrimon, N. (1993). Targeted gene expression as a means of altering cell fates and generating dominant phenotypes. *Development* 118, 401–415.

Carpenter, A. T. C. (1975). Electron microscopy of meiosis in *Drosophila melanogaster* females. *Chromosoma* 51, 157–182. doi: 10.1007/BF00319833

Carter, W. O., Naraynan, P. K., and Robinson, J. P. (1994). Intracellular hydrogen peroxide and superoxide anion detection in endothelial cells. *J. Leukoc. Biol.* 55, 253–258. doi: 10.1002/jlb.55.2.253

Carvalho, K. F., Machado, T. S., Garcia, B. M., Zangirolamo, A. F., Macabelli, C. H., Sugiyama, F. H. C., et al. (2020). Mitofusin 1 is required for oocyte growth and communication with follicular somatic cells. *FASEB J.* 34, 7644–7660. doi: 10.1096/fj.201901761R

Chan, D. C. (2012). Fusion and fission: interlinked processes critical for mitochondrial health. *Annu. Rev. Genet.* 46, 265–287. doi: 10.1146/annurev-genet-110410-132529

Cogliati, S., Frezza, C., Soriano, M. E., Varanita, T., Quintana-Cabrera, R., Corrado, M., et al. (2013). Mitochondrial cristae shape determines respiratory chain supercomplexes assembly and respiratory efficiency. *Cell* 155, 160–171. doi: 10.1016/j.cell.2013.08.032

Cox, R. T. and Spradling, A. C. (2003). A Balbiani body and the fusome mediate mitochondrial inheritance during *Drosophila* oogenesis. *Development* 130, 1579–1590. doi: 10.1242/dev.00365

DeLuca, S. Z., and O'Farrell, P. H. (2012). Barriers to male transmission of mitochondrial DNA in sperm development. *Dev. Cell* 22, 660–668. doi: 10.1016/j.devcel.2011.12.021

Demarco, R., and Jones, D. L. (2019). Mitochondrial fission regulates germ cell differentiation by suppressing ROS-mediated activation of epidermal growth factor signaling in the *Drosophila* larval testis. *Sci. Rep.* 9:19695. doi: 10.1038/s41598-019-55728-0

Demarco, R., Uyemura, B. S., D'Alterio, C., and Jones, D. L. (2019). Mitochondrial fusion regulates lipid homeostasis and stem cell maintenance in the *Drosophila* testis. *Nat. Cell Biol.* 21, 710–720. doi: 10.1038/s41556-019-0332-3

Deng, Q., Guo, T., Zhou, X., Xi, Y., Yang, X., and Ge, W. (2016). Cross-talk between mitochondrial fusion and the hippo pathway in controlling cell proliferation during *Drosophila* development. *Genetics* 203, 1777–1788. doi: 10.1534/genetics.115.186445

Fang, D., Yan, S., Yu, Q., Chen, D., and Yan, S. S. (2016). Mfn2 is required for mitochondrial development and synapse formation in human induced pluripotent stem cells/hiPSC derived cortical neurons. *Sci. Rep.* 6:31462. doi: 10.1038/srep31462

Folmes, C. D. L., and Terzic, A. (2016). Energy metabolism in the acquisition and maintenance of stemness. *Semin. Cell Dev. Biol.* 52, 68–75. doi: 10.1016/j.semcdb.2016.02.010

Galloway, C. A., Lee, H., Nejjar, S., Jhun, B. S., Yu, T., Hsu, W., et al. (2012). Transgenic control of mitochondrial fission induces mitochondrial uncoupling and relieves diabetic oxidative stress. *Diabetes* 61, 2093–2104. doi: 10.2337/db11-1640

Gates, J., Nowotarski, S. H., Yin, H., Mahaffey, J. P., Bridges, T., Herrera, C., et al. (2009). Enabled and Capping protein play important roles in shaping cell behavior during *Drosophila* oogenesis. *Dev. Biol.* 333, 90–107. doi: 10.1016/j.ydbio.2009.06.030

Homem, C. C. F., Steinmann, V., Burkard, T. R., Jais, A., Esterbauer, H., and Knoblich, J. A. (2014). Ecdysone and mediator change energy metabolism to terminate proliferation in *Drosophila* neural stem cells. *Cell* 158, 874–888. doi: 10.1016/j.cell.2014.06.024

Hunter, M. V., Willoughby, P. M., Bruce, A. E. E., and Fernandez-Gonzalez, R. (2018). Oxidative stress orchestrates cell polarity to promote embryonic wound healing. *Dev. Cell* 47, 377–387.e4. doi: 10.1016/j.devcel.2018.10.013

Iannetti, E. F., Prigione, A., Smeitink, J. A. M., Koopman, W. J. H., Beyrath, J., and Renkema, H. (2019). Live-imaging readouts and cell models for phenotypic profiling of mitochondrial function. *Front. Genet.* 10:131. doi: 10.3389/fgene.2019.00131

Ito, K., and Suda, T. (2014). Metabolic requirements for the maintenance of self-renewing stem cells. *Nat. Rev. Mol. Cell Biol.* 15, 243–256. doi: 10.1038/nrm3772

Kai, T., Williams, D., and Spradling, A. C. (2005). The expression profile of purified *Drosophila* germline stem cells. *Dev. Biol.* 283, 486–502. doi: 10.1016/j.ydbio.2005.04.018

Khacho, M., Clark, A., Svoboda, D. S., Azzi, J., MacLaurin, J. G., Meghaizel, C., et al. (2016). Mitochondrial dynamics impacts stem cell identity and fate decisions by regulating a nuclear transcriptional program. *Cell Stem Cell* 19, 232–247. doi: 10.1016/j.stem.2016.04.015

Lieber, T., Jeedigunta, S. P., Palozzi, J. M., Lehmann, R., and Hurd, T. R. (2019). Mitochondrial fragmentation drives selective removal of deleterious mtDNA in the germline. *Nature* 570, 380–384. doi: 10.1038/s41586-019-1213-4

Liesa, M., and Shirihai, O. S. (2013). Mitochondrial dynamics in the regulation of nutrient utilization and energy expenditure. *Cell Metab.* 17, 491–506. doi: 10.1016/j.cmet.2013.03.002

Liu, Q., Kang, L., Wang, L., Zhang, L., and Xiang, W. (2016). Mitofusin 2 regulates the oocytes development and quality by modulating meiosis and mitochondrial function. *Sci. Rep.* 6:30561. doi: 10.1038/srep30561

Livak, K. J., and Schmittgen, T. D. (2001). Analysis of relative gene expression data using real-time quantitative PCR and the 2−ΔΔCT method. *Methods* 25, 402–408. doi: 10.1006/meth.2001.1262

Luchsinger, L. L., de Almeida, M. J., Corrigan, D. J., Mumau, M., and Snoeck, H.-W. (2016). Mitofusin 2 maintains haematopoietic stem cells with extensive lymphoid potential. *Nature* 529, 528–531. doi: 10.1038/nature16500

Mahowald, A. P., and Strassheim, J. M. (1970). Intercellular migration of centrioles in the germarium of *Drosophila melanogaster*. An electron microscopic study. *J. Cell Biol.* 45, 306–320. doi: 10.1083/jcb.45.2.306

Mishra, P., and Chan, D. C. (2016). Metabolic regulation of mitochondrial dynamics. *J. Cell Biol.* 212, 379–387. doi: 10.1083/jcb.201511036

Nunnari, J., and Suomalainen, A. (2012). Mitochondria: in sickness and in health. *Cell* 148, 1145–1159. doi: 10.1016/j.cell.2012.02.035

Osterfield, M., Berg, C. A., and Shvartsman, S. Y. (2017). Epithelial patterning, morphogenesis, and evolution: *Drosophila* eggshell as a model. *Dev. Cell* 41, 337–348. doi: 10.1016/j.devcel.2017.02.018

Pernas, L., and Scorrano, L. (2016). Mito-morphosis: mitochondrial fusion, fission, and cristae remodeling as key mediators of cellular function. *Annu. Rev. Physiol.* 78, 505–531. doi: 10.1146/annurev-physiol-021115-105011

Phillips, D., Aponte, A. M., French, S. A., Chess, D. J., and Balaban, R. S. (2009). Succinyl-CoA synthetase is a phosphate target for the activation of mitochondrial metabolism. *Biochemistry* 48, 7140–7149. doi: 10.1021/bi900725c

Picard, M., Wallace, D. C., and Burelle, Y. (2016). The rise of mitochondria in medicine. *Mitochondrion* 30, 105–116. doi: 10.1016/j.mito.2016.07.003

Ponte, S., Carvalho, L., Gagliardi, M., Campos, I., Oliveira, P. J., and Jacinto, A. (2020). Drp1-mediated mitochondrial fission regulates calcium and F-actin dynamics during wound healing. *Biol. Open* 9:bio048629. doi: 10.1242/bio.048629

Prudent, J., Popgeorgiev, N., Gadet, R., Deygas, M., Rimokh, R., and Gillet, G. (2016). Mitochondrial Ca2+ uptake controls actin cytoskeleton dynamics during cell migration. *Sci. Rep.* 6:36570. doi: 10.1038/srep 36570

Rafalski, V. A., Mancini, E., and Brunet, A. (2012). Energy metabolism and energy-sensing pathways in mammalian embryonic and adult stem cell fate. *J. Cell Sci.* 125, 5597–5608. doi: 10.1242/jcs.114827

Rai, M., Katti, P., and Nongthomba, U. (2014). *Drosophila* Erect wing (Ewg) controls mitochondrial fusion during muscle growth and maintenance by regulation of the Opa1-like gene. *J. Cell Sci.* 127, 191–203. doi: 10.1242/jcs.135525

Rowe, L. A., Degtyareva, N., and Doetsch, P. W. (2008). DNA damage-induced reactive oxygen species (ROS) stress response in *Saccharomyces cerevisiae*. *Free Radic. Biol. Med.* 45, 1167–1177. doi: 10.1016/j.freeradbiomed.2008.07.018

Sandoval, H., Yao, C.-K., Chen, K., Jaiswal, M., Donti, T., Lin, Y. Q., et al. (2014). Mitochondrial fusion but not fission regulates larval growth and synaptic development through steroid hormone production. *Elife* 3:e03558. doi: 10.7554/eLife.03558.023

Schägger, H. (2002). Respiratory chain supercomplexes of mitochondria and bacteria. *Biochim. Biophys. Acta Bioenerg.* 1555, 154–159. doi: 10.1016/S0005-2728(02)00271-2

Schindelin, J., Arganda-Carreras, I., Frise, E., Kaynig, V., Longair, M., Pietzsch, T., et al. (2012). Fiji: an open-source platform for biological-image analysis. *Nat. Methods* 9, 676–682. doi: 10.1038/nmeth.2019

Seo, B. J., Choi, J., La, H., Habib, O., Choi, Y., Hong, K., et al. (2020). Role of mitochondrial fission-related genes in mitochondrial morphology and energy metabolism in mouse embryonic stem cells. *Redox Biol.* 36:101599. doi: 10.1016/j.redox.2020.101599

Spurlock, B., Tullet, J., Hartman, J. L., and Mitra, K. (2020). Interplay of mitochondrial fission-fusion with cell cycle regulation: possible impacts on stem cell and organismal aging. *Exp. Gerontol.* 135:110919. doi: 10.1016/j.exger.2020.110919

Srinivas, U. S., Tan, B. W. Q., Vellayappan, B. A., and Jeyasekharan, A. D. (2019). ROS and the DNA damage response in cancer. *Redox Biol.* 25:101084. doi: 10.1016/j.redox.2018.101084

Teixeira, F. K., Sanchez, C. G., Hurd, T. R., Seifert, J. R. K., Czech, B., Preall, J. B., et al. (2015). ATP synthase promotes germ cell differentiation independent of oxidative phosphorylation. *Nat. Cell Biol.* 17, 689–696. doi: 10.1038/ncb3165

Tretter, L., and Adam-Vizi, V. (2000). Inhibition of krebs cycle enzymes by hydrogen peroxide: a key role of α-ketoglutarate dehydrogenase in limiting NADH production under oxidative stress. *J. Neurosci.* 20, 8972–8979. doi: 10.1523/JNEUROSCI.20-24-08972.2000

Trevisan, T., Pendin, D., Montagna, A., Bova, S., Ghelli, A. M., and Daga, A. (2018). Manipulation of mitochondria dynamics reveals separate roles for form and function in mitochondria distribution. *Cell Rep.* 23, 1742–1753. doi: 10.1016/j.celrep.2018.04.017

Tsogtbaatar, E., Landin, C., Minter-Dykhouse, K., and Folmes, C. D. L. (2020). Energy metabolism regulates stem cell pluripotency. *Front. Cell Dev. Biol.* 8:87. doi: 10.3389/fcell.2020.00087

Udagawa, O., Ishihara, T., Maeda, M., Matsunaga, Y., Tsukamoto, S., Kawano, N., et al. (2014). Mitochondrial fission factor Drp1 maintains oocyte quality via dynamic rearrangement of multiple organelles. *Curr. Biol.* 24, 2451–2458. doi: 10.1016/j.cub.2014.08.060

Varuzhanyan, G., Rojansky, R., Sweredoski, M. J., Graham, R. L. J., Hess, S., Ladinsky, M. S., et al. (2019). Mitochondrial fusion is required for spermatogonial differentiation and meiosis. *Elife* 8:e51601. doi: 10.7554/eLife.51601

Vazquez-Martin, A., Cufí, S., Corominas-Faja, B., Oliveras-Ferraros, C., Vellon, L., and Menendez, J. A. (2012). Mitochondrial fusion by pharmacological manipulation impedes somatic cell reprogramming to pluripotency: new insight into the role of mitophagy in cell stemness. *Aging* 4, 393–401. doi: 10.18632/aging.100465

Wang, Z.-H., Clark, C., and Geisbrecht, E. R. (2016). *Drosophila* clueless is involved in Parkin-dependent mitophagy by promoting VCP-mediated Marf degradation. *Hum. Mol. Genet.* 25, 1946–1964. doi: 10.1093/hmg/ddw067

Wang, Z.-H., Liu, Y., Chaitankar, V., Pirooznia, M., and Xu, H. (2019). Electron transport chain biogenesis activated by a JNK-insulin-Myc relay primes mitochondrial inheritance in *Drosophila*. *Elife* 8:e49309. doi: 10.7554/eLife.49309.043

Xu, S., and Chisholm, A. D. (2014). *C. elegans* epidermal wounding induces a mitochondrial ROS burst that promotes wound repair. *Dev. Cell* 31, 48–60. doi: 10.1016/j.devcel.2014.08.002

Zhang, H., Menzies, K. J., and Auwerx, J. (2018). The role of mitochondria in stem cell fate and aging. *Development* 145:dev143420. doi: 10.1242/dev.143420

Zhang, J., Khvorostov, I., Hong, J. S., Oktay, Y., Vergnes, L., Nuebel, E., et al. (2011). UCP2 regulates energy metabolism and differentiation potential of human pluripotent stem cells. *EMBO J.* 30, 4860–4873. doi: 10.1038/emboj.2011.401

Zhang, Y., Wang, Z.-H., Liu, Y., Chen, Y., Sun, N., Gucek, M., et al. (2019). PINK1 inhibits local protein synthesis to limit transmission of deleterious mitochondrial DNA mutations. *Mol. Cell* 73, 1127–1137.e5. doi: 10.1016/j.molcel.2019.01.013

Conflict of Interest: The authors declare that the research was conducted in the absence of any commercial or financial relationships that could be construed as a potential conflict of interest.

frontiers in Cell and Developmental Biology

ORIGINAL RESEARCH
published: 04 February 2021
doi: 10.3389/fcell.2021.624601

Consistent Long-Term Therapeutic Efficacy of Human Umbilical Cord Matrix-Derived Mesenchymal Stromal Cells After Myocardial Infarction Despite Individual Differences and Transient Engraftment

Tiago L. Laundos[1,2,3], *Francisco Vasques-Nóvoa*[1,2,4,5], *Rita N. Gomes*[1,2,3], *Vasco Sampaio-Pinto*[1,2,3], *Pedro Cruz*[6], *Hélder Cruz*[6], *Jorge M. Santos*[6], *Rita N. Barcia*[6], *Perpétua Pinto-do-Ó*[1,2,3] *and Diana S. Nascimento*[1,2,3]*

[1] *Instituto de Investigação e Inovação em Saúde (i3S), University of Porto, Porto, Portugal,* [2] *Instituto Nacional de Engenharia Biomédica (INEB), University of Porto, Porto, Portugal,* [3] *Instituto de Ciências Biomédicas Abel Salazar (ICBAS), University of Porto, Porto, Portugal,* [4] *Cardiovascular RandD Center, Faculty of Medicine of the University of Porto, Porto, Portugal,* [5] *Department of Internal Medicine, Centro Hospitalar Universitário São João, Porto, Portugal,* [6] *ECBio S.A., Amadora, Portugal*

Human mesenchymal stem cells gather special interest as a universal and feasible add-on therapy for myocardial infarction (MI). In particular, human umbilical cord matrix-derived mesenchymal stromal cells (UCM-MSC) are advantageous since can be easily obtained and display high expansion potential. Using isolation protocols compliant with cell therapy, we previously showed UCM-MSC preserved cardiac function and attenuated remodeling 2 weeks after MI. In this study, UCM-MSC from two umbilical cords, UC-A and UC-B, were transplanted in a murine MI model to investigate consistency and durability of the therapeutic benefits. Both cellular products improved cardiac function and limited adverse cardiac remodeling 12 weeks post-ischemic injury, supporting sustained and long-term beneficial therapeutic effect. Donor associated variability was found in the modulation of cardiac remodeling and activation of the Akt-mTOR-GSK3β survival pathway. *In vitro*, the two cell products displayed similar ability to induce the formation of vessel-like structures and comparable transcriptome in normoxia and hypoxia, apart from UCM-MSCs proliferation and expression differences in a small subset of genes associated with MHC Class I. These findings support that UCM-MSC are strong candidates to assist the treatment of MI whilst calling for the discussion on methodologies to characterize and select best performing UCM-MSC before clinical application.

Keywords: mesenchymal stromal (or stem) cells, Wharton's jelly, myocardial infarction, regeneration/repair, umbilical cord matrix derived mesenchymal stromal cells (hUCM-MSCs), cell therapy, donor variability, cardiac fibrosis

OPEN ACCESS

Edited by:
Susana Solá,
University of Lisbon, Portugal

Reviewed by:
Gianandrea Pasquinelli,
University of Bologna, Italy
Marco Tatullo,
University of Bari Medical School, Italy

***Correspondence:**
Diana S. Nascimento
dsn@ineb.up.pt

Specialty section:
This article was submitted to Stem Cell Research, a section of the journal Frontiers in Cell and Developmental Biology

Received: *31 October 2020*
Accepted: *11 January 2021*
Published: *04 February 2021*

Citation:
Laundos TL, Vasques-Nóvoa F, Gomes RN, Sampaio-Pinto V, Cruz P, Cruz H, Santos JM, Barcia RN, Pinto-do-Ó P and Nascimento DS (2021) Consistent Long-Term Therapeutic Efficacy of Human Umbilical Cord Matrix-Derived Mesenchymal Stromal Cells After Myocardial Infarction Despite Individual Differences and Transient Engraftment. Front. Cell Dev. Biol. 9:624601. doi: 10.3389/fcell.2021.624601

INTRODUCTION

Cardiovascular diseases are the leading cause of morbidity and mortality worldwide (Benjamin et al., 2019), with ischemic heart disease representing the largest single cause of death in countries of all income levels (Nowbar et al., 2019). Myocardial Infarction (MI) occurs upon blockage of coronary arteries and impaired regional blood supply to the myocardium. As result of nutrient and oxygen deprivation, extensive cardiomyocyte death triggers a sequence of key inflammatory and fibrotic mechanisms that, coupled with the limited regenerative capacity of the adult heart (Sampaio-Pinto et al., 2020), lead to the formation of a non-functional collagen-based scar that negatively impacts on myocardial function and contribute to the development of heart failure. Despite tremendous improvement in the treatment and prognosis of MI, achieved with early reperfusion and optimized pharmacological therapy, some patients with severe and diffuse coronary disease still experience significant ventricular remodeling, myocardial dysfunction and high morbidity and mortality.

Cardiac cell-based therapies aimed at regeneration and/or instructing a more favorable repair have been explored in clinical settings, including skeletal myoblasts, embryonic stem cells (ESCs), bone marrow mononuclear cells (BMMNCs), cardiac stem cells (CSCs), hematopoietic stem cells (HSCs), mesenchymal stromal cells (MSCs), and recently, induced pluripotent stem cells (iPSCs)-derived cardiomyocytes in pre-clinical studies (Madigan and Atoui, 2018). The existence of CSCs in the adult myocardium has raised controversy in particular what concerns their capacity to generate cardiomyocytes (Valente et al., 2014; Maliken and Molkentin, 2018), as their therapeutic effect has been associated to immunomodulatory and paracrine mechanisms also observed in human MSCs (Wagner et al., 2020). Indeed, envisioning the development of a universal and feasible therapy, MSCs are of particular interest (Ballini et al., 2017). Contrarily to other candidates for cell therapy, MSCs do not express MHC Class II and display low levels of MHC Class I proteins, as such seen as immune evasive (Ankrum et al., 2014) and thus suitable for MHC mismatched allogeneic transplantation. These cells can be procured from a variety of adult sources as the bone marrow and adipose tissue, and neonatal sources, including the placenta, umbilical cord blood or umbilical cord matrix (UCM; Wharton's Jelly). Among these, UCM-MSC are particularly attractive since the source tissue can be obtained in a non-invasive and more efficient fashion, have higher expansion potential, higher differentiation range and were shown to be stronger immunomodulators by repressing T-cell activation and promoting Treg expansion more efficiently (Santos et al., 2013).

Our previous work showed that human MSCs isolated from the UCM [obtained using proprietary technology (UCX®)] preserved cardiac function and attenuated cardiac remodeling 2 weeks after MI through paracrine mechanisms (Nascimento et al., 2014). To date, one phase 1/2 clinical trial was completed to evaluate safety and efficacy of UCM-MCSs specifically in the treatment of acute MI with ST elevation (Gao et al., 2015), followed by two others directed to heart failure with reduced ejection fraction (Zhao et al., 2015; Bartolucci et al., 2017). While intravascular delivery of UCM-MSC appears safe and leads to improvement of heart function and other clinical indicators (Thompson et al., 2020), little is known regarding the extent of engraftment and whether donor-to-donor variability may influence the therapeutic potency of these cellular products or their derivatives, e.g., conditioned media and extracellular vesicles. Moreover, donor variability is a concern transversal to all MSCs based therapies, independently of tissue sources, as it could potentially lead to confounding effects when only one donor is selected to represent an experimental group. Studies with multiple donors' functional assays *in vivo* have highlighted this issue, with reports of umbilical cord blood (UCB)-MSCs donor variability in response to hypoxic preconditioning and amelioration of limb ischemia (Kang et al., 2018), as well as in a rat model of MI in which therapeutic efficacy was positively correlated with n-cadherin expression (Lee et al., 2012). In the latter work, cell-cell contact mediated by n-cadherin induced activation of ERK and upregulation of VEGF as shown by overexpression and blocking approaches (Lee et al., 2012).

In this study, UCM-MSC from two umbilical cords were isolated and their therapeutic efficacy after MI was compared to evaluate consistency and long-term effect. Intramyocardial delivery of both cellular products in a murine MI model attenuated cardiac dysfunction and minimized adverse cardiac remodeling 12 weeks post ischemic injury, supporting a sustained and long-term beneficial therapeutic effect for this cell product. Despite this beneficial effect, donor associated variability in the modulation of cardiac remodeling and activation of survival pathways was evident. *In vitro*, the two cell products showed equal ability to boost the formation of vessel-like structures and a similar transcriptome in normoxia and hypoxia, apart from expression differences in a small subset of genes associated with MHC Class I. These findings support that UCM-MSC are a strong candidate as add-on therapy for MI whilst calling for the discussion on methodologies to characterize and select best performing UCM-MSC before application in cellular therapies, or alternatives to overcome this limitation.

METHODS

Ethics and Regulation—Umbilical Cord Samples

This study was performed in accordance with the Declaration of Helsinki and approved by the Ethics Committee at the Cascais Hospital Dr. José de Almeida, in the scope of a research protocol between ECBio–Research and Development in Biotechnology, S.A., and HPP Saúde–Parcerias Cascais, S.A. Umbilical cord donations were obtained with written informed consents according to Directive 2004/23/EC of the European Parliament (Portuguese Law 22/2007 of June 29).

Ethics and Regulation—Animal Procedures

All animal procedures are in conformity with the Directive 2010/63/EU of the European Parliament and were approved by the IBMC-INEB (Instituto de Biologia Molecular e Celular–Instituto de Engenharia Biomédica) Animal Ethics Committee

and Direcção Geral de Alimentação e Veterinária (permit 022793). Humane endpoints were followed according to the Organization for Economic Cooperation and Development Guidance Document on the Recognition, Assessment, and Use of Clinical Signs as Humane Endpoints for Experimental Animals Used in Safety Evaluation (2000).

UCM-MSC Isolation

Human UCM-MSC were isolated according to Martins et al. (2014) and patented proprietary technology (PCT/IB2008/054067; WO 2009044379) developed by ECBio. The procedure includes three recovery phases to ensure a high cell yield and high isolation success rates. Furthermore, the UCM-MSC used in this study were obtained and processed under protocols compliant with a certifiable advanced therapy medicinal product (ATMP), compliant with clinical cell therapy. Modifications include steps for avoiding microbiological and endotoxin contamination of the final cell product, use of clinical grade enzymes, human serum as fetal bovine serum (FBS) substitute, short initial antibiotic/antimycotic decontamination in place of sustained treatment; all can be reviewed in Martins et al. (2014). Isolated UCM-MSC were cultured (up to P8) in Minimum Essential Medium α (α-MEM; Gibco, 2 mM L-glutamine, 1 g/L glucose, 2.2 g/L sodium bicarbonate), buffered with 10 mM HEPES (Gibco), hereafter designated UCM Basal Medium (BM), supplemented with 10% human serum (HS; Lonza; except otherwise stated), in a humidified incubator at 37°C, 21%O2 and 5% CO_2. UCM-MSCs characterization procedures can be found in the **Supplementary Data**.

Myocardial Infarction and UCM-MSC Delivery

Eight to twelve weeks old adult C57BL/6 mice (Charles River), independent of gender, were subjected to MI by permanent ligation of the left anterior descending (LAD) coronary artery, as previously described (Michael et al., 1995; Nascimento et al., 2014). UCM-MSC from two umbilical cord donors (UC-A and UC-B) were thawed in alpha-MEM containing 10% HS and resuspended in phosphate-buffered saline (PBS). UCM-MSC (2×10^5 cells/heart) were delivered after LAD ligation by four intramyocardial injections of 5 μl each using a Hamilton syringe (30 Gauge, PST45°, 1701N, Hamilton Company). A group of control animals injected with vehicle (PBS, $n = 6$) was subjected to the same surgical procedure and post-operative care. UCM-MSC preparations were kept in ice throughout the surgical procedures and preparations older than 3–4 h were discarded. Analgesia and fluid therapy were performed by intraperitoneal (IP) injection of buprenorphine (Butador; Richter Pharma AG) and subcutaneous injection of 5% w/v Glucose Intravenous Infusion (B Braun), respectively. This procedure was repeated every 12 h up to 72 h after surgery or until full recovery.

Transthoracic Echocardiography

Transthoracic echocardiography was performed 12 weeks after LAD coronary artery ligation and UCM-MSC delivery by using a Vevo 2100 microultrasound platform fitted with a high resolution 38 MHz microscan transducer (both from FujiFilm VisualSonics Inc.) and data analyzed by a blinded operator. Anesthesia was induced with 5% isoflurane, animals were placed on left lateral decubitus position and anesthesia maintained at 2% isoflurane throughout the procedure for data acquisition. Fractional shortening (FS) and ejection fraction (EF) were determined in parasternal long-axis (PSLAX) B-mode, using a modified Simpson's method as previously described (Sampaio-Pinto et al., 2018). Cardiac output was determined by computing stroke volume (SV) in the left ventricle outflow track (LVOT) determined using the Pulse wave (PW)-doppler mode in the subapical view, diameter of the aortic root (B-mode) and Heart Rate (HR). The Myocardial Performance Index (MPI), also known as the Tei index, was determined based on the isovolumetric contraction and relaxation times (IVCT and IVRT) and LV ejection time (LVET), all determined by PW-doppler at the mitral valve level.

Histologic Procedures and Morphometric Analysis

At 12 weeks after surgery, hearts were collected for representative histological sampling as previously described (Valente et al., 2015). Briefly, animals were deeply anesthetized by IP injection of pentobarbital (Eutasil; CEVA, 400 mg/kg). After 4M potassium chloride (Sigma-Aldrich) injection into de left ventricle chamber, diastole-arrested hearts were harvested, briefly washed in PBS, and fixed in 10% formalin neutral buffer (Prolabo; VWR International) up to 16 h at room temperature before paraffin embedding. Representative sampling of the LV was obtained by transverse sectioning (3 μm thick) from the apex to the base of paraffin-embedded hearts with an interval of 300 μm between sections. Infarct-size assessment was performed by staining paraffin sections with modified Masson Trichrome staining (MT), according to the Trichrome (Masson) Stain kit (Sigma-Aldrich), with the following modifications: nuclei were pre-stained with Celestine Blue solution after staining with Gill's Hematoxylin and incubation for 1 h in aqueous Bouin solution to promote uniform staining. Infarcted area, infarcted midline and LV dilation were calculated using the semi-automatic MIQuant Software (Nascimento et al., 2011). LV infarcted wall thickness was determined manually using ImageJ as follows: for each section with a transmural infarction, the thickness of the wall from the epicardial to the endocardial border was measured in five equidistant points and the average for each section was determined. The results shown per heart represent the average of all infarcted sections.

Immunofluorescence

After heat-induced epitope retrieval with Tris-EDTA buffer (95°C water bath, 35 min, ph = 9.0, Tris 1 mM and EDTA 10 mM), tissue was permeabilized with 0.2% Triton X-100 (Sigma-Aldrich) for 5 min and blocked for 1 h in 4% FBS/1% BSA in PBS. For CD31 detection, sections were incubated overnight at room temperature (RT) with goat anti-mouse CD31 (sc1506; Santa Cruz Biotechnology, Dallas, TX, USA), diluted 1:250 in the blocking solution. Thereafter, sections were incubated with AlexaFluor-568-conjugated donkey anti-goat IgG (A11057; Invitrogen) diluted 1:1000 in blocking solution for 1 h at RT and

mounted using Fluoroshield containing DAPI (F6057; Sigma—Aldrich). For quantification of $CD31^+$ cells, fluorescence images of stained sections were acquired with the INCell Analyzer 2000 (GE Healthcare) high-throughput microscope with a 40x dry objective (0.60 NA) and processed semi-automatically using the embedded system software. A study blinded operator established thresholds and criteria for detection and performed the analysis.

Lentiviral Transduction of UCX®

A premade lentiviral vector encoding a cytomegalovirus (CMV) promoter-driven cassette containing the transgene for firefly luciferase (FCT005; Kerafast) was used to produce UCM-MSC lines from either donor with constitutive bioluminescence capacity, hereafter referred to as UC-A-FLuc and UC-B-FLuc. Vectors also carried a puromycin resistance gene (puro) and a woodchuck hepatitis virus post-transcriptional regulatory element (WPRE) downstream of the transgene. Transduction was performed as described in Lin et al. (2012). Briefly, UCM-MSC were cultured (since P3) in Minimum Essential Medium α with 2 mM L-Glutamine (α-MEM; Gibco) containing 20% FBS (Gibco) and 1% P/S (100 U/ml Penicillin and 100 μg/ml Streptomycin). Cells were sub-cultured at P4 (10^4 cells/cm^2) in six-well plates and transduction initiated after 12 h with 0.5 mL/well of complete media containing 100 μg/mL protamine sulfate (P4020; Sigma) with a multiplicity of infection of 5. After 8 h, 0.5 mL of complete media containing protamine sulfate was added to compensate for evaporation. After 24 h of initiating transduction the medium was replaced, cells allowed to recover for 48 h, and sub-cultured in complete medium containing 0.05 μg/mL puromycin up to P7 and UCM-MSC-Fluc cells were cryopreserved in FBS containing 10% DMSO. Non-transduced cells to control purification efficiency we treated with puromycin in parallel.

Whole-Body Bioluminescence Imaging

UC-A-FLuc and UC-B-FLuc were delivered into mice hearts subjected to LAD coronary artery permanent ligation as described above. A group of animals subjected to sham surgery ($n = 2$, no ligation) was also prepared. Imaging was performed daily from day 1 to day 7, 15 min after subcutaneous injection of 3 mg D-luciferin (BT11, Biothema) in PBS (30 mg/mL). The IVIS Lumina III system was used coupled with the XGI-8 Gas Anesthesia System (both PerkinElmer) to induce anesthesia. Signal intensity analysis was performed in identical circular regions of interest centered in the thoracic cavity expressed as radiance (photons/second/cm^2/steradian) using Living Image software (PerkinElmer) and normalized in each animal to the value read at day 1 (results presented as percentage of Day 1 for individual animals).

Immunoblotting

Immunoblotting was performed as previously described (Vasques-Nóvoa et al., 2018). Briefly, samples were homogenized in modified RIPA buffer, proteins were separated by sodium dodecyl sulfate-polyacrylamide gel electrophoresis (SDS-PAGE) and then electroblotted onto nitrocellulose membranes (Bio-Rad). After blocking, blots were incubated with primary antibodies (**Supplementary Table 1**), which were subsequently detected with 700 or 800 nm infra-red dye-conjugated secondary antibodies. Protein phosphorylation status was evaluated incubating the membrane simultaneously with host mismatched primary antibodies targeting total and phosphorylated forms, which were identified with different fluorochrome-coupled secondary antibodies. Membranes were imaged by scanning at both 800 and 700 nm with Odyssey Infrared Imaging System (LICOR Biosciences). GAPDH was used as internal control.

Hypoxia Induction

UCM-MSC seeded at 1 x 10^4 cells/cm^2 (37°C, 21%O_2, 5%CO_2) were allowed to adapt to low serum concentrations [5% human serum (HS)] until they reached 90% confluency. At this point, cells were submitted to hypoxic environment (1%O_2; Normoxia groups kept at 21%O_2) for 24h to mimic oxygen deprivation found upon transplantation into infarcted tissue. After one serum free wash, media was replenished with α-MEM without HS (25 mL to a 175 cm^2 T-flask) and conditioning was carried for more 24 h. Finally, media was collected, concentrated with 3-kDa cut-off spin concentrators, and stored at−80°C until further use.

Targeted Transcriptome Sequencing

Total RNA from UCM-MSC submitted to normoxia or hypoxia for 24 h was isolated using the RNeasy Plus Mini Kit (QIAGEN). Ion Torrent sequencing libraries were prepared according to the AmpliSeq Library prep kit protocol, and as published (Li and Zhang, 2015). RNA concentration and total RNA integrity number (RIN) were obtained using Qubit 3.0 fluorimeter and Agilent 2100 Bioanalyzer, respectively. Briefly, 10 ng of total RNA with high RIN (Average ± SD for $n = 3$ was UC-A_N = 8.87 ± 0.58, UC-A_H = 9.10 ± 0.37, UC-B_N = 8.63 ± 0.12, UC-B_H = 9.30 ± 0.41) was reverse transcribed, the resulting cDNA was amplified for 12 cycles by adding PCR Master Mix, and the AmpliSeq human transcriptome gene expression primer pool (targeting 18,574 protein-coding mRNAs and 2,228 non-coding ncRNAs, based on UCSC hg19). Amplicons were digested with the proprietary FuPa enzyme, then barcoded adapters were ligated onto the target amplicons. The library amplicons were bound to magnetic beads, and residual reaction components were washed off. Libraries were amplified, purified and individually quantified using Agilent TapeStation High Sensitivity tape. Individual libraries were diluted to a final concentration of 50 pM and pooled equally, with twelve individual samples per pool for further processing. Emulsion PCR, templating and 550 chip loading was performed with an Ion Chef Instrument (Thermo-Fisher). Sequencing was performed on an Ion S5XL™ sequencer (Thermo-Fisher). Results from 3 independent conditioning experiments were analyzed on Transcriptome Analysis Console and only genes with a fold-change $> \pm 2$ and FDR p-value < 0.05 were considered. Heatmaps were done using the Average Linkage Clustering Method and the used distance measurement method was Spearman Rank Correlation. Gene ontology and KEGG pathways for up and downregulated terms were analyzed using Enrichr.

In vitro Tubulogenesis Assay

The tubulogenesis assay was performed as described in Arnaoutova and Kleinman (2010), with slight alterations. Primary human myocardial microvascular endothelial cells (HMVEC-Cs), a potential clinical target of angiogenic mechanisms after MI, were maintained in EGM2-MV media (both from Lonza) and used at Passage 6. Matrigel growth factor reduced (10 μL, Corning) was used to coat a 15-well Angiogenesis μ-Slide (81506; Ibidi) and allowed to polymerize at 37°C for 30 min. HMVEC-C were suspended in complete media (EGM2-MV), Conditioned Media (CM) or concentrated negative control (a-MEM no cells) diluted in basal media (EBM), with a final CM concentration of 5x, and seeded at 6.5 x 10^4 cells/cm^2 in a total of 50 μL per well. Conditioned media from 3 independent hypoxia inductions was run in parallel, along with technical triplicate wells for each condition. After 7.5 h incubation at 37°C and 5%CO_2 the center of each well was imaged using phase contrast microscopy on an inverted microscope Axiovert 200 (Carl Zeiss) with a 10x objective. Image analysis was performed on ImageJ (NIH) using the Angiogenesis Analyzer plugin (Carpentier, 2012).

RT-qPCR

RNA was extracted using RNeasy Plus Mini Kit (QIAGEN) according to the manufacturer's instructions, and cDNA was synthesized using PrimeScript RT reagent kit (Takara Bio). Real-time qPCR was performed using iQ Sybr Green Supermix (Bio-Rad) and N-Cadherin specific primers preciously published (Forward 5′-AGGGGACCTTTTCCTCAAGA-3′, Reverse 5′-CAATGTCAATGGGGTTCTCC-3′) (Lee et al., 2012). Reactions were run on iCycler iQ5 Real-Time PCR system (Bio-Rad) in triplicates. Relative gene expression was normalized to GAPDH expression.

Statistical Analysis

GraphPad Prism 8 was used for statistical analysis. Shapiro-wilk test was used to assess normality of the samples and F test or Brown-Forsythe test to probe equal variances. Datasets following a Gaussian distribution and showing same standard deviation were analyzed using independent sample Student's *t*-test and one-way ANOVA for two to three or more groups, respectively, followed by Tukey's *post-hoc* test for multiple comparisons. Statistical significance of non-parametric data was tested with Kruskal-Wallis test, followed by the FDR method of Benjamini and Hochberg adjustment for multiple comparisons.

RESULTS

We had previously shown that UCM-MSC attenuate remodeling after myocardial infarction upon intramyocardial delivery by proangiogenic, antiapoptotic, and endogenous cell-activation mechanisms as observed 2 weeks after MI. Herein, using the same murine MI model, the efficiency of UC-A and UC-B was evaluated in a long-term scenario of 12 weeks. UC-A and UC-B were collected from different donors using proprietary technology and updated protocols compliant with cell therapy in a clinical setting (Martins et al., 2014). Both cell lines meet the minimal criteria defined by the International Society for Cellular Therapy (Dominici et al., 2006), namely plastic cell-adherence, expression of CD73, CD105, CD90, and CD44 and absence of CD45, CD34, CD31, CD19 and HLA-DR surface markers (**Supplementary Figures 1A,B**, **Supplementary Tables 2**, **3**). Despite similar MSC profile, UC-B displayed greater proliferation rates as demonstrated by higher levels of histone H3 phosphorylation (ph3) and greater metabolic activity (**Supplementary Figures 1B,C**). This resulted in 9.6 million cells/cm and 2.3 M/cm of cord in UC-B and UC-A at P2, respectively (data not shown).

UCM-MSC Transplantation Consistently Improve Cardiac Function 12 Weeks After MI

Cardiac function was analyzed by high-resolution echocardiography ($n = 6$ in the Vehicle Group; $n = 5$ in UC-A; $n = 7$ in UC-B). Representative images of PSLAX view of each experimental group demonstrate an attenuation of left ventricle (LV) dysfunction in the transplanted groups, when compared to the vehicle control (**Figure 1A**). A consistent improvement of LV functional parameters in animals treated with UCM-MSC was observed. Ejection fraction was improved from 22.3 ± 6.0% in the vehicle treated groups to 40.5 ± 7.5% in UC-A ($p = 0.0012$) and 45.0 ± 11.8% in UC-B ($p = 0.0313$) (**Figure 1B**). Fractional shortening was also significantly improved between the vehicle and UC-B groups ($p = 0.0313$; from vehicle treated 8.3 ± 2.1% to 14.5 ± 5.5%), although UC-A showed a similar degree of improvement ($p = 0.0516$; to 14.4 ± 2.7%) albeit not reaching statistical significance potentially due to the small animal numbers on that group (**Figure 1C**). An overall trend for improved cardiac output (**Figure 1D**) and myocardial performance index (**Figure 1E**) was also observed in UCM-MSC treated groups compared to control vehicle. Of note, UC-B consistently improved cardiac function compared to UC-A, which induced minor functional benefits.

UC-B Outperforms UC-A in Reducing Adverse Cardiac Remodeling 12 Weeks After MI

In line with the echocardiographic functional evaluation, a beneficial effect of UCM-MSC was observed suggesting an attenuation of MI triggered cardiac remodeling in UCM-MSC treated groups. Masson's Trichrome stained heart sections were subjected to morphometric analysis to evaluate cardiac remodeling (LV dilation and wall thickness) and infarct size was calculated in the *MIQuant* software (**Figure 2A**). Infarct extension reduced from 36.8 ± 4.8% in control to 26.1 ± 2.7% in UC-A ($p = 0.0277$) and to 13.1 ± 8.3% in UC-B ($p < 0.0001$). Of note, the infarct size in UC-B was smaller compared to UC-A ($p = 0.0062$) (**Figure 2B**). Infarct midline showed the same trend for reduction, illustrating the therapeutic efficacy of UCM-MSC, although no significant differences were found between vehicle and UC-A (from 42.9 ± 9.3% to 34.7 ± 6.2%); once more, UC-B outperformed UC-A with a midline infarct size of 11.8 ± 11.2% ($p = 0.0024$) (**Figure 2C**). A trend for improvement

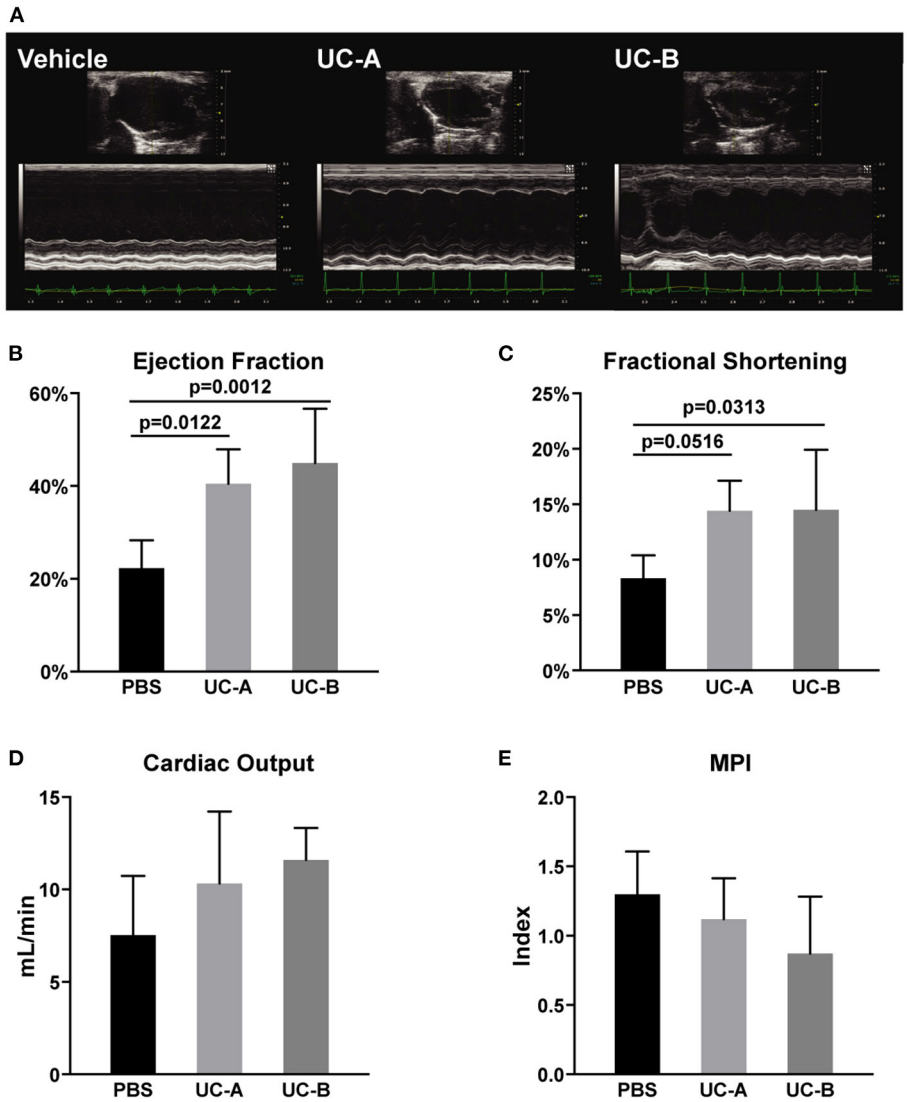

FIGURE 1 | Long term improvement in left ventricle systolic function 12 weeks after MI and UCM-MSC delivery from the 2 donors. **(A)** Representative PSLAX views in B- and M-mode. **(B)** Ejection fraction and **(C)** fractional shortening calculated using the Simpson's method (PSLAX B-mode). **(D)** Cardiac output determined through the quantification of the left ventricular outflow tract stroke volume (LVOT SV) in PW-doppler mode, aortic root diameter and Heart rate. **(E)** Myocardial Performance Index was assessed computing exclusively PW-doppler data (Mitral Valve Closure to Opening Time (MVCOT) and LV Ejection time). Mean ± SD.

but no statistically significant differences were observed between control and UC-A treated groups (26.0 ± 10.8% vs. 17.4 ± 4.0%), while UC-B showed less dilated LV with 6.9 ± 4.8% ($p = 0.0007$ vs. vehicle) (**Figure 2D**). Strikingly, no differences were observed for vehicle and UC-A (0.44 ± 0.41 mm vs. 0.41 ± 0.022 mm), with UC-B performing significantly better, with an infarcted wall thickness of 0.74 ± 0.25 mm ($p = 0.0248$ vs. vehicle and $p = 0.0261$ vs. UC-A) (**Figure 2E**). Increased neovascularization induced by this cellular product was observed previously 2 weeks after MI in the infarct borderzone (Nascimento et al., 2014). Herein, we did not find any differences in the number of endothelial cells in the infarcted area nor the borderzone (**Figures 2F–H**), indicating that the distinct efficacy of the cords does not relate with increased angiogenic capacity of the tissue in this chronic phase of MI.

UC-A and UC-B Following Myocardial Delivery Are Equally and Transiently Retained in the Myocardium

We hypothesized a key factor determining different efficacy of UCM-MSC could be their ability to reside and survive for substantially different time in the infarcted left ventricle wall undergoing nutrient and oxygen deprivation and inflammation. Moreover, higher proliferation observed *in vitro* in UC-B could result in a higher number of UCM-MSCs after transplantation of

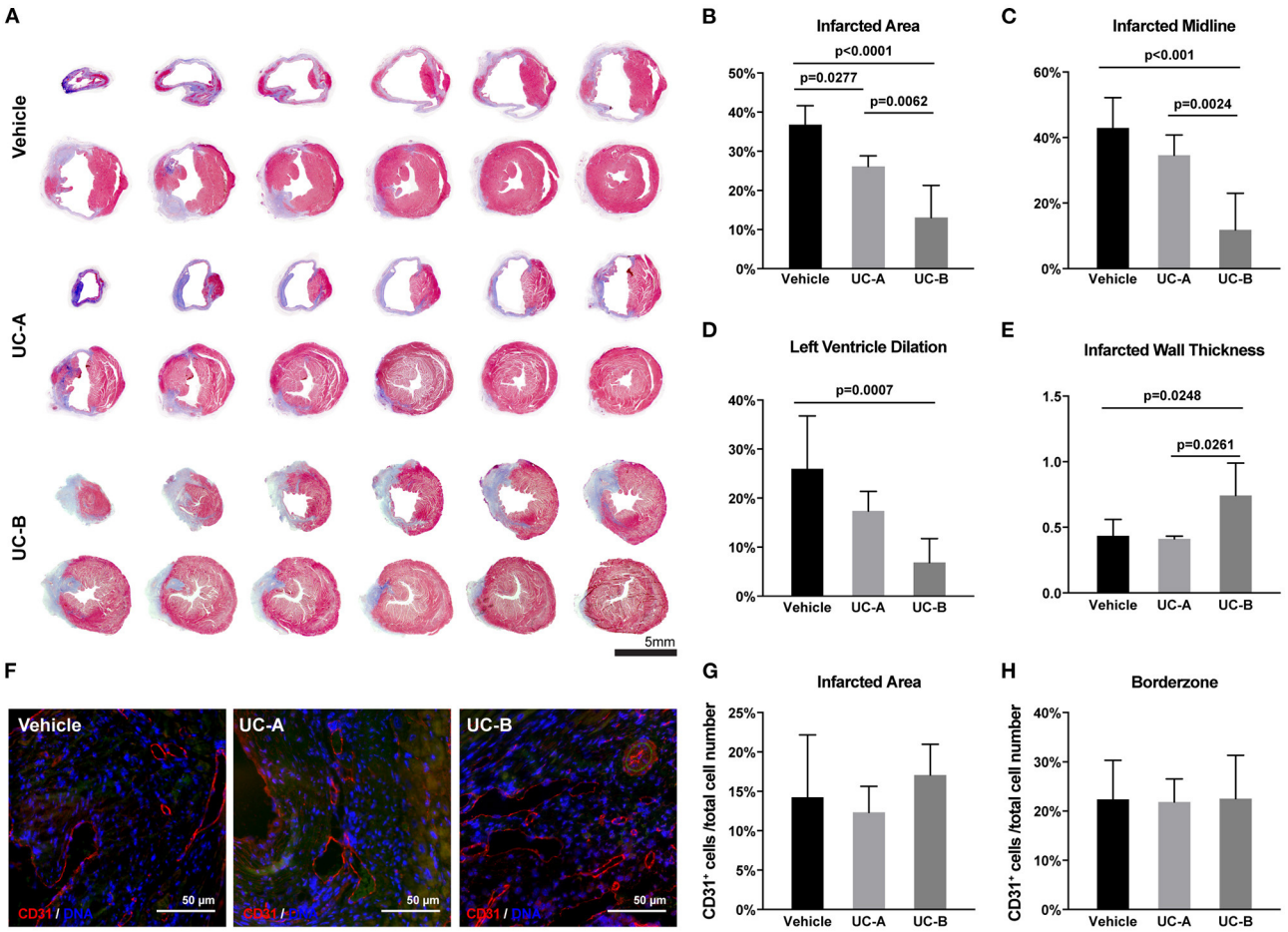

FIGURE 2 | UC-B and, at less extent UC-A, decrease cardiac remodeling 12 weeks after MI. **(A)** Representative transverse histological sections of hearts stained with Masson's Trichrome of each group. Collagen deposition (scarring) is identified in blue. **(B)** Left ventricular (LV) infarcted area, **(C)** infarcted midline, and **(D)** LV lumen dilation were quantified using the *MIQuant* Software. **(E)** Infarcted wall thickness (mm). **(F)** Representative immunofluorescence images of CD31 detection in the infarcted tissue (autofluorescence in green). **(G)** Percentage of CD31-expressing cells in the infarcted area and **(H)** borderzone. Each point represents the mean of the quantification for multiple 300 µm apart sections per heart.

similar cell numbers. To address this, UC-A and UC-B expressing firefly-luciferase under the constitutive CMV promotor after lentiviral transduction, were used in an *in vivo* longitudinal study to monitor their survival in our xenotransplant in immunocompetent infarcted mice (**Figures 3A,B**). UC-A-Luc and UC-B-Luc were delivered immediately upon coronary ligation in a group of 6 animals each. Upon administration of D-Luciferin at every 24 h, only viable cells carrying luciferase can produce bioluminescence. After day one, the number of cells reduced sharply and, from this point onward, ∼25% decreased every day, to negligible numbers by day 5 (**Figure 3B**). The clearance profile observed was the same for both cords. Of note, and albeit for a small number of animals, the decrease in viable cell numbers in sham controls is steeper from day 2 to day 3 and cannot be detected by day 4, suggesting the MI environment might extend their survival in the host tissue.

Activation of Akt Signaling in UC-B Treated Hearts Supports Improved Survival, Metabolism and Proliferation 48 h Post MI

Having established UC-A and UC-B have distinct performances *in vivo* and considering both persist for a short and similar period of time in the infarcted tissue, we assayed the short-term therapeutic potential of UC-A and UC-B after MI. For this purpose, LV borderzone was isolated 48 h after MI and UC-A and UC-B delivery ($N = 6$ per group) and main survival and inflammatory pathways were evaluated (**Figure 3C**). Increased Akt phosphorylation (Thr308) was observed in UC-B, suggesting higher Akt activity in UC-B treated hearts. Concurrently, GSK3β, a known repressor of metabolism, proliferation, and survival, showed significant increase in Akt-mediated inhibitory phosphorylation at Serine 9. Phosphorylation of mTOR, another downstream

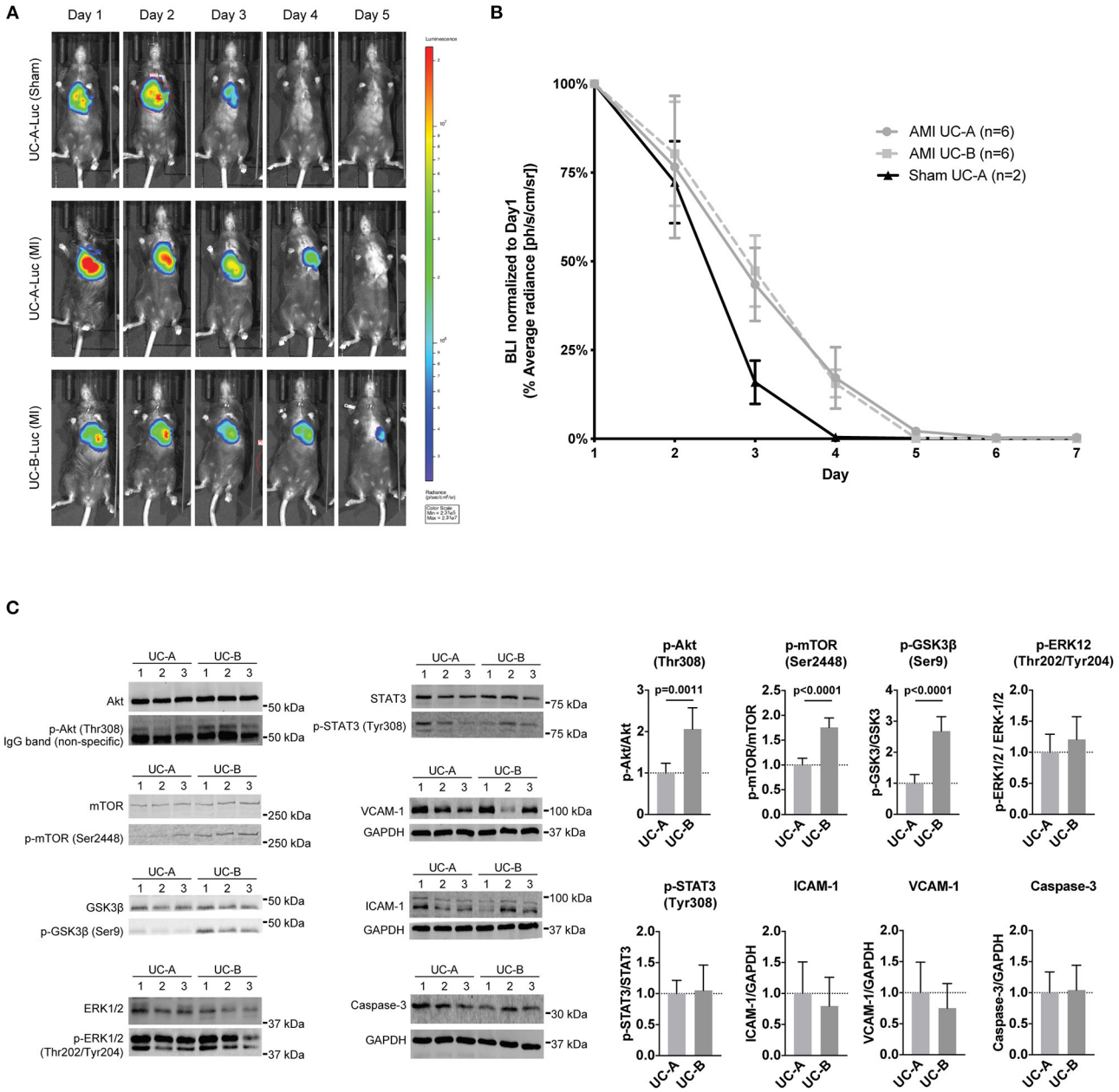

FIGURE 3 | UCM-MSC delivered into the LV show similar engraftment following myocardial infarction (MI) but differentially activate signaling pathways. **(A)** Representative images of time-course bioluminescence detection of luciferase expressing UC-A and UC-B delivered into the LV tissue after MI. **(B)** Average radiance determined in the thoracic cavity area using equivalent regions of interest for all animals in the study. Data shown as Average radiance ±SEM normalized to measurements of each animal at day 1. **(C)** Western-blot analysis of the LV borderzone at day 2 post MI and UCM-MSC myocardial delivery (blots shown for 3 animals per group; $n = 6$ per study group).

effector of Akt signaling, was also upregulated in the UC-B treated group suggesting increased Akt-mTOR-GSK3β signaling. STAT3 and ERK levels, pro-inflammatory and pro-remodeling pathways, showed similar activation levels in both cords. Furthermore, the expression of ICAM-1 and VCAM-1, regulated by inflammatory processes, and Caspase-3 seemed unchanged.

UC-A and UC-B Display Comparable Transcriptomic Profiles and Adaptation to Hypoxia Stimulus

Aiming at identifying gene expression differences correlating with enhanced therapeutic potential of UCM-MSC in ischemic conditions, the transcriptomic profile of the two cell-lines was compared under normoxia and hypoxic conditions, the latter

mimicking environmental changes installed in MI (**Figure 4A**). Unsupervised hierarchical clustering of the UC-A and UC-B datasets did not show an evident association between paired experiments, neither any effect of the hypoxic treatment (**Figure 4B**) suggesting homogenous datasets. Moreover, principal component analysis (PCA) (**Figure 4C**) showed that

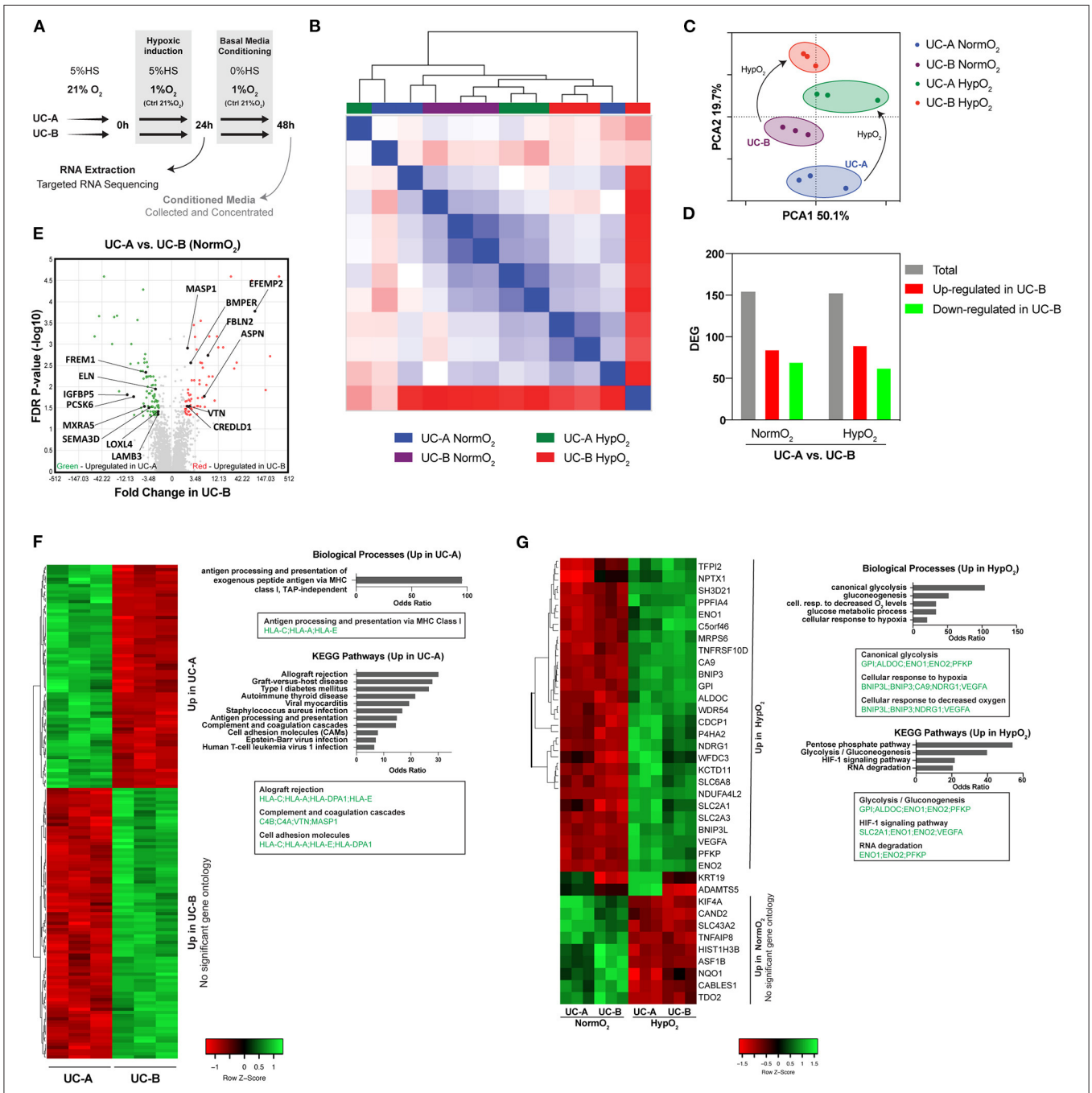

FIGURE 4 | Transcriptomic profiles of UC-A and UC-B in normoxia and in response to hypoxia. **(A)** Schematic overview of the experiment. **(B)** Unsupervised hierarchical clustering of RNA-Seq datasets obtained from 3 independent experiments of each conditionUCM-MSC line. **(C)** Principal component analysis (PCA) of the 12 RNA-Seq datasets showing an overlap on PCA1 and clustering on PCA2. **(D)** Number of total differentially expressed genes (DEG) and of genes up- and down-regulated in UC-B compared to UC-A, under normoxia and hypoxia conditions (fold-change> ±2, FDR < 0.05). **(E)** Volcano Plot of the DEG highlighting the statistically significant matrissome-associated genes. **(F)** Heatmap hierarchically organized by combined ranked score of DEG in normoxia conditions alongside the corresponding GO and KEGG pathways enrichment analysis. **(G)** Analysis of the DEG in normoxia vs. hypoxia for each UCM-MSC donor. Heatmap hierarchically organized by combined ranked score of the common DEG altered in the two donors in response to hypoxia; enriched GO and KEGG pathways are plotted.

datasets overlap on PCA1, explaining 50.1% of the sample's variance. On the PCA2 axis, which contributes 19.7% to dataset variance, both cords shift together under low oxygen levels, indicating an effect of the environmental oxygen levels, and a similar response of both UCM-MSC lines under these conditions. Regarding differential gene expression analysis (**Figures 4D–F**), UC-A and UC-B subjected to normoxia showed a total of 155 differentially expressed genes (DEG), of which 85 were up-regulated and 70 down-regulated in UC-B. Under hypoxia a comparable number of 153 total genes was found to be altered, with 90 upregulated and 63 downregulated in UC-B (fold change $> \pm 2$, FDR < 0.05). Since, the pro-reparative potential of MSC in the heart has been associated with paracrine signaling (Nascimento et al., 2014), we focused our analysis on matrisome-associated proteins (including ECM-affiliated proteins, ECM regulators and secreted factors). From the reported ∼1000 matrisome-associated genes (Naba et al., 2016), only 15 were differentially expressed, from which 7 and 8 were up- and down-regulated in UC-B, respectively (**Figure 4E**). GO enrichment analysis and pathway enrichment analysis (KEGG) of the differentially expressed genes under normoxia (**Figure 4F**) suggested increased activity associated with antigen presentation via MHC Class I with HLA-C, HLA-A, and HLA-E upregulated in UC-A. Pathway enrichment analysis (KEGG) supported this evidence, indicating higher transcription of genes associated with allograft rejection and cell adhesion molecules involved in inflammation (HLA-C, HLA-A, HLA-E, and HLA-DAPA1), as well as genes involved in complement and coagulation cascades (complement components, vitronectin and MASP1). Thirty seven genes showed altered expression in response to hypoxia in both UC-A and UC-B, 27 were upregulated and 9 downregulated on both cords (**Figures 4B,C,G**). The subset of upregulated genes showed an enrichment for processes related with cellular response to hypoxia and glycolysis; enriched KEGG pathways further hinted an adaptation of both cords to hypoxia, with enriched HIF-1 signaling pathway as well as Glycolysis and Gluconeogenesis, most notably, the upregulation of VEGF and Glucose-6-phosphate. As the two cords changed alongside in response to hypoxia, GO enrichment analysis and pathway enrichment analysis (KEGG) of the differentially expressed genes between the UC-A and UC-B after hypoxia retrieved similar results to the ones found in normoxia (data not shown). Overall, and despite similar transcriptomic profiles in normoxia and hypoxia, UC-B and UC-A expression differences were found regarding genes encoding for MHC class I molecules and complement activation-related proteins which are important elements of the inflammatory response.

UC-A and UC-B Present Equivalent Potential to Induce Tubulogenesis in Human Cardiac Endothelial Cells *in vitro*

We and others have previously indicated angiogenesis as one of the main mechanisms boosted by human UCM-MSC delivery upon MI (Zhang et al., 2013; Nascimento et al., 2014). As such, a classical tubulogenesis *in vitro* assay was performed to assess the angiogenic potency of the different donor-cord pairs in this study (**Figures 5A–C**). Human microvascular endothelial cells from cardiac origin were seeded onto a matrigel layer (growth factor reduced), in media conditioned by UC-A and UC-B and allowed to form tubes for 7.5 h. Results shown correspond to 3 independent conditioning experiments, and tubes quantified in triplicate wells for each condition/experiment. When compared to endothelial basal media (EBM), the conditioned media produced by the UCM-MSC, in either normoxia or hypoxia, increased tube number (by $98.2 \pm 21.7\%$ in UC-A-Normoxia (N), $94.0 \pm 21.7\%$ in UC-A-Hypoxia (N), $106.0 \pm 19.6\%$ in UC-B-N, and $106.5 \pm 21.1\%$ in UC-B-H), tube length (by $48.6 \pm 9.38\%$ in UC-A-N, $46.8\% \pm 8.15\%$ in UC-A-H, $51.6 \pm 5.58\%$ in UC-B-N, and $51.4 \pm 2.03\%$ in UC-B-H) and branching points/junctions (by $117 \pm 29.1\%$ in UC-A-N, $114.4 \pm 27.10\%$ in UC-A-H, $125.1 \pm 26.39\%$ in UC-B-N, and $131.3 \pm 28.21\%$ in UC-B-H). Notably, no significant differences were found between the two cords nor between UCM-MSC subjected to normoxia or hypoxia environmental conditions.

N-Cadherin Transcriptional Profile Is Identical Between Cords

It was previously suggested that transcriptional and translational levels of N-Cadherin positively correlated with the *in vivo* therapeutic efficacy of human UCB-MSCs in MI, in a study evaluating MSCs derived from a set of 4 cords (Lee et al., 2012). Based on this evidence, we assessed N-Cad expression levels on UC-A and UC-B at the end of the 3 independent conditioning experiments in an effort to predict therapeutic efficacy of our donor pair (**Figure 5D**). While we observe a marginal increase in the N-Cadherin levels in UC-B in normoxia, and similar trend between cords was observed in hypoxia, the differences were found to be statistically non-significant, thereby not supporting the discrepant effect observed between UC-A and UC-B.

DISCUSSION

Our previous research has shown that human UCM-MSC attenuate remodeling after MI in mice, albeit functional improvement was not attained likely a result of the limited time-frame (14 days) of the *in vivo* study. Whether this beneficial effect was sustained in the long term and/or was dependent of donor-to-donor variability, was not addressed. In the present study, we challenged that effect in a long-term scenario of 12 weeks and with cords derived from two different umbilical cord donors, UC-A and UC-B. Echocardiographic analysis showed that human UCM-MSC delivery in an acute phase resulted in sustained LV function, smaller infarct size and attenuated cardiac remodeling. To the best of our knowledge, this is the first evidence that transplantation of human UCM-MSC in the ischemic rodent heart provides a durable therapeutic effect at functional and histological levels. These results are consistent with the outcome reported in the preliminary work of López et al. (2013) in which functional improvement was found 32 weeks following UCM-MSC therapy. However, in this study, administered cells were isolated from rats, thus hindering translational relevance, and no systematic assessment of cardiac remodeling was performed.

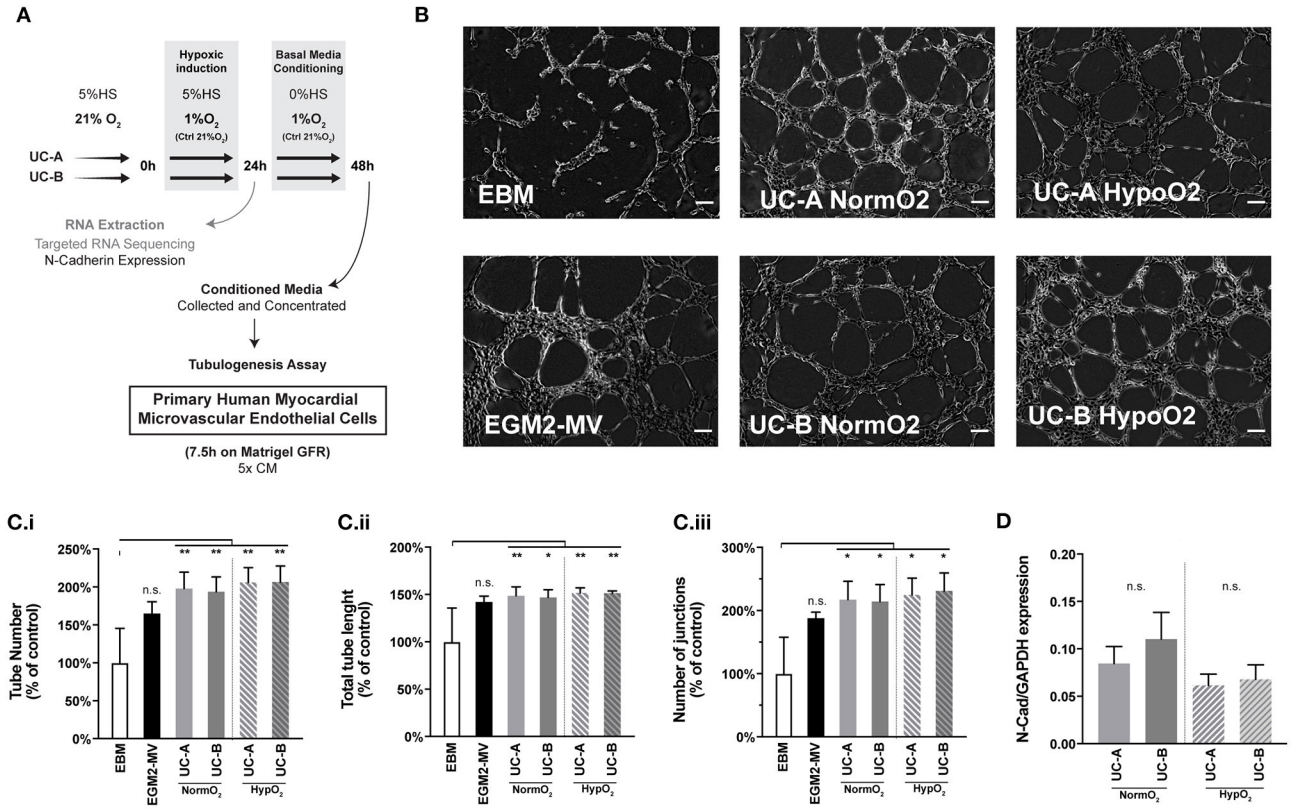

FIGURE 5 | UC-A and UC-B display equivalent *in vitro* angiogenic potential on cardiac microvascular endothelial cells. **(A)** Schematic overview of the experiment. **(B)** *In vitro* tubulogenesis assay of human myocardial microvascular endothelial cells. Representative images of the formed tubular-like structures 7.5 h after incubation with the conditioned media of the 4 experimental groups. EBM (basal media) and EGM-MV (complete media) controls are shown. Scale bar: 200 μm. **(C)** (i) Total tube number. **(C)** (ii) Total Tube length. **(C)** (iii) Number of Junctions. Results of 3 independent experiments are depicted. (*$p < 0.05$ and **$p < 0.01$) **(D)** Gene expression of N-Cadherin in UCM-MSC from the two donors from 3 independent hypoxia induction experiments ($p = 0.05$). n.s. - non-significant.

Another report by Hsiao et al. compared the therapeutic potential of human UCM-MSC primed or not with TGF-β2 in the context of MI. While showing attenuation of functional decline in the cell treated groups over the course of 16 weeks, no differences were shown at the endpoint vs. the control group, to support a long-term beneficial therapeutic effect (Hsiao et al., 2016).

We further show that in our model of xenotransplantation into immune competent mice, UCM-MSC transiently persisted in the infarcted myocardium for a period no longer than 5 days despite eliciting a durable therapeutic effect. Myocardial long-term engraftment of human cells has been demonstrated following delivery to immunodeficient/immunosuppressed (Chang et al., 2008; Gaebel et al., 2011; Latifpour et al., 2011; Roura et al., 2012; Im Cho et al., 2017) and immunocompetent animals (Berry et al., 2006; Zhang et al., 2013; Monguió-Tortajada et al., 2017). Of note, all these studies have assessed cellular integration in tissue sections at the experimental end-point by immunofluorescence or by using fluorescent cell tracking dyes. This contrasts with longitudinal studies in which bioluminescence has been used to trace transplanted cells. In these studies, animal derived cells transplanted into animals models showed clearance times similar to what we observed (Deuse et al., 2009; Wu et al., 2017) or at the most up to 30 days (Yan et al., 2013; Tu et al., 2019). Overall, these differences seem to reflect mostly the type of methodology used to assess engraftment. Whist *in vivo* bioluminescence is less sensitive than immunodetection to identify rare events of persistent cells, it allows reliable quantification of cell clearance/engraftment during the study. Herein, at the endpoint no human cell was detected using an anti-human antibody in histological sections (data not shown), reinforcing complete cell clearance. Moreover, differences in UCM-MSCs proliferation *in vitro* did not contribute to a higher cell number or longer survival *in vivo*. While the time for transplant clearance could be different in a human-to-human transplantation scenario, this data demonstrates that a short period of contact is sufficient for therapeutic benefits. This small time-window of engraftment is not compatible with a scenario of MSC differentiation in cardiac cells as has been demonstrated by others (Nagaya et al., 2004; Berry et al., 2006; Chang et al., 2008; Li et al., 2010). Instead, this scenario argues for the paracrine effects described for these cells in multiple reports (Nascimento et al., 2014; Yao et al., 2015; Cai et al., 2016) in which immunomodulatory properties, ECM remodeling ability and capacity to promote

angiogenesis are the main mechanisms (Guo et al., 2020). Several bioengineering strategies are under development to improve retention, survival, and engraftment of transplanted cells in the myocardium (Jiang et al., 2020). Of interest, a recently developed hydrogel-based combination of UCM-MSC with endothelial cells showed that *in vitro* maturation prior to transplantation promotes vasculogenic potential and cell survival/retention after transplantation in mice (Torres et al., 2020). Although, this approach may be a valuable delivery alternative for UCM-MSCs, whether longer retention will translate in better therapeutic efficacy still requires further investigation.

While being consistently beneficial and residing in the tissue for the same period of time, we show that the extent of LV function and morphology preservation at 12 weeks exerted by UC-B was superior to UC-A, even though the cells were isolated using a proprietary protocol envisaged to produce a homogeneous product (Martins et al., 2014). Moreover, UC-B delivery resulted in increased Akt-mTOR-GSK3β signaling in the infarcted myocardium 2 days post-MI. These observations are in line with abundant evidence demonstrating that the Akt-mTOR-GSK3β pathway is an important cardioprotection mechanism by promoting cardiomyocyte survival and metabolic homeostasis (Matsui et al., 2001; Shiraishi et al., 2004; Sussman et al., 2011; Lin et al., 2015). Also, the therapeutic effect of MCS delivery to the heart has been shown to encompass the secretion of a panoply of growth factors that activate mechanisms involving PI3K/Akt/mTOR pathway (Arslan et al., 2013; Cai et al., 2016). In agreement with this perspective and our findings, exosomes released by MSC promote cardiac functional restoration and improve remodeling following delivery to the ischemic heart (Arslan et al., 2013; Kang et al., 2015). Altogether, these findings support that Akt-mTOR-GSK3β pathway is a key target for therapy in ischemic diseases (Matsui et al., 2001; Shiraishi et al., 2004; Sussman et al., 2011; Lin et al., 2015).

In retrospect, and in an effort to identify features that could justify the observed differences in therapeutic potency and capacity to activate the Akt-mTOR-GSK3β pathway, we compared the transcriptome of these cells when cultured *in vitro*. Both cellular products were considered similar in normoxia apart from higher expression of HLA-I genes in UC-A, suggesting altered antigen processing via MHC Class I and allograft rejection. MHC Class I genes are present on all nucleated cells and mediate allogeneic rejection by presenting peptide antigens to $CD8^+$ T cells (Braciale, 1992), thus higher HLA-I expression on MSC following transplantation could increase the risk of rejection by the host. Yet, MSC are able to evade immune surveillance by downregulating HLA-I surface expression, even when primed with IFN-γ (Wang et al., 2019). In our study, given the high immunologic barrier to xenotransplantation, together with the hostile inflammatory milieu triggered by MI, UCM-MSC were cleared from the tissue up to 5 days post-transplant. Moreover, and regardless of having higher expression levels of MHC Class I genes, UC-A persisted in the myocardium for as long as UC-B, indicating that expression differences were not reflected on a faster clearance rate nor could justify the differential therapeutic efficacy of the two cords.

Contrasting with our previous results at 14 days after MI (Nascimento et al., 2014), hearts treated with UCM-MSC displayed a similar vascular network to the vehicle group, 12 weeks after MI. It is possible that neovascularization played a role in containing adverse remodeling and the expansion of the scar by preventing cardiomyocyte death in the border zone of the acute ischemic region and might have resolved to baseline levels at this stage. Our transcriptomic and *in vitro* angiogenesis functional analysis on human cardiac endothelial cells anticipate a similar angiogenic profile between cords, hence differences in angiogenesis may not be the cause of the observed *in vivo* variation between donors. Donor variability regarding MSCs therapeutic use have been described and linked mostly to angiogenesis. Kang et al. (2018) described a variable response to hypoxia on a set of UCB-MSCs derived from 7 cords on a panel of 4 genes (ANGPTL4, ADM, CDON, and GLUT3); better responders were associated with higher angiogenic potency *in vitro*, and showed better performance *in vivo* with 2 cords when challenged in a model of limb ischemia. Lee et al. (2012) showed different angiogenic potency that correlated with therapeutic potential of four hUCB-MSCs lines in a mouse model of MI, that could be linked to individual differences in the expression of N-cadherin, resulting in overactivated ERK that lead to increased VEGF signaling. Herein, N-cadherin nor VEGF were increased in the two cords, supporting our *in vitro* functional data regarding equivalent angiogenic induction performance. Regarding specifically MSCs derived from the UCM, Kim et al. (2019) compared the angiogenic capacity of different donor-derived UCM-MSC based of the tube forming assay and advanced four biomarkers (angiogenin, interleukin-8, monocyte chemoattractantprotein-1, and VEGF) to predict the pro-angiogenic potential of MSC *in vivo*. In our setting, hypoxia-primed cords upregulated VEGFA, but their conditioned media in normoxia vs. hypoxia showed equal potential to induce the formation of vessel-like structures by cardiac microvascular endothelial cells, meaning that VEGFA is not a key effector on its own in the angiogenic capacity of UCM-MSC.

CONCLUSION

This work is, to the best of our knowledge, the first evidence that transplantation of human UCM-MSC in the ischemic rodent heart provides a durable therapeutic effect at both functional and histological levels as observed 12 weeks after MI, despite transient engraftment.

Additionally, as far as we know, this is the first report of UCM-MSC donor-related variability in the ischemic heart. However, both donors performed equally good in the tube-forming assay, and therefore none of these assays was able to predict their therapeutic *in vivo* potential. As such, and despite that angiogenesis is a key mechanism for tissue repair after MI, other assays are needed to prospectively identify the best performing MSC to be used in clinical applications. In our setting, we show that therapeutic potency may not directly link with differential angiogenic potential nor variable response to hypoxia. Instead, we hypothesize other mechanisms may be at

play, such as differences in cardiac protection via Akt-mTOR-GSK3β as shown in our protein analysis 2 days after MI.

DATA AVAILABILITY STATEMENT

The datasets presented in this study can be found in online repositories. The names of the repository/repositories and accession number(s) can be found below: https://www.ebi.ac.uk/arrayexpress/, E-MTAB-9978.

ETHICS STATEMENT

The animal study was reviewed and approved by IBMC-INEB (Instituto de Biologia Molecular e Celular–Instituto de Engenharia Biomédica) Animal Ethics Committee and Direcção Geral de Alimentação e Veterinária (permit 022793).

AUTHOR CONTRIBUTIONS

TL: study design, data acquisition and analysis, writing original draft. FV-N, RG, and VS-P: data acquisition and analysis, review and editing. PC, HC, JS, and RB: conceptualization, funding, review and editing. PP-d-Ó: conceptualization, study design, funding, supervision, review and editing. DN: conceptualization, study design, funding, supervision, data acquisition and analysis, writing original draft, review and editing. All authors contributed to the article and approved the submitted version.

FUNDING

This work was funded by European Structural and Investment Funds (ESIF), under Lisbon Portugal Regional Operational Programme and National Funds through Fundação para a Ciência e Tecnologia (FCT) ([POCI-01-0145-FEDER-030985], [POCI-01-0145-FEDER-016385]); by FCT/Ministério da Ciência, Tecnologia e Inovação in the framework of individual funding [CEECINST/00091/2018] to DN and by QREN funds through the project ClinUCX (QREN 30196) and individual fellowships: [PD/BD/127997/2016] to TL, [SFRH/BD/144490/2019] to RG and [SFRH/BD/111799/2015] to VS-P. The funding bodies other than ECBio had no role in design, in the collection, analysis, and interpretation of data; in the writing of the manuscript; or in the decision to submit the manuscript for publication.

ACKNOWLEDGMENTS

The authors acknowledge the support of i3S scientific platforms: the Animal Facility caretakers, in particular to Sofia Lamas and Isabel Duarte for their invaluable support throughout the *in vivo* experiments. Joana Tavares from i3S/IBMC for the kind advice on implementing the *in vivo* bioluminescence assay. The Bioimaging Center for Biomaterials and Regenerative Therapies (b.IMAGE) and the Scientific Platform Advanced Light Microscopy (ALM), members of the national infrastructure PPBI-Portuguese Platform of BioImaging supported by [POCI-01-0145-FEDER-022122]. The Genomics platform (GenomePT project [POCI-01-0145-FEDER-022184]), and the HEMS, CCGEN, and TraCy. The authors are thankful to current and past members of Pinto-do-Ó laboratory for critical discussion.

SUPPLEMENTARY MATERIAL

The Supplementary Material for this article can be found online at: https://www.frontiersin.org/articles/10.3389/fcell.2021.624601/full#supplementary-material

REFERENCES

Ankrum, J. A., Ong, J. F., and Karp, J. M. (2014). Mesenchymal stem cells: immune evasive, not immune privileged. *Nat. Biotechnol.* 32, 252–260. doi: 10.1038/nbt.2816

Arnaoutova, I., and Kleinman, H. K. (2010). *In vitro* angiogenesis: endothelial cell tube formation on gelled basement membrane extract. *Nat. Protoc.* 5, 628–635. doi: 10.1038/nprot.2010.6

Arslan, F., Lai, R. C., Smeets, M. B., Akeroyd, L., Choo, A., Aguor, E. N., et al. (2013). Mesenchymal stem cell-derived exosomes increase ATP levels, decrease oxidative stress and activate PI3K/Akt pathway to enhance myocardial viability and prevent adverse remodeling after myocardial ischemia/reperfusion injury. *Stem Cell Res.* 10, 301–312. doi: 10.1016/j.scr.2013.01.002

Ballini, A., Scacco, S., Coletti, D., Pluchino, S., and Tatullo, M. (2017). Mesenchymal stem cells as promoters, enhancers, and playmakers of the translational regenerative medicine. *Stem Cells Int.* 2017:3292810. doi: 10.1155/2017/3292810

Bartolucci, J., Verdugo, F. J., González, P. L., Larrea, R. E., Abarzua, E., Goset, C., et al. (2017). Safety and efficacy of the intravenous infusion of umbilical cord mesenchymal stem cells in patients with heart failure: a phase 1/2 randomized controlled trial (rimecard trial [randomized clinical trial of intravenous infusion umbilical cord mesenchymal stem cells on cardiopathy]). *Circ. Res.* 121, 1192–1204. doi: 10.1161/circresaha.117.310712

Benjamin, E. J., Muntner, P., Alonso, A., Bittencourt, M. S., Callaway, C. W., Carson, A. P., et al. (2019). Heart disease and stroke statisticsand#x2014;2019 update: a report from the American Heart Association. *Circulation* 139, e56–e528. doi: 10.1161/CIR.0000000000000659

Berry, M. F., Engler, A. J., Woo, Y. J., Pirolli, T. J., Bish, L. T., Jayasankar, V., et al. (2006). Mesenchymal stem cell injection after myocardial infarction improves myocardial compliance. *Am. J. Physiol. Circ. Physiol.* 290, H2196–H2203. doi: 10.1152/ajpheart.01017.2005

Braciale, T. J. (1992). Antigen processing for presentation by MHC class I molecules. *Curr. Opin. Immunol.* 4, 59–62. doi: 10.1016/0952-7915(92)90126-y

Cai, M., Shen, R., Song, L., Lu, M., Wang, J., Zhao, S., et al. (2016). Bone marrow mesenchymal stem cells (BM-MSCs) improve heart function in swine myocardial infarction model through paracrine effects. *Sci. Rep.* 6, 28250. doi: 10.1038/srep28250

Carpentier, G. (2012). Angiogenesis analyzer for ImageJ. *ImageJ News*.

Chang, S.-A., Lee, E. J., Kang, H.-J., Zhang, S.-Y., Kim, J.-H., Li, L., et al. (2008). Impact of myocardial infarct proteins and oscillating pressure on the differentiation of mesenchymal stem cells: effect of acute myocardial infarction on stem cell differentiation. *Stem Cells* 26, 1901–1912. doi: 10.1634/stemcells.2007-0708

Deuse, T., Peter, C., Fedak, P. W., Doyle, T., Reichenspurner, H., Zimmermann, W. H., et al. (2009). Hepatocyte growth factor or vascular endothelial growth factor gene transfer maximizes mesenchymal stem cell-based myocardial salvage after acute myocardial infarction. *Circulation* 120(11 Suppl), S247–S254. doi: 10.1161/circulationaha.108.843680

Dominici, M., Le Blanc, K., Mueller, I., Slaper-Cortenbach, I., Marini, F., Krause, D., et al. (2006). Minimal criteria for defining multipotent mesenchymal stromal cells. The International Society for Cellular Therapy position statement. *Cytotherapy* 8, 315–317. doi: 10.1080/14653240600855905

Gaebel, R., Furlani, D., Sorg, H., Polchow, B., Frank, J., Bieback, K., et al. (2011). Cell origin of human mesenchymal stem cells determines a different healing performance in cardiac regeneration. *PLoS ONE* 6:e15652. doi: 10.1371/journal.pone.0015652

Gao, L. R., Chen, Y., Zhang, N. K., Yang, X. L., Liu, H. L., Wang, Z. G., et al. (2015). Intracoronary infusion of Wharton's jelly-derived mesenchymal stem cells in acute myocardial infarction: double-blind, randomized controlled trial. *BMC Med.* 13:162. doi: 10.1186/s12916-015-0399-z

Guo, Y., Yu, Y., Hu, S., Chen, Y., and Shen, Z. (2020). The therapeutic potential of mesenchymal stem cells for cardiovascular diseases. *Cell Death Dis.* 11:349. doi: 10.1038/s41419-020-2542-9

Hsiao, C.-Y., Tsai, P.-J., Chu, P.-C., Liu, S., Pan, C.-H., Chen, C., et al. (2016). Transplantation of Wharton's jelly mesenchymal stem cells to improve cardiacfunction in myocardial infarction rats. *J. Biomed. Sci.* 5:20. doi: 10.4172/2254-609X.100020

Im Cho, D., Seok Kang, W., Hwa Hong, M., Jin Kang, H., Ra Kim, M., Chul Kim, M., et al. (2017). The optimization of cell therapy by combinational application with apicidin-treated mesenchymal stem cells after myocardial infarction. *Oncotarget* 8:27. doi: 10.18632/oncotarget.17471

Jiang, B., Yan, L., Shamul, J. G., Hakun, M., and He, X. (2020). Stem cell therapy of myocardial infarction: a promising opportunity in bioengineering. *Adv. Ther.* 3:1900182. doi: 10.1002/adtp.201900182

Kang, I., Lee, B.-C., Choi, S. W., Lee, J. Y., Kim, J.-J., Kim, B.-E., et al. (2018). Donor-dependent variation of human umbilical cord blood mesenchymal stem cells in response to hypoxic preconditioning and amelioration of limb ischemia. *Exp. Mol. Med.* 50:35. doi: 10.1038/s12276-017-0014-9

Kang, K., Ma, R., Cai, W., Huang, W., Paul, C., Liang, J., et al. (2015). Exosomes secreted from CXCR4 overexpressing mesenchymal stem cells promote cardioprotection via akt signaling pathway following myocardial infarction. *Stem Cells Int.* 2015:659890. doi: 10.1155/2015/659890

Kim, H. K., Lee, S. G., Lee, S. W., Oh, B. J., Kim, J. H., Kim, J. A., et al. (2019). A subset of paracrine factors as efficient biomarkers for predicting vascular regenerative efficacy of mesenchymal stromal/stem cells. *Stem Cells* 37, 77–88. doi: 10.1002/stem.2920

Latifpour, M., Nematollahi-Mahani, S. N., Deilamy, M., Azimzadeh, B. S., Eftekhar-Vaghefi, S. H., Nabipour, F., et al. (2011). Improvement in cardiac function following transplantation of human umbilical cord matrix-derived mesenchymal cells. *Cardiology* 120, 9–18. doi: 10.1159/000332581

Lee, E. J., Choi, E.-K., Kang, S. K., Kim, G.-H., Park, J. Y., Kang, H.-J., et al. (2012). N-cadherin determines individual variations in the therapeutic efficacy of human umbilical cord blood-derived mesenchymal stem cells in a rat model of myocardial infarction. *Mol. Ther.* 20, 155–167. doi: 10.1038/mt.2011.202

Li, Q., Turdi, S., Thomas, D. P., Zhou, T., and Ren, J. (2010). Intra-myocardial delivery of mesenchymal stem cells ameliorates left ventricular and cardiomyocyte contractile dysfunction following myocardial infarction. *Toxicol. Lett.* 195, 119–126. doi: 10.1016/j.toxlet.2010.03.009

Li, Y., and Zhang, Z.-L. (2015). *Understanding Complex Networks Using Graph Spectrum*. Paper presented at the Proceedings of the 24th International Conference on World Wide Web, Florence, Italy.

Lin, P., Lin, Y., Lennon, D. P., Correa, D., Schluchter, M., and Caplan, A. I. (2012). Efficient lentiviral transduction of human mesenchymal stem cells that preserves proliferation and differentiation capabilities. *Stem Cells Transl. Med.* 1, 886–897. doi: 10.5966/sctm.2012-0086

Lin, Z., Zhou, P., von Gise, A., Gu, F., Ma, Q., Chen, J., et al. (2015). Pi3kcb links Hippo-YAP and PI3K-AKT signaling pathways to promote cardiomyocyte proliferation and survival. *Circ. Res.* 116, 35–45. doi: 10.1161/circresaha.115.304457

López, Y., Lutjemeier, B., Seshareddy, K., Trevino, E. M., Hageman, K. S., Musch, T. I., et al. (2013). Wharton's jelly or bone marrow mesenchymal stromal cells improve cardiac function following myocardial infarction for more than 32 weeks in a rat model: a preliminary report. *Curr. Stem Cell Res. Ther.* 8, 46–59. doi: 10.2174/1574888x11308010007

Madigan, M., and Atoui, R. (2018). Therapeutic use of stem cells for myocardial infarction. *Bioengineering* 5:28. doi: 10.3390/bioengineering5020028

Maliken, B. D., and Molkentin, J. D. (2018). Undeniable evidence that the adult mammalian heart lacks an endogenous regenerative stem cell. *Circulation* 138, 806–808. doi: 10.1161/CIRCULATIONAHA.118.035186

Martins, J. P., Santos, J. M., Almeida, J. M., Filipe, M. A., de Almeida, M. V. T., Almeida, S. C. P., et al. (2014). Towards an advanced therapy medicinal product based on mesenchymal stromal cells isolated from the umbilical cord tissue: quality and safety data. *Stem Cell Res. Ther.* 5:9. doi: 10.1186/scrt398

Matsui, T., Tao, J., Monte, F., d., Lee, K.-H., Li, L., et al. (2001). Akt activation preserves cardiac function and prevents injury after transient cardiac ischemia *in vivo*. *Circulation* 104, 330–335. doi: 10.1161/01.CIR.104.3.330

Michael, L. H., Entman, M. L., Hartley, C. J., Youker, K. A., Zhu, J., Hall, S. R., et al. (1995). Myocardial ischemia and reperfusion: a murine model. *Am. J. Physiol.* 269(6 Pt 2), H2147–2154. doi: 10.1152/ajpheart.1995.269.6.H2147

Monguió-Tortajada, M., Roura, S., Gálvez-Montón, C., Franquesa, M., Bayes-Genis, A., and Borràs, F. E. (2017). Mesenchymal stem cells induce expression of CD73 in human monocytes *in vitro* and in a swine model of myocardial infarction *in vivo*. *Front. Immunol.* 8:1577. doi: 10.3389/fimmu.2017.01577

Naba, A., Clauser, K. R., Ding, H., Whittaker, C. A., Carr, S. A., and Hynes, R. O. (2016). The extracellular matrix: tools and insights for the "omics" era. *Matrix Biol.* 49, 10–24. doi: 10.1016/j.matbio.2015.06.003

Nagaya, N., Fujii, T., Iwase, T., Ohgushi, H., Itoh, T., Uematsu, M., et al. (2004). Intravenous administration of mesenchymal stem cells improves cardiac function in rats with acute myocardial infarction through angiogenesis and myogenesis. *Am. J. Physiol.* 287, H2670–H2676. doi: 10.1152/ajpheart.01071.2003

Nascimento, D. S., Mosqueira, D., Sousa, L. M., Teixeira, M., Filipe, M., Resende, T. P., et al. (2014). Human umbilical cord tissue-derived mesenchymal stromal cells attenuate remodeling after myocardial infarction by proangiogenic, antiapoptotic, and endogenous cell-activation mechanisms. *Stem Cell Res. Ther.* 5:5. doi: 10.1186/scrt394

Nascimento, D. S., Valente, M., Esteves, T., de Pina, M., d., F., Guedes, J. G., et al. (2011). MIQuant – semi-automation of infarct size assessment in models of cardiac ischemic injury. *PLoS ONE* 6:e25045. doi: 10.1371/journal.pone.0025045

Nowbar, A. N., Gitto, M., Howard, J. P., Francis, D. P., and Al-Lamee, R. (2019). Mortality from ischemic heart disease. *Circulation* 12:e005375. doi: 10.1161/CIRCOUTCOMES.118.005375

Roura, S., Bagó, J. R., Soler-Botija, C., Pujal, J. M., Gálvez-Montón, C., Prat-Vidal, C., et al. (2012). Human umbilical cord blood-derived mesenchymal stem cells promote vascular growth *in vivo*. *PLoS ONE* 7:e49447. doi: 10.1371/journal.pone.0049447

Sampaio-Pinto, V., Rodrigues, S. C., Laundos, T. L., Silva, E. D., Vasques-Nóvoa, F., Silva, A. C., et al. (2018). Neonatal apex resection triggers cardiomyocyte proliferation, neovascularization and functional recovery despite local fibrosis. *Stem Cell Rep.* 10, 860–874. doi: 10.1016/j.stemcr.2018.01.042

Sampaio-Pinto, V., Silva, A. C., Pinto-do-Ó., P., and Nascimento, D. S. (2020). "Cardiac regeneration and repair: from mechanisms to therapeutic strategies," in *Concepts and Applications of Stem Cell Biology: A Guide for Students,* eds G. Rodrigues and B. A. J. Roelen (Cham: Springer International Publishing), 187–211.

Santos, J. M., Bárcia, R. N., Simões, S. I., Gaspar, M. M., Calado, S., Agua-Doce, A., et al. (2013). The role of human umbilical cord tissue-derived mesenchymal stromal cells (UCX®) in the treatment of inflammatory arthritis. *J. Transl. Med.* 11:18. doi: 10.1186/1479-5876-11-18

Shiraishi, I., Melendez, J., Ahn, Y., Skavdahl, M., Murphy, E., Welch, S., et al. (2004). Nuclear targeting of akt enhances kinase activity and survival of cardiomyocytes. *Circ. Res.* 94, 884–891. doi: 10.1161/01.RES.0000124394.01180.BE

Sussman, M. A., Völkers, M., Fischer, K., Bailey, B., Cottage, C. T., Din, S., et al. (2011). Myocardial AKT: the omnipresent nexus. *Physiol. Rev.* 91, 1023–1070. doi: 10.1152/physrev.00024.2010

Thompson, M., Mei, S. H. J., Wolfe, D., Champagne, J., Fergusson, D., Stewart, D. J., et al. (2020). Cell therapy with intravascular administration of mesenchymal stromal cells continues to appear safe: an updated systematic review and meta-analysis. *EClinicalMed.* 19:100249. doi: 10.1016/j.eclinm.2019.100249

Torres, A. L., Bidarra, S. J., Vasconcelos, D. P., Barbosa, J. N., Silva, E. A., Nascimento, D. S., et al. (2020). Microvascular engineering: dynamic changes in microgel-entrapped vascular cells correlates with higher vasculogenic/angiogenic potential. *Biomaterials* 228:119554. doi: 10.1016/j.biomaterials.2019.119554

Tu, Y., Qiu, Y., Liu, L., Huang, T., Tang, H., Liu, Y., et al. (2019). miR-15a/15b Cluster modulates survival of mesenchymal stem cells to improve its therapeutic efficacy of myocardial infarction. *J. Am. Heart Assoc.* 8:e010157. doi: 10.1161/JAHA.118.010157

Valente, M., Araújo, A., Esteves, T., Laundos, T. L., Freire, A. G., Quelhas, P., et al. (2015). Optimized heart sampling and systematic evaluation of cardiac therapies in mouse models of ischemic injury: assessment of cardiac remodeling and semi-automated quantification of myocardial infarct size. *Curr. Protoc. Mouse Biol.* 5, 359–391. doi: 10.1002/9780470942390.mo140293

Valente, M., Nascimento, D. S., Cumano, A., and Pinto-do-Ó, P. (2014). Sca-1+ cardiac progenitor cells and heart-making: a critical synopsis. *Stem Cells Dev.* 23, 2263–2273. doi: 10.1089/scd.2014.0197

Vasques-Nóvoa, F., Laundos, T. L., Cerqueira, R. J., Quina-Rodrigues, C., Soares-Dos-Reis, R., Baganha, F., et al. (2018). MicroRNA-155 amplifies nitric oxide/cGMP signaling and impairs vascular angiotensin II reactivity in septic shock. *Crit. Care Med.* 46, e945–e954. doi: 10.1097/ccm.0000000000003296

Wagner, M. J., Khan, M., and Mohsin, S. (2020). Healing the broken heart; the immunomodulatory effects of stem cell therapy. *Front. Immunol.* 11:639. doi: 10.3389/fimmu.2020.00639

Wang, Y., Huang, J., Gong, L., Yu, D., An, C., Bunpetch, V., et al. (2019). The plasticity of mesenchymal stem cells in regulating surface HLA-I. *iScience* 15, 66–78. doi: 10.1016/j.isci.2019.04.011

Wu, Z., Chen, G., Zhang, J., Hua, Y., Li, J., Liu, B., et al. (2017). Treatment of myocardial infarction with gene-modified mesenchymal stem cells in a small molecular hydrogel. *Sci. Rep.* 7:15826. doi: 10.1038/s41598-017-15870-z

Yan, X., Ray, P., Paulmurugan, R., Tong, R., Gong, Y., Sathirachinda, A., et al. (2013). A transgenic tri-modality reporter mouse. *PLoS ONE* 8:e73580. doi: 10.1371/journal.pone.0073580

Yao, Y., Huang, J., Geng, Y., Qian, H., Wang, F., Liu, X., et al. (2015). Paracrine action of mesenchymal stem cells revealed by single cell gene profiling in infarcted murine hearts. *PLoS ONE* 10:e0129164. doi: 10.1371/journal.pone.0129164

Zhang, W., Liu, X. C., Yang, L., Zhu, D. L., Zhang, Y. D., Chen, Y., et al. (2013). Wharton's jelly-derived mesenchymal stem cells promote myocardial regeneration and cardiac repair after miniswine acute myocardial infarction. *Coron Artery Dis.* 24, 549–558. doi: 10.1097/MCA.0b013e3283640f00

Zhao, X. F., Xu, Y., Zhu, Z. Y., Gao, C. Y., and Shi, Y. N. (2015). Clinical observation of umbilical cord mesenchymal stem cell treatment of severe systolic heart failure. *Genet Mol. Res.* 14, 3010–3017. doi: 10.4238/2015.April.10.11

Conflict of Interest: HC and PC were shareholders of ECBio S.A. JS and RB were employees of ECBio S.A.

The remaining authors declare that the research was conducted in the absence of any commercial or financial relationships that could be construed as a potential conflict of interest.

frontiers in Cell and Developmental Biology

REVIEW
published: 22 February 2021
doi: 10.3389/fcell.2021.626805

A Critical Perspective on 3D Liver Models for Drug Metabolism and Toxicology Studies

Ana S. Serras[1†], Joana S. Rodrigues[1†], Madalena Cipriano[2†], Armanda V. Rodrigues[1], Nuno G. Oliveira[1] and Joana P. Miranda[1]*

[1] Research Institute for Medicines (iMed.ULisboa), Faculty of Pharmacy, Universidade de Lisboa, Lisbon, Portugal,
[2] Fraunhofer Institute for Interfacial Engineering and Biotechnology IGB, Stuttgart, Germany

The poor predictability of human liver toxicity is still causing high attrition rates of drug candidates in the pharmaceutical industry at the non-clinical, clinical, and post-marketing authorization stages. This is in part caused by animal models that fail to predict various human adverse drug reactions (ADRs), resulting in undetected hepatotoxicity at the non-clinical phase of drug development. In an effort to increase the prediction of human hepatotoxicity, different approaches to enhance the physiological relevance of hepatic *in vitro* systems are being pursued. Three-dimensional (3D) or microfluidic technologies allow to better recapitulate hepatocyte organization and cell-matrix contacts, to include additional cell types, to incorporate fluid flow and to create gradients of oxygen and nutrients, which have led to improved differentiated cell phenotype and functionality. This comprehensive review addresses the drug-induced hepatotoxicity mechanisms and the currently available 3D liver *in vitro* models, their characteristics, as well as their advantages and limitations for human hepatotoxicity assessment. In addition, since toxic responses are greatly dependent on the culture model, a comparative analysis of the toxicity studies performed using two-dimensional (2D) and 3D *in vitro* strategies with recognized hepatotoxic compounds, such as paracetamol, diclofenac, and troglitazone is performed, further highlighting the need for harmonization of the respective characterization methods. Finally, taking a step forward, we propose a roadmap for the assessment of drugs hepatotoxicity based on fully characterized fit-for-purpose *in vitro* models, taking advantage of the best of each model, which will ultimately contribute to more informed decision-making in the drug development and risk assessment fields.

Keywords: *in vitro* liver model, fit-for-purpose models, hepatotoxicity, paracetamol, diclofenac, troglitazone, three-dimensional culture

OPEN ACCESS

Edited by:
Emmanuel S. Tzanakakis, Tufts University, United States

Reviewed by:
Natesh Parashurama, University at Buffalo, United States
Salman Khetani, University of Illinois at Chicago, United States

***Correspondence:**
Joana P. Miranda
jmiranda@ff.ulisboa.pt;
jmiranda@ff.ul.pt

† These authors have contributed equally to this work

Specialty section:
This article was submitted to Stem Cell Research, a section of the journal Frontiers in Cell and Developmental Biology

Received: *06 November 2020*
Accepted: *21 January 2021*
Published: *22 February 2021*

Citation:
Serras AS, Rodrigues JS, Cipriano M, Rodrigues AV, Oliveira NG and Miranda JP (2021) A Critical Perspective on 3D Liver Models for Drug Metabolism and Toxicology Studies. Front. Cell Dev. Biol. 9:626805. doi: 10.3389/fcell.2021.626805

INTRODUCTION

The process of development of new drugs is a costly investment with the pharmaceutical industry facing considerable challenges regarding the balance between the political pressure to increase drugs safety while reducing the cost of medicines. According to a recent study by Wouters et al. (2020), the median investment of bringing a new drug into the market, also accounting for failed

trials, was estimated at $985.3 million over the period of 2009–2018. It is a process that usually takes 10–15 years, with a success rate from phase I to launch of less than 10% (Dowden and Munro, 2019). This is mostly due to lack of drug efficacy or safety issues that occur essentially in the clinical phases IIb and III of drug development (Kola and Landis, 2004; Paul et al., 2010). Even after reaching the market (phase IV), there is still a relevant number of drug withdrawals for toxicological reasons. Approximately 18–30% of such withdrawals are caused by hepatotoxic effects, showing that the liver is the most frequent organ for adverse drug reactions (ADRs) (Onakpoya et al., 2016; Siramshetty et al., 2016; Zhang X. et al., 2020). Importantly, about 40–50% of the drug candidates associated with hepatotoxicity in humans did not present the same toxicological concern in animal models (van Tonder et al., 2013). Indeed, besides raising ethical issues, animal models often fail to correlate with human toxicity, since several toxic features disclosed in human trials were not predicted by animal studies (Olson et al., 2000; Shanks et al., 2009). One of the reasons for this discrepancy is the differential expression and activity of drug metabolizing enzymes between animals and humans that might confound the extrapolation of data derived from non-clinical species (Martignoni et al., 2006; Ruoß et al., 2020). Moreover, drug-induced liver injury (DILI) is a rare, but potentially fatal event, resultant from the poor translation between clinical trials and clinical practice and highlights the importance of targeting population variability at non-clinical stages (Jones et al., 2018). Within DILI, the idiosyncratic category is particularly difficult to identify by the pharmaceutical industry as it is almost undetectable in animal models (Kuna et al., 2018; Walker et al., 2020). Altogether, this has led to the proposal that the better the quality of non-clinical safety profiles, the higher the success rates for moving phase II upward (Cook et al., 2014; Walker et al., 2020). Consequently, *in vitro* liver models are growing strong while new drugs advance into clinical trials.

The search for more accurate non-clinical models along with the concern about animal welfare, reducing time and cost associated to drug development and the ever-increasing number of chemicals that need testing, made the establishment of relevant *in vitro* culture systems a priority in the toxicology assessment of drugs by the pharmaceutical industry, as these allow a higher-throughput capacity. Novel cell culture and tissue engineering technologies along with integrated endpoints have been adopted for improving liver cell metabolic performance *in vitro* and are expected to generate more robust data on the potential risks of pharmaceuticals (Davila et al., 2004; Andersen and Krewski, 2009, 2010; Krewski et al., 2009; Giri et al., 2010; Shukla et al., 2010; Balls, 2011; Mandenius et al., 2011). Existing strategies include three-dimensional (3D) structures, flow-based cultures, co-cultures and stem-cell differentiation.

In this review, we discuss the dissimilarities of the 3D *in vitro* hepatic systems currently used in research and drug development and their actual contribution for unraveling the mechanisms of drug-induced hepatotoxicity. Special emphasis is given to the features of 3D culture systems, cell organization and architecture, the effects of stirring and perfusion and how these characteristics modulate the phenotype and functionality of liver cells. In addition, we take a step forward by presenting a comparative analysis of the IC_{50} values for cytotoxicity and mechanistic endpoints, obtained either with two-dimensional (2D) and 3D *in vitro* systems for the classical hepatotoxic drugs paracetamol (acetaminophen), diclofenac and troglitazone. In this context, it seems clear the need for harmonized and fully characterized models. Moreover, it is also important to highlight that the hepatotoxicity assessment and the choice of the *in vitro* liver models depend on the questions that need to be addressed. These strategies stand out as crucial when evaluating the model's relevance value for mechanism-based hepatotoxicity assessment.

DRUG-INDUCED HEPATOTOXICITY: OVERVIEW, LIVER METABOLISM AND MECHANISMS OF TOXICITY

The liver is responsible for most of the metabolism of orally administered drugs since its anatomical proximity to the gastrointestinal tract and histological structure, including the sinusoidal space and the blood supply from the portal vein, allows the efficient transport of drugs and other xenobiotics (Vernetti et al., 2017). It is a complex organ composed by ∼60% of hepatocytes, parenchymal cells responsible for multiple functions, including metabolism. Non-parenchymal cells (NPCs) include cholangiocytes lining the bile ducts; sinusoidal endothelial cells, which constitute a permeable barrier between the blood and the space of Disse; Kupffer cells, the liver-resident macrophages; and stellate cells, which synthesize fat and produce vitamin A and collagen (Kuntz and Kuntz, 2008).

Drug-induced hepatotoxicity is defined as the hepatic damage caused by the exposure to prescription-only or over-the-counter medicines, herbs or other xenobiotics. DILI represents a major challenge for clinicians, the pharmaceutical industry, and regulatory agencies worldwide. As above mentioned, it corresponds to the leading cause of attrition of compounds in drug development, being also frequently associated to drug withdrawals from market or to use restrictions (Stevens and Baker, 2009; Devarbhavi, 2012; Jones et al., 2018).

Classically, DILI can be classified as intrinsic (e.g., caused by paracetamol) or idiosyncratic (e.g., caused by troglitazone) hepatotoxicity. Intrinsic hepatotoxicity is direct, dose-dependent and predictable, whereas idiosyncratic hepatotoxicity occurs without obvious dose-dependency, in an unpredictable fashion and with a short latency time, particularly after re-exposure (Russmann et al., 2009; Roth and Ganey, 2010). Idiosyncratic DILI can be an allergic immune-mediated hypersensitivity or the result of a non-allergic metabolic injury (Larson, 2010). DILI may also be categorized according to the duration (i.e., acute or chronic) and location/typology of the injury. The latter can be classified as hepatitis (mostly due to hepatocyte necrosis), cholestatic (i.e., bile duct damage or cholangiolitis) or mixed injury (Stefan and Hamilton, 2010). Despite the variety of its clinical presentations, DILI still does not display specific biomarkers, leading to abnormal liver tests and often the dysfunction is only identified by exclusion of other etiologies, which can lead to life-threatening clinical situations (Devarbhavi, 2012; Fu et al., 2020). Indeed, the identification of new molecular

biomarkers has been investigated in order to improve diagnosis and treatment of DILI. However, its applicability is still limited (Fu et al., 2020). Thus, DILI is largely unrecognized and underreported, such that the true incidence is unknown.

There are several examples of clinically relevant drugs that have received prescription restrictions or the inclusion of a black box warning for potential hepatotoxicity. Among hepatotoxic drugs, paracetamol is the most frequently studied. Nevertheless, the most commonly hepatotoxicity-associated pharmacological groups of orally administrated drugs are antibiotics (e.g., amoxicillin-clavulanate and rifampicin), antiretrovirals (e.g., nevirapine), non-steroidal anti-inflammatory drugs (NSAIDs, e.g., diclofenac and ibuprofen), antidepressants (e.g., paroxetine), and anticonvulsants (e.g., phenytoin, carbamazepine, and valproic acid) (EMEA, 2000; Paniagua and Amariles, 2018). Among intravenous administration, antibiotics, and antineoplastic drugs are the pharmacological groups mostly associated with hepatic toxicity (Ghabril et al., 2013). It should be mentioned that during the past decades, particularly in the last 20 years, several medicines such as troglitazone, bromfenac, trovafloxacin, ebrotidine, nimesulide, nefazodone, ximelagatran, lumiracoxib, pemoline, tolcapone, and sitaxentan have also been removed from the market in some countries in Europe and in the United States due to severe DILI (Fung et al., 2001; Qureshi et al., 2011; Babai et al., 2018).

Liver Metabolism

Drug metabolism is a major determinant of hepatotoxicity, as both detoxification and bioactivation processes can occur, and are most frequently responsible for inter-individual differences in drug-induced toxicity.

Liver metabolism encompasses phase I biotransformation reactions, also known as functionalization reactions, leading to the hydrolysis, oxidation, and reduction of a given drug or xenobiotic. Key enzymes in this phase belong to the CYP450 family, but can also be epoxide hydrolase and monoamine oxidase, among others. The metabolites generated can be detoxified or bioactivated by further phase I biotransformation or by conjugation through phase II metabolism (e.g., glucuronidation, sulfation, and acetylation). The role of liver transporters (e.g., organic anion-transporting polypeptides, OATP, multidrug resistance-associated proteins, and MRP) is of great importance for the excretion, being this step also known as phase III (Gomez-Lechon et al., 2010; Yuan and Kaplowitz, 2013). A significant feature of liver drug metabolism is that it may transform the parental compounds into chemically reactive intermediates or electrophilic metabolites (i.e., bioactivation) that attack tissue constituents, potentially leading to mutations, cancer or tissue necrosis (Pessayre, 1993). Drug-induced hepatotoxicity can thus be consequence of the toxicity of the parental drug *per se* or the result of one or more of its metabolites that arise from liver metabolism (**Figure 1**). Therefore, the toxicity of a given xenobiotic greatly depends on the equilibrium between detoxification and bioactivation. Hence, in a new drug development scheme, the biotransformation processes should be widely studied in order to predict the physiological effect of the new compound.

There are several prodrugs that take advantage of liver metabolism, e.g., cyclophosphamide (Preissner et al., 2015) and L-Dopa (Di Stefano et al., 2011), as the initial molecule is only active after biotransformation near the target site, decreasing its potential toxicity and also increasing its bioavailability. On the other hand, paracetamol is an interesting example in which hepatotoxicity is dose-dependent and occurs since its metabolic pathway switches at a high dose exposure from the detoxifying phase II metabolism to phase I metabolism, generating the hepatotoxic metabolite *N*-acetyl-*p*-benzoquinone imine (NAPQI). This metabolite can covalently react with proteins, leading to necrosis, apoptosis and, ultimately, to liver failure (Hinson et al., 2010). Additionally, phase II metabolism may also lead to hepatotoxic derivatives, such as for example carboxylic acids, e.g., bromfenac (and other NSAIDs) or valproic acid (Sidenius et al., 2004; Skonberg et al., 2008). These can be bioactivated to acyl-coenzyme A thioesters, which are intermediates in phase II conjugation reaction, and may lead to reactivity toward reduced glutathione (GSH) and covalent binding to endogenous proteins (Sidenius et al., 2004; Skonberg et al., 2008). Hence, factors including the inhibition or induction of any of the biotransformation enzymes, drug-drug interactions, or genetic polymorphisms, may lead to increased activity and toxicity or, on the other hand, to an absence of effect.

Several widely prescribed drugs are themselves potent CYP450 enzyme inducers, e.g., phenobarbital, carbamazepine and rifampicin, or inhibitors, e.g., fluoxetine, ritonavir, fluconazole, and ciprofloxacin (Baxter et al., 2010; Wooten, 2015; Wolverton and Wu, 2020). Subsequently, in the context of multiple drug prescription, the biotransformation of drugs that are substrates of CYP450 enzymes or other phase II enzymes and hepatic transporters can be severely altered when administered simultaneously. Some antiretroviral drugs, such as efavirenz (Grilo et al., 2017) or nevirapine (Pinheiro et al., 2017), may be simultaneously the substrate and the inducer of an enzyme, such as CYP3A4 and CYP2B6, and can regulate its own biotransformation (auto-inducer) (Kappelhoff et al., 2005). Indeed, enzyme induction is included within the pharmacokinetic (PK) tolerance concept, as it can lead to overdose reactions (higher parent drug/metabolite activation) or to sub-therapeutic exposures (lower parent drug/metabolite inactivation) to drugs when normal doses are administered (Dumas and Pollack, 2008; Omiecinski et al., 2011; Jaeschke, 2013). However, the effect that xenobiotics can exert on the induction or inhibition of biotransformation enzymes is especially difficult to predict with the currently existing *in vitro* and *in vivo* drug testing models, mainly due to interspecies and inter-individual differences, or decreased cells functionality (Reder-Hilz et al., 2004; Zanger et al., 2007; Godoy et al., 2013).

Genetic polymorphisms are particularly relevant risk factors regarding drug-metabolizing enzymes and may represent susceptibility biomarkers, important for predicting potential hepatotoxicity risks. Genetic polymorphisms are common gene variations that might encode for impaired/altered metabolic enzymes and generate different population subgroups in terms of metabolism assessment (Meyer and Zanger, 1997;

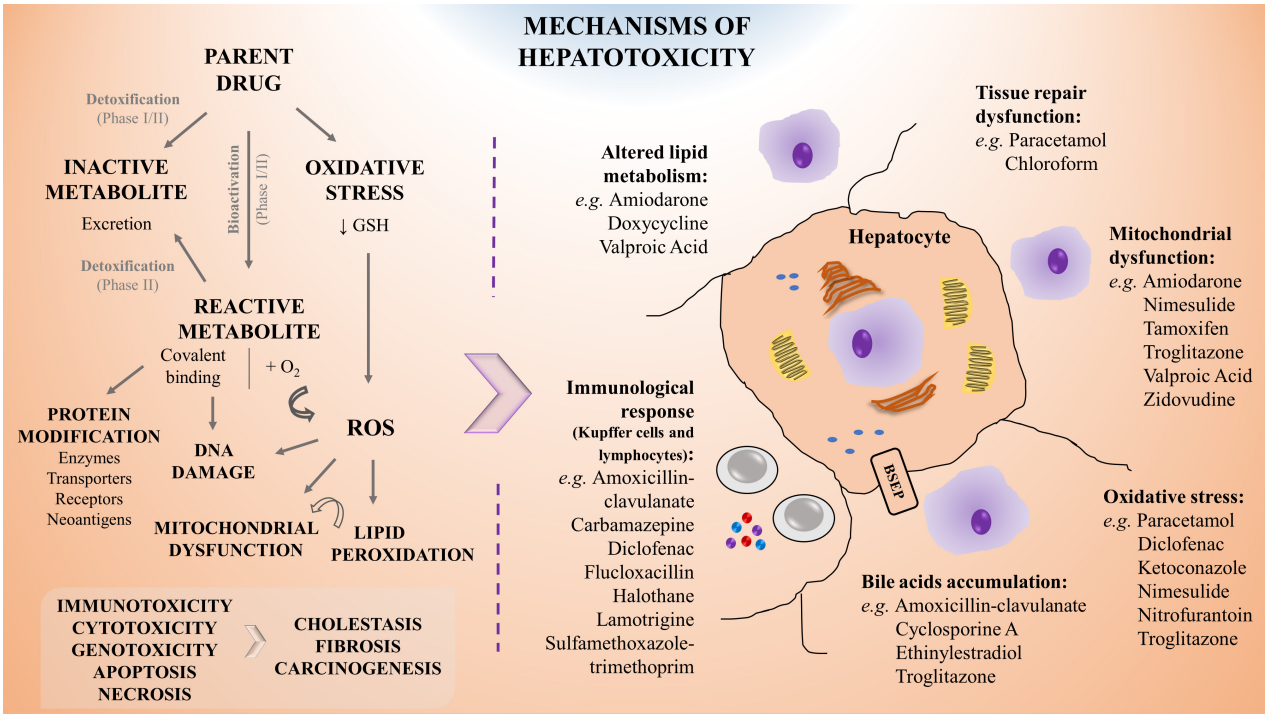

FIGURE 1 | Schematic representation of the mechanisms of hepatotoxicity including examples of associated drugs. Drug biotransformation (phase I and II metabolism) is based on the chemical modification of a parent drug into a metabolite which may become inactive (detoxification), leading to its rapid and innocuous excretion, or reactive (bioactivation), leading to potential toxicity. Specifically, hepatotoxicity may result from direct damage, from failure of repairing mechanisms or from immune-mediated responses, leading to alterations in lipids metabolism, mitochondrial dysfunction, oxidative stress and accumulation of bile, amongst others. Moreover, the saturation of cells stress defense mechanisms may lead to carcinogenic events and promote tissue necrosis or fibrosis, resulting in liver's functions impairment. For a given hepatotoxic compound different mechanisms of toxicity can be involved. GSH, reduced glutathione; ROS, reactive oxygen species.

Andrade et al., 2009; Ahmad and Odin, 2017). As this event is not rare, these subgroups need to be accounted in a drug development scheme and, thus, properly mimicked at the non-clinical stage. Interindividual variability concerning phase I, II, and III enzyme expression can also justify some cases of hepatotoxicity. Genetic polymorphisms are reported to affect the biotransformation of drugs dependent on CYP2C9, CYP2C19, CYP2B6, CYP2D6, CYP3A4, and CYP3A5 subfamilies, phase II enzymes uridine 5′-diphosphate glucuronosyltransferase (UGT) 1A1, UGT2B7 and *N*-acetyltransferase (NAT) 2, and hepatic transporters multidrug resistance protein (MDR) 1, breast cancer resistance protein (BCRP), MRPs, and OATP1B1, amongst others (Wienkers and Heath, 2005; Zanger et al., 2007; Brockmöller and Tzvetkov, 2008; Shah et al., 2015; Krasniqi et al., 2016; Saiz-Rodríguez et al., 2020). Some classical examples include CYP2D6, due to its clinical impact in the bioactivation of drugs such as codeine, tramadol, or tamoxifen within low or extensive metabolizers (Cavallari et al., 2019). Another classical example are NAT2 polymorphisms, reflected in slow, intermediate, and rapid acetylators of drugs, particularly isoniazid (anti-tuberculosis drug), in which the former presents potentially more ADRs than the latter (Brockmöller and Tzvetkov, 2008). Moreover, an inherited mutation in the adenosine triphosphate (ATP)-binding cassette subfamily B (ABCB) 11 gene, which encodes for bile salt export pump (BSEP), may lead to the diminishing of the bile acids transport and clearance, potentially leading to cholestasis (Kenna and Uetrecht, 2018).

Mechanisms of Hepatotoxicity

The liver is a prime target for drug-induced damage due to its central role for concentrating and metabolizing the majority of drugs. Therefore, earlier and better understanding of drug modes of action and toxicity are essential (Kola and Landis, 2004; Paul et al., 2010; Padda et al., 2011). As above mentioned, following exposure, the toxic effect of a given drug may be attributed directly to the interaction of the parent drug or the product of its biotransformation, with an endogenous target through covalent or non-covalent binding, hydrogen abstraction, electron transfer, or enzymatic reactions, resulting in dysfunction or destruction of the target molecules (Chan and Benet, 2017). Moreover, besides arising from direct damage by the molecule, hepatotoxicity may also be resultant from a failure of repair mechanisms or due to immune-mediated responses. The mechanisms of hepatotoxicity more frequently described are depicted in **Figure 1** and involve:

i) Mitochondrial dysfunction, an effect that may occur upon the exposure to different drugs, particularly amiodarone (Bethesda, 2012), nimesulide (Singh et al., 2010), troglitazone (Smith, 2003), or valproic acid (Xu et al., 2019);

ii) Oxidative stress, as observed for instance upon paracetamol or nitrofurantoin administration (Bethesda, 2012; Bruderer et al., 2015; Ramachandran and Jaeschke, 2018);
iii) Covalent binding with proteins that may impair their transporter function leading to accumulation of toxic elimination products and intrahepatic cholestasis (Boelsterli, 2003; Padda et al., 2011), as reported for ethinylestradiol and cyclosporine (Bethesda, 2012). It may also alter their conformation or structure as observed on the inhibition of hepatic synthesis of coagulation factors by exposure to coumarins (Grattagliano et al., 2009; Gregus, 2013);
iv) DNA damage, as suggested in the context of nevirapine toxicity (Kranendonk et al., 2014; Pinheiro et al., 2017; Marinho et al., 2019);
v) Depletion of enzymes or co-factors as observed upon paracetamol overdose (Mazaleuskaya et al., 2015; Ramachandran and Jaeschke, 2018);
vi) Dysfunction of cell repairing mechanisms that can result in: tissue necrosis, as for example by sulfasalazine, ketoconazole, or valproic acid (Kleiner, 2017); in fibrosis, by e.g., chronic exposure to methotrexate, high doses of retinol (vitamin A), and iron intoxication (Zhang et al., 2016); or in carcinogenesis, as a consequence of aflatoxin B1 exposure (Gregus, 2013; Jaeschke, 2013; Cai et al., 2020);
vii) Immunological-mediated tissue damage, that has been linked to NSAIDs such as diclofenac (Aithal et al., 2004), antibiotics such as amoxicillin-clavulanate (Bethesda, 2012) or flucloxacillin (Woolbright and Jaeschke, 2018) and anticonvulsants such as carbamazepine or lamotrigine (Bethesda, 2012).

These molecular mechanisms may intersect with each other leading to a cascade of key events. Indeed, an initial drug-related reactive oxygen species (ROS) formation may lead to lipid peroxidation on fatty acids chains in the cell membrane. In parallel, β-oxidation of lipids and oxidative stress may cause mitochondrial membrane permeabilization and dysfunction, ultimately leading to hepatocyte apoptosis. The rupture of the mitochondrial membrane can result in ATP depletion that accompanied by an increase in intracellular calcium concentration may generate liver necrosis. Conversely, inhibition of peroxisomal fatty acid β-oxidation may result in abnormal triglycerides accumulation in the hepatocyte and result in liver steatosis (Gregus, 2013). Adverse outcome pathways (AOPs) are promising tools in that regard, as they describe existing knowledge concerning the linkage between a direct molecular initiating event (MIE) and an adverse outcome through a number of key events (KEs) at a biological level of organization relevant to risk assessment (Gijbels and Vinken, 2017).

At the cellular level, the paracrine communication between hepatocytes and NPCs is also crucial for the response to a toxic insult. It has been reported that NPCs, after a primary injury of the hepatocyte, exhibit a secondary response that may aggravate or ameliorate the initial lesion, e.g., metabolic alterations and activation of immune cells, such as Kupffer cells and lymphocytes (**Figure 1**; Godoy et al., 2013; Kostadinova et al., 2013; Messner et al., 2013; Leite et al., 2016; Proctor et al., 2017; Bell et al., 2020; Li et al., 2020).

LIVER *IN VITRO* MODELS FOR TOXICOLOGICAL STUDIES

Both liver metabolism and the mechanisms of initial liver injury are important to comprehend the potential toxicity of a drug. Therefore, the development of efficient and fit-for-purpose *in vitro* models should mimic the complexity of the *in vivo* hepatic milieu. As such, when building a relevant liver *in vitro* model, the hepatic cell sources and tissue architecture, flow dynamics and the formation of molecular gradients need to be carefully considered.

No universally accepted hepatocyte source that provides robust, predictive and significant toxicological and pharmacological results is currently available. Cell source selection depends on cell availability and study requirements while understanding the limitations associated to each cell origin, namely metabolic competence, stability, and population representativeness (Soldatow et al., 2013). Regarding culture architecture, efforts have been focused in better mimic the *in vivo* microenvironment, giving special attention to culture three-dimensionality either by taking advantage of cell self-assembling capacity or by using natural polymers. More complex systems, such as bioreactors, micropatterning techniques, or microfluidic devices can also be employed (Miranda et al., 2010; Bell et al., 2016; Knospel et al., 2016; Adiels et al., 2017). Those platforms should also allow acute toxicity studies and long-term assessment so that the exposure to a xenobiotic generates relevant responses (Jiang et al., 2019). Overall, the value of an *in vitro* model depends on how well it reproduces the key physiological characteristics of an *in vivo* system. However, the criteria for defining liver function maintenance *in vitro* are not consensual, ranging from focusing on the preservation of hepatocyte phase I and II enzyme functions to the inclusion of a broader spectrum of tissue characteristics involved in human liver toxicity, such as the incorporation of NPCs for mimicking cells' crosstalk (Bale et al., 2014; Zeilinger et al., 2016; Langhans, 2018; Bell et al., 2020).

Some common evaluated features to compare hepatic cell-based *in vitro* culture systems' value for toxicological applications include cell morphology, viability, and functional stability; metabolic capacity; preservation of hepatic-specific gene expression under long-term cultures; and response to a panel of well-accepted reference drugs (e.g., paracetamol and valproic acid) capable of replicating human *in vivo* intrinsic DILI (Miranda et al., 2009, 2010; Leite et al., 2011; Mueller et al., 2011; Tostoes et al., 2011; Cipriano et al., 2017b; Pinheiro et al., 2017; Vinken and Hengstler, 2018; Bell et al., 2020). Moreover, the generated data should be able to be correlated to clinical observations, reproducible, comparable among laboratories, and analyzed properly to support decision-making with a clear definition of the models' applicability and limitations (Dash et al., 2009; Vinken and Hengstler, 2018; Albrecht et al., 2019).

Liver Cell-Based Versus Stem Cell-Based Models

Over the past decades, large efforts have been made to establish predictive *in vitro* liver test models. However, despite the number of reports available, a comprehensive and systematic comparison between cell culture systems adequate to objectively rank or select them for pharmacological and toxicological applications is still scarce.

Several *in vitro* human-based models for the prediction of hepatotoxicity have been developed using a range of cell sources and endpoints. These include the use of liver slices, genetically engineered cells, human hepatoma cell lines (e.g., HepG2, THLE, and HepaRG cells), primary hepatocytes or stem cell (SC)-derived models (Gomez-Lechon et al., 2008; Asha and Vidyavathi, 2010; Sirenko et al., 2016; Gao and Liu, 2017; Pinheiro et al., 2017; Nudischer et al., 2020). **Figure 2** summarizes the advantages and limitations of each cell source for *in vitro* testing, as well as their *in vivo* physiological relevance.

Liver slices and isolated perfused livers, containing both parenchymal and NPCs, retain liver's structure and thus maintain zone-specific enzymatic activity. However, within hours, the cell functionality decreases and necrosis takes place (Lerche-Langrand and Toutain, 2000; Boess et al., 2003; Haschek et al., 2009). It is associated with limited throughput and requires continuous animal experimentation and personnel expertise (Vernetti et al., 2017).

Alternatively, cell-based models are less complex and associated to higher throughput screening for the identification of hepatotoxic compounds. Primary hepatocytes, either obtained from human liver autopsies or biopsies or from animal livers, have been used for cytotoxicity, biotransformation, and PK studies (Vernetti et al., 2017). Human primary hepatocytes (hpHep), in particular, are considered the gold standard in human-relevant liver *in vitro* models for cytotoxicity and drug metabolism testing, retaining most of the native tissue's functionality, namely phase I and phase II enzymes (Godoy et al., 2013; Zeilinger et al., 2016). However, both the limited availability of primary human cells and its suitability only for short-term studies under monolayer cultures are major disadvantages. Indeed, in 2D conditions, it is observed a progressive loss of the hepatic phenotype in a process called de-differentiation, which is a consequence of the disruption of cell–cell and cell-matrix connections (Zeilinger et al., 2016). Additionally, hpHep display inter-donor variability and thus the use of different cell batches to validate results is advised, covering several metabolic genetic polymorphism and phenotypes (Godoy et al., 2013; Zeilinger et al., 2016). On the other hand, rat primary hepatocytes (rpHep), despite being more easily available, present relevant interspecies differences (Sandker et al., 1994; Li et al., 2008; Ménochet et al., 2012; Shen et al., 2012).

Human hepatoma cell lines, such as HepG2 and HepaRG, have no limitations in terms of cell numbers and are easy to culture, but display poor phenotype and functional match to *in vivo* hepatocytes (Gerets et al., 2012). The use of these cell lines do not consider populational differences and may reflect characteristics that primary cells do not have, e.g., being more sensitive to compounds with anti-proliferative properties (Sirenko et al., 2016). HepG2 present low levels of CYPs and normal levels of phase II enzymes except for UGTs (Westerink and Schoonen, 2007a,b), which make them appropriate for testing the toxicity of the parent compound but less suited for metabolite toxicity testing. Instead, HepaRG cell line composed of a mixture of both hepatocyte-like and biliary-like cells, have been reported to maintain hepatic functions and expression of liver-specific genes comparable to hpHep without the inter-donor variability and functional instability issues (Guillouzo et al., 2007). Nevertheless, it should be noted that a cell characterization study at the mRNA/gene expression and CYP activity levels, by Gerets et al. (2012), revealed that although it is a suitable model for induction studies, these cells were not as indicative as hpHep for the prediction of human hepatotoxic drugs, being comparable to HepG2 cells. On the other hand, Lübberstedt et al. (2011) showed that HepaRG presented similar or even higher CYP2C9, CYP2D6, and CYP3A4 enzyme activity than that of hpHep, whereas Aninat et al. (2006) confirmed the presence of relevant UGT1A1 and GST activity levels. Still, high metabolic capacity in cell lines does not necessarily correlate with high sensitivity for the hepatotoxicity detection (Gerets et al., 2012). Thus, unfortunately, even the most promising and differentiated hepatoma cells do not constitute an ideal surrogate system for human hepatocytes for hepatotoxicity studies, as they do not reproduce the drug-metabolizing enzyme pattern of human hepatocytes. An alternative approach to overcome the limitations of hepatic cell lines is to genetically modify cells with vectors encoding for human CYP enzymes and other genes involved in xenobiotic metabolism (Coecke et al., 2001; Kanamori et al., 2003; Gomez-Lechon et al., 2008; Prakash et al., 2008; Godoy et al., 2013). However, the number of enzymes that can be satisfactorily transfected into cells is low and the metabolic profiles differ from those of primary hepatocytes (Frederick et al., 2011; Godoy et al., 2013).

To overcome the limitations of the above mentioned cell sources, SC-derived human hepatocyte-like cells (HLCs) have been suggested as a reliable alternative (Szkolnicka et al., 2014; Takayama et al., 2014; Freyer et al., 2016; Cipriano et al., 2017a,b, 2020; **Figure 2**). SCs represent normal primary cells with a mostly stable genotype than hepatoma cell lines. Moreover, compared to hpHep, present unlimited supply, can be maintained for long-term and may also represent a broad patient population (Godoy et al., 2013; Horvath et al., 2016). As such, stem or progenitor cells are an exciting prospect for drug metabolism studies and cell transplantation, providing that high levels of hepatocyte-like functions can be induced and tumorigenicity concerns are overcome. Many protocols have been developed for differentiating SCs into HLCs with different approaches, such as mimicking liver development through the sequential addition of growth factors and cytokines (Cai et al., 2007; Hay et al., 2008b; Brolén et al., 2010), modulation of signaling pathways (Hay et al., 2008a) or by using epigenetic modifiers (Sharma et al., 2006; Dong et al., 2009; Norrman et al., 2013). Currently, most work has been developed using induced pluripotent SCs (iPSCs) isolated from adult tissues in an non-invasive way, with

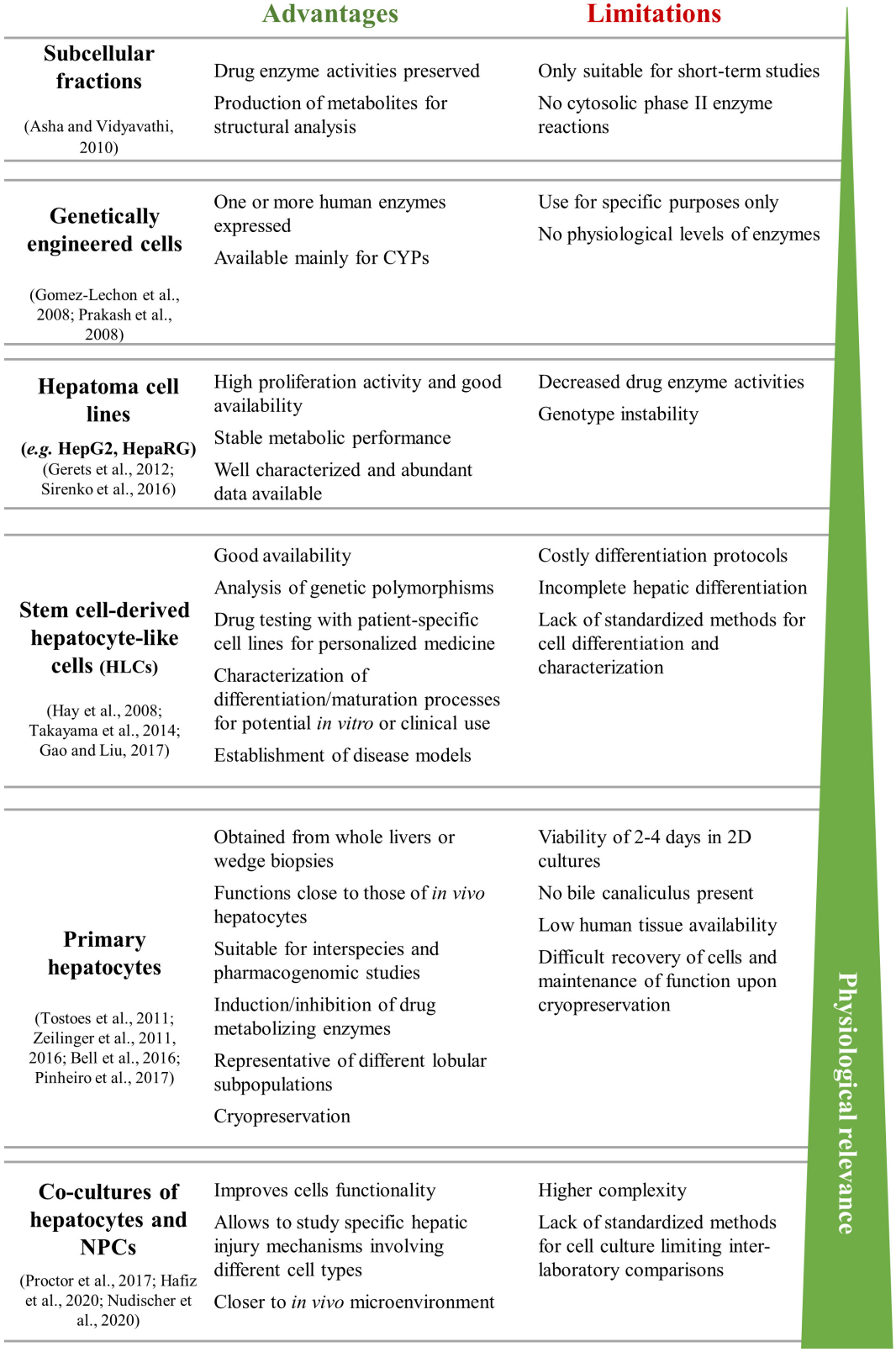

FIGURE 2 | Summary of the advantages and limitations of commonly used cell sources for *in vitro* liver models. HLCs, hepatocyte-like cells; hpHep, human primary hepatocytes; NPCs, non-parenchymal cells.

promising outcomes (Sauer et al., 2014; Sirenko et al., 2016; Yamashita et al., 2018; Pareja et al., 2020). An example is the work from Gao and Liu (2017), that revealed that iPSC-derived HLCs resembled hpHep more closely than most hepatoma cell lines in global gene expression profiles, specifically in the expression of genes involved in hepatotoxicity, drug-metabolizing enzymes, transporters, and nuclear receptors. Interestingly, Freyer et al. (2016) detected CYP1A2, CYP2B6, and CYP3A4 activities in iPSC-derived HLCs, but also at a lower level than in hpHep. Likewise, Takayama et al. (2014) showed that iPSC-derived HLCs retained donor-specific drug metabolism capacity and drug responsiveness, reflecting interindividual differences, but lower CYP1A2, CYP2C9, CYP2D6, and CYP3A4 activities when compared to the correspondent hpHep donors. Besides hepatocytes, efforts have also been made to generate NPCs from iPSCs, including cholangiocytes (Ogawa et al., 2015; Sampaziotis et al., 2015), Kupffer cells (Tasnim et al., 2019), LSECs (Koui et al., 2017), and hepatic stellate cells (Koui et al., 2017; Coll et al., 2018). Nevertheless, iPSC technology has some limitations related to the genomic instability and to residual iPSC-specific methylation patterns that links these cells to their tissue of origin, which ultimately may affect their final differentiation (Robinton and Daley, 2012). Still, iPSC-derived HLCs show powerful value not only for toxicology applications but also for disease modeling and personalized drug therapy.

Alternatively, adult liver SCs (LSCs) are a particularly interesting SC source. LSCs can be obtained from liver biopsies, propagated *in vitro* and differentiated into mature hepatocytes (Huch et al., 2015; Wang et al., 2015; Luo et al., 2018). LSCs are located in the epithelium of the canals of Hering and contribute to liver regeneration in response to an injury (Overi et al., 2018). LSCs are bipotent, being able to differentiate into hepatocytes or cholangiocytes. As such, these cells express SC (e.g., SRY-box transcription factor 9, Sox9), cholangiocyte (CK-19), and hepatocyte (CK-18) markers (Overi et al., 2018). The identification of populations of proliferating and self-renewing cells that can replace injured hepatocytes can be performed with lineage tracing approaches using *Wnt*-responsive genes such as *Axin2* or *Lgr5* (Huch et al., 2013; Wang et al., 2015).

Mesenchymal SCs (MSCs) including liver, bone-marrow, adipose, or umbilical cord tissue-derived MSCs have also been used for deriving human HLCs (Snykers et al., 2006, 2007; Banas et al., 2007; Kazemnejad et al., 2008; Okura et al., 2010; Yin et al., 2015; Fu et al., 2016; Yang et al., 2020). From those, human neonatal MSCs stand as a promising choice due to the non-invasive access and to its more primitive origin (Hass et al., 2011; Lee et al., 2012; Cipriano et al., 2017a; Yu Y. B. et al., 2018. The first report using human neonatal umbilical cord tissue-derived MSCs (hnMSCs) was from Campard et al. (2008). Therein, hnMSCs were differentiated into HLCs with impressive results, i.e., presenting hepatic-specific markers, urea production, glycogen accumulation, and CYP3A4 activity. Afterward, other researchers also differentiated hnMSCs into HLCs exhibiting hepatic markers, urea and albumin (ALB) production. However, their biotransformation activity was not assessed (Zhang et al., 2009; Zhao et al., 2009; Zhou et al., 2014). More recently, Cipriano et al. (2017a) generated hnMSC-derived HLCs with more partial hepatic phenotype, sharing expression of gene groups with hpHep that was not observed between HepG2 and hnMSCs, as shown by genome-wide analysis (Cipriano et al., 2017a). Importantly, when resorting to the 3D culture technology, MSC-derived HLCs demonstrate an improvement in phase I biotransformation activity, urea and ALB production, as well as relevant diclofenac and nevirapine biotransformation capacity, which supports its potential usefulness for toxicological studies (Cipriano et al., 2017b, 2020). Nevertheless, despite the growing efforts made in this research field a complete mature hepatocyte phenotype of HLCs derived from MSCs has not yet been achieved. Perhaps liver MSCs may be the best choice, because they are originally committed to hepatic lineage, but an accurate comparison of hepatocytes derived from human liver MSCs and other sources must still be done (Kholodenko et al., 2019; Shi et al., 2020).

All these strategies are not deprived of challenges as they require specialized personnel and expensive culture medium supplementation, whereas a complete mature phenotype has not yet been achieved. The fetal HLC phenotype is still a challenge, revealing the need to further understand hepatic differentiation mechanisms and optimizing differentiation strategies (Raju et al., 2018; Raasch et al., 2019). Moreover, the use of diverse differentiation protocols across different laboratories hinders the robustness assessment of the use of HLCs for toxicology applications. To address this issue, some authors proposed a set of cellular markers and functional assays to control the quality of iPSC-derived cells, since these are the most common type of SCs used *in vitro* (Daston et al., 2015; Beken et al., 2016). Although the specific metrics to monitor cell characteristics may vary according to the differentiation protocol and cell line used, this guide provides an important reference for quality control of other types of SC-based models. For HLCs, the most important markers to be analyzed are CYP3A4, CYP2B6, CYP1A1/2, CYP2C9, CYP2C19, CYP2D6, alpha-fetoprotein (AFP), ALB, Sox17, C-X-C motif chemokine receptor 4 (CXCR4), hepatocyte growth factor (HGF), hepatocyte nuclear factor 4 alpha (HNF-4α), tyrosine aminotransferase (TAT), transthyretin (TTR) while functional assays include urea and ALB synthesis, glycogen uptake, fibrinogen secretion, ATP, and GSH levels, CYP3A activity in particular, phase II activities and drug transporter capacity (Beken et al., 2016). Nonetheless, due to overall unsatisfactory phenotype of the currently available cell sources, at least for some hepatic features, the improvement of the cell culture system has been explored as will be further described in the following sections.

Three-Dimensional Liver Systems

The major shortcoming of the currently available *in vitro* liver preparations lays on insufficient hepatocyte-like functions and metabolic competence. In fact, none of the hpHep-, HepG2-, or HepaRG-based 2D models are suitable to indicate the risk of hepatotoxicity for novel chemical entities unless PK data are incorporated in the study, supporting the need to employ more sophisticated technologies to increase prediction sensitivity (Sison-Young et al., 2017). Accordingly, recent reports emphasize a shift, by the industry, from 2D *in vitro*

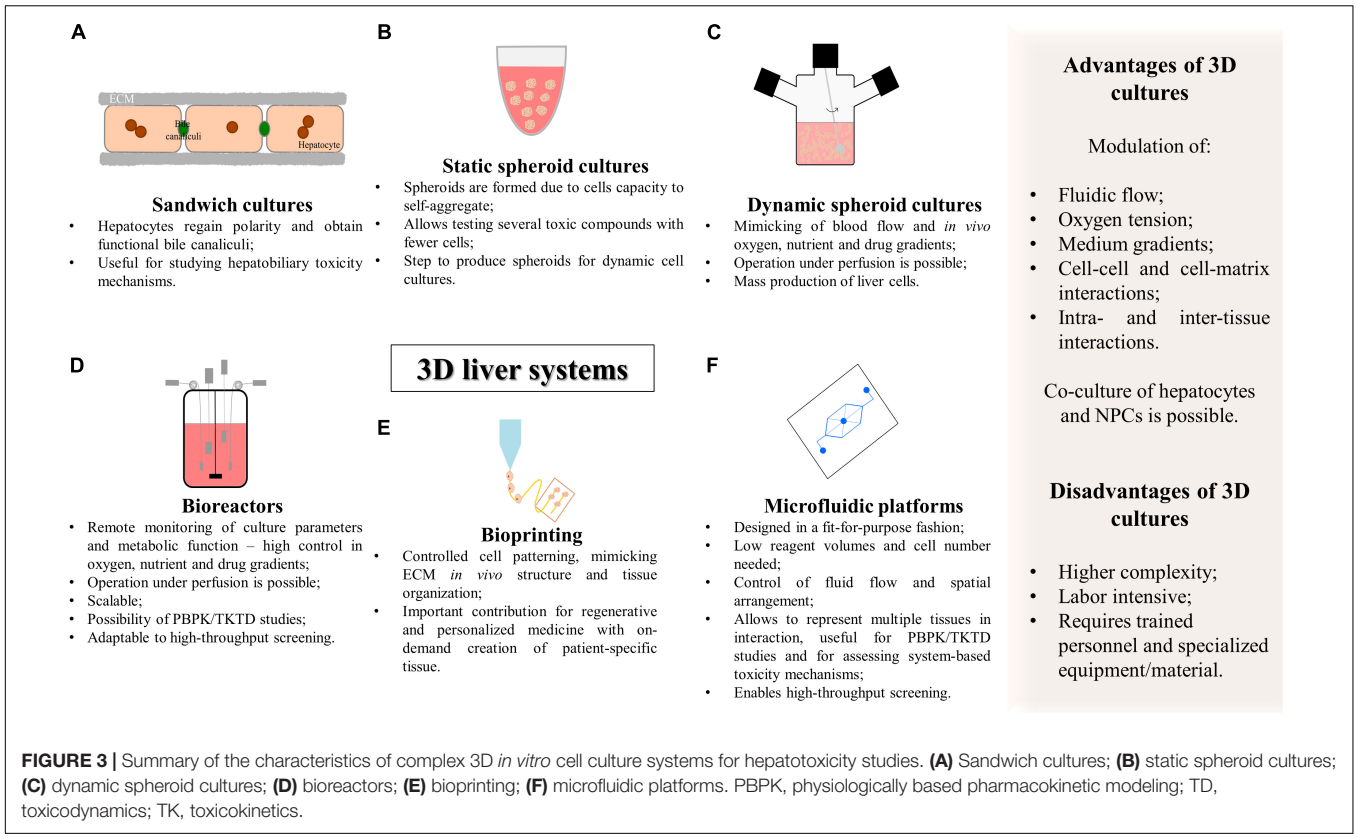

FIGURE 3 | Summary of the characteristics of complex 3D *in vitro* cell culture systems for hepatotoxicity studies. **(A)** Sandwich cultures; **(B)** static spheroid cultures; **(C)** dynamic spheroid cultures; **(D)** bioreactors; **(E)** bioprinting; **(F)** microfluidic platforms. PBPK, physiologically based pharmacokinetic modeling; TD, toxicodynamics; TK, toxicokinetics.

approaches to more complex 3D assays where multicellular microphysiological devices are being evaluated within a vision to replicate the characteristics and response of human tissues *in vivo* (Vivares et al., 2015).

Traditionally, 2D cultures are employed as *in vitro* models due to their ease of use to quickly screen large numbers of compounds. However, this culture approach negatively impacts cell expression profiles (Engler et al., 2006) and causes primary hepatocytes to rapidly lose their differentiation markers (Treyer and Müsch, 2013), compromising long-term and repeated dose studies. On the other hand, 3D cell culture systems have been shown to improve the biotransformation capacities in primary hepatocytes (Tibbitt and Anseth, 2009; Miranda et al., 2010; Mandenius et al., 2011; Mueller et al., 2011; Zeilinger et al., 2011; Schyschka et al., 2013), hepatoma cell lines (Fey and Wrzesinski, 2012; Molina-Jimenez et al., 2012; Wrzesinski et al., 2014) and SC-derived HLCs (Gieseck et al., 2014; Freyer et al., 2016; Cipriano et al., 2017b, 2020) over time in culture.

In general, as summarized in **Figure 3** and **Table 1**, 3D cell culture systems are prone to high-throughput adaptation and scale up but vary in complexity and on remote monitoring of cell culture parameters. Three-dimensional systems can comprise extracellular matrix (ECM) sandwich cultures (Chatterjee et al., 2014; Deharde et al., 2016), spheroid and organoid cultures (Miranda et al., 2009; Leite et al., 2011, 2012; Tostoes et al., 2011; Wrzesinski et al., 2014; Huch et al., 2015; Bell et al., 2016; Peng et al., 2018; Ramli et al., 2020), cells adherent to a scaffold (Kazemnejad et al., 2008; Lin and Chang, 2008; Haycock, 2011), or more complex cellular systems such as hollow-fiber bioreactors (Darnell et al., 2011, 2012; Lübberstedt et al., 2011; Mueller et al., 2011; Zeilinger et al., 2011; Hoffmann et al., 2012; Cipriano et al., 2017b), bioartificial livers (Chan et al., 2004), multi-well perfused bioreactors (Domansky et al., 2010; Vivares et al., 2015; Aeby et al., 2018; Mannaerts et al., 2020), and more recently bioprinted systems (Lauschke et al., 2016; Goulart et al., 2019) and microfluidic platforms (MP) (Rennert et al., 2015; Ma C. et al., 2016; Bauer et al., 2017; Danoy et al., 2019).

Three-dimensional cell cultures can also be achieved using either static or dynamic systems. Static systems are less complex and do not include medium flow, while dynamic systems might be stirred and/or perfused, depending on the cell culture system complexity (Miranda et al., 2009, 2010; Tostoes et al., 2011). Static culture systems are compliant with high-throughput and are usually adopted for the optimization of culture medium constitution, to test a diversity of toxic compounds using fewer cells or as a step to produce spheroids to be used in more complex 3D culture systems, e.g., bioreactors (Wrzesinski et al., 2014; Fey et al., 2020). In contrast, stirring conditions facilitate oxygen diffusion as well as medium homogenization, further resembling the physiological blood flow, and create a hydro-dynamic shear stress that must be balanced, by improving cell performance while avoiding cellular stress and death (Conway et al., 2009). Also, a continuously perfused system is particularly interesting in hepatocyte cell culture and in xenobiotic metabolism studies, avoiding fluctuations of basic cell culture parameters such as pH, oxygen, glucose, and lactate concentration and the accumulation

TABLE 1 | Advanced 3D liver cell models commercially available.

Commercial name	Cell model	Features	Studies employing the advanced liver model
LiverChip/PhysioMimix Liver-on-Chip	Human or rat primary hepatocytes cultured with NPCs (e.g., liver sinusoidal endothelial cells, LSECs; stellate and Kupffer cells)	Liver tissue-engineered perfused bioreactor; Viability for at least 1 month; Scalable; Allows to mimic liver zonation; Allows PBPK studies; Allows prediction of *in vivo* hepatic clearances; Expression of genes of phase I, phase II, and phase III similar to freshly thawed hepatocytes	Domansky et al., 2010; Vivares et al., 2015; Tsamandouras et al., 2017
HμREL Technology	Human, primate, dog or rat primary hepatocytes cultured with NPCs	Compartments designed to represent tissue-functional units (microfluidic devices); Viability for at least 10 days; Phase I and phase II enzymes activity similar to freshly thawed hepatocytes; Allows prediction of *in vivo* hepatic clearance, particularly with low clearance compounds; Enables multi-parametric and repeated-dose readouts	Chao et al., 2009; Bonn et al., 2016; Hultman et al., 2016; Novik et al., 2017
HepaPredict	Human primary hepatocytes cultured with Kupffer, stellate and biliary cells	Spheroids in well-plates; Viability for at least 35 days; Allows to study inter-individual variability; Expression of genes of metabolic enzymes, drug and bile transporters similar to isolated hepatocytes; CYP1A2, CYP2C8, CYP2C9, CYP2D6, and CYP3A4 activity; Polarized cellular organization with functional bile canaliculi; Enables studies of chronic toxicity, long-term metabolic analyses, enzyme induction assays, drug target validation and disease modeling	Bell et al., 2016, 2017; Hendriks et al., 2016; Vorrink et al., 2017
HepatoPac	Human, monkey, dog or rat primary hepatocytes supported by mouse embryonic 3T3 fibroblasts	Micropatterned plates; Viability for at least 4 weeks; Phase I, phase II, and phase III enzymes activity similar to primary hepatocytes; Allows prediction of *in vivo* hepatic clearance, particularly with low clearance compounds	Khetani and Bhatia, 2008; Wang et al., 2010; Chan et al., 2013; Kratochwil et al., 2018
3D InSightLiver Microtissues	Human, monkey, dog or rat primary hepatocytes cultured with Kupffer cells and LSECs	96-well format, 1 microtissue per well; Viability up to 28 days; Albumin secretion; Activity of cytochrome P450; Polarized cellular organization with functional bile canaliculi; High mitochondrial function; Allows hepatotoxicity assessment and disease modeling	Messner et al., 2013, 2018; Proctor et al., 2017
MIMETAS OrganoPlate®	Human primary hepatocytes, HepaRG, iPSC-derived, UpCytes, and HepG2 cultured with stellate cells, Kupffer cells, bile duct, and LSECs	Supports up to 96 tissues on a single well-plate; Viability for at least 2 weeks; Polarized cellular organization with functional bile canaliculi; Perfusion supports long-term culture and formation of adjacent LSECs tubular structure; Defined ECMs tailored to support liver cells; Allows PBPK studies; Allows disease modeling	Jang et al., 2015
Liver-Chip	Human, dog or rat primary hepatocytes cultured with NPCs	Microfluidic device; Viability up to 2 weeks; Albumin and urea secretion; CYP1A2, CYP2B6, and CYP3A4 activity; Polarized cellular organization with functional bile canaliculi; Allows energy metabolism studies; Allows the recapitulation of different hepatotoxicity mechanisms (e.g., steatosis, cholestasis, and fibrosis)	Jang et al., 2019

of metabolites that influence the PK of a specific compound (Conway et al., 2009; Miranda et al., 2009; Shvartsman et al., 2009; Mueller et al., 2011; Tostoes et al., 2011; Vinci et al., 2011; Zeilinger et al., 2011; Lauschke et al., 2016; McCarty et al., 2016; Prodanov et al., 2016). In addition, stirred and/or perfused systems promote a liver-like mass transfer which might mimic liver zonation *in vitro* (Allen et al., 2005; McCarty et al., 2016; Tomlinson et al., 2019). This wide variety of studies employs distinct cell sources and distinct approaches for creating 3D culture systems, showing encouraging results for *in vitro* hepatotoxicity models.

Sandwich Cultures

The sandwich culture system consists of culturing hepatocytes between two layers of ECM, usually gelled collagen or Matrigel® (**Figure 3A**). The ECM constitution influences cell disposition and function as the underlay matrix in sandwich cultures controls cell morphology and multicellular arrangement while the overlay matrix impacts bile excretion behavior (Deharde et al., 2016; Langhans, 2018). Sandwich-cultured hepatocytes regain polarity, maintaining proper basolateral and canalicular transporters localization and functional bile canaliculi. This 3D culture system is particularly important for the estimation of

transport clearance, enzyme-transporter interplay, and bile acid mediated hepatotoxicity (Tuschl et al., 2009; Chatterjee et al., 2014; Deharde et al., 2016; Yang et al., 2016; Zeigerer et al., 2017). Data generated with sandwich models can also be used to establish quantitative relationships between intracellular bile acid accumulation and cytotoxicity and this information can be incorporated into pharmacology models for DILI and hepatic clearance predictions (Ogimura et al., 2011; Camenisch and Umehara, 2012; Umehara and Camenisch, 2012; Yang et al., 2016). Indeed, Chatterjee et al. (2014) used sandwich culture systems from hpHep and rpHep and evaluated the system with a set of compounds correctly flagging clinically known cholestatic compounds (eight out of the nine). The major limitation of sandwich cultures of hpHep is that in the long-term it has been reported leakage, bile canaliculi damage and development of cholestasis in a time-dependent manner (Deharde et al., 2016; Zeigerer et al., 2017). This indicates the need to improve culture conditions and increase the stability of the bile canalicular network necessary to model hepatobiliary excretion processes *in vitro* (Rowe et al., 2013; Deharde et al., 2016; Zeigerer et al., 2017; Bell et al., 2018). Nevertheless, sandwich cultures are a valuable tool for short-term studies of hepatobiliary drug disposition and for assessing the underlying mechanisms of hepatotoxicity.

Multicellular Spheroid Cultures

Three-dimensional systems of multicellular spheroids take advantage of the self-assembling capacity of cells to form aggregates and maintain cell viability, over an extended time in culture while keeping a better hepatocyte-like functional phenotype when compared to 2D cultures (Messner et al., 2013; Wrzesinski et al., 2014; Bell et al., 2016; Leite et al., 2016). The different systems for culturing multicellular spheroids are summarized in **Table 2**.

Non-adhesive surfaces, hanging-drop method, hydrogels, and nanoimprinted structures are some examples of small-scale 3D systems that allow the formation of organoids or multicellular spheroids of hepatocytes (Messner et al., 2013, 2018; Bell et al., 2016; Koyama et al., 2018; Peng et al., 2018), hepatic cell lines (Ramaiahgari et al., 2014; Leite et al., 2016) or other cell types (Huch et al., 2015; Asai et al., 2017; Cipriano et al., 2017b, 2020; Takebe et al., 2017; Wang S. et al., 2019; Wang Z. et al., 2019; Ramli et al., 2020; **Table 2**).

The use of non-adhesive surfaces (**Figure 3B**) is the least complex and easier strategy to establish spheroid cultures as it does not require specialized equipment. Herein, spheroid size is controlled by the cell density, media volume and serum concentration. Using ultra-low attachment plates, Bell et al. (2016) showed that cryopreserved hpHep spheroids may constitute a promising *in vitro* system to study liver function; liver diseases such as steatosis, cholestasis, and viral hepatitis; drug targets, and delayed onset of DILI reactions since proteomic analysis of the spheroid cultures closely resembled intact liver tissues and could reflect inter-individual variability. The adequacy of the model for long-term dosing tests was also demonstrated by the higher sensitivity of 3D cultures to a panel of hepatotoxic agents (Bell et al., 2016). Moreover, spheroids of hepatic cell lines demonstrated an improved phenotype, displaying higher ALB and apolipoprotein B (ApoB) secretion and higher expression of genes related to phase I metabolism, glucose, and lipid metabolism (Nakamura et al., 2011; Takahashi et al., 2015). More recently, immortalized and expandable human liver progenitor-like cells spheroids (iHepLPCs-3D) revealed enhanced hepatic-specific functions and markers and successfully predicted individual heterogeneous toxicities of several drugs (Wang Z. et al., 2019).

Non-parenchymal cells have a key role in liver injury. Thus, the incorporation of stellate cells, Kupffer cells, and sinusoidal endothelial cells in liver cell models has been attempted for improving the prediction of drug toxicity (Messner et al., 2013; Bell et al., 2016; Leite et al., 2016; Proctor et al., 2017; Hafiz et al., 2020; Nudischer et al., 2020). Proctor et al. (2017) demonstrated the higher predictive value of 3D human liver microtissues (multicellular spheroids), consisting of a co-culture of hpHep, Kupffer cells and liver endothelial cells, due to the increased sensitivity in identifying hepatotoxic drugs within a panel of 110 compounds, when compared to 2D-cultured hpHep (Proctor et al., 2017). Spheroid co-cultures of HepaRG with human hepatic stellate cells also led to the development of a 3D *in vitro* fibrosis model, maintaining the metabolic competence of the organoid over 21 days (Leite et al., 2016). This 3D model enabled the identification of compounds that induce liver fibrosis, being suitable for repeated dosage studies and displayed differential toxicity and hepatic stellate cell activation profile according to the nature of the compound (Leite et al., 2016).

Dynamic Cell Culture Systems Applied to Hepatic Spheroids

A limitation of static cultures is that these types of culture do not mimic the blood flow and oxygen, nutrient, and drug gradients that occur *in vivo*. Therefore, dynamic cell culture systems have been developed to create physiologically relevant versions of such gradients (Miranda et al., 2009, 2010; Leite et al., 2011; Tostoes et al., 2011).

The NASA rotary system, a milestone in dynamic 3D culturing, is a rotating cell culture vessel that simulates a microgravity condition. The low shear force allows spheroid growth as well as high mass transfer of nutrients in media preventing cell death within the spheroid core (Brown et al., 2003). This system has been used to culture spheroids of primary hepatocytes, presenting functional bile canaliculi, up-regulation of hepatocyte-specific functional genes, glycogen storage, as well as ALB production and phase I and II enzymatic activity (Brown et al., 2003; Nelson et al., 2010; Chang and Hughes-Fulford, 2014). It also enabled culturing aggregates of iPSC-derived HLCs or of hepatic cell lines with increased up-regulation of metabolic and hepatocyte-specific gene transcripts, and expression of tight junction proteins providing a more physiologically relevant system that has even been used for the study of hepatitis viruses infections (Chang and Hughes-Fulford, 2009; Sainz et al., 2009; Berto et al., 2013; Yamashita et al., 2018). Nevertheless, translating this technology to absorption, distribution, metabolism, excretion, and toxicity (ADMET) studies has been challenging due to the expensive equipment and

TABLE 2 | Advantages and limitations of spheroid forming techniques for *in vitro* toxicity testing applications.

Spheroid forming techniques	Advantages	Limitations	References
Non-adhesive surface Ultra-low attachment plate	Low cost Easy to perform Co-culture of different cell types	Variation in size/cell number/shape	Leite et al., 2011, 2016; Bell et al., 2016
Hanging drop	Inexpensive Easy to perform Well-controlled spheroid size Fast spheroid formation Easy to trace spheroid assembly Co-culture of different cell types	Labor intensive Difficult massive production	Messner et al., 2013
Micromolding Nanoimprinting	Well-controlled spheroid size Designed aggregate geometry Co-culture of different cell types	High complexity Requires specialized facilities	Nakamura et al., 2011; Yoshii et al., 2011; Chan et al., 2013
Stirred system	Low complexity Massive production Long-term culture Dynamic control of culture conditions Adaptable to perfusion Adaptable to online monitoring Easy to scale up Co-culture of different cell types	Requires specialized equipment Requires trained personnel	Miranda et al., 2009, 2010; Leite et al., 2011
Hydrogels/scaffolds	Availability of a wide range of natural or synthetic materials Mimic cues of native ECM Biodegradable Protection from shear stress	Batch-to-batch variability of natural materials Requires trained personnel Labor intensive	Miranda et al., 2010; Tostoes et al., 2011; Tripathi and Melo, 2015; Christoffersson et al., 2019

labor intensive loading, maintenance, and harvesting (Hammond et al., 2016).

Alternatively, the spinner flask suspension cultures (**Figure 3C**) are maintained in a simple and effective stirred system that has been previously described for culturing primary hepatocytes (Sakai et al., 1996; Kamihira et al., 1997; Glicklis et al., 2004; Miranda et al., 2009; Tostoes et al., 2011; Pinheiro et al., 2017), hepatic cell lines (Werner et al., 2000; Chen et al., 2014), and HLCs (Subramanian et al., 2011; Schneeberger et al., 2020). Spinner flask hepatic cultures have been used for mass production of cells for treating liver failure (Sakai et al., 1996; Kamihira et al., 1997; Schneeberger et al., 2020) and for maintaining hepatic cells for toxicological and pharmacological studies (Miranda et al., 2009; Pinheiro et al., 2017). This cell culture system offers the possibility for up-scaling (i.e., 125 mL to 36 L of working volume); adaptation to a perfusion system; online culture monitoring (Tostoes et al., 2011); and sampling of cells or cell culture medium for several analyses (Pinheiro et al., 2017), which is particularly interesting for PK studies (Miranda et al., 2009). Some studies resort to the encapsulation of hepatic cells to protect from shear stress while conferring ECM characteristics which may result in enhanced cell performance (Miranda et al., 2010; Chen et al., 2014).

By resorting to spinner flasks, primary hepatocyte spheroids (both of human and rat origin) preserved ALB and urea secretion and biotransformation activity of phase I and phase II enzymes up to 3 weeks (Miranda et al., 2009, 2010; Leite et al., 2011; Tostoes et al., 2011) and were able to metabolize diphenhydramine and troglitazone (Miranda et al., 2009); while hepatoma spheroids demonstrated gradual increase in ALB synthesis and ammonia elimination with increases in rotation speed (Chen et al., 2014). Using a similar system, Pinheiro et al. (2017) also demonstrated the maintenance of the hepatic phenotype through the presence of ALB, cytokeratin (CK)-18, HNF-4α, MRP2, and OATP-C, along with the production of urea and ALB. Stable activity levels of phase I (7-ethoxycoumarin-*O*-deethylation, ECOD, and 7-ethoxyresorufin-*O*-deethylase, EROD, activities) and phase II (sulfotransferase, SULT1A1) enzymes, modulated by nevirapine and its metabolites were also observed (Pinheiro et al., 2017). Positive results have also been obtained with co-cultures of hepatocytes and fibroblasts which demonstrates the importance of ECM interactions in hepatic phenotype (Leite et al., 2011). Moreover, spinner cultures improved *CYP3A4*, *ALB*, and *MRP2* expression in HLCs and increased ALB and urea production when compared to static cultures (Schneeberger et al., 2020) and were reported for the mass production of liver organoids presenting up-regulated hepatic markers (Subramanian et al., 2011).

Bioreactor Systems

Bioreactors are containers that provide the optimal requirements for biochemical reactions for the synthesis of a desired product at an industrial scale (e.g., pharmaceuticals, vaccines, or antibodies), and have been primarily developed to grow yeast, bacteria, or animal cells (Mustafa et al., 2018). Bioreactors differ from the previously mentioned dynamic systems by enabling the remote monitoring of cultures, i.e., the accurate control of cell culture parameters that may provide the appropriate stable

microenvironment for liver cell cultures (**Figure 3D**; Tostoes et al., 2012; Lübberstedt et al., 2015; Farzaneh et al., 2020). Culture parameters include medium flow, gas tension, temperature, pH, glucose metabolism, lactate production along with the specific determination of hepatic metabolic activity revealed by ammonia detoxification, urea, and ALB secretion, enabling to extrapolate at the cell functional level. As an example, online monitoring of oxygen concentration, which is related with changes in metabolic activity, allows the estimation of cell viability in real time (Mueller et al., 2011; Rowe et al., 2018).

Bioreactors generally operate under linear or circular perfusion. The continuous addition of nutrients, mixing and removal of metabolic by-products ensures that hepatocytes experience smaller gradients of nutrients and hormones which enhance hepatocyte functionality (Tostoes et al., 2011, 2012). Accordingly, when comparing perfusion feeding with 50% medium replacement, the former showed improved ALB synthesis in non-encapsulated rpHep spheroids whilst urea synthesis and phase I drug metabolizing enzyme activity were improved in alginate encapsulated spheroids (Tostoes et al., 2011). Furthermore, the possibility of running in recirculation and feed mode allows repeated dose testing, reflecting more closely the *in vivo* situation (Mueller et al., 2011). Tostoes et al. (2012) evaluated the feasibility of using hpHep spheroids for repeated drug dose testing in an automated perfusion bioreactor for 3–4 weeks. These conditions allowed the maintenance of phase I and II enzyme expression and activity responding to induction stimuli, the presence of hepatic markers (HNF-4α, CK-18, CYP3A, and ALB) and the maintenance of ALB and urea synthesis rate. The presence of polarity markers and bile canaliculi function further supported the applicability of this system for long-term and repeated drug dose tests (Tostoes et al., 2012).

The hollow-fiber bioreactor is an example of a 3D perfused bioreactor system (Darnell et al., 2011, 2012; Mueller et al., 2011; Hoffmann et al., 2012; Freyer et al., 2016; Knospel et al., 2016; Cipriano et al., 2017b). This system was originally developed to function as extracorporeal liver support system and designed to accommodate a 3D perfusion, high-density culture of human liver cells within a cell compartment volume of 800 mL (Gerlach et al., 1994, 2003). It consists on a complex capillary network for arterio-venous medium perfusion, oxygen supply, and carbon dioxide removal, with an electronically controlled perfusion device with pumps for medium feed and recirculation, temperature control, and a valve regulated by a gas mixing unit (Darnell et al., 2011; Mueller et al., 2011). Aiming for drug testing applications, the same system was later miniaturized to cell compartment volumes of 8, 2, and 0.5 mL which enabled a significant reduction of the required cell amounts and reagents while maintaining cell function similar to larger devices (Zeilinger et al., 2011; Lübberstedt et al., 2015; Knospel et al., 2016). Human primary liver cells cultured in such small-scale hollow-fiber bioreactors preserved CYP1A2, CYP2D6, and CYP3A4/5 activities as well as the drug transporters BCRP, MDR1, and MRP2 up to 2 weeks in culture (Zeilinger et al., 2011; Hoffmann et al., 2012). Notably, these systems also displayed relevant biotransformation and toxicity profiles for several drugs, including paracetamol and diclofenac, along with the formation of biliary structures (Hoffmann et al., 2012; Lübberstedt et al., 2015; Knospel et al., 2016).

The implementation of alternative *in vitro* systems resorting to SC-derived HLCs culture in a bioreactor has also been described (Songyang et al., 2015; Freyer et al., 2016; Cipriano et al., 2017b; Farzaneh et al., 2020). Under such conditions, HLCs present glycogen storage ability, expression of hepatic-specific markers and transporters, including *CK-18, ALB, HNF-4α, CYP1A2, MRP2,* and *OATP-C*, formation of bile duct-like structures, higher ALB production and diclofenac biotransformation (Songyang et al., 2015; Freyer et al., 2016; Cipriano et al., 2017b). Taking advantage of the controlled microenvironment provided by bioreactors, Farzaneh et al. (2020) demonstrated the potent impact of oxygen concentration in the expression of liver-specific genes, ALB and urea secretion and CYP3A4 activity in human hepatic organoids derived from iPSCs.

Bioprinting

The recent emergence of 3D printer technology (bioprinting), along with the development of biocompatible materials (e.g., hydrogels), has been translated into tissue engineering, constituting a novel fabrication technique. This technology resorts to cell-laden biomaterials as bioinks (**Figure 3E**) and involves layer-by-layer deposition of cell-embedded polymers guided by a computer-aided design (CAD) software (Ma et al., 2018). It is considered a precise, versatile, and flexible technique that allows controlled cell patterning, thus contributing to create defined heterotypic cell contacts (Nguyen et al., 2016). It may also mimic *in vivo* ECM and, ultimately, enables to generate a functional tissue or organ. Bioprinting not only constitutes a renewed promise for regenerative and personalized medicine, with the development of patient-specific tissue designs and on-demand creation of complex structures within a short time (Aimar et al., 2019; Tamay et al., 2019), but also constitutes an opportunity for the development of the next-generation devices for toxicology and drug-screening purposes.

Currently, there are already available examples of 3D bioprinting approaches with enhanced liver cell functionalities *in vitro*. Liver organoids of HepaRG and human stellate cells printed for mimicking liver lobule presented higher *ALB* and *CYP3A4* expression than HepaRG monolayer cultures (Grix et al., 2018). Similarly, a physiologically relevant bioink allowed hpHep and liver stellate cells to maintain urea and ALB production over 2 weeks while responding to drug treatment appropriately (Mazzocchi et al., 2018). Additionally, Nguyen et al. (2016) developed human 3D bioprinted liver tissues with patient-derived hepatocytes and NPCs stable for 4 weeks in culture and identified trovafloxacin toxicity signatures at clinically relevant doses for the first time. Moreover, Kizawa et al. (2017) created a human bioprinted liver tissue maintaining stable drug, glucose metabolism and bile secretion for at least 23 days in culture.

The combination of iPSC-derived hepatic cells and bioprinting technologies has also been reported (Kazemnejad et al., 2008; Ma X. et al., 2016; Goulart et al., 2019; Yu et al., 2019). A 3D-bioprinted structure mimicking liver lobule pattern with iPSC-derived hepatic progenitor cells and human umbilical

vein endothelial cells and adipose-derived SCs as supporting cells improved the expression of hepatic-specific markers, biotransformation enzymes, and ALB and urea production (Ma X. et al., 2016). Moreover, by taking advantage of the innate biochemical constituents and ultrastructure of the native ECM, Yu et al. (2019) used decellularized ECM and iPSC-derived HLCs as bioink in a hexagonal structure digitally designed, demonstrating the potential of these engineering personalized human tissue platforms.

Despite all the advances brought by 3D bioprinting, an important limitation is that this technology does not consider post-printing processes that are necessary to better mimic the *in vivo* environment such as changes in scaffold shape throughout time, resulting from, e.g., coating, cell self-organization, and matrix deposition. To address this issue, a novel technique termed "Four-dimensional (4D) bioprinting" has recently emerged in which constructs continue to evolve after being printed over time, i.e., the fourth dimension (Gao et al., 2016). Four-dimensional adds the advantages of 3D printing while using smart materials able to reshape themselves in response to different stimuli (e.g., pH, temperature, and light) to closely mimic the dynamic responses of tissues (Tamay et al., 2019). The expectation is that using 4D bioprinting technology will produce bioprinted human liver tissues containing human liver cell lines and immunocompetent cells within a defined architecture, with the aim of detecting DILI during the non-clinical phase (Poietis, 2018). Altogether, these technologies seem very promising in the quest for *in vitro* liver relevant and functional models and motivate further development for advanced pharmaceutical applications. Nevertheless, limitations such as biocompatible materials that can be printed, the inability to create microstructures and low bioprinting speeds are still some important challenges that have been hampering the possibility of running screening studies for toxicology applications (Gao et al., 2016; Mazzocchi et al., 2019; Tamay et al., 2019).

Microfluidic Platforms

The combination of microfabrication techniques, such as photolithography frequently used to manufacture computer chips, together with the rapid development of tissue engineering led to the establishment and expansion of systems with dimensions in the micrometer scale for cell culture purposes, i.e., the MP or organ-on-a-chip (OoC) systems (**Figure 3F**; Bhatia and Ingber, 2014).

Although 3D liver models allow maintenance of *in vivo*-like phenotype for several days or even weeks, the static culture conditions do not enable the removal of medium accumulated substances or metabolites, that can be toxic or introduce self-feedback inhibition of cells functionality/viability, as is the case of urea or ammonia accumulation. The need for flow-based systems granted MP or liver-on-a-chip an enormous potential, as they may recapitulate the *in vivo* flow rate by removing the metabolites and functional products. Moreover, due to its small size, the experimental costs, reagent volumes, and cell number needed within MP are lower, which is particularly interesting for high-throughput experimentation, while enabling high microenvironment control (Bhatia and Ingber, 2014; Loskill et al., 2015; Sosa-Hernández et al., 2018). Most importantly, by resorting to the microfluidic technology, it is possible to numerically define a downscaling factor of a living tissue into an *in vitro* tissue-representative functional unit that will support quantitative *in vitro* to *in vivo* extrapolations using physiologically-based modeling and PK studies, which may represent an important step toward the replacement and reduction of animal models in the non-clinical phase (Bauer et al., 2017).

Organ-on-a-chip systems display high design and experimental flexibility, offering the possibility to be planned according to the aim of the study, i.e., in a more fit-for-purpose fashion. OoC contain the minimal functional unit of a tissue, recapitulating the *in vivo* organ's dynamics, architecture, functionality, and (patho)physiological response under real-time monitoring (Bhatia and Ingber, 2014; Mastrangeli et al., 2019), e.g., quantification of oxygen and glucose concentrations and cytokine detection (Zhou et al., 2015; Bavli et al., 2016). As such, some of the most important aspects to consider for the establishment of a OoC system are the chip design; the cell sources and cell types as well as cell density and disposition to enable the formation of functional tissues; the medium composition for each cell type; flow rate, direction, and type of perfusion; and the ability to perform functional endpoint assessment of the tissues in the chip.

Within the OoC technology, modulation of fluid flow, both in terms of direction and rate, have an impact in cells phenotype while enabling media sampling for analyses throughout culture period (Domansky et al., 2005; Wikswo, 2014; Vivares et al., 2015; Sosa-Hernández et al., 2018; Mastrangeli et al., 2019; Busche et al., 2020). MP also enable a more physiological cell-to-media ratio, avoiding dilution of signaling molecules and metabolites. High cell-to-media ratios cannot be achieved in higher scale cell culture systems without extreme costs on cell production and without compromising the maintenance of cell viability (Becker et al., 2014). Interestingly, a recent quantitative comparison on liquid-to-cell volume ratios and metabolic burden between the human body and *in vitro* systems revealed a systemic liquid-to-cell ratio of 0.3 in the human body, with 0.06 nL of liquid per hepatocyte, while the *in vitro* systems range from 375 to 0.5 depending on the scale and perfusion system (Wang et al., 2018). The functional importance of high density cell culture in low volume systems was demonstrated by Haque et al. (2016) that observed the accumulation of higher and more physiological concentrations of cytokines (which triggers autocrine signals) and increased ALB production, MRP-2 presence, bile canaliculi formation as well as CYP3A4 and 1A1 activities and *CYP1A2* expression.

The spatial arrangement of the cells is another important factor to enhance the functionality of hepatocytes, by maintaining cell polarity and tissue-specific activity (Lee et al., 2007; Kang et al., 2015; Rennert et al., 2015; Busche et al., 2020). Within MP, cells can be seeded in high densities in either a 2D or a 3D fashion (Sosa-Hernández et al., 2018). Tightly packed hepatocytes in a MP designed to simulate the liver sinusoid structure promoted properties of a functional liver sinusoid such as extensive cell–cell contact, continuous nutrient exchange and defined tissue, and

fluid transport regions (Lee et al., 2007). A further advantage of these systems is that different cell types can be cultured in the same system in separate chambers, having representative cells of the same tissue or even from different organs in interaction through paracrine or endocrine chemical signals like *in vivo*, constituting multi-organ systems (Zhou et al., 2015; Liu et al., 2019). This enables the study of organ-level responses to a potential toxic compound that involve the interaction of different tissues (Ronaldson-Bouchard and Vunjak-Novakovic, 2018).

At the single organ level, Rennert et al. (2015) used a two-channel MP (Becker et al., 2014) to create a 3D liver model integrating a vascular layer, composed of endothelial cells and tissue macrophages, and a hepatic layer, comprising stellate cells co-cultured with HepaRG cells, separated by a suspended membrane simulating the space of Disse. The complexity of this model enhanced hepatocyte polarity and allowed the observation of hepatobiliary function (Rennert et al., 2015). Moreover, it incorporated a sensor for online oxygen measurement, useful for toxicological screening, as reported earlier (Rennert et al., 2015). On the other hand, Danoy et al. (2019) optimized a culture of iPSC-derived HLCs in a biochip and showed that the microfluidic environment led to a higher degree of mature HLCs than in traditional 2D cultures. In a follow-up study, the same microfluidic culture was used to mimic liver zonation based on the formation of an oxygen gradient in the biochip (Danoy et al., 2020). Moreover, when co-cultured iPSC-derived endothelial cells, iPSC-derived HLCs were able to metabolize quercetin into its active metabolites (Yu et al., 2020).

At the multi-organ level, OoC systems have been developed to recreate the first pass metabolism dynamics by connecting gut epithelial cells and liver cells (Choe et al., 2017). With these systems it is possible to consider the gut-liver axis, including immune cells to study inflammatory responses, important for diabetes and fatty liver disease models (Jeon et al., 2020). These systems can also be used to mimic an oral administration route resorting to liver–intestine co-culture (Maschmeyer et al., 2015); to mimic systemic administration routes using endothelialized liver–skin co-culture (Maschmeyer et al., 2015); and to restitute pancreas-liver functional coupling through insulin release from pancreatic islet microtissues in response to a glucose load that promoted glucose uptake by liver spheroids (Bauer et al., 2017). Finally, they can also be adequate to study drug distribution through the connection of, for example, up to ten different microphysiological systems (MPSs), including liver, gut, lung, endometrium, heart, pancreas, brain, skin, kidney, and muscle (Edington et al., 2018). In sum, MP can indeed represent a game changer for personalized medicine applications and in the development of *in vitro* non-clinical models (Wang et al., 2018; Ingber, 2020; Sohn et al., 2020).

In vitro Hepatotoxicity Studies: 3D Versus 2D

The evaluation of the capacity of a given model system to detect and mimic prototypical types of liver toxicity allows to determine its ultimate predictive ability. This toxicity must be assessed both in a short-term (24–48 h) and a long-term (weeks to months) culture conditions as it is known that DILI mechanisms may be developed not only after an acute exposure but also from a chronic type (e.g., by development of drug tolerance or deposition of elimination products) (Jiang et al., 2019). Moreover, the assessment of a prolonged exposure to each compound leads to substantially lower IC_{50} values obtained in standard cytotoxicity assays, representing a cumulative effect often seen in the clinic and not only in an overdose scheme following isolated supratherapeutic administrations. Therefore, for a more complete evaluation of the strategies used in different studies, it is important to gather the existing data regarding well-known hepatotoxicants. In this work, we selected three of the *most DILI-concern* medicines, ranked by the United States Food and Drug Administration, based on their impact in human health, either because they are indeed highly prescribed (diclofenac and paracetamol) or are paradigmatic examples in Toxicology (troglitazone) (Chen et al., 2020). In fact, molecules such as paracetamol or diclofenac display a well-known diversity of mechanisms of hepatotoxicity that may help to further validate new *in vitro* liver models. Several hepatotoxicity studies that evaluate paracetamol (**Supplementary Table 1**), diclofenac (**Supplementary Table 2**), and troglitazone (**Supplementary Table 3**) consider distinct cell sources, culture conditions, and endpoints. However, the available data is not homogeneous and thus it is somehow difficult to compare results between groups, especially considering 3D liver models. Indeed, full characterization of the *in vitro* liver models regarding metabolic and toxicity capacity is not always described, which may represent one of the reasons limiting their acceptance by the regulatory authorities and further effective application in toxicological studies.

As shown in **Supplementary Tables 1–3**, toxicities of test drugs are often investigated by evaluation of cytotoxicity biomarkers such as cell viability (e.g., tetrazolium reduction MTT or MTS assays), membrane lysis (e.g., LDH release) or depletion of cellular ATP. However, these represent only late-stage toxicity associated with apoptotic or necrotic events and thus do not permit a proper mechanistic evaluation of the toxicological events (O'Brien et al., 2006). Therefore, additional mechanistic endpoints have gained increasing importance when assessing drug safety with the pharmaceutical industry and the scientific community proposing complementary biomarkers' assessment, in order to obtain and cover different mechanisms of injury to diminish hepatotoxicity risk. These include mitochondrial dysfunction, bile salt transporter modification, lipids accumulation, reactive metabolite formation through conjugation with GSH or covalent binding and calcium homeostasis alteration that need to be assessed in a representative number of compounds with different toxicity mechanisms within high-content and high-throughput platforms (Xu et al., 2004; O'Brien et al., 2006; Khetani et al., 2013; Trask et al., 2014; Schadt et al., 2015; Bell et al., 2016; Williams et al., 2020; Zhang C. et al., 2020). Hence, besides including the different hepatic cell source and cell culture systems, **Supplementary Tables 1–3** were incorporated to not only accommodate the cytotoxicity data but also the metabolic activity and mechanistic endpoints assessed in each study. The few studies that evaluate these mechanistic

biomarkers are essential to identify also the models' ability to mimic processes related to cholestasis, steatosis, genotoxicity, and viral hepatitis (Shen et al., 2012; Bell et al., 2016; Hendriks et al., 2016; Leite et al., 2016; Prill et al., 2016; Williams et al., 2020), amongst others.

Paracetamol

Paracetamol is a widely used antipyretic and non-opioid analgesic agent that constitutes an example of a safe drug at therapeutic doses, but overdosage causes predictable and reproducible hepatotoxicity through mitochondrial dysfunction and centrilobular necrosis in the liver (Hinson et al., 2010).

Paracetamol is metabolized mainly by conjugation with sulfate and glucuronic acid (Riches et al., 2009) and, in a less extent, by oxidation by CY2E1, CYP1A2, CYP2D6, CYP2A6, and CYP3A4 (Mazaleuskaya et al., 2015). As previously stated, its oxidation generates NAPQI that is detoxified by GSH conjugation, through glutathione S-transferases (GSTs) GSTP1, GSTT1, and GSTM1. When large quantities of NAPQI are formed, liver GSH pool can be critically depleted, meaning that excess NAPQI is not detoxified and cell injury occurs, namely trough the modification of cellular proteins. Protein binding leads to oxidative stress and mitochondrial damage (McGill and Jaeschke, 2013; Caparrotta et al., 2018). Paracetamol toxicity is also related to calcium accumulation and activation of endonucleases, DNA damage (Boelsterli, 2003), ATP depletion, *Jnk* activation, up-regulation of electron transport chain protein components and activation of *p53* signaling (Davis and Stamper, 2016).

Supplementary Table 1 summarizes the collected *in vitro* data for paracetamol. It suggests that mouse primary hepatocytes are more sensitive to paracetamol, with lower IC_{50} values (Jemnitz et al., 2008; Kučera et al., 2017), followed by rpHep, hepatic cell lines HepG2 and HepaRG, hpHep and HLCs (Lewerenz et al., 2003; Jemnitz et al., 2008; Riches et al., 2009; Zhang et al., 2011; Tasnim et al., 2015; Bell et al., 2017), highlighting not only the interspecies differences but also the importance of choosing a representative cell type (Carmo et al., 2004; Reder-Hilz et al., 2004).

Paracetamol IC_{50} values compiled in **Supplementary Table 1** further suggest that 2D cultures are less sensitive to paracetamol toxicity than 3D cultures (Gunness et al., 2013; Jang et al., 2015; Gaskell et al., 2016; Bell et al., 2017; Li et al., 2020). It was demonstrated increased sensitivity of 3D human liver microtissues, with subsequently lower IC_{50} values for a panel of known hepatotoxicants, including paracetamol, in comparison with 2D-plated hpHep (Proctor et al., 2017). Moreover, by using a 3D liver-sinusoid-on-a-chip of HepG2, Deng et al. (2019) showed that not only this system was able to improve cell functions, but also its sensitivity to paracetamol when compared to 2D-plated HepG2. Besides, even within 3D systems, different culture strategies may lead to different results for the same drug. Jang et al. (2015) tested HepG2 in a 3D static Matrigel® culture and in a 3D microfluidic chip and obtained a higher sensitivity for hepatotoxicity in the latter, justified by its improved maintenance of hepatic functions. Foster et al. (2019) found also an increased sensitivity in 3D co-culture systems of hpHep and NPCs compared to hpHep spheroids. Likewise, Li et al. (2020) observed an augmented toxicity to paracetamol in the co-culture spheroids group (hpHep and Kupffer cells). Interestingly, when both systems were co-treated with lipopolysaccharides (mimicking inflammatory conditions), a higher protective role was detected in the co-culture system, mainly due to Kupffer cells, when comparing to hpHep spheroids. In fact, exposure and response to paracetamol under healthy or pre-inflammatory states may lead to different cytokine release profiles with distinct activation of immune cells (Kim et al., 2017; Li et al., 2020). Although it is generally acknowledged that paracetamol has only very weak anti-inflammatory properties, it should be highlighted that is commonly administered already under an inflammatory condition. This reinforces the need of considering co-cultures for an early identification of possible drug-induced hepatotoxic immunological responses depending on the patient health state.

Although mechanistic endpoints are not often represented in the majority of studies using paracetamol as hepatotoxicant, the reports that present this important information assess mainly mitochondrial dysfunction and oxidative stress (Bruderer et al., 2015; Goda et al., 2016; Zhang C. et al., 2020), followed by reactive metabolites formation and liver cholestasis or steatosis (Lewerenz et al., 2003; Prot et al., 2012; Prill et al., 2016; Kučera et al., 2017; Williams et al., 2020) and liver fibrosis (Leite et al., 2016). Nevertheless, the drastic differences in sensitivity to paracetamol, may be due not only to the cell type but also to the different culture conditions, highlighting the importance of both the cell architecture and the presence of other liver cell types for the study of distinct pathways that may be involved in drug toxicity.

Diclofenac

Diclofenac is one of the most worldwide prescribed NSAID. It has been linked with rare, albeit significant, cases of severe hepatotoxicity with a fatality rate of 10% (Aithal, 2004). Diclofenac is mainly metabolized by CYP2C9 into 4-OH-diclofenac and in a lower extent converted into 5-OH-diclofenac by CYP3A4. Diclofenac and its metabolites are conjugated with glucuronic acid by UGT2B7 and excreted across the canalicular plasma membrane into the bile via MRP-2 (Aithal, 2004). There is evidence that individuals that present increased glucuronidation activity as a consequence of a genetic polymorphism in UGT2B7 (C-161T allele) exhibit a 9-fold increased risk of adverse hepatic reactions (Daly et al., 2007). Diclofenac-acyl-glucuronide may also conjugate with GSH forming a diclofenac glutathione thioester (Syed et al., 2016). Thus, diclofenac metabolism comprises phase I, II, and III activities and its toxic effects can be associated to the reactive metabolites 4-OH-diclofenac, diclofenac-acyl-glucuronide, diclofenac glutathione thioester, and 4-OH-diclofenac-acyl-glucuronide (Aithal, 2004) that cause ATP depletion resulting in mitochondrial toxicity (Syed et al., 2016). As such, diclofenac constitutes an example of a hepatotoxicant dependent on bioactivation.

Compared to paracetamol, the available studies of diclofenac addressing the toxicity in 2D versus 3D cell cultures are fewer (**Supplementary Table 2**). Most importantly, regarding mechanistic biomarkers of toxicity, only a minority of studies assess endpoints for mitochondrial dysfunction (Goda et al., 2016), reactive metabolite formation, calcium homeostasis

(Ponsoda et al., 1995), and liver cholestasis or steatosis (Bell et al., 2016; Williams et al., 2020).

As shown in **Supplementary Table 2**, Gaskell et al. (2016) and Cipriano et al. (2017b) obtained IC_{50} values for the 3D spheroid cultures of HepG2/C3A and HLCs, respectively, lower than for the corresponding 2D cultures. This may be due to an increase in phase II (glucuronidation) activity, indicating that the 3D system may be more representative of the biological response. Ramaiahgari et al. (2014) attained higher sensitivity to diclofenac in the 3D culture of HepG2 compared to 2D but the IC_{50} values were higher than those reported by Gaskell et al. (2016). Yu K. N. et al. (2018) also demonstrated that the addition of both phase I and II enzymes in a 3D miniaturized Hep3B cell system led to a more predictive assessment of diclofenac's toxicity when compared to the 3D system groups with only CYP450 enzymes or human liver microsomes added and its 2D counterpart. Also, Atienzar et al. (2014) proved that the co-culture of dog hepatocytes with NPCs present similar sensitivity to diclofenac compared to HepG2 but less sensitivity than hpHep in a 5-day exposure culture. This IC_{50} variation is transversal to the majority of reports presented in **Supplementary Table 2**, in which most of the studies only evaluate one type of culture system (Wang et al., 2002; Xu et al., 2003; Lauer et al., 2009; Lin et al., 2012; Goda et al., 2016; Knospel et al., 2016; Sarkar et al., 2017), hindering the comparison between both types of cultures. Besides the relevance of the culture system, this observation reinforces the importance to include mechanistic insights in early toxicity assessments rather than rely solely on cell viability quantification. A competent and complete *in vitro* model may provide a higher amount of valuable information if more variables are taken into account.

Troglitazone

Troglitazone (TGZ) is a thiazolidinedione derivative developed for the treatment of type II diabetes. Soon after being approved, TGZ was withdrawn from the marked in Europe and 3 years afterward in the United States due to non-immune idiosyncratic toxicity (Chojkier, 2005). It is a classic example of a drug whose toxicity failed to be predicted during drug development. TGZ is extensively metabolized by CYP3A4 and GST, it is a CYP3A and 2B6 inducer and is able, as well as its sulfate conjugate, to inhibit BSEP (Sahi et al., 2000; Kassahun et al., 2001). This leads to an increased formation of TGZ metabolites along with its intracellular accumulation, resulting in intrahepatic cholestasis, mitochondrial dysfunction, covalent binding to proteins, and macromolecular damage ultimately leading to apoptosis (Smith, 2003; Chojkier, 2005). TGZ is more toxic in humans than in rodent models (Shen, 2007; Kostadinova et al., 2013). In view of this, TGZ was only identified as hepatotoxic after reaching the market. TGZ is, thus, an example of the importance of identifying species-specific toxicity. In fact, Shen et al. (2012), using 3D gel entrapped rat and human hepatocytes, observed that at clinical doses of TGZ, hepatotoxicity was absent in rat hepatocytes, but present in human hepatocytes. Similarly, Kostadinova et al. (2013) reported TGZ-induced cytotoxicity in human 3D liver cells but only minor effects in rat 3D liver.

In addition, as summarized in **Supplementary Table 3**, and in accordance with clinical observations, 3D human liver models show increased sensitivity to TGZ toxicity which may be related to higher formation of metabolites as consequence of the higher induction ability of 3D models. Nonetheless, Gunness et al. (2013) obtained discrepant results, with the 3D model of HepaRG cells being 10-fold less sensitive to TGZ than the monolayer model. On the other hand, this decreased sensitivity might reflect a higher clearance, commonly increased in 3D cultures due to the cellular architecture. Moreover, HepaRG cells present higher CYP3A4 activity (Aninat et al., 2006) that might interfere with drug and metabolite clearances since TGZ metabolites may also be hepatotoxic (Tolosa et al., 2018). Another explanation could be the known TGZ-induced BSEP inhibition (Jackson et al., 2018), not investigated in this study. Hendriks et al. (2016) assessed BSEP inhibition in two long-term 3D spheroid models of HepaRG and hpHep with repeated drug exposure and bile acids co-exposure and was able to detect the cholestatic effect of several compounds, including TGZ, in both cell types. Independently of the studied mechanisms, the co-culture of hpHep (Kostadinova et al., 2013; Proctor et al., 2017; Li et al., 2020) or hepatoma cell lines (Granitzny et al., 2017) with NPCs displayed a higher sensitivity to TGZ toxicity (Kostadinova et al., 2013).

Using HLCs as alternative sources to hpHep, Tasnim et al. (2016) found similar sensitivity between 3D hESC/hiPSC-HLCs and hpHep upon exposure to TGZ for 24 h, whereas when comparing to its 2D counterpart, 3D cellulosic scaffold cultured hiPSC-HLCs showed a slightly lower sensitivity. On the other hand, Takayama et al. (2013) showed that 3D-cultured iPSC-HLCs presented a decreased sensitivity to TGZ after 24 h of exposure when compared to hpHep, but a better sensitivity compared to 3D-cultured HepG2. Moreover, Holmgren et al. (2014) was able to use hiPSC-HLCs in a long-term culture and successfully detected steatosis in the cells exposed to TGZ for 2 days. This is an important step to show that these HLCs may reveal the mechanistic pattern of TGZ hepatotoxicity and stand as a good alternative for hpHep.

CHALLENGES WITHIN THE ASSESSMENT OF DRUGS HEPATOTOXICITY USING *IN VITRO* LIVER MODELS

The pharmaceutical industry is clearly interested on the early identification of toxicity cues in models covering different aspects of human liver (patho)physiology (Bale et al., 2014). On the other hand, the chemical/cosmetic industry has been politically stressed to use advanced alternatives for animal testing for hazard identification and characterization. Although each type of industry presents different needs and goals, the early identification of potential hepatotoxic substances and deep understanding of hepatotoxic mechanisms in relevant *in vitro* models will profit both industries.

In this section, we propose a roadmap with the essential steps to assess drugs hepatotoxicity using *in vitro* liver models.

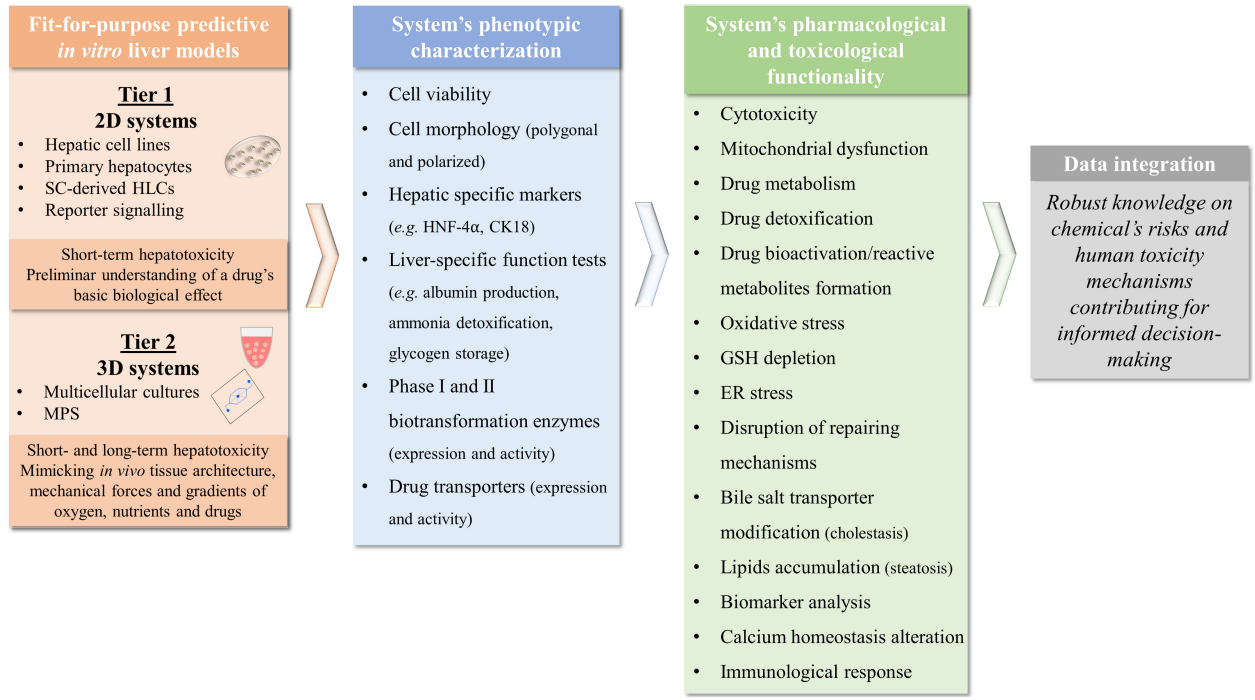

FIGURE 4 | Roadmap for assessing drugs hepatotoxicity mechanisms using *in vitro* models that might be used alone or in combination at different points and on different scales. Tier 1 comprises single-cell systems that report on immediate chemical/biological effects such as cytotoxicity and bioactivation while Tier 2 includes more complex systems containing liver cells in a more physiologic state, enabling assessment of the consequences of acute and chronic drug exposure. Moreover, phenotypic characterization and the pharmacological and toxicological functionality of a system and the ability to identify toxicity mechanisms needs to be considered before undertaking toxicological investigations to ensure that the most appropriate methods are used. Depending on the complexity, each model might be able to represent one or more liver functional endpoints and can be used alone or in combination depending on the hepatotoxicity mechanisms that are intended to study. To integrate findings from different test systems and to dissect the multilevel impact of compounds, bioinformatics and machine learning models may also be useful, which will ultimately contribute to more informed decision-making in the drug development and risk assessment fields. SC, stem cells; HLCs, hepatocyte-like cells; MPS, microphysiological system.

As no single currently used model can recapitulate all human hepatotoxicity mechanisms, we further support the need for a systematic tiered approach for drug hepatotoxicity assessment combining more than one model. Indeed, the model systems with increased biological complexity might be efficiently and effectively used alone or in combination, at different points, and on different scales of the drug development process. The final goal is thus to cover the different human hepatotoxicity mechanisms needed to provide accurate hazard identification and risk assessment (**Figure 4**). Finally, the data generated in such non-clinical assays should be integrated to deliver robust information to drug regulators to improve the decision-making process (**Figures 4**, **5**).

Firstly, the cell source needs to be carefully considered to ensure the appropriate tissue context. Hepatotoxicity involves different mechanisms in a multistep and multicellular process (Grattagliano et al., 2009; Gregus, 2013). As such, there is no single model or test that can evaluate a chemical's risk of inducing liver injury, but rather a set of well-characterized hepatic models with well-defined purposes to be used in a multistep manner. This approach may vary in terms of cell source and culture complexity, allowing to assess specific toxicity mechanisms as well as to properly mimic the different types and stages of liver toxicity.

In particular, human-derived cells, namely hpHep or SC-derived HLCs, contribute to more relevant *in vitro* systems by allowing to capture population heterogeneity and to represent healthy and disease conditions. On the other hand, simpler and single-cell system based on, e.g., hepatic cell lines and monolayer cultures enable high-throughput applications for testing a wide set of conditions and allow to preliminarily understand a drug's basic biological effects in human cells (**Figure 4**, tier 1). Conversely, more complex systems, such as 3D-based cultures improve data accuracy not only concerning cytotoxicity, but also biotransformation activity and drug accumulation by mimicking tissue architecture, mechanical forces and gradients of oxygen, nutrients, and drugs that are found *in vivo* (**Figure 4**, tier 2). Additionally, complex models that include different liver cell types, e.g., hepatocytes and stellate cells or immune cells, allow to explore additional biological responses such as cholestasis, steatosis, fibrosis, and inflammation (Leite et al., 2016; Jeon et al., 2020).

A crucial step within the development and selection of a relevant *in vitro* model for non-clinical studies is its thorough characterization. The systems' phenotype and functionality need to be assessed to understand which pharmacology and toxicology mechanisms can be accurately represented

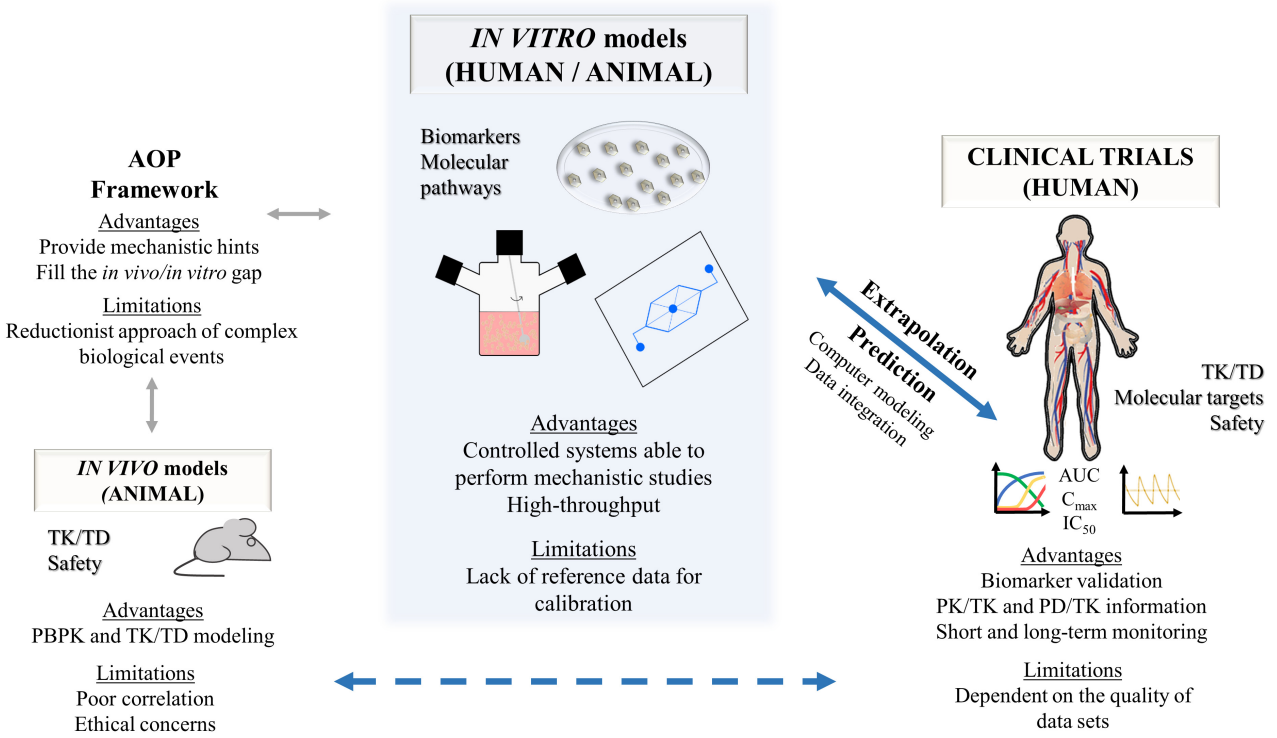

FIGURE 5 | Data integration from non-clinical assays for prediction of clinical conditions. A shift in paradigm where fit-for-purpose human-based *in vitro* models, particularly using *in vitro* 3D systems and causality-inferring bioinformatic approaches, might provide high-quality data for relevant extrapolation of human toxicokinetics and toxicodynamics, ultimately leading to the prediction of human hepatotoxicity mechanisms and molecules' risk assessment. As a consequence, animal models will then become progressively less used with the increasing complexity and relevance of these strategies. AOP, adverse outcome pathway; AUC, area under the curve; C_{max}, maximum plasma concentration; IC_{50}, half maximal inhibitory concentration; PBPK, physiologically based pharmacokinetic; PK, pharmacokinetic; PD, pharmacodynamic; TD, toxicodynamics; TK, toxicokinetics.

and evaluated in each model. Importantly, the capacity of the models for both short and/or long-term exposures should be evaluated as well (**Figure 4**). Indeed, the models' comparison presented in section "*In vitro* Hepatotoxicity Studies: 3D Versus 2D" revealed to be challenging and little informative because most of the hepatotoxicity studies available in the literature focus on cytotoxicity estimation instead of analyzing specific functional endpoints of hepatotoxicity such as altered conversion of primary and secondary metabolites, disruption of repairing mechanisms, immunological response, mitochondrial dysfunction, bile salt transporter modification, lipids accumulation, or calcium homeostasis alteration, which highlight hepatic injury mechanisms such as inflammation, cholestasis, steatosis, fibrosis, or genotoxicity (Xu et al., 2004; O'Brien et al., 2006; Khetani et al., 2013; Trask et al., 2014; Schadt et al., 2015; Bell et al., 2016; Leite et al., 2016; Jeon et al., 2020; Williams et al., 2020; Zhang C. et al., 2020).

Retrospective analysis of approved or failed drugs with a known mechanism displaying the expected hepatic response is a common approach to determine the capability of an *in vitro* system to accurately recapitulate the human liver biological response (Jemnitz et al., 2008; Kostadinova et al., 2013; Messner et al., 2013; Hendriks et al., 2016; Bell et al., 2017; Cipriano et al., 2017b; Proctor et al., 2017; Sarkar et al., 2017; Foster et al., 2019; Williams et al., 2020), e.g., paracetamol for induced necrosis, valproic acid for induced steatosis, or cyclosporine A for induced cholestasis (Vinken and Hengstler, 2018). The data generated with these systems should then be compared with clinical data as well as with other *in vitro* methods to understand applicability and limitations of each system for assessing the inherent risk of a chemical or a new molecular entity (Beken et al., 2016; **Figure 5**). Models are commonly assessed by direct comparison of *in vitro* to the *in vivo* maximum plasma concentration (C_{max}) (Godoy et al., 2013; Shah et al., 2015; Proctor et al., 2017), often multiplied by a factor of 20× to 100× (O'Brien et al., 2006; Xu et al., 2008; Khetani et al., 2013; Proctor et al., 2017; Vorrink et al., 2018; Yu K. N. et al., 2018). Thus, knowing that the C_{max} of paracetamol, diclofenac, and TGZ is 165.38 μM, 10.13 μM (Regenthal et al., 1999) and 2.82 μM (Loi et al., 1999), respectively, it is possible to comprehend by **Supplementary Tables 1–3** that, in general, 3D models present better capability of predicting cytotoxicity than 2D models. However, this comparison assumes that the ratio of test compounds in blood or plasma *in vivo* is the same in the cell culture medium *in vitro* (Vinken and Hengstler, 2018) and that cells response *in vivo* is the same *in vitro*. Also, within the same drug, such a big range of concentration (20× to 100× C_{max}) may represent different mechanisms of toxicity (Albrecht et al., 2019).

A paradigm change from selecting a list of reference chemicals that cause cytotoxicity, to selecting a group of positive and negative mechanistic controls, coupled to a mechanistic-based selection of functional endpoints, including biomarkers assessment, is thus essential for using advanced *in vitro* models to its full potential. An example of a mechanistic positive control for a test system where biliary excretion is measured would be TGZ since it is a known BSEP inhibitor associated with bile acid accumulation (Funk et al., 2001; Jackson et al., 2018). Moreover, the combination of advanced 3D hepatic *in vitro* models with other advanced endpoint methodologies and systems biology employing *-omics* approaches (e.g., RNA-seq, Epigenetics, and ChIP-seq proteomics) could further support better prediction of hepatotoxicity.

Finally, the integration of the biological data obtained with the selected *in vitro* models may support a deeper understanding of the models' potential to predict specific mechanisms of detoxification and toxicity. The inclusion of relevant positive and negative controls that validate the obtained data will support robust knowledge on chemical's risks and human toxicity mechanisms that has not been detected so far using monolayers of a single cell type.

CONCLUSION

There has been major progress toward the development of more physiologically relevant hepatic *in vitro* models, namely through the application of 3D culture techniques. Despite the wide variety of available cellular models along with distinct cell sources, 3D-based liver systems and co-culture strategies improve hepatic-specific functions and sustain the culture through longer periods than 2D counterparts, emphasizing the value-added capacity of such systems to mimic the multicellular mechanisms involved both in intrinsic and idiosyncratic liver toxicity. This has been demonstrated in paracetamol, diclofenac and TGZ toxicities studies where IC_{50} values from 3D cultures confirmed its higher sensitivity.

Nevertheless, the appropriate *in vitro* system's evaluation and proper extrapolation of the *in vitro* data requires a paradigm shift from quantitative cytotoxicity assessment to a comprehensive mechanistic evaluation of the response to chemicals. Advanced 3D systems provide the opportunity to investigate mechanistic hepatotoxicology if accompanied by a careful selection of adequate positive and negative controls and systems toxicology data coupled to disease-related functional endpoints. Despite the advances in creating more physiologically relevant culture systems, a major difficulty is still the standardization of protocols across laboratories and the selection of critical positive and negative controls to assess the transferability and reproducibility of models across different groups. Importantly, advanced endpoint methodologies are essential to identify the applicability of each hepatic system, further allowing comparison between studies. Such a detailed and complete *in vitro* evaluation will support future decision on the adequate model to be used in chemical risk assessment and in a non-clinical drug development scheme.

AUTHOR CONTRIBUTIONS

JM, MC, JR, and AS: conception and design. JM, MC, JR, AS, AR, and NO: writing and critically review the manuscript. JR, AS, and AR: figure design and elaboration. JM: directing manuscript. All authors contributed to the article and approved the submitted version.

FUNDING

This research has been supported by FCT (Portugal) through the research grants and scholarship PTDC/MED-TOX/29183/2017, UIDB/04138/2020, UIDP/04138/2020, and SFRH/BD/144130/2019 to JR and by the H2020, European Commission, though the MSCA-IF-EF-ST – Standard EF to MC (GA-845147-LIV-AD-ON-A-CHIP).

SUPPLEMENTARY MATERIAL

The Supplementary Material for this article can be found online at: https://www.frontiersin.org/articles/10.3389/fcell.2021.626805/full#supplementary-material

REFERENCES

Adiels, C. B., Goksör, M., Wölfl, S., Paukštyte, J., Banaeiyan, A. A., and Theobald, J. (2017). Design and fabrication of a scalable liver-lobule-on-a-chip microphysiological platform. *Biofabrication* 9:015014. doi: 10.1088/1758-5090/9/1/015014

Aeby, E. A., Misun, P. M., Hierlemann, A., and Frey, O. (2018). Microfluidic hydrogel hanging-drop network for long-term culturing of 3D microtissues and simultaneous high-resolution imaging. *Adv. Biosyst.* 2, 1–11. doi: 10.1002/adbi.201800054

Ahmad, J., and Odin, J. A. (2017). Epidemiology and genetic risk factors of drug hepatotoxicity. *Clin. Liver Dis.* 21, 55–72. doi: 10.1016/j.cld.2016.08.004

Aimar, A., Palermo, A., and Innocenti, B. (2019). The role of 3D printing in medical applications: a state of the art. *J. Healthc. Eng.* 2019:5340616. doi: 10.1155/2019/5340616

Aithal, G. P. (2004). Diclofenac-induced liver injury: a paradigm of idiosyncratic drug toxicity. *Expert Opin. Drug Saf.* 3, 519–523. doi: 10.1517/14740338.3.6.519

Aithal, G. P., Ramsay, L., Daly, A. K., Sonchit, N., Leathart, J. B. S., Alexander, G., et al. (2004). Hepatic adducts, circulating antibodies, and cytokine polymorphisms in patients with diclofenac hepatotoxicity. *Hepatology* 39, 1430–1440. doi: 10.1002/hep.20205

Albrecht, W., Kappenberg, F., Brecklinghaus, T., Stoeber, R., Marchan, R., Zhang, M., et al. (2019). Prediction of human drug-induced liver injury (DILI) in relation to oral doses and blood concentrations. *Arch. Toxicol.* 93, 1609–1637. doi: 10.1007/s00204-019-02492-9

Allen, J. W., Khetani, S. R., and Bhatia, S. N. (2005). In vitro zonation and toxicity in a hepatocyte bioreactor. *Toxicol. Sci.* 84, 110–119. doi: 10.1093/toxsci/kfi05

Andersen, M. E., and Krewski, D. (2009). Toxicity testing in the 21st century: bringing the vision to life. *Toxicol. Sci.* 107, 324–330. doi: 10.1093/toxsci/kfn255

Andersen, M. E., and Krewski, D. (2010). The vision of toxicity testing in the 21st century: moving from discussion to action. *Toxicol. Sci.* 117, 17–24. doi: 10.1093/toxsci/kfq188

Andrade, R., Agundez, J., Lucena, M., Martinez, C., Cueto, R., and Garcia-Martin, E. (2009). Pharmacogenomics in Drug Induced Liver Injury. *Curr. Drug Metab.* 10, 956–970. doi: 10.2174/138920009790711805

Aninat, C., Piton, A., Glaise, D., Le Charpentier, T., Langouët, S., Morel, F., et al. (2006). Expression of cytochromes P450, conjugating enzymes and nuclear receptors in human hepatoma HepaRG cells. *Drug Metab. Dispos.* 34, 75–83. doi: 10.1124/dmd.105.006759

Asai, A., Aihara, E., Watson, C., Mourya, R., Mizuochi, T., Shivakumar, P., et al. (2017). Paracrine signals regulate human liver organoid maturation from induced pluripotent stem cells. *Development* 144, 1056–1064. doi: 10.1242/dev.142794

Asha, S., and Vidyavathi, M. (2010). Role of human liver microsomes in in vitro metabolism of drugs-a review. *Appl. Biochem. Biotechnol.* 160, 1699–1722. doi: 10.1007/s12010-009-8689-6

Atienzar, F. A., Novik, E. I., Gerets, H. H., Parekh, A., Delatour, C., Cardenas, A., et al. (2014). Predictivity of dog co-culture model, primary human hepatocytes and HepG2 cells for the detection of hepatotoxic drugs in humans. *Toxicol. Appl. Pharmacol.* 275, 44–61. doi: 10.1016/j.taap.2013.11.022

Babai, S., Auclert, L., and Le-Louët, H. (2018). Safety data and withdrawal of hepatotoxic drugs. *Therapie* [Epub ahead of print]. doi: 10.1016/j.therap.2018.02.004

Bale, S. S., Vernetti, L., Senutovitch, N., Jindal, R., Hegde, M., Gough, A., et al. (2014). In vitro platforms for evaluating liver toxicity. *Exp. Biol. Med.* 239, 1180–1191. doi: 10.1177/1535370214531872

Balls, M. (2011). Modern alternative approaches to the problem of drug-induced liver injury. *ATLA Altern. to Lab. Anim.* 39, 103–107. doi: 10.1177/026119291103900205

Banas, A., Teratani, T., Yamamoto, Y., Tokuhara, M., Takeshita, F., Quinn, G., et al. (2007). Adipose tissue-derived mesenchymal stem cells as a source of human hepatocytes. *Hepatology* 46, 219–228. doi: 10.1002/hep.21704

Bauer, S., Wennberg Huldt, C., Kanebratt, K. P., Durieux, I., Gunne, D., Andersson, S., et al. (2017). Functional coupling of human pancreatic islets and liver spheroids on-a-chip: towards a novel human ex vivo type 2 diabetes model. *Sci. Rep.* 7, 1–11. doi: 10.1038/s41598-017-14815-w

Bavli, D., Prill, S., Ezra, E., Levy, G., Cohen, M., Vinken, M., et al. (2016). Real-time monitoring of metabolic function in liver-on-chip microdevices tracks the dynamics of mitochondrial dysfunction. *Proc. Natl. Acad. Sci. U.S.A.* 113, E2231–E2240. doi: 10.1073/pnas.1522556113

Baxter, M. A., Rowe, C., Alder, J., Harrison, S., Hanley, K. P., Park, B. K., et al. (2010). Generating hepatic cell lineages from pluripotent stem cells for drug toxicity screening. *Stem Cell Res.* 5, 4–22. doi: 10.1016/j.scr.2010.02.002

Becker, H., Schulz, I., Mosig, A., Jahn, T., and Gärtner, C. (2014). Microfluidic devices for cell culture and handling in organ-on-a-chip applications. *Microfluid. BioMEMS Med. Microsyst.* 8976:89760N. doi: 10.1117/12.2037237

Beken, S., Kasper, P., and van Der Laan, J. W. (2016). Regulatory acceptance of alternative methods in the development and approval of pharmaceuticals. *Adv. Exp. Med. Biol.* 856, 33–64. doi: 10.1007/978-3-319-33826-2_3

Bell, C. C., Chouhan, B., Andersson, L. C., Andersson, H., Dear, J. W., Williams, D. P., et al. (2020). Functionality of primary hepatic non-parenchymal cells in a 3D spheroid model and contribution to acetaminophen hepatotoxicity. *Arch. Toxicol.* 94, 1251–1263. doi: 10.1007/s00204-020-02682-w

Bell, C. C., Dankers, A. C. A., Lauschke, V. M., Sison-Young, R., Jenkins, R., Rowe, C., et al. (2018). Comparison of hepatic 2D sandwich cultures and 3d spheroids for long-term toxicity applications: a multicenter study. *Toxicol. Sci.* 162, 655–666. doi: 10.1093/toxsci/kfx289

Bell, C. C., Hendriks, D. F. G., Moro, S. M. L., Ellis, E., Walsh, J., Renblom, A., et al. (2016). Characterization of primary human hepatocyte spheroids as a model system for drug-induced liver injury, liver function and disease. *Sci. Rep.* 6:25187. doi: 10.1038/srep25187

Bell, C. C., Lauschke, V. M., Vorrink, S. U., Palmgren, H., Duffin, R., Andersson, T. B., et al. (2017). Transcriptional, functional, and mechanistic comparisons of stem cell-derived hepatocytes, HepaRG cells, and three-dimensional human hepatocyte spheroids as predictive in vitro systems for drug-induced liver injury. *Drug Metab. Dispos.* 45, 419–429. doi: 10.1124/dmd.116.074369

Berto, A., Van der Poel, W. H. M., Hakze-van der Honing, R., Martelli, F., La Ragione, R. M., Inglese, N., et al. (2013). Replication of hepatitis E virus in three-dimensional cell culture. *J. Virol. Methods* 187, 327–332. doi: 10.1016/j.jviromet.2012.10.017

Bethesda (2012). *LiverTox: Clinical and Research Information on Drug-Induced Liver Injury [Internet]*. Bethesda, MD: National Institute of Diabetes and Digestive and Kidney Diseases.

Bhatia, S. N., and Ingber, D. E. (2014). Microfluidic organs-on-chips. *Nat. Biotechnol.* 32, 760–772. doi: 10.1038/nbt.2989

Boelsterli, U. A. (2003). *Mechanistic Toxicology: The Molecular Basis of How Chemicals Disrupt Biological Targets. First*. Boca Raton, FL: CRC Press.

Boess, F., Kamber, M., Romer, S., Gasser, R., Muller, D., Albertini, S., et al. (2003). Gene expression in two hepatic cell lines, cultured primary hepatocytes, and liver slices compared to the in vivo liver gene expression in rats: possible implications for toxicogenomics use of in vitro systems. *Toxicol. Sci.* 73, 386–402. doi: 10.1093/toxsci/kfg064

Bonn, B., Svanberg, P., Janefeldt, A., Hultman, I., and Grime, K. (2016). Determination of human hepatocyte intrinsic clearance for slowly metabolized compounds: comparison of a primary hepatocyte/stromal cell co-culture with plated primary hepatocytes and hepaRG. *Drug Metab. Dispos.* 44, 527–533. doi: 10.1124/dmd.115.067769

Brockmöller, J., and Tzvetkov, M. V. (2008). Pharmacogenetics: data, concepts and tools to improve drug discovery and drug treatment. *Eur. J. Clin. Pharmacol.* 64, 133–157. doi: 10.1007/s00228-007-0424-z

Brolén, G., Sivertsson, L., Björquist, P., Eriksson, G., Ek, M., Semb, H., et al. (2010). Hepatocyte-like cells derived from human embryonic stem cells specifically via definitive endoderm and a progenitor stage. *J. Biotechnol.* 145, 284–294. doi: 10.1016/j.jbiotec.2009.11.007

Brown, L. A., Arterburn, L. M., Miller, A. P., Cowger, N. L., Hartley, S. M., Andrews, A., et al. (2003). Maintenance of liver functions in rat hepatocytes cultured as spheroids in a rotating wall vessel. *Vitr. Cell. Dev. Biol. Anim.* 39, 13–20.

Bruderer, R., Bernhardt, O. M., Gandhi, T., Miladinoviæ, S. M., Cheng, L. Y., Messner, S., et al. (2015). Extending the limits of quantitative proteome profiling with data-independent acquisition and application to acetaminophen-treated three-dimensional liver microtissues. *Mol. Cell. Proteomics* 14, 1400–1410. doi: 10.1074/mcp.M114.044305

Busche, M., Tomilova, O., Schütte, J., Werner, S., Beer, M., Groll, N., et al. (2020). HepaChip-MP - a twenty-four chamber microplate for a continuously perfused liver coculture model. *Lab Chip* 20, 2911–2926. doi: 10.1039/d0lc00357c

Cai, J., Zhao, Y., Liu, Y., Ye, F., Song, Z., Qin, H., et al. (2007). Directed differentiation of human embryonic stem cells into functional hepatic cells. *Hepatology* 45, 1229–1239. doi: 10.1002/hep.21582

Cai, P., Zheng, H., She, J., Feng, N., Zou, H., Gu, J., et al. (2020). Molecular mechanism of aflatoxin-induced hepatocellular carcinoma derived from a bioinformatics analysis. *Toxins* 12:203. doi: 10.3390/toxins12030203

Camenisch, G., and Umehara, K. (2012). Predicting human hepatic clearance from in vitro drug metabolism and transport data: a scientific and pharmaceutical perspective for assessing drug-drug interactions. *Biopharm. Drug Dispos.* 33, 179–194. doi: 10.1002/bdd.1784

Campard, D., Lysy, P. A., Najimi, M., and Sokal, E. M. (2008). Native umbilical cord matrix stem cells express hepatic markers and differentiate into hepatocyte-like cells. *Gastroenterology* 134, 833–848. doi: 10.1053/j.gastro.2007.12.024

Caparrotta, T. M., Antoine, D. J., and Dear, J. W. (2018). Are some people at increased risk of paracetamol-induced liver injury? A critical review of the literature. *Eur. J. Clin. Pharmacol.* 74, 147–160. doi: 10.1007/s00228-017-2356-6

Carmo, H., Hengstler, J. G., de Boer, D., Ringel, M., Carvalho, F., Fernandes, E., et al. (2004). Comparative metabolism of the designer drug 4-methylthioamphetamine by hepatocytes from man, monkey, dog, rabbit, rat and mouse. *Naunyn Schmiedebergs Arch. Pharmacol.* 369, 198–205. doi: 10.1007/s00210-003-0850-0

Cavallari, L. H., Van Driest, S. L., Prows, C. A., Bishop, J. R., Limdi, N. A., Pratt, V. M., et al. (2019). Multi-site investigation of strategies for the clinical implementation of CYP2D6 genotyping to guide drug prescribing. *Genet. Med.* 21:2255–2263. doi: 10.1038/s41436-019-0484-3

Chan, C., Berthiaume, F., Nath, B. D., Tilles, A. W., Toner, M., and Yarmush, M. L. (2004). Hepatic tissue engineering for adjunct and temporary liver support: critical technologies. *Liver Transplant.* 10, 1331–1342. doi: 10.1002/lt.20229

Chan, R., and Benet, L. Z. (2017). Evaluation of DILI predictive hypotheses in early drug development. *Chem. Res. Toxicol.* 30, 1017–1029. doi: 10.1021/acs.chemrestox.7b00025

Chan, T. S., Yu, H., Moore, A., Khetani, S. R., and Tweedie, D. (2013). Meeting the challenge of predicting hepatic clearance of compounds slowly metabolized by cytochrome P450 using a novel hepatocyte model, HepatoPac. *Drug Metab. Dispos.* 41, 2024–2032. doi: 10.1124/dmd.113.053397

Chang, T. T., and Hughes-Fulford, M. (2009). Monolayer and spheroid culture of human liver hepatocellular carcinoma cell line cells demonstrate distinct global gene expression patterns and functional phenotypes. *Tissue Eng. Part A* 15, 559–567. doi: 10.1089/ten.tea.2007.0434

Chang, T. T., and Hughes-Fulford, M. (2014). Molecular mechanisms underlying the enhanced functions of three-dimensional hepatocyte aggregates. *Biomaterials* 35, 2162–2171. doi: 10.1016/j.biomaterials.2013.11.063

Chao, P., Maguire, T., Novik, E., Cheng, K. C., and Yarmush, M. L. (2009). Evaluation of a microfluidic based cell culture platform with primary human hepatocytes for the prediction of hepatic clearance in human. *Biochem. Pharmacol.* 78, 625–632. doi: 10.1016/j.bcp.2009.05.013

Chatterjee, S., Richert, L., Augustijns, P., and Annaert, P. (2014). Hepatocyte-based in vitro model for assessment of drug-induced cholestasis. *Toxicol. Appl. Pharmacol.* 274, 124–136. doi: 10.1016/j.taap.2013.10.032

Chen, M., Suzuki, A., Thakkar, S., Yu, K., Hu, C., and Tong, W. (2020). *U. S. Food and Drug Administration. Drug Induc. Liver Inj. Rank Dataset*. Available online at: https://www.fda.gov/science-research/liver-toxicity-knowledge-base-ltkb/drug-induced-liver-injury-rank-dilirank-dataset (accessed September 25, 2020).

Chen, Y., Yu, C., Lv, G., Cao, H., Yang, S., Zhang, Y., et al. (2014). Rapid large-scale culturing of microencapsulated hepatocytes: a promising approach for cell-based hepatic support. *Transplant. Proc.* 46, 1649–1657. doi: 10.1016/j.transproceed.2014.03.002

Choe, A., Ha, S. K., Choi, I., Choi, N., and Sung, J. H. (2017). Microfluidic Gut-liver chip for reproducing the first pass metabolism. *Biomed. Microdevices* 19, 1–11. doi: 10.1007/s10544-016-0143-2

Chojkier, M. (2005). Troglitazone and liver injury: in search of answers. *Hepatology* 41, 237–246. doi: 10.1002/hep.20567

Christoffersson, J., Aronsson, C., Jury, M., and Selegård, R. (2019). Fabrication of modular hyaluronan-PEG hydrogels to support 3D cultures of hepatocytes in a perfused liver-on-a-chip device. *Biofabrication* 11:015013. doi: 10.1088/1758-5090/aaf657

Cipriano, M., Correia, J. C., Camões, S. P., Oliveira, N. G., Cruz, P., Cruz, H., et al. (2017a). The role of epigenetic modifiers in extended cultures of functional hepatocyte-like cells derived from human neonatal mesenchymal stem cells. *Arch. Toxicol.* 91, 2469–2489. doi: 10.1007/s00204-016-1901-x

Cipriano, M., Freyer, N., Knöspel, F., Oliveira, N. G., Barcia, R., Cruz, P. E., et al. (2017b). Self-assembled 3D spheroids and hollow-fibre bioreactors improve MSC-derived hepatocyte-like cell maturation in vitro. *Arch. Toxicol.* 91, 1815–1832. doi: 10.1007/s00204-016-1838-0

Cipriano, M., Pinheiro, P. F., Sequeira, C. O., Rodrigues, J. S., Oliveira, N. G., Antunes, A. M. M., et al. (2020). Nevirapine biotransformation insights: an integrated in vitro approach unveils the biocompetence and glutathiolomic profile of a human hepatocyte-like cell 3D model. *Int. J. Mol. Sci.* 21, 1–18. doi: 10.3390/ijms21113998

Coecke, S., Bogni, A., Langezaal, I., Worth, A., Hartung, T., and Monshouwer, M. (2001). The use of genetically engineered cells for assessing CYP2D6-related polymorphic effects. *Toxicol. Vitr.* 15, 553–556. doi: 10.1016/S0887-2333(01)00061-3

Coll, M., Perea, L., Boon, R., Leite, S. B., Vallverdú, J., Mannaerts, I., et al. (2018). Generation of hepatic stellate cells from human pluripotent stem cells enables in vitro modeling of liver fibrosis. *Cell Stem Cell* 23, 101.e7–113.e7. doi: 10.1016/j.stem.2018.05.027

Conway, D. E., Sakurai, Y., Weiss, D., Vega, J. D., Taylor, W. R., Jo, H., et al. (2009). Expression of CYP1A1 and CYP1B1 in human endothelial cells: regulation by fluid shear stress. *Cardiovasc. Res.* 81, 669–677. doi: 10.1093/cvr/cvn360

Cook, D., Brown, D., Alexander, R., March, R., Morgan, P., Satterthwaite, G., et al. (2014). Lessons learned from the fate of AstraZeneca's drug pipeline: a five-dimensional framework. *Nat. Rev. Drug Discov.* 13, 419–431. doi: 10.1038/nrd4309

Daly, A. K., Aithal, G. P., Leathart, J. B. S., Swainsbury, R. A., Dang, T. S., and Day, C. P. (2007). Genetic susceptibility to diclofenac-induced hepatotoxicity: contribution of UGT2B7, CYP2C8, and ABCC2 genotypes. *Gastroenterology* 132, 272–281. doi: 10.1053/j.gastro.2006.11.023

Danoy, M., Bernier, M. L., Kimura, K., Poulain, S., Kato, S., Mori, D., et al. (2019). Optimized protocol for the hepatic differentiation of induced pluripotent stem cells in a fluidic microenvironment. *Biotechnol. Bioeng.* 116, 1762–1776. doi: 10.1002/bit.26970

Danoy, M., Poulain, S., Lereau-Bernier, M., Kato, S., Scheidecker, B., Kido, T., et al. (2020). Characterization of liver zonation-like transcriptomic patterns in HLCs derived from hiPSCs in a microfluidic biochip environment. *Biotechnol. Prog.* 36:e3013. doi: 10.1002/btpr.3013

Darnell, M., Schreiter, T., Zeilinger, K., Urbaniak, T., Söderdahl, T., Rossberg, I., et al. (2011). Cytochrome P450-dependent metabolism in HepaRG cells cultured in a dynamic three-dimensional bioreactor. *Drug Metab. Dispos.* 39, 1131–1138. doi: 10.1124/dmd.110.037721

Darnell, M., Ulvestad, M., Ellis, E., Weidolf, L., and Andersson, T. B. (2012). In vitro evaluation of major in vivo drug metabolic pathways using primary human hepatocytes and HepaRG cells in suspension and a dynamic three-dimensional bioreactor system. *J. Pharmacol. Exp. Ther.* 343, 134–144. doi: 10.1124/jpet.112.195834

Dash, A., Inman, W., Hoffmaster, K., Sevidal, S., Kelly, J., Obach, R. S., et al. (2009). Liver tissue engineering in the evaluation of drug safety. *Expert Opin. Drug Metab. Toxicol.* 5, 1159–1174. doi: 10.1517/17425250903160664

Daston, G., Knight, D. J., Schwarz, M., Gocht, T., Thomas, R. S., Mahony, C., et al. (2015). SEURAT: Safety Evaluation Ultimately Replacing Animal Testing — recommendations for future research in the field of predictive toxicology. *Arch. Toxicol.* 89, 15–23. doi: 10.1007/s00204-014-1421-5

Davila, J. C., Cezar, G. G., Thiede, M., Strom, S., Miki, T., and Trosko, J. (2004). Use and application of stem cells in toxicology. *Toxicol. Sci.* 79, 214–223. doi: 10.1093/toxsci/kfh100

Davis, M., and Stamper, B. D. (2016). TAMH: a useful in vitro model for assessing hepatotoxic mechanisms. *Biomed Res. Int.* 2016:4780872. doi: 10.1155/2016/4780872

Deharde, D., Schneider, C., Hiller, T., Fischer, N., Kegel, V., Lübberstedt, M., et al. (2016). Bile canaliculi formation and biliary transport in 3D sandwich-cultured hepatocytes in dependence of the extracellular matrix composition. *Arch. Toxicol.* 90, 2497–2511. doi: 10.1007/s00204-016-1758-z

Deng, J., Zhang, X., Chen, Z., Luo, Y., Lu, Y., Liu, T., et al. (2019). A cell lines derived microfluidic liver model for investigation of hepatotoxicity induced by drug-drug interaction. *Biomicrofluidics* 13:024101. doi: 10.1063/1.5070088

Devarbhavi, H. (2012). An Update on Drug-induced Liver Injury. *J. Clin. Exp. Hepatol.* 2, 247–259. doi: 10.1016/j.jceh.2012.05.002

Di Stefano, A., Sozio, P., Serafina Cerasa, L., and Iannitelli, A. (2011). L-dopa prodrugs: an overview of trends for improving parkinsons disease treatment. *Curr. Pharm. Des.* 17, 3482–3493. doi: 10.2174/138161211798194495

Domansky, K., Inman, W., Serdy, J., Dash, A., Lim, M. H. M., and Griffith, L. G. (2010). Perfused multiwell plate for 3D liver tissue engineering. *Lab Chip* 10, 51–58. doi: 10.1039/B913221J

Domansky, K., Inman, W., Serdy, J., and Griffith, L. G. (2005). Perfused microreactors for liver tissue engineering. *Annu. Int. Conf. IEEE Eng. Med. Biol. Proc.* 7, 7490–7492. doi: 10.1109/iembs.2005.1616244

Dong, X. J., Zhang, G. R., Zhou, Q. J., Pan, R. L., Chen, Y., Xiang, L. X., et al. (2009). Direct hepatic differentiation of mouse embryonic stem cells induced by valproic acid and cytokines. *World J. Gastroenterol.* 15, 5165–5175. doi: 10.3748/wjg.15.5165

Dowden, H., and Munro, J. (2019). Trends in clinical success rates and therapeutic focus. *Nat. Rev. Drug Discov.* 18, 495–496. doi: 10.1038/d41573-019-00074-z

Dumas, E. O., and Pollack, G. M. (2008). Opioid tolerance development: a pharmacokinetic/pharmacodynamic perspective. *AAPS J.* 10, 537–551. doi: 10.1208/s12248-008-9056-1

Edington, C. D., Chen, W. L. K., Geishecker, E., Kassis, T., Soenksen, L. R., Bhushan, B. M., et al. (2018). Interconnected microphysiological systems for quantitative biology and pharmacology studies. *Sci. Rep.* 8:4530. doi: 10.1038/s41598-018-22749-0

EMEA (2000). *Public Statement on Viramune (Nevirapine) - Severe and Life-Threatening Cutaneous and Hepatic Reactions*. Available online at:

https://www.ema.europa.eu/en/news/public-statement-viramune-nevirapine-severe-life-threatening-cutaneous-hepatic-reactions (accessed May 30, 2020).

Engler, A. J., Sen, S., Sweeney, H. L., and Discher, D. E. (2006). Matrix elasticity directs stem cell lineage specification. *Cell* 126, 677–689. doi: 10.1016/j.cell.2006.06.044

Farzaneh, Z., Abbasalizadeh, S., Asghari-Vostikolaee, M. H., Alikhani, M., Cabral, J. M. S., and Baharvand, H. (2020). Dissolved oxygen concentration regulates human hepatic organoid formation from pluripotent stem cells in a fully controlled bioreactor. *Biotechnol. Bioeng.* 117, 3739–3756. doi: 10.1002/bit.27521

Fey, S. J., Korzeniowska, B., and Wrzesinski, K. (2020). Response to and recovery from treatment in human liver-mimetic clinostat spheroids: a model for assessing repeated-dose drug toxicity. *Toxicol. Res.* 9, 379–389. doi: 10.1093/toxres/tfaa033

Fey, S. J., and Wrzesinski, K. (2012). Determination of drug toxicity using 3D spheroids constructed from an immortal human hepatocyte cell line. *Toxicol. Sci.* 127, 403–411. doi: 10.1093/toxsci/kfs122

Foster, A. J., Chouhan, B., Regan, S. L., Rollison, H., Amberntsson, S., Andersson, L. C., et al. (2019). Integrated in vitro models for hepatic safety and metabolism: evaluation of a human Liver-Chip and liver spheroid. *Arch. Toxicol.* 93, 1021–1037. doi: 10.1007/s00204-019-02427-4

Frederick, D. M., Jacinto, E. Y., Patel, N. N., Rushmore, T. H., Tchao, R., and Harvison, P. J. (2011). Cytotoxicity of 3-(3,5-dichlorophenyl)-2,4-thiazolidinedione (DCPT) and analogues in wild type and CYP3A4 stably transfected HepG2 cells. *Toxicol. Vitr.* 25, 2113–2119. doi: 10.1016/j.tiv.2011.09.015

Freyer, N., Knöspel, F., Strahl, N., Amini, L., Schrade, P., Bachmann, S., et al. (2016). Hepatic differentiation of human induced pluripotent stem cells in a perfused three-dimensional multicompartment bioreactor. *Biores. Open Access* 5, 235–248. doi: 10.1089/biores.2016.0027

Fu, S., Wu, D., Jiang, W., Li, J., Long, J., Jia, C., et al. (2020). Molecular biomarkers in drug-induced liver injury: challenges and future perspectives. *Front. Pharmacol.* 10:1667. doi: 10.3389/fphar.2019.01667

Fu, Y., Deng, J., Jiang, Q., Wang, Y., Zhang, Y., Yao, Y., et al. (2016). Rapid generation of functional hepatocyte-like cells from human adipose-derived stem cells. *Stem Cell Res. Ther.* 7:105. doi: 10.1186/s13287-016-0364-6

Fung, M., Thornton, A., Mybeck, K., Wu, J. H. H., Hornbuckle, K., and Muniz, E. (2001). Evaluation of the characteristics of safety withdrawal of prescription drugs from worldwide pharmaceutical markets-1960 to 1999. *Ther. Innov. Regul. Sci.* 35, 293–317. doi: 10.1177/009286150103500134

Funk, C., Ponelle, C., Scheuermann, G., and Pantze, M. (2001). Cholestatic potential of troglitazone as a possible factor contributing to troglitazone-induced hepatotoxicity: in vivo and in vitro interaction at the canalicular bile salt export pump (Bsep) in the rat. *Mol. Pharmacol.* 59, 627–635. doi: 10.1124/MOL.59.3.627

Gao, B., Yang, Q., Zhao, X., Jin, G., Ma, Y., and Xu, F. (2016). 4D bioprinting for biomedical applications. *Trends Biotechnol.* 34, 746–756. doi: 10.1016/j.tibtech.2016.03.004

Gao, X., and Liu, Y. (2017). A transcriptomic study suggesting human iPSC-derived hepatocytes potentially offer a better in vitro model of hepatotoxicity than most hepatoma cell lines. *Cell Biol. Toxicol.* 33, 407–421. doi: 10.1007/s10565-017-9383-z

Gaskell, H., Sharma, P., Colley, H. E., Murdoch, C., Williams, D. P., and Webb, S. D. (2016). Characterization of a functional C3A liver spheroid model. *Toxicol. Res.* 5, 1053–1065. doi: 10.1039/c6tx00101g

Gerets, H. H. J., Tilmant, K., Gerin, B., Chanteux, H., Depelchin, B. O., Dhalluin, S., et al. (2012). Characterization of primary human hepatocytes, HepG2 cells, and HepaRG cells at the mRNA level and CYP activity in response to inducers and their predictivity for the detection of human hepatotoxins. *Cell Biol. Toxicol.* 28, 69–87. doi: 10.1007/s10565-011-9208-4

Gerlach, J. C., Encke, J., Hole, O., Müller, C., Ryan, C. J., and Neuhaus, P. (1994). Bioreactor for a larger scale hepatocyte in vitro perfusion. *Transplantation* 58, 984–988. doi: 10.1097/00007890-199411150-00002

Gerlach, J. C., Mutig, K., Sauer, I. M., Schrade, P., Efimova, E., Mieder, T., et al. (2003). Use of primary human liver cells originating from discarded grafts in a bioreactor for liver support therapy and the prospects of culturing adult liver stem cells in bioreactors: a morphologic study. *Transplantation* 76, 781–786. doi: 10.1097/01.TP.0000083319.36931.32

Ghabril, M., Fontana, R., Rockey, D., Jiezhun, G., and Chalasani, N. (2013). Drug-induced liver injury caused by intravenously administered medications: the drug-induced liver injury network experience. *J. Clin. Gastroenterol.* 47, 553–558. doi: 10.1097/MCG.0b013e318276bf00

Gieseck, R. L. III, Hannan, N. R. F., Bort, R., Hanley, N. A., Drake, R. A. L., Cameron, G. W. W., et al. (2014). Maturation of induced pluripotent stem cell derived hepatocytes by 3D-culture. *PLoS One* 9:e86372. doi: 10.1371/journal.pone.0086372

Gijbels, E., and Vinken, M. (2017). An update on adverse outcome pathways leading to liver injury. *Appl. Vitr. Toxicol.* 3, 283–285. doi: 10.1089/aivt.2017.0027

Giri, S., Nieber, K., and Bader, A. (2010). Hepatotoxicity and hepatic metabolism of available drugs: current problems and possible solutions in preclinical stages. *Expert Opin. Drug Metab. Toxicol.* 6, 895–917. doi: 10.1517/17425251003792521

Glicklis, R., Merchuk, J. C., and Cohen, S. (2004). Modeling mass transfer in hepatocyte spheroids via cell viability, spheroid size, and hepatocellular functions. *Biotechnol. Bioeng.* 86, 672–680. doi: 10.1002/bit.20086

Goda, K., Takahashi, T., Kobayashi, A., Shoda, T., Kuno, H., and Sugai, S. (2016). Usefulness of in vitro combination assays of mitochondrial dysfunction and apoptosis for the estimation of potential risk of idiosyncratic drug induced liver injury. *J. Toxicol. Sci.* 41, 605–615. doi: 10.2131/jts.41.605

Godoy, P., Hewitt, N. J., Albrecht, U., Andersen, M. E., Ansari, N., Bhattacharya, S., et al. (2013). Recent advances in 2D and 3D in vitro systems using primary hepatocytes, alternative hepatocyte sources and non-parenchymal liver cells and their use in investigating mechanisms of hepatotoxicity, cell signaling and ADME. *Arch. Toxicol.* 87, 1315–1530. doi: 10.1007/s00204-013-1078-5

Gomez-Lechon, M., Donato, M., Lahoz, A., and Castell, J. (2008). Cell lines: a tool for in vitro drug metabolism studies. *Curr. Drug Metab.* 9, 1–11. doi: 10.2174/138920008783331086

Gomez-Lechon, M. J., Lahoz, A., Gombau, L., Castell, J. V., and Donato, M. T. (2010). In vitro evaluation of potential hepatotoxicity induced by drugs. *Curr. Pharm. Des.* 16, 1963–1977. doi: 10.2174/138161210791208910

Goulart, E., de Caires-Junior, L. C., Telles-Silva, K. A., Araujo, B. H. S., Rocco, S. A., et al. (2019). 3D bioprinting of liver spheroids derived from human induced pluripotent stem cells sustain liver function and viability in vitro. *Biofabrication* 12:015010. doi: 10.1088/1758-5090/ab4a30

Granitzny, A., Knebel, J., Müller, M., Braun, A., Steinberg, P., Dasenbrock, C., et al. (2017). Evaluation of a human in vitro hepatocyte-NPC co-culture model for the prediction of idiosyncratic drug-induced liver injury: a pilot study. *Toxicol. Rep.* 4, 89–103. doi: 10.1016/j.toxrep.2017.02.001

Grattagliano, I., Bonfrate, L., Diogo, C. V., Wang, H. H., Wang, D. Q. H., and Portincasa, P. (2009). Biochemical mechanisms in drug-induced liver injury: certainties and doubts. *World J. Gastroenterol.* 15, 4865–4876. doi: 10.3748/wjg.15.4865

Gregus, Z. (2013). "Chapter 3: mechanisms of toxicity," in *Casarett and Doull's Toxicology: Basic Science of Poisons* -, 8th Edn, ed. C. D. Klaassen (San Francisco: McGraw-Hill, Medical Publishing Division), 45–107.

Grilo, N. M., João Correia, M., Miranda, J. P., Cipriano, M., Serpa, J., Matilde Marques, M., et al. (2017). Unmasking efavirenz neurotoxicity: time matters to the underlying mechanisms. *Eur. J. Pharm. Sci.* 105, 47–54. doi: 10.1016/j.ejps.2017.05.010

Grix, T., Ruppelt, A., Thomas, A., Amler, A., Noichl, B., Lauster, R., et al. (2018). Bioprinting Perfusion-Enabled Liver Equivalents for Advanced Organ-on-a-Chip Applications. *Genes* 9:176. doi: 10.3390/genes9040176

Guillouzo, A., Corlu, A., Aninat, C., Glaise, D., Morel, F., and Guguen-Guillouzo, C. (2007). The human hepatoma HepaRG cells: a highly differentiated model for studies of liver metabolism and toxicity of xenobiotics. *Chem. Biol. Interact.* 168, 66–73. doi: 10.1016/j.cbi.2006.12.003

Gunness, P., Mueller, D., Shevchenko, V., Heinzle, E., Ingelman-Sundberg, M., and Noor, F. (2013). 3D organotypic cultures of human heparg cells: a tool for in vitro toxicity studies. *Toxicol. Sci.* 133, 67–78. doi: 10.1093/toxsci/kft021

Hafiz, E. O. A., Bulutoglu, B., Mansy, S. S., Chen, Y., Abu-Taleb, H., Soliman, S. A. M., et al. (2020). Development of liver microtissues with functional biliary ductular network. *Biotechnol. Bioeng.* 118, 17–29. doi: 10.1002/bit.27546

Hammond, T., Allen, P., and Birdsall, H. (2016). Is there a space-based technology solution to problems with preclinical drug toxicity testing? *Pharm. Res.* 33, 1545–1551. doi: 10.1007/s11095-016-1942-0

Haque, A., Gheibi, P., Gao, Y., Foster, E., Son, K. J., You, J., et al. (2016). Cell biology is different in small volumes: endogenous signals shape phenotype of primary hepatocytes cultured in microfluidic channels. *Sci. Rep.* 6, 1–15. doi: 10.1038/srep33980

Haschek, W. M., Rousseaux, C. G., and Wallig, M. A. (2009). Fundamentals of toxicologic pathology: second edition. *Fundam. Toxicol. Pathol.* 2009, 1–691. doi: 10.1016/C2009-0-02051-0

Hass, R., Kasper, C., Böhm, S., and Jacobs, R. (2011). Different populations and sources of human mesenchymal stem cells (MSC): a comparison of adult and neonatal tissue-derived MSC. *Cell Commun. Signal.* 9:12. doi: 10.1186/1478-811X-9-12

Hay, D. C., Fletcher, J., Payne, C., Terrace, J. D., Gallagher, R. C. J., Snoeys, J., et al. (2008a). Highly efficient differentiation of hESCs to functional hepatic endoderm requires ActivinA and Wnt3a signaling. *Proc. Natl. Acad. Sci. U.S.A.* 105, 12301–12306. doi: 10.1073/pnas.0806522105

Hay, D. C., Zhao, D., Fletcher, J., Hewitt, Z. A., McLean, D., Urruticoechea-Uriguen, A., et al. (2008b). Efficient differentiation of hepatocytes from human embryonic stem cells exhibiting markers recapitulating liver development in vivo. *Stem Cells* 26, 894–902. doi: 10.1634/stemcells.2007-0718

Haycock, J. W. (2011). *3D Cell Culture: A Review of Current Approaches and Techniques*. Totowa, NJ: Humana Press.

Hendriks, D. F. G., Puigvert, L. F., Messner, S., Mortiz, W., and Ingelman-Sundberg, M. (2016). Hepatic 3D spheroid models for the detection and study of compounds with cholestatic liability. *Sci. Rep.* 6:35434. doi: 10.1038/srep35434

Hinson, J. A., Roberts, D. W., and James, L. P. (2010). Mechanisms of acetaminophen-induced liver necrosis. *Handb. Exp. Pharmacol.* 196, 396–405. doi: 10.1007/978-3-642-00663-0_12

Hoffmann, S. A., Müller-Vieira, U., Biemel, K., Knobeloch, D., Heydel, S., Lübberstedt, M., et al. (2012). Analysis of drug metabolism activities in a miniaturized liver cell bioreactor for use in pharmacological studies. *Biotechnol. Bioeng.* 109, 3172–3181. doi: 10.1002/bit.24573

Holmgren, G., Sjögren, A. K., Barragan, I., Sabirsh, A., Sartipy, P., Synnergren, J., et al. (2014). Long-term chronic toxicity testing using human pluripotent stem cell-derived hepatocytes. *Drug Metab. Dispos.* 42, 1401–1406. doi: 10.1124/dmd.114.059154

Horvath, P., Aulner, N., Bickle, M., Davies, A. M., Del Nery, E., Ebner, D., et al. (2016). Screening out irrelevant cell-based models of disease. *Nat. Rev. Drug Discov.* 15, 751–769. doi: 10.1038/nrd.2016.175

Huch, M., Dorrell, C., Boj, S. F., Van Es, J. H., Li, V. S. W., Van De Wetering, M., et al. (2013). In vitro expansion of single Lgr5 + liver stem cells induced by Wnt-driven regeneration. *Nature* 494, 247–250. doi: 10.1038/nature11826

Huch, M., Gehart, H., Van Boxtel, R., Hamer, K., Blokzijl, F., Verstegen, M. M. A., et al. (2015). Long-term culture of genome-stable bipotent stem cells from adult human liver. *Cell* 160, 299–312. doi: 10.1016/j.cell.2014.11.050

Hultman, I., Vedin, C., Abrahamsson, A., Winiwarter, S., and Darnell, M. (2016). Use of HμREL human coculture system for prediction of intrinsic clearance and metabolite formation for slowly metabolized compounds. *Mol. Pharm.* 13, 2796–2807. doi: 10.1021/acs.molpharmaceut.6b00396

Ingber, D. E. (2020). Is it time for reviewer 3 to request human organ chip experiments instead of animal validation studies? *Adv. Sci.* 2020:2002030. doi: 10.1002/advs.202002030

Jackson, J. P., Freeman, K. M., St. Claire, R. L., Black, C. B., and Brouwer, K. R. (2018). Cholestatic drug induced liver injury: a function of bile salt export pump inhibition and farnesoid X receptor antagonism. *Appl. Vitr. Toxicol.* 4, 265–279. doi: 10.1089/aivt.2018.0011

Jaeschke, H. (2013). "Chapter 13: toxic responses of the liver," in *Casarett and Doull's Toxicology: Basic Science of Poisons* -, 8th Edn, ed. C. D. Klaassen (San Francisco: McGraw-Hill, Medical Publishing Division), 557–583.

Jang, M., Kleber, A., Ruckelshausen, T., Betzholz, R., and Manz, A. (2019). Differentiation of the human liver progenitor cell line (HepaRG) on a microfluidic-based biochip. *J. Tissue Eng. Regen. Med.* 13, 482–494. doi: 10.1002/term.2802

Jang, M., Neuzil, P., Volk, T., Manz, A., and Kleber, A. (2015). On-chip three-dimensional cell culture in phaseguides improves hepatocyte functions in vitro. *Biomicrofluidics* 9:034113. doi: 10.1063/1.4922863

Jemnitz, K., Veres, Z., Monostory, K., Kóbori, L., and Vereczkey, L. (2008). Interspecies differences in acetaminophen sensitivity of human, rat, and mouse primary hepatocytes. *Toxicol. Vitr.* 22, 961–967. doi: 10.1016/j.tiv.2008.02.001

Jeon, J. W., Choi, N., Lee, S. H., and Sung, J. H. (2020). Three-tissue microphysiological system for studying inflammatory responses in gut-liver Axis. *Biomed. Microdevices* 22:65. doi: 10.1007/s10544-020-00519-y

Jiang, J., Pieterman, C. D., Ertaylan, G., Peeters, R. L. M., and de Kok, T. M. C. M. (2019). *The Application of Omics-Based Human Liver Platforms for Investigating the Mechanism of Drug-Induced Hepatotoxicity in Vitro*. Berlin: Springer.

Jones, S. C., Kortepeter, C., and Brinker, A. D. (2018). "Postmarketing surveillance of drug-induced liver injury," in *Methods in Pharmacology and Toxicology*, ed. K. Y. James (New York, NY: Springer), 459–474.

Kamihira, M., Yamada, K., Hamamoto, R., and Iijima, S. (1997). Spheroid formation of hepatocytes using synthetic polymer. *Ann. N. Y. Acad. Sci.* 831, 398–407. doi: 10.1111/j.1749-6632.1997.tb52213.x

Kanamori, Y., Fujita, K. I, Nakayama, K., Kamataki, T., and Kawai, H. (2003). Large-scale production of genetically engineered CYP3A4 in *E. coli*: application of a Jarfermenter. *Drug Metab. Pharmacokinet.* 18, 42–47. doi: 10.2133/dmpk.18.42

Kang, Y. B. A., Sodunke, T. R., Lamontagne, J., Cirillo, J., Rajiv, C., Bouchard, M. J., et al. (2015). Liver sinusoid on a chip: long-term layered co-culture of primary rat hepatocytes and endothelial cells in microfluidic platforms. *Biotechnol. Bioeng.* 112, 2571–2582. doi: 10.1002/bit.25659

Kappelhoff, B. S., Van Leth, F., MacGregor, T. R., Lange, J. M. A., Beijnen, J. H., and Huitema, A. D. R. (2005). Nevirapine and efavirenz pharmacokinetics and covariate analysis in the 2NN study. *Antivir. Ther.* 10, 145–155.

Kassahun, K., Pearson, P. G., Tang, W., McIntosh, I., Leung, K., Elmore, C., et al. (2001). Studies on the metabolism of troglitazone to reactive intermediates in vitro and in vivo. Evidence for novel biotransformation pathways involving quinone methide formation and thiazolidinedione ring scission. *Chem. Res. Toxicol.* 14, 62–70. doi: 10.1021/tx000180q

Kazemnejad, S., Allameh, A., Seoleimani, M., Gharehbaghian, A., Mohammadi, Y., Amirizadeh, N., et al. (2008). Functional hepatocyte-like cells derived from human bone marrow mesenchymal stem cells on a novel 3-dimensional biocompatible nanofibrous scaffold. *Int. J. Artif. Organs* 31, 500–507. doi: 10.1177/039139880803100605

Kenna, J. G., and Uetrecht, J. (2018). Do In Vitro assays predict drug candidate idiosyncratic drug-induced liver injury risk? *Drug Metab. Dispos.* 46, 1658–1669. doi: 10.1124/dmd.118.082719

Khetani, S. R., and Bhatia, S. N. (2008). Microscale culture of human liver cells for drug development. *Nat. Biotechnol.* 26, 120–126. doi: 10.1038/nbt1361

Khetani, S. R., Kanchagar, C., Ukairo, O., Krzyzewski, S., Moore, A., Shi, J., et al. (2013). Use of micropatterned cocultures to detect compounds that cause drug-induced liver injury in humans. *Toxicol. Sci.* 132, 107–117. doi: 10.1093/toxsci/kfs326

Kholodenko, I. V., Kurbatov, L. K., Kholodenko, R. V., Manukyan, G. V., and Yarygin, K. N. (2019). Mesenchymal stem cells in the adult human liver: hype or hope? *Cells.* 8:1127. doi: 10.3390/cells8101127

Kim, D. E., Jang, M.-J., Kim, Y. R., Lee, J.-Y., Cho, E. B., Kim, E., et al. (2017). Prediction of drug-induced immune-mediated hepatotoxicity using hepatocyte-like cells derived from human embryonic stem cells. *Toxicology* 387, 1–9. doi: 10.1016/j.tox.2017.06.005

Kizawa, H., Nagao, E., Shimamura, M., Zhang, G., and Torii, H. (2017). Scaffold-free 3D bio-printed human liver tissue stably maintains metabolic functions useful for drug discovery. *Biochem. Biophys. Rep.* 10, 186–191. doi: 10.1016/j.bbrep.2017.04.004

Kleiner, D. E. (2017). The histopathological evaluation of drug-induced liver injury. *Histopathology* 70, 81–93. doi: 10.1111/his.13082

Knospel, F., Jacobs, F., Freyer, N., Damm, G., De Bondt, A., van den Wyngaert, I., et al. (2016). In vitro model for hepatotoxicity studies based on primary human hepatocyte cultivation in a perfused 3D bioreactor system. *Int. J. Mol. Sci.* 17:584. doi: 10.3390/ijms17040584

Kola, I., and Landis, J. (2004). Can the pharmaceutical industry reduce attrition rates? *Nat. Rev. Drug Discov.* 3, 711–716. doi: 10.1038/nrd1470

Kostadinova, R., Boess, F., Applegate, D., Suter, L., Weiser, T., Singer, T., et al. (2013). A long-term three dimensional liver co-culture system for improved

prediction of clinically relevant drug-induced hepatotoxicity. *Toxicol. Appl. Pharmacol.* 268, 1–16. doi: 10.1016/j.taap.2013.01.012

Koui, Y., Kido, T., Ito, T., Oyama, H., Chen, S. W., Katou, Y., et al. (2017). An in vitro human liver model by iPSC-derived parenchymal and non-parenchymal cells. *Stem Cell Rep.* 9, 490–498. doi: 10.1016/j.stemcr.2017.06.010

Koyama, S., Arakawa, H., Itoh, M., Masuda, N., Yano, K., Kojima, H., et al. (2018). Evaluation of the metabolic capability of primary human hepatocytes in three-dimensional cultures on microstructural plates. *Biopharm. Drug Dispos.* 39, 187–195. doi: 10.1002/bdd.2125

Kranendonk, M., Alves, M., Antunes, P., and Rueff, J. (2014). Human sulfotransferase 1A1-dependent mutagenicity of 12-hydroxy-nevirapine: the missing link? *Chem. Res. Toxicol.* 27, 1967–1971. doi: 10.1021/tx5003113

Krasniqi, V., Dimovski, A., Domjanovic, I. K., Bilic, I., and Bozina, N. (2016). How polymorphisms of the cytochrome P450 genes affect ibuprofen and diclofenac metabolism and toxicity. *Arh. Hig. Rada Toksikol.* 67, 1–8. doi: 10.1515/aiht-2016-67-2754

Kratochwil, N. A., Triyatni, M., Mueller, M. B., Klammers, F., Leonard, B., Turley, D., et al. (2018). Simultaneous assessment of clearance, metabolism, induction, and drug-drug interaction potential using a long-term in vitro liver model for a novel hepatitis b virus inhibitor. *J. Pharmacol. Exp. Ther.* 365, 237–248. doi: 10.1124/jpet.117.245712

Krewski, D., Andersen, M. E., Mantus, E., and Zeise, L. (2009). Toxicity testing in the 21st century: implications for human health risk assessment: perspective. *Risk Anal.* 29, 474–479. doi: 10.1111/j.1539-6924.2008.01150.x

Kučera, O., Endlicher, R., Rychtrmoc, D., Lotková, H., Sobotka, O., and Červinková, Z. (2017). Acetaminophen toxicity in rat and mouse hepatocytes in vitro. *Drug Chem. Toxicol.* 40, 448–456. doi: 10.1080/01480545.2016.1255953

Kuna, L., Bozic, I., Kizivat, T., Bojanic, K., Mrso, M., Kralj, E., et al. (2018). Models of drug induced liver injury (DILI) – current issues and future perspectives. *Curr. Drug Metab.* 19, 830–838. doi: 10.2174/1389200219666180523095355

Kuntz, E., and Kuntz, H.-D. (2008). *Hepatology Textbook and Atlas*, 3rd Edn. Berlin: Springer.

Langhans, S. A. (2018). Three-dimensional in vitro cell culture models in drug discovery and drug repositioning. *Front. Pharmacol.* 9:6. doi: 10.3389/fphar.2018.00006

Larson, A. M. (2010). Diagnosis and management of acute liver failure. *Curr. Opin. Gastroenterol.* 26, 214–221. doi: 10.1097/MOG.0b013e32833847c5

Lauer, B., Tuschl, G., Kling, M., and Mueller, S. O. (2009). Species-specific toxicity of diclofenac and troglitazone in primary human and rat hepatocytes. *Chem. Biol. Interact.* 179, 17–24. doi: 10.1016/j.cbi.2008.10.031

Lauschke, V. M., Hendriks, D. F. G., Bell, C. C., Andersson, T. B., and Ingelman-Sundberg, M. (2016). Novel 3D culture systems for studies of human liver function and assessments of the hepatotoxicity of drugs and drug candidates. *Chem. Res. Toxicol.* 29, 1936–1955. doi: 10.1021/acs.chemrestox.6b00150

Lee, H. J., Jung, J., Cho, K. J., Lee, C. K., Hwang, S. G., and Kim, G. J. (2012). Comparison of in vitro hepatogenic differentiation potential between various placenta-derived stem cells and other adult stem cells as an alternative source of functional hepatocytes. *Differentiation* 84, 223–231. doi: 10.1016/j.diff.2012.05.007

Lee, P. J., Hung, P. J., and Lee, L. P. (2007). An artificial liver sinusoid with a microfluidic endothelial-like barrier for primary hepatocyte culture. *Biotechnol. Bioeng.* 97, 1340–1346. doi: 10.1002/bit.21360

Leite, S. B., Roosens, T., El Taghdouini, A., Mannaerts, I., Smout, A. J., Najimi, M., et al. (2016). Novel human hepatic organoid model enables testing of drug-induced liver fibrosis in vitro. *Biomaterials* 78, 1–10. doi: 10.1016/j.biomaterials.2015.11.026

Leite, S. B., Teixeira, A. P., Miranda, J. P., Tostões, R. M., Clemente, J. J., Sousa, M. F., et al. (2011). Merging bioreactor technology with 3D hepatocyte-fibroblast culturing approaches: improved in vitro models for toxicological applications. *Toxicol. Vitr.* 25, 825–832. doi: 10.1016/j.tiv.2011.02.002

Leite, S. B., Wilk-Zasadna, I., Zaldivar, J. M., Airola, E., Reis-Fernandes, M. A., Mennecozzi, M., et al. (2012). Three-dimensional HepaRG model as an attractive tool for toxicity testing. *Toxicol. Sci.* 130, 106–116. doi: 10.1093/toxsci/kfs232

Lerche-Langrand, C., and Toutain, H. J. (2000). Precision-cut liver slices: characteristics and use for in vitro pharmaco-toxicology. *Toxicology* 153, 221–253. doi: 10.1016/S0300-483X(00)00316-4

Lewerenz, V., Hanelt, S., Nastevska, C., El-Bahay, C., Röhrdanz, E., and Kahl, R. (2003). Antioxidants protect primary rat hepatocyte cultures against acetaminophen-induced DNA strand breaks but not against acetaminophen-induced cytotoxicity. *Toxicology* 191, 179–187. doi: 10.1016/S0300-483X(03)00256-7

Li, F., Cao, L., Parikh, S., and Zuo, R. (2020). Three-Dimensional Spheroids With Primary Human Liver Cells and Differential Roles of Kupffer Cells in Drug-Induced Liver Injury. *J. Pharm. Sci.* 109, 1912–1923. doi: 10.1016/j.xphs.2020.02.021

Li, M., Yuan, H., Li, N., Song, G., Zheng, Y., Baratta, M., et al. (2008). Identification of interspecies difference in efflux transporters of hepatocytes from dog, rat, monkey and human. *Eur. J. Pharm. Sci.* 35, 114–126. doi: 10.1016/j.ejps.2008.06.008

Lin, J., Schyschka, L., Mühl-Benninghaus, R., Neumann, J., Hao, L., Nussler, N., et al. (2012). Comparative analysis of phase I and II enzyme activities in 5 hepatic cell lines identifies Huh-7 and HCC-T cells with the highest potential to study drug metabolism. *Arch. Toxicol.* 86, 87–95. doi: 10.1007/s00204-011-0733-y

Lin, R.-Z., and Chang, H.-Y. (2008). Recent advances in three-dimensional multicellular spheroid culture for biomedical research. *Biotechnol. J.* 3, 1172–1184. doi: 10.1002/biot.200700228

Liu, H., Wang, Y., Cui, K., Guo, Y., Zhang, X., and Qin, J. (2019). Advances in hydrogels in organoids and organs-on-a-chip. *Adv. Mater.* 31, 1–28. doi: 10.1002/adma.201902042

Loi, C. M., Alvey, C. W., Vassos, A. B., Randinitis, E. J., Sedman, A. J., and Koup, J. R. (1999). Steady-state pharmacokinetics and dose proportionality of troglitazone and its metabolites. *J. Clin. Pharmacol.* 39, 920–926. doi: 10.1177/00912709922008533

Loskill, P., Marcus, S. G., Mathur, A., Reese, W. M., and Healy, K. E. (2015). μOrgano: a lego®-like plug & play system for modular multi-organ-chips. *PLoS One* 10:e0139587. doi: 10.1371/journal.pone.0139587

Lübberstedt, M., Müller-Vieira, U., Biemel, K. M., Darnell, M., Hoffmann, S. A., Knöspel, F., et al. (2015). Serum-free culture of primary human hepatocytes in a miniaturized hollow-fibre membrane bioreactor for pharmacological in vitro studies. *J. Tissue Eng. Regen. Med.* 9, 1017–1026. doi: 10.1002/term.1652

Lübberstedt, M., Müller-Vieira, U., Mayer, M., Biemel, K. M., Knöspel, F., Knobeloch, D., et al. (2011). HepaRG human hepatic cell line utility as a surrogate for primary human hepatocytes in drug metabolism assessment in vitro. *J. Pharmacol. Toxicol. Methods* 63, 59–68. doi: 10.1016/j.vascn.2010.04.013

Luo, X., Gupta, K., Ananthanarayanan, A., Wang, Z., Xia, L., Li, A., et al. (2018). Directed differentiation of adult liver derived mesenchymal like stem cells into functional hepatocytes. *Sci. Rep.* 8:2818. doi: 10.1038/s41598-018-20304-5

Ma, C., Zhao, L., Zhou, E. M., Xu, J., Shen, S., and Wang, J. (2016). On-chip construction of liver lobule-like microtissue and its application for adverse drug reaction assay. *Anal. Chem.* 88, 1719–1727. doi: 10.1021/acs.analchem.5b03869

Ma, J., Wang, Y., and Liu, J. (2018). Bioprinting of 3D tissues/organs combined with microfluidics. *RSC Adv.* 8, 21712–21727. doi: 10.1039/C8RA03022G

Ma, X., Qu, X., Zhu, W., Li, Y. S., Yuan, S., Zhang, H., et al. (2016). Deterministically patterned biomimetic human iPSC-derived hepatic model via rapid 3D bioprinting. *Proc. Natl. Acad. Sci. U.S.A.* 113, 2206–2211. doi: 10.1073/pnas.1524510113

Mandenius, C. F., Andersson, T. B., Alves, P. M., Batzl-Hartmann, C., Björquist, P., Carrondo, M. J. T., et al. (2011). Toward preclinical predictive drug testing for metabolism and hepatotoxicity by using in vitro models derived from human embryonic stem cells and human cell lines - A report on the vitrocellomics EU-project. *ATLA Altern. Lab. Anim.* 39, 147–171. doi: 10.1177/026119291103900210

Mannaerts, I., Eysackers, N., Anne van Os, E., Verhulst, S., Roosens, T., Smout, A., et al. (2020). The fibrotic response of primary liver spheroids recapitulates in vivo hepatic stellate cell activation. *Biomaterials* 261:120335. doi: 10.1016/j.biomaterials.2020.120335

Marinho, A. T., Miranda, J. P., Caixas, U., Charneira, C., Gonçalves-Dias, C., Marques, M. M., et al. (2019). Singularities of nevirapine metabolism: from

sex-dependent differences to idiosyncratic toxicity. *Drug Metab. Rev.* 51, 76–90. doi: 10.1080/03602532.2019.1577891

Martignoni, M., Groothuis, G. M. M., and de Kanter, R. (2006). Species differences between mouse, rat, dog, monkey and human CYP-mediated drug metabolism, inhibition and induction. *Expert Opin. Drug Metab. Toxicol.* 2, 875–894. doi: 10.1517/17425255.2.6.875

Maschmeyer, I., Hasenberg, T., Jaenicke, A., Lindner, M., Lorenz, A. K., Zech, J., et al. (2015). Chip-based human liver-intestine and liver-skin co-cultures - A first step toward systemic repeated dose substance testing in vitro. *Eur. J. Pharm. Biopharm.* 95, 77–87. doi: 10.1016/j.ejpb.2015.03.002

Mastrangeli, M., Millet, S., Orchid Partners, T., and Van den Eijnden-van Raaij, J. (2019). Organ-on-chip in development: towards a roadmap for organs-on-chip. *ALTEX* 36, 650–668. doi: 10.14573/altex.1908271

Mazaleuskaya, L. L., Sangkuhl, K., Thorn, C. F., Fitzgerald, G. A., Altman, R. B., and Klein, T. E. (2015). PharmGKB summary: pathways of acetaminophen metabolism at the therapeutic versus toxic doses. *Pharmacogenet. Genomics* 25, 416–426. doi: 10.1097/FPC.0000000000000150

Mazzocchi, A., Devarasetty, M., Huntwork, R., Soker, S., and Skardal, A. (2018). Optimization of collagen type I-hyaluronan hybrid bioink for 3D bioprinted liver microenvironments. *Biofabrication* 11:015003. doi: 10.1088/1758-5090/aae543

Mazzocchi, A., Soker, S., and Skardal, A. (2019). 3D bioprinting for high-throughput screening: drug screening, disease modeling, and precision medicine applications. *Appl. Phys. Rev.* 6:011302. doi: 10.1063/1.5056188

McCarty, W. J., Usta, O. B., and Yarmush, M. L. (2016). A microfabricated platform for generating physiologically-relevant hepatocyte zonation. *Sci. Rep.* 6:26868. doi: 10.1038/srep26868

McGill, M. R., and Jaeschke, H. (2013). Metabolism and disposition of acetaminophen: recent advances in relation to hepatotoxicity and diagnosis. *Pharm. Res.* 30, 2174–2187. doi: 10.1007/s11095-013-1007-6

Ménochet, K., Kenworthy, K. E., Houston, J. B., and Galetin, A. (2012). Use of mechanistic modeling to assess interindividual variability and interspecies differences in active uptake in human and rat hepatocytes. *Drug Metab. Dispos.* 40, 1744–1756. doi: 10.1124/dmd.112.046193

Messner, S., Agarkova, A., Moritz, W., and Kelm, J. M. (2013). Multi-cell type human liver microtissues for hepatotoxicity testing. *Arch. Toxicol.* 87, 209–213. doi: 10.1007/s00204-012-0968-2

Messner, S., Fredriksson, L., Lauschke, V. M., Roessger, K., Escher, C., Bober, M., et al. (2018). Transcriptomic, proteomic, and functional long-term characterization of multicellular three-dimensional human liver microtissues. *Appl. Vitr. Toxicol.* 4, 1–12. doi: 10.1089/aivt.2017.0022

Meyer, U. A., and Zanger, U. M. (1997). Molecular mechanisms of genetic polymorphisms of drug metabolism. *Annu. Rev. Pharmacol. Toxicol.* 37, 269–296. doi: 10.1146/annurev.pharmtox.37.1.269

Miranda, J. P., Leite, S. B., Muller-Vieira, U., Rodrigues, A., Carrondo, M. J. T., and Alves, P. M. (2009). Towards an extended functional hepatocyte in vitro culture. *Tissue Eng. Part C Methods* 15, 157–167. doi: 10.1089/ten.tec.2008.0352

Miranda, J. P., Rodrigues, A., Tostoes, R. M., Leite, S., Zimmerman, H., Carrondo, M. J. T., et al. (2010). Extending hepatocyte functionality for drug-testing applications using high-viscosity alginate-encapsulated three-dimensional cultures in bioreactors. *Tissue Eng. Part C Methods* 16, 1223–1232. doi: 10.1089/ten.TEC.2009.0784

Molina-Jimenez, F., Benedicto, I., Dao Thi, V. L., Gondar, V., Lavillette, D., Marin, J. J., et al. (2012). Matrigel-embedded 3D culture of Huh-7 cells as a hepatocyte-like polarized system to study hepatitis C virus cycle. *Virology* 425, 31–39. doi: 10.1016/j.virol.2011.12.021

Mueller, D., Tascher, G., Muller-Vieira, U., Knobeloch, D., Nuessler, A. K., Zeilinger, K., et al. (2011). In-depth physiological characterization of primary human hepatocytes in a 3D hollow-fiber bioreactor. *J. Tissue Eng. Regen. Med.* 5, e207–e218. doi: 10.1002/term.418

Mustafa, M. G., Khan, M. G. M., Nguyen, D., and Iqbal, S. (2018). "Techniques in biotechnology," in *Omics Technologies and Bio-Engineering*, ed. V. Azevedo (Amsterdam: Elsevier), 233–249.

Nakamura, K., Kato, N., Aizawa, K., Mizutani, R., Yamauchi, J., and Tanoue, A. (2011). Expression of albumin and cytochrome P450 enzymes in HepG2 cells cultured with a nanotechnology-based culture plate with microfabricated scaffold. *J. Toxicol. Sci.* 36, 625–633. doi: 10.2131/jts.36.625

Nelson, L. J., Walker, S. W., Hayes, P. C., and Plevris, J. N. (2010). Low-shear modelled microgravity environment maintains morphology and differentiated functionality of primary porcine hepatocyte cultures. *Cells Tissues Organs* 192, 125–140. doi: 10.1159/000308893

Nguyen, D. G., Funk, J., Robbins, J. B., and Crogan-grundy, C. (2016). Bioprinted 3D primary liver tissues allow assessment of organ-level response to clinical drug induced toxicity in vitro. *PLoS One* 11:e0158674. doi: 10.1371/journal.pone.0158674

Norrman, K., Strömbeck, A., Semb, H., and Ståhlberg, A. (2013). Distinct gene expression signatures in human embryonic stem cells differentiated towards definitive endoderm at single-cell level. *Methods* 59, 59–70. doi: 10.1016/j.ymeth.2012.03.030

Novik, E. I., Dwyer, J., Morelli, J. K., Parekh, A., Cho, C., Pludwinski, E., et al. (2017). Long-enduring primary hepatocyte-based co-cultures improve prediction of hepatotoxicity. *Toxicol. Appl. Pharmacol.* 336, 20–30. doi: 10.1016/j.taap.2017.09.013

Nudischer, R., Renggli, K., Hierlemann, A., Roth, A. B., and Bertinetti-Lapatki, C. (2020). Characterization of a long-term mouse primary liver 3D tissue model recapitulating innate-immune responses and drug-induced liver toxicity. *PLoS One* 15:e0235745. doi: 10.1371/journal.pone.0235745

O'Brien, P. J., Irwin, W., Diaz, D., Howard-Cofield, E., Krejsa, C. M., Slaughter, M. R., et al. (2006). High concordance of drug-induced human hepatotoxicity with in vitro cytotoxicity measured in a novel cell-based model using high content screening. *Arch. Toxicol.* 80, 580–604. doi: 10.1007/s00204-006-0091-3

Ogawa, M., Ogawa, S., Bear, C. E., Ahmadi, S., Chin, S., Li, B., et al. (2015). Directed differentiation of cholangiocytes from human pluripotent stem cells. *Nat. Biotechnol.* 33, 853–861. doi: 10.1038/nbt.3294

Ogimura, E., Sekine, S., and Horie, T. (2011). Bile salt export pump inhibitors are associated with bile acid-dependent drug-induced toxicity in sandwich-cultured hepatocytes. *Biochem. Biophys. Res. Commun.* 416, 313–317. doi: 10.1016/j.bbrc.2011.11.032

Okura, H., Komoda, H., Saga, A., Kakuta-Yamamoto, A., Hamada, Y., Fumimoto, Y., et al. (2010). Properties of hepatocyte-like cell clusters from human adipose tissue-derived mesenchymal stem cells. *Tissue Eng. Part C Methods* 16, 761–770. doi: 10.1089/ten.TEC.2009.0208

Olson, H., Betton, G., Robinson, D., Thomas, K., Monro, A., Kolaja, G., et al. (2000). Concordance of the toxicity of pharmaceuticals in humans and in animals. *Regul. Toxicol. Pharmacol.* 32, 56–67. doi: 10.1006/rtph.2000.1399

Omiecinski, C. J., Vanden Heuvel, J. P., Perdew, G. H., and Peters, J. M. (2011). Xenobiotic metabolism, disposition, and regulation by receptors: from biochemical phenomenon to predictors of major toxicities. *Toxicol. Sci.* 120, S49–S75. doi: 10.1093/toxsci/kfq338

Onakpoya, I. J., Heneghan, C. J., and Aronson, J. K. (2016). Post-marketing withdrawal of 462 medicinal products because of adverse drug reactions: a systematic review of the world literature. *BMC Med.* 14:10. doi: 10.1186/s12916-016-0553-2

Overi, D., Carpino, G., Cardinale, V., Franchitto, A., Safarikia, S., Onori, P., et al. (2018). Contribution of resident stem cells to liver and biliary tree regeneration in human diseases. *Int. J. Mol. Sci.* 19:2917. doi: 10.3390/ijms19102917

Padda, M. S., Sanchez, M., Akhtar, A. J., and Boyer, J. L. (2011). Drug-induced cholestasis. *Hepatology* 53, 1377–1387. doi: 10.1002/hep.24229

Paniagua, A. C., and Amariles, P. (2018). "Hepatotoxicity by drugs," in *Pharmacokinetics and Adverse Effects of Drugs - Mechanisms and Risks Factors*, (Ntambwe Malangu: IntechOpen). doi: 10.5772/intechopen.72005

Pareja, E., Gómez-Lechón, M. J., and Tolosa, L. (2020). Induced pluripotent stem cells for the treatment of liver diseases: challenges and perspectives from a clinical viewpoint. *Ann. Transl. Med.* 8:566. doi: 10.21037/atm.2020.02.164

Paul, S. M., Mytelka, D. S., Dunwiddie, C. T., Persinger, C. C., Munos, B. H., Lindborg, S. R., et al. (2010). How to improve R&D productivity: the pharmaceutical industry's grand challenge. *Nat. Rev. Drug Discov.* 9, 203–214. doi: 10.1038/nrd3078

Peng, W. C., Logan, C. Y., Fish, M., Anbarchian, T., Aguisanda, F., Álvarez-Varela, A., et al. (2018). Inflammatory cytokine TNFα promotes the long-term expansion of primary hepatocytes in 3D culture. *Cell* 175, 1607.e15–1619.e15. doi: 10.1016/j.cell.2018.11.012

Pessayre, D. (1993). Cytochromes P450 and formation of reactive metabolites. Role in hepatotoxicity of drugs. *Therapie* 48, 537–548.

Pinheiro, P. F., Pereira, S. A., Harjivan, S. G., Martins, I. L., Marinho, A. T., Cipriano, M., et al. (2017). Hepatocyte spheroids as a competent in vitro system for drug biotransformation studies: nevirapine as a bioactivation case study. *Arch. Toxicol.* 91, 1199–1211. doi: 10.1007/s00204-016-1792-x

Poietis (2018). *Servier and Poietis Announce Scientific Partnership in 4D Bioprinting of Liver Tissues*. Available online at: https://poietis.com/servier-and-poietis-announce-scientific-partnership-in-4d-bioprinting-of-liver-tissues/ (accessed May 8, 2020).

Ponsoda, X., Bort, R., Jover, R., Gómez-lechón, M. J., and Castell, J. V. (1995). Molecular mechanism of diclofenac hepatotoxicity: association of cell injury with oxidative metabolism and decrease in ATP levels. *Toxicol. Vitr.* 9, 439–444. doi: 10.1016/0887-2333(95)00035-7

Prakash, C., Sharma, R., Gleave, M., and Nedderman, A. (2008). In vitro screening techniques for reactive metabolites for minimizing bioactivation potential in drug discovery. *Curr. Drug Metab.* 9, 952–964. doi: 10.2174/138920008786485209

Preissner, S., Simmaco, M., Gentile, G., and Preissner, R. (2015). Personalized cancer therapy considering cytochrome P450 variability. *Adv. Pharmacol.* 74, 113–130. doi: 10.1016/bs.apha.2015.03.004

Prill, S., Bavli, D., Levy, G., Ezra, E., Schmälzlin, E., Jaeger, M. S., et al. (2016). Real-time monitoring of oxygen uptake in hepatic bioreactor shows CYP450-independent mitochondrial toxicity of acetaminophen and amiodarone. *Arch. Toxicol.* 90, 1181–1191. doi: 10.1007/s00204-015-1537-2

Proctor, W. R., Foster, A. J., Vogt, J., Summers, C., Middleton, B., Pilling, M. A., et al. (2017). Utility of spherical human liver microtissues for prediction of clinical drug-induced liver injury. *Arch. Toxicol.* 91, 2849–2863. doi: 10.1007/s00204-017-2002-1

Prodanov, L., Jindal, R., Bale, S. S., Hegde, M., Mccarty, W. J., Golberg, I., et al. (2016). Long-term maintenance of a microfluidic 3D human liver sinusoid. *Biotechnol. Bioeng.* 113, 241–246. doi: 10.1002/bit.25700

Prot, J. M., Bunescu, A., Elena-Herrmann, B., Aninat, C., Snouber, L. C., Griscom, L., et al. (2012). Predictive toxicology using systemic biology and liver microfluidic "on chip" approaches: application to acetaminophen injury. *Toxicol. Appl. Pharmacol.* 259, 270–280. doi: 10.1016/j.taap.2011.12.017

Qureshi, Z. P., Seoane-Vazquez, E., Rodriguez-Monguio, R., Stevenson, K. B., and Szeinbach, S. L. (2011). Market withdrawal of new molecular entities approved in the United States from 1980 to 2009. *Pharmacoepidemiol. Drug Saf.* 20, 772–777. doi: 10.1002/pds.2155

Raasch, M., Fritsche, E., Kurtz, A., Bauer, M., and Mosig, A. S. (2019). Microphysiological systems meet hiPSC technology – New tools for disease modeling of liver infections in basic research and drug development. *Adv. Drug Deliv. Rev.* 140, 51–67. doi: 10.1016/j.addr.2018.06.008

Raju, R., Chau, D., Notelaers, T., Myers, C. L., Verfaillie, C. M., and Hu, W. S. (2018). In vitro pluripotent stem cell differentiation to hepatocyte ceases further maturation at an equivalent stage of e15 in mouse embryonic liver development. *Stem Cells Dev.* 27, 910–921. doi: 10.1089/scd.2017.0270

Ramachandran, A., and Jaeschke, H. (2018). Acetaminophen toxicity: novel insights into mechanisms and future perspectives. *Gene Expr.* 18, 19–30. doi: 10.3727/105221617X15084371374138

Ramaiahgari, S. C., Den Braver, M. W., Herpers, B., Terpstra, V., Commandeur, J. N. M., Van De Water, B., et al. (2014). A 3D in vitro model of differentiated HepG2 cell spheroids with improved liver-like properties for repeated dose high-throughput toxicity studies. *Arch. Toxicol.* 88, 1083–1095. doi: 10.1007/s00204-014-1215-9

Ramli, M. N., Bin, Lim, Y. S., Koe, C. T., Demircioglu, D., Tng, W., et al. (2020). Human pluripotent stem cell-derived organoids as models of liver disease. *Gastroenterology* 159, 1471.e12–1486.e12. doi: 10.1053/j.gastro.2020.06.010

Reder-Hilz, B., Ullrich, M., Ringel, M., Hewitt, N., Utesch, D., Oesch, F., et al. (2004). Metabolism of propafenone and verapamil by cryopreserved human, rat, mouse and dog hepatocytes: comparison with metabolism in vivo. *Naunyn. Schmiedebergs. Arch. Pharmacol.* 369, 408–417. doi: 10.1007/s00210-004-0875-z

Regenthal, R., Krueger, M., Koeppel, C., and Preiss, R. (1999). Drug levels: therapeutic and toxic serum/plasma concentrations of common drugs. *J. Clin. Monit. Comput.* 15, 529–544. doi: 10.1023/A:1009935116877

Rennert, K., Steinborn, S., Gröger, M., Ungerböck, B., Jank, A. M., Ehgartner, J., et al. (2015). A microfluidically perfused three dimensional human liver model. *Biomaterials* 71, 119–131. doi: 10.1016/j.biomaterials.2015.08.043

Riches, Z., Bloomer, J., Patel, A., Nolan, A., and Coughtrie, M. (2009). Assessment of cryopreserved human hepatocytes as a model system to investigate sulfation and glucuronidation and to evaluate inhibitors of drug conjugation. *Xenobiotica* 39, 374–381. doi: 10.1080/00498250902763440

Robinton, D. A., and Daley, G. Q. (2012). The promise of induced pluripotent stem cells in research and therapy. *Nature* 481, 295–305. doi: 10.1038/nature10761

Ronaldson-Bouchard, K., and Vunjak-Novakovic, G. (2018). Organs-on-a-chip: a fast track for engineered human tissues in drug development. *Cell Stem Cell* 22, 310–324. doi: 10.1016/j.stem.2018.02.011

Roth, R. A., and Ganey, P. E. (2010). Intrinsic versus idiosyncratic drug-induced hepatotoxicity - Two villains or one? *J. Pharmacol. Exp. Ther.* 332, 692–697. doi: 10.1124/jpet.109.162651

Rowe, C., Gerrard, D. T., Jenkins, R., Berry, A., Durkin, K., Sundstrom, L., et al. (2013). Proteome-wide analyses of human hepatocytes during differentiation and dedifferentiation. *Hepatology* 58, 799–809. doi: 10.1002/hep.26414

Rowe, C., Shaeri, M., Large, E., Cornforth, T., Robinson, A., Kostrzewski, T., et al. (2018). Perfused human hepatocyte microtissues identify reactive metabolite-forming and mitochondria-perturbing hepatotoxins. *Toxicol. Vitr.* 46, 29–38. doi: 10.1016/j.tiv.2017.09.012

Ruoß, M., Vosough, M., Königsrainer, A., Nadalin, S., Wagner, S., Sajadian, S., et al. (2020). Towards improved hepatocyte cultures: progress and limitations. *Food Chem. Toxicol.* 138:111188. doi: 10.1016/j.fct.2020.111188

Russmann, S., Kullak-Ublick, G., and Grattagliano, I. (2009). Current concepts of mechanisms in drug-induced hepatotoxicity. *Curr. Med. Chem.* 16, 3041–3053. doi: 10.2174/092986709788803097

Sahi, J., Hamilton, G., Sinz, M., Barros, S., Huang, S. M., Lesko, L. J., et al. (2000). Effect of troglitazone on cytochrome P450 enzymes in primary cultures of human and rat hepatocytes. *Xenobiotica* 30, 273–284. doi: 10.1080/004982500237668

Sainz, B., Tencate, V., and Uprichard, S. L. (2009). Three-dimensional Huh7 cell culture system for the study of Hepatitis C virus infection. *Virol. J.* 6, 1–8. doi: 10.1186/1743-422X-6-103

Saiz-Rodríguez, M., Almenara, S., Navares-Gómez, M., Ochoa, D., Román, M., Zubiaur, P., et al. (2020). Effect of the most relevant CYP3A4 and CYP3A5 polymorphisms on the pharmacokinetic parameters of 10 CYP3A substrates. *Biomedicines* 8:94. doi: 10.3390/biomedicines8040094

Sakai, Y., Naruse, K., Nagashima, I., Muto, T., and Suzuki, M. (1996). Large-scale preparation and function of porcine hepatocyte spheroids. *Int. J. Artif. Organs* 19, 294–301. doi: 10.1177/039139889601900507

Sampaziotis, F., De Brito, M. C., Madrigal, P., Bertero, A., Saeb-Parsy, K., Soares, F. A. C., et al. (2015). Cholangiocytes derived from human induced pluripotent stem cells for disease modeling and drug validation. *Nat. Biotechnol.* 33, 845–852. doi: 10.1038/nbt.3275

Sandker, G. W., Vos, R. M. E., Delbressine, L. P. C., Slooff, M. J. H., Meijer, D. K. F., and Groothuis, G. M. M. (1994). Metabolism of three pharmacologically active drugs in isolated human and rat hepatocytes: analysis of interspecies variability and comparison with metabolism in vivo. *Xenobiotica* 24, 143–155. doi: 10.3109/00498259409043228

Sarkar, U., Ravindra, K. C., Large, E., Young, C. L., Rivera-Burgos, D., Yu, J., et al. (2017). Integrated assessment of diclofenac biotransformation, pharmacokinetics, and omics-based toxicity in a three-dimensional human liver-immunocompetent coculture systems. *Drug Metab. Dispos.* 45, 855–866. doi: 10.1124/dmd.116.074005

Sauer, V., Roy-Chowdhury, N., Guha, C., and Roy-Chowdhury, J. (2014). Induced pluripotent stem cells as a source of hepatocytes. *Curr. Pathobiol. Rep.* 2, 11–20. doi: 10.1007/s40139-013-0039-2

Schadt, S., Simon, S., Kustermann, S., Boess, F., McGinnis, C., Brink, A., et al. (2015). Minimizing DILI risk in drug discovery - A screening tool for drug candidates. *Toxicol. Vitr.* 30, 429–437. doi: 10.1016/j.tiv.2015.09.019

Schneeberger, K., Sánchez-Romero, N., Ye, S., Steenbeek, F. G., Oosterhoff, L. A., Pla Palacin, I., et al. (2020). Large-Scale Production of LGR5-positive bipotential human liver stem cells. *Hepatology* 72, 257–270. doi: 10.1002/hep.31037

Schyschka, L., Sánchez, J. J. M., Wang, Z., Burkhardt, B., Müller-Vieira, U., Zeilinger, K., et al. (2013). Hepatic 3D cultures but not 2D cultures preserve

specific transporter activity for acetaminophen-induced hepatotoxicity. *Arch. Toxicol.* 87, 1581–1593. doi: 10.1007/s00204-013-1080-y

Shah, F., Leung, L., Barton, H. A., Will, Y., Rodrigues, A. D., Greene, N., et al. (2015). Setting clinical exposure levels of concern for drug-induced liver injury (DILI) using mechanistic in vitro assays. *Toxicol. Sci.* 147, 500–514. doi: 10.1093/toxsci/kfv152

Shanks, N., Greek, R., and Greek, J. (2009). Are animal models predictive for humans? *Philos. Ethics Humanit. Med.* 4:2. doi: 10.1186/1747-5341-4-2

Sharma, N. S., Shikhanovich, R., Schloss, R., and Yarmush, M. L. (2006). Sodium butyrate-treated embryonic stem cells yield hepatocyte-like cells expressing a glycolytic phenotype. *Biotechnol. Bioeng.* 94, 1053–1063. doi: 10.1002/bit.20936

Shen, C., Meng, Q., and Zhang, G. (2012). Species-specific toxicity of troglitazone on rats and human by gel entrapped hepatocytes. *Toxicol. Appl. Pharmacol.* 258, 19–25. doi: 10.1016/j.taap.2011.10.020

Shen, M. M. (2007). Nodal signaling: developmental roles and regulation. *Development* 134, 1023–1034. doi: 10.1242/dev.000166

Shi, D., Xin, J., Lu, Y., Ding, W., Jiang, J., Zhou, Q., et al. (2020). Transcriptome profiling reveals distinct phenotype of human bone marrow mesenchymal stem cell-derived hepatocyte-like cells. *Int. J. Med. Sci.* 17, 263–273. doi: 10.7150/ijms.36255

Shukla, S. J., Huang, R., Austin, C. P., and Xia, M. (2010). The future of toxicity testing: a focus on in vitro methods using a quantitative high-throughput screening platform. *Drug Discov. Today* 15, 997–1007. doi: 10.1016/j.drudis.2010.07.007

Shvartsman, I., Dvir, T., Harel-Adar, T., and Cohen, S. (2009). Perfusion cell seeding and cultivation induce the assembly of thick and functional hepatocellular tissue-like construct. *Tissue Eng. Part A* 15, 751–760. doi: 10.1089/ten.tea.2008.0024

Sidenius, U., Skonberg, C., Olsen, J., and Hansen, S. H. (2004). In vitro reactivity of carboxylic acid-CoA thioesters with glutathione. *Chem. Res. Toxicol.* 17, 75–81. doi: 10.1021/tx034127o

Singh, B. K., Tripathi, M., Pandey, P. K., and Kakkar, P. (2010). Nimesulide aggravates redox imbalance and calcium dependent mitochondrial permeability transition leading to dysfunction in vitro. *Toxicology* 275, 1–9. doi: 10.1016/j.tox.2010.05.001

Siramshetty, V. B., Nickel, J., Omieczynski, C., Gohlke, B. O., Drwal, M. N., and Preissner, R. (2016). WITHDRAWN - A resource for withdrawn and discontinued drugs. *Nucleic Acids Res.* 44, D1080–D1086. doi: 10.1093/nar/gkv1192

Sirenko, O., Hancock, M. K., Hesley, J., Hong, D., Cohen, A., Gentry, J., et al. (2016). Phenotypic characterization of toxic compound effects on liver spheroids derived from ipsc using confocal imaging and three-dimensional image analysis. *Assay Drug Dev. Technol.* 14, 381–394. doi: 10.1089/adt.2016.729

Sison-Young, R. L., Lauschke, V. M., Johann, E., Alexandre, E., Antherieu, S., Aerts, H., et al. (2017). A multicenter assessment of single-cell models aligned to standard measures of cell health for prediction of acute hepatotoxicity. *Arch. Toxicol.* 91, 1385–1400. doi: 10.1007/s00204-016-1745-4

Skonberg, C., Olsen, J., Madsen, K. G., Hansen, S. H., and Grillo, M. P. (2008). Metabolic activation of carboxylic acids. *Expert Opin. Drug Metab. Toxicol.* 4, 425–438. doi: 10.1517/17425255.4.4.425

Smith, M. T. (2003). Mechanisms of troglitazone hepatotoxicity. *Chem. Res. Toxicol.* 16, 679–687. doi: 10.1021/tx034033e

Snykers, S., Vanhaecke, T., De Becker, A., Papeleu, P., Vinken, M., Van Riet, I., et al. (2007). Chromatin remodeling agent trichostatin A: a key-factor in the hepatic differentiation of human mesenchymal stem cells derived of adult bone marrow. *BMC Dev. Biol.* 7:24. doi: 10.1186/1471-213X-7-24

Snykers, S., Vanhaecke, T., Papeleu, P., Luttun, A., Jiang, Y., Vander Heyden, Y., et al. (2006). Sequential exposure to cytokines reflecting embryogenesis: the key for in vitro differentiation of adult bone marrow stem cells into functional hepatocyte-like cells. *Toxicol. Sci.* 94, 330–341. doi: 10.1093/toxsci/kfl058

Sohn, L. L., Schwille, P., Hierlemann, A., Tay, S., Samitier, J., Fu, J., et al. (2020). How can microfluidic and microfabrication approaches make experiments more physiologically relevant? *Cell Syst.* 11, 209–211. doi: 10.1016/j.cels.2020.07.003

Soldatow, V. Y., Lecluyse, E. L., Griffith, L. G., and Rusyn, I. (2013). In vitro models for liver toxicity testing. *Toxicol. Res.* 2, 23–39. doi: 10.1039/c2tx20051a

Songyang, R., Irudayam, J., Contrearas, D., Sareen, D., Talavera-Adame, D., Svendsen, C. N., et al. (2015). Bioartificial liver device based on induced pluripotent stem cell-derived hepatocytes. *J. Stem Cell Res. Ther.* 5, 1–9. doi: 10.4172/2157-7633.1000263

Sosa-Hernández, J. E., Villalba-Rodríguez, A. M., Romero-Castillo, K. D., Aguilar-Aguila-Isaías, M. A., García-Reyes, I. E., Hernández-Antonio, A., et al. (2018). Organs-on-a-chip module: a review from the development and applications perspective. *Micromachines* 9:536. doi: 10.3390/mi9100536

Stefan, D., and Hamilton, J. P. (2010). Drug-induced liver injury. *US Gastroenterol. Hepatol. Rev.* 6, 73–80.

Stevens, J. L., and Baker, T. K. (2009). The future of drug safety testing: expanding the view and narrowing the focus. *Drug Discov. Today* 14, 162–167. doi: 10.1016/j.drudis.2008.11.009

Subramanian, K., Owens, D. J., O'Brien, T. D., Verfaillie, C. M., and Hu, W. S. (2011). Enhanced differentiation of adult bone marrow-derived stem cells to liver lineage in aggregate culture. *Tissue Eng. Part A* 17, 2331–2341. doi: 10.1089/ten.tea.2010.0667

Syed, M., Skonberg, C., and Hansen, S. H. (2016). Mitochondrial toxicity of diclofenac and its metabolites via inhibition of oxidative phosphorylation (ATP synthesis) in rat liver mitochondria: possible role in drug induced liver injury (DILI). *Toxicol. Vitr.* 31, 93–102. doi: 10.1016/j.tiv.2015.11.020

Szkolnicka, D., Farnworth, S. L., Lucendo-Villarin, B., Storck, C., Zhou, W., Iredale, J. P., et al. (2014). Accurate prediction of drug-induced liver injury using stem cell-derived populations. *Stem Cells Transl. Med.* 3, 141–148. doi: 10.5966/sctm.2013-0146

Takahashi, Y., Hori, Y., Yamamoto, T., Urashima, T., Ohara, Y., and Tanaka, H. (2015). 3D spheroid cultures improve the metabolic gene expression profiles of HepaRG cells. *Biosci. Rep.* 35, 1–7. doi: 10.1042/BSR20150034

Takayama, K., Kawabata, K., Nagamoto, Y., Kishimoto, K., Tashiro, K., Sakurai, F., et al. (2013). 3D spheroid culture of hESC/hiPSC-derived hepatocyte-like cells for drug toxicity testing. *Biomaterials* 34, 1781–1789. doi: 10.1016/j.biomaterials.2012.11.029

Takayama, K., Morisaki, Y., Kuno, S., Nagamoto, Y., Harada, K., Furukawa, N., et al. (2014). Prediction of interindividual differences in hepatic functions and drug sensitivity by using human iPS-derived hepatocytes. *Proc. Natl. Acad. Sci. U.S.A.* 111, 16772–16777. doi: 10.1073/pnas.1413481111

Takebe, T., Sekine, K., Kimura, M., Yoshizawa, E., Ayano, S., Koido, M., et al. (2017). Massive and reproducible production of liver buds entirely from human pluripotent stem cells. *Cell Rep.* 21, 2661–2670. doi: 10.1016/j.celrep.2017.11.005

Tamay, D. G., Usal, T. D., Alagoz, A. S., and Yucel, D. (2019). 3D and 4D printing of polymers for tissue engineering applications. *Front. Bioeng. Biotechnol.* 7:164. doi: 10.3389/fbioe.2019.00164

Tasnim, F., Phan, D., Toh, Y. C., and Yu, H. (2015). Cost-effective differentiation of hepatocyte-like cells from human pluripotent stem cells using small molecules. *Biomaterials* 70, 115–125. doi: 10.1016/j.biomaterials.2015.08.002

Tasnim, F., Toh, Y. C., Qu, Y., Li, H., Phan, D., Narmada, B. C., et al. (2016). Functionally enhanced human stem cell derived hepatocytes in galactosylated cellulosic sponges for hepatotoxicity testing. *Mol. Pharm.* 13, 1947–1957. doi: 10.1021/acs.molpharmaceut.6b00119

Tasnim, F., Xing, J., Huang, X., Mo, S., Wei, X., Tan, M. H., et al. (2019). Generation of mature kupffer cells from human induced pluripotent stem cells. *Biomaterials* 192, 377–391. doi: 10.1016/j.biomaterials.2018.11.016

Tibbitt, M. W., and Anseth, K. S. (2009). Hydrogels as extracellular matrix mimics for 3D cell culture. *Biotechnol. Bioeng.* 103, 655–663. doi: 10.1002/bit.22361

Tolosa, L., Jiménez, N., Pérez, G., Castell, J. V., Gómez-Lechón, M. J., and Donato, M. T. (2018). Customised in vitro model to detect human metabolism-dependent idiosyncratic drug-induced liver injury. *Arch. Toxicol.* 92, 383–399. doi: 10.1007/s00204-017-2036-4

Tomlinson, L., Hyndman, L., Firman, J. W., Bentley, R., Kyffin, J. A., Webb, S. D., et al. (2019). In vitro liver zonation of primary rat hepatocytes. *Front. Bioeng. Biotechnol.* 7:17. doi: 10.3389/fbioe.2019.00017

Tostoes, R. M., Leite, S. B., Miranda, J. P., Sousa, M., Wang, D. I. C., Carrondo, M. J. T., et al. (2011). Perfusion of 3D encapsulated hepatocytes-a synergistic effect enhancing long-term functionality in bioreactors. *Biotechnol. Bioeng.* 108, 41–49. doi: 10.1002/bit.22920

Tostoes, R. M., Leite, S. B., Serra, M., Jensen, J., Bjorquist, P., Carrondo, M. J., et al. (2012). Human liver cell spheroids in extended perfusion bioreactor culture for repeated-dose drug testing. *Hepatology* 55, 1227–1236. doi: 10.1002/hep.24760

Trask, O. J., Moore, A., and Lecluyse, E. L. (2014). A micropatterned hepatocyte coculture model for assessment of liver toxicity using high-content imaging analysis. *Assay Drug Dev. Technol.* 12, 16–27. doi: 10.1089/adt.2013.525

Treyer, A., and Müsch, A. (2013). Hepatocyte polarity. *Compr. Physiol.* 3, 243–287. doi: 10.1002/cphy.c120009

Tripathi, A., and Melo, J. S. (2015). Preparation of a sponge-like biocomposite agarose-chitosan scaffold with primary hepatocytes for establishing an in vitro 3D liver tissue model. *RSC Adv.* 5, 30701–30710. doi: 10.1039/c5ra04153h

Tsamandouras, N., Kostrzewski, T., Stokes, C. L., Griffith, L. G., Hughes, D. J., and Cirit, M. (2017). Quantitative assessment of population variability in hepatic drug metabolism using a perfused three-dimensional human liver microphysiological system. *J. Pharmacol. Exp. Ther.* 360, 95–105. doi: 10.1124/jpet.116.237495

Tuschl, G., Hrach, J., Walter, Y., Hewitt, P. G., and Mueller, S. O. (2009). Serum-free collagen sandwich cultures of adult rat hepatocytes maintain liver-like properties long term: a valuable model for in vitro toxicity and drug-drug interaction studies. *Chem. Biol. Interact.* 181, 124–137. doi: 10.1016/j.cbi.2009.05.015

Umehara, K. I., and Camenisch, G. (2012). Novel in vitro-in vivo extrapolation (IVIVE) method to predict hepatic organ clearance in rat. *Pharm. Res.* 29, 603–617. doi: 10.1007/s11095-011-0607-2

van Tonder, J. J., Steenkamp, V., and Gulumi, M. (2013). "Pre-clinical assessment of the potential intrinsic hepatotoxicity of candidate drugs," in *New Insights into Toxicity and Drug Testing*, ed. S. Gowder (IntechOpen). doi: 10.5772/54792

Vernetti, L. A., Vogt, A., Gough, A., and Taylor, D. L. (2017). Evolution of experimental models of the liver to predict human drug hepatotoxicity and efficacy. *Clin. Liver Dis.* 21, 197–214. doi: 10.1016/j.cld.2016.08.013

Vinci, B., Duret, C., Klieber, S., Gerbal-Chaloin, S., Sa-Cunha, A., Laporte, S., et al. (2011). Modular bioreactor for primary human hepatocyte culture: medium flow stimulates expression and activity of detoxification genes. *Biotechnol. J.* 6, 554–564. doi: 10.1002/biot.201000326

Vinken, M., and Hengstler, J. G. (2018). Characterization of hepatocyte-based in vitro systems for reliable toxicity testing. *Arch. Toxicol.* 92, 2981–2986. doi: 10.1007/s00204-018-2297-6

Vivares, A., Salle-Lefort, S., Arabeyre-Fabre, C., Ngo, R., Penarier, G., Bremond, M., et al. (2015). Morphological behaviour and metabolic capacity of cryopreserved human primary hepatocytes cultivated in a perfused multiwell device. *Xenobiotica* 45, 29–44. doi: 10.3109/00498254.2014.944612

Vorrink, S. U., Ullah, S., Schmidt, S., Nandania, J., Velagapudi, V., Beck, O., et al. (2017). Endogenous and xenobiotic metabolic stability of primary human hepatocytes in long-term 3D spheroid cultures revealed by a combination of targeted and untargeted metabolomics. *FASEB J.* 31, 2696–2708. doi: 10.1096/fj.201601375R

Vorrink, S. U., Zhou, Y., Ingelman-Sundberg, M., and Lauschke, V. M. (2018). Prediction of drug-induced hepatotoxicity using long-term stable primary hepatic 3D spheroid cultures in chemically defined conditions. *Toxicol. Sci.* 163, 655–665. doi: 10.1093/toxsci/kfy058

Walker, P. A., Ryder, S., Lavado, A., Dilworth, C., and Riley, R. J. (2020). The evolution of strategies to minimise the risk of human drug-induced liver injury (DILI) in drug discovery and development. *Arch. Toxicol.* 94, 2559–2585. doi: 10.1007/s00204-020-02763-w

Wang, B., Zhao, L., Fish, M., Logan, C. Y., and Nusse, R. (2015). Self-renewing diploid Axin2+ cells fuel homeostatic renewal of the liver. *Nature* 524, 180–185. doi: 10.1038/nature14863

Wang, K., Shindoh, H., Inoue, T., and Horii, I. (2002). Advantages of in vitro cytotoxicity testing by using primary rat hepatocytes in comparison with established cell lines. *J. Toxicol. Sci.* 27, 229–237. doi: 10.2131/jts.27.229

Wang, S., Wang, X., Tan, Z., Su, Y., Liu, J., Chang, M., et al. (2019). Human ESC-derived expandable hepatic organoids enable therapeutic liver repopulation and pathophysiological modeling of alcoholic liver injury. *Cell Res.* 29, 1009–1026. doi: 10.1038/s41422-019-0242-8

Wang, W. W. W., Khetani, S. R., Krzyzewski, S., Duignan, D. B., and Obach, R. S. (2010). Assessment of a micropatterned hepatocyte coculture system to generate major human excretory and circulating drug metabolites. *Drug Metab. Dispos.* 38, 1900–1905.

Wang, Y. I., Carmona, C., Hickman, J. J., and Shuler, M. L. (2018). Multiorgan microphysiological systems for drug development: strategies, advances, and challenges. *Adv. Healthc. Mater.* 7:201701000. doi: 10.1002/adhm.201701000

Wang, Z., Li, W., Jing, H., Ding, M., Fu, G., Yuan, T., et al. (2019). Generation of hepatic spheroids using human hepatocyte-derived liver progenitor-like cells for hepatotoxicity screening. *Theranostics* 9, 6690–6705. doi: 10.7150/thno.34520

Werner, A., Duvar, S., Müthing, J., Büntemeyer, H., Lünsdorf, H., Strauss, M., et al. (2000). Cultivation of immortalized human hepatocytes HepZ on macroporous CultiSpher G microcarriers. *Biotechnol. Bioeng.* 68, 59–70.

Westerink, W. M. A., and Schoonen, W. G. E. J. (2007a). Cytochrome P450 enzyme levels in HepG2 cells and cryopreserved primary human hepatocytes and their induction in HepG2 cells. *Toxicol. Vitr.* 21, 1581–1591. doi: 10.1016/j.tiv.2007.05.014

Westerink, W. M. A., and Schoonen, W. G. E. J. (2007b). Phase II enzyme levels in HepG2 cells and cryopreserved primary human hepatocytes and their induction in HepG2 cells. *Toxicol. Vitr.* 21, 592–602. doi: 10.1016/j.tiv.2007.06.017

Wienkers, L. C., and Heath, T. G. (2005). Predicting in vivo drug interactions from in vitro drug discovery data. *Nat. Rev. Drug Discov.* 4, 825–833. doi: 10.1038/nrd1851

Wikswo, J. P. (2014). The relevance and potential roles of microphysiological systems in biology and medicine. *Exp. Biol. Med.* 239, 1061–1072. doi: 10.1177/1535370214542068

Williams, D. P., Lazic, S. E., Foster, A. J., Semenova, E., and Morgan, P. (2020). Predicting drug-induced liver injury with bayesian machine learning. *Chem. Res. Toxicol.* 33, 239–248. doi: 10.1021/acs.chemrestox.9b00264

Wolverton, S. E., and Wu, J. J. (2020). *Comprehensive Dermatologic Drug Therapy*, 4th Edn. Cham: Springer.

Woolbright, B. L., and Jaeschke, H. (2018). Mechanisms of inflammatory liver injury and drug-induced hepatotoxicity. *Curr. Pharmacol. Rep.* 4, 346–357. doi: 10.1007/s40495-018-0147-0

Wooten, J. M. (2015). Rules for improving pharmacotherapy in older adult patients: part 2 (Rules 6-10). *S. Med. J.* 108, 97–104. doi: 10.14423/SMJ.0000000000000243

Wouters, O. J., McKee, M., and Luyten, J. (2020). Estimated research and development investment needed to bring a new medicine to market, 2009-2018. *JAMA J. Am. Med. Assoc.* 323, 844–853. doi: 10.1001/jama.2020.1166

Wrzesinski, K., Rogowska-Wrzesinska, A., Kanlaya, R., Borkowski, K., Schwämmle, V., Dai, J., et al. (2014). The cultural divide: exponential growth in classical 2D and metabolic equilibrium in 3D environments. *PLoS One* 9:e0106973. doi: 10.1371/journal.pone.0106973

Xu, J., Ma, M., and Purcell, W. M. (2003). Characterisation of some cytotoxic endpoints using rat liver and HepG2 spheroids as in vitro models and their application in hepatotoxicity studies. II. Spheroid cell spreading inhibition as a new cytotoxic marker. *Toxicol. Appl. Pharmacol.* 189, 112–119. doi: 10.1016/S0041-008X(03)00090-5

Xu, J. J., Diaz, D., and O'Brien, P. J. (2004). Applications of cytotoxicity assays and pre-lethal mechanistic assays for assessment of human hepatotoxicity potential. *Chem. Biol. Interact.* 150, 115–128. doi: 10.1016/j.cbi.2004.09.011

Xu, J. J., Henstock, P. V., Dunn, M. C., Smith, A. R., Chabot, J. R., and de Graaf, D. (2008). Cellular imaging predictions of clinical drug-induced liver injury. *Toxicol. Sci.* 105, 97–105. doi: 10.1093/toxsci/kfn109

Xu, S., Chen, Y., Ma, Y., Liu, T., Zhao, M., Wang, Z., et al. (2019). Lipidomic profiling reveals disruption of lipid metabolism in valproic acid-induced hepatotoxicity. *Pharmacology* 10:819. doi: 10.3389/fphar.2019.00819

Yamashita, T., Takayama, K., Sakurai, F., and Mizuguchi, H. (2018). Billion-scale production of hepatocyte-like cells from human induced pluripotent stem cells. *Biochem. Biophys. Res. Commun.* 496, 1269–1275. doi: 10.1016/j.bbrc.2018.01.186

Yang, B., Duan, W., Wei, L., Zhao, Y., Han, Z., Wang, J., et al. (2020). Bone marrow mesenchymal stem cell-derived hepatocyte-like cell exosomes reduce hepatic ischemia/reperfusion injury by enhancing autophagy. *Stem Cells Dev.* 29, 372–379. doi: 10.1089/scd.2019.0194

Yang, K., Guo, C., Woodhead, J. L., St Claire, R. L., Watkins, P. B., Siler, S. Q., et al. (2016). Sandwich-cultured hepatocytes as a tool to study drug disposition and drug-induced liver injury. *J. Pharm. Sci.* 105, 443–459. doi: 10.1016/j.xphs.2015.11.008

Yin, L., Zhu, Y., Yang, J., Ni, Y., Zhou, Z., Chen, Y., et al. (2015). Adipose tissue-derived mesenchymal stem cells differentiated into hepatocyte-like cells in vivo and in vitro. *Mol. Med. Rep.* 11, 1722–1732. doi: 10.3892/mmr.2014.2935

Yoshii, Y., Waki, A., Yoshida, K., Kakezuka, A., Kobayashi, M., Namiki, H., et al. (2011). The use of nanoimprinted scaffolds as 3D culture models to facilitate spontaneous tumor cell migration and well-regulated spheroid formation. *Biomaterials* 32, 6052–6058. doi: 10.1016/j.biomaterials.2011.04.076

Yu, C., Ma, X., Zhu, W., Wang, P., Miller, K. L., Stupin, J., et al. (2019). Scanningless and continuous 3D bioprinting of human tissues with decellularized extracellular matrix. *Biomaterials* 194, 1–13. doi: 10.1016/j.biomaterials.2018.12.009

Yu, F., Goh, Y. T., Li, H., Chakrapani, N. B., Ni, M., Xu, G. L., et al. (2020). A vascular-liver chip for sensitive detection of nutraceutical metabolites from human pluripotent stem cell derivatives. *Biomicrofluidics* 14:034108. doi: 10.1063/5.0004286

Yu, K. N., Nadanaciva, S., Rana, P., Lee, D. W., Ku, B., Roth, A. D., et al. (2018). Prediction of metabolism-induced hepatotoxicity on three-dimensional hepatic cell culture and enzyme microarrays. *Arch. Toxicol.* 92, 1925–1310. doi: 10.1007/s00204-017-2126-3

Yu, Y. B., Song, Y., Chen, Y., Zhang, F., and Qi, F. Z. (2018). Differentiation of umbilical cord mesenchymal stem cells into hepatocytes in comparison with bone marrow mesenchymal stem cells. *Mol. Med. Rep.* 18, 2009–2016. doi: 10.3892/mmr.2018.9181

Yuan, L., and Kaplowitz, N. (2013). Mechanisms of drug-induced liver injury. *Clin. Liver Dis.* 17, 507–518. doi: 10.1016/j.cld.2013.07.002

Zanger, U. M., Klein, K., Saussele, T., Blievernicht, J., Hofmann, M. H., and Schwab, M. (2007). Polymorphic CYP2B6: molecular mechanisms and emerging clinical significance. *Pharmacogenomics* 8, 743–759. doi: 10.2217/14622416.8.7.743

Zeigerer, A., Wuttke, A., Marsico, G., Seifert, S., Kalaidzidis, Y., and Zerial, M. (2017). Functional properties of hepatocytes in vitro are correlated with cell polarity maintenance. *Exp. Cell Res.* 350, 242–252. doi: 10.1016/j.yexcr.2016.11.027

Zeilinger, K., Freyer, N., Damm, G., Seehofer, D., and Knöspel, F. (2016). Cell sources for in vitro human liver cell culture models. *Exp. Biol. Med.* 241, 1684–1698. doi: 10.1177/1535370216657448

Zeilinger, K., Schreiter, T., Darnell, M., Söderdahl, T., Lübberstedt, M., Dillner, B., et al. (2011). Scaling down of a clinical three-dimensional perfusion multicompartment hollow fiber liver bioreactor developed for extracorporeal liver support to an analytical scale device useful for hepatic pharmacological in vitro studies. *Tissue Eng. Part C Methods* 17, 549–556. doi: 10.1089/ten.tec.2010.0580

Zhang, C., Zhang, Q., Li, J., Yu, L., Li, F., Li, W., et al. (2020). Integration of in vitro data from three dimensionally cultured HepaRG cells and physiologically based pharmacokinetic modeling for assessment of acetaminophen hepatotoxicity. *Regul. Toxicol. Pharmacol.* 114:104661. doi: 10.1016/j.yrtph.2020.104661

Zhang, C. Y., Yuan, W. G., He, P., Lei, J. H., and Wang, C. X. (2016). Liver fibrosis and hepatic stellate cells: etiology, pathological hallmarks and therapeutic targets. *World J. Gastroenterol.* 22, 10512–10522. doi: 10.3748/wjg.v22.i48.10512

Zhang, S., Tong, W., Zheng, B., Susanto, T. A. K., Xia, L., Zhang, C., et al. (2011). A robust high-throughput sandwich cell-based drug screening platform. *Biomaterials* 32, 1229–1241. doi: 10.1016/j.biomaterials.2010.09.064

Zhang, X., Jiang, T., Chen, D., Wang, Q., and Zhang, L. W. (2020). Three-dimensional liver models: state of the art and their application for hepatotoxicity evaluation. *Crit. Rev. Toxicol.* 50, 279–309. doi: 10.1080/10408444.2020.1756219

Zhang, Y. N., Lie, P. C., and Wei, X. (2009). Differentiation of mesenchymal stromal cells derived from umbilical cord Wharton's jelly into hepatocyte-like cells. *Cytotherapy* 11, 548–558. doi: 10.1080/14653240903051533

Zhao, Q., Ren, H., Li, X., Chen, Z., Zhang, X., Gong, W., et al. (2009). Differentiation of human umbilical cord mesenchymal stromal cells into low immunogenic hepatocyte-like cells. *Cytotherapy* 11, 414–426. doi: 10.1080/14653240902849754

Zhou, Q., Patel, D., Kwa, T., Haque, A., Matharu, Z., Stybayeva, G., et al. (2015). Liver injury-on-a-chip: microfluidic co-cultures with integrated biosensors for monitoring liver cell signaling during injury. *Lab Chip* 15, 4467–4478. doi: 10.1039/c5lc00874c

Zhou, R., Li, Z., He, C., Li, R., Xia, H., Li, C., et al. (2014). Human umbilical cord mesenchymal stem cells and derived hepatocyte-like cells exhibit similar therapeutic effects on an acute liver failure mouse model. *PLoS One* 9:e0104392. doi: 10.1371/journal.pone.0104392

Conflict of Interest: The authors declare that the research was conducted in the absence of any commercial or financial relationships that could be construed as a potential conflict of interest.

frontiers in Cell and Developmental Biology

ORIGINAL RESEARCH
published: 22 March 2021
doi: 10.3389/fcell.2021.555248

Evaluation of the *ex vivo* Effects of Tamoxifen on Adipose-Derived Stem Cells: A Pilot Study

Ilena Boemi[1,2†], Andrea Vittorio Emanuele Lisa[3,4†], Eleonora Vitali[1], Nurçin Liman[1], Andrea Battistini[3,4], Federico Barbera[3,4], Luca Maione[3,4,5], Valeriano Vinci[3,4], Marco Ettore Attilio Klinger[3,4] and Andrea Gerardo Antonio Lania[1,6]*

[1] Laboratory of Cellular and Molecular Endocrinology, Humanitas Clinical and Research Center, Istituto di Ricovero e Cura a Carattere Scientifico (IRCCS), Rozzano, Italy, [2] Department of Medical Biotechnology and Translational Medicine BIOMETRA, University of Milan, Milan, Italy, [3] Department of Medical Biotechnology and Translational Medicine BIOMETRA, Reconstructive and Aesthetic Plastic Surgery School, University of Milan, Milan, Italy, [4] Plastic Surgery Unit, Humanitas Clinical and Research Center, Istituto di Ricovero e Cura a Carattere Scientifico (IRCCS), Rozzano, Italy, [5] Plastic Surgery Unit, Clinica San Carlo, Paderno Dugnano, Italy, [6] Department of Biomedical Sciences, Humanitas University, Pieve Emanuele, Italy

OPEN ACCESS

Edited by:
Joana Paiva Miranda,
University of Lisbon, Portugal

Reviewed by:
Toshiaki Saeki,
Saitama Medical University International Medical Center, Japan
Ana Sofia Fernandes,
Universidade Lusófona Research Center for Biosciences and Health Technologies, Portugal

***Correspondence:**
Ilena Boemi
ilena.boemi@gmail.com

† These authors have contributed equally to this work

Specialty section:
This article was submitted to Stem Cell Research, a section of the journal Frontiers in Cell and Developmental Biology

Received: 24 April 2020
Accepted: 23 February 2021
Published: 22 March 2021

Citation:
Boemi I, Lisa AVE, Vitali E, Liman N, Battistini A, Barbera F, Maione L, Vinci V, Klinger MEA and Lania AGA (2021) Evaluation of the ex vivo Effects of Tamoxifen on Adipose-Derived Stem Cells: A Pilot Study. Front. Cell Dev. Biol. 9:555248. doi: 10.3389/fcell.2021.555248

Autologous fat grafting (AFG) is a safe and minimally invasive procedure to correct soft tissue defects. The benefit of AFG is attributed to adipose-derived stem cells (ASCs) in fat tissue graft. This technique is useful also in patients undergoing reconstructive surgery following quadrantectomy for breast cancer. However, these patients are frequently treated with tamoxifen. We evaluated the *ex vivo* effects of tamoxifen on ASCs to understand if cellular functions of ASCs are affected. We selected 24 female patients; 10 of which were breast cancer patients treated with quadrantectomy and tamoxifen. As control group, we selected 14 healthy female subjects (9 premenopausal and 5 menopausal). We found that tamoxifen has no effect on cellular proliferation, VEGF secretion or apoptosis of ASCs. The gene expression assessment demonstrated no impairment in differentiation capacity of ASCs. Our results showed that tamoxifen has no effect on cellular functions of ASCs for the first time in an *ex vivo* single-center study.

Keywords: adipose-derived stem cells, cell therapies, tamoxifen, autologous fat grafting, breast cancer

INTRODUCTION

Autologous fat grafting (AFG), also called fat transplantation or lipofilling, is a safe and minimally invasive surgical procedure to correct soft tissue defects in reconstructive surgery (Pearl et al., 2012). In women, among cancers, the most frequently diagnosed is breast cancer. Breast cancer is also the leading cause of death from cancer in women worldwide (Tao et al., 2015). It is common medical practice to surgically remove primary tumor mass in breast cancer patients and consequently, there is a population of women in need of reconstructive surgery following the tumor excision. So, AFG can be applied first and foremost in breast reconstruction following breast conserving surgery (BCS) of breast cancer patients, providing a remarkable solution to common sequelae of BCS such as post-surgical local deformities and pain syndromes (Caviggioli et al., 2011, 2016; Maione et al., 2014). It can also be used as an alternative therapy in radiotherapy-induced dystrophic tissues (Rigotti et al., 2007), chronic ulcers, scar tissues (Klinger et al., 2015), and degenerative diseases such as systemic sclerosis (Del Papa et al., 2015).

Adipose tissue, commonly known as fat, was initially considered solely as a simple storage organ of excess energy, thermal insulation, and mechanical cushion. It is indeed a metabolically dynamic organ functioning as the primary site of excess energy storage as well as an endocrine organ synthesizing various biologically active compounds. More importantly regarding its application in reconstructive medicine, autologous adipose tissue is biocompatible. The surgical techniques of AFG have changed within the last few years. In the past, it had limited benefits due to the free transfer of intact adipose tissue. More specifically, the technique is based on free composite fat-cell transplantation strategies (Simonacci et al., 2016). Indeed, given the high incidence of breast cancer in women, new techniques for post-surgical breast reconstruction continuously develop, such as the cell-assisted lipotransfer (CAL). CAL consist of transplanting fat with adipose-derived stem cells (Matsumoto et al., 2006). Human adipose-derived stem cells are multipotent mesenchymal stem cells, and they are one of the components of the stromal vascular fraction (SVF) of adipose tissue (Simonacci et al., 2017). The stromal vascular fraction is formed by multiple cell types, including circulating blood cells, fibroblasts, pericytes, endothelial cells, and adipose-derived stem cells (Gir et al., 2012). ASCs, present in the SVF, have been shown to be metabolically active, secreting angiogenic factors such as vascular endothelial growth factor (VEGF) and differentiating into a wide range of cell types in all three embryonic cell lineages. Within the mesodermal lineage, ASCs can differentiate into chondrocytes, myocytes and osteoblasts, whereas only neurogenic differentiation of ASCs has been observed within the ectodermal lineage (Mizuno and Hyakusoku, 2010; Yu et al., 2011; Jung Ho and Yoon, 2019). Current literature also describes hepatic and pancreatic differentiation capacity of ASCs, therefore completing the trigerminal lineage potential (Frese et al., 2016). Consequently, AFG is now a common practice following surgery of breast cancer patients who are frequently under hormone therapy such as tamoxifen prior to surgery (Caviggioli et al., 2011; Maione et al., 2014; Stark et al., 2018).

Tamoxifen (TAM) is a synthetic non-steroidal anti-estrogen that is the hormone therapy of choice in estrogen receptor positive breast cancer pre-menopausal patients (Osborne, 1998). Its anti-estrogenic effect in target tissues (e.g., mammary and adipose tissues) stems from competitive binding to estrogen receptors. Tamoxifen is recommended as a long-term prophylaxis for patients at high risk for developing breast cancer based on reduced recurrence rates (Cuzick et al., 2007). It is also used for the treatment of invasive breast cancer before and/or after surgery, for preventing invasive breast cancer in women at high risk for developing breast cancer, and lastly for post-operative medical management of ductal carcinoma *in situ* (DCIS) (Early Breast Cancer Trialists' Collaborative Group [EBCTCG], 2011).

However, in 2015 Pike et al. concluded that *in vitro* exposure to tamoxifen has cytotoxic effects on ASCs in terms of increased apoptosis and inhibition of proliferation as well as reduction of multipotent differentiation capacity in a dose and time dependent manner (Pike et al., 2015). A systematic review of patient factors affecting ASC viability indicated a reduction of proliferation and differentiation potential of ASCs with increasing age, body mass index, diabetes mellitus and exposure to radiotherapy and tamoxifen; although, the latter was not uniformly seen across all studies (Varghese et al., 2017). Moreover, in some human and animal models tamoxifen has been shown to inhibit proliferation of endothelial cell lines and decrease VEGF production (Blackwell et al., 2000; McNamara et al., 2001). On the other hand, concerning the unpredictable and relatively high rates of fat graft resorption in AFG, recent clinical observations suggest that tamoxifen exposure reduces resorption and fibrosis rates of injected fat grafts, resulting in a better integration of autologous fat grafts (Silva et al., 2018).

AFG following hormone therapy in breast cancer patients is increasingly used, however in literature there is not yet a clear understanding about this procedure in TAM treated patients. The aim of this study is to investigate the *ex vivo* effects of tamoxifen on ASCs obtained from ER-positive breast cancer patients and to compare the cellular functions of ASCs obtained from TAM treated patients with that of control group subjects. In further detail, ASCs extracted from SVF of liposuctioned adipose tissue of breast cancer patients previously treated with tamoxifen have been examined in terms of proliferation, apoptosis, VEGF secretion and multipotent differentiation capacity, and compared with that of control group subjects. Our results showed that tamoxifen has no effect on cellular functions of adipose-derived stem cells and suggested that even in patients with breast cancer, treated with tamoxifen, AFG can be remarkable solution to common sequelae of BCS.

MATERIALS AND METHODS

Patients Selection

The study was approved by the Ethical Committee of Humanitas Research Hospital (study number: 1960, ID of the experimentation: 545, authorization date: 08-03-2018). Informed consent was obtained from all patients involved in the study. The research was carried out according to The Code of Ethics of the World Medical Association (Declaration of Helsinki).

For this study we selected a total of 24 female patients; 10 of which were pre-menopausal ER positive breast cancer patients treated with tamoxifen (20 mg per day for at least 6 months). As the control group, we selected 14 healthy females, 9 pre-menopausal and 5 menopausal subjects. The age of our patients ranged between 18 and 64 years and the mean age is of 42 years. In detail, the subjects enrolled in the study were divided into three groups. The first group was composed of women in daily treatment with tamoxifen (for at least 6 months) for oncological reasons suffering from post-mastectomy pain syndrome and needing autologous fat grafting. The tamoxifen dose was fixed at 20 mg/day and we included all the patients that were taken the drug with the fixed protocol. The second group was composed of fertile women presenting with retractile scars requiring autologous fat grafting (hormonal status was confirmed by FSH and LH blood test, subjects assuming hormones were excluded). The third group was composed of post-menopausal women (at least 1 year from the last menstruation) treated with autologous fat grafting for aesthetic purpose. All tamoxifen

treated subjects included in the study were compliant. In all the subjects enrolled in the study there were no co-morbidity, and they were not receiving other concomitant therapies. The exclusion criteria included: tobacco, pregnancy, body mass index (BMI) >25 or <19, and any other comorbidity. For each sample, fat tissue was drawn bilaterally from the flanks. Infiltration solution was made of saline and adrenaline (1 cc in 500 mL). No local anesthetic was used during the procedure. Procession is obtained through Coleman technique (centrifugation 3,000 rpm for 3 min). The adipose tissue of breast cancer patients was obtained while they were still continuing the tamoxifen therapy. The patients would take the treatment early in the morning and the adipose tissue collection was performed later in the day. Subjects enrolled in the study were not treated with antithrombotic DVT prophylaxis. **Supplementary Table S1** describes, in detail, participant information.

Isolation and Cell Culture

Adipose-derived stem cells (ASCs) were obtained from side lipoaspiration. Liposuctioned adipose tissue was washed with PBS (Sigma-Aldrich) and then digested with collagenase I (1 mg/ml) (Merck Millipore) for 1 h at 37°. After tissue centrifugation at 1,200 g for 10 min, cells were resuspended in 160 mM NH_4Cl to remove erythrocytes. ASCs were then cultured in phenol red free DMEM medium (Gibco) and supplemented with 10% FBS (Sigma-Aldrich), 100 U/ml penicillin (Lonza), 100 μg/ml streptomycin (Lonza) and 1 mM L-glutamine (Lonza). The cells were submitted for the experiment at passages 2–6.

HUVEC cells were kindly provided by Dr. Elisa Zaghi (Humanitas Clinical and Research Hospital, Rozzano, Italy). Cells were grown on plates coated with collagen (50 μg/ml) in EGM2 medium (Lonza) supplemented with 5% FBS. HUVECs that were ∼80% confluent were used for experiment.

Immunophenotype

Immunophenotype of ASCs was analyzed between passage 1–2 of culture. The cells were stained with the following fluorescent-conjugated antibodies: CD44FITC, CD90(Thy1)PE/Cy5, CD105PE/Cy7, CD73(Ecto-5′-nucleotidase)PerCP/Cy5.5, CD45PB, CD34APC/Cy7. All the antibodies were purchased from Biolegend. The samples were acquired using FACS SYMPHONY (BD Biosciences) and the results were analyzed using FACSDiva software (BD Biosciences). The gating strategy and the representative histograms of ASCs expression marker are shown in **Supplementary Figure S1**.

Proliferation Assay

Cells were plated in 96-well plates (15×10^3 cells/well) and after 4 and 8 days of culture cell proliferation was analyzed using the CyQUANT Cell Proliferation Assay Kit (Invitrogen) according to the manufacturer's protocol. The fluorescent intensity was read in a microplate reader with the appropriate filters.

Apoptosis Assay

Detection of apoptosis was performed using FITC Annexin V Apoptosis Detection Kit with 7-AAD (#640922, Biolegend), according to the manufacturer's protocol. After 48 h of culture cells were double-stained with the Fluorochrome-labeled Annexin V and the fluorescent 7-AAD dye for 15 min at room temperature in the dark. The percentage of apoptotic cells was determined by flow cytometry using FACS SYMPHONY (BD Biosciences). The results were analyzed using FACSDiva software (BD Biosciences).

Multilineage Differentiation

For adipogenic differentiation, ASCs were cultured in adipogenic induction medium containing phenol red free DMEM medium (Gibco), supplemented with 10% FBS (Sigma-Aldrich), 100 U/ml penicillin (Lonza), 100 μg/ml streptomycin (Lonza), 1 mM L-glutamine (Lonza), 1 μM dexamethasone, 500 nM IBMX, 50 μM indomethacin and 10 μg/mL human insulin for 21 days. After 3 weeks cells were fixed and stained with fresh Oil Red-O solution (Sigma-Aldrich) to identify lipid droplets.

For osteogenic differentiation, ASCs were cultured in osteogenic induction medium containing phenol red free DMEM medium (Gibco), supplemented with 10% FBS (Sigma-Aldrich), 100 U/ml penicillin (Lonza), 100 μg/ml streptomycin (Lonza), 1 mM L-glutamine (Lonza), 50 μM ascorbic acid, 100 nM dexamethasone and 10 mM β-glycerophosphate for 21 days. After 3 weeks cell fixed and stained with Alizarin Red Staining Solution (Merck) to identify calcium deposits.

Images acquired with EVOS XL Imaging System (LifeTecnologies).

VEGF Secretion and Expression

To analyze VEGF-A secretion, ASCs were cultured for 4 and 8 days. At each time point the collected supernatants were used to measured human VEGF-A secretion with ELISA kit (Duo-Set ELISA, R&D Systems), according to manufacturer protocol. The absorbance was measured in a microplate reader at 450 nm. The experiment was performed in triplicate for each sample. To analyzed VEGF-A gene expression, ASC were cultured for 24 h and then harvested for RNA extraction. As controls we used HUVEC cells untreated or treated with 10 nM phorbol-12-myristate-13-acetate (PMA) (Sigma-Aldrich) for 24 h. Then HUVECs were harvested for RNA extraction.

Quantitative RT-PCR Analysis

Total RNA (200 ng) was extracted from cultured ASCs, for each sample, and HUVECs with SV Total RNA Isolation System (Promega) and converted to cDNA using GoTaq(R) 2-Step RT-qPCR System (Promega) according to the manufacturer protocol. mRNA levels were quantified with Viia7 (Applied Biosystems) using SYBR Green Real-Time PCR [GoTaq(R) 2-Step RT-qPCR System, Promega] according to manufacturer protocol. Glyceraldehyde 3-phosphate dehydrogenase (GAPDH) was used as internal control. Primers used to detect the specific genes are detailed in **Supplementary Table S2**.

Statistical Analysis

GraphPad Prism 7.0 was used to perform statistical analyses. Comparison among multiple groups were done with ANOVA

test and *post hoc* Bonferroni's correction, whereas comparisons between two groups were done with unpaired *t*-test. A value of $p < 0.05$ was considered statistically significant. All data are shown as mean ± S.E.M.

RESULTS

Tamoxifen Did Not Affect Proliferation of ASCs

In order to evaluate the *ex vivo* effects of tamoxifen we firstly assessed the ability to proliferate of ASCs. Prior to submit the cells for experiments, between passage 1–2, ASCs were checked for immunophenotype at FACS SYMPHONY (BD Biosciences) (**Supplementary Figure S1**). As shown in **Figure 1**. we evaluated cell proliferation at two different time point, day 4 and day 8 of culture, and we observed no difference between ASCs from pre- and menopausal patients compared to tamoxifen treated ones. This data suggest that tamoxifen didn't affect cell proliferation of *ex vivo* ASCs.

Tamoxifen Did Not Increase Apoptosis

To investigate the effect of tamoxifen on apoptosis of ASCs, cells from pre-, menopausal and tamoxifen treated patients were plated for 48 h and then apoptosis was analyzed by flow cytometry. As shown in **Figure 2**, tamoxifen did not increase the apoptosis of ASCs from treated patients compared to ASCs of control ones.

Effects of Tamoxifen on VEGF

We wanted to analyze the ability of ASCs from TAM-treated patients to secrete VEGF-A. ASCs form pre-, menopausal and tamoxifen patients were cultured for 4 and 8 days, then VEGF secretion was assessed on supernatant. As shown in **Figure 3**, there was no difference in the secretion of VEGF by tamoxifen group compare to control group, moreover ASCs from TAM-treated patients displayed the same trend of control ones. To confirm our data, we also performed qRT-PCR for the expression of VEGF-A (**Supplementary Figure S2**) and we used as controls

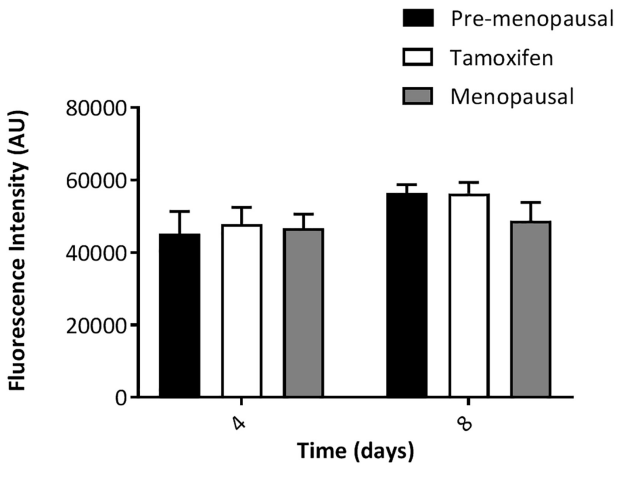

FIGURE 1 | *Ex vivo* effect of tamoxifen on ASCs proliferation. ASCs were left in culture for 4 or 8 days and then proliferation rate was evaluated. Data represent mean ± S.E.M. of three independent experiments each performed in triplicates.

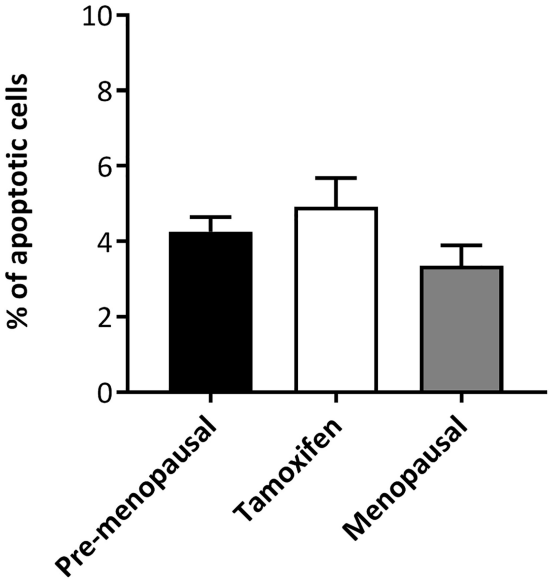

FIGURE 2 | *Ex vivo* effect of tamoxifen on apoptosis of ASCs. TAM did not significantly increased apoptosis of ASCs. Cells were plated for 48 h and then apoptosis was analyzed by flow cytometry, apoptotic cells were defined as Annexin V + 7-AAD-. Data represent mean ± S.E.M. of three independent experiments.

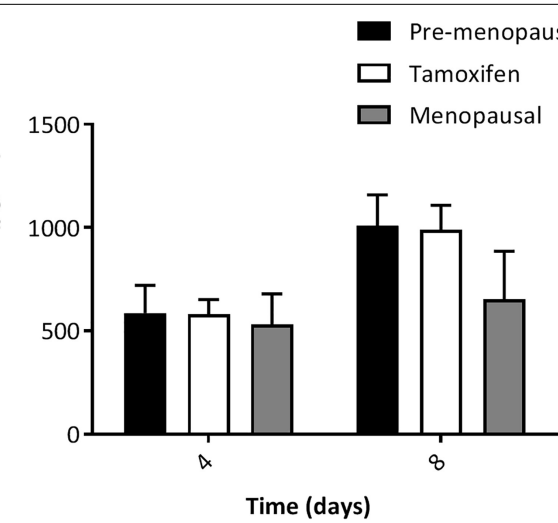

FIGURE 3 | VEGF-A secretion by ASCs. ELISA analysis of VEGF released (pg/ml) by ASCs at 4 and 8 days of culture. ASCs from TAM treated patients did not display lower secretion and at day 8 they were able to secret a higher amount of VEGF compared to day 4; same behavior observed as for ASCs from pre- and post- menopausal patients. Data represent mean ± S.E.M. of three independent experiments each performed in triplicates.

HUVEC cells and HUVEC cells treated for 24 h with PMA, that is known from the literature to increase VEGF expression. As shown by the real time analyses, there was no differences in the expression of VEGF by tamoxifen group compare to control group. Taken together our results indicate that tamoxifen didn't affect VEGF secretion and expression.

Effects of Tamoxifen on Multilineage Differentiation

We assessed the effects of tamoxifen on multilineage differentiation of ASCs after 21 days. As shown in **Figure 4A** ASC from pre-, post- menopausal and TAM treated patients exhibit capacity for osteogenic and adipogenic differentiation, when cultured with the specific induction media, and stained with Alizarin Red and Oil-O-Red, respectively. The quantification of Alizarin Red and Oil-O-Red staining highlight no differences in the ability of differentiate between the 3 groups (**Figure 4B**).

We performed also quantitative real-time RT-PCR for osteogenic and adipogenic marker, OST (Osteocalcin), ALP (Alkaline Phosphatase) and LEPTIN, FABP4 (Fatty Acid-Binding Protein 4) respectively. No significant alterations were founded in the expression of adipogenic marker between the 3 groups and moreover all ASC extracted from pre-, post- menopausal and TAM treated patients upregulate LEPTIN and FAPB4 after 21 days with the induction media compared to day 0, indicated that ASCs were able to differentiate into adipocytes (**Figures 5A,B**).

We assed also the osteogenic potential and as highlighted by qRT-PCR analysis; no differences were observed in ALP expression level and all the ASC had a higher expression at day 21 compared to day 0 (**Figure 6A**). OST analysis reveals that ASCs from TAM treated patients had a lower expression of this gene compared to pre-menopausal ASCs but not to post-menopausal ones. Despite this ASC extracted from pre, post- menopausal and TAM treated patients upregulate OST after 21 days with the induction media compared to day 0 (**Figure 6B**).

ASCs Expression of ERα and ERβ

ER presences in ASCs were evaluated using qRT-PCR. As shown in **Figures 7A,B**, both ER-α (ESR1) and ER-β (ESR2) were detected in human ASCs. Quantitative RT-PCR analysis reveals that ER-α levels in ASCs were higher than ER-β; moreover, despite no differences within the 3 groups in ER-β levels we observed that ASCs from pre-menopausal patients have a significantly high level of ER-α compare to the others two groups. No differences were observed in the levels of ER-α between ASC from TAM treated patients and post-menopausal one.

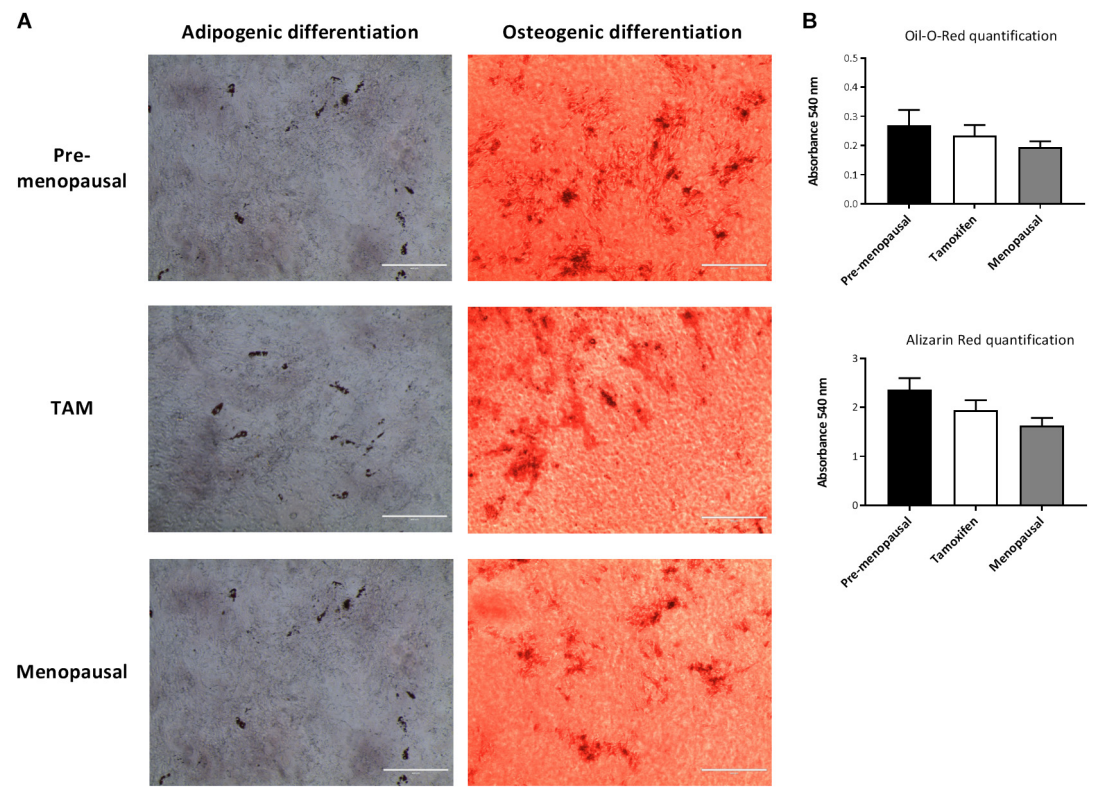

FIGURE 4 | Effects of tamoxifen on multilineage differentiation. ASCs were cultured for 3 weeks with appropriated induction media for adipogenic or osteogenic differentiation to assess the multilineage differentiation capabilities. **(A)** Representative images of Oil Red O (left panels) and Alizarin Red (right panels) staining of ASCs. Oli Red O stains intracellular lipids, while Alizarin Red stains calcified extracellular matrix. Scale bar: 400 μm. **(B)** Quantification of Oil Red O and Alizarin Red staining of ASCs shown no differences in multilineage differentiation capabilities between the three groups. Data represent mean ± S.E.M.

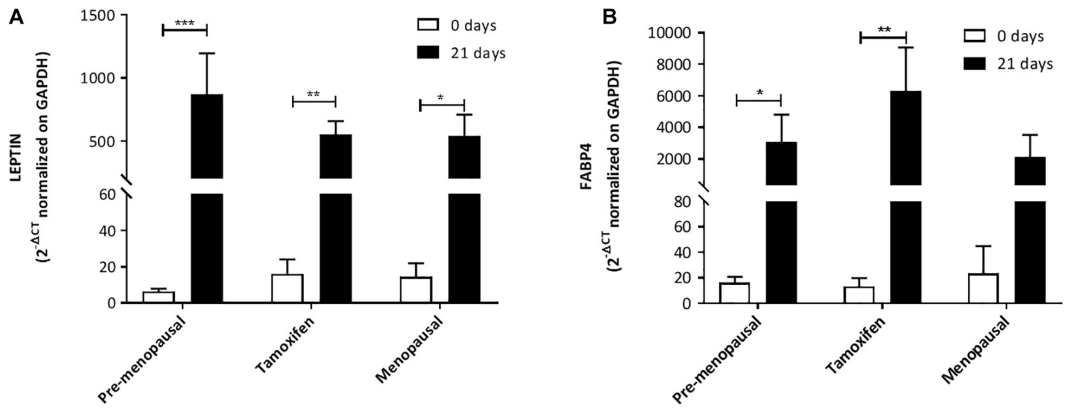

FIGURE 5 | Expression of adipogenic markers. Expression of adipogenic markers LEP **(A)** and FABP4 **(B)** mRNA levels from qRT-PCR analysis highlight that there is no significant alteration between the three groups. Moreover, the analysis confirmed that ASCs from all three groups are able to increase the expression of LEP and FABP4 after 21 days of culture with the induction media compared to day 0. Data in all graphs are presented as mean ± S.E.M. $^{*}p < 0.05$, $^{**}p < 0.01$, and $^{***}p < 0.001$.

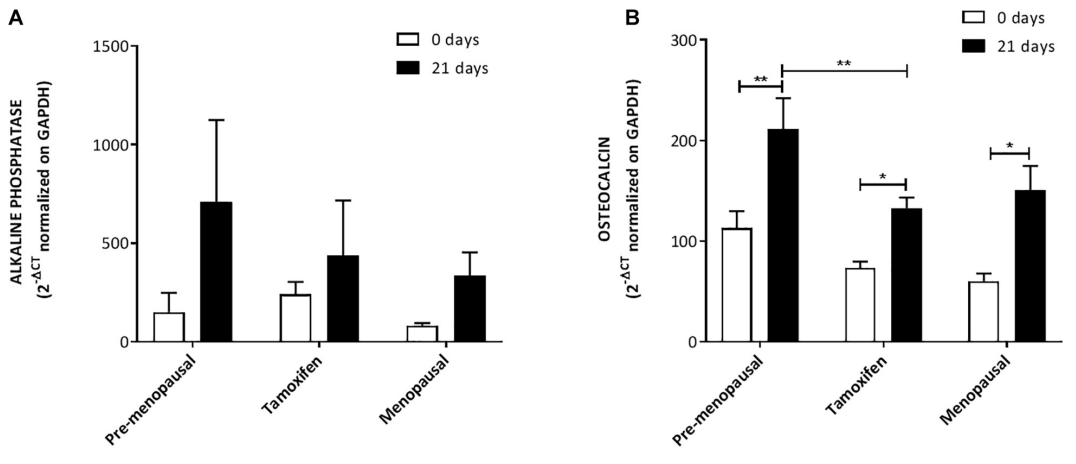

FIGURE 6 | Expression of osteogenic markers. Expression of osteogenic markers OST **(A)** and ALP **(B)** mRNA levels from qRT-PCR analysis. the analysis confirmed that ASCs from all three groups are able to increase the expression of ALP and OST after 21 days of culture with the induction media compared to day 0. Data in all graphs are presented as mean ± S.E.M. $^{*}p < 0.05$ and $^{**}p < 0.01$.

DISCUSSION

This study evaluated the *ex vivo* effects of tamoxifen treatment on adipose-derived stem cells. It aims to provide a further understanding of the impact of endocrine therapy adjuvant to surgical approaches in breast cancer patients, and more specifically of selective estrogen receptor modulators such as tamoxifen, on adipose-derived stem cells present in autologous fat grafts used for breast reconstruction. Our findings suggest that tamoxifen has no significant effect on the cellular functions of adipose-derived stem cells, justifying autologous fat grafting as the standard treatment for breast reconstruction in post-surgical breast cancer patients treated with tamoxifen.

Given the anti-apoptotic, angiogenic and anti-oxidant features of adipose-derived stem cells, autologous fat grafting enriched with adipose-derived stem cells has become the standard surgical practice (Serra-Renom et al., 2010; Sterodimas et al., 2010; Nie et al., 2011). Autologous fat grafting is a safe and minimally invasive surgical procedure to correct soft tissue defects in the field of reconstructive surgery (Pearl et al., 2012). The latter procedure is frequently performed in breast cancer patients after surgical removal of the mammary tumor mass (Caviggioli et al., 2011; Maione et al., 2014; Stark et al., 2018). It comprises of obtaining a fat graft from a donor site through liposuction and re-injecting it immediately into the region of interest through syringes. For more successful graft survival, these fat grafts can be augmented with adipose-derived stem cells. Most laboratories digest the lipoaspirate with collagenase following centrifugation to generate the stromal vascular fraction, which consists of multiple cell types including adipose-derived stem cells (Gir et al., 2012). However, most of these patients are treated with adjuvant endocrine therapy, tamoxifen being the first choice in premenopausal women (Osborne, 1998). In consideration of this concomitance, it is necessary to study the effects of

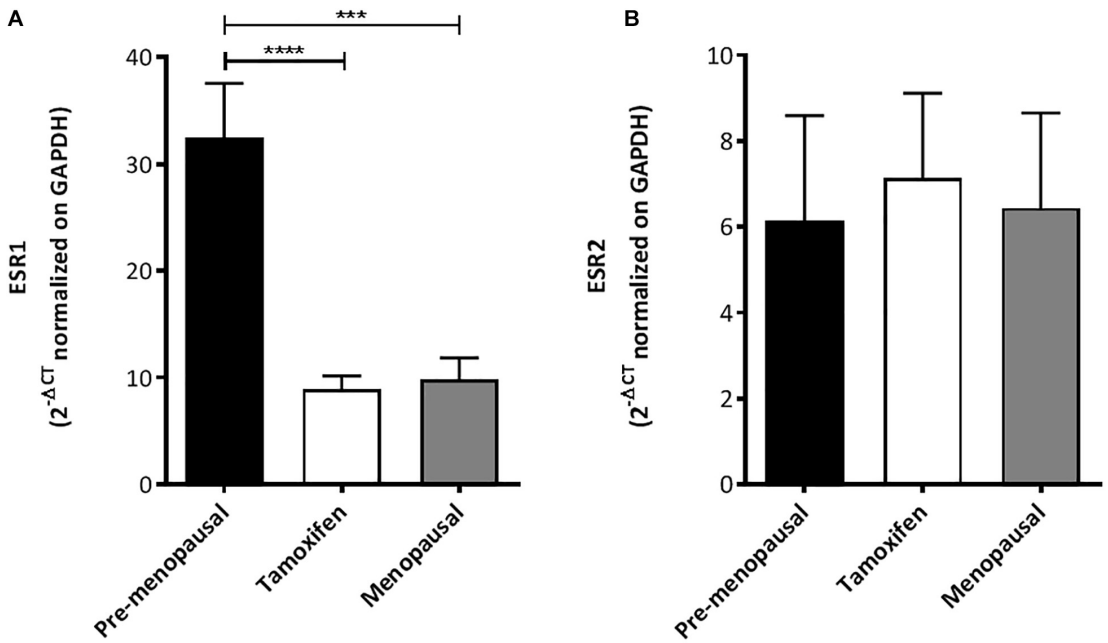

FIGURE 7 | Expression of estrogen receptor by ASCs. **(A)** qRT-PCR analysis for ESR1 (ER-α) shown that ASCs from pre-menopausal patients have a significantly high level of ER-α compare to the others two groups. **(B)** No differences were found in ESR2 (ER-β) mRNA levels within the three group as shown by qRT-PCR analysis. ***$p < 0.001$ and ****$p < 0.0001$.

tamoxifen on adipose-derived stem cells, present in the SVF, to further investigate its impact on autologous fat grafts used in breast reconstruction.

Tamoxifen is a non-steroidal selective estrogen receptor modulator (SERM) that inhibits the growth of breast cancer cells by competitive antagonism of the estrogen receptor (ER) (Osborne, 1998). The current literature on the impact of tamoxifen on adipose-derived stem cells commonly used to augment autologous fat grafts is limited. Pike and colleagues studied the impact of tamoxifen on adipose-derived stem cells in *in vitro* conditions and demonstrated that tamoxifen (at a concentration above 2 μM) has cytotoxic effects on adipose-derived stem cells in terms of apoptosis induction and proliferation inhibition. However, the cell cycle in adipose-derived stem cells was unchanged. In the same study, tamoxifen also appears to decrease the multipotent differentiation capacity of adipose-derived stem cells (Pike et al., 2015). These findings are in line with previous work in which it was shown that high concentrations of tamoxifen induce caspase dependent apoptosis (Mandlekar and Kong, 2001). Furthermore, *in vitro* cells are exposed to an entirely non-metabolized pharmacological compound, whereas *in vivo* cells are in contact with a pool of metabolites of the parent drug at diverse concentrations in relation to bioavailability and distribution. In this respect, the study conducted by Lien et al. showed how tamoxifen and its active metabolites are distributed in tissues from rat and human. In the rat, tamoxifen was present with the highest concentration in the lung and liver. In the other tissues, researchers found that the levels of TAM and its metabolites were 8- to 70-fold higher than in serum. Concentration fluctuations of tamoxifen and its metabolites were observed during one dosing interval in most tissues, except fat and testes, in which the drug concentrations were relatively stable. In the adipose tissue TAM active metabolites were present just in a tiny amount. Experiments were conducted also in human healthy and malignant tissues and the concentration of TAM and its active metabolites, present in these tissues, confirmed the conclusions drawn in the aforementioned experiments on rats. The concentration of tamoxifen was 10- to 60-fold higher in human tissues compared to serum, and, as seen in the rat, TAM was present with the highest level in the lung and liver. The greater quantity of the drug was retained by pancreas, pancreatic tumor, brain metastases from breast cancer and primary breast cancer. Concerning the active metabolites, their concentration was higher in most tissues, except fat.

Adipose tissue contained high concentration of the parent drug and low concentrations of its active metabolites (Lien et al., 1991). Our studies suggest that tamoxifen treatment does not significantly affect the proliferation capacity and apoptosis rates of *ex vivo* adipose-derived stem cells of patients subjected to prolonged treatment in comparison to that of control group composed of both pre-menopausal and menopausal women.

Angiogenesis is an important component in the fat graft survival due to the necessity of vascular supply to the newly implanted tissues (Nishimura et al., 2000). Volume reduction followed by failure of autologous fat grafts is an increasingly incident event in reconstructive surgeries. A novel technique to overcome this issue is augmenting the autologous fat grafts with adipose-derived stem cells innately present in the SVF of adipose tissues. The better preservation of fat tissue architecture

in autologous fat grafts enriched with adipose-derived stem cells (ASCs) is mainly attributed to the angiogenic properties of ASCs (Gentile et al., 2012). However, one of the target population for this procedure, namely breast cancer patients, are commonly treated with tamoxifen prior to autologous fat grafting. For this reason, it is imperative to investigate if tamoxifen has any influence on the angiogenesis of adipose-derived stem cells. In our study the angiogenesis of ASCs is quantitated in terms of vascular endothelial growth factor (VEGF-A) secretion and expression by the adipose-derived stem cells. Regarding the role of VEGF in wound healing, a study showed that during wound repair the expression of VEGF and its receptor increased, indicating a significant role for this mediator in wound angiogenesis (Frank et al., 1995). Besides angiogenesis, another study concluded that VEGF stimulates wound healing via multiple mechanisms including collagen deposition and epithelization (Bao et al., 2009). Therefore, VEGF secretion by adipose-derived stem cells is essential for its angiogenic features utilized in the autologous fat grafting. In this manner, analysis of VEGF-A secretion by the adipose-derived stem cells enable us to indirectly measure the angiogenic capabilities of our cells. In our studies we found that there was no significant difference in the secretion and expression of VEGF-A by the ASCs of the group of tamoxifen treated patients compared to that of the control group. Moreover, ASCs of tamoxifen treated patients displayed the same trend as that of control group; in both groups, VEGF secretion increased with longer duration of culture. Based on these two observations, it can be suggested that tamoxifen did not affect VEGF-A secretion and expression by adipose-derived stem cells.

Human adipose-derived stem cells (ASCs), originating from the vascular stromal compartment of adipose tissue, are multipotent cells able to differentiate into several cells types including osteoblasts, chondrocytes and adipocytes (Lindroos et al., 2011). Such multipotency and easy accessibility of adipose-derived stem cells make it a suitable candidate for use in many diverse regenerative therapies for damaged bones, myocardial tissues, chronic wounds and many others (Gimble et al., 2007). One such application of ASCs in reconstructive surgery is the autologous fat grafting augmented with adipose-derived stem cells for breast reconstruction in women with breast cancer. However, there are significant confounders including adjuvant endocrine therapy such as tamoxifen, in evaluating the success rates of such procedures this population of patients. Given the complex and cytotoxic nature of the therapeutic regimens for most cancer patients, the efficacy of ASC augmentation has been questioned by many practitioners. According to previous reports, bone marrow derived mesenchymal stem cells are resistant to chemotherapeutic agents and irradiation (Chen et al., 2006). Nevertheless, there is limited and contradicting literature on the effects of cytotoxic therapies on adipose-derived stem cells. A recent study outlined that ASCs are resistant to drugs widely used for chemotherapy, such as cisplatin, comptothecin, and vincristine, and that they can preserve their phenotype and the ability to differentiate *in vitro* after treatment (Liang et al., 2011). In contrast, another study showed that the capacity for multilineage differentiation was down-regulated in ASCs exposed to 5μM of tamoxifen (Pike et al., 2015). In light of these conflicting results, we studied the multilineage differentiation capacity of the adipose-derived stem cells obtained from our control group and tamoxifen-treated patients. We compared the ability to differentiate at day 0 and after 21 days of culture with the induction medium. As shown in the graphs, all groups are able to induce the gene after 21 days of culture, and this induction, with the exception of ALP gene, is statistically significant compare to day 0. The results of the real time for LEP and ALP gene shown a non-statistically significant trend comparing TAM treated patients and pre-menopausal subjects. It is interesting to note that TAM treated patients are mostly similar to post-menopausal subjects, in terms of differentiation capacity, compare to pre-menopausal ones. A recent study shown that at a transcriptome level ASCs from pre- e post- menopausal women are different (Xie et al., 2020), this could, at least partially, explaining the trend and why TAM-treated ASCs and ASCs from post-menopausal subjects appear to be more similar and slightly different from pre-menopausal one. At the best our knowledge our study is the first implying *ex vivo* ASCs from TAM-treated patients and pre- and post-menopausal subjects, indeed in light of the trend we found and the above-mentioned study, further studies to better clarify this point are needed. Overall, in our study, there is no significant difference in terms of multilineage differentiation capacity among all of the ASCs obtained from pre-menopausal subjects, menopausal subjects and tamoxifen treated patients. This finding is in parallel with the literature on bone marrow derived mesenchymal stem cells as well as the report on cisplatin, comptothecin, and vincristine (Frank et al., 1995; Chen et al., 2006).

Estrogen is an endogenous hormone essential for growth of various types of cells including those in mammary and adipose tissues. Estrogen exerts these effects through two nuclear estrogen receptors, namely ERα and ERβ (Molina et al., 2017). Estrogen receptor expression at the time of diagnosis of breast cancer is an invaluable prognostic factor also used for personalizing targeted therapies (Thomas and Gustafsson, 2011). The mechanism of action of one of the adjuvant endocrine therapy, namely selective estrogen receptor modulators such as tamoxifen, involves these estrogen receptors expressed in the breast cancer cells. The estrogen receptor antagonism exerted by tamoxifen inhibits the growth signal in breast cancer and so, the initially estrogen dependent tumor mass undergoes regression upon deprivation of their supporting hormone. Endocrine treatment, concurrently or not with chemotherapy, has been shown to reduce the recurrence and mortality rates in breast cancer positive for ER (Early Breast Cancer Trialists' Collaborative Group [EBCTCG], 2018). However, estrogen receptor expression is considerably ubiquitous and indeed, the effect of tamoxifen is beyond the scope of breast cancer cells only (Hua et al., 2018). Concerning the effects of estrogen receptor activation in ASCs, the available scientific literature is limited. A recent study found that adults stem cells from adipose tissues expressed both ERα and ERβ at the mRNA level and ERβ at the protein level (Pike et al., 2015). Another study, performed on ASC from mouse, concluded that both ERα and ERβ act as positive regulators improving ASC proliferation, migration and wound healing (Zhang et al., 2016). Likewise, our study involved a preliminary evaluation of the expression

of estrogen receptors in our adipose-derived stem cells. Both of ERα and ERβ were detected in the human adipose-derived stem cells with ERα levels higher than that of ERβ. This finding is in parallel with previous studies concluding ERα to be the main mediator of proliferation, wound healing and migration in mouse adipose-derived stem cells (Zhang et al., 2016). Although no significant differences in ERβ levels were observed among the three groups, the ASCs obtained from pre-menopausal subjects had a significantly higher level of ERα expression compared to that of other two groups with equivalent levels. Nevertheless, the roles of ERα and ERβ in adipose-derived stem cell biology will require further elucidation.

Breast reconstruction following breast cancer surgery is well known to improve quality of life. Autologous fat grafting has become a standard of care in the repair of volume and contour defects, and in improving unaesthetic results such as indurations, scar contractures, tissue deficits and breast asymmetry. In spite of the overall positive patient and surgeon reported outcomes, the concomitant administration of long-term adjuvant endocrine therapy confounds the success rate analysis of autologous fat grafting in breast cancer populations (Liang et al., 2011; Millet et al., 2016; Lindegren et al., 2019). Our work focused on the *ex vivo* effects of tamoxifen, another antiestrogen therapy, on cellular functions of adipose-derived stem cells. In this study we shown, for the first time in an *ex vivo* single-center study, that tamoxifen does not impair the cellular functions of ASCs. For this reason, we hypothesize that tamoxifen treatment, post-mastectomy, should not contraindicate autologous fat grafting in breast cancer patients.

DATA AVAILABILITY STATEMENT

The original contributions presented in the study are included in the article/**Supplementary Material**, further inquiries can be directed to the corresponding author/s.

ETHICS STATEMENT

The studies involving human participants were reviewed and approved by the Ethical Committee of Humanitas Research Hospital (study number: 1960, ID of the experimentation: 545, authorization date: 08-03-2018). The patients/participants provided their written informed consent to participate in this study.

AUTHOR CONTRIBUTIONS

IB, AVL, MK, and AGL: conceptualization. IB: methodology and formal analysis. IB, AVL, EV, and NL: validation. IB and AVL: investigation. IB, AVL, MK, AGL, EV, AB, and VV: resources. IB, AVL, FB, LM, and VV: data curation. IB, AVL, and NL: writing—original draft preparation. IB, AVL, NL, EV, MK, and AGL: writing—review and editing. IB, AVL, AB, and LM: visualization. MK and AGL: supervision, project administration, and funding acquisition. All authors have read and agreed to the published version of the manuscript.

ACKNOWLEDGMENTS

We would like to thank Dr. Elisa Zaghi, Dr. Francesca Calcaterra, and Dr. Floriana Maria Farina for their assistance with the HUVEC cells culture and experiment.

SUPPLEMENTARY MATERIAL

The Supplementary Material for this article can be found online at: https://www.frontiersin.org/articles/10.3389/fcell.2021.555248/full#supplementary-material

REFERENCES

Bao, P., Kodra, A., Tomic-Canic, M., Golinko, M. S., Ehrlich, H. P., and Brem, H. (2009). The role of vascular endothelial growth factor in wound healing. *J. Surg. Res.* 153, 347–358. doi: 10.1016/j.jss.2008.04.023

Blackwell, K. L., Haroon, Z. A., Shan, S., Saito, W., Broadwater, G., Greenberg, C. S., et al. (2000). Tamoxifen inhibits angiogenesis in estrogen receptor-negative animal models. *Clin. Cancer Res.* 6, 4359–4364.

Caviggioli, F., Maione, L., Forcellini, D., Klinger, F., and Klinger, M. (2011). Autologous fat graft in postmastectomy pain syndrome. *Plast. Reconstr. Surg.* 128, 349–352. doi: 10.1097/PRS.0b013e31821e70e7

Caviggioli, F., Maione, L., Klinger, F., Lisa, A., and Klinger, M. (2016). Autologous fat grafting reduces pain in irradiated breast: a review of our experience. *Stem Cells Int.* 2016:2527349. doi: 10.1155/2016/2527349

Chen, M.-F., Lin, C.-T., Chen, W.-C., Yang, C.-T., Chen, C.-C., Liao, S.-K., et al. (2006). The sensitivity of human mesenchymal stem cells to ionizing radiation. *Int. J. Radiat. Oncol.* 66, 244–253. doi: 10.1016/j.ijrobp.2006.03.062

Cuzick, J., Forbes, J. F., Sestak, I., Cawthorn, S., Hamed, H., Holli, K., et al. (2007). Long-term results of tamoxifen prophylaxis for breast cancer-96-month follow-up of the randomized IBIS-I trial. *J. Natl. Cancer Inst.* 99, 272–282. doi: 10.1093/jnci/djk049

Del Papa, N., Caviggioli, F., Sambataro, D., Zaccara, E., Vinci, V., Luca, G., et al. (2015). Autologous fat grafting in the treatment of fibrotic perioral changes in patients with systemic sclerosis. *Cell Transplant.* 24, 63–72. doi: 10.3727/096368914X674062

Early Breast Cancer Trialists' Collaborative Group [EBCTCG] (2011). Relevance of breast cancer hormone receptors and other factors to the efficacy of adjuvant tamoxifen: patient-level meta-analysis of randomised trials. *Lancet* 378, 771–784. doi: 10.1016/S0140-6736(11)60993-8

Early Breast Cancer Trialists' Collaborative Group [EBCTCG] (2018). Long-term outcomes for neoadjuvant versus adjuvant chemotherapy in early breast cancer: meta-analysis of individual patient data from ten randomised trials. *Lancet Oncol.* 19, 27–39. doi: 10.1016/S1470-2045(17)30777-5

Frank, S., Hübner, G., Breier, G., Longaker, M. T., Greenhalgh, D. G., and Werner, S. (1995). Regulation of vascular endothelial growth factor expression in cultured keratinocytes. *J. Biol. Chem.* 270, 12607–12613. doi: 10.1074/jbc.270.21.12607

Frese, L., Dijkman, P. E., and Hoerstrup, S. P. (2016). Adipose tissue-derived stem cells in regenerative medicine. *Transfus. Med. Hemother.* 43, 268–274. doi: 10.1159/000448180

Gentile, P., Orlandi, A., Scioli, M. G., Di Pasquali, C., Bocchini, I., Curcio, C. B., et al. (2012). A comparative translational study: the combined use of enhanced stromal vascular fraction and platelet-rich plasma improves fat grafting maintenance in breast reconstruction. *Stem Cells Transl. Med.* 1, 341–351. doi: 10.5966/sctm.2011-0065

Gimble, J. M., Katz, A. J., and Bunnell, B. A. (2007). Adipose-derived stem cells for regenerative medicine. *Circ. Res.* 100, 1249–1260. doi: 10.1161/01.RES.0000265074.83288.09

Gir, P., Oni, G., Brown, S. A., Mojallal, A., and Rohrich, R. J. (2012). Human adipose stem cells: current clinical applications. *Plast. Reconstr. Surg.* 129, 1277–1290. doi: 10.1097/PRS.0b013e31824ecae6

Hua, H., Zhang, H., Kong, Q., and Jiang, Y. (2018). Mechanisms for estrogen receptor expression in human cancer. *Exp. Hematol. Oncol.* 7:24. doi: 10.1186/s40164-018-0116-7

Jung Ho, W., and Yoon, H.-J. (2019). Differentiation into various cell lineages of adipose derived stem cells. *Glob. Pharm. Res.* 5, 1–2. doi: 10.15761/GPR.1000105

Klinger, M., Lisa, A., Klinger, F., Giannasi, S., Veronesi, A., Banzatti, B., et al. (2015). Regenerative approach to scars, ulcers and related problems with fat grafting. *Clin. Plast. Surg.* 42, 345–352. doi: 10.1016/j.cps.2015.03.008

Liang, W., Xia, H., Li, J., and Zhao, R. C. (2011). Human adipose tissue derived mesenchymal stem cells are resistant to several chemotherapeutic agents. *Cytotechnology* 63, 523–530. doi: 10.1007/s10616-011-9374-5

Lien, E. A., Solheim, E., and Ueland, P. M. (1991). Distribution of tamoxifen and its metabolites in rat and human tissues during steady-state treatment. *Cancer Res.* 51, 4837–4844.

Lindegren, A., Schultz, I., and Wickman, M. (2019). Improved patient-reported outcomes after autologous fat transplantation and corrective surgery after breast surgery. *J. Plast. Surg. Hand Surg.* 53, 111–118. doi: 10.1080/2000656X.2018.1561456

Lindroos, B., Suuronen, R., and Miettinen, S. (2011). The potential of adipose stem cells in regenerative medicine. *Stem Cell Rev. Rep.* 7, 269–291. doi: 10.1007/s12015-010-9193-7

Maione, L., Vinci, V., Caviggioli, F., Klinger, F., Banzatti, B., Catania, B., et al. (2014). Autologous fat graft in postmastectomy pain syndrome following breast conservative surgery and radiotherapy. *Aesthetic Plast. Surg.* 38, 528–532. doi: 10.1007/s00266-014-0311-9

Mandlekar, S., and Kong, A. N. T. (2001). Mechanisms of tamoxifen-induced apoptosis. *Apoptosis* 6, 469–477. doi: 10.1023/a:1012437607881

Matsumoto, D., Sato, K., Gonda, K., Takaki, Y., Shigeura, T., Sato, T., et al. (2006). Cell-assisted lipotransfer: supportive use of human adipose-derived cells for soft tissue augmentation with lipoinjection. *Tissue Eng.* 12, 3375–3382. doi: 10.1089/ten.2006.12.3375

McNamara, D. A., Harmey, J., Wang, J. H., Kay, E., Walsh, T. N., and Bouchier-Hayes, D. J. (2001). Tamoxifen inhibits endothelial cell proliferation and attenuates VEGF-mediated angiogenesis and migration in vivo. *Eur. J. Surg. Oncol.* 27, 714–718. doi: 10.1053/ejso.2001.1177

Millet, E., Haik, J., Ofir, E., Mardor, Y., Winkler, E., Harats, M., et al. (2016). The impact of autologous fat grafting on breast cancer: an experimental model using magnetic resonance imaging. *Isr. Med. Assoc. J.* 18, 283–285. doi: 10.1210/endo-25-6-1013

Mizuno, H., and Hyakusoku, H. (2010). Review article: fat grafting to the breast and adipose-derived stem cells: recent scientific consensus and controversy. *Aesthetic Surg. J.* 30, 381–387. doi: 10.1177/1090820X10373063

Molina, L., Figueroa, C. D., Bhoola, K. D., and Ehrenfeld, P. (2017). GPER-1/GPR30 a novel estrogen receptor sited in the cell membrane: therapeutic coupling to breast cancer. *Expert Opin. Ther. Targets* 21, 755–766. doi: 10.1080/14728222.2017.1350264

Nie, C., Yang, D., Xu, J., Si, Z., Jin, X., and Zhang, J. (2011). Locally administered Adipose-derived stem cells accelerate wound healing through differentiation and vasculogenesis. *Cell Transplant.* 20, 205–216. doi: 10.3727/096368910X520065

Nishimura, T., Hashimoto, H., Nakanishi, I., and Furukawa, M. (2000). Microvascular angiogenesis and apoptosis in the survival of free fat grafts. *Laryngoscope* 110, 1333–1338. doi: 10.1097/00005537-200008000-00021

Osborne, K. C. (1998). Tamoxifen in the treatment of breast cancer. *N. Engl. J. Med.* 339, 1609–1618. doi: 10.1056/NEJM199811263392207

Pearl, R. A., Leedham, S. J., and Pacifico, M. D. (2012). The safety of autologous fat transfer in breast cancer: lessons from stem cell biology. *J. Plast. Reconstr. Aesthetic Surg.* 65, 283–288. doi: 10.1016/j.bjps.2011.07.017

Pike, S., Zhang, P., Wei, Z., Wu, N., Klinger, A., Chang, S., et al. (2015). In vitro effects of tamoxifen on adipose-derived stem cells. *Wound Repair Regen.* 23, 728–736. doi: 10.1111/wrr.12322

Rigotti, G., Marchi, A., Galiè, M., Baroni, G., Benati, D., Krampera, M., et al. (2007). Clinical treatment of radiotherapy tissue damage by lipoaspirate transplant: a healing process mediated by adipose-derived adult stem cells. *Plast. Reconstr. Surg.* 119, 1409–1422. doi: 10.1097/01.prs.0000256047.47909.71

Serra-Renom, J. M., Muñoz-Olmo, J. L., and Serra-Mestre, J. M. (2010). Fat grafting in postmastectomy breast reconstruction with expanders and prostheses in patients who have received radiotherapy: formation of new subcutaneous tissue. *Plast. Reconstr. Surg.* 125, 12–18. doi: 10.1097/PRS.0b013e3181c49458

Silva, A. B. D., Haupenthal, F., Morais, A. D., Ascenço, A. S. K., Sebastião, A. P. M., Cavalcanti, M. A. R., et al. (2018). Relationship between tamoxifen and the absorption of subfascial autologous fat grafts. *Plast. Reconstr. Surg.* 141, 1408–1415. doi: 10.1097/PRS.0000000000004415

Simonacci, F., Bertozzi, N., Grieco, M. P., Grignaffini, E., and Raposio, E. (2016). Autologous fat transplantation for breast reconstruction: a literature review. *Ann. Med. Surg.* 12, 94–100. doi: 10.1016/j.amsu.2016.11.012

Simonacci, F., Bertozzi, N., Grieco, M. P., Grignaffini, E., and Raposio, E. (2017). Procedure, applications, and outcomes of autologous fat grafting. *Ann. Med. Surg.* 20, 49–60. doi: 10.1016/j.amsu.2017.06.059

Stark, R. Y., Mirzabeigi, M. N., Vonderhaar, R. J., and Bucky, L. P. (2018). Utilizing large volume fat grafting in breast reconstruction after nipple sparing mastectomies. *Gland Surg.* 7, 337–346. doi: 10.21037/gs.2018.05.01

Sterodimas, A., de Faria, J., Nicaretta, B., and Pitanguy, I. (2010). Tissue engineering with adipose-derived stem cells (ADSCs): current and future applications. *J. Plast. Reconstr. Aesthetic Surg.* 63, 1886–1892. doi: 10.1016/J.BJPS.2009.10.028

Tao, Z. Q., Shi, A., Lu, C., Song, T., Zhang, Z., and Zhao, J. (2015). Breast cancer: epidemiology and etiology. *Cell Biochem. Biophys.* 72, 333–338. doi: 10.1007/s12013-014-0459-6

Thomas, C., and Gustafsson, J.-A. (2011). The different roles of ER subtypes in cancer biology and therapy. *Nat. Rev. Cancer* 11, 597–608. doi: 10.1038/nrc3093

Varghese, J., Griffin, M., Mosahebi, A., and Butler, P. (2017). Systematic review of patient factors affecting adipose stem cell viability and function: implications for regenerative therapy. *Stem Cell Res. Ther.* 8:45. doi: 10.1186/s13287-017-0483-8

Xie, Y., Fang, B., Liu, W., Li, G., Huang, R. L., Zhang, L., et al. (2020). Transcriptome differences in adipose stromal cells derived from pre- And postmenopausal women. *Stem Cell Res. Ther.* 11, 1–11. doi: 10.1186/s13287-020-01613-x

Yu, J. M., Bunnell, B. A., and Kang, S.-K. (2011). "Neural Differentiation of Human Adipose Tissue-Derived Stem Cells," in *Adipose-Derived Stem Cells: Methods and Protocols*, eds J. M. Gimble and B. A. Bunnell (Totowa, NJ: Humana Press), 219–231.

Zhang, W., Schmull, S., Du, M., Liu, J., Lu, Z., Zhu, H., et al. (2016). Estrogen receptor α and β in mouse: adipose-derived stem cell proliferation, migration, and brown adipogenesis in vitro. *Cell. Physiol. Biochem.* 38, 2285–2299. doi: 10.1159/000445583

Conflict of Interest: Since 1st December 2020, IB has been employed by Frontiers Media SA. IB declared his/her affiliation with Frontiers, and the handling editor states that the process nevertheless met the standards of a fair and objective review.

The remaining authors declare that the research was conducted in the absence of any commercial or financial relationships that could be construed as a potential conflict of interest.

frontiers in Cell and Developmental Biology

ORIGINAL RESEARCH
published: 13 April 2021
doi: 10.3389/fcell.2021.629430

DAND5 Inactivation Enhances Cardiac Differentiation in Mouse Embryonic Stem Cells

José Manuel Inácio[1], João von Gilsa Lopes[1], Ana Mafalda Silva[1], Fernando Cristo[1], Sara Marques[1], Matthias E. Futschik[2] and José António Belo[1]**

[1] iNOVA4Health, CEDOC, NOVA Medical School, NMS, Universidade Nova de Lisboa, Lisbon, Portugal, [2] Faculty of Medicine, School of Public Health, Imperial College London, Medical School, St. Mary's Hospital, London, United Kingdom

OPEN ACCESS

Edited by:
Joana Paiva Miranda, University of Lisbon, Portugal

Reviewed by:
Michel Puceat, Institut National de la Santé et de la Recherche Médicale (INSERM), France
Vera Marisa Costa, University of Porto, Portugal

***Correspondence:**
José António Belo
jose.belo@nms.unl.pt
José Manuel Inácio
jose.inacio@nms.unl.pt

Specialty section:
This article was submitted to Stem Cell Research, a section of the journal Frontiers in Cell and Developmental Biology

Received: *14 November 2020*
Accepted: *18 March 2021*
Published: *13 April 2021*

Citation:
Inácio JM, von Gilsa Lopes J, Silva AM, Cristo F, Marques S, Futschik ME and Belo JA (2021) DAND5 Inactivation Enhances Cardiac Differentiation in Mouse Embryonic Stem Cells. Front. Cell Dev. Biol. 9:629430. doi: 10.3389/fcell.2021.629430

Deciphering the clues of a regenerative mechanism for the mammalian adult heart would save millions of lives in the near future. Heart failure due to cardiomyocyte loss is still one of the significant health burdens worldwide. Here, we show the potential of a single molecule, DAND5, in mouse pluripotent stem cell-derived cardiomyocytes specification and proliferation. *Dand5* loss-of-function generated the double of cardiac beating foci compared to the wild-type cells. The early formation of cardiac progenitor cells and the increased proliferative capacity of *Dand5* KO mESC-derived cardiomyocytes contribute to the observed higher number of derived cardiac cells. Transcriptional profiling sequencing and quantitative RT-PCR assays showed an upregulation of early cardiac gene networks governing cardiomyocyte differentiation, cell cycling, and cardiac regenerative pathways but reduced levels of genes involved in cardiomyocyte maturation. These findings prompt DAND5 as a key driver for the generation and expansion of pluripotent stem cell-derived cardiomyocytes systems with further clinical application purposes.

Keywords: cardiomyocyte proliferation, cardiac progenitor cell, cardiac differentiation, *Dand5*, embryonic stem cells

INTRODUCTION

Cardiomyocyte loss is a significant process underlying heart failure prevalence in our aging society (Virani et al., 2020). From inherited cardiomyopathies, myocardial infarction to oncological treatments, the causes for cardiomyocyte death are vast, and its regeneration scarce or null (Leone et al., 2015; Yuan and Braun, 2017). The natural replication of cardiomyocytes is present during mammalian embryo and fetus development, but stops irreversibly within the first weeks of postnatal life (Payan et al., 2020). Cardiac development starts on both sides of the embryo, with cells from the heart-forming regions migrating from the anterior region of the primitive streak to the midline, forming the heart tube (Buckingham et al., 2005; Kelly et al., 2014; Meilhac et al., 2015). After a series of coordinated cell movements, the heart tube loops and fuses to form the 4-chamber structured heart. With the gradual differentiation of cardiac cells, cycles of contraction and relaxation, related

to heart function, emerge consistently, allowing the entire organism's blood supply. Thus, for cardiac morphogenesis and function, the specification, proliferation, migration, differentiation, and maturation of the heart precursor cells are essential. These processes require a precise spatial and temporal coordination of several signaling pathways at multiple levels since many of them are involved in more than one molecular mechanism and sometimes with opposite regulatory readouts (Brand, 2003; Olson et al., 2006; Bruneau, 2013; Paige et al., 2015). Over the last decade, we have expanded our knowledge on the regulatory network that is essential for cardiac development, regeneration, and remodeling during disease, namely due to the advances in "omics" technologies (O'Meara et al., 2015; Uosaki et al., 2015; Liu et al., 2019; Wang et al., 2020; Xiong and He, 2020; Zhou and Wang, 2020). During mesoderm specification, the T-box transcription factors T and EOMES activate the expression of the early cardiac transcription factor MESP-1 while repressing genes related to pluripotency (Bondue and Blanpain, 2010; Devine et al., 2014). Subsequently, the GATA zinc-finger family (e.g., GATA4), the T-box protein family (TBX5), the NK homeodomain family (NKX2-5), the MADS-box family (MEF2, SRF), are triggered to promote the differentiation of cardiac progenitor cells (Lien et al., 1999; Bruneau et al., 2001; Gottlieb et al., 2002; Dodou et al., 2004; Phan et al., 2005; Qian et al., 2012). In addition, the isoform switching of contractile genes, such as the later expression cardiac troponin T3 in comparison with the fetal cTnT1 isoform, plays a role in the maturation of the cardiomyocytes (Taegtmeyer et al., 2010; Ames et al., 2013). Nevertheless, even with all the datasets and information currently available, identifying key regulatory genes and developmental gene networks remains a challenge.

DAND5 is an extracellular protein belonging to the family of TGF-β/Nodal signaling antagonists Cerberus/DAN (Belo et al., 2000, 2009). DAND5-mediated antagonism of Nodal signaling requires DAND5 binding to the ligand Nodal, and most likely, to Nodal (co)receptors, which consequently prevents agonist-receptor interaction and subsequent signaling activation. Furthermore, some Cerberus/Dan family members, including DAND5, are multivalent antagonists that also bind to and inhibit BMP and Wnt ligands (Belo et al., 2009). Interestingly, we have reported that loss-of-function of DAND5 in mice leads to a massive increase of the ventricular heart wall's thickness caused by an increased mitotic index of the cardiomyocytes (CMs) at the compact myocardium (Araújo et al., 2014; Belo et al., 2017). Allied to these, increased levels of phosphorylated-SMAD2 and increased *Ccnd1* expression levels were detected in the hearts of *Dand5* knockout (*Dand5* KO) neonatal mice (Araújo et al., 2014). Although the significant mortality rate observed in *Dand5* knockout newborn mice is linked with the increased mitotic index of the cardiomyocytes, the notion that the proliferative and regenerative capacity of cardiac cells from the diseased heart can be stimulated by the modulation of a single endogenous signaling antagonist is exciting and open new therapeutic avenues.

To explore this hypothesis and further clarify the function of DAND5 in the molecular control of cardiomyogenesis, we successfully derived a *Dand5* KO mouse embryonic stem cell line that proved to be a valuable *in vitro* cardiac differentiation model. Using this cellular tool, we show that *Dand5* loss-of-function dramatically increases the proportion of FLK-1^+/PDGFR-α^+ cardiac progenitor cells. In addition, the knockout of *Dand5* activates cell-cycle regulators, augmenting cardiomyocyte proliferation. Furthermore, we provide regulatory information on the signaling pathways enriched in *Dand5* KO mESC-derived cardiomyocytes. In conclusion, the modulation of *Dand5* expression levels seems to play an important role in the output of cardiomyocytes derived from pluripotent stem cell systems. Thus, the modulation of DAND5 levels could be used for the generation of better mature-ready iPS-CM for use in cell therapies to heal a diseased heart.

MATERIALS AND METHODS

Mice

The animals were maintained at 22 ± 1°C in a 12-h light-dark cycle. The mouse line used in this work was the *Dand5* knockout (*Dand5* KO) generated using E14 embryonic stem cells and currently in an 129 background (Marques et al., 2004). Embryonic stage E0.5 was considered at noon of the plugs detection day. All animal experiments were performed in accordance with the European Union (EU) guidelines for animal research and welfare, and in compliance with the Portuguese law and approved by the Consultative Commission of the Veterinary Agency from Portuguese Ministry of Agriculture (Directive 2010/63/EU of the European Parliament). All animal experiments were conducted under DGAV Permit No. 0421/000/000/2016.

Derivation and Primary Culture of Mouse *Dand5* KO ESC Lines

Three days after vaginal plug detection, pregnant females were sacrificed by cervical dislocation and the uterine horns were surgically removed and immediately placed on a pre-heated M2 culture medium (EmbryoMax®, Millipore). The blastocysts were flushed, washed, and incubated with Acidic Tyrode's solution [137 mM NaCl; 2.7 mM KCl; 1.6 mM $CaCl_2.2H_2O$; 0.5 mM $MgCl_2.6H_2O$; 5.6 mM glucose; 0.4% Polyvinylpyrrolidone (PVP), pH 2.5] to remove the zona pellucida.

One blastocyst was plated per 6-well plate well, on mitotically inactivated MEF feeders, containing ES cell medium composed by Knockout-DMEM medium (Thermo Fisher Scientific) supplemented with 15% FBS (HyClone, UT, United States), 1% MEM Non-Essential Amino Acids (Thermo Fisher Scientific), 1% Penicillin/Streptomycin, 2 mM L-glutamine, and 0.1 mM β-Mercaptoethanol (Thermo Fisher Scientific). In order to maintain pluripotency conditions, 1000 U mouse LIF (ESGRO® Millipore) was added, as well as 1 μM PD0325901 (Calbiochem® Millipore) and 2 μM CHIRON99021 (Calbiochem® Millipore) inhibitors. Blastocysts were incubated at 37°C, 5% CO_2 for 48 h, avoiding any disturbance during this period to allow its attachment to the feeder layer. On day 3 after flushing, half of the medium was replenished. During days 3–7, the outgrowths were monitored daily, and the medium was renewed every day.

At day 7, the cells were dissociated and transferred onto new inactivated feeder layers. The incipient mESC line is at Passage 1

(P1), and the medium was daily renewed. After 3–4 days, mESC colonies started to be distinguishable.

Karyotyping

Dand5 KO mESC lines chromosome analysis was performed using GTG high-resolution banding technique by the Department of Genetics, Faculty of Medicine of the University of Porto – São João Hospital. In total, 15 metaphases were analyzed for each ES cell line.

mESCs Differentiation Through Embryoid Bodies Formation

Undifferentiated *Dand5* KO and the respective E14 WT control mESC lines were used to test cells pluripotency potential and spontaneous differentiation by the hanging droplet method (Bover et al., 2018). Briefly, cells were dissociated into a single cell suspension and resuspended in fresh mESC medium without LIF. Then, mESCs were cultured in hanging drops (500 cells per droplet) for 48 h until the formation of embryoid bodies (EBs). Then, the EBs were cultured in static suspension until day 5, followed by adherent culture in 0.1% gelatin-coated wells up to day 10, prompting spontaneous differentiation. The culture medium was renewed every day.

RNA Isolation for cDNA Synthesis and RT-qPCR

Total RNA was extracted from mouse mESCs, MEF cells, and EBs, at several days of differentiation, using TRI Reagent® (Sigma) and the Direct-zol™ RNA MiniPrep Kit (Zymo Research) according to the manufacturer's instructions. The RNA samples were evaluated relating to quantity and quality using a spectrophotometer (Nanodrop 2000, Thermo Fisher Scientific). Only samples with 260/280 nm and 260/230 nm ratios equal or superior to 2.0 were considered. First strand cDNA was synthesized through reverse transcription reaction using RevertAid Reverse Transcriptase, Oligo (dT) primers, RiboLock RNase Inhibitor, and dNTP (Thermo Fisher Scientific). RT-qPCR reactions were performed in triplicate using a SensiFAST SYBR Lo-ROX mix (BIOLINE) (the primers listed in **Supplementary Table 1**) on a 7300 Real-Time PCR system (Applied Biosystems). Relative quantification of expression was performed using the ddCt method (Bustin, 2000) and normalized to GAPDH as a housekeeping gene and with E14 mESC line as reference.

Fluorescent Immunocytochemistry

Undifferentiated or differentiated mESCs were fixed in 4% paraformaldehyde, incubated with primary antibodies (diluted in 1x PBS, 1% Bovine Serum Albumin, 0.05% sodium azide solution) overnight at 4°C, listed in **Supplementary Table 2**, followed by appropriated secondary antibody incubation, overnight at 4°C. Nuclei were stained with DAPI at room temperature and cell images were acquired with Zeiss Axio Imager Z2 microscope or Zeiss LSM710 confocal microscope (Carl Zeiss). Images were taken in sequential mode and posteriorly adjusted in ImageJ.

Flow Cytometry

To detect and quantify cardiac progenitor cells, EBs were dissociated into a single cell suspension and incubated with the following antibodies: Phycoerythrin (PE)- conjugated Flk-1 (eBioscience; 1:50), Allophycocyanin (APC)-conjugated-PdgfR-α (eBioscience; 1:100) at 4°C for 30 min.

To analyze cardiomyocyte proliferation, newly synthesized DNA was labeled by incubating EBs with EdU for 90 min. EdU detection was done following the Click-iT EdU Alexa Fluor 488 Imaging Kit (Thermo Fisher Scientific) instructions and then incubated with antibodies for MLC2v at 4°C for 30 min. Relative fluorescence intensity of cells was detected by Becton Dickinson FACSCanto II (BD Biosciences). Analysis of results was performed using FlowJo v10 software (BD). A minimum of 30,000 events were acquired for each condition.

RNA-Sequencing

Total RNA was extracted from three biological replicates within each time point as mentioned above. Libraries were constructed using Stranded mRNA Library Prep Kit. Pair-end libraries were sequenced on an Illumina PE150 Platform with an output of ∼40 M reads per sample. The quality of the reads was assessed using FastQC software and mapping of reads was performed applying the STAR (version 2.7.5c) aligner using murine genome from GENCODE Release M25 as reference (Dobin and Gingeras, 2015). In particular, the primary genome sequence assembly GRCm38 together with corresponding annotations was used. To obtain the read counts per gene, the featureCount function of the Bioconductor package Rsubread (version 2.2.6) was executed (Liao et al., 2019a). As a measure of gene expression, the transcripts per million (TPM) were subsequently calculated. Finally, the analysis of differential gene expression was performed using Bioconductor edgeR package (version 3.30.3) with a biological coefficient of variation of 0.2 (McCarthy et al., 2012). *P*-value correction for multiple testing was performed using the Benjamini Hochberg (FDR) method. Mappings of Ensembl IDs to gene symbols were extracted from Bioconductor package org.Mm.eg.db for murine genome annotation (version 3.11.4). As functional enrichment analysis for KEGG pathway categories, Over-Representation Analysis of differentially expressed genes was conducted using WebGestalt (Liao et al., 2019b). As input, differentially expressed genes with FDR lower than 0.01 and with either positive or negative logged (base 2) fold changes larger than 2 or smaller than −2 were selected. Using genes that associated with Heart Cardiomyopathy and Dilated Cardiomyopathy terms of KEGG, a heat map was produced based on Z Scores, which were calculated by subtracting the overall average log2 TPM from the log2 TPM of the respective sample, and dividing that result by the standard deviation of all log2 TPM values across all samples.

Statistical Analysis

Statistical Analysis was performed using GraphPad Prism 7 software (GraphPad Software, Inc.; San Diego, CA, United States). All the experimental values are reported as mean ± SD.

In the case of the RT-PCR experiments, statistical differences between the two groups (mutant and control groups) were determined by applying the unpaired Student's *t*-test. Also, a one-way ANOVA test was applied when more than two groups were compared. To reject the null hypothesis, the probability values of $^{*}p < 0.05$. were considered statistically significant.

RESULTS

Generation and Characterization of *Dand5* KO mESC Line

To uncover the role of DAND5 in the mechanisms of cardiac mesoderm differentiation and in the number of *in vitro* produced cardiomyocytes, we successfully derived a mouse ES cell line from *Dand5* knockout (*Dand5* KO) mouse blastocysts. To access the blastocysts, pregnant females were sacrificed at stage E3.5, and the uterus was flushed, allowing the collection and handling of embryos (**Figure 1A**). The blastocysts were then incubated with Acidic Tyrode's solution to disrupt the zona pellucida (Khalifa et al., 1992), which promotes blastocyst hatching. The mouse blastocysts were then plated in feeder cells and maintained in culture until clusters of outgrowths started to be visible (**Figure 1B**). Since the first passage, the *Dand5* KO mESCs colonies adopted an oval morphology with clear light boundaries, and within cells showed a large nucleus compared with a reduced cytoplasm (**Figure 1C**). *Dand5* KO mESCs were cocultured with freshly MEFs feeders up to passage 3, which promoted an efficient derivation and pluripotency maintenance. For subsequent passages, the cells were cultured on 0.1% gelatin-coated plates.

To ensure *Dand5* KO mESCs quality and purity, we performed a full characterization of the undifferentiated cells relating to its chromosomic and genetic stability, pluripotency, and differentiation capacities. Firstly, to authenticate the new *Dand5* KO mESCs, we successfully confirmed the knockout genotype of the derived cells according to what was established before (Marques et al., 2004; **Supplementary Figure 1A**). In addition, the male gender identification resulted from the positive amplification of a specific region of the *Sry* gene, classified as the master regulator involved in the early male phenotype (Polanco and Koopman, 2007), was also determined (**Supplementary Figure 1B**). Chromosomic integrity and stability were analyzed by karyotyping. In a total of 15 metaphases evaluated, we observed that *Dand5* KO mESC line presents a normal chromosomic number (40, XY), without any translocation detected. Likewise, the karyotype results confirmed the male gender, firstly identified by the PCR technique (**Figure 1D**).

To validate the pluripotency properties of the *Dand5* KO mESCs, we started by assessing the expression of pluripotency genes *Nanog*, *Oct4*, and *Sox2,* by quantitative RT-PCR at Passage 6. The results indicated that the *Dand5* KO mESC line shows expression levels comparable to the mESCs control cells for all these pluripotency genes (**Figure 1E**). In this experiment, RNA isolated from mouse embryonic fibroblast cells was used as a negative control, and as expected, these cells did not express any of these pluripotency genes. Then, protein expression for pluripotency markers was examined by immunofluorescence. The derived mESCs expressed nucleus markers – NANOG and OCT4 – and the surface marker SSEA-1 positively, confirming the stemness of the *Dand5* KO mESCs (**Figure 1F**). Testing the spontaneous differentiation capacity in the three germ layers is a crucial validation step to guarantee the pluripotency properties of any given ES cell line. To do so, we prepared cells to form embryoid bodies using the hanging drop differentiation. The results clearly show that some *Dand5* KO mESCs spontaneously differentiate to the endoderm lineage, positively marked with AFP, while others differentiate to the mesoderm lineage, positively marked with α-Actinin sarcomeric, and others differentiate to the ectoderm lineage, positively marked with Vimentin (**Figure 1G**). Altogether, these data demonstrated that we efficiently derivated and expanded an mESC line from blastocyst-stage *Dand5* KO embryos. The line shows pluripotent ground-state properties and capacity to differentiate into three germ layers from which all cell lineages that compose an organism derive.

Cardiac Progenitor Numbers Are Increased During *Dand5* KO mESCs Cardiomyocyte Differentiation

After the pluripotency properties and stability of the derived cell lines were confirmed, we used this model to study the role of DAND5 in cardiomyogenesis *in vitro*. The differentiation of pluripotent KO cells into cardiomyocytes was induced by the hanging drop method leading to Embryoid Bodies' formation (EBs) (**Figure 2A**). This protocol was performed in three independent experiments using *Dand5* KO mESCs and E14 WT mESC lines control in parallel. Through a spontaneous differentiation process, cardiac cells originated with observable rhythmic beating foci along 10 days. Interestingly, beating foci areas started to be visible in the KO differentiated cells prior to the WT cell line (**Figure 2C**). At day 6, their contractile movements were notorious in all the plated EBs at different rhythmic rates, while in the control line, the beating foci areas start to show contractile movements only between days 7 and 8 in a sporadic number of EBs (**Figure 2C**). By performing the statistical analysis of the counted contractile areas, we observed that each KO EB originates the double of beating foci areas compared to the WT EBs during the entire differentiation protocol. From day 7 to day 10, the differences between the two cell lines were statistically significant, indicating that the mutant *Dand5* cells have a higher capacity to develop beating foci areas from the initial to the final stages of differentiation. To confirm that this observed phenotype results in earlier differentiation and organization of cardiomyocytes, we performed an immunostaining against sarcomeric α-actinin (**Figure 2D**). At day 6, Dand5 KO mESCs showed clear and organized α-actinin positive foci while the control line displayed a scattered signal. Additionally, defined sarcomeric structures' appearance indicated that the cardiac program is enhanced in Dand5 KO cells (**Figure 2D**). This earlier and higher activation of cardiomyocyte differentiation was confirmed by α-*MHC* expression, already upregulated at day 6 of differentiation (**Figure 3A**). These results suggest that DAND5

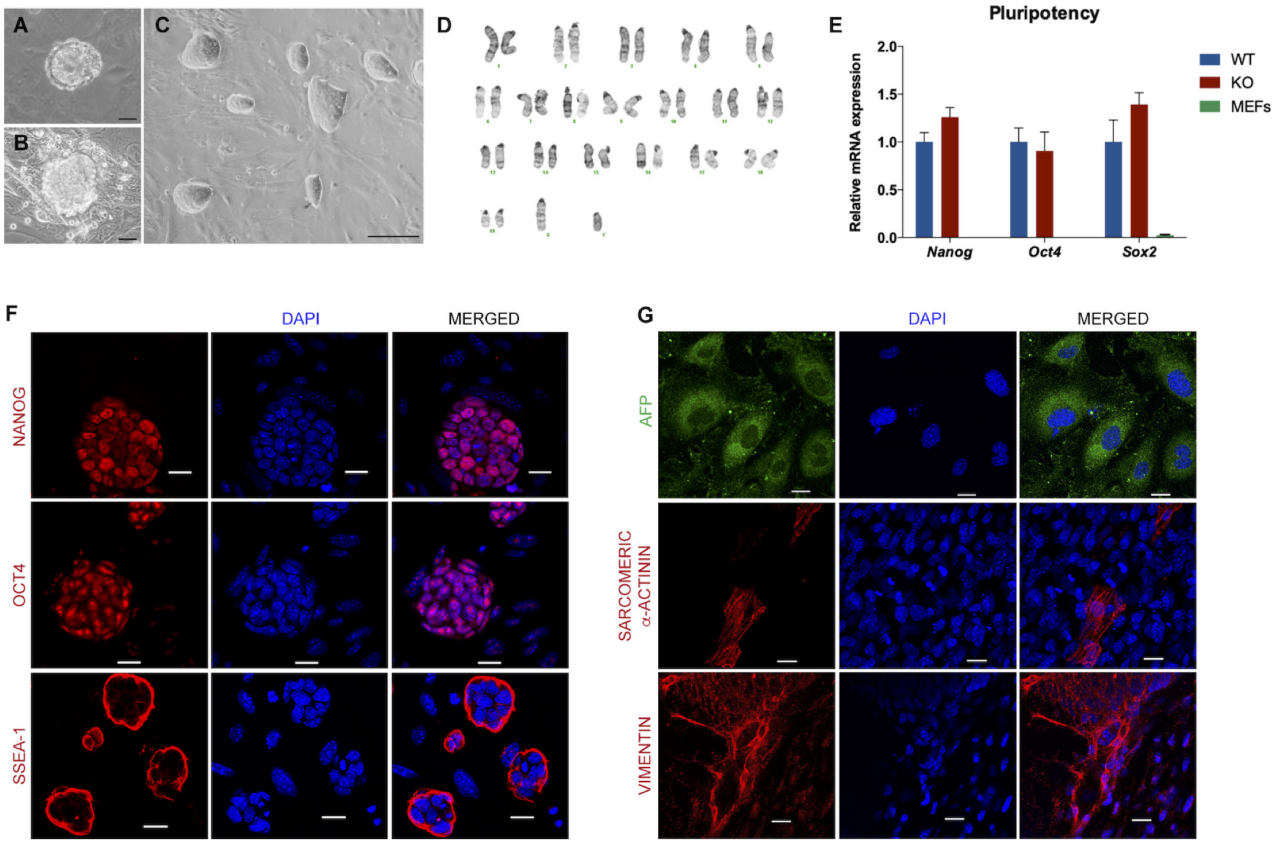

FIGURE 1 | Characterization of the *Dand5* knockout mouse embryonic stem cell line. **(A)** Morphology of mouse blastocyst at stage E3.5, with well-defined ICM and blastocyst cavity; **(B)** Morphology of blastocyst hatched on MEF feeder at day 3 after collection; **(C)** Morphology of *Dand5* KO mESC line colonies cocultured with MEFs (scale bar: 100 μm); **(D)** Karyotype of a representative metaphase showing normal 40 chromosomes (XY); **(E)** Expression of *Nanog*, *Oct4,* and *Sox2* of the derived mouse *Dand5* KO ES cells by qRT-PCR (*n = 3*). Experiments were performed in triplicate for each one. The expression level of each pluripotency gene is represented relative to the referred E14 ESC line, used as a positive control; **(F)** Immunofluorescence analysis show positive expression of NANOG, OCT4, and SSEA-1 in *Dand5* KO mESCs (scale bars: 20 μm); **(G)** The presence of AFP (endoderm), α-Actinin sarcomeric (mesoderm), and Vimentin (ectoderm) markers were positively detected at day 10 of differentiation by immunofluorescence analysis (scale bars: 20 μm).

influences the commitment, number, and electrophysiological capabilities of cardiac progenitor cells (CPCs). To determine whether the loss-of-function of the *Dand5* gene could promote an early formation of CPCs, we analyzed the population of FLK-1$^+$/PDGFR-α$^+$ cells from both *Dand5* KO and WT EBs by FACS. At day 4, we found that *Dand5* KO EBs have ∼40% more cardiovascular precursors cells than the WT EBs (**Figure 2E**). While there was an expected increase in the numbers of FLK-1$^+$/PDGFR-α$^+$ cells on both DAND5 KO and WT at day 5, we still observed significantly more FLK-1$^+$/PDGFR-α$^+$ cells in the Dand5 KO EBs when compared to the WT counterparts (**Figure 2E**).

Since the *Dand5* KO cell line differentiates into more CPC than the WT line, we investigated if the expression levels of cardiac mesoderm genes in the KO cell line are increased during the early stages of cardiomyocyte differentiation by quantitative RT-PCR. Firstly, we confirmed that *Dand5* is not expressed in the KO mESCs (**Figure 2B**). Cardiac-specific genes, including *Mesp-1*, *Isl1*, *Nkx2.5*, α*-MHC*, and *cTnT* along with *Brachyury(T)*, *Bmp2*, and *Fzd4* were assayed as markers to study the cardiac differentiation and specification along time. Interestingly, we observed an earlier expression pattern of almost all analyzed genes during the differentiation of the *Dand5* KO mESCs when compared to the WT mESC line (**Figures 3**, **4**). High *Mesp-1* mRNA relative expression was found at day 3 of differentiation in the KO cells, and only at day 4 in the WT line. In addition, we observed that *Dand5* KO cells show a significantly higher peak of *Mesp-1* expression relative to the WT cells (**Figure 4**). This data suggests that in the absence of *Dand5*, ES cells demonstrate a faster and increased capacity for mesoderm formation toward the *Mesp-1* cardiogenic mesoderm lineage. Accordingly, *Brachyury(T)*, which is co-expressed along with *Mesp-1* in the mesodermal cells of the primitive streak (David et al., 2011), was also highly expressed in *Dand5* KO cells (**Figure 4**). The expression of *Fzd4*, a lateral plate mesoderm marker, was also higher in the KO cells when compared to the control line (**Figure 4**). The First Heart Field (FHF) progenitor's marker, *Nkx2.5*, was significantly upregulated in the differentiated *Dand5* KO mESCs (**Figure 4**), marking the stage of cells' commitment into the first

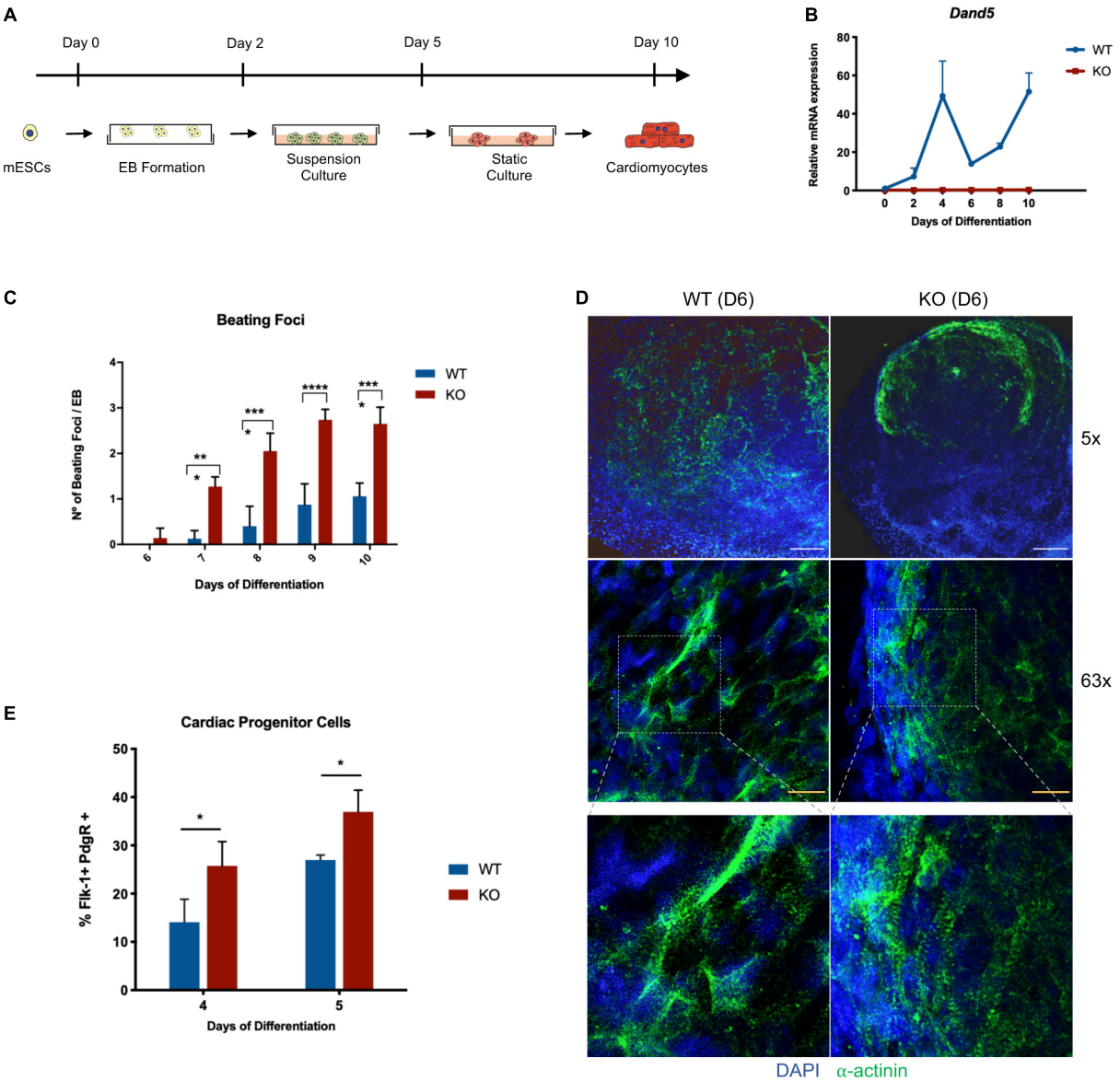

FIGURE 2 | Analysis of *Dand5* KO mESCs during cardiomyocyte differentiation. **(A)** Schematic representation of the cardiomyocytes' differentiation using the hanging drop technique; **(B)** Relative *Dand5* expression throughout cardiac differentiation. **(C)** Measurement of beating foci per KO and WT EBs. Results are expressed as the total number of beating foci with respect to the total number of plated EBs; **(D)** Whole-mount EB immunofluorescence analysis show positive expression of sarcomeric α-actinin on *Dand5* KO and WT EBs differentiated for 6 days. DAPI was used as a positive control for nuclear staining (scale bars: white 200 μm; yellow 20 μm). **(E)** Analysis of FLK-1 and PDGFR-α expression by flow cytometry. All the results represent the mean ± SD of three independent biological experiments. Unpaired Student's *t*-test was applied to compare the differences between WT and KO groups in each day of differentiation. Statistically significant results were considered when $^{*}p < 0.05$, $^{**}p < 0.01$, $^{***}p < 0.001$, and $^{****}p < 0.0001$.

myocardial lineage. Besides, levels of *Isl1* expression increased substantially at day 4, reaching the peak at day 5 for the mutant and the control lines (**Figure 4**). Expression of *Isl1* is commonly used to identify cells of the second Heart as the late cardiac progenitors to commit into the myocardial cells (Moretti et al., 2006). Comparing the relative levels of *Isl1* expression at day 5, the differentiated *Dand5* KO mESCs present higher gene expression levels than the control line (**Figure 4**). Taken together, these results corroborate the hypothesis that loss-of-function of the *Dand5* gene, in differentiating mESCs, increases the number of cardiac progenitors, which in turn results in a higher capacity to develop beating foci and, therefore, production of functional cardiomyocytes. Interestingly, *Dand5* displays two peaks of expression, at day 4 and by day 8–10 of differentiation (**Figure 2B**). Consequently, we can hypothesize that DAND5 may be relevant to regulate pathways involved in the specification and in the proliferation of cardiomyocytes at those two time-windows.

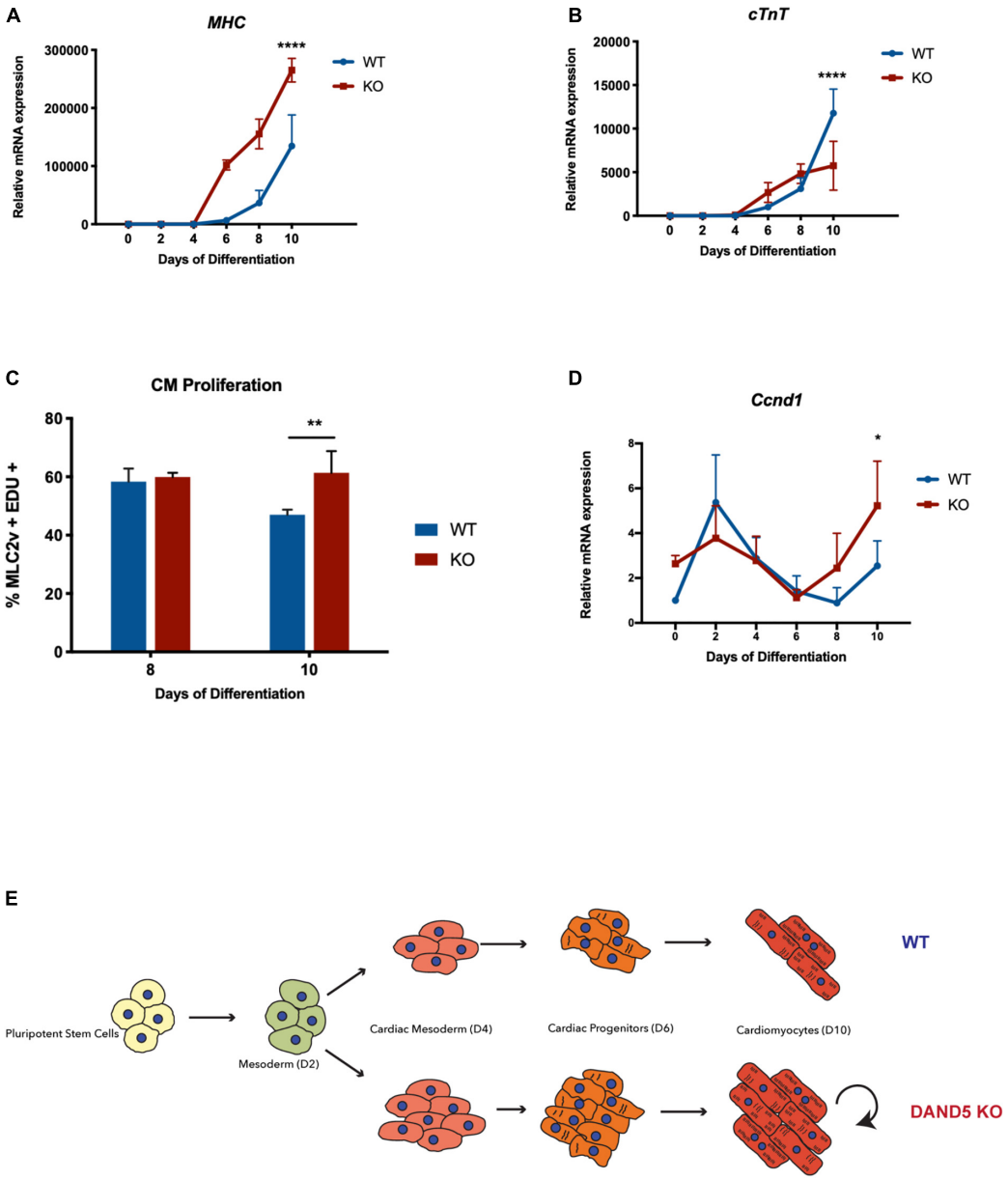

FIGURE 3 | *Dand5* KO leads to increased cardiomyocyte proliferation **(A)** Relative mRNA expression of *MHC* in *Dand5* KO and WT differentiated cells; **(B)** Relative *cTNT* expression throughout cardiac differentiation *of Dand5* KO and WT cells; **(C)** Analysis of cardiomyocyte proliferation by labeling newly synthesized DNA using EdU incubation for 1.5 h. Relative fluorescence intensity of cells was analyzed by flow cytometry; **(D)** Relative mRNA expression of *Ccnd1* gene in *Dand5* KO and WT differentiated cells. **(E)** Summary of the results: the increased formation of cardiac progenitor cells and the increased proliferative capacity of *Dand5* KO mESC-derived cardiomyocytes contribute to the observed higher number of derived cardiac cells. All the results represent the mean ± SD of three independent biological experiments. Unpaired Student's *t*-test was applied to compare the differences between WT and KO groups in each day of differentiation. Statistically significant results were considered when $^{*}p < 0.05$, $^{**}p < 0.01$, and $^{****}p < 0.0001$.

Dand5 KO Increases the Proliferation of ESC-Derived Cardiomyocytes

To examine the functionality and maturation state of the *Dand5* KO mESC-derived cardiomyocytes, we analyzed the expression of α-myosin heavy chain (α-*MHC)* and cardiac troponin T (*cTnT)* genes (**Figure 3**). Myosin is a protein that contributes to the generation of the contractile movements during the early mouse heart development through the mediation of ATP molecules (Ng et al., 2010). The qRT-PCR results identified an up-regulation of α-*MHC* gene expression in the KO line when compared to the WT line, already evident by day 6 and still persisting at day 10 of differentiation (**Figure 3A**). This result suggests again an increased stimulation cardiomyogenesis resulting from the loss-of-function of *Dand5*. In contrast, *cTnT* expression levels

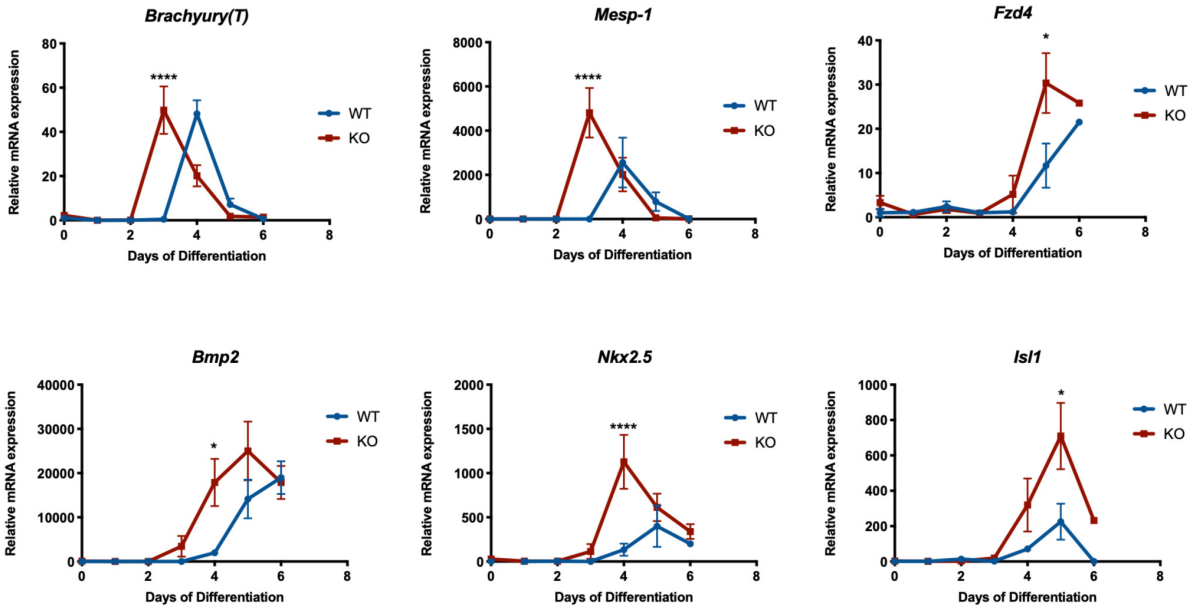

FIGURE 4 | Relative mRNA expression of *Brachyury(T)*, *Mesp-1*, *Fzd4*, *Bmp2*, *Nkx2.5*, and *Isl1* genes in *Dand5* KO and WT differentiated cells. All the results represent the mean ± SD of three independent biological experiments. Unpaired Student's *t*-test was applied to compare the differences between WT and KO groups in each day of differentiation. Statistically significant results were considered when $^{*}p < 0.05$ and $^{****}p < 0.0001$.

were significantly lower in the differentiating *Dand5* KO cells compared to WT cells at day 10 (**Figure 3B**). cTnT is one of the main regulatory proteins capable of controlling the ionic Ca^{2+} variations and anchor the other troponin components, essential for myocardium contraction (Nishii et al., 2008). Thus, this result indicated a possible structural commitment delay of the *Dand5* KO mESC-derived cardiomyocytes characterized by a reduced number of cTnT proteins at the sarcomere level and, consequently, impairment in their phenotypic maturation. Curiously, comparing *Bmp2* expression at CPC stage (day 4–5), we observed that *Dand5* KO cells have higher *Bmp2* expression than the WT (**Figure 3E**). It has been demonstrated that ectopic expression of *Bmp2* stimulates proliferation and blocks fully cardiomyocyte differentiation in embryoid bodies (Prados et al., 2018). To confirm the proliferation state of the *Dand5* KO mESC-derived cardiomyocytes, a proliferation assay consisting of labeling newly synthesized DNA with EdU and posterior fluorescence labeling using the Click-iT EdU Kit was performed at day 8 and day 10 of differentiation (**Figure 3C**). The results of this assay indicate that the knockout of DAND5 increases the proliferation of cardiomyocytes derived from the *Dand5* KO mESC line. Moreover, a statistically significant increase in the expression of the cardiac cell cycle regulator *Ccnd1* was found in the KO cells at day 10 (**Figure 3D**). This explains the observed increased levels of α-*MHC* and the decreased levels of *cTnT* expression in the differentiated *Dand5* KO cardiomyocytes. *cTnT* is usually upregulated in a more mature cardiomyocyte phenotype state. Therefore, our results suggest that *Dand5* KO mESC-derived cardiomyocytes sustain their self-renewal and immature state instead of long-term maturation, being capable to proliferate more than the WT line.

Transcriptional Changes Toward a Cardiomyocyte Fate Are More Advanced in *Dand5* KO Cells

To examine the difference between the global transcriptional profile of *Dand5* KO and WT mESC, we performed next generation RNA-sequencing (RNA-seq), and compared the transcriptomes of undifferentiated cells and differentiated cells at day 5 (EBs in suspension), day 6 (24 h after EB plating), day 8, and day 10. Principal component analysis (PCA) indicated that *Dand5* KO samples, except for the undifferentiated and day 10 cells, were consistently closer to WT samples of later days than the corresponding WT samples themselves (**Figure 5A**). This suggests that *Dand5* KO EBs progressed faster through cardiac mesoderm induction and differentiation. Next, we decided to confirm the existence of different expression patterns under the absence of DAND5 during EB differentiation on a gene level. We obtained an overall picture of the genetic expression across the time series by visualization and clustering of genes that were detected by RNA seq. As the resulting heat map displays, expression patterns of *Dand5* KO samples are distinct from their WT counterparts, mainly at days 5, 6, and 8 (**Figure 5B**). Differences can still be observed at day 10 samples, but not in the same degree as in the other days, which is in accordance with the PCA analysis (**Figure 5A**).

Focusing our analysis at day 6, when visible beating foci areas in the *Dand5* KO cells start to emerge, we generated a Volcano Plot and selected the genes with FDR lower than 0.01 and absolute log FC higher than 2 between *Dand5* KO and WT samples (**Figure 5C**). Then, a KEGG pathway enrichment analysis of the differentially expressed genes was carried out

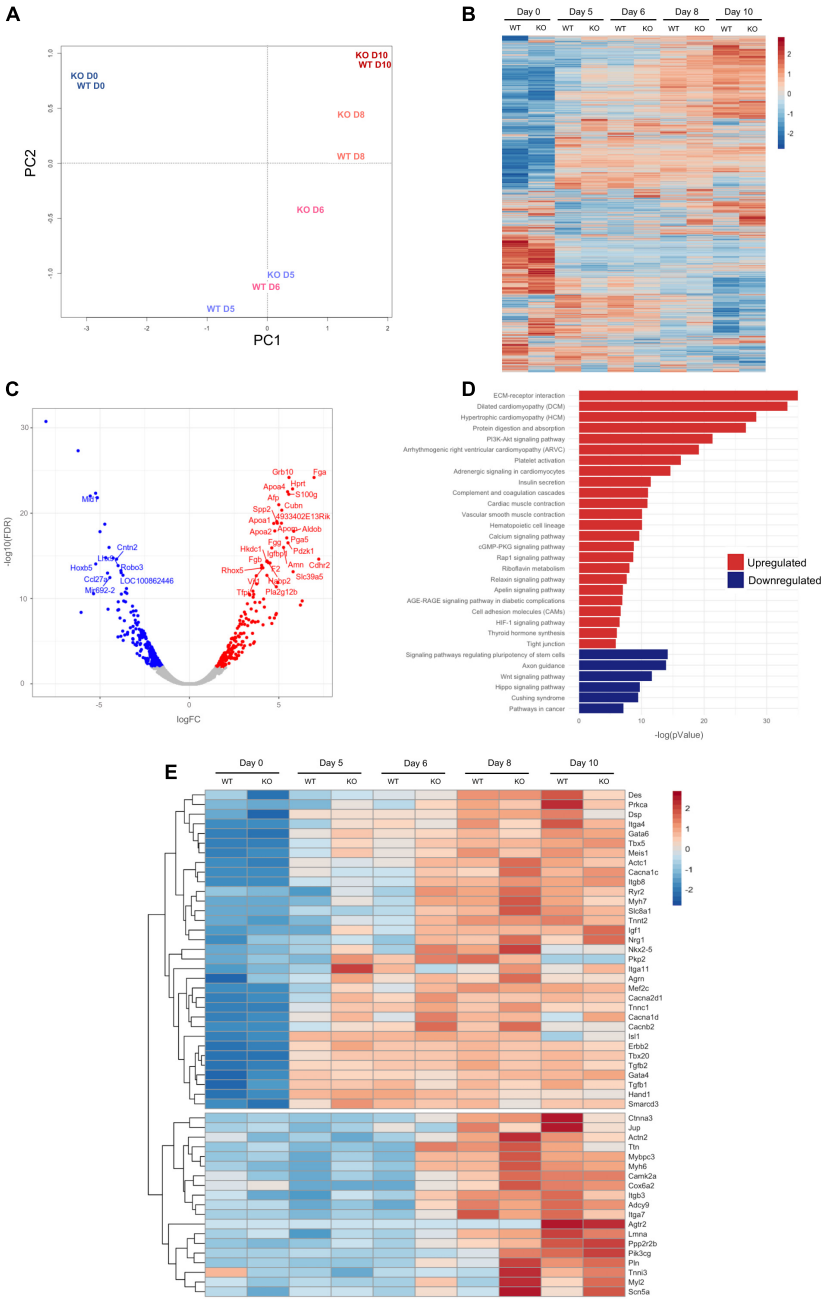

FIGURE 5 | RNA-seq Analysis of EB differentiation up to day 10. **(A)** Principal Component Analysis (PCA) of WT and *Dand5* KO samples from EB differentiation from mESC (D0) to day 10 of differentiation (D10); **(B)** Heat Map of all the genes commonly counted in all the samples. Profiles of expression of each gene were hierarchically clustered; **(C)** Volcano plot of genes differentially expressed at day 6 of EB differentiation. Genes with FDR < 0.01 were colored in red. Results are relative to WT data. **(D)** Pathway enrichment analysis of genes differentially expressed at day 6 of EB differentiation. Results are relative to WT data; **(E)** Heat Map of genes related with Heart Cardiomyopathy and Dilated Cardiomyopathy terms of KEGG. Profiles of expression of each gene were hierarchically clustered.

and suggested that upregulated differentially expressed genes were involved in pathways such as dilated cardiomyopathy, hypertrophic cardiomyopathy, PI3K-Akt signaling pathway, cardiac muscle contraction or calcium signaling pathway (**Figure 5D**). On the other hand, we observed that the downregulated differentially expressed genes were associated with pathways such as pluripotency maintenance, Wnt, or Hippo signaling (**Figure 5D**). This is in line with the expected results for *Dand5* KO differentiating cells, which were already committing to a cardiac lineage, with an increased proliferative capacity, while their WT counterparts are still delayed in this process.

Next, we evaluated a panel of well-studied genes involved in different cardiomyogenic processes in more detail. Notably, the clustered heat map for the differential expression (**Figure 5E**) reveals two distinct gene expression signatures that can be interpreted as two different transcriptional waves. The first cluster contains genes known to be related to early cardiac induction and being expressed before day 5, which explains the similar levels of expression for these genes (e.g., *Isl1* and *Hand1*). Genes related to early cardiomyocyte differentiation, cardiovascular morphogenesis, and function, as *Nkx2.5*, *Tbx5*, *Mef2c,* or *Tnnc1*, are also in the first cluster. These genes started being upregulated in *Dand5* KO compared to corresponding WT samples as early as day 5, and their relative upregulation persists until genes show full induction in the WT samples. These results are in agreement with the PCR measurements, validating the RNA-seq results. The transcriptome analyses also indicated that the knockout of *Dand5* changed the expression of genes associated with cardiovascular morphogenesis and function. Genes like *MHC* (*Myh7*), *cTnT* (*Tnnt2*), *TNNI* (*Tnni3*), *Myl2*, were upregulated in the absence of *Dand5*. The second cluster of genes displays a different expression pattern, with main differences in transcription arising at days 6 and 8. Genes in this cluster are related with cardiomyocyte commitment, such as *Titin* (*Ttn*), usually a marker of cardiomyocyte maturation, *Ryr2*, that encodes a Ca^{2+} channel, or *Itgb7*, and integrin subunit related with cardiomyocyte interaction with ECM and other cells. Additionally, we observed an up-regulation of genes related with cardiomyocyte proliferation, *Agrn1* at day 8, and of *Igf1* and *Nrg1* at day 10 on *Dand5* KO samples. These findings suggested an increased cell proliferation in the *Dand5* KO cells, which is in line with the results from the cardiomyocyte proliferation assay.

DISCUSSION

In this study, we found that suppression of DAND5 leads to an increase in the number of cardiac progenitor cells and augments the proliferative state of the mESCs-derived cardiomyocytes. During the differentiation of the *Dand5* KO mESCs, a significant difference in the number of beating foci areas in the mutant cells compared to the control line was observed. This result is concomitant with the detected upregulation of *Mesp-1*, *Isl1*, and *Nkx2.5* within the period of cardiac mesoderm formation. During *in vivo* cardiogenesis, MESP1 proteins start to be recruited to the mouse primitive streak at E6.5 (Meilhac et al., 2014). Its expression is transient during the phase of mesoderm formation, and there are about 150–250 $MESP1^{+}$ progenitor cells that will contribute to cardiac morphogenesis (Meilhac et al., 2014; Chabab et al., 2016; Meilhac and Buckingham, 2018). In the case of DAND5 absence, our data predict that this number of cells is increased, leading to abnormal migration of cells to the heart and posterior high numbers of cardiac cells. In agreement, the high levels of relative *Nkx2.5* and *Isl1* expression in the *Dand5* mutant also revealed that the production of cardiac progenitors, derived from the First and Second Heart Fields, could be increased. The First Heart Field cardiac lineage, which can be identified through the positive expression of the *Nkx2.5* gene, contributes primarily to the formation of the linear heart tube and ultimately to the origin of the mature cardiac cells that will populate the left ventricle (Buckingham et al., 2005). Second Heart Field cells are often identified by the positive expression of *Isl1* being these cells the late cardiac progenitors for myocardial, endothelial, and smooth muscle cells (Moretti et al., 2006). Our results also demonstrated that the absence of DAND5 changes strikingly the population of FLK-1^{+}/PDGFR-α^{+} cardiac progenitor cells in differentiating mESCs. Moreover, it is noted that the size of the mature heart will depend on how the number of cardiac progenitor cells scales up (Chabab et al., 2016). Combining these previous findings with our new results suggests that the increase of the *Mesp-1*, *Isl1*, and *Nkx2.5* expression during mouse cardiogenesis may coincide with a larger number of FHF and SHF progenitors capable of forming a robust myocardium tissue. These combined features could provide an explanation for the progressive increase of the trabecular and compact myocardium observed in the DAND5 null-mutant embryos (Araújo et al., 2014).

Cardiomyocytes are derived from the lateral plate mesoderm, which is composed of cells that migrated from the primitive streak toward both these anterior lateral regions of the embryo. This population of cells is characterized by *Fzd4* expression. The abundance of FZD4 is positively correlated with higher cardiomyocytes yield (Yoon et al., 2018). In our experiment, *Fzd4* expression was upregulated during the differentiation of *Dand5* KO mESCs, which is in line with the expanded cardiogenic capacity demonstrated by DAND5 mutant cells. The observed expression pattern of *Bmp2* was also interesting. In mice, ectopic expression of *Bmp2* in the chamber myocardium maintains the cardiomyocyte in a primitive and proliferative state leading to heart dysmorphogenesis and embryonic death (Prados et al., 2018). In contrast, the upregulation of *Bmp2* in the DAND5 mutant cells could contribute to the proliferation and expansion of the cardiac progenitor cells while not affecting cardiac differentiation. Indeed, levels of expression of genes essential for proper cardiomyocytes contraction (α-*MHC* and *cTnT*) demonstrated so. The high levels of relative α-*MHC* expression detected in the knockout cells are compatible with a high number of derived-cardiomyocytes. Moreover, these cells display enhanced sarcomere structures at early differentiation stages, explaining the previous contractility of the *Dand5* KO EBs. Curiously, the decreased levels of *cTnT* expression found in the differentiated *Dand5* KO mESCs at latter differentiation stages, indicates that the produced cardiomyocytes were not fully mature. This agrees with prior results that demonstrated a decrease in *cTnT* expression in the mutant mouse embryos at E13 and E15 (Araújo et al., 2014).

Cyclins and cyclin-dependent kinase (CDKs) are defined as regulatory molecules during embryonic cardiomyocyte division (Ikenishi et al., 2012). During this development process, it was reported that the Wnt/β-catenin pathway is capable of interfering in the proliferation capacity, mainly in the ventricular cardiomyocytes (Buikema et al., 2013). The recruitment of CCND1 and CCND2 (Cyclin D1 and Cyclin D2) proteins is one of the key triggers of the cardiac cell cycle. In the present data, we found a statistical increase of *Ccnd1* in the

Dand5 KO cells at day 10, explaining the high number of derived cardiomyocytes. Moreover, our proliferation assay also highlighted the difference between the *Dand5* KO mESC-derived cardiomyocytes' proliferative capacity and the control cell line.

Transcriptomic analysis supported the notion that *Dand5* has a broad and important biological significance during cardiac development. Clear differences in the differentiation process were observed in PCA following knockdown of *Dand5*, especially a temporal shift toward an anticipated cardiac transcriptional program. Genes affected included those commonly related with cardiac morphogenesis and function underlying proliferation and differentiation of specific populations of heart precursor cells (Buckingham et al., 2005; Srivastava, 2006; Epstein, 2010; Ikenishi et al., 2012), such as cardiac transcription factors (e.g., *Nkx2.5*, *Isl1*), structural genes (*MHC*, *cTnT*), or cell cycle regulators (e.g., *Ccnd1*), which have been also validated by the RT-PCR results. Nevertheless, taking advantage of the power of genome-level approach, *Dand5* KO cells revealed significant changes in genes related to ECM-receptor interaction, dilated cardiomyopathy, hypertrophic cardiomyopathy, adrenergic signaling in cardiomyocytes, cardiac muscle contraction, calcium signaling, cell adhesion molecules, tight junctions, among other biological processes. Similarly, signaling pathways associated with cell-cycle regulation, the Hippo, IGF-PI3K-Akt, and Neuregulin were also altered. From all the factors involved in stimulating cardiomyocyte proliferation, *Meis1*, *Nrg*, and *Igf1*, were the ones that attained our attention. *Meis1* has been associated with *Hox* genes and found to be involved in the cell cycle regulation of cardiomyocytes (Paul et al., 2020). Cardiac-specific deletion of *Meis1* expression increases the proliferative capacity of the cardiomyocytes of newborn mice, whereas overexpression of *Meis1* decreases neonatal cardiomyocyte regenerative window (Mahmoud et al., 2013). *Meis1* was downregulated in *Dand5* KO mESCs, which prompted the deactivation of the regulatory mechanism of cardiomyocyte cell-cycle arrest and may have resulted in a continued division and proliferation of CMs. In contrast, *Nrg1* and *Igf1* were upregulated in *Dand5* KO embryoid bodies. Several studies have shown that the overexpression of *Nrg1* not only promotes cardiomyocyte proliferation in mice but also improves cardiac function after heart injury (D'Uva et al., 2015; Gemberling et al., 2015; Santoro and Sahara, 2015). Ectopic *Igf* signaling also fosters cardiomyocyte proliferation by increasing cell-cycle activity in adult mice cardiomyocytes (Samarel, 2002). *Igf1* expression was also increased in *Dand5* KO cells when compared to the control line. All these observations indicated that the obtained results of the transcriptional analysis are a valuable starting tool to explore the function of *Dand5* as a regulator during the cardiomyocyte-specific differentiation and proliferation.

In conclusion, we successfully derived and characterized a stable *Dand5* knockout mouse embryonic stem cell line with the purpose to uncover the first insights related to the role of DAND5 as an important endogenous regulator of the mechanisms controlling differentiation and proliferation of cardiomyocytes during the first stages of life. Moreover, our findings suggest that DAND5 drives distinctive transcriptional programs associated with the differentiation and proliferative networks of CMs that could be explored as a novel therapeutical approach for a diseased heart.

DATA AVAILABILITY STATEMENT

The datasets presented in this study can be found in online repositories. The names of the repository/repositories and accession number(s) can be found below: https://www.ebi.ac.uk/arrayexpress/, E-MTAB-9986.

ETHICS STATEMENT

The animal study was reviewed and approved by the Veterinary Agency from Portuguese Ministry of Agriculture (DGAV), Portugal.

AUTHOR CONTRIBUTIONS

JI and JB conceived and designed the study. JI, JG, AS, FC, and SM performed the experiments. JI, JG, and MF analyzed the RNA-Seq data. JI, JG, FC, and JB wrote the original draft. All authors critically read and approved the final manuscript.

FUNDING

This work was supported by the Fundação para a Ciência e a Tecnologia (PTDC/BIM-MED/3363/2014) and Scientific Employment Stimulus to JI (Norma Transitória 8189/2018), pre-doctoral fellowship to JG (FCT; PD/BD/136919/2018) and post-doctoral fellowship to FC (DAI/ 2019/08/SAICTPAC/0047/2015), and iNOVA4Health-UID/Multi/04462/2013, a program financially supported by Fundação para a Ciência e a Tecnologia/Ministério da Educação e Ciência, through national funds and co-funded by FEDER under the PT2020 Partnership Agreement.

ACKNOWLEDGMENTS

The authors want to thank all CEDOC facilities, but mostly the Rodent Facility and Flow Cytometry Facility; and the Cogento Consortium for Genetically Tractable Organisms.

SUPPLEMENTARY MATERIAL

The Supplementary Material for this article can be found online at: https://www.frontiersin.org/articles/10.3389/fcell.2021.629430/full#supplementary-material

REFERENCES

Ames, E. G., Lawson, M. J., Mackey, A. J., and Holmes, J. W. (2013). Sequencing of mRNA identifies re-expression of fetal splice variants in cardiac hypertrophy. *J. Mol. Cell. Cardiol.* 62, 99–107. doi: 10.1016/j.yjmcc.2013.05.004

Araújo, A. C., Marques, S., and Belo, J. A. (2014). Targeted inactivation of cerberus like-2 leads to left ventricular cardiac hyperplasia and systolic dysfunction in the mouse. *PLoS One* 9:e102716. doi: 10.1371/journal.pone.0102716

Belo, J. A., Bachiller, D., Agius, E., Kemp, C., Borges, A. C., Marques, S., et al. (2000). Cerberus-like is a secreted BMP and nodal antagonist not essential for mouse development. *Genesis* 26, 265–270.

Belo, J. A., Marques, S., and Inácio, J. M. (2017). The role of Cerl2 in the establishment of left-right asymmetries during axis formation and heart development. *J. Cardiovasc. Dev. Dis.* 4:23. doi: 10.3390/jcdd4040023

Belo, J. A., Silva, A. C., Borges, A.-C., Filipe, M., Bento, M., Gonçalves, L., et al. (2009). Generating asymmetries in the early vertebrate embryo: the role of the Cerberus-like family. *Int. J. Dev. Biol.* 53, 1399–1407. doi: 10.1387/ijdb.072297jb

Bondue, A., and Blanpain, C. (2010). Mesp1: a key regulator of cardiovascular lineage commitment. *Circ. Res.* 107, 1414–1427. doi: 10.1161/CIRCRESAHA.110.227058

Bover, O., Justo, T., Pereira, P. N. G., Facucho-Oliveira, J., Inacio, J. M., Ramalho, J. S., et al. (2018). Loss of Ccbe1 affects cardiac-specification and cardiomyocyte differentiation in mouse embryonic stem cells. *PLoS One* 13:e0205108. doi: 10.1371/journal.pone.0205108

Brand, T. (2003). Heart development: molecular insights into cardiac specification and early morphogenesis. *Dev. Biol.* 258, 1–19. doi: 10.1016/S0012-1606(03)00112-X

Bruneau, B. G. (2013). Signaling and transcriptional networks in heart development and regeneration. *Cold Spring Harb. Perspect. Biol.* 5:a008292. doi: 10.1101/cshperspect.a008292

Bruneau, B. G., Nemer, G., Schmitt, J. P., Charron, F., Robitaille, L., Caron, S., et al. (2001). A murine model of Holt-Oram syndrome defines roles of the T-box transcription factor Tbx5 in cardiogenesis and disease. *Cell* 106, 709–721. doi: 10.1016/s0092-8674(01)00493-7

Buckingham, M., Meilhac, S., and Zaffran, S. (2005). Building the mammalian heart from two sources of myocardial cells. *Nat. Rev. Genet.* 6, 826–835. doi: 10.1038/nrg1710

Buikema, J. W., Mady, A. S., Mittal, N. V., Atmanli, A., Caron, L., Doevendans, P. A., et al. (2013). Wnt/β-catenin signaling directs the regional expansion of first and second heart field-derived ventricular cardiomyocytes. *Development* 140, 4165–4176. doi: 10.1242/dev.099325

Bustin, S. A. (2000). Absolute quantification of mRNA using real-time reverse transcription polymerase chain reaction assays. *J. Mol. Endocrinol.* 25, 169–193. doi: 10.1677/jme.0.0250169

Chabab, S., Lescroart, F., Rulands, S., Mathiah, N., Simons, B. D., and Blanpain, C. (2016). Uncovering the number and clonal dynamics of Mesp1 progenitors during heart morphogenesis. *Cell Rep.* 14, 1–10. doi: 10.1016/j.celrep.2015.12.013

David, R., Jarsch, V. B., Schwarz, F., Nathan, P., Gegg, M., Lickert, H., et al. (2011). Induction of MesP1 by Brachyury(T) generates the common multipotent cardiovascular stem cell. *Cardiovasc. Res.* 92, 115–122. doi: 10.1093/cvr/cvr158

Devine, W. P., Wythe, J. D., George, M., Koshiba-Takeuchi, K., and Bruneau, B. G. (2014). Early patterning and specification of cardiac progenitors in gastrulating mesoderm. *Elife* 3:e03848. doi: 10.7554/eLife.03848

Dobin, A., and Gingeras, T. R. (2015). Mapping RNA-seq reads with STAR. *Curr. Protoc. Bioinforma.* 51, 11.14.1–11.14.19. doi: 10.1002/0471250953.bi1114s51

Dodou, E., Verzi, M. P., Anderson, J. P., Xu, S.-M., and Black, B. L. (2004). Mef2c is a direct transcriptional target of ISL1 and GATA factors in the anterior heart field during mouse embryonic development. *Development* 131, 3931–3942. doi: 10.1242/dev.01256

D'Uva, G., Aharonov, A., Lauriola, M., Kain, D., Yahalom-Ronen, Y., Carvalho, S., et al. (2015). ERBB2 triggers mammalian heart regeneration by promoting cardiomyocyte dedifferentiation and proliferation. *Nat. Cell Biol.* 17, 627–638. doi: 10.1038/ncb3149

Epstein, J. A. (2010). Franklin H. epstein lecture. Cardiac development and implications for heart disease. *N. Engl. J. Med.* 363, 1638–1647. doi: 10.1056/NEJMra1003941

Gemberling, M., Karra, R., Dickson, A. L., and Poss, K. D. (2015). Nrg1 is an injury-induced cardiomyocyte mitogen for the endogenous heart regeneration program in zebrafish. *Elife* 4:e05871. doi: 10.7554/eLife.05871

Gottlieb, P. D., Pierce, S. A., Sims, R. J., Yamagishi, H., Weihe, E. K., Harriss, J. V., et al. (2002). Bop encodes a muscle-restricted protein containing MYND and SET domains and is essential for cardiac differentiation and morphogenesis. *Nat. Genet.* 31, 25–32. doi: 10.1038/ng866

Ikenishi, A., Okayama, H., Iwamoto, N., Yoshitome, S., Tane, S., Nakamura, K., et al. (2012). Cell cycle regulation in mouse heart during embryonic and postnatal stages. *Dev. Growth Differ.* 54, 731–738. doi: 10.1111/j.1440-169X.2012.01373.x

Kelly, R. G., Buckingham, M. E., and Moorman, A. F. (2014). Heart fields and cardiac morphogenesis. *Cold Spring Harb. Perspect. Med.* 4:a015750. doi: 10.1101/cshperspect.a015750

Khalifa, E. A., Tucker, M. J., and Hunt, P. (1992). Cruciate thinning of the zona pellucida for more successful enhancement of blastocyst hatching in the mouse. *Hum. Reprod.* 7, 532–536. doi: 10.1093/oxfordjournals.humrep.a137685

Leone, M., Magadum, A., and Engel, F. B. (2015). Cardiomyocyte proliferation in cardiac development and regeneration: a guide to methodologies and interpretations. *Am. J. Physiol. Hear. Circ. Physiol.* 309, H1237–H1250. doi: 10.1152/ajpheart.00559.2015

Liao, Y., Smyth, G. K., and Shi, W. (2019a). The R package Rsubread is easier, faster, cheaper and better for alignment and quantification of RNA sequencing reads. *Nucleic Acids Res.* 47:e47. doi: 10.1093/nar/gkz114

Liao, Y., Wang, J., Jaehnig, E. J., Shi, Z., and Zhang, B. (2019b). WebGestalt 2019: gene set analysis toolkit with revamped UIs and APIs. *Nucleic Acids Res.* 47, W199–W205. doi: 10.1093/nar/gkz401

Lien, C. L., Wu, C., Mercer, B., Webb, R., Richardson, J. A., and Olson, E. N. (1999). Control of early cardiac-specific transcription of Nkx2-5 by a GATA-dependent enhancer. *Development* 126, 75–84.

Liu, Y., Lu, P., Wang, Y., Morrow, B. E., Zhou, B., and Zheng, D. (2019). Spatiotemporal gene coexpression and regulation in mouse cardiomyocytes of early cardiac morphogenesis. *J. Am. Heart Assoc.* 8:e012941. doi: 10.1161/JAHA.119.012941

Mahmoud, A. I., Kocabas, F., Muralidhar, S. A., Kimura, W., Koura, A. S., Thet, S., et al. (2013). Meis1 regulates postnatal cardiomyocyte cell cycle arrest. *Nature* 497, 249–253. doi: 10.1038/nature12054

Marques, S., Borges, A. C., Silva, A. C., Freitas, S., Cordenonsi, M., and Belo, J. A. (2004). The activity of the nodal antagonist Cerl-2 in the mouse node is required for correct L/R body axis. *Genes Dev.* 18, 2342–2347. doi: 10.1101/gad.306504

McCarthy, D. J., Chen, Y., and Smyth, G. K. (2012). Differential expression analysis of multifactor RNA-Seq experiments with respect to biological variation. *Nucleic Acids Res.* 40, 4288–4297. doi: 10.1093/nar/gks042

Meilhac, S. M., and Buckingham, M. E. (2018). The deployment of cell lineages that form the mammalian heart. *Nat. Rev. Cardiol.* 15, 705–724. doi: 10.1038/s41569-018-0086-9

Meilhac, S. M., Lescroart, F., Blanpain, C., and Buckingham, M. E. (2014). Cardiac cell lineages that form the heart. *Cold Spring Harb. Perspect. Med.* 4:a013888. doi: 10.1101/cshperspect.a013888

Meilhac, S. M., Lescroart, F., Blanpain, C., and Buckingham, M. E. (2015). Cardiac cell lineages that form the heart. *Cold Spring Harb. Perspect. Med.* 5:a026344. doi: 10.1101/cshperspect.a026344

Moretti, A., Caron, L., Nakano, A., Lam, J. T., Bernshausen, A., Chen, Y., et al. (2006). Multipotent embryonic isl1+ progenitor cells lead to cardiac, smooth muscle, and endothelial cell diversification. *Cell* 127, 1151–1165. doi: 10.1016/j.cell.2006.10.029

Ng, S. Y., Wong, C. K., and Tsang, S. Y. (2010). Differential gene expressions in atrial and ventricular myocytes: insights into the road of applying embryonic stem cell-derived cardiomyocytes for future therapies. *Am. J. Physiol. Cell Physiol.* 299, C1234–C1249. doi: 10.1152/ajpcell.00402.2009

Nishii, K., Morimoto, S., Minakami, R., Miyano, Y., Hashizume, K., Ohta, M., et al. (2008). Targeted disruption of the cardiac troponin T gene causes sarcomere disassembly and defects in heartbeat within the early mouse embryo. *Dev. Biol.* 322, 65–73. doi: 10.1016/j.ydbio.2008.07.007

Olson, E. N., Moretti, A., Caron, L., Nakano, A., Lam, J. T., Bernshausen, A., et al. (2006). Targeted disruption of the cardiac troponin T gene causes sarcomere disassembly and defects in heartbeat within the early mouse embryo. *Am. J. Physiol. Cell Physiol.* 322, 1151–1165.

O'Meara, C. C., Wamstad, J. A., Gladstone, R. A., Fomovsky, G. M., Butty, V. L., Shrikumar, A., et al. (2015). Transcriptional reversion of cardiac myocyte fate during mammalian cardiac regeneration. *Circ. Res.* 116, 804–815. doi: 10.1161/CIRCRESAHA.116.304269

Paige, S. L., Plonowska, K., Xu, A., and Wu, S. M. (2015). Molecular regulation of cardiomyocyte differentiation. *Circ. Res.* 116, 341–353. doi: 10.1161/CIRCRESAHA.116.302752

Paul, S., Zhang, X., and He, J.-Q. (2020). Homeobox gene Meis1 modulates cardiovascular regeneration. *Semin. Cell Dev. Biol.* 100, 52–61. doi: 10.1016/j.semcdb.2019.10.003

Payan, S. M., Hubert, F., and Rochais, F. (2020). Cardiomyocyte proliferation, a target for cardiac regeneration. *Biochim. Biophys. Acta Mol. Cell Res.* 1867:118461. doi: 10.1016/j.bbamcr.2019.03.008

Phan, D., Rasmussen, T. L., Nakagawa, O., McAnally, J., Gottlieb, P. D., Tucker, P. W., et al. (2005). BOP, a regulator of right ventricular heart development, is a direct transcriptional target of MEF2C in the developing heart. *Development* 132, 2669–2678. doi: 10.1242/dev.01849

Polanco, J. C., and Koopman, P. (2007). Sry and the hesitant beginnings of male development. *Dev. Biol.* 302, 13–24. doi: 10.1016/j.ydbio.2006.08.049

Prados, B., Gómez-Apiñániz, P., Papoutsi, T., Luxán, G., Zaffran, S., Pérez-Pomares, J. M., et al. (2018). Myocardial Bmp2 gain causes ectopic EMT and promotes cardiomyocyte proliferation and immaturity. *Cell Death Dis.* 9:399. doi: 10.1038/s41419-018-0442-z

Qian, L., Huang, Y., Spencer, C. I., Foley, A., Vedantham, V., Liu, L., et al. (2012). In vivo reprogramming of murine cardiac fibroblasts into induced cardiomyocytes. *Nature* 485, 593–598. doi: 10.1038/nature11044

Samarel, A. M. (2002). IGF-1 overexpression rescues the failing heart. *Circ. Res.* 90, 631–633. doi: 10.1161/01.res.0000015425.11187.19

Santoro, F., and Sahara, M. (2015). A specified therapeutic window for neuregulin-1 to regenerate neonatal heart muscle. *Ann. Transl. Med.* 3:249. doi: 10.3978/j.issn.2305-5839.2015.09.38

Srivastava, D. (2006). Genetic regulation of cardiogenesis and congenital heart disease. *Annu. Rev. Pathol.* 1, 199–213. doi: 10.1146/annurev.pathol.1.110304.100039

Taegtmeyer, H., Sen, S., and Vela, D. (2010). Return to the fetal gene program. *Ann. N. Y. Acad. Sci.* 1188, 191–198. doi: 10.1111/j.1749-6632.2009.05100.x

Uosaki, H., Cahan, P., Lee, D. I., Wang, S., Miyamoto, M., Fernandez, L., et al. (2015). Transcriptional landscape of cardiomyocyte maturation. *Cell Rep.* 13, 1705–1716. doi: 10.1016/j.celrep.2015.10.032

Virani, S. S., Alonso, A., Benjamin, E. J., Bittencourt, M. S., Callaway, C. W., Carson, A. P., et al. (2020). Heart disease and stroke statistics—2020 update: a report from the American Heart Association. *Circulation* 141, e139–e596. doi: 10.1161/CIR.0000000000000757

Wang, Y., Yi, N., Hu, Y., Zhou, X., Jiang, H., Lin, Q., et al. (2020). Molecular signatures and networks of cardiomyocyte differentiation in humans and mice. *Mol. Ther. Nucleic Acids* 21, 696–711. doi: 10.1016/j.omtn.2020.07.011

Xiong, H., and He, A. (2020). Single-cell transcriptomic analysis of cardiac progenitor differentiation. *Curr. Cardiol. Rep*. 22:38. doi: 10.1007/s11886-020-01285-2

Yoon, C., Song, H., Yin, T., Bausch-Fluck, D., Frei, A. P., Kattman, S., et al. (2018). FZD4 marks lateral plate mesoderm and signals with norrin to increase cardiomyocyte induction from pluripotent stem cell-derived cardiac progenitors. *Stem Cell Reports* 10, 87–100. doi: 10.1016/j.stemcr.2017.11.008

Yuan, X., and Braun, T. (2017). Multimodal regulation of cardiac myocyte proliferation. *Circ. Res.* 121, 293–309. doi: 10.1161/CIRCRESAHA.117.308428

Zhou, B., and Wang, L. (2020). Transcriptional profiling of single cardiomyocytes in health and disease. *Curr. Cardiol. Rep.* 22:92. doi: 10.1007/s11886-020-01346-6

Conflict of Interest: The authors declare that the research was conducted in the absence of any commercial or financial relationships that could be construed as a potential conflict of interest.

Advantages of publishing in Frontiers

OPEN ACCESS
Articles are free to read for greatest visibility and readership

FAST PUBLICATION
Around 90 days from submission to decision

HIGH QUALITY PEER-REVIEW
Rigorous, collaborative, and constructive peer-review

TRANSPARENT PEER-REVIEW
Editors and reviewers acknowledged by name on published articles

Frontiers
Avenue du Tribunal-Fédéral 34
1005 Lausanne | Switzerland

Visit us: www.frontiersin.org
Contact us: frontiersin.org/about/contact

REPRODUCIBILITY OF RESEARCH
Support open data and methods to enhance research reproducibility

DIGITAL PUBLISHING
Articles designed for optimal readership across devices

FOLLOW US
@frontiersin

IMPACT METRICS
Advanced article metrics track visibility across digital media

EXTENSIVE PROMOTION
Marketing and promotion of impactful research

LOOP RESEARCH NETWORK
Our network increases your article's readership